

TM 5-858-3

TECHNICAL MANUAL

**DESIGNING FACILITIES
TO RESIST
NUCLEAR WEAPON EFFECTS
STRUCTURES**

**HEADQUARTERS, DEPARTMENT OF THE ARMY
6 JULY 1984**

REPRODUCTION AUTHORIZATION/RESTRICTIONS

This manual has been prepared by or for the Government and, except to the extent indicated below, is public property and not subject to copyright.

Copyrighted material included in the manual has been used with the knowledge and permission of the proprietors and is acknowledged as such at point of use. Anyone wishing to make further use of any copyrighted material, *by itself and apart from this text*, should seek necessary permission directly from the proprietors.

Reprints or republications of this manual should include a credit substantially as follows: "Department of the Army, USA, Technical Manual TM 5-858-3, Designing Facilities to Resist Nuclear Weapon Effects, Structures.

If the reprint or republication includes *copyrighted* material, the credit should also state: "Anyone wishing to make further use of copyrighted material, *by itself and apart from this text*, should seek necessary permission directly from the proprietors."

This manual includes copyright material reproduced by permission of the Agabian Associates Engineers and Consultants.

TECHNICAL MANUAL

No. 5-858-3

HEADQUARTERS
DEPARTMENT OF THE ARMY
WASHINGTON, DC 6 JULY 1984

DESIGNING FACILITIES TO RESIST NUCLEAR WEAPON EFFECTS

STRUCTURES

REPORTING OF ERRORS

You can improve this bulletin by reporting errors, omissions, and recommendations for improvements. Reports should be submitted on DA Form 2028 (Recommended Changes to Publications and Blank Forms) and forwarded directly to Commander, US Army Corps of Engineers, ATTN: DAEN-ECE-T, Washington, DC, 20314.

A reply will be furnished directly to you.

	Paragraph	Page
CHAPTER 1. INTRODUCTION		
General	1-1	1-1
TM 5-858-3: Structures	1-2	1-1
CHAPTER 2. BASIC OBJECTIVES OF THE STRUCTURE		
Objectives vs. Availability Requirements	2-1	2-1
CHAPTER 3. DESIGN REQUIREMENTS		
Introduction	3-1	3-1
Functional Requirements	3-2	3-1
Technical Requirements	3-3	3-1
Technical Design Criteria	3-4	3-1
CHAPTER 4. DESIGN PHILOSOPHY		
Major Elements	4-1	4-1
Design Procedure	4-2	4-2
Depth Selection	4-3	4-2
Selection of Structural Concept	4-4	4-2
Development of Structure Concepts	4-5	4-9
Preliminary Design	4-6	4-10
Final Design Detailing	4-7	4-10
Design Verification	4-8	4-10
CHAPTER 5. MATERIAL PROPERTIES		
Materials of Interest	5-1	5-1
Material Properties Required for Design	5-2	5-1
Assignment of Numerical Values	5-3	5-1
Static Properties of Structural Steel	5-4	5-2
Dynamic Properties of Steel	5-5	5-3
Conventional-Strength Concrete	5-6	5-12
High-Strength Concrete	5-7	5-18
Ultra-High-Strength Concrete	5-8	5-19
Plastics and Other Materials	5-9	5-20
Properties of Soils	5-10	5-21
Properties of Rock	5-11	5-29
Stress/Strain Models	5-12	5-44

*This manual together with TM 5-858-1, 31 October 1983 and TM 5-858-3 through TM 5-858-8 supersedes TM 5-856-1, 1 July 1959; TM 5-856-2, 15 March 1957; TM 5-856-3, 15 March 1957; TM 5-856-4, 15 March 1957; TM 5-856-5, 15 January 1958; TM 5-856-6, 15 January 1960; TM 5-856-7, 15 January 1958; TM 5-856-8, 15 January 1960; and TM 5-856-9, 15 January 1960.

CHAPTER	TITLE	<i>Paragraph</i>	<i>Page</i>
CHAPTER 6.	BEHAVIOR OF STRUCTURAL ELEMENTS		
	Load Capacity of Structural Elements	6-1	6-1
	Flexural Strength of Structural Steel	6-2	6-1
	Shear Strength of Structural Steel	6-3	6-3
	Combined Flexural and Axial Loads on Structural Steel	6-4	6-6
	Flexural and Shear Strength of Reinforced Concretes	6-5	6-7
	Combined Flexural and Axial Loads on Reinforced Concrete	6-6	6-11
	Ultimate Load for Two-Way Slabs	6-7	6-12
	Composite Beam Slabs	6-8	6-16
	Composite Slabs with Steel Liners	6-9	6-18
	Fiber-Reinforced Concrete	6-10	6-20
CHAPTER 7.	NONDETERIORATING DESIGN DETAILS		
	Introduction	7-1	7-1
	Multiple Loading of Steel Members	7-2	7-1
	Guidelines for Connection Details	7-3	7-5
	Multiple Loading of Reinforced-Concrete Members	7-4	7-6
CHAPTER 8.	DYNAMIC STRUCTURAL ANALYSIS		
	Introduction	8-1	8-1
	Reduction to a System with Few Degrees of Freedom	8-2	8-1
	Resistance Function and Spring Constant	8-3	8-1
	Dynamic Design Factors	8-4	8-2
	Dynamic Design of Structural Elements	8-5	8-19
	Analysis of Complex Structures	8-6	8-27
CHAPTER 9.	NUMERICAL METHODS FOR STRUCTURE DESIGN VERIFICATION		
	Introduction	9-1	9-1
	Static Analysis	9-2	9-1
	Response Spectrum	9-3	9-2
	Dynamic Response by Normal Mode Method	9-4	9-3
	Dynamic Response by Direct Integration Method	9-5	9-4
	Nonlinear Dynamic Analysis	9-6	9-6
	Modeling Techniques	9-7	9-7
CHAPTER 10.	ABOVEGROUND STRUCTURES		
	General	10-1	10-1
	Resistance/Geometry Selection	10-2	10-1
	Construction Material Selection	10-3	10-1
	Design for Airblast	10-4	10-1
	Frame Structures Under Blast Loads	10-5	10-20
	Shear Wall Structures	10-6	10-26
	Arches	10-7	10-34
	Domes	10-8	10-37
CHAPTER 11.	FLUSH, PARTIALLY BURIED, AND SHALLOW-BURIED STRUCTURES		
	Design Threats	11-1	11-1
	Site Properties	11-2	11-1
	Structure/Medium Interaction	11-3	11-1
	Loads on Earth-Mounded Structures	11-4	11-6
	Loads on Silos and Vertical Shafts	11-5	11-8
	Loads on Shallow-Buried Structures	11-6	11-14
	Design of Shallow-Buried Structures	11-7	11-22
	Analysis for Design Verification	11-8	11-28
CHAPTER 12.	DEEP-BURIED STRUCTURES		
	Introduction	12-1	12-1
	Distance to Adjacent Openings	12-2	12-1
	Geometry/Orientation	12-3	12-1
	Absolute Size	12-4	12-3
	Reinforcement	12-5	12-8
	Design Procedures for Opening Reinforcement	12-6	12-10
	Excavation Method	12-7	12-48

	<i>Page</i>
APPENDIX A Probability Design of Hardened Structures Under Uncertainties	A-1
APPENDIX B Finite Element Method of Structural Analysis	B-1
APPENDIX C Computer Software for Finite Element Analysis	C-1
APPENDIX D Glossary	D-1
APPENDIX E Bibliography	E-1

LIST OF ILLUSTRATIONS

<i>Figure</i>	<i>Title</i>	<i>Page</i>
4-1	Example of Aboveground Structure	4-4
4-2	Example of Flush Structures	4-6
4-3	Examples of Partially Buried Structures	4-7
4-4	Examples of Shallow-Buried Structures	4-8
4-5	Example of a Deep-Buried System	4-9
5-1	Partial Stress/Strain Curve for A36 Steel	5-4
5-2	Stress/Strain Curves for Specified Minimum Values	5-4
5-3	Mill Tests of Structural Steel	5-5
5-4	Ultimate and Yield Strengths at Elevated Temperatures	5-6
5-5	Effect of Rate of Strain on Stress/Strain Curve for Mild Steel, ASTM A-7 (Discontinued)	5-7
5-6	Effect of Rate of Strain on Yield Stress, ASTM A-7 (Discontinued)	5-8
5-7	Effect of Rate of Strain on Yield Stress in Reinforcing Steel	5-8
5-8	Percent Increase in Yield Stress vs. Equivalent Average Stress Rate for Reinforcing Steel	5-9
5-9	Percent Increase in Yield Stress vs. Equivalent Average Strain Rate for Reinforcing Steel	5-10
5-10	Transition from Ductile to Brittle Behavior of Mild Structural Steel	5-11
5-11	Effect of State of Stress on Failure	5-11
5-12	Effect of Rate of Strain on Stress/Strain Curve for Concrete Compression Tests	5-13
5-13	Dynamic Increase Factor (DIF) for the Compressive Strength of Concrete	5-13
5-14	Effect of Age on Compression Strength, f'_c	5-14
5-15	Effect of Biaxial Compression on Yield Strength of Concrete	5-15
5-16	Axial Compressive Stress (f'_{cc}) as a Function of the Other Compressive Stresses (σ_2, σ_3)	5-15
5-17	Normalized Triaxial Compression Data	5-16
5-18	Stress/Strain Curve for Concrete Confined by Rectangular Hoops	5-18
5-19	Influence of Quantity of Hoops on Stress/Strain Curve for Concrete	5-18
5-20	Idealized Stress/Strain Curves of Potential Backpacking Materials	5-22
5-21	Pore Pressure Parameters	5-24
5-22	Pressure vs. Volumetric Strain for Watching Hills Clay Subjected to Hydrostatic Compression	5-25
5-23	Shear Stress/Strain Relations for McCormick Ranch Sand	5-26
5-24	Deviatoric Stress/Strain Relations for a Sand in a Test Where the Mean Normal Stress is Constant	5-27
5-25	Shear Modulus of Sand Increasing with Confining Pressure	5-28
5-26	Breakdown Stress Associated with an Increase in Poisson's Ratio and a Linear Relation between Stiffness and Confining Stress	5-30
5-27	Shear Stress/Strain Relations for Watching Hill Clay	5-31
5-28	Influence of Time to Failure on the Normalized Secant Moduli at an Axial Strain of 1 Percent	5-32
5-29	Variations of the Shear Secant Modulus as a Function of Shearing Strain	5-33
5-30	Fit of Ramberg-Osgood Curves to Soil Data	5-34
5-31	Stress/Strain Relation for Nugget Sandstone	5-36
5-32	Shear Stress/Axial Relation for Coconino Sandstone	5-37
5-33	Stress/Strain Relation for Cedar City Granite	5-38
5-34	Stress/Strain Relation for Marble Subjected to Proportional Loading ($\sigma_3/\sigma_1 = 0.338$)	5-39
5-35	Ductility of Several Common Rocks Varying with Confining Pressure	5-40
5-36	Average Strength-Pressure Curves of Different Rock Types	5-41
5-37	Strength of Dunham Dolomite under Triaxial Compression and Triaxial Extension Stress States	5-42
5-38	Five Typical Modes of Joint Strength and Displacement	5-43
5-39	Failure Envelopes Expected for Rock Masses	5-45
5-40	Stress/Strain Behavior for Steel	5-45
5-41	Virgin Loading and Unloading/Reloading Behavior of Concrete Model in Compression	5-46
5-42	Behavior of Concrete Model Under Cracking and Rebonding	5-46
5-43	Idealized Model for Geologic Materials	5-48
5-44	Uniaxial Stress/Strain Fit for Backfill Material	5-51

<i>Figure</i>	<i>Title</i>	<i>Page</i>
6-1	Ramberg-Osgood Function	6-2
6-2	Hysteresis Loop	6-3
6-3	Comparison of Load Deflection Curves A36 and A441 Steels	6-4
6-4	Comparison of Equal Strength and Equal Stiffness Designs	6-5
6-5	Typical Beam Section Reinforced to Prevent Web Buckling	6-7
6-6	Approximate Interaction Equation for Wide-Flange Section (Strong Axis Bending, Short Column)	6-8
6-7	Approximate Interaction Equation for Wide-Flange Section (Weak Axis Bending, Short Column)	6-8
6-8	Axial-Load/Moment-Capacity Curve for Reinforced Concrete Columns	6-11
6-9	Yield Lines for a Square Slab	6-13
6-10	Yield Lines for a Rectangular Slab	6-13
6-11	Characteristic Load-Deflection Curves for Structural Walls	6-15
6-12	Structural Wall Test Model	6-15
6-13	Dynamic Ultimate Load Ratios vs. Ratio of Panel Influence Factor to Column Influence Factor	6-16
6-14	Composite Beam-Slab Section	6-17
6-15	Plastic Stress Distribution in Composite Beam	6-17
6-16	Dimensions of Channel Shear Connectors	6-19
6-17	Composite Closure Configuration	6-19
7-1	Beam-Column Connection, Type I, Detail Showing Test Device	7-1
7-2	Alternative Beam-Column Connection, Type II	7-2
7-3	Alternative Beam-Column Connection, Type III	7-2
7-4	Alternative Beam-Column Connection, Type V	7-3
7-5	Flexural Hysteresis Loops for Reinforced Concrete	7-4
7-6	Definition of Ductility Factor μ	7-5
7-7	Shear Hysteresis Loops for Reinforced Concrete	7-8
7-8	Diagonal Reinforcing for Plastic Hinges	7-9
7-9	Experimental Deep Beam with Additional Diagonal Reinforcement to Carry Shear	7-10
7-10	Interior Connection with Diagonal Longitudinal Steel and Hoops for Additional Web Shear	7-11
7-11	Concrete Crushing Inside Curved Bar	7-11
7-12	Exterior Connection with Additional Diagonal Steel and Hoops for Additional Web Shear	7-12
7-13	L-Shaped (Corner) Connection with Additional Diagonal Steel and Hoops	7-13
7-14	Shear Wall Design for Protective Structures	7-13
7-15	Diagonal Reinforcement for Deep Beam	7-14
8-1	Resistance-Deflection Diagrams for Beams	8-3
8-2	General Resistance-Deflection Diagram for Structural Elements	8-4
8-3	Uniformly Loaded Square Interior Flat Slab, Assumed Maximum Moments and Failure Lines	8-20
8-4	Tee-Beam Design Factor for Spring Constant	8-21
8-5	Tee-Beam Design Factor for Resistance and Negative Moment	8-22
8-6	Tee-Beam Design Factor for Positive Moment	8-23
8-7	Model and Notation for General Single-Degree-of-Freedom System	8-25
8-8	Maximum Response of Simple Spring Mass System to Initially Peaked Triangular Force Pulse	8-26
8-9	Forces and Reactions on a Simple Slab Subjected to Uniform Blast Load	8-28
8-10	Design Chart for Maximum Dynamic Shear in a One-Way Slab	8-29
8-11	Design Chart for Elastic Rebound	8-30
9-1	Meshing Techniques	9-9
9-2	Modeling Techniques	9-10
9-3	Building Models	9-12
10-1	Variation of Pressure in a Blast Wave	10-2
10-2	Normal Reflection Factor in Sea Level Air vs. Incident Overpressure	10-3
10-3	Reflected Pressure Coefficient vs. Angle of Incidence	10-4
10-4	Object Drag Coefficients	10-5
10-5	Surface Drag Coefficients	10-7
10-6	Average Drag Coefficients C_S on Front Face of a Wedge	10-8
10-7	Effects of Inclination and Length on Flat Plate Drag Force at Low Overpressure (less than 20 psi)	10-12
10-8	Stages in the Diffraction of a Blast Wave by a Structure without Openings (plan view)	10-13
10-9	Loading on Aboveground, Closed, Rectangular Structure	10-14
10-10	Net Horizontal Loading on a Structure in the Shock Direction	10-16
10-11	Loading on a Circular Arch Element for Axially Approaching Blast Wave	10-16
10-12	Deflected Shape of Arch During Early Stages of Blast Loading Normal to Arch Axis	10-17
10-13	Approximate Modal Loadings from Imposed Blast Loadings	10-18
10-14	Approximate Modal Loadings	10-19
10-15	Plan and Sectional Views of a Typical Dome	10-20
10-16	Single-Story Frame Model and Column Load Conditions	10-21
10-17	Shear Resistance and Bending Moments in a Column Subjected to Lateral Displacement and Vertical Load	10-22

Figure	Title	Page
10-18	Effect of Girder Flexibility on Resistance-Deflection Diagram of Multibay Frames	10-22
10-19	Single-Span Support Assumptions for Design of Frame Girders	10-25
10-20	Multistory Frame Building and the Equivalent Dynamic System	10-25
10-21	Multistory Frame Building with Participating Walls and the Equivalent Dynamic System	10-26
10-22	Simple Shear Wall Structure	10-27
10-23	Forces Acting on Shear Wall	10-28
10-24	Shear Wall Structure with Steel Framing	10-29
10-25	Shear Wall Structure with Interior Shear Wall	10-30
10-26	Idealized Resistance Function for a One-Story Shear Wall	10-31
10-27	Two-Story Shear Wall	10-31
10-28	Shear Wall with Openings and Equivalent Frame	10-32
10-29	Forces Acting upon Structure as a Rigid Body	10-33
10-30	Force Acting upon Two-Story Structure	10-34
10-31	Vibrational Shape Associated with the Lowest Natural Frequency of a Two-Hinged Arch in the Compression Mode ..	10-35
10-32	Vibrational Shape Associated with Lowest Natural Frequency of a Fixed-End Arch in the Compression Mode	10-35
10-33	Sample Arch	10-36
10-34	Vibrational Shape Associated with Lowest Natural Frequency of a Two-Hinged Arch in the Deflection Mode	10-37
10-35	Vibration Parameter C_3 as a Function of the Central Angle θ for a Two-Hinged Arch in the Deflection Mode	10-38
10-36	Vibrational Shape Associated with Lowest Natural Frequency of a Fixed-End Arch in the Deflection Mode	10-40
10-37	Vibrational Parameter C_4 as a Function of the Central Angle θ for a Fixed-End Arch in the Deflection Mode	10-41
10-38	Location and Direction of Maximum Deflections of an Arch Subjected to Deflection Mode Loadings	10-42
10-39	Idealized Resistance Function	10-42
10-40	Relative Values of Parameters in the Deflection Mode	10-43
10-41	Buckled Shape and Distribution of Critical Pressures for a Two-Hinged Arch	10-43
10-42	Buckled Shape and Distribution of Critical Pressure for a Fixed-End Arch	10-44
10-43	Buckling Parameter k as a Function of the Central Angle θ for a Fixed-End Arch	10-45
10-44	Sources of Lateral Resistance on Spread-Footing Foundations	10-46
11-1	Free-Field Geological Profile of Representative Site Obtained from Borings and Seismic Surveys	11-2
11-2	Soil Failure as a Result of Downward Motion of a Flexible Structure	11-3
11-3	Medium/Structure Interaction	11-4
11-4	Effects of Shock Wave Propagating along Longitudinal Axis of Structure	11-7
11-5	Pressures Acting on Windward Face of Soil Mounded over a Structure	11-8
11-6	Minimum Cover for Fully-Buried Condition	11-9
11-7	Deformation of a Vertical Cylinder	11-10
11-8	Horizontal Static Stress Distribution against Vertical Cylinder	11-11
11-9	Magnitude of Horizontal Static Stress on Cylinder at Infinite Depth	11-12
11-10	Site of Underground Reinforced-Concrete Structure Subjected to Overhead Blast Loading	11-13
11-11	Simplified Nonlinear Properties	11-14
11-12	Static Loads on Shallow-Buried Slab	11-16
11-13	Dynamic Loads on Shallow-Buried Rectangular Structure	11-17
11-14	Settlements that Affect Loads on Structures	11-18
11-15	Relationship Between $(r/t_d)^2$ and Γ/Λ	11-20
11-16	Loading Assumptions for Iowa Formula	11-21
11-17	Sliding Wedge Theory of Failure of Buried Flexible Conduit Due to Surface Pressure P above Half of Cylindrical Conduit	11-22
11-18	Simple Equivalent Loads for Arch Design	11-24
11-19	Thrust (T) Due to Ground-Surface-Air Overpressure (P_o) for a Hinged Arch	11-25
11-20	Shear (S) Due to Ground-Surface-Air Overpressure (P_o) for a Hinged Arch	11-26
11-21	Moment (M) Due to Ground-Surface-Air Overpressure (P_o) for a Hinged Arch	11-27
11-22	Springing Line Reactions from Dead Loads for a Two-Hinged Arch	11-28
11-23	Thrust (T) Due to Earth Loads for a Hinged Arch	11-29
11-24	Shear (S) Due to Earth Loads for a Hinged Arch	11-30
11-25	Moment (M) Due to Earth Loads for a Hinged Arch	11-31
11-26	Illustrative Example of Time-Dependent Deformed Shapes of Buried Structure	11-32
12-1	Vertical, Circular, Cylindrical Opening Subjected to Ground Shock and Overburden Stresses	12-4
12-2	Definition of Angle θ for Three Types of Openings: (1) Horizontal Circular and Elliptical Cylinders, (2) Spheres, and (3) Prolate Spheroids	12-5
12-3	Quasi-Static Components of Free-Field Ground Shock	12-6
12-4	Ratio of in situ Strength to Laboratory Strength as a Function of Opening Diameter to Joint Spacing	12-8
12-5	Geometry of Rock/Liner System	12-11
12-6	Examples of Bilinear Fits to Effective Resistance and Mass Functions	12-12
12-7	Curves for Tunnel-Liner Systems, $C = 0$ and $\bar{t}_r = 0$	12-13
12-8	Curves for Tunnel-Liner Systems, $C = 0$ and $\bar{t}_r = 0.5$	12-14
12-9	Curves for Tunnel-Liner Systems, $C = 0$ and $\bar{t}_r = 1$	12-15

<i>Figure</i>	<i>Title</i>	<i>Page</i>
12-10	Curves for Tunnel-Liner Systems, $C = 0$ and $\bar{t}_r = 2$	12-16
12-11	Curves for Tunnel-Liner Systems, $C = 0.1$ and $\bar{t}_r = 0$	12-17
12-12	Curves for Tunnel-Liner Systems, $C = 0.1$ and $\bar{t}_r = 0.5$	12-18
12-13	Curves for Tunnel-Liner Systems, $C = 0.1$ and $\bar{t}_r = 1$	12-19
12-14	Curves for Tunnel-Liner Systems, $C = 0.1$ and $\bar{t}_r = 5$	12-20
12-15	Curves for Tunnel-Liner Systems, $C = 0.3$ and $\bar{t}_r = 0$	12-21
12-16	Curves for Tunnel-Liner Systems, $C = 0.3$ and $\bar{t}_r = 0.5$	12-22
12-17	Curves for Tunnel-Liner Systems, $C = 0.3$ and $\bar{t}_r = 1$	12-23
12-18	Curves for Tunnel-Liner Systems, $C = 0.3$ and $\bar{t}_r = 5$	12-24
12-19	Curves for Tunnel-Liner Systems, $C = 0.5$ and $\bar{t}_r = 0$	12-25
12-20	Curves for Tunnel-Liner Systems, $C = 0.5$ and $\bar{t}_r = 0.5$	12-26
12-21	Curves for Tunnel-Liner Systems, $C = 0.5$ and $\bar{t}_r = 1$	12-27
12-22	Curves for Tunnel-Liner Systems, $C = 0.5$ and $\bar{t}_r = 5$	12-28
12-23	Curves for Tunnel-Liner Systems, $C = 0.7$ and $\bar{t}_r = 0$	12-29
12-24	Curves for Tunnel-Liner Systems, $C = 0.7$ and $\bar{t}_r = 0.5$	12-30
12-25	Curves for Tunnel-Liner Systems, $C = 0.7$ and $\bar{t}_r = 1$	12-31
12-26	Curves for Tunnel-Liner Systems, $C = 0.7$ and $\bar{t}_r = 5$	12-32
12-27	Curves for Tunnel-Liner Systems, $C = 1$ and $\bar{t}_r = 0$	12-33
12-28	Curves for Tunnel-Liner Systems, $C = 1$ and $\bar{t}_r = 0.5$	12-34
12-29	Curves for Tunnel-Liner Systems, $C = 1$ and $\bar{t}_r = 1$	12-35
12-30	Curves for Tunnel-Liner Systems, $C = 1$ and $\bar{t}_r = 5$	12-36
12-31	Mechanical Failure of a Rock Cavity	12-43
12-32	Three Patterns of Planes of Weakness	12-44
12-33	Construction of Incremental Free-Field Acceleration History	12-45
12-34	Liner Reinforcement	12-46

LIST OF TABLES

<i>Table</i>	<i>Title</i>	<i>Page</i>
2-1	Basic Objectives of the Structure	2-1
4-1	Cost-Effective Structure Concepts and Hardness Levels vs. Depth Classification	4-3
5-1	Allowable Ductility Factors for Structures	5-2
5-2	Backpacking Materials	5-23
5-3	Variation of Properties of Geologic Materials at a Selected Site	5-50
6-1	Effective Length Factors	6-2
8-1	Dynamic Design Factors: Beams and One-Way Slabs	8-5
8-2	Dynamic Design Factors: Two-Way Slabs and Circular Slabs, Uniform Load	8-8
8-3	Dynamic Design Factors for Flat Slabs: Square Interior Uniform Load	8-16
8-4	Dynamic Design Factors for Tee-Beams	8-17
8-5	Deep Beams: Uniform Load, Elastic Range	8-18
8-6	Trusses: Simply Supported Uniform Load	8-18
8-7	Summary of Test Data for Structural Elements	8-24
9-1	Comparison of Different Methods of Dynamic Analysis	9-8
10-1	Drag and Lift Coefficients for Structural Shapes of Infinite Length at Low Overpressures (less than 20 psi)	10-10
10-2	Drag Coefficients for Rectangular Bodies at Low Overpressures (less than 20 psi)	10-11
12-1	Reinforcement Concepts for Rock Openings	12-10

CHAPTER 1 INTRODUCTION

1-1. General.

a. This series of manuals, entitled *Designing Facilities to Resist Nuclear Weapon Effects*, is organized as follows:

- TM 5-858-1 Facilities System Engineering
- TM 5-858-2 Weapon Effects
- TM 5-858-3 Structures
- TM 5-858-4 Shock Isolation Systems
- TM 5-858-5 Air Entrainment, Fasteners, Penetration Protection, Hydraulic-Surge Protective Devices, EMP Protective Devices
- TM 5-858-6 Hardness Verification
- TM 5-858-7 Facility Support Systems
- TM 5-858-8 Illustrative Examples

A list of references pertinent to each manual is placed in an appendix. Additional appendixes and bibliographies are used, as required, for documentation of supporting information. Pertinent bibliographic material is identified in the text with the author's name placed in parentheses. Such bibliographic material is not necessary for the use of this manual; the name and source of publications related to the subject of this manual is provided for information purposes.

b. The purpose of this series of manuals is to provide guidance to engineers engaged in designing facilities that are required to resist nuclear weapon effects. It has been written for systems, structural, mechanical, electrical, and test engineers possessing state-of-the-art expertise in their respective disciplines, but having little knowledge of nuclear weapon effects on facilities. While it is applicable as general design guidelines to all Corps of Engineers specialists who participate in designing permanent military facilities, it has been written and organized on the assumption a systems-engineering group will coordinate design of the facilities.

c. Technical Manual 5-858 addresses only the designing of hardened facilities; other techniques to achieve survival capacity against nuclear weapon attacks are deception, duplication, dispersion, nomadization, reconstitution, and active defense. A facility is said to be hardened if it has been designed to directly resist and mitigate the weapon effects. Most of the hardening requirements are allocated to the subsidiary facilities, which house, support, and protect the prime mission materiel/personnel (PMMP). This manual is applicable to permanent facilities, such as those associated with weapon systems, materiel stockpiles, command centers, manufacturing centers, and communications centers.

d. The nuclear weapon threats considered are listed below. Biological, chemical, and conventional weapon attacks are not considered.

- Weapons aimed at the facility itself or at nearby targets
- A range from many, relatively small-yield weapons to a single super-yield weapon
- Weapon yields from tens of kilotons to hundreds of megatons
- Weapon delivery by aerial bombing, air-to-surface missile, surface-to-surface missile, or satellite-launched vehicle
- Detonation (burst) of a weapon in the air, at the ground surface, or beneath the ground surface
- Direct-overhead bursts for a deep-buried facility
- Near-miss bursts for a near-surface facility, producing peak over-pressures from tens to thousands of psi at the facility

e. The designing of facilities resistant to nuclear weapon effects is an evolving specialty that uses a relatively narrow data base that incorporates both random and systematic uncertainties. The range of these uncertainties may vary from significant (order of 1 to 2 magnitudes) to normal (10 to 100 percent variation from average values). The applicable uncertainty value depends on the specific weapon effect or hardening objective under consideration. Loading uncertainty is generally more significant than resistance uncertainty. Awareness of the appropriate uncertainty (extent of ignorance) factor is essential not only for system engineering trade-offs, but in the utilization of available analysis or test procedures. Studies and experiments are being conducted to improve methodology, to better define random uncertainties, and to reduce systematic uncertainties. This manual will be revised as significant improvements occur in either methodology or data base.

1-2. TM 5-858-3. Structures

a. This volume delineates methodology for the designing of structural elements and structures. Aboveground, partially buried, and fully buried structures are treated. Emphasis is placed on providing resistance (hardness) to the airblast and ground-shock weapon effects.

b. In addition to airblast and ground-shock loading, protective structures must be evaluated for loads imposed by other nuclear weapon effects such as thermal and nuclear radiation and ejecta/debris impact. Normally, buried structures have adequate protection against these other effects because of the shielding provided by the ground. Aboveground structures and

flush or partially buried structures are more susceptible to radiation and debris effects. When reinforced concrete is used for construction, the concrete thickness (mass) required to resist the airblast and ground-shock loads provides shielding against radiation and debris impact. However, whether this shielding is adequate depends on the thickness of the concrete, the nuclear weapon effects environment, and the fragility/tolerance levels of the personnel and equipment within the structure. Techniques for predicting the environments are provided in TM 5-858-2, *Weapon Effects*. Techniques for determining required nuclear-radiation shielding or attenuation associated with various construction materials and permissible radiation levels for personnel and equipment can be obtained from several sources. (See, for example, Abbot et al., 1971.)

c. As a rule, radiation considerations will not be the governing factor in a hardened design but must be checked once the structure concept has been selected and preliminary sizing of structural components established. The design may need modification if additional radiation attenuation is required. At very high levels of free-field radiation, materials may be damaged by photon or neutron energy deposition within exposed structural members.

d. Thermal radiation from the fireball can also damage exposed structural materials, and may require installation of sacrificial surface materials on exposed structural members. Glasstone and Dolan (1977) discuss this subject in detail.

e. Cratering ejecta/debris or man-made objects that are transported by the blast wave may impact hardened structures. The latter will be the type of debris usually associated with tornado-tossed objects or missiles, such as construction materials, pipes, telephone poles, vehicles, etc. Crater ejecta includes earth clods and rock missiles, and the resulting load

on a structure is related to the static weight of the ejecta plus the dynamic load due to impact. In this case, the overall response of structural elements is based on energy momentum balance or the impact forcing function. Overall response includes flexure and reaction shear in the structural element.

f. The effect of impact by man-made debris depends on the material and geometrical properties of the impacting object. The impact phenomenology can be analyzed as either a localized or a gross effect. Local damage may include penetration perforation, scabbing, or punching shear in the region of impact on the structure. The gross effect requires an analysis of the overall response of the structural element and must consider the "softness" or crushing of the impacting object. The deformation characteristics of the debris are used to develop an applied force time history and the analysis for overall response to the force is performed as for an impulsive load. In analyzing the gross effect of a hard impact, energy and momentum balance techniques are used to predict maximum response.

g. In recent years a considerable number of analyses and tests have been performed to support hazard safety analysis of nuclear plant facilities under impact from tornado-tossed debris missiles. Existing ballistic-missile impact equations have been changed as a result of the analyses and new empirical equations have been developed on the basis of results from simulated tornado-missile impact tests. There are several references that provide design approaches to localized effects and to structural response when considering the gross effect of debris impact on a structural element. (See Kennedy, 1975; ASCE, 1976; and McDonald, 1977.) The approach used for gross structural response analysis follows procedures similar to those provided in chapter 8.

CHAPTER 2 BASIC OBJECTIVES OF THE STRUCTURE

2-1. Objectives vs. availability requirements

a. The structure, which is one system of the multisystem facility, has three basic objectives or functions to fulfill:

- House the prime-mission materiel/personnel.
- Mitigate hostile external natural environments to levels tolerable to the prime-mission materiel/personnel.
- Mitigate nuclear weapon effects to levels tolerable to the prime-mission materiel/personnel.

These basic objectives, along with typical second-level objectives, are listed in table 2-1 and coded for their availability requirements for the preattack, transattack, and postattack time frames. Preattack availability is defined as the probability, at any random time until button-up or the first weapon detonation, that the system will be in a fully operable state. Transattack availability is required from button-up or detonation of the first weapon until the attack is completed. Postattack availability is required from the end of the attack until the facility objectives are fulfilled. Procedures for determining the values to be

Table 2-1. Basic Objectives of the Structure

Functional Requirement			Applicability*	
			Prime-Mission Materiel	Prime-Mission Personnel
1. HOUSE				
PROVIDE	Space	FOR	○ ● ●	○ ● ●
ACCOMMODATE	Access/egress	OF	○ ▲ ●	○ ▲ ●
	Installation		○	
	Maintenance		○ ▲ ▲	
2. MITIGATE HOSTILE EXTERNAL NATURAL ENVIRONMENTS				
MITIGATE	Meteorological	TO LEVELS TOLERABLE TO	○ ● ●	○ ● ●
	Hydrologic		○ ● ●	○ ● ●
	Tectonic		○ ● ●	○ ● ●
	Chemical		○ ● ●	○ ● ●
	Biological		○ ● ●	○ ● ●
3. MITIGATE NUCLEAR-WEAPON EFFECTS				
MITIGATE	Initial nuclear radiation	TO LEVELS TOLERABLE TO	●	●
	EMP		●	●
	Fireball		●	●
	Thermal radiation		●	●
	Airblast		●	●
	Airblast-induced ground shock		●	●
	Crater-induced ground shock		●	●
	Crater		● ●	● ●
	Ejecta/debris impact		●	●
	Ejecta/debris depth		● ●	● ●
	Dust		● ●	● ●
	Firestorm		● ●	● ●
	Residual nuclear radiation		● ●	● ●

* Applicability	Preattack	Transattack	Postattack
Applicable to most missions	○	●	●
Mission-peculiar applicability	△	▲	▲

assigned to each time-frame duration are described in TM 5-858-1.

b. In general, design procedures to satisfy requirements for preattack availability follow conventional standards of design that meet structure integrity, cost, and environmental requirements. Appropriate military building codes will be applicable for housing and for mitigation of hostile external natural environments. Special considerations of seismic risk will be considered for seismically active regions. Because of the need to mitigate nuclear weapon effects (harden the system), conditions imposed by transattack and postattack availability requirements will result in hardened system concepts that will dictate supplementary design criteria for preattack availability. Subsystems beyond the structure itself that require extraordinary design because of hardening the facility are delineated in TM 5-858-4, TM 5-858-5, and TM 5-858-7.

c. Transattack and postattack availability requirements will dictate the design criteria for mitigation of nuclear weapon effects. The design objectives are threefold: (1) the structure and its contents must be able to experience tolerable levels of nuclear weapon effects (attenuation of input); (2) they must survive the effects (resisting capacity); and (3) essential functions must remain intact (uninterrupted performance).

d. The structure is the principal facility subsystem that provides transattack availability. Attenuation mitigates most of the nuclear weapon effects to tolerable levels; depth of burial, thickness of concrete, steel liners, sealed environments, and isolators are various methods employed. The effects of airblast, ground shock, and, in some cases, ejecta impact have to be further mitigated by designing structural elements that have the resisting capacity to maintain structural integrity—elements with sufficient strength and ability to deform.

e. Design objectives for postattack availability are dictated by endurance criteria. Attenuated levels of nuclear weapon effects such as radiation, dust, and firestorm have to be maintained until the external hostile environment allows egress. Furthermore, the postattack mission may have to be carried out in such an environment. The endurance period is therefore a totally or partially buttoned-up period during which the structure must provide the housing for prime-mission materiel and personnel.

f. Multiple attacks may occur and facilities may have to be designed to resist them. If the intervals are very short (seconds or minutes), the entire multi-attack period is a transattack availability period. For longer periods (hours, days), transattack-postattack-transattack sequences must be considered. For multiple attack, design procedures must include nondeteriorating design details as provided in chapter 7.

CHAPTER 3 DESIGN REQUIREMENTS

3-1. Introduction.

a. The structure design must meet a set of requirements prescribed by the facilities system engineering group or its equivalent. These requirements will be continually refined as the facility develops.

b. General design and construction for preattack environment will, at the least, adhere to standard practice as defined by military specifications and standards, such as those pertaining to reliability, maintainability, and safety. In seismically active regions, design requirements will be specified.

c. One or more of the following 13 nuclear weapon effects will be specified, depending on the specific threat and facility:

- Initial nuclear radiation
- Electromagnetic pulse (EMP)
- Fireball
- Thermal radiation
- Airblast
- Airblast-induced ground shock
- Crater-induced ground shock
- Crater
- Ejecta/debris impact
- Ejecta/debris depth
- Dust
- Firestorm
- Residual nuclear radiation

These specifications will be presented as curves, tabulated data, and mathematical relationships. Volume TM 5-858-2 discusses nuclear weapon effects.

d. Environmental compatibility requirements may be imposed. Typical requirements will be related to:

- Construction environment abatement
- Site-conforming structure
- Site disturbance and renovation

3-2. Functional requirements

The functional requirements of the structure will be defined by the facilities system engineering group. The group will state the time frame in which each function must be accomplished and the beginning and end conditions of each function. The structure objectives listed in chapter 2 represent very sketchy delineations of first-level functional requirements.

3-3. Technical requirements

Each functional requirement will be translated into a set of quantitative technical requirements. Examples of technical requirements are:

- Volumes, areas, and dimensions
- Size and location of penetrations (access/egress and umbilical)
- Loads imposed by the housed materiel and personnel, such as heat, moisture, pressure, vibration, chemical, forces, etc.
- Fragility levels imposed by materiel and personnel, such as radiation, pressure, shock, dimensional distortion, rigid body rotation, loss of gas or liquid seal, etc.

3-4. Technical design criteria

a. *Site.* The site will be characterized as defined in chapters 1 through 9 of TM 5-858-1.

b. *Service life.* The service life will be specified as a minimum period during which the structure provides specified functions without requiring major rehabilitation. The service life specified for the structure will, in general, be 20 years. Often, a design is required to be adaptable to upgrading for extended life.

c. *Availability.* The structure availability will be specified as a minimum percent of time during a given preattack period wherein the structure must be in a committable state at the start of the attack, when the attack occurs at an unknown (random) point in time. Structure availability will, in general, be specified as ≥ 99.9 percent in any calendar year.

d. *Hardness.* Specifications of design hardness will, in general, take the following deterministic form:

Design the structure for the _____
name of weapon
_____ and attendant effects from _____ kt (or
effect number yield
Mt) weapon(s) detonated at a range of _____ ft
and a height of _____ ft.

Such a specification will be repeated for each weapon effect appropriate to the facility of interest. An equivalent single-weapon attack representing the effects resulting from a certain number of bursts may be specified, or the designer may be given multiple-weapon attack criteria so that the effects of material degradation can be included.

e. *Endurance.* The structure endurance will be specified as a minimum period of time that the structure must successfully perform its functions after having absorbed the first burst or after button-up. This period can range from minutes to months.

f. *Design reliability.* In general, it will be specified that the design be based on mean (average or expected) value of any design parameter whose inherent uncertainty leads to significant perturbation of the total system cost. A conservative bounding will be

TM 5-858-3

used for all other parameters. For example, mean values would be used for the cost-significant parameters of the following generic variables, as required:

- Weather conditions
- Atmospheric conditions
- Geologic conditions

- Weapon-effect parameters
- Physical, mechanical, thermal, electrical, and chemical properties
- Dimensions, areas, volumes
- Analysis assumptions
- Failure levels
- Workmanship

CHAPTER 4 DESIGN PHILOSOPHY

4-1. Major elements

a. Introduction. Because of the high cost of structural hardening and the probabilistic nature of success (or failure) of a system subjected to a nuclear weapon attack, the design philosophy for translating the requirements presented in chapter 3 into rational, cost-effective hardening designs will have many unique provisions.

b. Select structure failure mode. In addition to structure collapse, one or more of the following—when excessive—might constitute structural failure, depending on the tolerance criteria of the housed system:

- Radiation rise inside the structure
- Pressure rise inside the structure
- Dimensional distortion of the structure
- Rigid-body rotation or tilt of the structure
- Degradation of the structure material due to nuclear radiation, heating, or straining
- Loss of gas or liquid seal
- Quantities of projectiles, debris, or dust penetrating the structure
- Quantities of projectiles, debris, or dust generated within the structure
- Transmission of shock to structure contents

It may be cost effective to conceptualize the structure and (as required) the housed system and facility materiel so that structure collapse is the predominant and overriding structure failure mode. The reconception of the system and facility materiel is a facilities/system engineering responsibility (TM 5-858-1).

c. Maximize energy absorption. It will be cost effective to maximize the inelastic energy absorption capacity of a structure whose failure mode is structure collapse. This can be accomplished by designing a ductile structure. Deflections beyond the dynamic yield point of the material are defined by a ductility factor, μ , which is the ratio of maximum acceptable transient deflection, δ_m , to deflection at effective elastic yield point, δ_y . The allowable value of μ to be used depends on the material properties and the failure mode used for each individual element. When the failure mode is structure collapse, large inelastic deformations are permissible up to the threshold of collapse. However, very large deformations of structures may cause instability. Although individual structural elements may have very large permissible ductility factors, the ductility factor for the complete structure should be determined by consideration of the overall response of the structure. When failure is defined by deformation tolerances, it is sometimes

necessary to design the element to remain elastic; i.e., a ductility factor of unity is used.

d. Minimize synergistic damage. In order to minimize the attractiveness of multiple-warhead attacks, minimize synergistic damage (total damage greater than the sum of the increments). The most common examples of synergistic damage are the $P - \delta$ effect in severely distorted structural members, the local buckling of steel structural members, and the shear resistance degradation of concrete structural members in areas of high bending moment. ($P - \delta$ effects are secondary moments in axially loaded structural elements resulting from the drift or distortion, due to lateral forces, of the member.) The $P - \delta$ effect and local buckling can be minimized by judicious selection of the state of incipient structure collapse used as a failure criterion. The effect of shear resistance degradation in concrete members can be minimized by proper detailing, as discussed in chapter 7.

e. Minimize air-borne debris. Protect structures sensitive to impact from air-borne debris, such as radar faces and antenna structures, by controlling unhardened construction on the site. Unhardened structures should be located far enough from the hardened structure so that particles of debris carried by the overpressure shock wave will drop to the ground before they can reach the structure. If, for functional reasons, such structures must be located within this critical distance, they should be so designed that they will not become a source of debris.

f. Separate design and refined analysis activities. Computerized analyses, such as dynamic, inelastic, and two- and three-dimensional analyses for structure/medium interaction or structure response, will provide: (1) inputs and validation to the ongoing design, and (2) postdesign validation. The design group will direct and integrate all analyses (which may be executed by others) with the designing.

g. Quantify uncertainties. Properties of structural materials, behavior of structural members, and applied loads are not fully predictable and are therefore sources of uncertainty. As a result, the safety and serviceability of a proposed structure cannot be achieved in an absolute manner. A rational structural design procedure must consider all uncertainties involved in the design process and maintain a desired level of reliability for a proposed structure.

(1) The desired levels of reliability are obtained by assigning acceptably small values to the probabilities of undesirable response. Because of the uncertainties and risk involved, such a design procedure must be based on the theory of probability and

be developed at the concept stage. Loads and resistances must be defined for final design.

(2) Assessment of failure probability requires quantification of the following uncertainties:

- Applied Loads (peak value, duration, waveform)
- Material Properties (elastic limit, ultimate strength, modulus, Poisson's ratio)
- Resistance Models (flexural, shear, axial, and bearing resistance capacities)
- Natural Frequencies and Mode Shapes
- Structural Damping
- Approximations in Mathematical Models
- Quality Control of Construction

Methods of estimating these uncertainties are discussed in appendix A.

4-2. Design procedure

a. Step 1. Determine the mean and coefficient of variation values of all load and resistance terms, accounting for uncertainties and for errors in modeling. Use both statistical data and theoretical models as input. (See typical examples in appendix A.)

b. Step 2. Determine component reliabilities against various failure modes, using failure modes specified by the facilities system engineering group (TM 5-858-1).

c. Step 3. Determine design parameters such as safety factors, capacity and reduction factors, and load factors, using values derived in steps 1 and 2 as input.

d. Step 4. With design parameters determined, proceed as for deterministic design. The values calculated for steps 1, 2, and 3 will vary from site to site, from structure to structure, and even for different points within a structure.

4-3. Depth selection

a. Depth classifications. The depth at which the structure is constructed has a profound influence on the structure concept, hardness, cost, and design procedure. Cost-effective structure concepts and hardness levels are shown in table 4-1 for five generic depths. The resistance/geometry lists in table 4-1 are presented in the order of increasing hardness. Choice of structure configuration must consider the resistance levels, site conditions, and operational requirements. Unless the intended function dictates aboveground construction, or unless the required resistance levels are quite low, construction belowground will be most cost-effective.

b. Aboveground. A structure is classified as aboveground when all or a portion of the structure projects above the ground surface (fig. 4-1).

c. Flush. A structure is classified as flush when it is countersunk in the ground so that the structure roof is level with the ground surface (fig. 4-2).

d. Partially buried. A structure is classified as partially buried when it is beneath a soil cover deep enough to defeat initial radiation, ejecta/debris impact, and residual radiation, but shallower than one half of the structure diameter (fig. 4-3). (Consider structures with mounding slopes steeper than 1:4 to be aboveground structures subject to overpressure and ground-shock loadings.)

e. Shallow buried. A structure is classified as shallow-buried when it is covered by soil at least one half of the structure diameter in depth, yet the structure is still close enough to the surface that it cannot absorb direct overhead bursts (fig. 4-4).

f. Deep buried. A structure is classified as deeply buried when it is buried to a depth that allows the structure to absorb direct overhead bursts (fig. 4-5).

4-4. Selection of structural concept

a. Tradeoff analysis. If the structure design requirements do not dictate or implicitly suggest the depth classification, the structure designer is faced with performing tradeoff analyses among the candidate classifications. All other things assumed to be equal, select the classification that minimizes the number of applicable weapon effects (table 4-1). Study carefully the operations and equipment to be housed, since these determine acceptable clear spans and acceptable space configurations. The availability of good foundation material is also an important factor in the choice of structure type.

b. Resistance level. For efficient use of construction material, shell configurations (arch, dome, cylinder) are superior to box structures (flat slab and wall elements). Slab thicknesses become excessive with increasing combinations of loading and span. When large clear spans are required for functional reasons, the shell type of structure may be demanded.

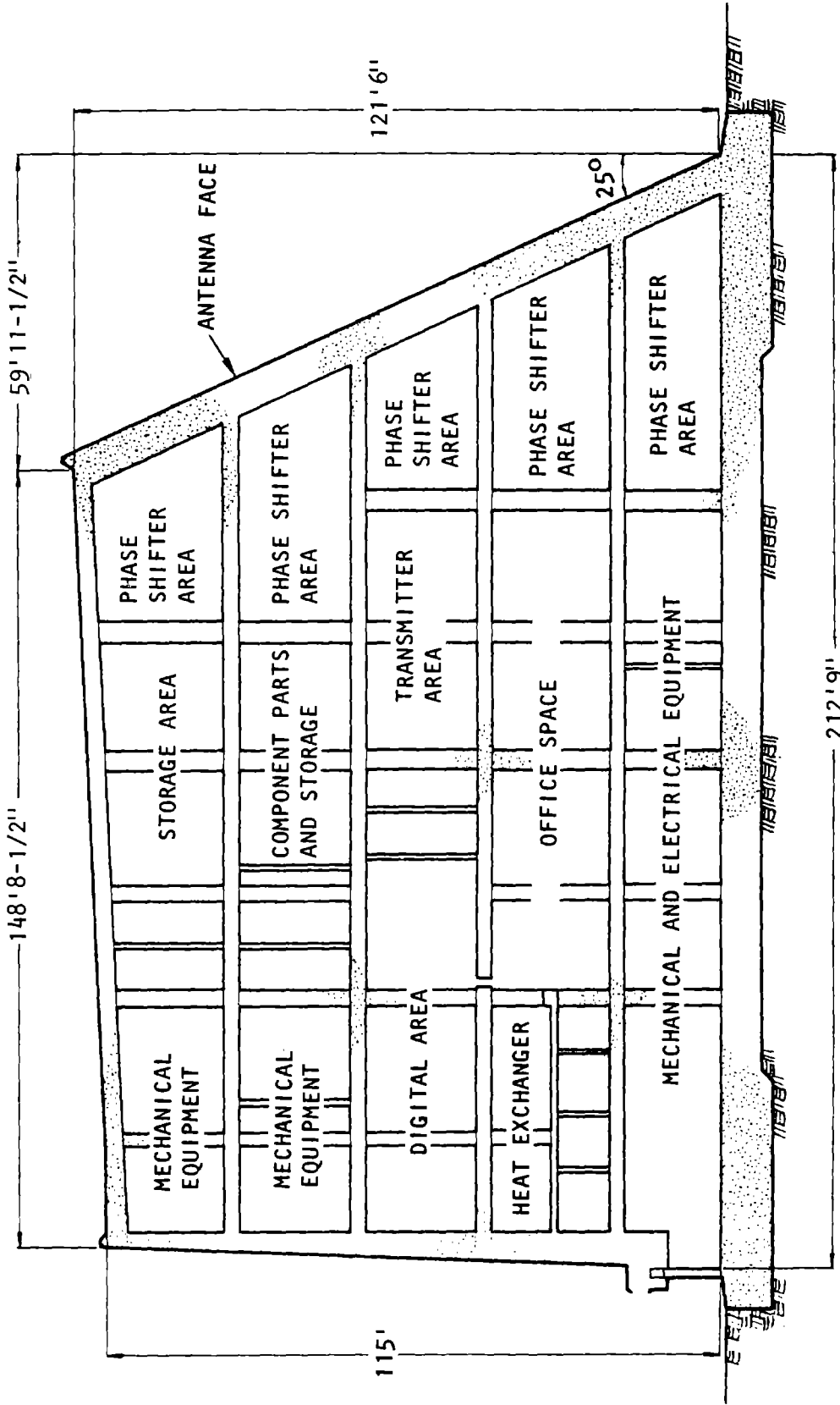
c. Space utilization. Space is better used by box structures since the interior clear height does not decrease near the exterior walls as it does in shell structures. Using space in zones of reduced headroom may be difficult and can result in wasted floor area.

d. Foundation design. With box structures the vertical load is transmitted to the foundation material by many columns and walls and is thereby distributed over the entire area of the structure. Foundation loads for arch and dome structures are concentrated at the perimeter and may require installing massive footings or carrying the foundation deeper in order to reach rock or more competent soil.

Table 4-1. Cost-Effective Structure Concepts and Hardness Levels vs. Depth Classification

Depth Classification	Structure Concept		Cost Effective Design Hardness	Applicable Weapon Effects
	Resistance/Geometry	Construction Material		
Aboveground	<ul style="list-style-type: none"> • Rigid frame • Shear wall • Box • Arch • Dome • Shell 	<ul style="list-style-type: none"> • Reinforced concrete • Steel • Composite 	<ul style="list-style-type: none"> • Several to tens of psi 	<ul style="list-style-type: none"> • All 13 nuclear weapon effects • Airblast crucial
Partially buried	<ul style="list-style-type: none"> • Box • Arch • Dome • Shell 	<ul style="list-style-type: none"> • Reinforced concrete • Steel • Composite 	<ul style="list-style-type: none"> • Tens to thousands of psi 	<ul style="list-style-type: none"> • Most effects reduced • Airblast crucial • Ground shock crucial
Flush	<ul style="list-style-type: none"> • Box • Vertical cylindrical shell 	<ul style="list-style-type: none"> • Reinforced concrete 	<ul style="list-style-type: none"> • Tens to thousands of psi 	<ul style="list-style-type: none"> • Ground shock crucial • Ejecta crucial • Airblast (overpressure only) • Nuclear, thermal, other effects reduced
Shallow-buried	<ul style="list-style-type: none"> • Shell 	<ul style="list-style-type: none"> • Reinforced concrete • Steel • Composite 	<ul style="list-style-type: none"> • Hundreds to thousands of psi 	<ul style="list-style-type: none"> • Ground shock crucial • Other effects reduced
Deep-buried	<ul style="list-style-type: none"> • Unlined • Rock bolted • Liner • Backpacker liner 	<ul style="list-style-type: none"> • Liner • Reinforced concrete • Steel • Composite 	<ul style="list-style-type: none"> • Direct overhead bursts absorbed 	<ul style="list-style-type: none"> • Ground shock from cratering crucial • EMP still effective

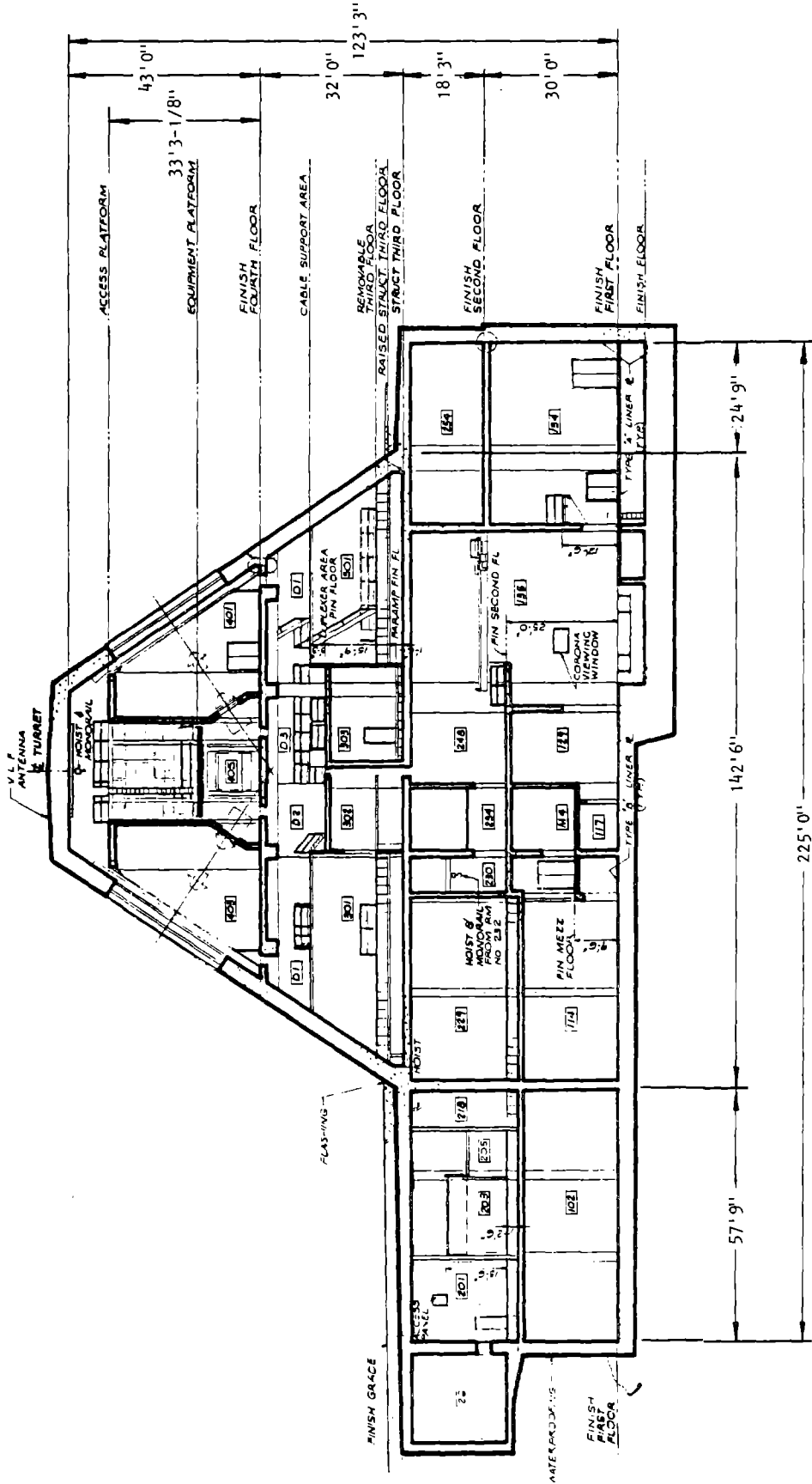
U.S. Army Corps of Engineers



(a) Safeguard Perimeter Acquisition Radar Building (PARB)

U.S. Army Corps of Engineers

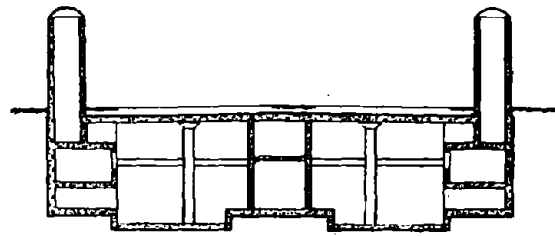
Figure 4-1. Example of Aboveground Structure (1 of 2)



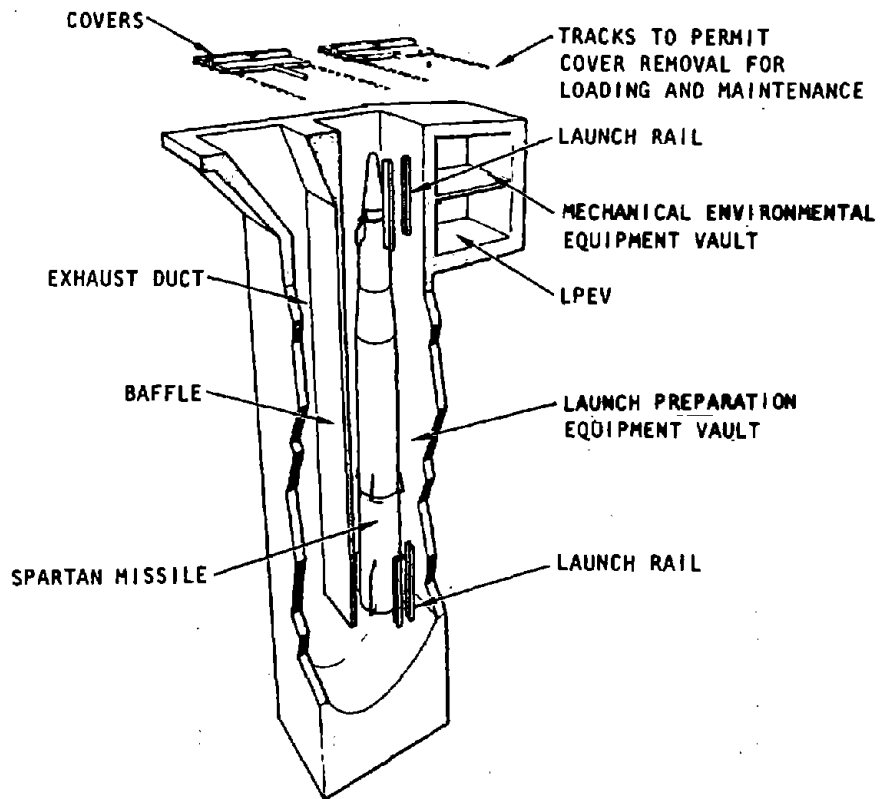
(b) Safeguard Missile Site Control Building (MSCB)

Figure 4-1. Example of Aboveground Structure (2 of 2)

U.S. Army Corps of Engineers



(a) Safeguard radar power plant (box type)

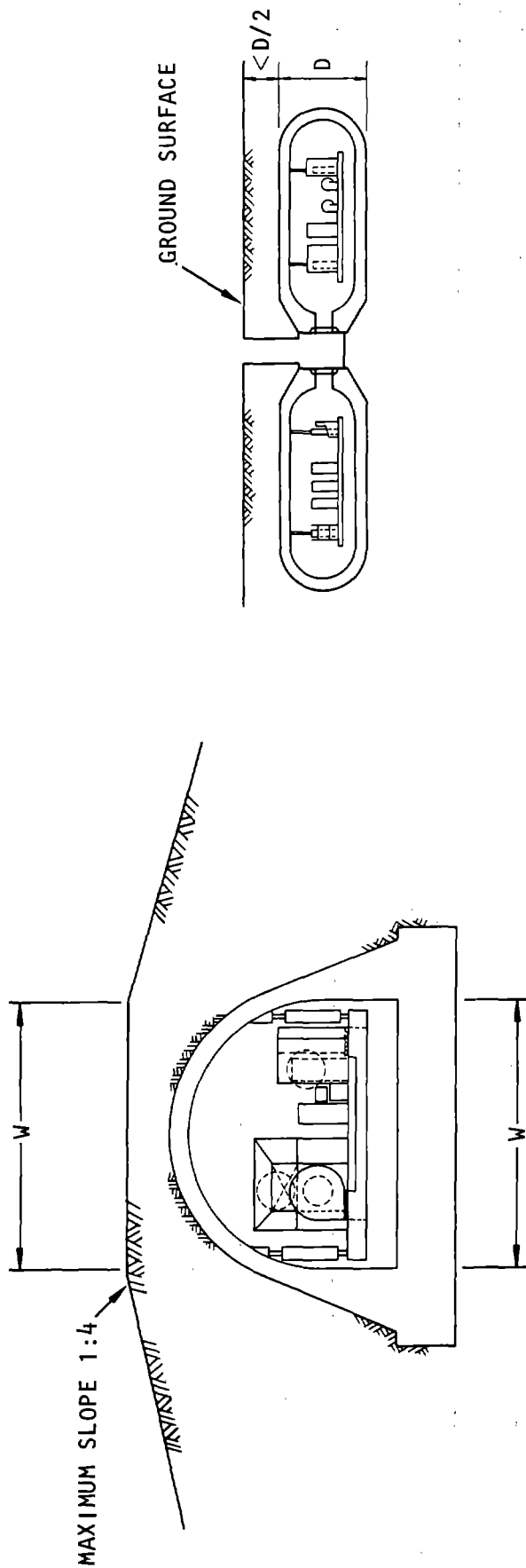


NOTE: SHOCK ISOLATION SYSTEM NOT SHOWN

(b) Spartan launch cell (silo)

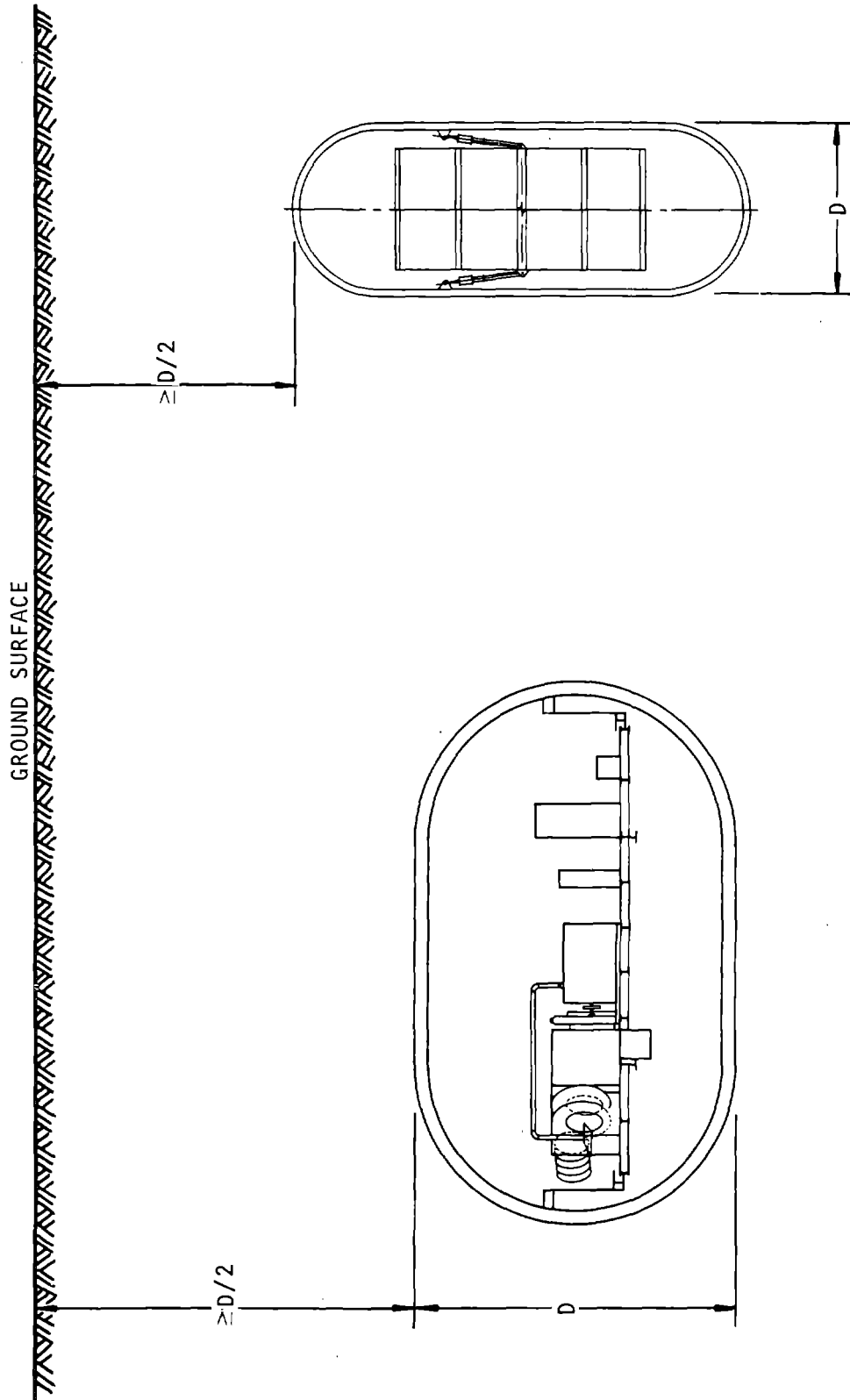
U.S. Army Corps of Engineers

Figure 4-2. Example of Flush Structures



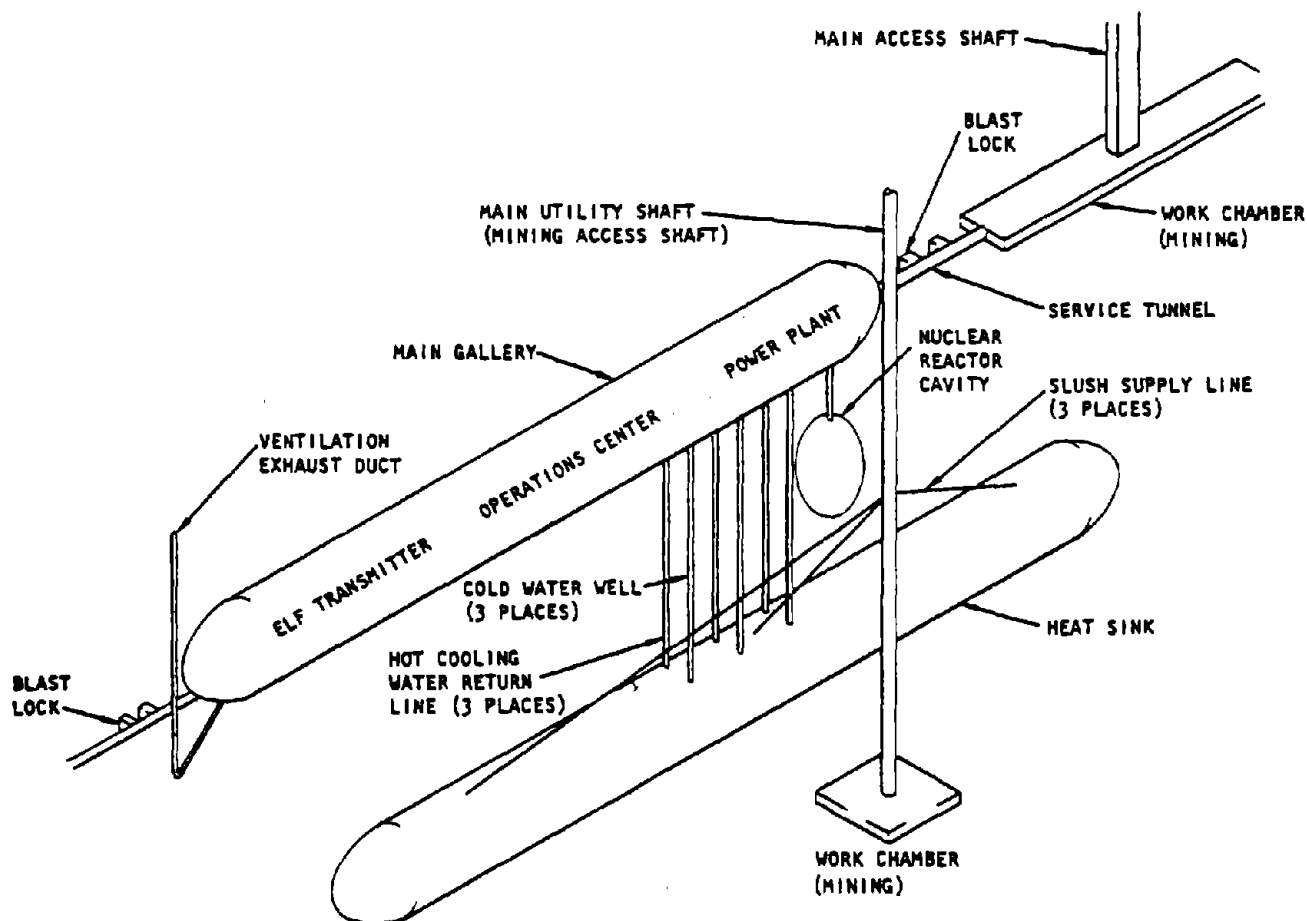
U.S. Army Corps of Engineers

Figure 4-3. Examples of Partially Buried Structures



U.S. Army Corps of Engineers

Figure 4-4. Examples of Shallow-Buried Structures



U.S. Army Corps of Engineers

Figure 4-5. Example of a Deep-Buried System.

4-5. Development of structure concepts

a. Requirements. Final design of a hardened structure must be preceded by a systematic effort to arrive at the optimum configuration that satisfies all functional and protective requirements. In brief, the requirements the structural system must satisfy are:

- Meet the functional requirements of the system it will house by providing space and the desired environment
- Protect the contained equipment, materiel, personnel, and internal environment against specified weapon effects
- Be designed for economical construction within reasonable time schedules

There are, at times, special additional requirements. For example, it may be specified that an underground military center be designed to remain sufficiently intact after multiple attacks so that access/egress at a predetermined time is possible.

b. Selection of candidate concepts. Select several geometric concepts for feasibility of construction, for specific advantages in the internal layout of space, and for necessary structural resistance to both static and dynamic loads.

c. Evaluation of candidate concepts. Evaluate constructibility in terms of cost and schedules. Evaluate each concept for its adaptability to the changing requirements of the system it will house.

d. Selection of preferred concept. The preferred concept must satisfy at least all functional requirements and it should meet schedules for beneficial occupancy. If several candidate concepts meet these requirements, the results of a cost-effectiveness analysis should be the criteria for final selection.

e. Design considerations during concept selection. Consider the following:

(1) Where possible, use curved surfaces to resist blast pressures with membrane stresses. Arch and dome structures with flat foundations require base slabs that resist soil reactions by flexural and shear stresses. Cylindrical structures with hemispherical or ellipsoidal ends and spherical structures resist all loads primarily by membrane action.

(2) Reinforce openings in the shells for blast valves and doors with a thickened section of the shell in the form of a ring. Localized bending at the ring and membrane stresses should be resisted by the reinforcement.

(3) In relatively rigid structural elements, such as reinforced-concrete slabs, stresses are usually determined by assuming a uniform application of the blast pressures. However, any effects of nonuniformities in loading should be resisted by the proper placing of reinforcing bars. For structures with flexible walls, such as corrugated metal tunnels and shafts, design the structures to maintain their stability under dynamic and static loading. Consider also the effect of nonuniform loading as the blast wave travels along the structure.

(4) Even small relative motions as the blast wave travels along the structure are critical at rigid connections, such as junctions of pipes with structures, tunnels with structures, and any point of stress concentration where relative movement is possible between two structural elements. Minimize the number and amplitude of these movements.

(5) Downdrag forces developing between soil and the structures buried in soil are often significant. These are forces that are applied to the exterior walls of a structure as the soil around the structure is compressed by the blast overpressure. The maximum value that the downdrag can attain is the shear strength of the soil. Downdrag forces are usually a large percentage of the total dynamic load.

(6) Equipment and personnel inside the structure are often placed on shock-isolated platforms. The shock-isolated internal structures are supported from the external structure by hangers, columns, or beams, depending upon the shock-isolation system used, and space for relative motion is allowed. The shock-isolation system to be used has a strong influence on the final configuration of the structure (TM 5-858-4).

(7) The housed system and the facility may be designed concurrently. Therefore, if changes in the housed system are made while the facility is being designed, changes in structure design (sometimes drastic) must be accommodated with minimum change in concept. The design assumption that everything will end up larger than originally specified is safe but expensive. System changes should be anticipated as far in advance as possible.

4-6. Preliminary design

a. Define the interface between the facility and the housed system. Analyze all housed system requirements and evaluate their effect on the design of the structural system.

b. Specify the nuclear weapon effects in the form of design criteria and develop this information with relation to the site and structural concept selected.

c. Identify design loads: Overpressure, ground shock, earth loads, dead loads, and live loads. For example, calculate the attenuation of overpressure with depth, the load distribution on the structure, the ef-

fect of load duration relative to the natural period of the structure, and the downdrag forces.

d. Determine the allowable stresses and the allowable ductility factors for the various elements.

e. Specify, in outline form, structural materials and the required properties, as well as the type of construction, backfill, and finishing.

f. Compute sizes, thicknesses, basic dimensions, and layout of all structural elements.

g. Include enough detail in the drawings that a preliminary design of the structural system may be clearly expressed in terms of plans, elevations, and sections.

4-7. Final design detailing

a. *Concrete detailing.* Detail the members and connections for continuity, ductility, and resistance to loads in any direction. Diagonal tension reinforcement should be perpendicular to the member axis because inclined bars form planes of weakness under conditions of shear reversal (rebound). Doubly reinforced members with the reinforcing adequately tied are more ductile than singly reinforced sections. Joints should be detailed for ductile behavior of the completed element. Overreinforced members fail by crushing the compression concrete without tension reinforcement yielding. Avoid this type of brittle failure in hardened construction by using underreinforced design procedures. When heavy concentrations of longitudinal reinforcing are required, provide for adequate transverse reinforcement using ties, stirrups, or transverse bars to prevent bond failure where splitting of the concrete occurs.

b. *Steel and composite construction.* Arch or circular sections for underground construction, steel beams for composite construction, and steel doors/closures are examples of economical steel construction. Ductility, continuity, and development of full plastic strengths at joints are also required for steel construction. Design the connections so that ductile behavior takes place in the member. Design the connections for tension members to develop the yield strength of the member. Properly detailed welded joints provide maximum structure continuity and a minimum of local stress concentration. High-strength bolted joints for shop or field connections are acceptable substitutes for welded connections. Bolted connections utilizing A-307 bolts should not be used in blast hardening design. Proceed with final design detailing after all major design decisions have been made.

4-8. Design verification

Verify structure performance under specified weapon effects by performing design verification analyses, described in chapter 9. (Read also TM 5-858-6 for expanded discussion of methodology and procedures in verification analyses.)

CHAPTER 5

MATERIAL PROPERTIES

5-1. Materials of interest

There are five materials commonly encountered in unhardened structure design that are also of interest in design of hardened structures:

- Concrete and reinforced concretes
- Steels
- Plastics and reinforced plastics
- Soils (gravels, sands, silts, and clays)
- Rock masses

Because of the rebound characteristics, prestressed concrete should not be used in hardened structures. Plastics are sometimes used as an integral part of a rugged mechanical or structural system. The last two are, of course, the geologic materials of the structure site. To achieve ground-shock attenuation between a rock site and the structure, backpacking materials such as concrete, plastic, select gravel, and select sand can be used.

5-2. Material properties required for design

a. Knowledge of physical, mechanical, and thermal properties of materials is required for hardened design. Corrosion and aging will modify several of the properties and must be accounted for during design.

b. Physical properties of interest are:

- Unit weight
- Porousness
- Permeability
- Moisture content
- Grain size and distribution
- Planes of weakness (macroscopic)

c. Mechanical properties:

- Moduli of deformation
- Creep rate
- Yield strength
- Fracture strength
- Shear strength
- Cohesive strength
- Fatigue strength
- Ductility
- Internal damping

d. Thermal properties:

- Coefficient of expansion
- Conductivity
- Specific heat
- Ignition temperature
- Melting-point temperature
- Boiling-point temperature
- Heat of fusion
- Heat of vaporization

e. Understanding the physical and mechanical properties is required for design against initial radia-

tion, airblast, ground shock, ejecta/debris impact, and dust erosion. Understanding the physical and thermal properties is required for design against EMP, fireball, thermal radiation, and firestorm effects.

f. Understanding the properties of the structural materials is more important for protective construction design than for conventional design because the loadings from nuclear weapon effects are unusually severe and because construction costs must be minimized without jeopardizing critical functional requirements. Consider the deformations and stresses induced in members as they approach or exceed the yield. Also, allow for the special changes that occur in the engineering properties of loading rate sensitive materials subjected to rapidly applied loads.

g. Understanding the physical properties of soil and rock is required for predicting the ground shock from a nuclear detonation at a particular site, predicting the cost of excavation, and comparing structural concepts. This knowledge is required when the selection of a site is still flexible. In the early stages of site selection, before borings and soil tests have been made, it is usually necessary to enlist the aid of a trained geologist in predicting the types of materials to be encountered.

5-3. Assignment of numerical values

a. Assign numerical values to the properties of materials that will reflect the material in place on a specified attack date and under specified type and rate of load application. In general, the modifying effects of nuclear radiation and load interaction (e.g., the effect of temperature on yield strength) are small but both should be examined. Some loads require exceptional design, e.g., a sacrificial material thickness (real or calculated) used to absorb intense nuclear and thermal radiation.

b. Definition of physical properties is generally based on laboratory testing of enough specimens to establish minimum and average values; refer to TM 5-858-6 for the statistical sample size of specimens required to establish minimum and average values.

c. Disparity between specified minimum values and average in-place values is most pronounced for mechanical properties of structural materials. Average in-place strengths of concretes and steels, for example, can exceed the minimum specified by several tens of percent. Use an enhancement factor of 1.15 for estimating the in-place average yield point of steel. To estimate the mean value (q_u) of the unconfined compressive strength of concrete, three

separate enhancement factors must be applied to the specified minimum strength as indicated in the following equation:

$$\bar{q}_u = f'_c(F_Q)(F_G)(F_D) \quad (5-1)$$

where

$F_Q = 1.15$ (average enhancement of design mix to assure the specified minimum)

$F_G = R/100$ (enhancement due to aging)

$$R = 10^{[17.0156 - (\log_{10} \text{days} - 2.76343)^2]^{1/2}} - 1.909356$$

$F_D = 1.25$ (dynamic enhancement)

The above values for enhancement are typical suggested averages each of which may be modified or refined depending on the information available. As an example, F_Q may be reduced to 1.1 or less when very careful control is exercised; this often is done in constructing test structures. In analyzing existing structures when a record of the cylinder tests is available, F_Q may be modified to account for the difference in the specified minimum and the average cylinder breaking strength. The equation for computing F_G is based on moist curing at 73°F for the number of days indicated up to 580 days (F_G assumed to remain constant after 580 days). If moist curing is discontinued after a time, the F_Q for the days of moist curing should be added to 0.03 percent per day for the days in dry air; when cured only in dry air, assume moist curing for 7 to 13 days depending on how massive the section and the relative surface area exposed to air. The dynamic enhancement factor (F_D) is dependent upon the rate of strain, discussed in paragraph 5-6b for concrete and paragraph 5-5b for reinforcing steel.

d. In defining thermal properties it should be noted that the coefficient of expansion will vary several tens of percent over the range of possible thermal responses (from cold weather temperatures to near melting temperatures); however, a single equivalent value of the coefficient is adequate for all stages of design. The modeling of the more highly temperature-dependent conductivity and specific heat parameters (several hundred percent variation) should reflect the criticality of the response. The temperature dependence of the coefficient of expansion, conductivity, and specific heat is well documented for the five generic materials of interest.

e. Design and detailing of structures must ensure ductile behavior. Except where system requirements mandate that stresses in structural elements not exceed yield values, take advantage of the yielding of the material. However, where yielding occurs and the amount of yielding must be limited, select appropriate values for the ductility factor μ (the ratio of maximum allowable deformation to the yield deformation). The allowable value of μ will depend on the function of the particular element, the type of failure mode, and the construction material. Table 5-1 gives recommended μ values for structural steel and reinforced concrete.

5-4. Static properties of structural steel

a. Metals can be grouped in two classes based on their lattice structures. The first class is the face-centered cubic, and includes aluminum, copper, and steels that are heat-treated or cold-worked until they lose the definitive yield point characteristic of these metals. The second class of metals is the body-centered cubic lattice, and includes structural and alloy steels.

Table 5-1. Allowable Ductility Factors for Structures*

Design Controlled	Structural Steel	Reinforced Concrete
Flexure	5.0	3.0
Shear	5.0	1.3
Axial Compression	1.3	1.3
Ring Compression	2.5	1.3

*Chapter 8 contains ductility data for elements

U.S. Army Corps of Engineers

Metals of this class have a yield level that is influenced by the rate of loading. An effect of carbon and other additives is to produce steels with a distinct yield strength, ultimate strength, and elongation at fracture. The most commonly used structural steel is A36, which is a mild, or low-carbon, steel capable of withstanding large strains at fracture. High-strength steels are produced by adding various percentages of alloying elements that increase the yield and ultimate strengths while decreasing the elongation at fracture.

b. The stress/strain curve in figure 5-1 demonstrates a number of the mechanical properties of steel. In addition to the terms shown in figure 5-1, the following are important:

(1) Shear modulus of elasticity, G , is the ratio of shearing stress to shearing strain within the elastic range, and may be determined by the expression

$$G = \frac{E}{2(1 + \nu)} \quad (5-1)$$

where

ν = Poisson's ratio

E = Modulus of elasticity

For steel, the common value of ν ranges from 0.25 to 0.33 in the elastic range.

(2) Impact strength is the ability of the steel to absorb energy at high rates of loading.

c. The stress/strain curves for a number of steels are shown in figure 5-2. These curves are for minimum properties defined by the corresponding American Society for Testing and Materials (ASTM) standard. The actual tensile properties may differ from these values significantly. Figure 5-3 shows the distribution of upper yield strengths of mild steel specimens representing 33,000 tons of steel procured for nine different projects over a 13-year period.

d. In reinforced concrete structural members which are underreinforced, the energy absorption is directly related to the strength and elongation of the yielding reinforcing bars. (Elongation is a measure of the ductility of steel and the ability of the structural member to absorb energy. At fracture, elongation varies from about 20 to 34 percent). In the rolling of deformed bars, the steel is cold-worked or strain-hardened which increases the strength but reduces the elongation. The minimum tensile strengths of deformed bars and wires and the minimum allowable elongations are specified by ASTM.

e. Steel plates varying in thickness from 1/2 to 2 in. have been heated continuously at high temperatures and tested, with the results shown in figure 5-4. The modulus of elasticity of structural steel decreases as the temperature increases. Up to a temperature of 900°F, the decrease in the modulus is approximately linear and is equal to about 650,000 psi per 100°F increase. Above 900°F, the modulus of

elasticity decreases at a greater rate (Bresler et al., 1968).

5-5. Dynamic properties of steel

a. Figure 5-5 shows the effect of dynamic loading on the stress/strain diagram for mild steel. It is seen that the yield stress increases to some dynamic value f_{ds} , the yield-point strain increases, the modulus of elasticity remains constant, and the ultimate strength increases slightly. The most important dynamic property is the increased yield strength, shown in figure 5-6 for mild steel.

b. The effect of dynamic loading is the same for deformed reinforcing bars as it is for structural steel. Figure 5-7 shows the dynamic yield stress for intermediate and structural grades of reinforcing steel loaded at various rates. Intermediate-grade reinforcing bars with static yield stresses from 39.5 ksi to 54.6 ksi were tested at loading times as fast as 5.0 msec (Keenan-Feldman, 1960). The average stress rate is plotted against percent increase in yield stress in figure 5-8 and the average strain rate is plotted against increase in yield stress in figure 5-9.

c. Lateral stress, temperature, and rate of loading all have an influence on whether steel will behave in a brittle or ductile manner. Under normal conditions, steel loaded uniaxially behaves in a ductile manner, yielding when slip due to high shear stress occurs along certain cleavage planes. The shear stress at which slip occurs along these cleavage planes is the yield strength and the maximum principal tension stress at fracture is the brittle strength. The brittle strength of steel is not affected appreciably by temperature variations and increases slightly with impact loading (Bresler, et al., 1968; Gaylord-Gaylord, 1968) (fig. 5-10). Yield strength, on the other hand, increases both at lower temperatures (fig. 5-4b) and with increased loading rates (fig. 5-5).

d. The effect of state of stress can be seen by comparing two simple elements: one loaded uniaxially and one loaded triaxially, with both lateral stresses equal (fig. 5-11). In the uniaxial element, yielding occurs when the axial stress exceeds two times the shear stress (V_u). This stress at yield is less than the brittle strength and the material will have a ductile behavior. The triaxial element, on the other hand, yields when the maximum principal stress (σ_2) exceeds the lateral stress (σ_x) plus two times the shear stress (V_u). This higher principal stress represents a higher yield stress. If the lateral stress (σ_x) is large enough, then the yield stress in the primary direction will exceed the brittle strength and the steel will fracture without yielding. This difference in material behavior is significant for structural elements that are confined in the direction perpendicular to the loading, such as closures with edge restraints under normal loading.

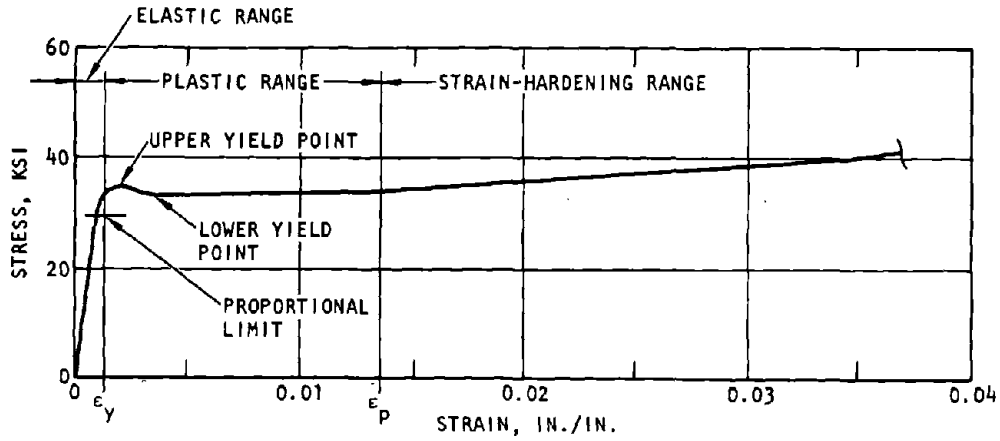


Figure 5-1. Partial Stress/Strain Curve for A36 Steel (Bresler-Sculzi, 1968)

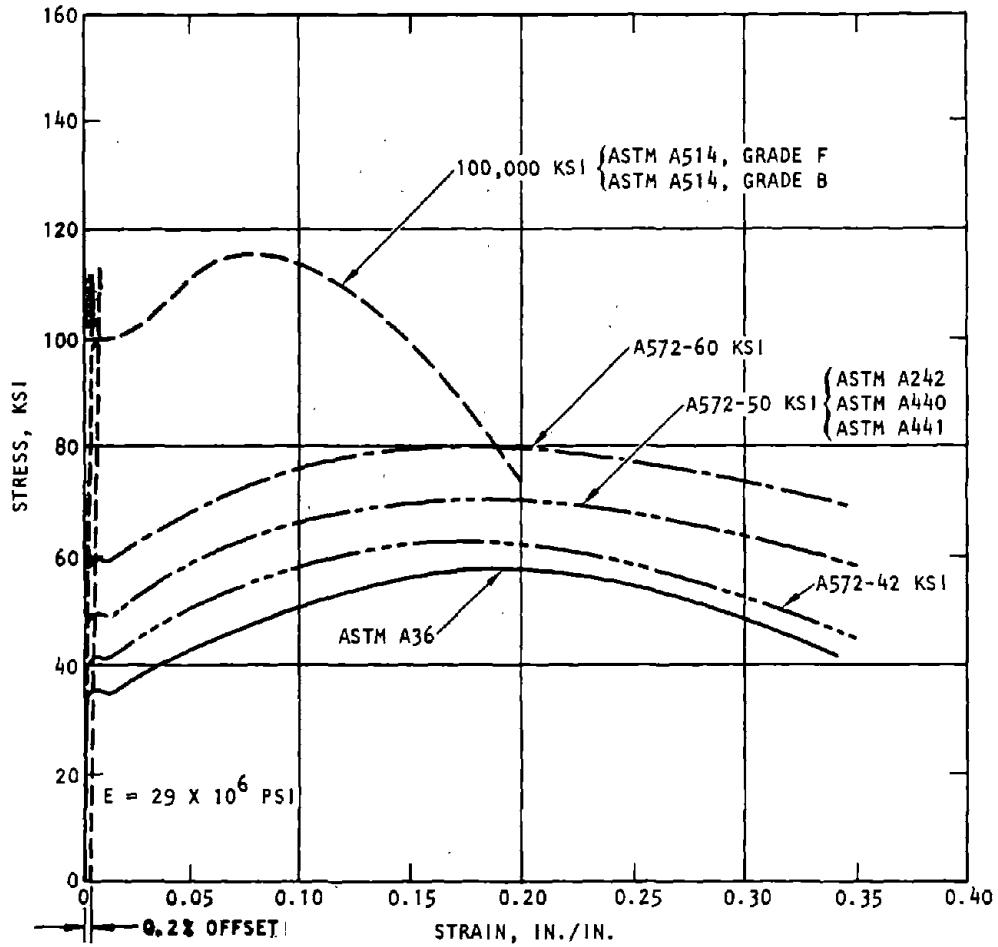


Figure 5-2. Stress/Strain Curves for Specified Minimum Values (Bresler-Sculzi, 1968)

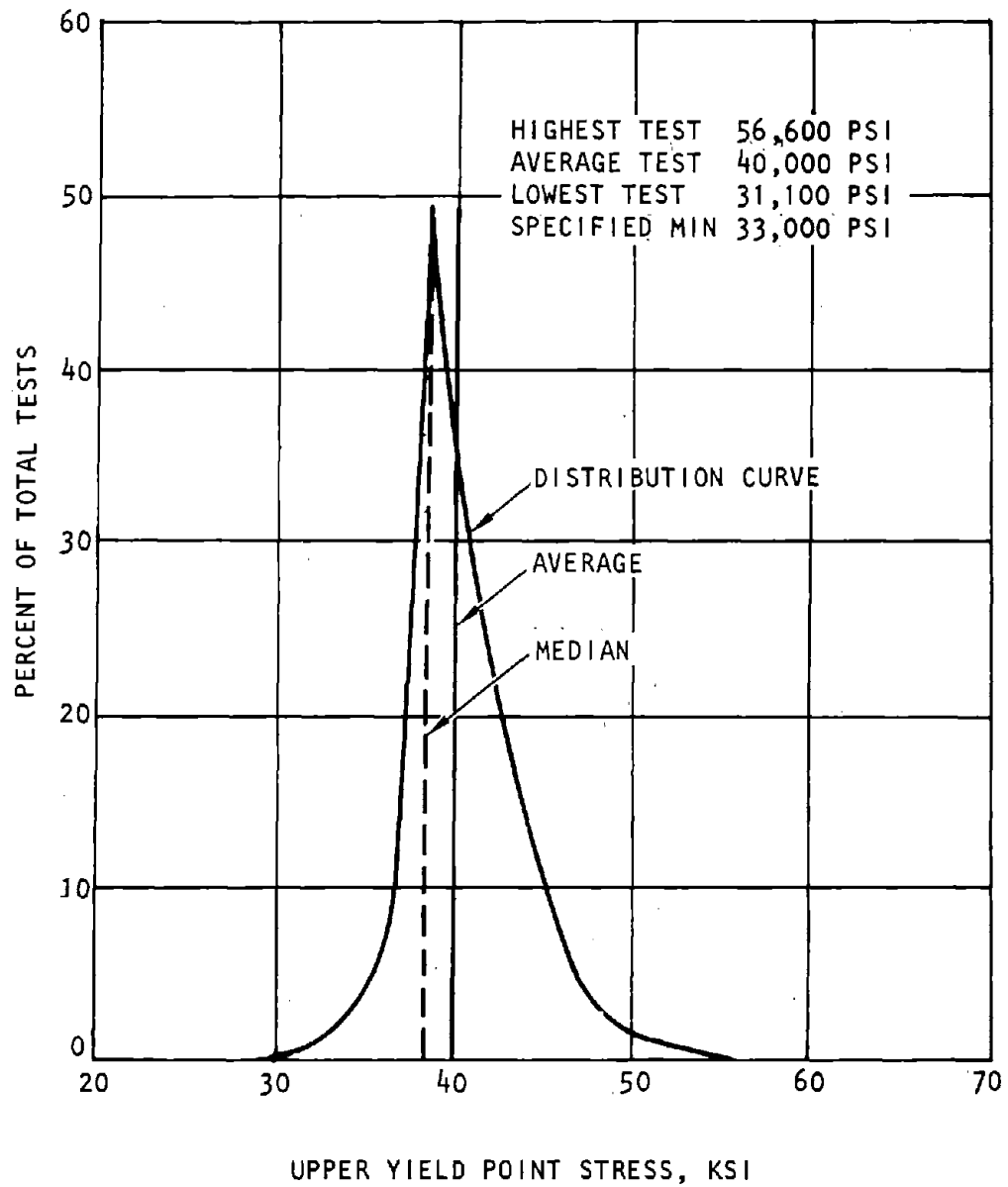
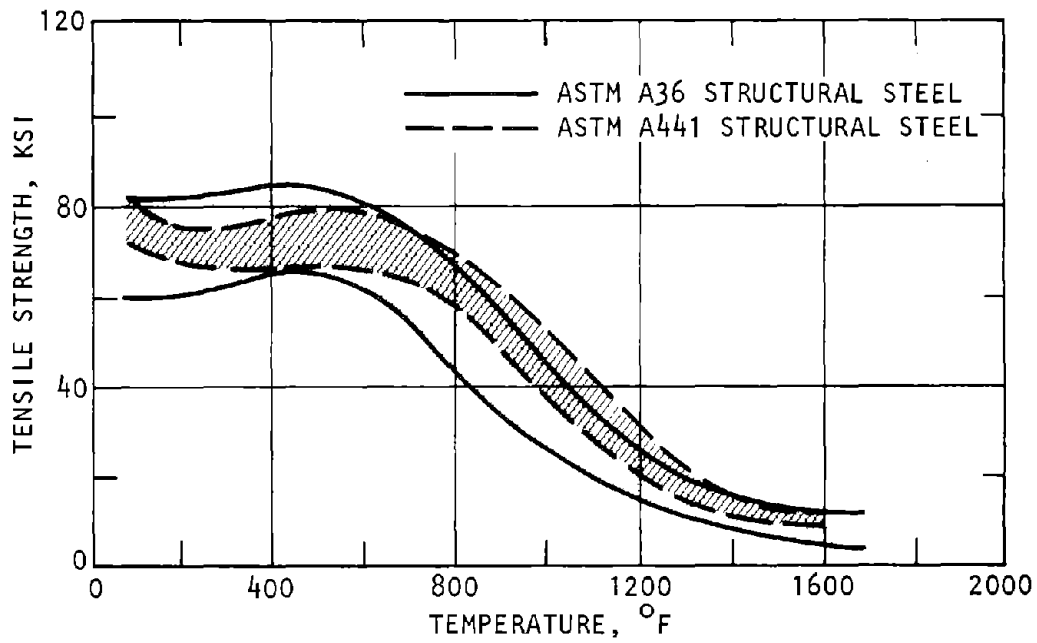
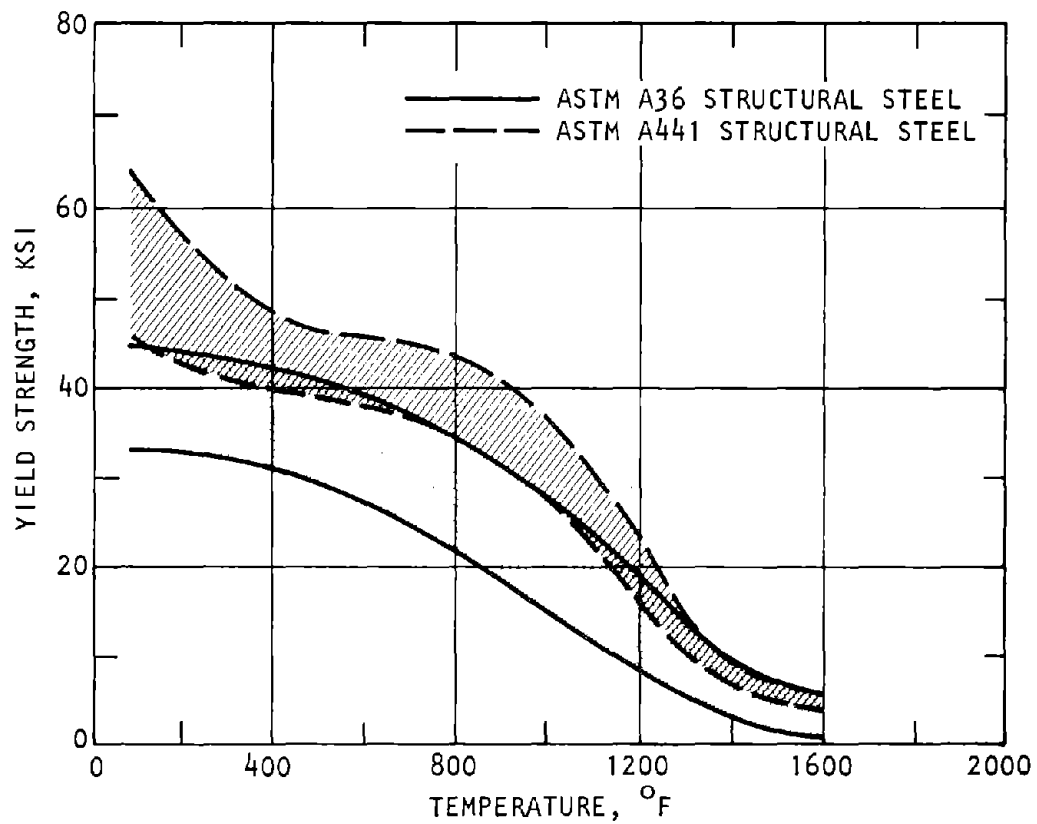


Figure 5-3. Mill Tests of Structural Steel (COE, 1965)



(a) Ultimate strength



(b) Yield strength

Figure 5-4. Ultimate and Yield Strengths at Elevated Temperatures (Bresler et al., 1968)

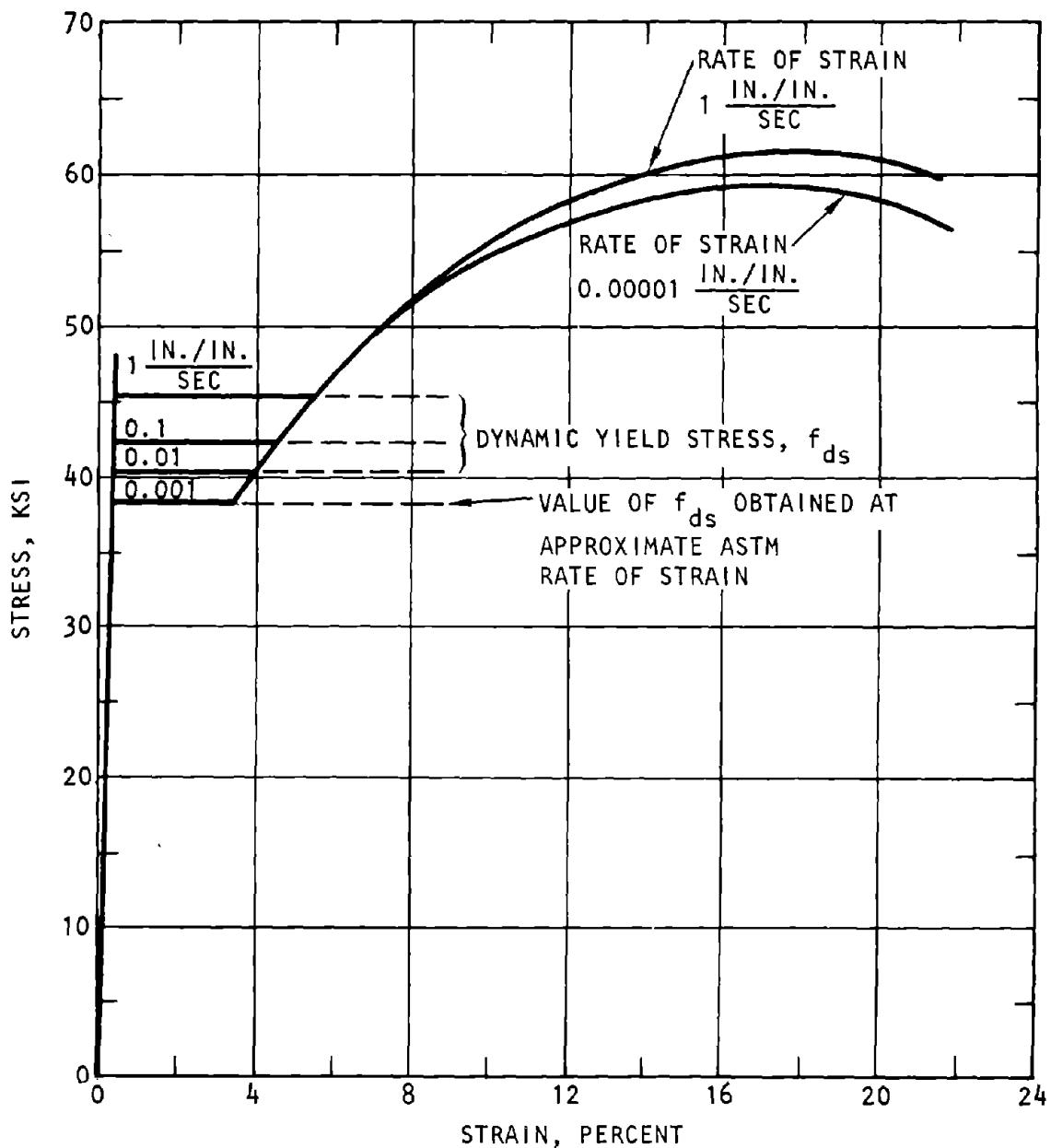


Figure 5-5. Effect of Rate of Strain on Stress/Strain Curve for Mild Steel, ASTM A-7 (Discontinued) (COE, 1965)

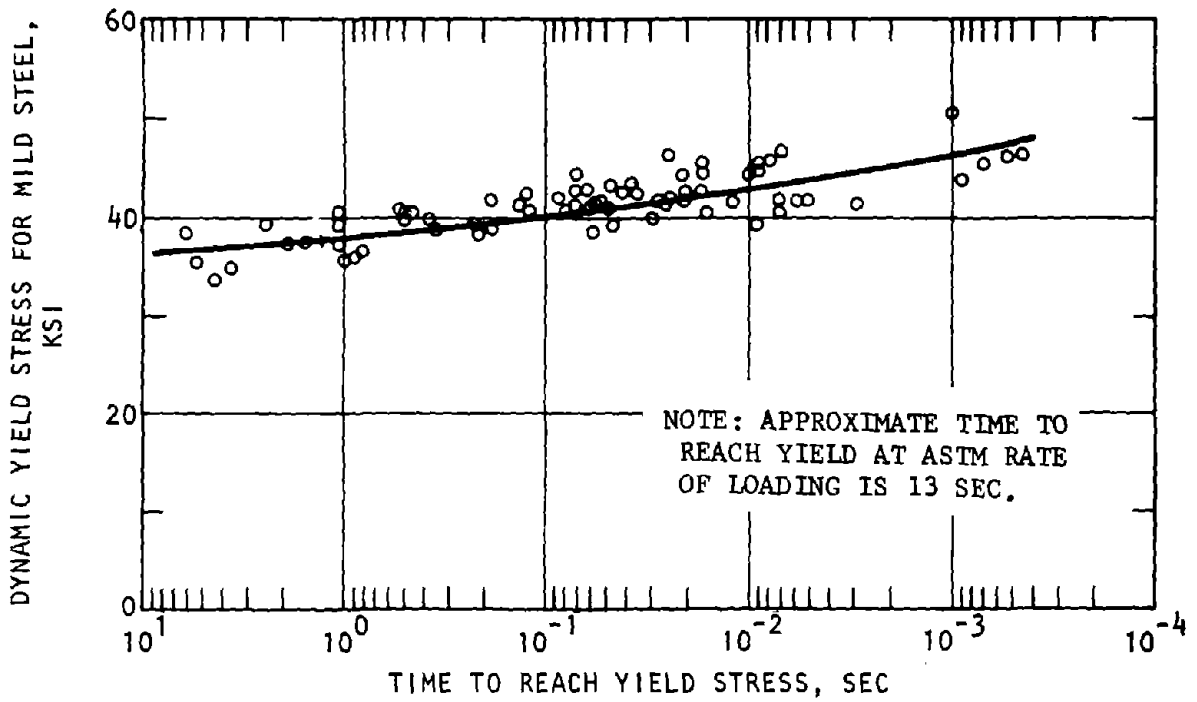


Figure 5-6. Effect of Rate of Strain on Yield Stress, ASTM A-7 (Discontinued) (Norris et al., 1959)

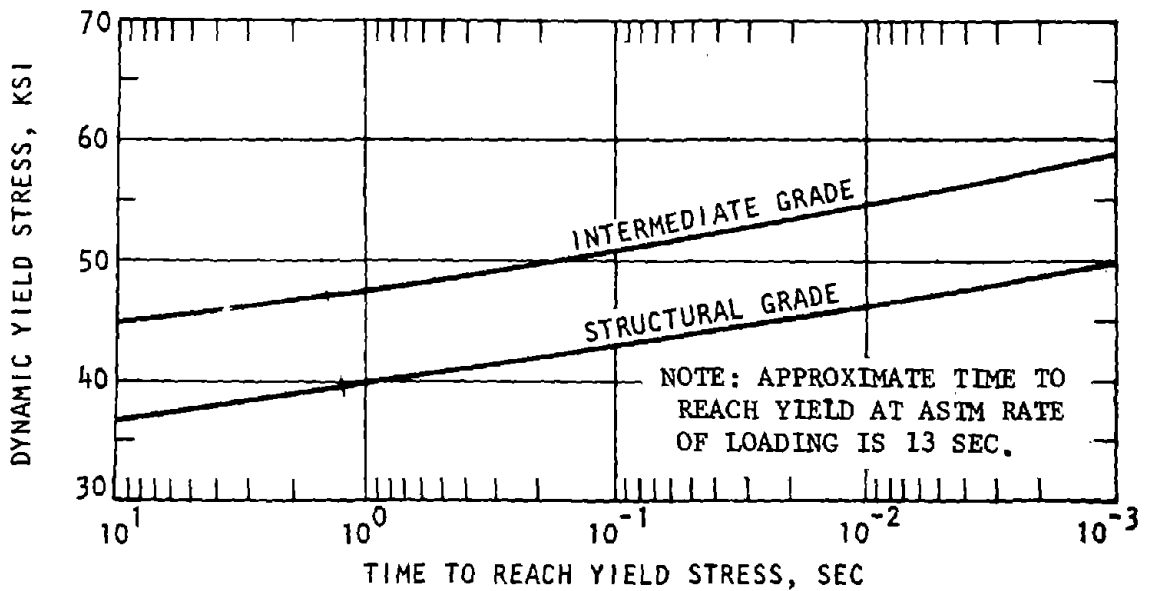


Figure 5-7. Effect of Rate of Strain on Yield Stress in Reinforcing Steel (COE, 1965)

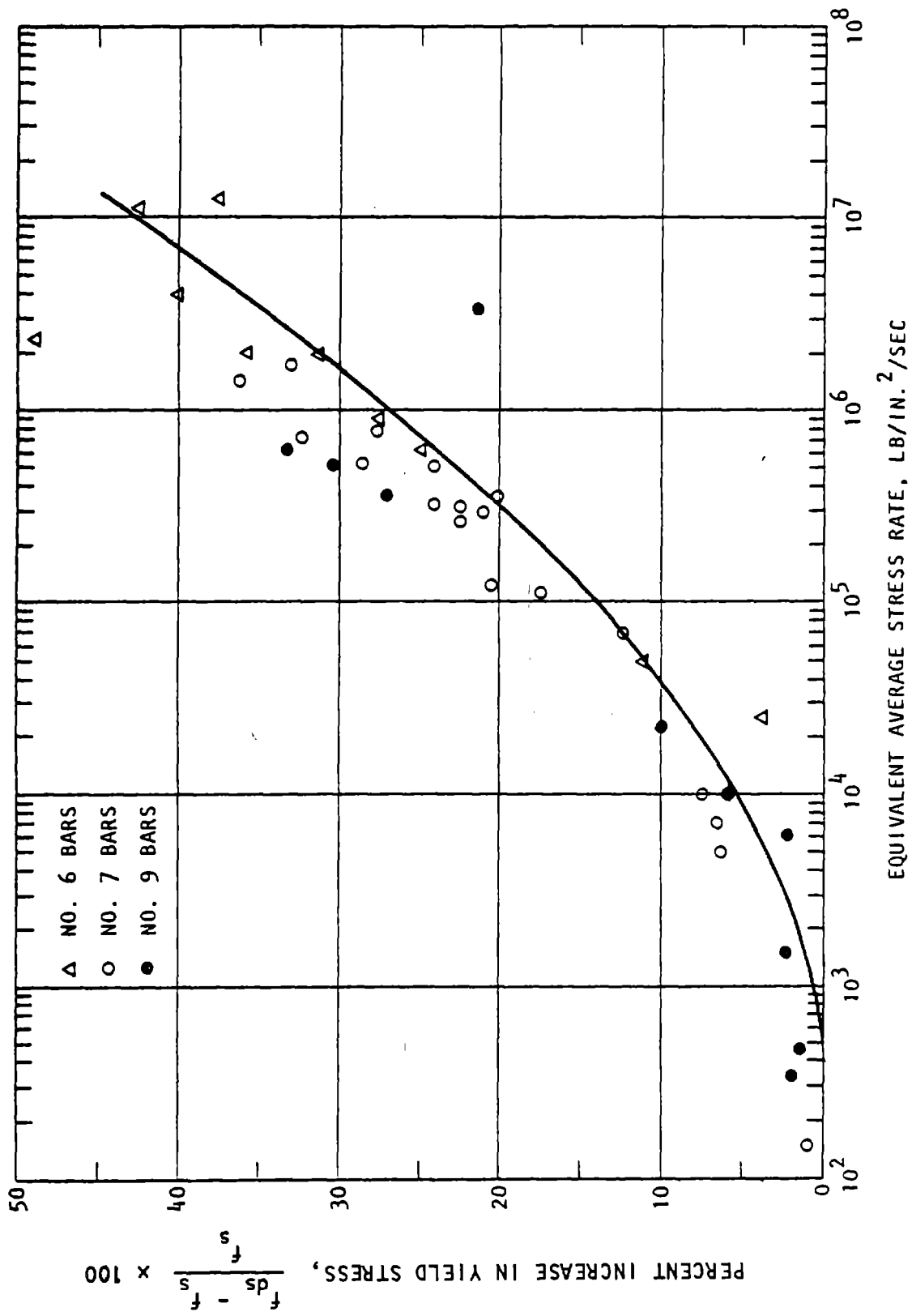


Figure 5-8. Percent Increase in Yield Stress vs. Equivalent Average Stress Rate for Reinforcing Steel (Keenan-Feldman, 1960)

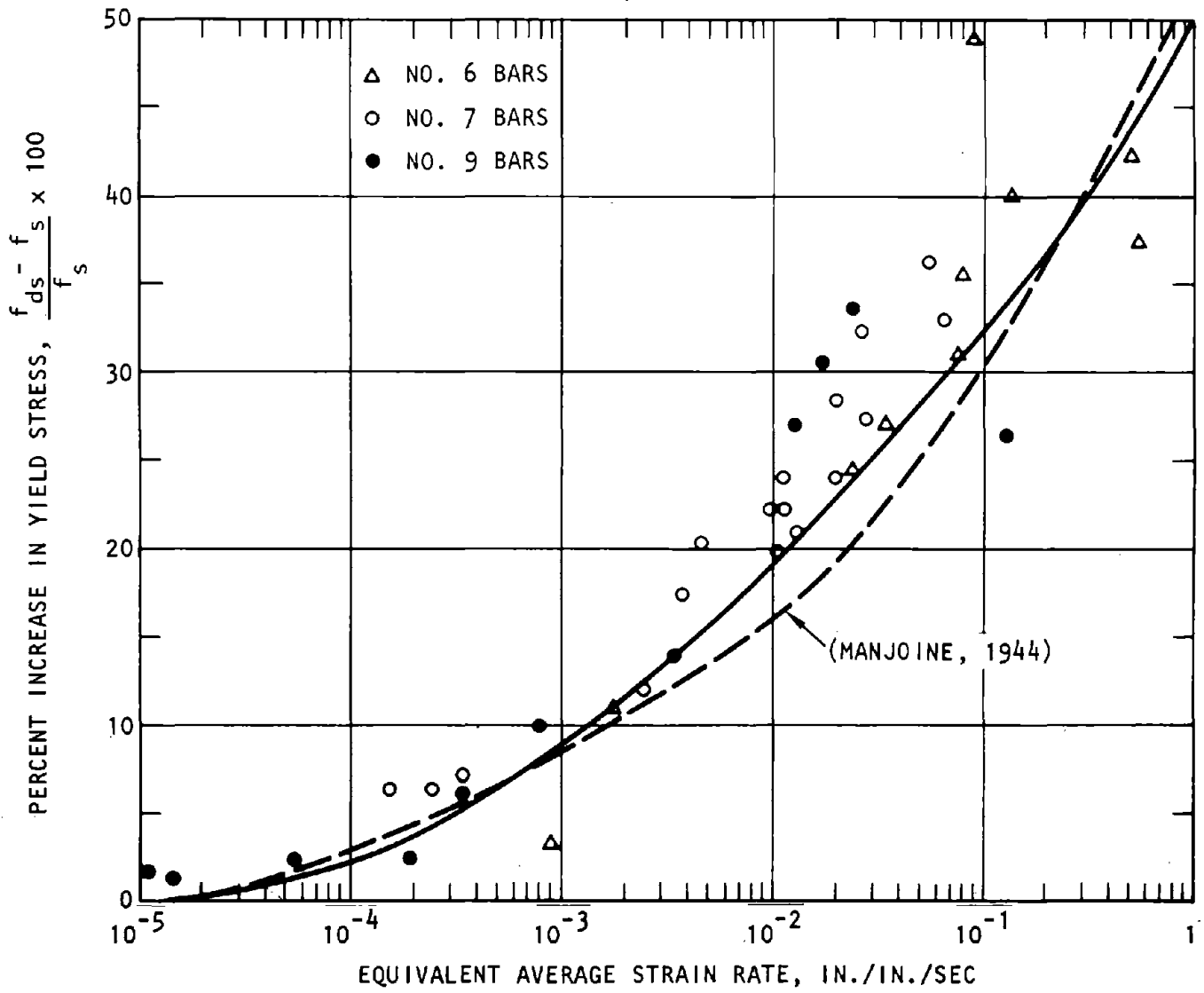


Figure 5-9. Percent Increase in Yield Stress vs. Equivalent Average Strain Rate for Reinforcing Steel (Keenan-Feldman, 1960)

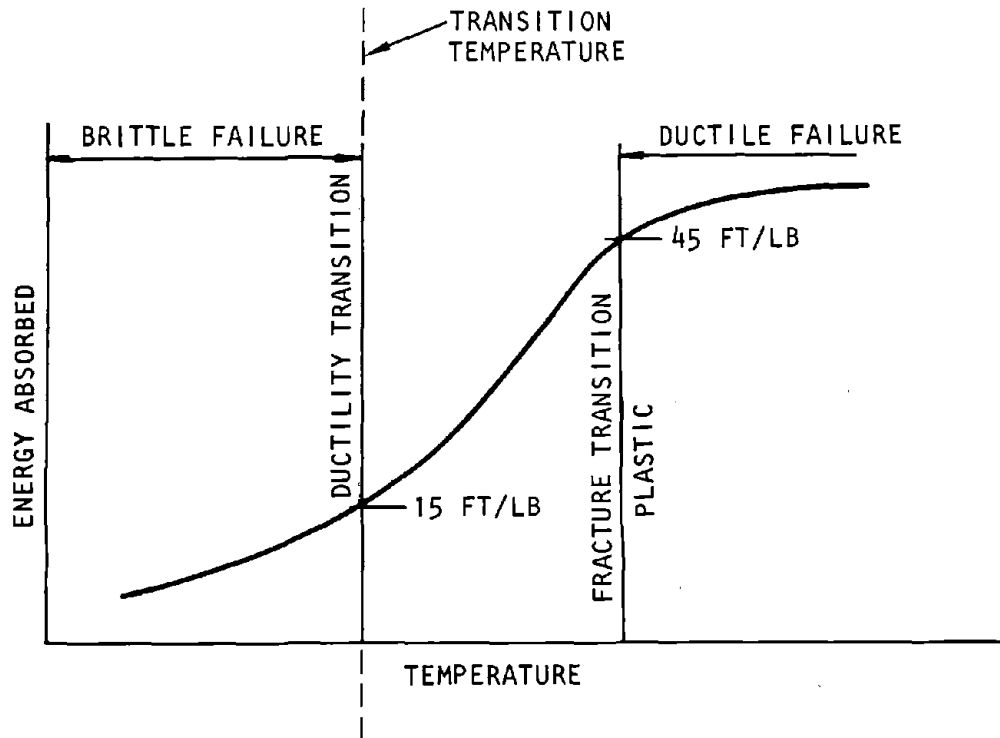


Figure 5-10. Transition from Ductile to Brittle Behavior of Mild Structural Steel (Gaylord-Gaylord, 1968)

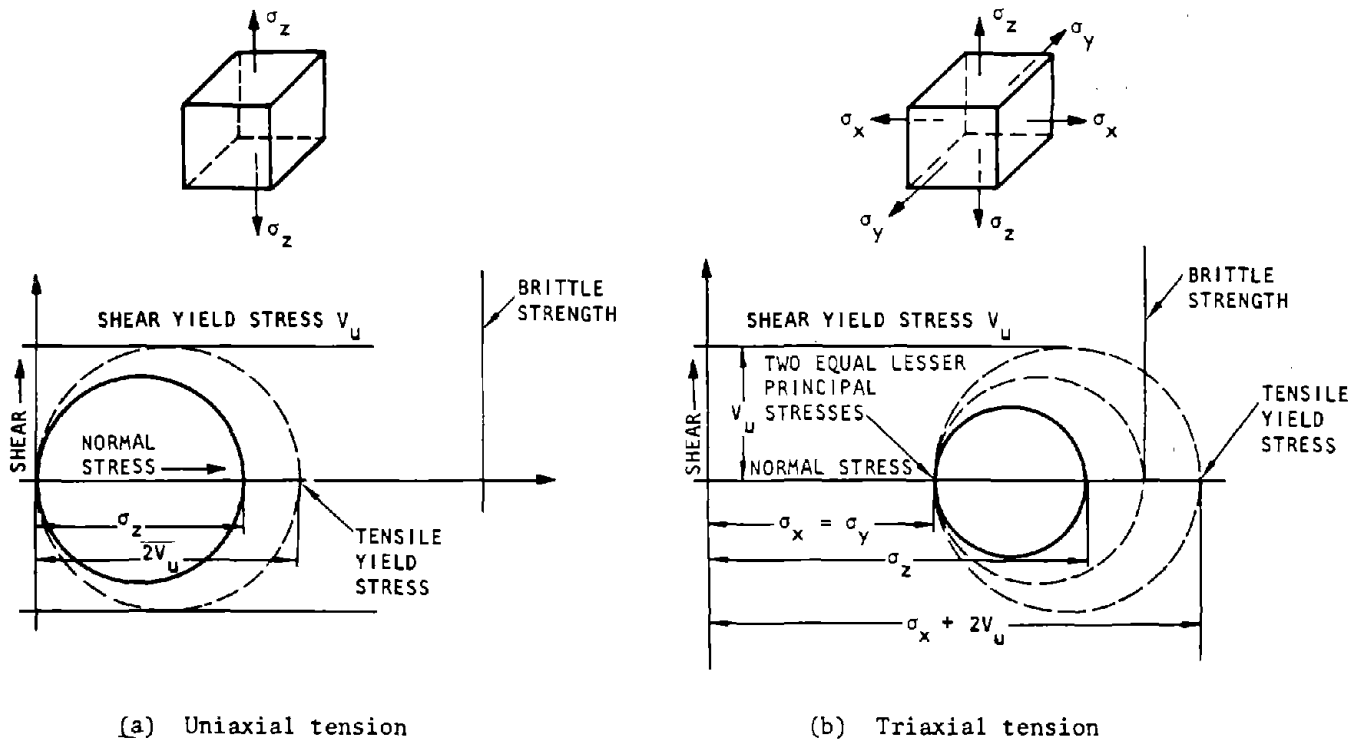


Figure 5-11. Effect of State of Stress on Failure (Bresler et al., 1968)

e. Residual stresses provide lateral stresses in an element. This condition increases the yield stress in the primary direction and makes brittle fracture more likely. In structural members, residual stresses are produced by rolling, which strain-hardens the steel, and by differential cooling rates at various points in the structural shape. Effect of residual stresses must be included in analysis when the allowable stresses are at yield level. The heat of welding, particularly improper welding, produces differential temperatures in the steel member, causing residual stresses. Bolt holes cause high residual stresses at points of maximum load stress.

f. A measure of the ductility or brittleness of steel is determined from the Charpy V-notch test (ASTM, 1972). In this test a standard rectangular beam with a V-notch at midlength is struck by a pendulum. Each steel alloy has a characteristic brittle transition temperature, below which the steel exhibits brittle behavior. The energy absorbed as determined by the Charpy V-notch test at the transition temperature is 15 ft-lb. As the temperature is increased above the brittle transition temperature, a second transition to ductile behavior occurs with Charpy V-notch energy absorption of 45 ft-lb, as shown in figure 5-11. Steels with lower transition temperatures are less likely to experience brittle fracture. A few typical transition temperatures corresponding to 15 ft-lb of energy, as determined by Charpy V-notch test, are tabulated below:

Steel	Transition Temperature, °F
A36	+30
A441	+15
A514	-50

g. A number of factors in the welding process can degrade weld metal, decreasing the strength of the weld. Such defects may not be visible. It is essential to follow the welding and inspection procedures established by the American Welding Society (AWS). In good welding the metal is normally stronger than the adjacent parent metal. For full penetration welds, most specifications prescribe tensile, compressive, and shear stresses equal to or greater than the adjacent parent metal. AWS specifications and the American Institute of Steel Construction (AISC) manual should be consulted for minimum mechanical properties for various electrodes. The AISC Manual (latest edition) specifies the recommended design stresses. The same general mechanism that produces dynamic increase in the yield strength of the parent metal produces a comparable dynamic increase in the weld metal. Since the weld is designed to be stronger than the parent metal for static conditions, it will also be stronger for dynamic loading. Enhancement factors can be applied to the minimum stresses specified in the AISC Manual.

h. Since standard unfinished bolts normally show little or no yielding, bolted joints should not use A-307 bolts. High-strength bolts should be used for all shop and field connections. The proof load, which is the required AISC tension load for bolts, is taken as 0.7 times the ASTM designated tensile strength of the bolt. In computing tensile loads, use tensile stress area as defined in the AISC Manual. For shear capacity, take either the shank area or the root area through the threaded section, depending on where the shear plane is. The minimum strength specifications for various types of bolts are given by ASTM (1968). In blast design, friction-type joints are not permitted.

5-6. Conventional-strength concrete

a. Reinforced concrete adapts readily to unusual configurations and loading conditions. Even though concrete is brittle, reinforced-concrete structures can be designed to respond to dynamic loading in a ductile manner and are well-adapted to survive dynamic loading conditions. Chapter 7 describes special design details that insure inelastic behavior with minimum deterioration in stiffness and energy dissipation under repeated loadings.

b. The unconfined (uniaxial) compressive strength of concrete f'_c increases with rate of loading (fig. 5-12). As the rate of straining increases, f'_c increases and the modulus of elasticity E_c corresponding to the initial slope of the stress/strain curves increases slightly, but the strain at maximum stress remains nearly constant. However, a constant value for E_c should be used. Figure 5-13 shows an average curve for the dynamic increase in concrete compressive strength with increase in rate of strain. A range of strain rates is shown for average concrete structural members under dynamic loads. For rates of straining between 0.03 and 0.3 in./in./sec, the increase in compressive strength will usually vary from 20 to 40 percent, with 25% assumed as the average increase. Determine the average rate of strain by dividing the yield-point strain by the time to reach yield point. Use dynamic analysis to determine time to reach yield point; using the known yield-point strain (normally assumed as 0.002), obtain the average rate of strain. A dynamic increase factor corresponding to the actual rate of strain can then be determined from figure 5-13. The dynamic strength of concrete in compression, f'_{dc} , is normally assumed to be 1.25 f'_c , unless otherwise determined from data similar to figure 5-13. The ultimate strength of concrete in tension, shear, and bond may also increase under rapid rates of strain. However, because conclusive data on the effects of strain rate are lacking, no increases for dynamic loading should be made of these states of stress.

c. The design strength of concrete is usually specified as the minimum strength achieved 28 days after pouring. However, cement continues to hydrate;

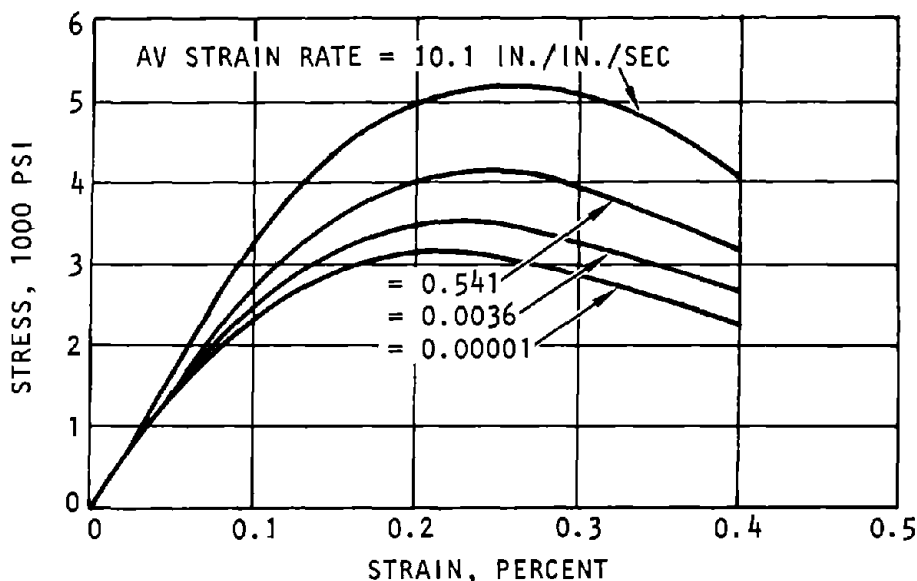


Figure 5-12. Effect of Rate of Strain on Stress/Strain Curve for Concrete Compression Tests (Watstein-Boresi, 1952)

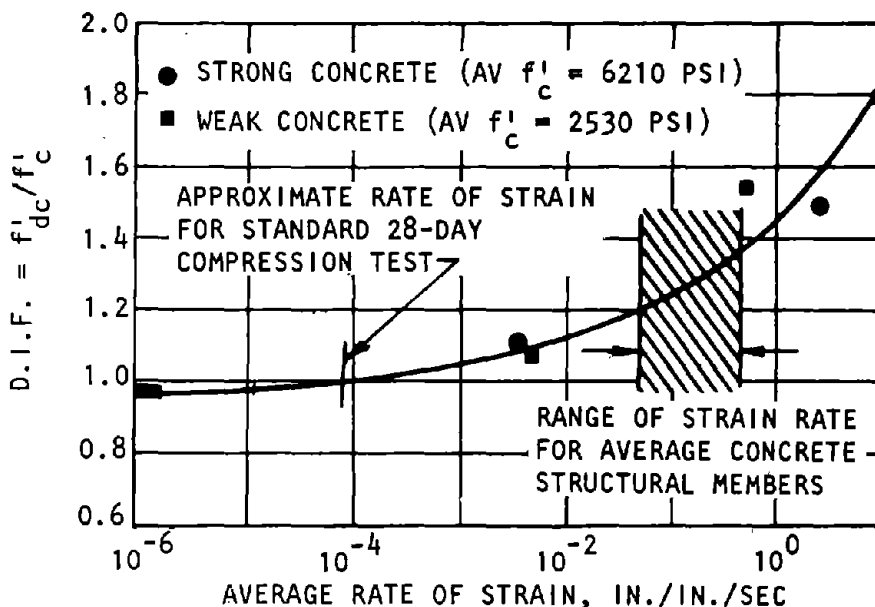


Figure 5-13. Dynamic Increase Factor (DIF) for the Compressive Strength of Concrete (Watstein-Boresi, 1952)

consequently, concrete continues to increase in strength after 28 days, although at a decreasing rate. Figure 5-14 shows a typical curve of this increase. In protective construction, an increase of as much as 20 percent over the 28-day concrete strength can be used (and is included in the enhancement factor at paragraph 5-3c) when the controlling design is based on nuclear weapon effects.

d. Concrete members are normally subject to direct and shear stresses. However, combined stresses can be reduced to three principal stresses acting at right angles to each other on an appropriately oriented elementary cube in the material. Shear stresses acting in planes of principal stresses are zero. Biaxial stress behavior results when one of the principal

stresses is zero; if two of them are zero, a uniaxial stress condition exists.

e. Criteria for the strength of concrete subjected to uniaxial, biaxial, and triaxial stress are based primarily on test data. Concrete is stronger under multiaxial compressive stress. This increase in strength is advantageous in the design of protective structures, since there are many situations in which concrete is confined by the surrounding material. For example, buried shells loaded primarily in compression and concrete wall surfaces will normally be under a biaxial stress condition.

f. Biaxial strength of concrete f'_{bc} may be 15 percent higher than the uniaxial strength f'_c when equal

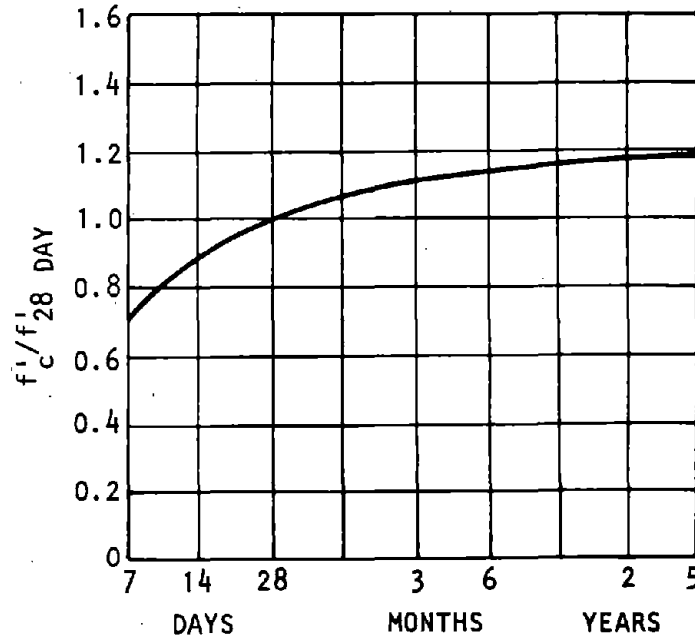


Figure 5-14. Effect of Age on Compression Strength f'_c (Winter-Nilson, 1973)

compression stresses act in two perpendicular directions (figure 5-15). Reading the figure, one sees that the increase in compression strength can be about 25 percent if the lateral compression stress is about 70 percent of the uniaxial strength.

g. Under triaxial compression the strength and ductility of concrete increases even more significantly (Park-Paulay, 1975) used data based primarily on tests of concrete cylinders loaded axially to failure while subjected to confining-fluid pressures to provide the following relationships:

$$f'_{cc} = f'_c + 4.1 \sigma_\ell \quad (5-3)$$

where

- f'_{cc} = Axial compressive strength of confined specimen
- f'_c = Uniaxial compressive strength of unconfined specimen
- σ_ℓ = Lateral confining pressure

However, equation 5-1 is not applicable to nonuniform lateral confining pressures, which are more typical for protective structure design. For nonuniform confining pressures, equation 5-3 may be rewritten by substituting the average of the two principal confining pressures, σ_2 and σ_3 , for the lateral confining fluid pressure, σ_ℓ , and using β in place of 4.1 as an experimental parameter representing a lateral stress coefficient. These substitutions result in the following equation:

$$f'_{cc} = f'_c + \beta \frac{\sigma_2 + \sigma_3}{2} \quad (5-4)$$

where

- f'_{cc} = Compressive strength in direction of σ_1
- f'_c = Unconfined compressive strength of concrete
- β = Experimental parameter
- σ_2, σ_3 = Principal normal confining stresses

This effect is illustrated in figure 5-16, which shows that the parameter β can range from 0 for no confinement to roughly 4 for triaxial confinement.

h. A series of biaxial and triaxial tests of concrete cube specimens of 4000-psi nominal unconfined compression strength is documented by Endebrock and Traina (1972). Figure 5-17 shows the relationships among the three principal stresses at failure when all stresses are compressive. For the biaxial stress ($\sigma_3 = 0$) condition, a confining pressure (σ_2) of $0.3\sigma_1$ increases the strength of concrete by about 25 percent. For a triaxial stress condition in which a uniform lateral confining pressure of $0.2\sigma_1$ is used ($\sigma_2 = \sigma_3 = 0.2\sigma_1$), the compressive strength is higher by a factor of 5.50 as compared to the unconfined compressive strength f'_c . Results from this test indicated that a triaxial state of stress resulted in much higher strength increases than indicated by equation 5-3. This disparity characterizes the inadequacy of the present state of the art for predicting the failure characteristics of concrete under triaxial stresses. Extending the results to real structures and to variations in concrete strengths is unreliable, since most experimental work has been carried out at constant concrete strength. However, the limited data available indicate that concrete strengths under triaxial loading conditions are significantly higher than

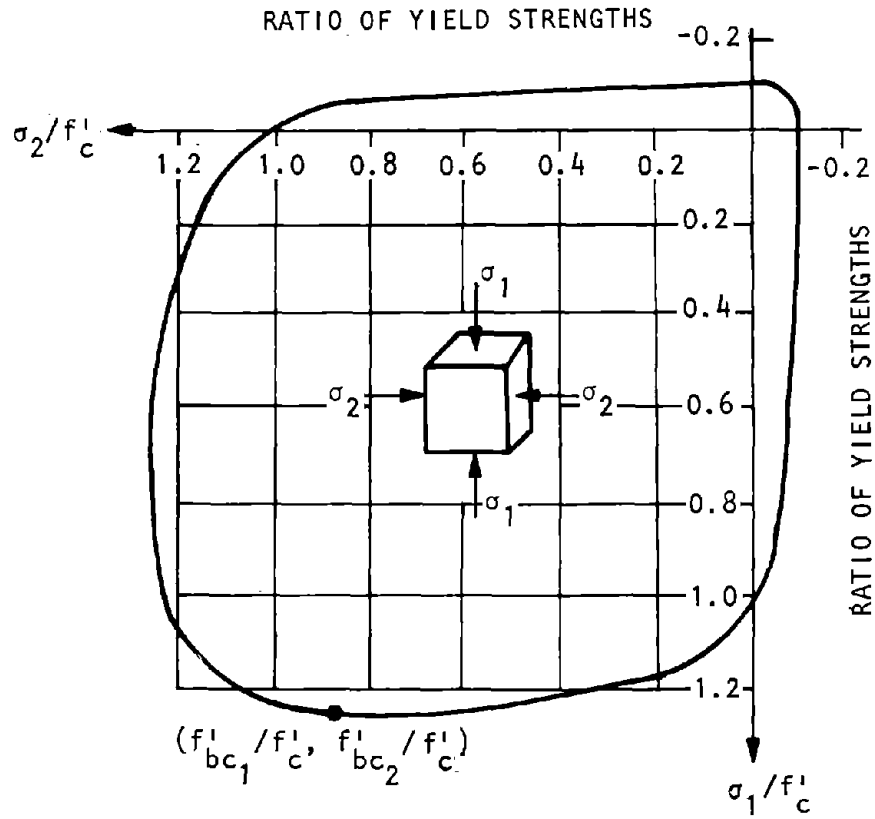


Figure 5-15. Effect of Biaxial Compression on Yield Strength of Concrete (Park-Paulay, 1975)

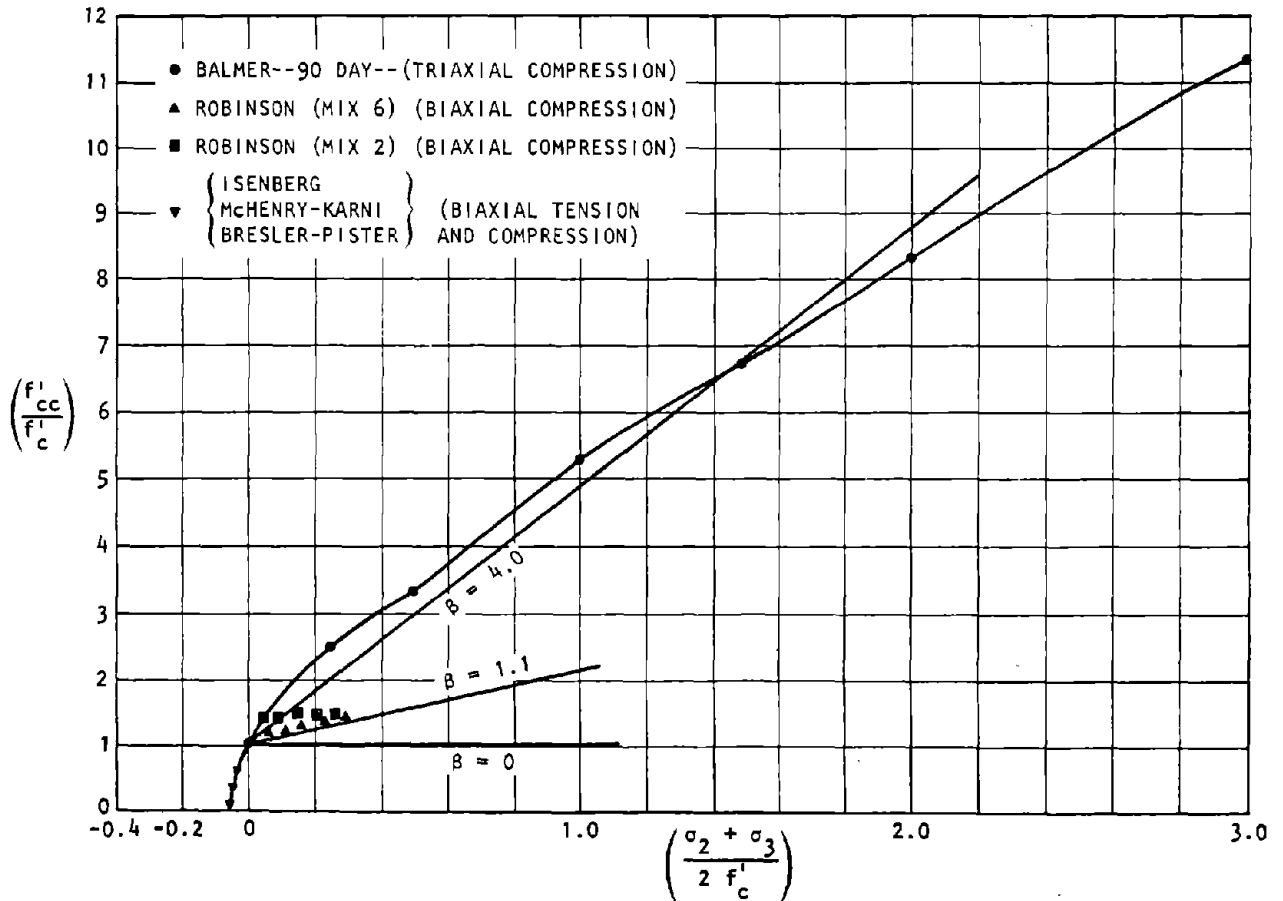


Figure 5-16. Axial Compressive Strength (f'_{cc}) as a Function of the Other Compressive Stresses (σ_2, σ_3) (AA, 1975)

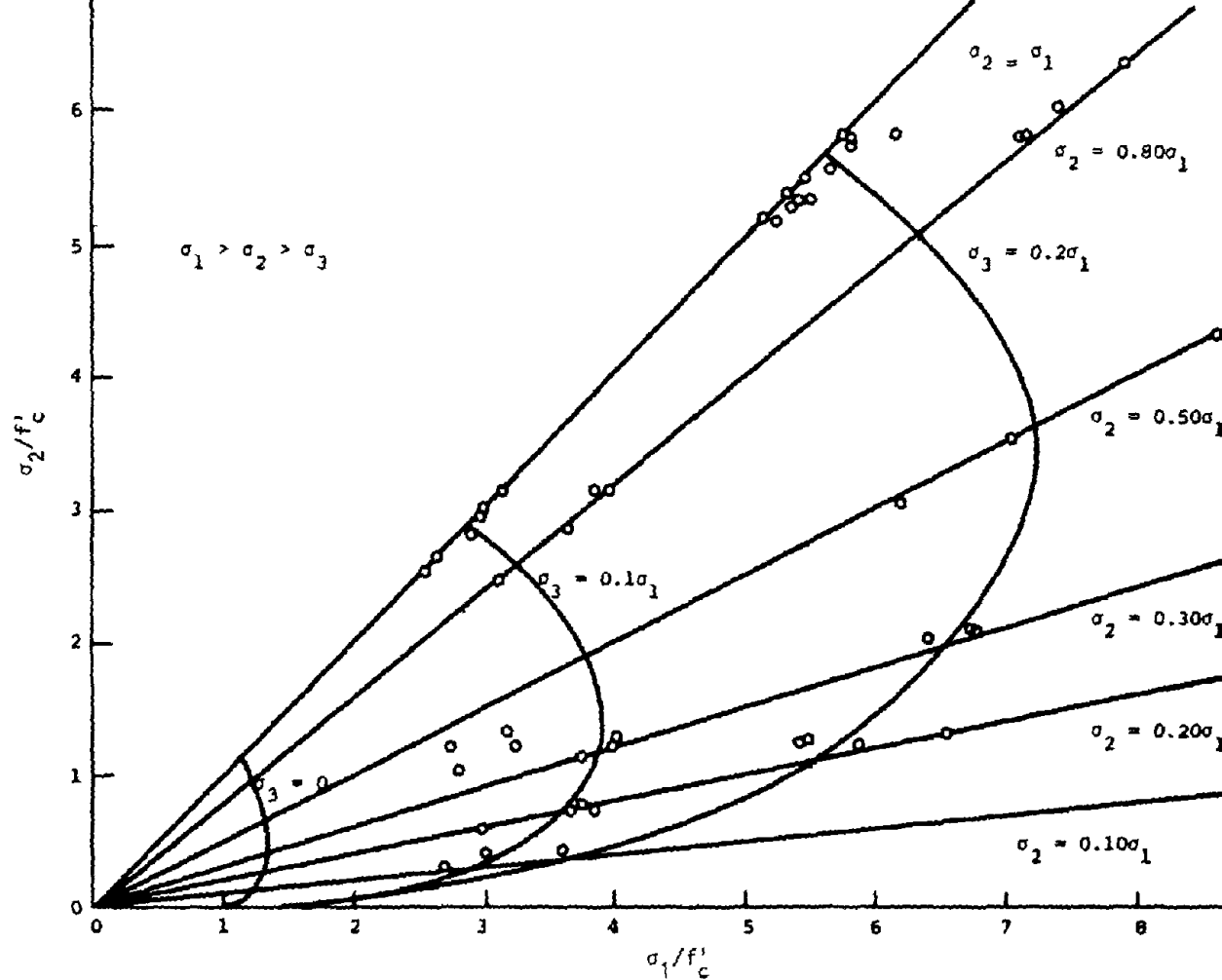


Figure 5-17. Normalized Triaxial Compression Data (Endebroek-Traina, 1972)

those obtained from normal unconfined compressive strength tests. Specific recommendations on the use of higher concrete strengths because of biaxial or triaxial loading conditions will have to be deferred until more testing has been performed, especially tests in which the concrete strength is varied.

i. Concrete used for protective construction is normally massive in section and heavily reinforced. In addition, a steel plate may be anchored to concrete surfaces as primary or secondary reinforcing or as EMP protection. Because of these factors, concrete will normally be subjected to some degree of confinement that will justify increasing maximum allowable compressive stresses. The amount of confinement should be computed and figure 5-16 used to determine the increased allowable stress.

j. A common example of concrete confinement by transverse reinforcement is the use of closely spaced steel spirals or hoops in members subjected to axial loads. See SEAOC (1975) for column tie details. When the concrete is heavily loaded and stresses approach the uniaxial strength of the concrete, transverse

strains become high because of progressive cracking. The concrete bears out again transverse reinforcement which then applies a confining reaction to the concrete. Numerous tests have shown that confinement by transverse reinforcement can considerably improve the stress/strain characteristics and ductility of concrete at high strains.

k. For strength of concrete confined by steel spirals the relationships given by equation 5-15 apply approximately (Richart et al., 1928). The spirals are sufficiently close (conventional spacing meets this criterion) to apply a near-uniform confining pressure. To calculate the confining pressure from the helical tension developed by the spiral reinforcing. The confining pressure σ_l on the concrete reaches a maximum when the spiral reinforcing reaches its yield strength f_s . Yield strength can be static or dynamic depending on strain rate. From equilibrium of forces acting on the half-turn of a spiral,

$$\sigma_l = \frac{2f_s A_s}{Ds}$$

where

- A_s = Area of spiral reinforcing bar
- D = Diameter of spiral
- s = Pitch of spiral

equation 5-5 is similar to the relationship developed in ACI 317 (1977) commentary on spiral reinforcement for ductile frame columns subject to flexure and axial loads. Substituting equation 5-5 into equation 5-3 gives the axial compressive strength of concrete confined by a spiral as follows:

$$f'_{cc} = f'_c + 8.2 \frac{f_s A_s}{Ds} \quad (5-6)$$

l. Hoops are less effective than circular spirals for confining the concrete. Because the pressure of the concrete against the sides of the hoops tends to bend the bars outward, confining reactions occur only near the corners of the hoops. A considerable portion of the concrete cross section remains unconfined.

m. Park and Paulay (1975) suggest the use of the stress/strain curve proposed by Ken and Park (1971) for concrete confined by rectangular hoops (fig. 5-18). The characteristics of the suggested curve are as follows:

Region AB: $\epsilon_c \leq 0.002$

$$\sigma_c = f'_c \left[\frac{2\epsilon_c}{0.002} - \left(\frac{\epsilon_c}{0.002} \right)^2 \right] \quad (5-7)$$

Region BC: $0.002 \leq \epsilon_c \leq \epsilon_{20c}$

$$\sigma_c = f'_c [1 - Z(\epsilon_c - 0.002)] \quad (5-8)$$

where

$$Z = \frac{0.5}{\epsilon_{50u} + \epsilon_{50h} - 0.002}$$

$$\epsilon_{50u} = \frac{3 + 0.002 f'_c}{f'_c - 1000}$$

$$\epsilon_{50h} = \frac{3}{4} a_v \sqrt{\frac{w}{s}}$$

a_v = Ratio of volume of transverse reinforcement to volume of concrete core measured to outside of hoops

w = Width of confined concrete measured to outside of hoops

s = Spacing of hoops

Region CD: $\epsilon_c \geq \epsilon_{20c}$

$$\sigma_c = 0.2 f'_c \quad (5-9)$$

The relationships given in equation 5-8 assume that the maximum stress reached by the confined concrete

is the cylinder strength f'_c , although there is evidence that rectangular hoops will cause an increase in strength. The principal advantages of confinement by hoops are increased ductility and improved stress/strain characteristics after yielding of the concrete, as evidenced by the ability to sustain increased stresses at very large strains. Figure 5-19 shows the influence of rectangular steel hoops on the stress/strain curve defined above when the concrete cylinder strength is 4000 psi and $s/w = 0.5$.

n. The ACI commentary determines the lateral confining pressure provided by hoop reinforcing by developing the cross-sectional area of one leg of a single hoop used to provide confinement to the rectangular core of a compression member. This approach assumes that the same average compressive stress exists in the rectangular core as would exist in the core of an equivalent circular spiral compression member having equal gross area, core area, center-to-center spacing of lateral reinforcement, and strength of concrete and lateral reinforcement. From equilibrium of the forces acting on one hoop,

$$\sigma_h = \frac{2A_s f_y}{sw} \quad (5-10)$$

where

- A_s = Area of hoop reinforcing bar
- s = Spacing of hoops
- w = Hoop dimension normal to lateral confining pressure

However, for equal confinement of concrete, rectangular hoops are not as efficient as spirals in providing lateral confinement to the concrete. The American Concrete Institute (ACI) assumes a 50 percent reduction in efficiency—

$$\sigma_h = \frac{A_s f_y}{sw} \quad (5-11)$$

Substituting equation 5-11 into equation 5-3 gives the axial compressive strength of concrete confined by a hoop as follows:

$$f'_{cc} = f'_c + 4.1 \frac{A_s f_s}{sw} \quad (5-12)$$

o. Individual reinforcing ties can also be used to confine the concrete by anchoring the main reinforcing, similar to the use of hoops in anchoring column reinforcement. Confining stresses will rely on the effectiveness of the main reinforcing steel to prevent lateral displacement of the concrete, on the yield strength of the ties, on the spacing of the ties in each direction, and on embedment or anchorage of the ties.

p. A steel plate is sometimes used to line the interior surface of concrete structures with circular cross sections, such as tunnels, cylinders,

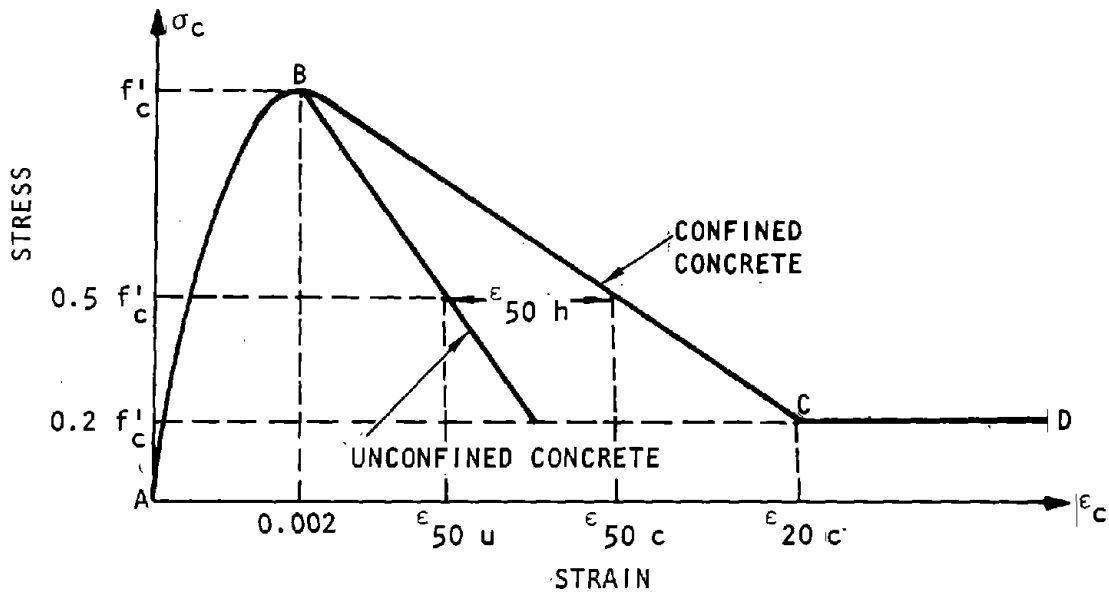


Figure 5-18. Stress/Strain Curve for Concrete Confined by Rectangular Hoops (Kent-Park, 1971)

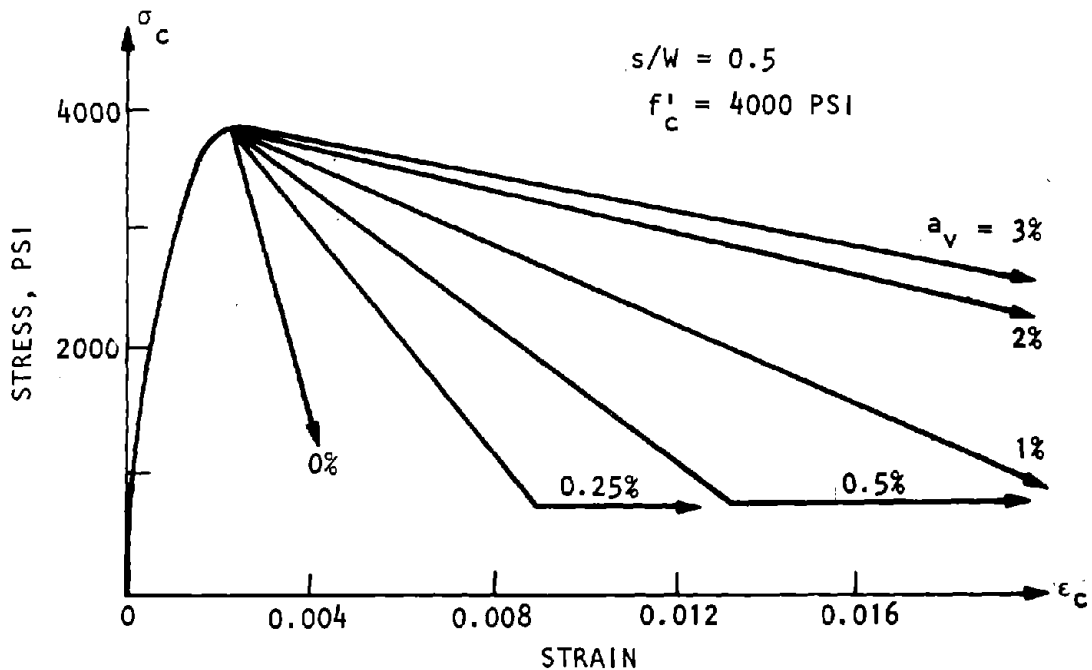


Figure 5-19. Influence of Quantity of Hoops on Stress/Strain Curve for Concrete (Park-Paulay, 1975)

hemispheres, etc. The liner plate is anchored to the concrete by shear lugs and provides reinforcement as well as confinement of the concrete. Assume the amount of confinement provided by the liner as

$$\sigma_l \leq \frac{f_s W}{R} \quad (5-13)$$

where

- σ_l = Confining pressure on concrete
- f_s = Static or dynamic yield strength of the liner depending on strain rate
- R = Liner mean radius
- W = Liner thickness

Account for the buckling of the cylindrical plate in calculating the maximum confining pressure provided by the liner. Plates with $R/W < 150$ will provide confinement without buckling.

5-7. High-strength concrete

a. At increasing hardness levels, consider the use of high-strength concrete as an alternative to the more conventional structural concrete. Concrete with a compressive strength of 5,000 psi or more can be considered high-strength concrete. Although concrete that approaches a compressive strength of 10,000 psi

or more after 90 days has been developed for special applications, the use of concrete having strengths in excess of 6,000 psi has been limited, and routine production practices are not as well established for high-strength as for conventional concrete strengths. Nevertheless, high-strength concrete has been successfully used in dynamic simulation tests of protective structures.

b. The dimensions of structural members can be reduced by designing for high-strength concrete. However, building codes control the length-to-thickness ratio of compression members and restrict deflections of flexural members. In hardened structures not occupied by personnel, building code limitations on deflections of flexural members may be exceeded if the design assures that the strength requirements will be met. For hardened structures occupied by personnel during the preattack period, building code deflection should be adhered to. Also, the ACI code reduces the depth of the equivalent rectangular compressive stress block used in ultimate design for each increment of 1,000 psi above 4,000 psi concrete. This reduction for high-strength design penalizes its use (Saucier, 1965), which may or may not be realistic when high-strength concrete is used for hardened structures. However, the ACI approach is recommended until further research and tests support a change.

c. Despite these limitations, high-strength concrete appears attractive in the design of hardened facilities. Many of these structures are buried circular shells or arches where the walls act primarily as compression members and buckling stability is the limiting criterion for thickness. In addition to the radial compression loads, buried shells will also experience asymmetric loads that are influenced by the stiffness of the shell. Asymmetric loadings induce progressively higher bending stresses as the section thickens. The reduced shell thickness made possible by increasing the concrete strength will help minimize bending stresses.

d. The in-place cost of high-strength concrete is greater than for conventional concrete because of the additional cement per cubic yard, better quality aggregate, and the extra control required in its production, compaction, and curing. However, it is possible that the total cost of the facility may be less because of reduced concrete thickness and less excavation.

5-8. Ultra-high-strength concretes

a. New construction materials under development will produce ultra-high-strength concretes. The Portland Cement Association reports that concrete strengths as high as 11,000 psi are being ready-mixed at the job site and strengths of 15,000 psi are being

produced in the laboratory using normal-weight aggregate. Concrete-polymer composite materials are also being developed to produce high-strength concrete (NTIS, 1978). Polymer concrete, in which the polymerized monomer acts as the binder for the aggregate, can produce strengths up to 20,000 psi. Portland cement concrete can be impregnated with a monomer, which is subsequently polymerized in situ, to increase the compressive strength by two-fold or more. US Army Waterways Experiment Station (WES) developed a granite-simulant grout mixture to produce strengths of approximately 20,000 psi. However, before these ultra-high-strength concretes can be considered for full-scale application to hardened structures, additional investigation, demonstration, and experience will be necessary, especially in determining in-place material costs.

b. Randomly dispersed steel fibers of short length and small cross section can be intermixed with ordinary concrete. Length of the fiber normally varies from 3/4 to 1-1/2 in, depending on concrete mix and application. The diameters of wire fibers range from 10 to 16 mils. Rectangular fibers of comparable thickness produced by shearing sheets or flattening wire are also available. Crimped or deformed steel fibers improve the physical properties of the concrete, notably because they: increase first-crack flexural strength; increase ability to carry load after cracking by arresting crack growth; improve ductility and fatigue strength; and provide high spall resistance. The improvement in concrete properties depends on the volume, aspect ratio, shape, and bond characteristics of the fiber. Generally, fiber concrete properties are directly proportional to fiber volume for a given fiber and a given concrete mix, up to a volume of fibers of about 4 percent. A minimum fiber content is normally considered as 0.25 percent by volume.

c. Steel fibers in concentration of up to 4% by volume have been found to increase the first-crack flexural strength of concrete up to 2.5 times the strength of plain concrete (ACI, 1973).

d. The effectiveness of steel fibers to increase the compressive strength of concrete has not been firmly established. Results from research and field applications of fiber reinforcing indicate a range from little increase to as much as 100 percent increase in strength over the plain concrete. The addition of 5 to 6 fibers by volume can be estimated conservatively to increase the compressive strength by 10 to 20 percent. The establishment of f'_c for fiber-reinforced concrete is by strength testing similar to plain concrete except that splitting tensile strength tests are used. This f'_c is then enhanced in the same manner as conventional concrete (par. 5-3c).

e. A series of tests of beams designed to fail in shear which were cast with steel-fiber-reinforced concrete

was reported by Paul and Sinnamon (1975). In addition to the randomly dispersed steel fibers, the test beams were reinforced with a single, conventional reinforcing bar but with no shear reinforcement. Test results were used to develop a rationale for predicting the ultimate shear capacity of fiber-reinforced-concrete beams subject to bending and shear. The approach was to modify the ACI code formula for determining shear capacity of conventional beams without shear reinforcement. (It was assumed that the code relationships were related primarily to the compressive strength of the concrete.) However, it was known that the tensile capacity of fiber concrete varies with fiber content and is not related well to the compressive strength. To incorporate this relationship into a shear capacity formula, the modulus of rupture was introduced to reflect the effect of fiber content on the tensile strength of the fiber concrete. Fitting test results to the modified code formula provided the following relationship for ultimate shear capacity of fiber-reinforced concrete beams:

$$\frac{7.5}{F} \frac{S}{WH} = 1.07 + 155,000 \frac{a_s S_u H}{F M_u} \quad (5-14)$$

where

- S = Ultimate shear capacity of concrete at section
- H = Effective depth of beam
- W = Width of beam
- d = Effective depth of the beam
- F = Modulus of rupture of fiber-reinforced concrete
- a_s = Steel to concrete ratio, A_s/WH
 A_s = Area of tension steel reinforcement
- S_u = Total applied design shear at the section
- M_u = Applied design load moment at the section

When a member is subjected to axial compression as well as moment and shear, the shear capacity of the member is increased. Based on the ACI code, an amplification factor can be used to increase the shear capacity due to thrust. In the absence of data on the effect of axial force on shear capacity for fiber-reinforced concrete members, it is suggested that the following amplification factor be used as given in the ACI code.

$$\text{Amplification Factor} = 1 + 0.0005 \frac{N_u}{WH} \quad (5-15)$$

where

- N_u = Design axial load normal to the cross section occurring simultaneously with V_u , to be taken as positive for compression and to include the effects of tension due to shrinkage and creep, lb

WH = Gross area of section

f. Steel fibers do not significantly affect the modulus of elasticity or Poisson's ratio for concrete.

g. Fiber-reinforced concrete has certain characteristics that may be applicable, under unique conditions, to the design of hardened structures. The uniform dispersal but random orientation of the steel fibers provides isotropic strength properties not common to conventionally reinforced concrete. The increased ultimate strength and the improved ductility after first cracking are desirable properties for conditions requiring special construction materials. There has not been enough experience in mix design and testing to specify strength and physical characteristics of fiber-reinforced concrete based on the relationship between design strength of the concrete and the fiber content, specified as a percentage by volume and the properties and shape of the fiber. The mechanism that controls the first crack strength or the ultimate strength is not well understood, but important in determining strength are: volume, spacing, orientation, aspect ratio (length to diameter or thickness), bond characteristics, and specific surface of the steel fibers. A recent investigation (Agabian Associates, 1978) of fiber-reinforced concrete spheres subjected to hydrostatic compression showed that the average wall stress at implosion was 2.2 times the unconfined compression strength. Previously the same ratio for plain concrete spheres had been found to be 1.4 (Haynes, 1976). This shows the additional enhancement of strength under confinement provided by fiber reinforcement. The Agabian investigation also showed the external pressure at implosion to be 1.49 times the pressure at the development of in-plane cracks, usually interpreted as the onset of inelasticity. This ratio for plain concrete spheres was 1.25. This shows the improvement in ductility after first cracking as a result of fiber reinforcement.

h. Fiber-reinforced concrete has an application in blast-resistant construction because it exhibits greater ductility and resistance to spalling and fragmentation than plain concrete. However, as with other high-strength concretes, more experience is needed to relate strength to mix designs and to determine construction costs and quality control requirements. Fiber-reinforced concrete should be used in conjunction with conventional forms of reinforcing and not as a substitute for steel reinforcement.

5-9. Plastics and other materials

a. A crushable backpacking material is sometimes used in the design of hardened facilities sited in rock. Placed between the structure or element to be protected and the rock excavation, the backpacking material dissipates the ground-shock energy reaching the structure. Energy is reflected because of the

mismatch in shock impedance and is absorbed because of inelastic straining, thereby reducing the peak stresses and peak accelerations in the structure.

b. A suitable backpacking material should possess a relatively low crushing strength and a high degree of compressibility without a significant increase in applied stress. Also, the backpacking material must possess a multiple-attack loading capability; be resistant to aging effects and to the infiltration of groundwater; be relatively insensitive to strain-rate changes; be readily available in most areas; be easy to handle and place; and be reasonably inexpensive to fabricate and install.

c. Stress/strain properties of backpacking materials are normally based on confined static properties because data available from dynamic test programs are limited. The two basic types of idealized stress/strain curves for potential backpacking materials (fig. 5-20) define the properties of a variety of materials. The elastoplastic material shown in figure 5-20a typifies insulating concretes and plastic foams. The plastoelastic material shown in figure 5-20b typifies many granular materials. Since multiple-attack considerations will require the most efficient energy absorbers, elastoplastic materials are more applicable to protective construction.

d. Properties for materials that generally exhibit elastoplastic behavior are given in table 5-2. These materials include low-density concretes, rigid foamed plastics, and foamed glass. Note that such materials are available for a wide range of properties.

e. Two types of low-density concretes are available: cellular concrete and concrete using vermiculite or polystyrene as the aggregate. A wide range of compressive strengths can be obtained depending on the cement paste, the admixture, and the aggregate used. When exposed to groundwater for long periods, the strength of low-density concrete decreases owing to chemical attack and degradation; laboratory tests should simulate these conditions in order to establish design values. These concretes can be emplaced with conventional construction equipment and techniques and have a low cost-per-unit volume compared to that of plastic backpacking materials.

f. Closed-cell or rigid foam plastics generally exhibit elastoplastic behavior, while the open-cell or flexible plastics usually exhibit a plastoelastic stress/strain behavior. Foamed plastics can be foamed in place or be precast and placed in slabs around structures. Use a closed-cell type in a groundwater environment and choose the material constituents that will have the highest possible percentage of closed cells in the foam. A wide range of strengths and densities are available. The more common types of foamed plastics considered for backpacking are polystyrene, polyurethane, epoxy, and phenolic. Foamed plastic materials are more costly than other types of backpacking.

g. Foamed glass comes in precast elements that must be fitted around structures and may not be convenient for backpacking large areas. However, foamed glass is impermeable to groundwater and its cost is between low-density concrete at low cost and foamed plastics at high cost.

h. Gravel is a common backpacking material that exhibits plastoelastic behavior if not fully compacted when placed. The modulus of elasticity can be varied by specifying the degree of compaction, but a value of approximately 30,000 to 40,000 psi provides reasonable characteristics for backpacking materials.

5-10. Properties of soils

a. A large part of this chapter is a summary of material prepared for the Defense Nuclear Agency (DNA) in *Nuclear Geoplosics, Part 2 Section 3 (AA, 1972)*. (For further background and detailed test results, see the reference.)

b. The properties of all soils are influenced by initial void ratio, degree of saturation, stress history, loading path, and rate of loading. The stresses that develop within the soil mass depend on the relative compressibilities of the soil skeletons and pore fluid. Strength and stiffness are related to effective stress (Skempton, 1961). Effective stress is defined as the total stress minus the pore fluid pressure.

c. During airblast or ground-shock loading, the rate of loading is generally faster than the rate at which pore fluid can be expelled. Since the fluid is generally much less compressible than the soil skeleton, pressure builds up in the pore fluid. In soils with less than 100 percent saturation, large volume changes occur during dynamic loading as air is compressed in the voids. In soils with 100 percent saturation, a large percentage of the total stress will be taken up by the pore fluid.

d. If the saturation is very low (less than 30 percent), the effective stress is greater than the total stress because pore pressures are negative due to the surface tension of the water adhering to the soil particles. The surface tension lessens as the degree of saturation increases. If the initial saturation is high enough that the soil reaches 100 percent saturation as it is compressed, the subsequent increase in mean normal stress is practically all accounted for by an increase in pore water pressure. At high stresses, where voids are eliminated, plastic flow or melting of the solid constituent occurs. Typical pore-pressure parameters are shown in figure 5-21 which relates the pore pressures to total stress in uniaxial strain hydrostatic compression, and triaxial compression experiments.

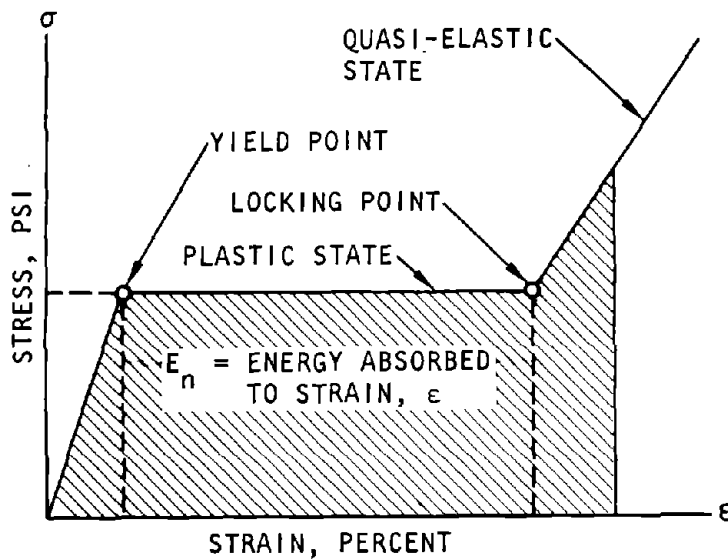
e. Dry, coarse-grained soil under hydrostatic compression exhibits three distinct phases in the mean normal-stress/volumetric-strain (P/μ) relationship. The first phase occurs at low stress levels (below 10 bars) where the soil behavior is influenced by the in-

initial void ratio and the initial state of stress (Vesic-Clough, 1968; Ko-Scott, 1967). The second phase occurs when intergranular stresses become high enough to cause crushing of the soil grains (below about 100 bars). The third phase occurs after the influence of the initial void ratio and crushing have diminished. Most of the energy absorption, however, occurs in the initial phase. At stresses above 10 bars, the soil unloads nearly along the loading path.

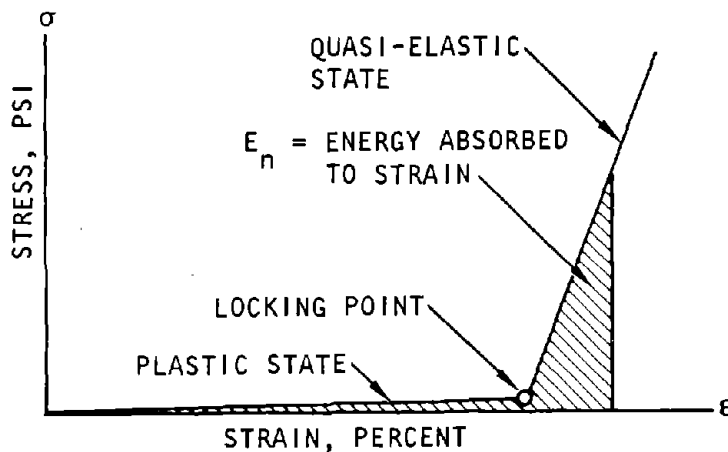
f. Fine-grained soils (clays) are more cohesive than coarse-grained soils and behave differently under stress. Because most fine-grained soils, though mixed with coarser particles, are more flocculated than

dispersed, the application of external stresses may cause irrecoverable deformations and impose important stress-history effects on the soil. In partially saturated clays irrecoverable volumetric strains as high as 60 percent of the maximum can occur (fig. 5-22). Note that during unloading significant hysteresis begins when the transition zone is reached.

g. Coarse-grained soils exhibit several typical shear stress/strain relations, as shown in figures 5-23, 5-24, and 5-25. The following observations can be made: (1) The shear stress/strain curves are concave to the shear strain axis and shear strains are irreversible; (2) the initial shear modulus increases with the



(a) Elastoplastic materials

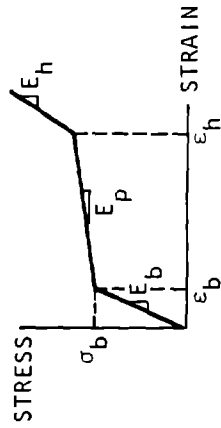


(b) Plastoelastic materials

U.S. Army Corps of Engineers

Figure 5-20. Idealized Stress/Strain Curves of Potential Backpacking Materials

Table 5-2. Backpacking Materials (AJA, 1968)



Material	Yield Stress σ_b' psi	Yield Strain ϵ_b' %	Hard Strain ϵ_H' %	Elastic Modulus E_b' psi	Plastic Modulus E_p' psi	Locking Modulus E_h' psi	Density γ_b' pcf
Vermiculite Concrete	75	3.0	40	2,500	0	500	40
Foamed Glass	150	6.0	40	2,500	0	NO DATA	10
Foamed Polyurethane							
Foamed Epoxy Plastic							
Vermiculite Concrete	75	1.5	40	5,000	200	1,000	40
Cellular Concrete	150	3.0	40	5,000	150	1,500	25
Polystyrene Concrete							
Vermiculite Concrete	150	1.5	40	10,000	400	2,000	45
Cellular Concrete							
Polystyrene Concrete							
Vermiculite Concrete	300	3.0	40	10,000	500	3,000	45
Polystyrene Concrete							
Vermiculite Concrete	150	0.8	40	20,000	500	3,000	45
Polystyrene Concrete							
Vermiculite Concrete	300	1.5	40	20,000	500	3,000	50
Cellular Concrete							
Foamed Phenolic Plastic	600	3.0	40	20,000	800	NO DATA	15
Vermiculite Concrete	300	0.8	40	40,000	500	3,000	50
Cellular Concrete							
Vermiculite Concrete	600	1.5	40	40,000	800	3,000	70

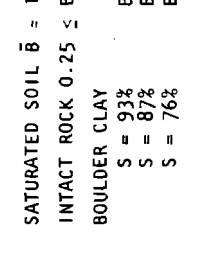
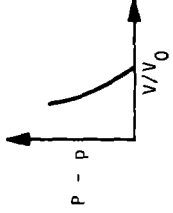
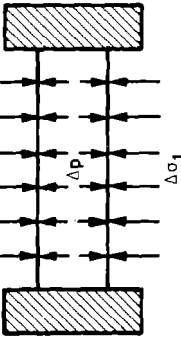
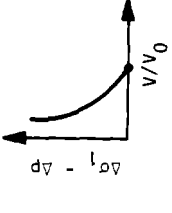
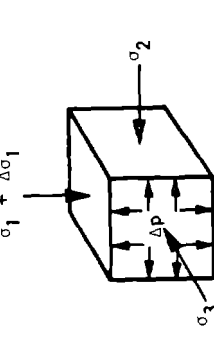
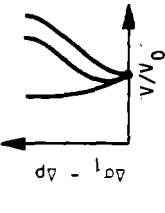
LOAD CONDITIONS	VOLUME CHANGE VS. EFFECTIVE STRESS	PORE PRESSURE PARAMETER	REMARKS
<p>HYDROSTATIC COMPRESSION</p>  <p>$P = \text{PORE PRESSURE}$</p>		$\bar{B} = \Delta p / \Delta P$	<p>SATURATED SOIL $\bar{B} \approx 1$</p> <p>INTACT ROCK $0.25 \leq B \leq 0.55$</p> <p>BOULDER CLAY</p> <p>S = 93% B = 0.69</p> <p>S = 87% B = 0.33</p> <p>S = 76% B = 0.10</p>
<p>ONE-DIMENSIONAL COMPRESSION</p> 		$\bar{C} = \Delta p / \Delta \sigma_1$	<p>SATURATED SOIL $\bar{C} \approx 1$</p> <p>PARTIALLY SATURATED SOIL $0 < \bar{C} < 1$</p>
<p>TRIAXIAL COMPRESSION</p>  <p>$\sigma_2 = \sigma_3$</p>		$\Delta p = \bar{B} \Delta \sigma_3 + \bar{A} (\Delta \sigma_1 - \Delta \sigma_3) $ <p>S = 100%</p> $\bar{A} = \frac{(\Delta p - \Delta \sigma_3)}{(\Delta \sigma_1 - \Delta \sigma_3)}$	<p>S = 100% AT FAILURE</p> <p>VERY LOOSE FINE SAND $\bar{A} = 2 \text{ TO } 3$</p> <p>SENSITIVE CLAY NORMALLY CONSOLIDATED CLAY $\bar{A} = 1.5 \text{ TO } 2.5$</p> <p>LIGHTLY OVERCONSOLIDATED CLAY $\bar{A} = 0.7 \text{ TO } 1.3$</p> <p>HEAVILY OVERCONSOLIDATED CLAY $\bar{A} = 0.3 \text{ TO } 0.7$</p> <p>(Skempton, 1954 and 1961)</p>

Figure 5-21. Pore Pressure Parameters (AA, 1972)

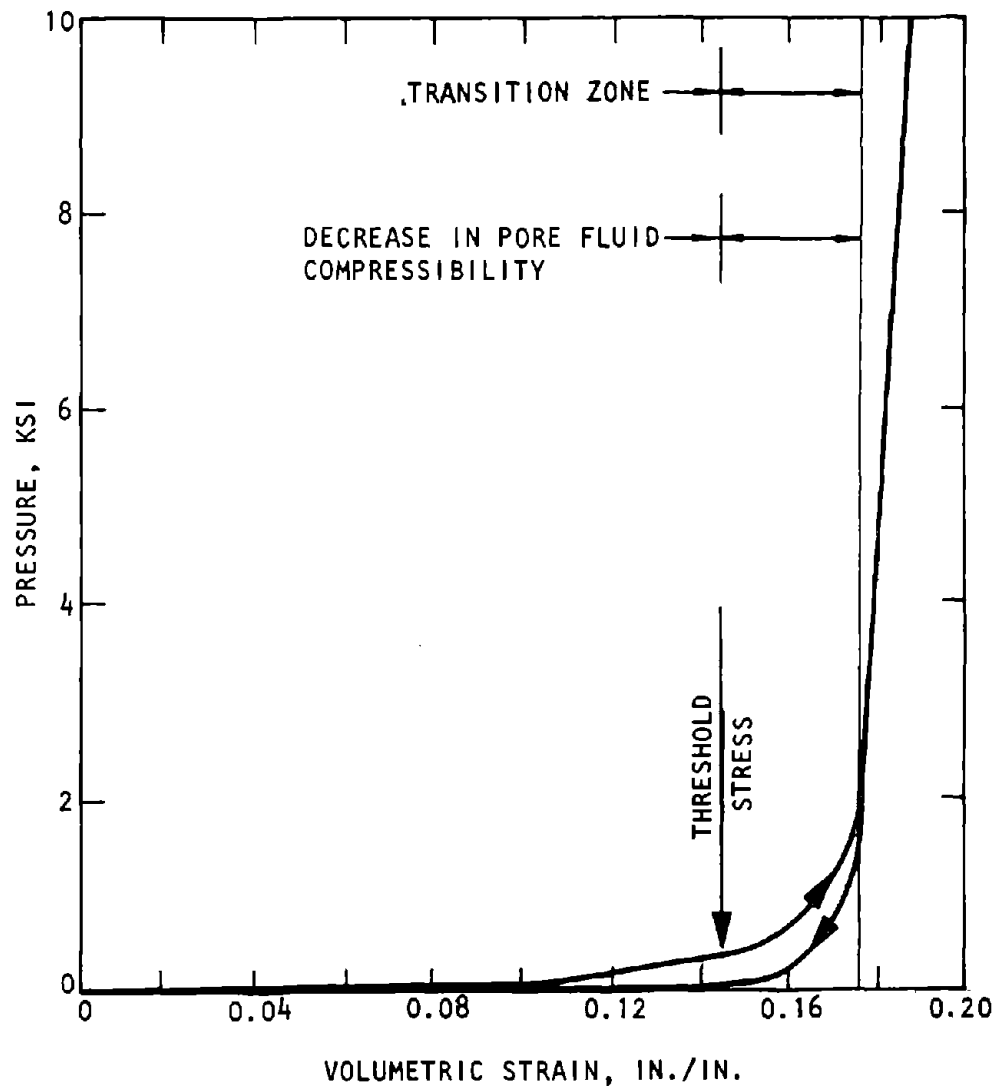
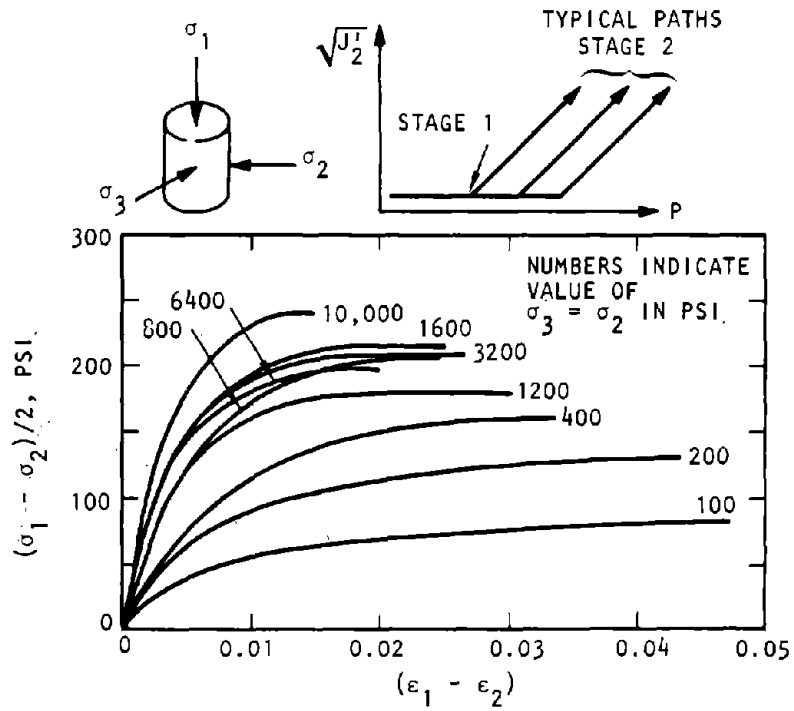
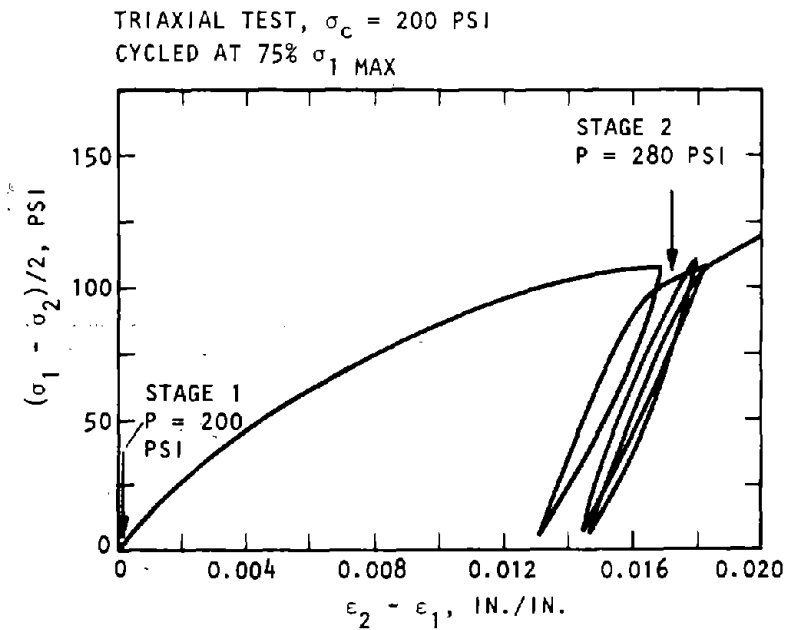


Figure 5-22. Pressure vs Volumetric Strain for Watching Hills Clay Subjected to Hydrostatic Compression (Mazanti-Holland, 1970)



(a) Triaxial compression tests



(b) Cyclic loading in triaxial compression

Figure 5-23. Shear Stress/Strain Relations for McCormick Ranch Sand (Mazanti-Holland, 1970)

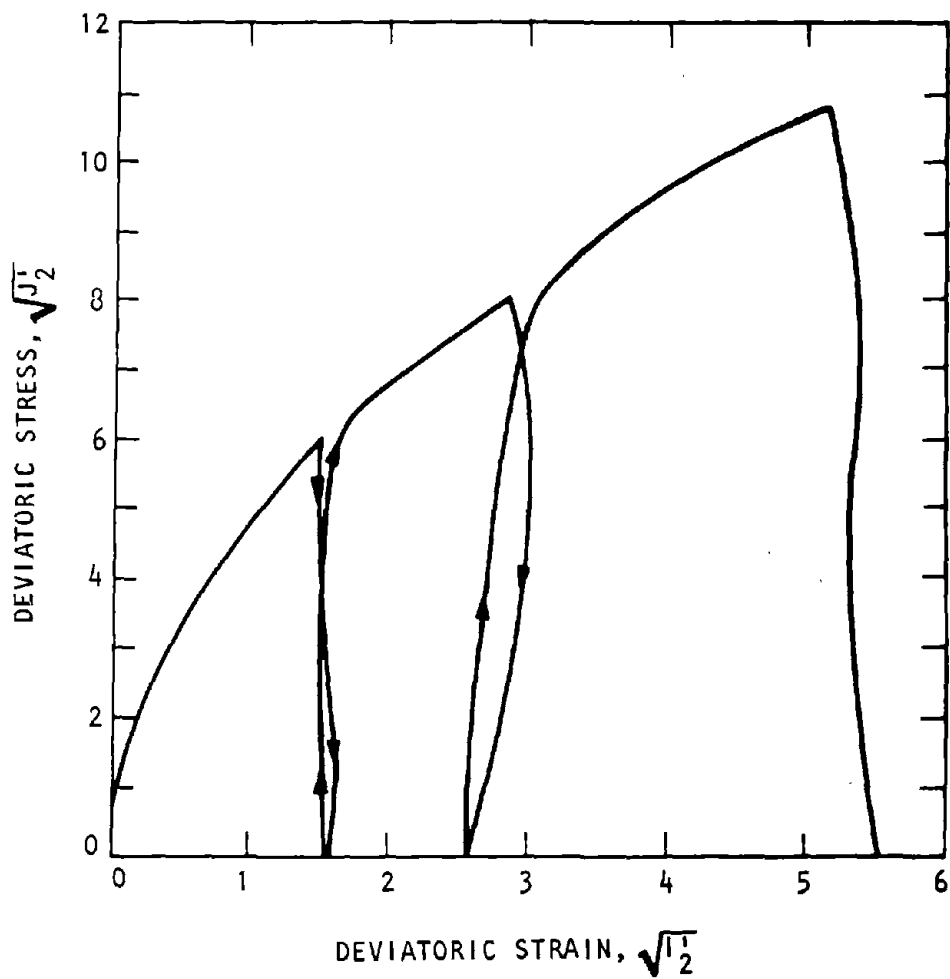
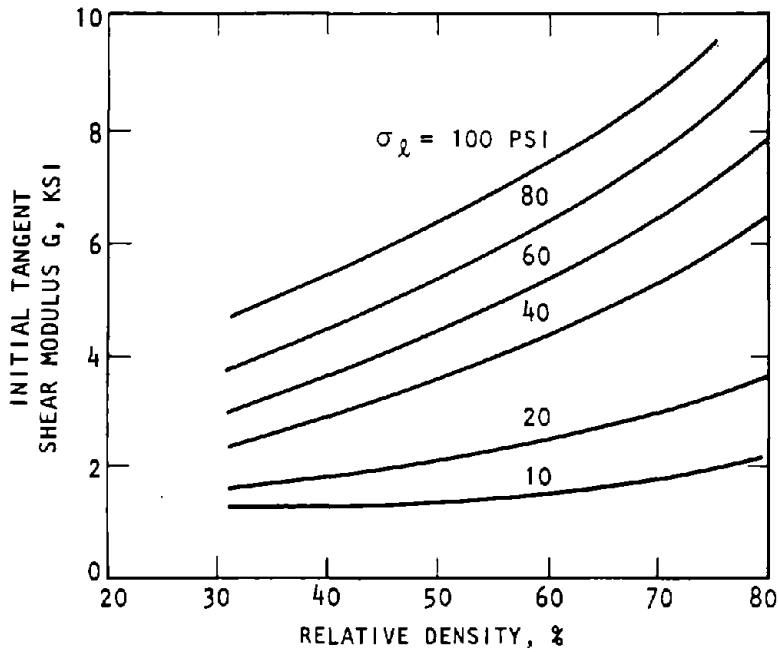
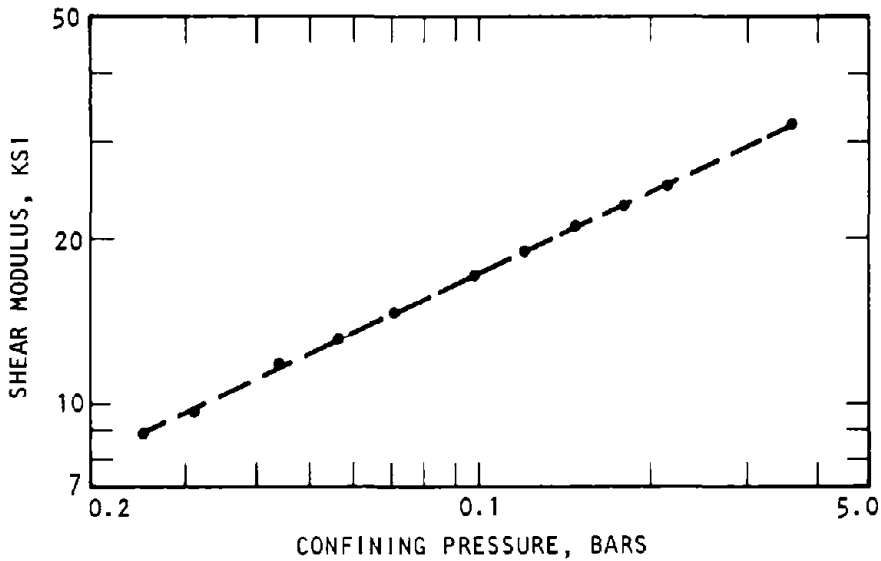


Figure 5-24. Deviatoric Stress/Strain Relations for a Sand in a Test Where the Mean Normal Stress is Constant (AA, 1972)



(a) Initial tangent shear modulus depends on confinement and relative density ("A Study of Bulk and Shear Moduli of a Sand"; L. Domaschuk and N. H. Wade; Proc. ASCE Soil Mech. Div., 95:SM 2, Mr. 1969; copyright 1969 ASCE; reprinted with permission of ASCE)



(b) Initial shear modulus of a dry sand increases with confining pressure ("Instruments and Apparatus for Soil and Rock Mechanics", B. O. Hardin and J. Music, fig. 8, page 68; ASTM-STP-392, 1965; copyright 1965 ASTM; reprinted with permission of ASTM)

Figure 5-25. Shear Modulus of Sand Increasing with Confining Pressure

amount of initial effective confining pressure and with relative density; (3) the maximum shear stress increases with effective confining pressure; (4) after several cycles of unloading and reloading, if the previous maximum shear stress is not exceeded, the unloading/reloading shear stress/strain relations are approximately linear; and (5) the shear modulus is influenced by both the level of shear stress and the mean normal stress.

h. There is an important level of pressure called the "breakdown" stress that affects the shear stress/strain relations and shear strength. At pressures higher than the breakdown stress, the grain is crushed and the shear strength, unaffected by initial void ratio, increases linearly, along with the tangent moduli, with increasing mean normal stress (fig. 5-26).

i. Shear stress/strain relations for fine-grained, partially saturated soils have the characteristics shown in figure 5-27. The influence of the confining stress on the shear modulus and strength is significant until it exceeds the transition zone in the hydrostatic-pressure/volumetric-strain curve. Beyond the transition zone, the influence of the confining pressure is slight. This is because a large portion of the increase in the external hydrostatic stress is taken up by the pore fluid.

j. Dynamic behavior of dry soil is not rate sensitive but loading rate effects especially the pore pressure of saturated soils. For normally consolidated clay soils, rate sensitivity at small strains (<0.5 percent) is related to distortion, whereas at larger strains (>5 percent) related to a volume change. Dynamic triaxial tests on compacted clay indicate that the secant modulus is highly dependent upon the rate of loading. Typical results to 1 percent strain are shown in figure 5-28. When dynamic loading rates on the order of 6 msec to peak are compared to laboratory rates of a few minutes to peak, a factor of two is shown to exist between fast-loading and quasi-static tests.

k. Appropriate laboratory and field tests will be required to determine the required soil stiffness. An appropriate approximation of shear modulus is the secant modulus corresponding to the strains that will be experienced by the soil. Variations of the shear secant modulus as a function of shearing strain are given in figure 5-29 for representative sands and saturated clays.

l. Formulas developed by Richart (1975) for the low strain shear modulus G_o are presented below in figure 5-30. For sands:

$$G_o = \rho V_s^2 \tag{5-16}$$

where

$$V_s = \begin{cases} \text{Shear wave velocity} \\ (170 - 78.2e) (\sigma_o)^{1/4}, \text{ for round-grained} \\ \text{clean sands } (e < 0.80) \\ (159 - 53.5e) (\sigma_o)^{1/4}, \text{ for angular-grained} \\ \text{clean sands} \end{cases}$$

ρ = Mass density of the soil
 σ_o = Average confining pressure
 e = Void ratio
 γ = Shearing strain amplitude

For clays:

$$G_o = 2300 V_s \tag{5-17}$$

where V_s = the undrained shear strength

Alternatively, fit curves to equation 5-17.

$$\frac{\gamma}{\gamma_r} = \frac{\tau}{\tau_m} \left[1 + \alpha \left| \frac{\tau}{c_1 \tau_m} \right|^{R-1} \right] \tag{5-18}$$

where γ is the shearing strain and τ is the shearing stress. Other parameters are given in figure 5-30. Note that τ_m is the maximum shearing stress where the tangent modulus of the stress/strain curve is equal to zero and $\tau_m = \gamma_r G_o$. To obtain shearing strengths, multiply τ_m by a safety factor of 1.50 for static loads and 1.25 for dynamic loads. The secant shear modulus may be obtained by the definition:

$$G = \tau/\gamma \tag{5-19}$$

5-11. Properties of rock

a. The mechanical properties of rock for ground-shock effects include rock stiffnesses, ductility, strength, and postfailure behavior. (Agbabian Associates, 1972). These properties are functions of temperature and interstitial fluid pressure of stress state and magnitude, and loading path and rate. A distinction is made between the mechanical properties of competent rock and rock masses that have weakness planes such as bedding planes, joints, or faults. When properties of the in situ rock mass are defined from properties of competent specimens and from examination of the orientation, spatial distribution, areal extent, and mechanical properties of the weakness planes, categorize the mass: (1) Anisotropic continuum with average or effective mechanical properties (or isotropic and homogeneous in the most idealized case); (2) Discontinuous with different properties for the blocks of competent rock and for the discontinuities (bedding planes, clay seams, joints, or faults) separating the blocks.

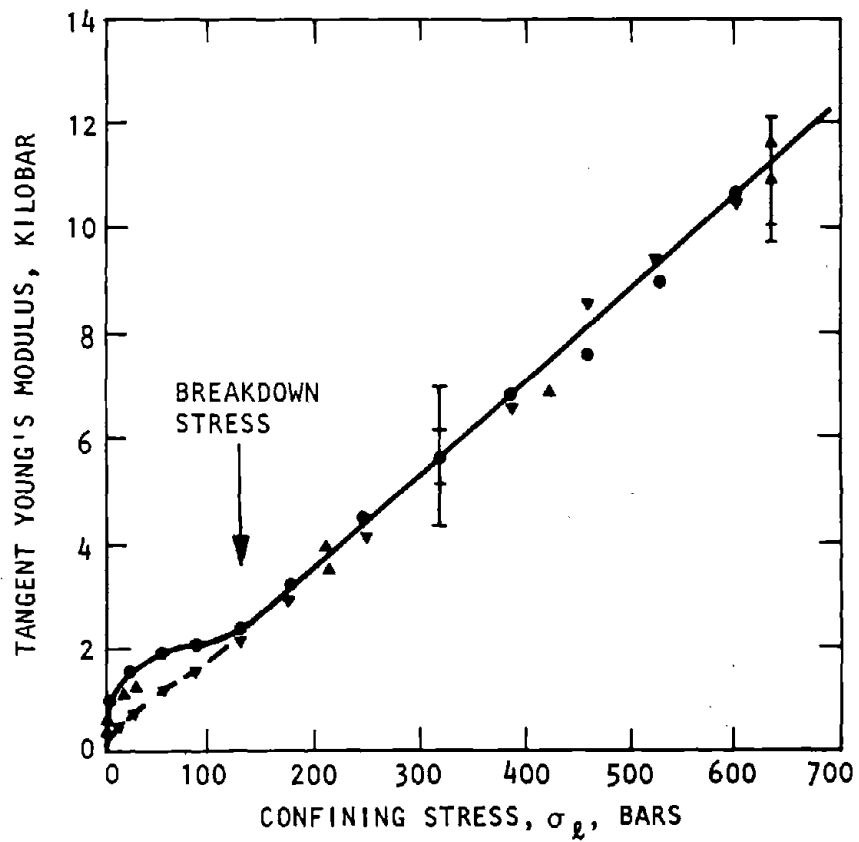
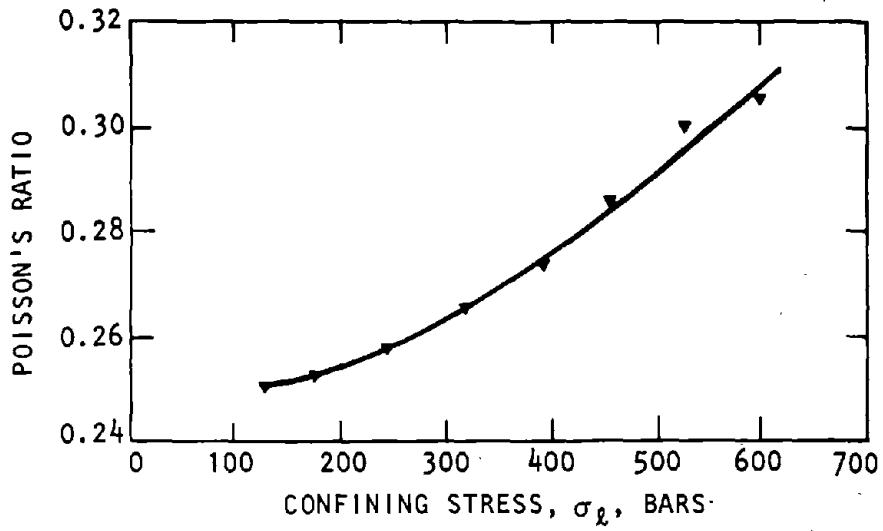


Figure 5-26. Breakdown Stress Associated with an Increase in Poisson's Ratio and a Linear Relation between Stiffness and Confining Stress (AA, 1972)

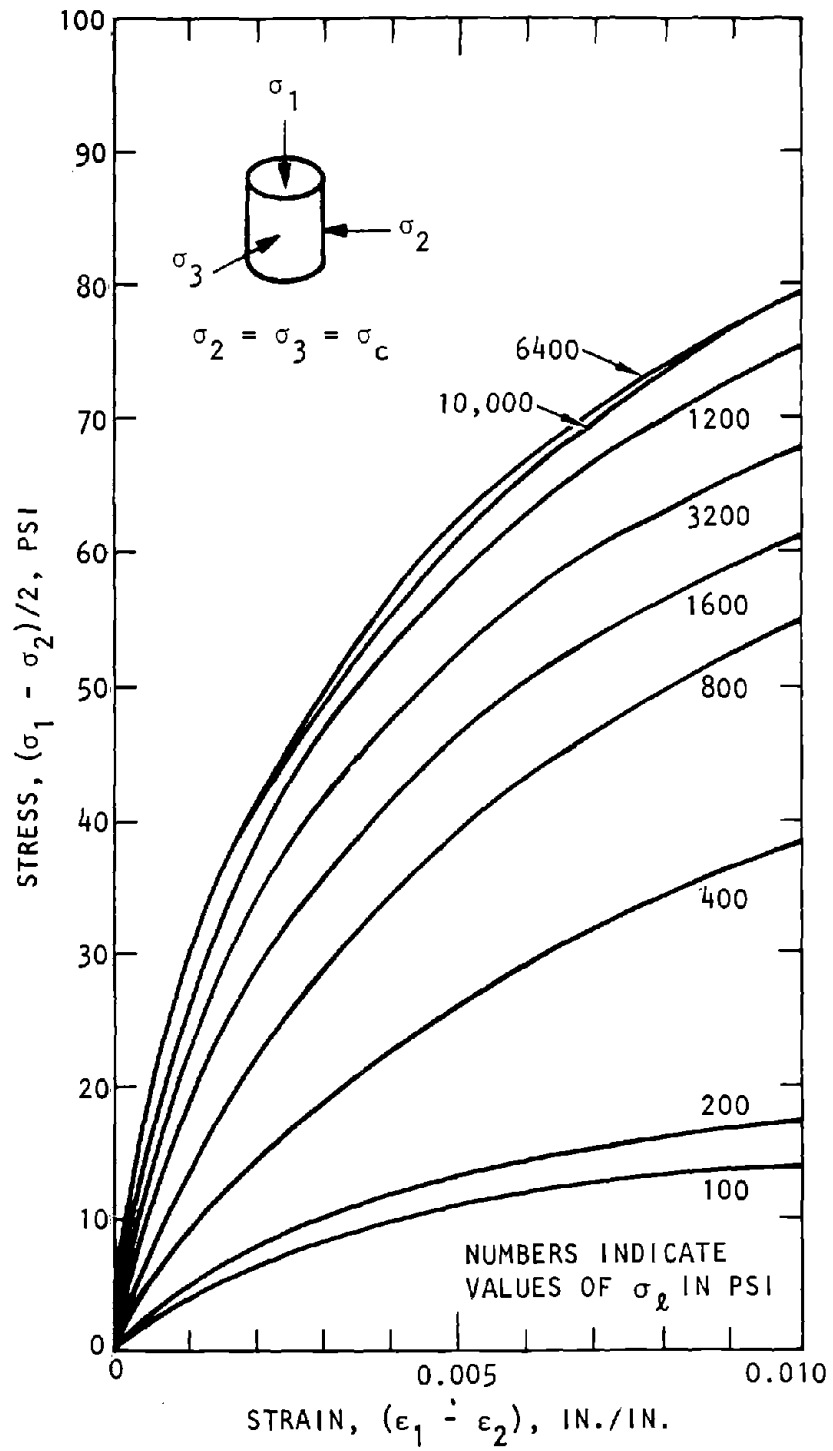


Figure 5-27. Shear Stress/Strain Relations for Watching Hill Clay (Mazanti-Holland, 1970)

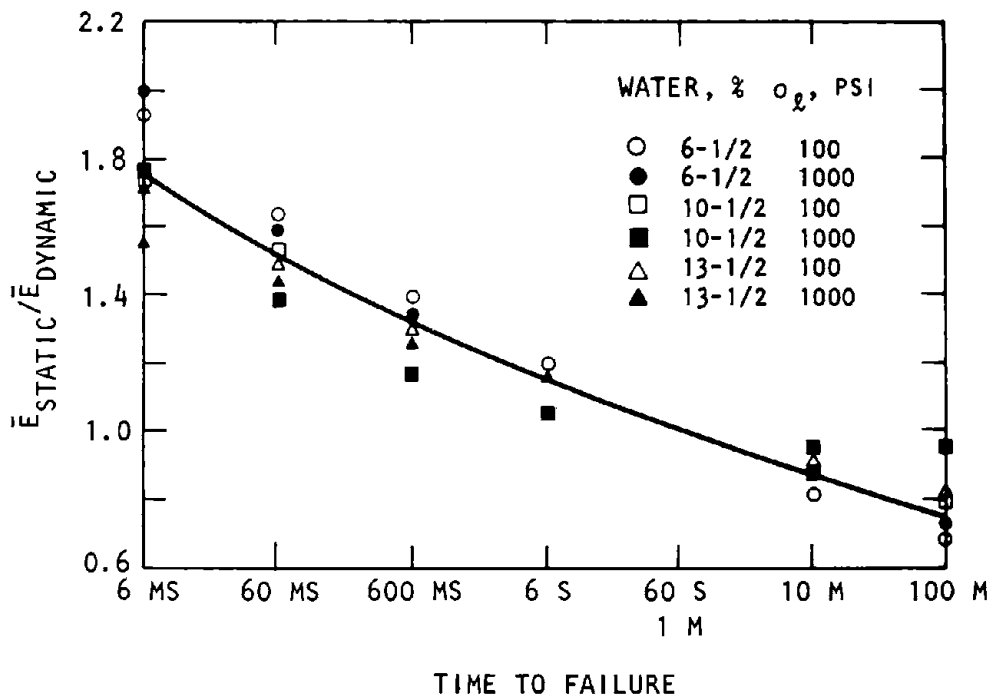
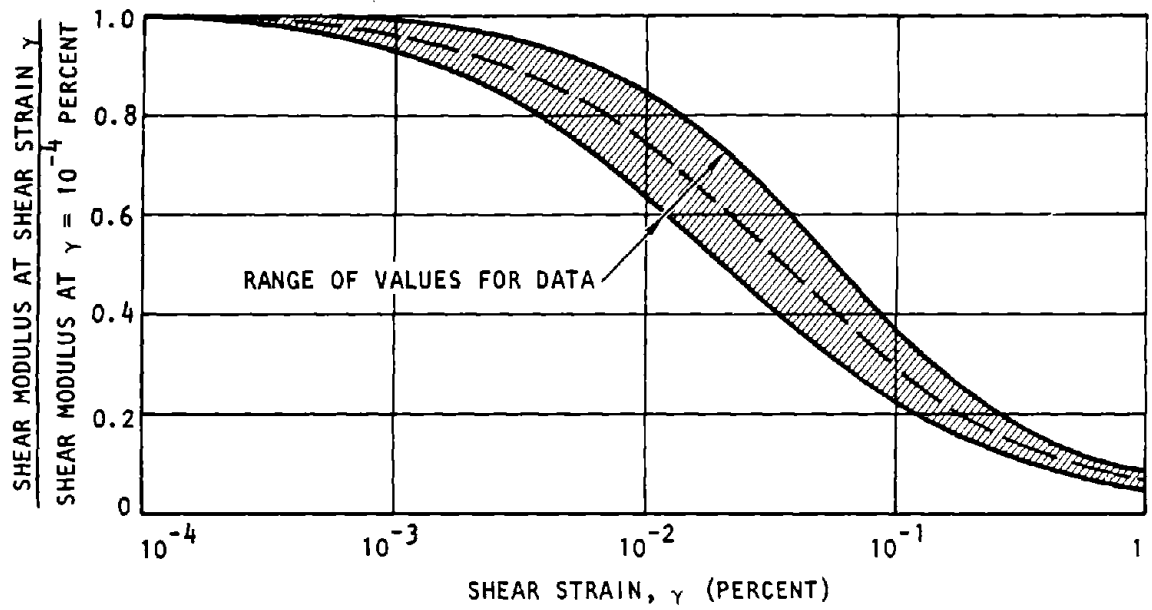
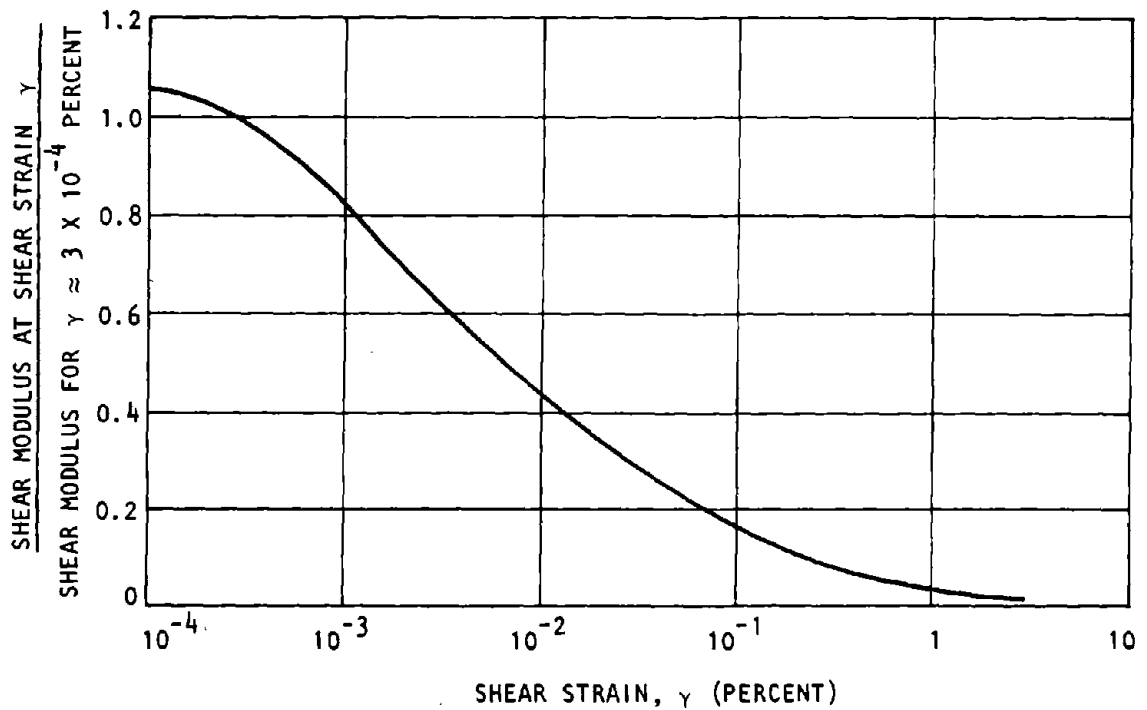


Figure 5-28. Influence of Time to Failure on the Normalized Secant Moduli at an Axial Strain of 1 percent (Olson-Parola, 1967)



(a) For sands



(b) For saturated clays

Figure 5-29. Variations of the Shear Secant Modulus as a Function of Shearing Strain (Seed-Idriss, 1970)

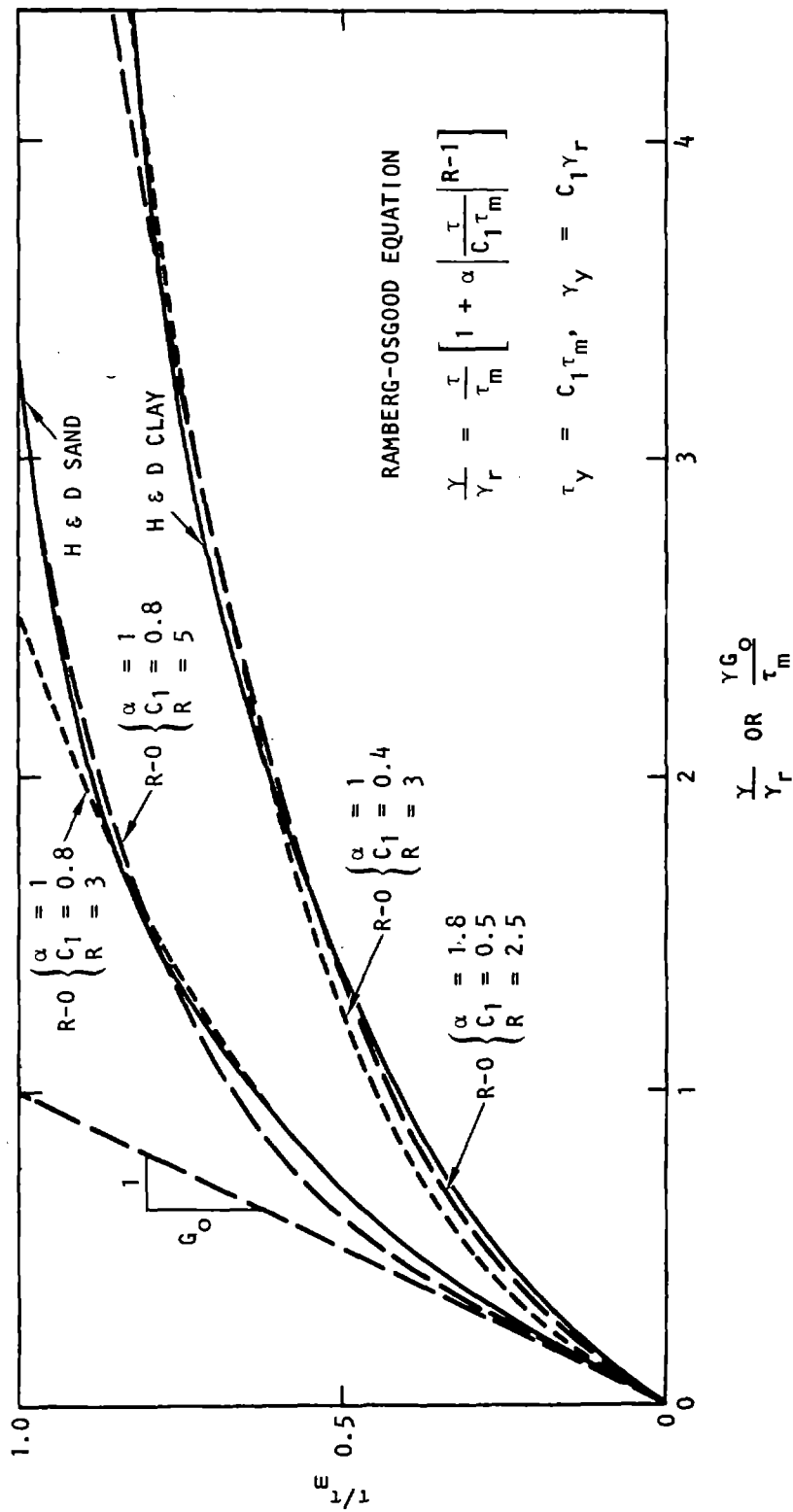


Figure 5-30. Fit of Ramberg-Osgood Curves to Soil Data (Richart, 1975)

b. Stiffness is defined as the effective bulk and shear moduli and is determined from experimental data. Bulk modulus is usually obtained from plots of mean stress vs. mean strain or volumetric strain; shear modulus is obtained from plots of maximum shear stress, $1/2(\sigma_1 - \sigma_3)$, vs. maximum shear strain, $\epsilon_1 - \epsilon_3$.

c. Figures 5-31, 5-32, and 5-33 show typical data for sandstone and granite. Generally, the stress/strain behavior is highly non-linear and the rock properties are very site dependent. The increase in rock stiffness as hydrostatic pressure increases depends upon the initial porosity of the rock. With increasing hydrostatic pressure, weakly consolidated and altered rock will show a very rapid increase in stiffness as preexisting cracks close and pores collapse.

d. The shear stress/strain behavior of rock depends on mean stress. Rapid changes of the effective shear moduli (proportional to the slopes of the curves $1/2(\sigma_1 - \sigma_3)$ vs. $(\epsilon_1 - \epsilon_3)$) both at low and high shear stress are typical of weakly consolidated and altered rock types.

e. General data defining the relationship between stress/strain behavior, loading history, loading path, and strain rate are sparse. At high stress levels, loading history is important because of deformation-induced anisotropy. Rock properties thus become directionally dependent. Loading history also determines the stress/strain behavior of rock during unloading. Stress path appears to have little influence on rock behavior in triaxial compression ($\sigma_1 > \sigma_2 = \sigma_3$) but may be significant in multiaxial compression ($\sigma_1 \neq \sigma_2 = \sigma_3$). Measurements on granite at strain rates up to 100 in./in./sec and up to 1 kbar of hydrostatic pressure indicate that the effective moduli and the strains at fracture increase by no more than approximately 10 to 20 percent compared with quasi-statically determined values.

f. Yield strength is commonly defined as the stress or stress difference at which plots of σ_1 or $\sigma_1 - \sigma_3$ vs. ϵ_1 depart significantly from linearity (fig. 5-34). Sometimes yielding is defined as the stress that produces a predetermined amount of strain, say 2 to 5 percent. This definition of yield strength is ambiguous unless it is normalized, for example, with respect to an elastic modulus of the rock. Similar difficulties arise in defining ductility. The term is almost always used in a qualitative sense to indicate the strain prior to failure.

g. Figure 5-35 shows "ductility" data for a variety of rock types. Yield strength and ductility generally increase rapidly with increasing hydrostatic pressure. Above a certain threshold value of hydrostatic confinement, the yield stress of some rocks appears to depend much less on confinement. From what is now known, however, such behavior is more an exception than a rule. Experimental evidence

indicates that ductility is substantially lowered with increasing magnitude of the intermediate principal stress. Both yield stress and rock ductility depend strongly on temperature and strain rate; yield stress decreases and ductility increases at elevated temperature and/or at low strain rate.

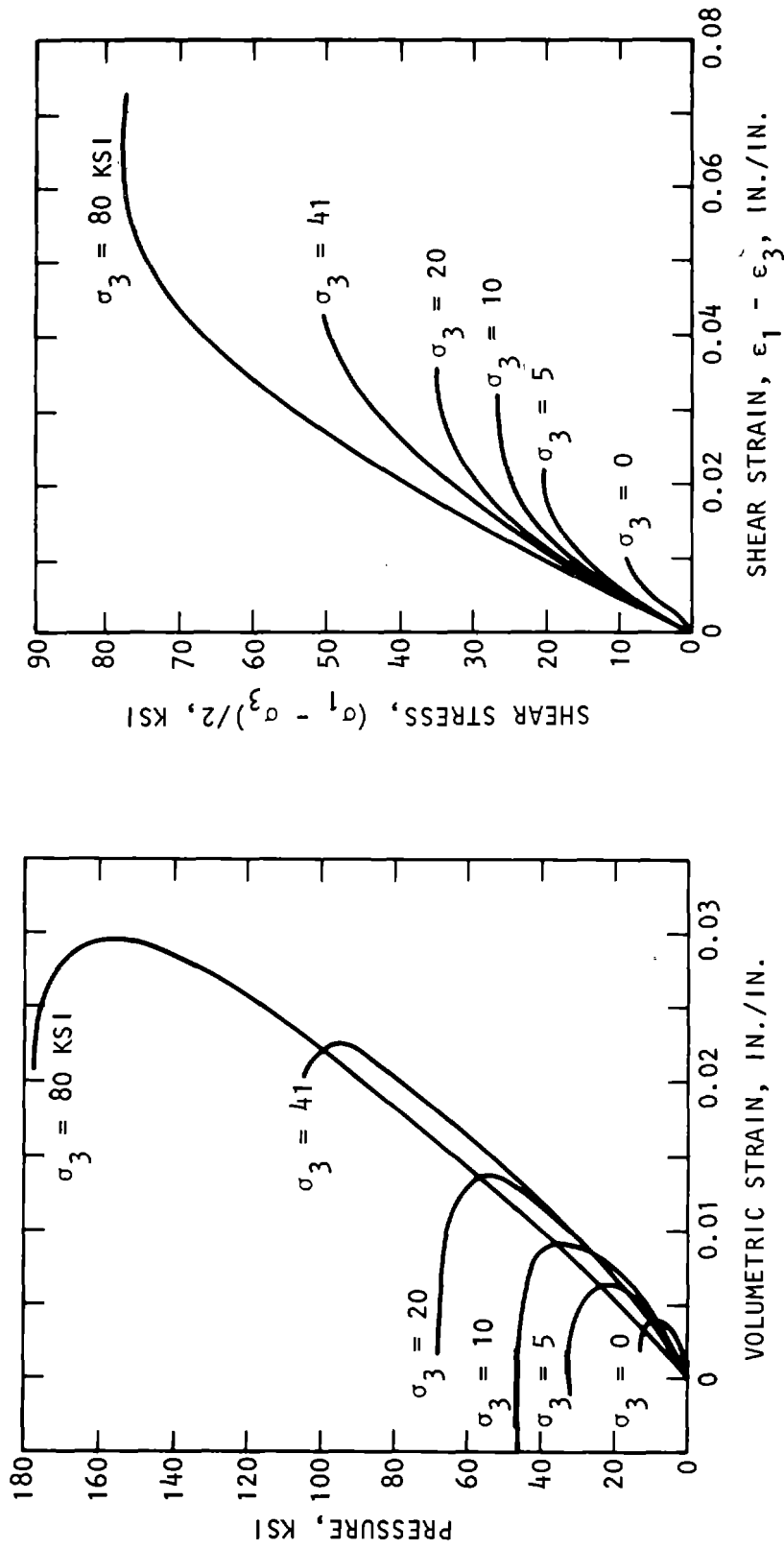
h. Ultimate strength is defined as the maximum stress difference or deviatoric stress that rock can sustain. Ultimate strengths of several types of rocks are shown in figure 5-36. The strength of rock increases rapidly with increasing hydrostatic pressure. The actual relationship between strength and confining pressure is generally not the same as the relationship between yield stress and pressure. Strength also depends on the intermediate principal stress, as shown in figure 5-37. If strength is expressed only as a function of the hydrostatic component of stress, neglecting the influence of the intermediate principal stress, then the predicted strength will always be less than the actual strength. However, high intermediate principal stresses, if they exist, should be considered because they change rock behavior by making it more brittle; an increase in strength is accompanied by a decrease in ductility.

i. The influence of stress path on the strength of isotropic rock is generally negligible. Strain rates produce a relatively small increase in the strength of dry rocks. Interstitial fluid pressure and temperature can be important.

j. Mechanical properties of failure planes must be known to predict postfailure behavior. The relationship between shear stress and displacement, as well as the variation of shear strength of joints with relative displacement of joint surfaces, depends on joint geometry. Figure 5-38 shows a typical set of records of shear stress vs. displacement parallel to the joint surfaces. Once the initial shear stress has been reached, the strength of joints varies in one of five ways (most common are (2) and (3) below):

- (1) The shear strength remains constant.
- (2) The shear strength decreases monotonically to the residual shear strength. In this case, the initial shear strength equals the maximum shear strength.
- (3) The shear strength increases to "maximum shear strength" and then decreases to the residual shear strength.
- (4) The shear strength drops to a local "minimum shear strength," increases again, and subsequently drops to the residual shear strength.
- (5) The shear strength increases, approaching the residual shear strength asymptotically. In this case the maximum shear strength equals the residual shear strength.

k. Figure 5-39 shows schematic plots that define the maximum shear strength τ_m as a function of normal stress (σ_n), joint roughness, and joint grouting for joints in a particular rock type. Intact rock is also



(a) Pressure/volumetric-strain relation (b) Shear stress/strain relation

Figure 5-31. Stress/Strain Relation for Nugget Sandstone (Swanson, 1969)

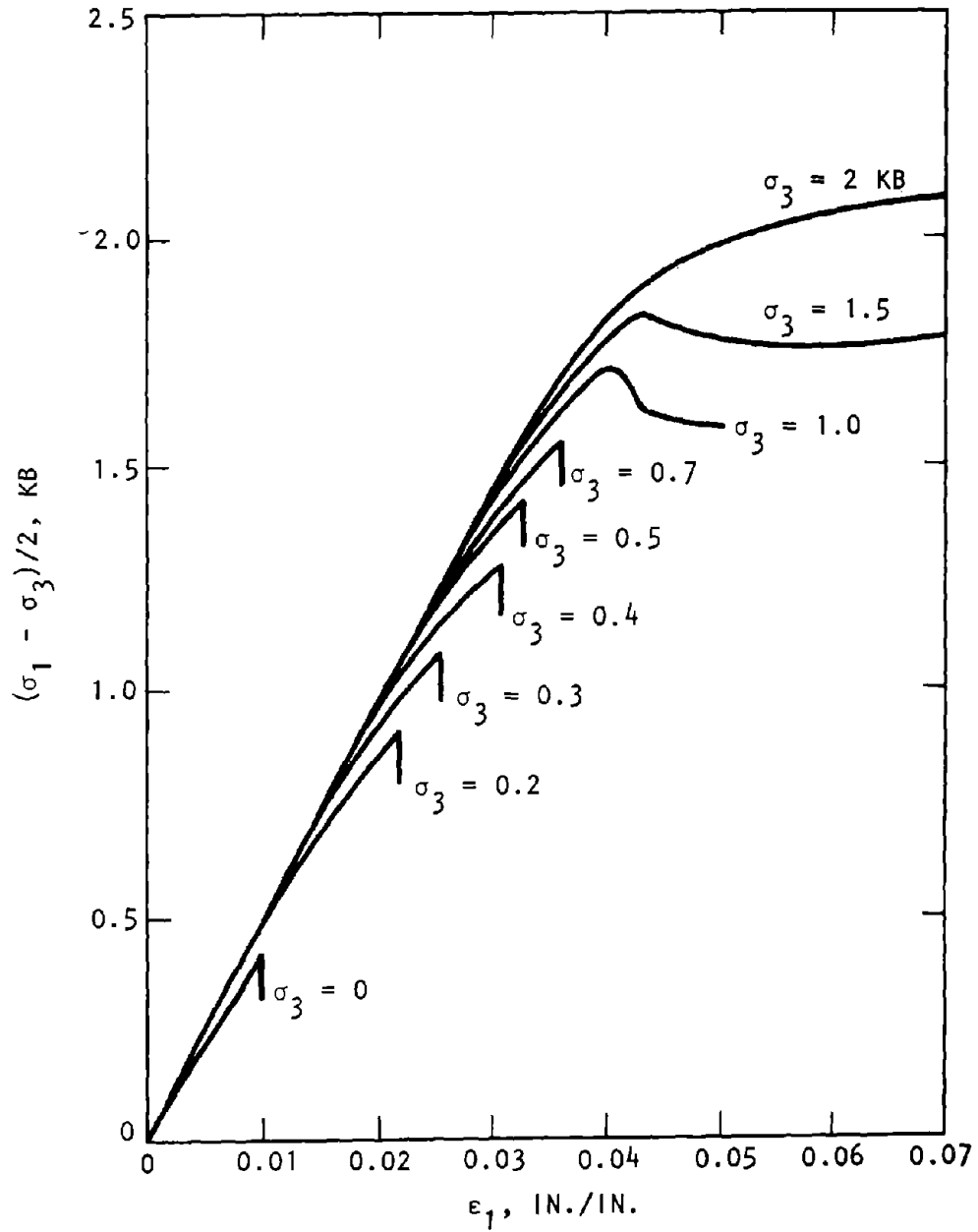
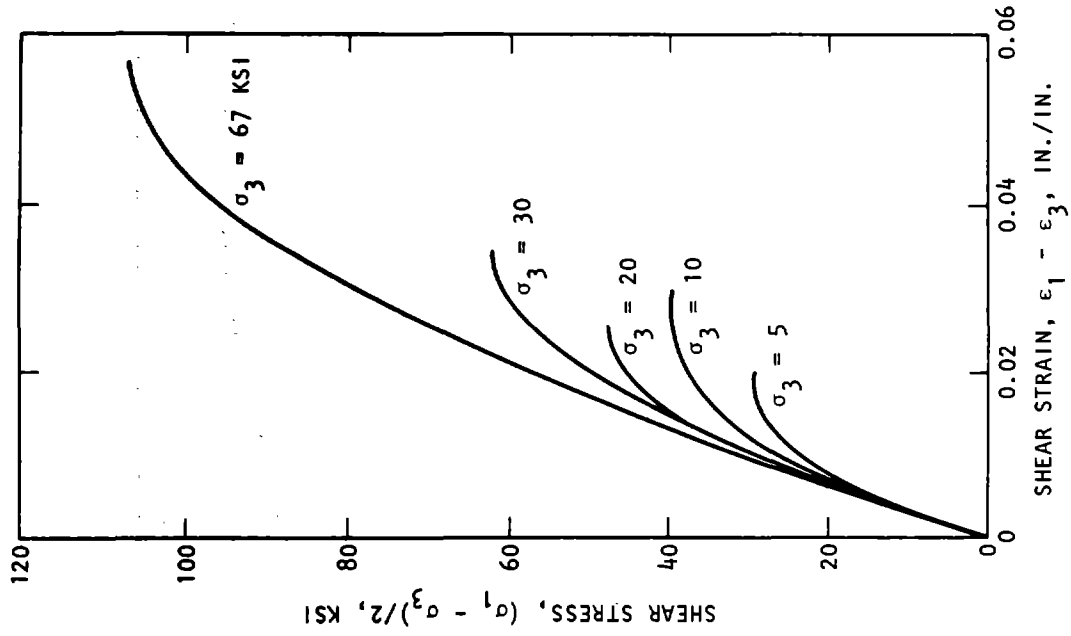
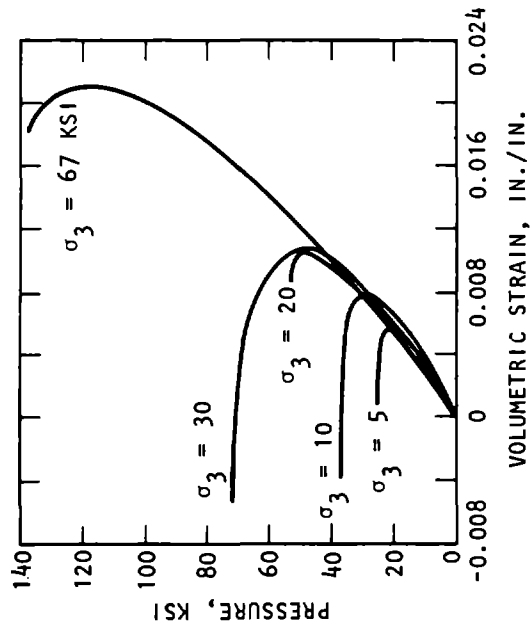


Figure 5-32. Shear Stress/Axial Strain Relations for Coconino Sandstone (Swolfs, 1971)

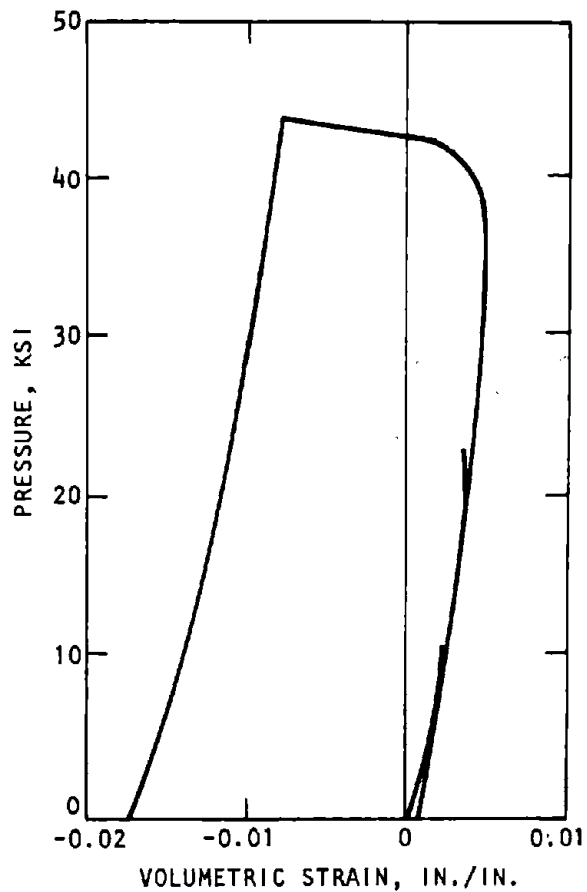


(b) Shear stress/strain relation

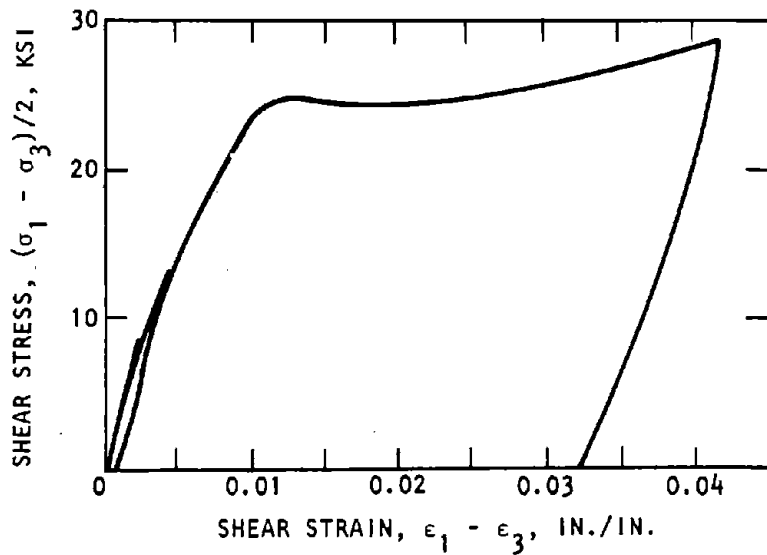


(a) Pressure/volumetric-strain relation

Figure 5-33. Stress/Strain Relation for Cedar City Granite (Swanson, 1969)



(a) Pressure/volumetric-strain relation



(b) Shear stress/strain relation

Figure 5-34. Stress/Strain Relation for Marble Subjected to Proportional Loading ($\sigma_3/\sigma_1 = 0.338$) (Swanson, 1969)

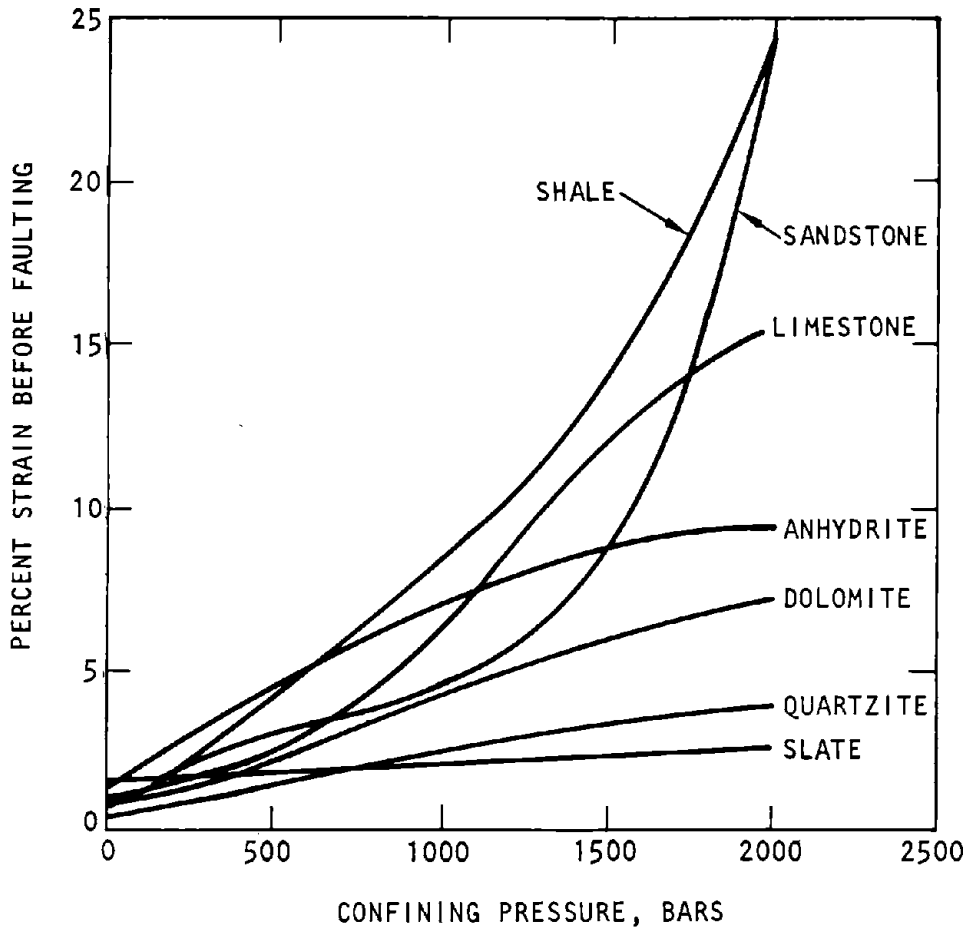


Figure 5-35. Ductility of Several Common Rocks Varying with Confining Pressure (Donath, 1970)

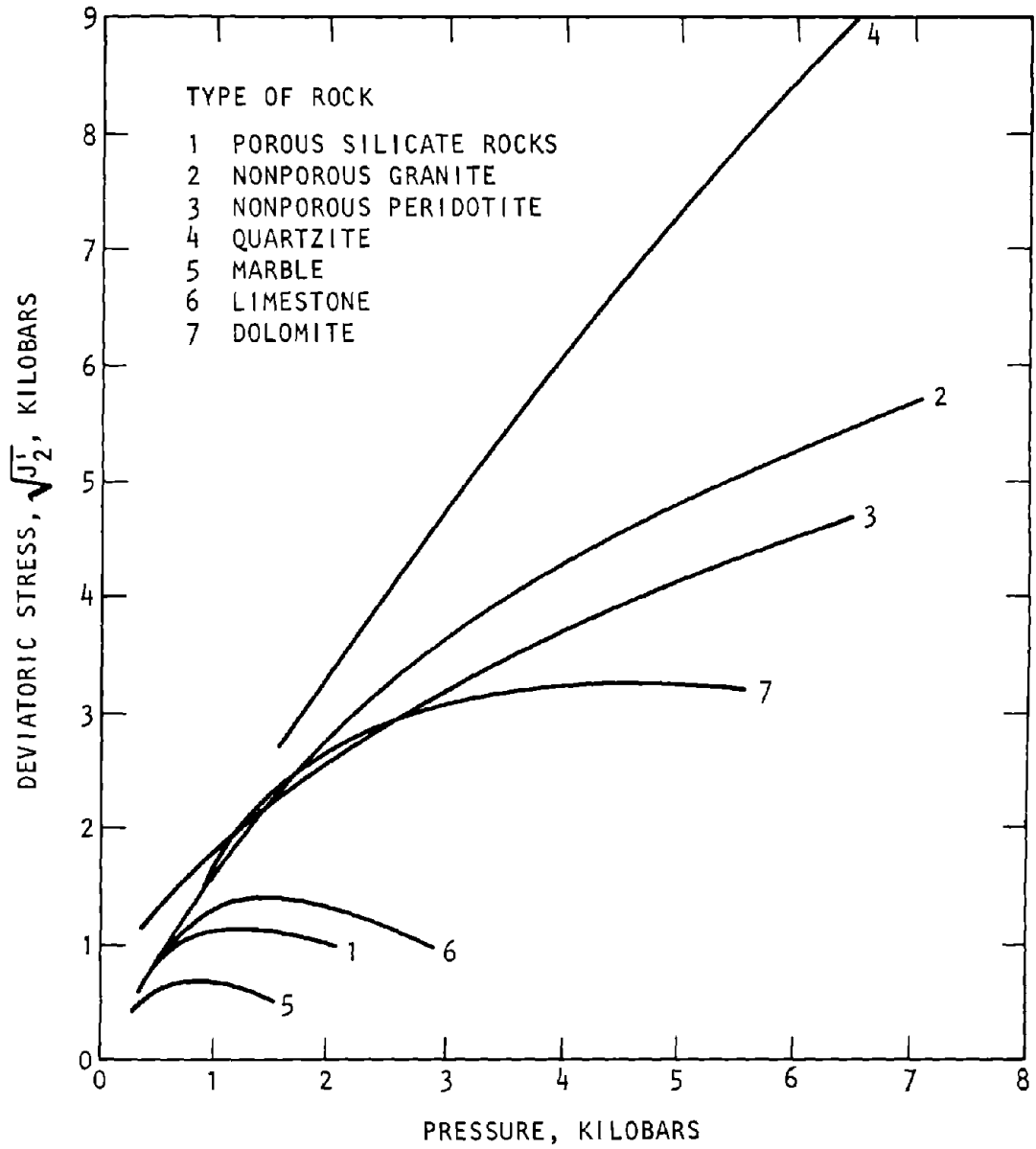


Figure 5-36. Average Strength-Pressure Curves of Different Rock Types (Mogi, 1966)

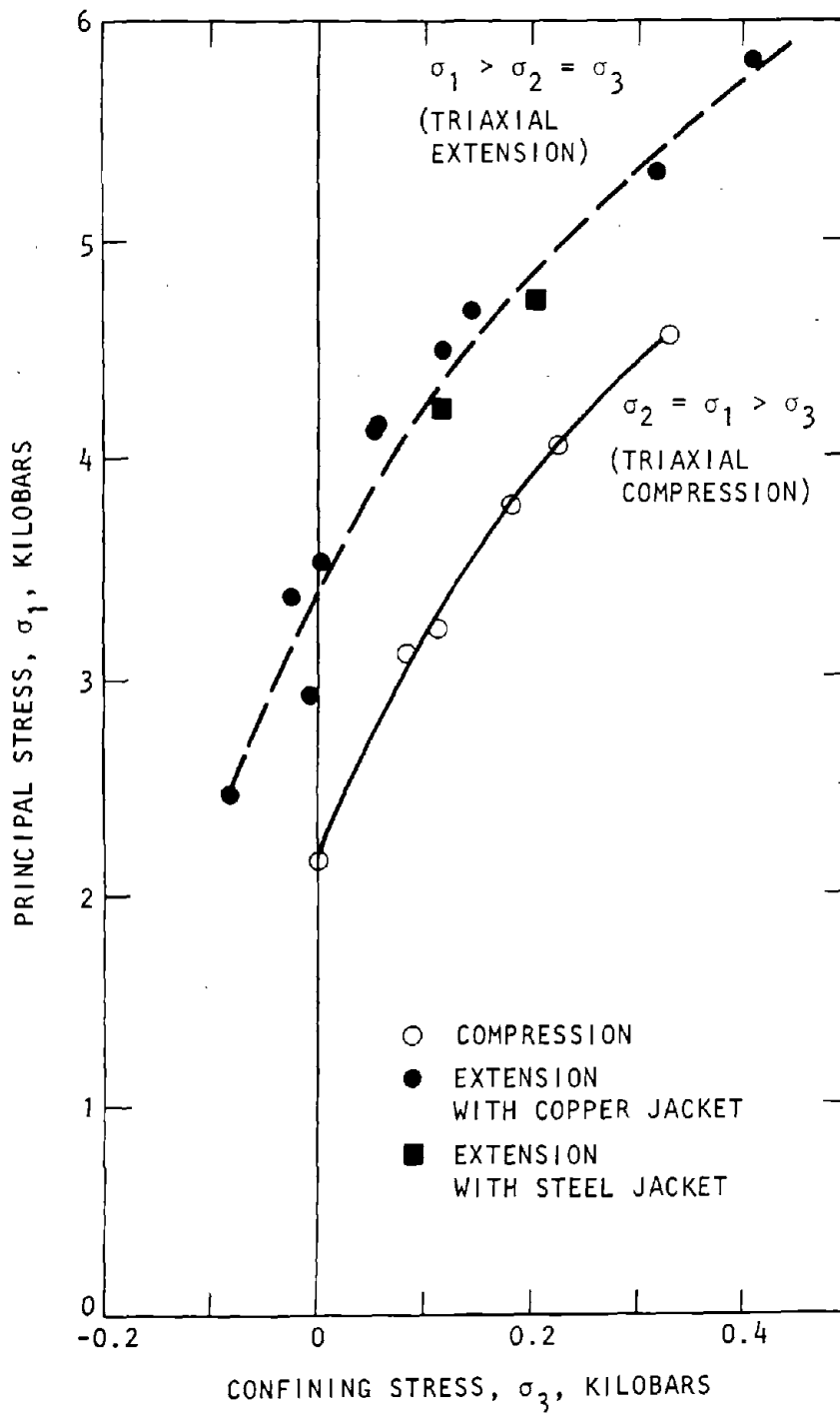
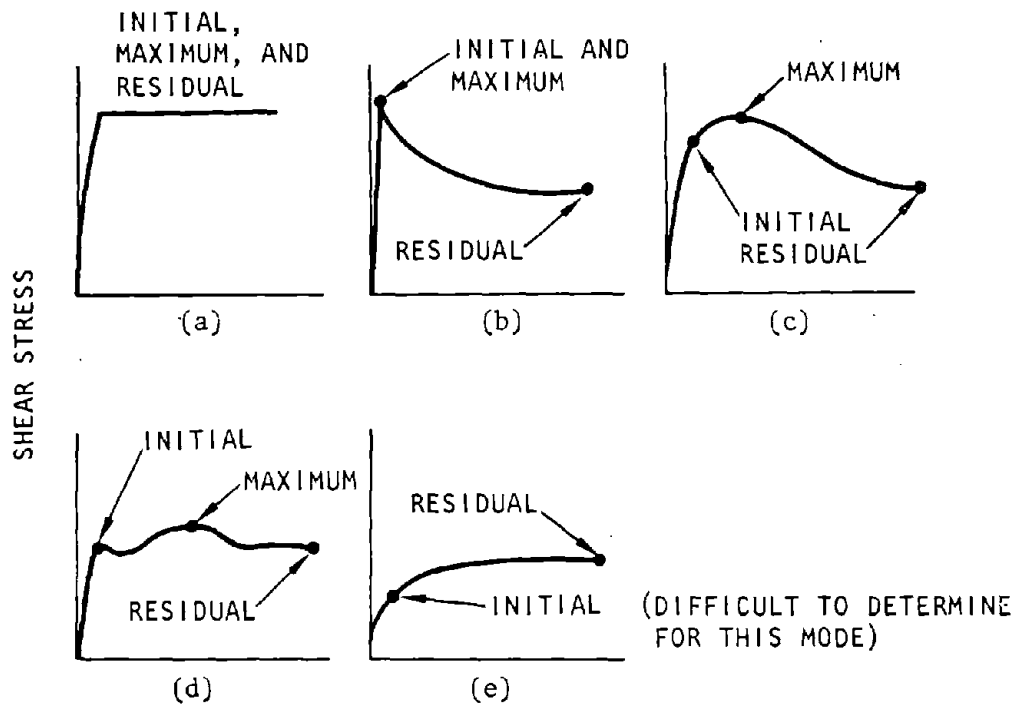


Figure 5-37. Strength of Dunham Dolomite Under Triaxial Compression and Triaxial Extension Stress States (Mogi, 1967)



DISPLACEMENT ALONG JOINT IN DIRECTION OF SHEAR STRESS

NOTE: INITIAL STRENGTH DETERMINED BY
POINT OF MAXIMUM CURVATURE

Figure 5-38. Five Typical Modes of Joint Strength and Displacement (Coulson, 1970; Wallace et al., 1970; Jaeger-Cook, 1971)

shown. The variation of shear strength of joints is generally related to the magnitude of the frictional resistance that can be mobilized.

$$\tau_m = C_j + C_f \sigma_n = C_j + \sigma_n (\tan \phi) \quad (5-20)$$

where

- C_j = Joint cohesion at zero normal stress
- C_f = Coefficient of friction
- ϕ = Friction angle

For most rock, C_f varies in the narrow range between 0.4 to 0.7, and ϕ between 22 deg and 35 deg. The influence of interstitial water pressure is taken into account by subtracting the pore pressure from C_j and σ_n .

5-12. Stress/strain models

a. Experimental data are used to develop analytical models of materials for use in design or analysis of the response of protective structures and their surrounding geological medium. The designer/analyst has freedom to adapt such material property models to the special requirements of the structure/medium systems. The mathematical models described below are complex exemplaries of structural and geologic materials used for design verification.

b. The stress/strain behavior for structural steel is generally assumed to be linearly elastic and perfectly plastic, and is identical for both tension and compression. Initial loading, unloading and reloading follow a path whose slope is the same, as shown in figure 5-40, a diagram applicable for either structural steel or reinforcing steel.

c. A reinforced-concrete model may be obtained by combining the separate properties of the plain concrete and the steel. The model is orthotropic, homogeneous, and possesses the main characteristics of both materials.

d. Plain concrete is represented by a variable modulus model in which the elastic moduli in orthogonal directions under virgin compressive loading are assumed to be functions of both the strain and the confinement (AA, 1975a). The functional relationships of the two elastic moduli for a biaxially stressed element, originally suggested by Liu et al. (1972), are given by:

$$E_c^i = \frac{E_c \left[1 - \left(\frac{\epsilon_i}{\epsilon_m} \right)^2 \right]}{\left[1 + \left(\frac{1}{1 - \nu \beta_i} \frac{E_c \epsilon_m}{\sigma_m} - 2 \right) \left(\frac{\epsilon_i}{\epsilon_m} \right) + \left(\frac{\epsilon_i}{\epsilon_m} \right)^2 \right]^2}$$

$$G_{ij} = \frac{E_c^i E_c^j}{(1 + \nu) (E_c^i + E_c^j)} \quad (5-21)$$

in which

- E_c^i, E_c^j = Tangent moduli in two orthotropic directions
- G_{ij} = Shear modulus between the two orthogonal directions
- E_c = Initial tangent modulus of concrete, constant for all directions (tangent modulus corresponding to zero strain)
- ϵ_i = Strain in the direction considered
- σ_m = Peak stress in biaxial compressive loading
- ϵ_m = Strain corresponding to the peak stress
- ν = Poisson's ratio for concrete, assumed to be a constant
- $\beta_i = \frac{\sigma_i}{\sigma_1}$ = Ratio of principal stress in orthogonal direction to principal stress in direction considered

The directions of orthotropy are assumed to coincide with the principal directions of stresses until tensile cracking occurs, after which they remain permanently rigid. Unloading and reloading in compression assume a constant modulus equal to the initial modulus E_c . The complete loading, unloading, and reloading characteristics of the plain concrete are shown in figure 5-41. In tension, a constant E_c is assumed in all cases until cracking occurs (fig. 5-42). Then the concrete modulus is set to zero until rebonding. After rebonding, the postrebonding modulus is set to a value lower than E_c , usually selected as $0.5 E_c$.

e. The cracking strength of concrete f_{cr} , where $\sigma_z \leq f_{cr}$ in the direction of σ_z , is assumed to be

$$f_{cr} = f_c - \eta \sigma_x \quad (5-22)$$

for $\sigma_x < \sigma_y$ and $\sigma_x \leq 0$; σ_x and σ_y are the confinement stress components in which

- f_c = Unconfined tensile strength of concrete
- η = Slope of cracking envelope = f_c/f'_c in which f'_c is the unconfined compressive strength of concrete
- σ_x = Minimum nonpositive stress normal to σ_z

The stress/strain behavior of concrete in tension is depicted in figure 5-42.

f. The main properties of the reinforcing steel treated in the composite model are the area of the steel (percentage of steel area) and its stress/strain behavior. Both of these properties are prescribed in directions parallel to the axes of the steel bars. These areas are then transformed to the principal directions of orthotropy, where they are incorporated with the tangent moduli of the steel to form the composite moduli. The stress/strain behavior of the steel is

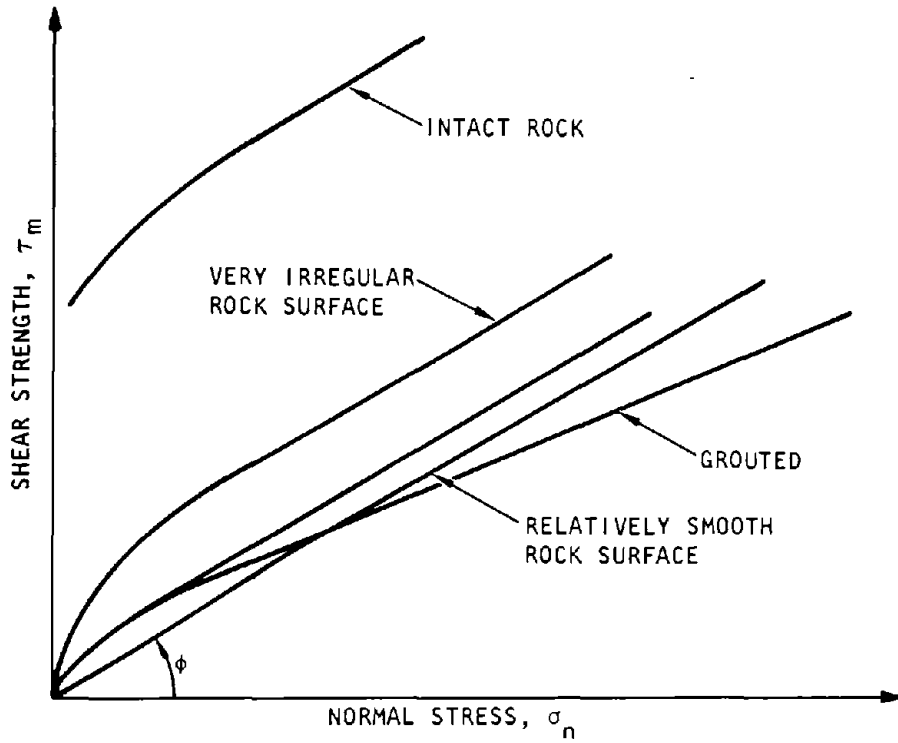
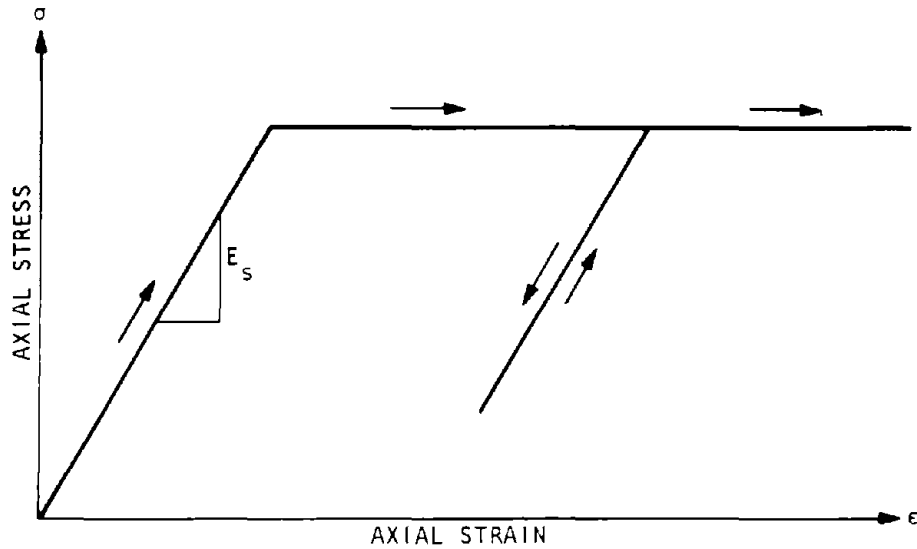
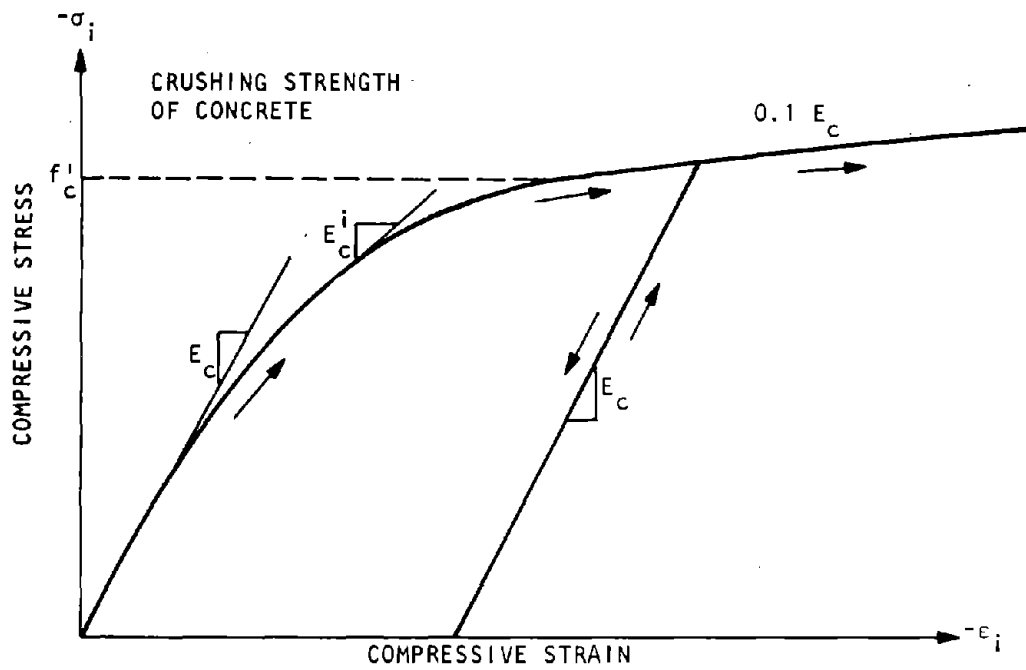


Figure 5-39. Failure Envelopes Expected to Rock Masses (Coulson, 1970; Deere et al, 1967)



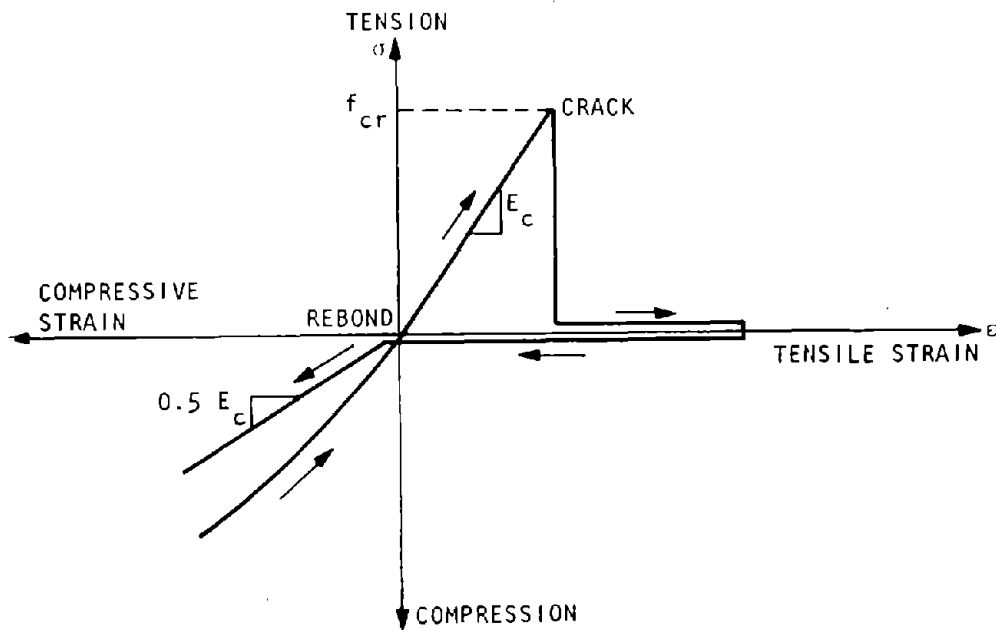
U.S. Army Corps of Engineers

Figure 5-40. Stress/Strain Behavior for Steel



U.S. Army Corps of Engineers

Figure 5-41. Virgin Loading and Unloading/Reloading Behavior of Concrete Model in Compression



U.S. Army Corps of Engineers

Figure 5-42. Behavior of Concrete Model Under Cracking and Rebonding

assumed to be linearly elastic and perfectly plastic and is identical for both tension and compression (fig. 5-41).

g. Based on the transformed percentage of steel areas in the three principal directions of orthotropy, the effective modulus E_r of the uncracked composite material for each direction is given by the weighted mean between steel and concrete moduli, using respective steel-area percentages as weighting factors in each orthotropic direction:

$$E_r = E_c a_c + E_s a_s \quad (5-23)$$

where

E_c = Elastic modulus of plain concrete (eq. 5-21)

E_s = Elastic modulus of steel

a_s = Projected fraction of steel area in the direction considered

$a_c = 1 - A_s =$ Fraction of concrete area

After the occurrence of cracking, one or all of the directions of orthotropy are fixed. The effective modulus using projected areas for that direction is then given by

$$E_r = \frac{(E_c a_c + E_s a_s) E_s a_s}{E_s a_s + (1 - \lambda) E_c a_c} \quad (5-24)$$

in which λ is a bond-slip parameter that is based on experimental data. This parameter may be defined approximately by

$$\lambda = 1 - \frac{10X}{3} \quad \text{for } X \leq 0.15$$

$$= \frac{10(1 - X)}{17} \quad \text{for } 0.15 < X \leq 1.0$$

where X is the ratio of tensile stress to yield stress. The onset of cracking is determined when the stress carried by concrete, σ_c , has exceeded its tensile strength, that is, whenever $\sigma_c > f_{cr}$ where σ_c is calculated by

$$\sigma_c = \frac{E_c \sigma_r}{E_c a_c + E_s a_s} \quad (5-25)$$

in which σ_r is the effective average principal stress computed for the element of interest and f_{cr} is given by equation 5-22.

h. After cracking and before the occurrence of "rebonding," concrete is assumed to lose all its strength in the cracked direction and the stress in the reinforcement is not allowed to exceed the yield stress of steel. The effective modulus of the composite

material during loading, unloading, or reloading is given by

$$E_r = E_s a_s \quad (5-26)$$

In the absence of reinforcement ($a_s = 0$) the effective modulus is set equal to a nominal minimal value to avoid numerical difficulties.

i. Rebonding occurs when, during unloading, the strain becomes negative (i.e., compressive). The composite modulus is composed of a weighted average (according to the percentage of steel area) of the steel modulus and a fraction of the virgin-concrete modulus. Thus

$$E_r = n E_c a_c + E_s a_s \quad (5-27)$$

where n may be taken to be approximately 0.5 in the absence of experimental data.

j. Models that represent soil layers may assume a hysteretic, piecewise linear stress/strain behavior and a Mohr-Coulomb-type failure envelope as shown in figure 5-43. These models must be curve-fitted to experimental data of a given site. Empirical constants as well as measurable material properties are required to develop such models. Definitions of terms and relationships shown in the figure are given below:

Virgin Loading for $\mu \leq \mu_m, \dot{\mu} \leq 0$

$$\left. \begin{aligned} B &= B_1 \text{ for } \mu < \mu_2 \\ B &= B_2 \text{ for } \mu_1 > \mu \geq \mu_2 \end{aligned} \right\} \quad (5-28)$$

$$G = \frac{3B(1 - 2\nu)}{2(1 + \nu)} \quad (5-29)$$

Unloading/Reloading for $\mu > \mu_m, B = B_1 \quad (5-30)$

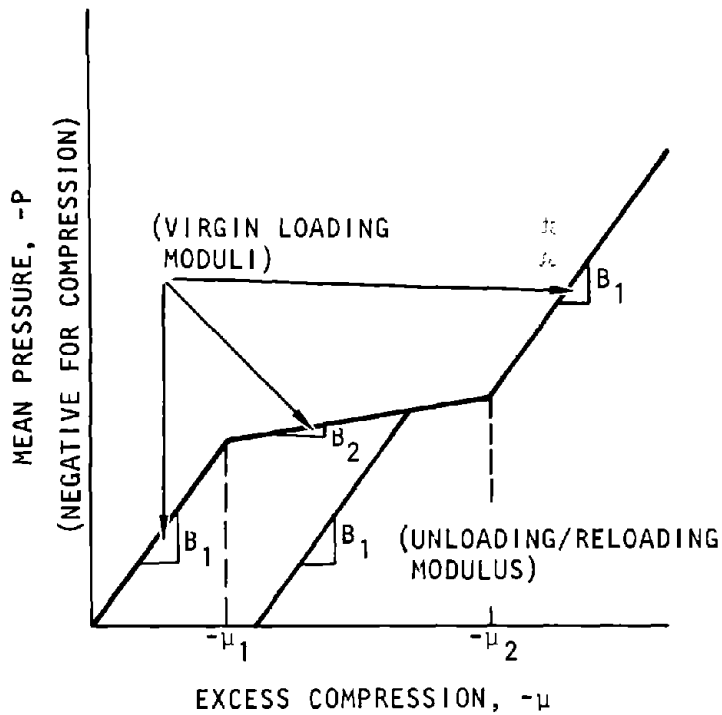
$$\left. \begin{aligned} F &= Y_{11} + Y_{12} J_1 - \sqrt{J_2} \geq 0 \\ F &= Y_{25} - J_1 \geq 0 \end{aligned} \right\} \text{ (for } J_1 \geq Y_{10} \text{)}$$

$$F = Y_{16} - \sqrt{J_2} \geq 0 \quad \text{(for } J_1 < Y_{10} \text{)}$$

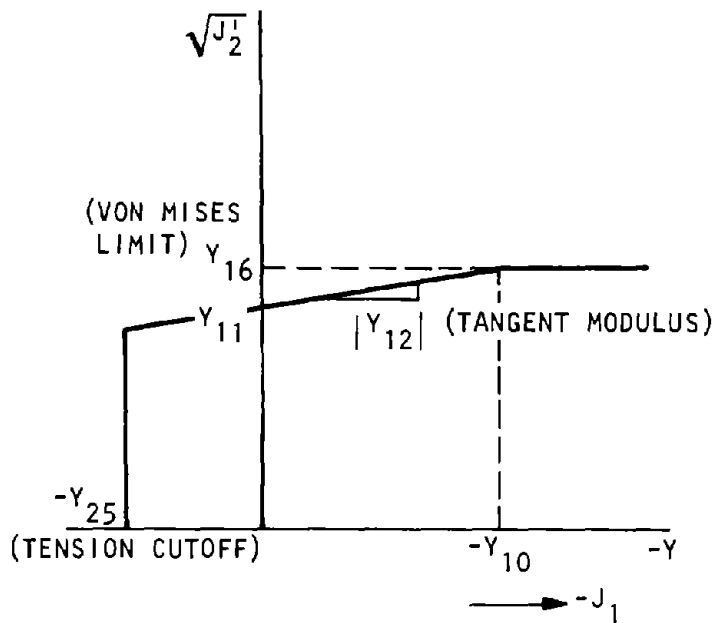
$$F < 0 \text{ not permitted} \quad (5-31)$$

In these equations

- J_1 = First stress invariant (σ_{ii})
- J_2 = Second stress deviator invariant $\frac{1}{2} (\sigma_{ij} \sigma_{ij})$
- B = Bulk modulus
- G = Shear modulus
- ν = Poisson's ratio (assumed to be constant)
- μ = $(1 + \epsilon_r) (1 + \epsilon_2) (1 + \epsilon_\theta) - 1$
- = Excess compression (negative for compressive strains)



(a) Pressure/volume change curve



(b) Failure envelope

Figure 5-43. Idealized Model for Geologic Materials

- $\dot{\mu}$ = Time derivative of μ
- μ_m = Maximum excess compression reached in previous load history
- $\epsilon_r, \epsilon_z,$ and ϵ_θ are the three axial strains
- $B_1, B_2, \mu_1, \mu_2, Y_{11}, Y_{12}, Y_{16},$ and Y_{25} are empirical constants, as shown in figure 5-44

As an illustration of the application of the above relationships, table 5-3 shows the material properties at a site for which laboratory data were available. (The profile of this site is shown in figure 11-1.)

k. An idealized uniaxial-loading stress/strain curve for material backfilled around a buried structure is shown in figure 5-44. This example is included to show that the piecewise linear uniaxial stress/strain curve obtained from laboratory data may be approximated by a single continuous high-order polynomial curve. In this example, the variable modulus model is obtained as a fourth-order polynomial. The laboratory data are given in the figure.

Virgin Loading for $\mu \leq \mu_m, \dot{\mu} \leq 0$

$$B = D_0 + D_1\mu + D_2\mu^2 + D_3\mu^3 \quad (5-32)$$

$$G = \frac{B(1 - 2\nu)}{2(1 + \nu)} \quad (5-33)$$

Unloading/Reloading for $\mu > \mu_m$

$$B_m = D_0 + D_1\mu_m + D_2\mu_m^2 + D_3\mu_m^3 \quad (5-34)$$

$$P_m = \left[\sigma_x(\mu_m) + \sigma_y(\mu_m) + \sigma_z(\mu_m) \right] / 3 \quad (5-35)$$

$$\mu_R = \left[1 - \exp \frac{\mu_m}{\mu_0} \right] \bar{\mu} \quad (5-36)$$

$$B'_0 = B_m + \frac{P_m - B_m(\mu_m - \mu_R)}{\mu^* \left[1 - \exp \left(\frac{\mu_R - \mu_m}{\mu^*} \right) \right]} \quad (5-37)$$

$$B = B_m - [B_m - B'_0] \exp [- (\mu - \mu_R) / \mu^*]$$

for $B'_0 < B_m$

$$B = B_m \text{ (or maximum B) encountered in load history}$$

for $B'_0 \geq B_m$

(5-38)

$$G = \text{Maximum of } \frac{3}{2} B_m \frac{(1 - 2\nu_u)}{(1 + \nu_u)} \text{ or largest G encountered in load history}$$

Yield Criteria

$$\left. \begin{aligned} F &= Y_{11} + Y_{12}J_1 - \sqrt{J_2'} \geq 0 \\ F &= Y_{25} - J_1 \geq 0 \\ F &= Y_{16} - \sqrt{J_2'} \geq 0 \end{aligned} \right\} \begin{aligned} &\text{(for } J_1 \geq Y_{10}) \\ &\text{(for } J_1 < Y_{10}) \end{aligned}$$

$$F < 0 \text{ not permissible} \quad (5-39)$$

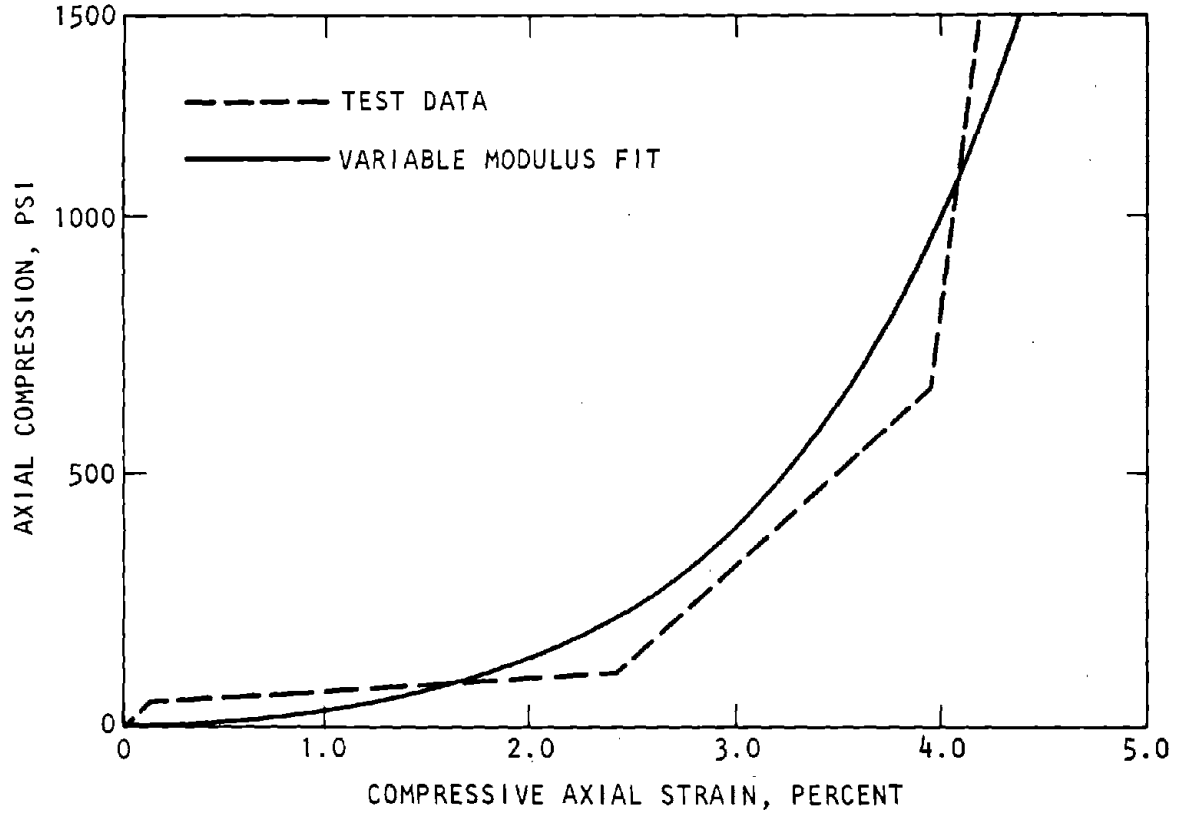
in which

ν_u = Unloading Poisson's ratio
 $D_0, D_1, D_2, \mu_0, \mu^*, \bar{\mu},$ and Y_{10} are empirical constants determined from the loading/unloading uniaxial stress/strain curve and the yield criteria.

All other variables are as defined for the soil model by equations 5-28 through 5-31.

Table 5-3. Variation of Properties of Geologic Materials at a Selected Site (Endebrook-Traina, 1972; Lee-Agbabian, 1976)

Mat'l No.	Material Description	Depth, ft	Density, psf	Poisson's Ratio, ν	Excess Compression, in./in.		Bulk Modulus, psi				Yield Criteria			
					μ_1	μ_2	B_1 Loading	B_2 Loading	B_u Tensile	B_u Unloading	Y_T , psi Tension Cutoff	Y_{11} , psi Cohesion	Y_{12} Envelope Slope	
1	Dry Clay	0 to 8.75	110	0.4	-2.41×10^{-4}	-0.02	4.15×10^4	2.66×10^4	4.15×10^4	4.15×10^4	4.15×10^4	10	100	-0.0033
2	Wet Clay	8.75 to 16.25	130	0.4	-1.57×10^{-5}	-0.005	6.37×10^5	5.78×10^5	6.37×10^5	6.37×10^5	6.37×10^5	30	10	-0.0033
3	Limestone	16.25 to 20.45	167	0.35	-8.3×10^{-7}	-0.005	1.205×10^7	4.88×10^6	1.20×10^7	1.20×10^7	1.20×10^7	48	5000	-0.1667
4	Interbedded Limestone and Shale	20.45 to 32.85	160	0.36	-6.4×10^{-6}	-0.005	1.56×10^6	8.79×10^5	1.56×10^6	1.56×10^6	1.56×10^6	76	500	-0.1
5	Limestone	32.85 to 35.25	167	0.35	-8.3×10^{-7}	-0.005	1.20×10^7	4.88×10^6	1.20×10^7	1.20×10^7	1.20×10^7	101	5000	-0.1667
6	Shale	35.25 to 41.65	155	0.38	-5.86×10^{-6}	-0.005	1.70×10^6	1.13×10^6	1.70×10^6	1.70×10^6	1.70×10^6	115	5000	-0.1
7	Coal	41.65 to 45.25	90	0.41	-8.0×10^{-6}	-0.005	1.25×10^6	8.69×10^5	1.25×10^6	1.25×10^6	1.25×10^6	129	500	-0.1
8	Shale	45.25 to 51.75	155	0.38	-5.86×10^{-6}	-0.005	1.70×10^6	1.13×10^6	1.70×10^6	1.70×10^6	1.70×10^6	143	500	-0.1
9	Limestone	51.75 to 60.85	167	0.35	-8.3×10^{-7}	0.005	12.05×10^7	4.88×10^6	1.205×10^7	1.205×10^7	1.20×10^7	169	5000	-0.1667



UNIAXIAL TEST DATA FOR BACKFILL MATERIAL

RANGE OF AXIAL STRAIN, IN./IN.	CONSTRAINT MODULUS M_c , PSI
$\epsilon > -0.0015$	31,111
$-0.0015 > \epsilon > -0.0244$	2,667
$-0.0244 > \epsilon > -0.0394$	37,037
$-0.0394 > \epsilon$	310,588

Figure 5-44. Uniaxial Stress/Strain Fit for Backfill Material (Less-Agbabian, 1976)

CHAPTER 6

BEHAVIOR OF STRUCTURAL ELEMENTS

6-1. Load capacity of structural elements

a. The load-carrying capacity of structural elements depends on their material properties, shape and size of cross section, dimensions and support conditions, and load distribution. Material properties are discussed in chapter 5. In this section, the load-carrying capacity of reinforced concrete and steel elements as influenced by shape and size of cross section is presented. Dimensions, support conditions, and load distribution are discussed to the extent that they influence the stress distribution across a cross section and thereby the load-carrying capacity of the element. For example, the presence of an axial load could reduce the moment-carrying capacity of the element, or a laterally braced column could carry increased axial loads by allowing the column to yield without becoming unstable prematurely.

b. Generally, the load-carrying capacity is determined by static considerations. The dynamic load-carrying capacity is obtained by replacing properties of the material under static load with the properties under dynamic load. Where there is insufficient data on dynamic behavior and it is known that the static load conditions are the lower bound of the load-carrying capacity, the static load-carrying capacity is taken to be the measure of the dynamic load-carrying capacity of the structural element.

6-2. Flexural strength of structural steel

a. Plastic design in structural steel is a standard procedure for protective construction. The flexural strength of structural shapes is obtained from the expression

$$M_P = f_s \cdot Z_x \text{ or } f_s \cdot Z_y \quad (6-1)$$

where

$$\begin{aligned} M_P &= \text{Plastic moment} \\ f_s &= \text{Yield strength of the steel} \\ Z_x, Z_y &= \text{Plastic section modulus with respect} \\ &\quad \text{to the major and minor axes,} \\ &\quad \text{respectively} \end{aligned}$$

For rectangular sections of width W and depth H

$$Z_x = \frac{WH^2}{4} = 1.5 \text{ times the elastic section modulus} \quad (6-2)$$

For rolled sections, the plastic section modulus is 1.10 to 1.23 times the elastic section modulus. The AISC *Manual of Steel Construction* (AISC, latest edition) includes plastic design selection tables based the plastic

section moduli of rolled sections. Plastic section modulus is the summation of static moment of the tension and compression areas of the structural member about the neutral axis.

b. An important consideration in the evaluation of the plastic flexural strength of structural steel elements is the lateral support of the beam's compression flange. The compression flange should not buckle before reaching the flexural strength of the beam. This and other restrictions, such as width/thickness ratio of the projecting elements of the compression flange and depth/thickness ratio of the web, have led to semiempirical formulas that are specified by the AISC Manual. Design procedures should generally comply with these guidelines in order to preclude premature failure of structural shapes. Equivalent length coefficients for laterally unsupported beams are given in table 6-1.

c. The load-deflection diagram of structural steel is usually taken as elastoplastic if ductility factors are selected such that deformations do not reach the strain-hardening phase of the steel. Nonlinear load-deflection relationships, however, may be used if a more accurate description of the response of the structural element is required.

d. A typical nonlinear load-deflection relationship is given by the Ramberg-Osgood functions, as shown in figure 6-1 (Popov-Pinkney, 1968). The equation for computing deflection for a given load is:

$$\frac{\delta}{\delta_p} = \frac{P}{P_p} \left[1 + \alpha \left| \frac{P}{P_p} \right|^{\kappa-1} \right] \quad (6-3)$$

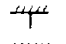


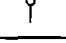
where P and δ are the load and deflection, P_p is the plastic load, δ_p is the deflection at $P = P_p$, and α and κ are positive real numbers for curve fitting. The exponent κ is a measure of the sharpness of curvature of the load-deflection curve. Test results show that $\alpha = 0.5$ and $\kappa = 8$ are practical average values for use in the Ramberg-Osgood equations.

e. The area enclosed by a hysteresis loop (loading and unloading of the steel number) is given by the approximate relation

$$\text{Hysteresis Loop Area} = \left(\frac{\kappa - 1}{\kappa + 1} \right) (P_2 - P_1)^{\delta'} \quad (6-4)$$

The hysteresis loop area can be used to estimate structural damping (AA, 1975a). The relationships for the loading and unloading branches of the load-deflection curve are shown in figure 6-2. In the figure, β is the slope factor (a measure of the stiffness of the structural element); it is usually close to unity.

Table 6-1. Effective Length Factors (AISC, 1969)

Buckled shape of column is shown by dashed line	(a)	(b)	(c)	(d)	(e)	(f)
Theoretical K value	0.5	0.7	1.0	1.0	2.0	2.0
Recommended design value when ideal conditions are approximated	0.65	0.80	1.2	1.0	2.10	2.0
End condition code	   	Rotation fixed and translation fixed Rotation free and translation fixed Rotation fixed and translation free Rotation free and translation free				

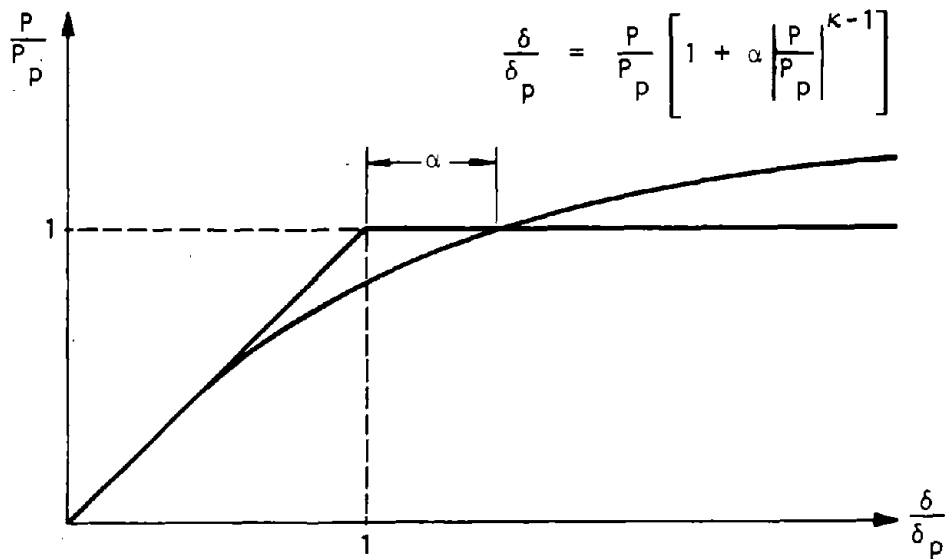


Figure 6-1. Ramberg-Osgood Function (Popov-Pinkney, 1968)

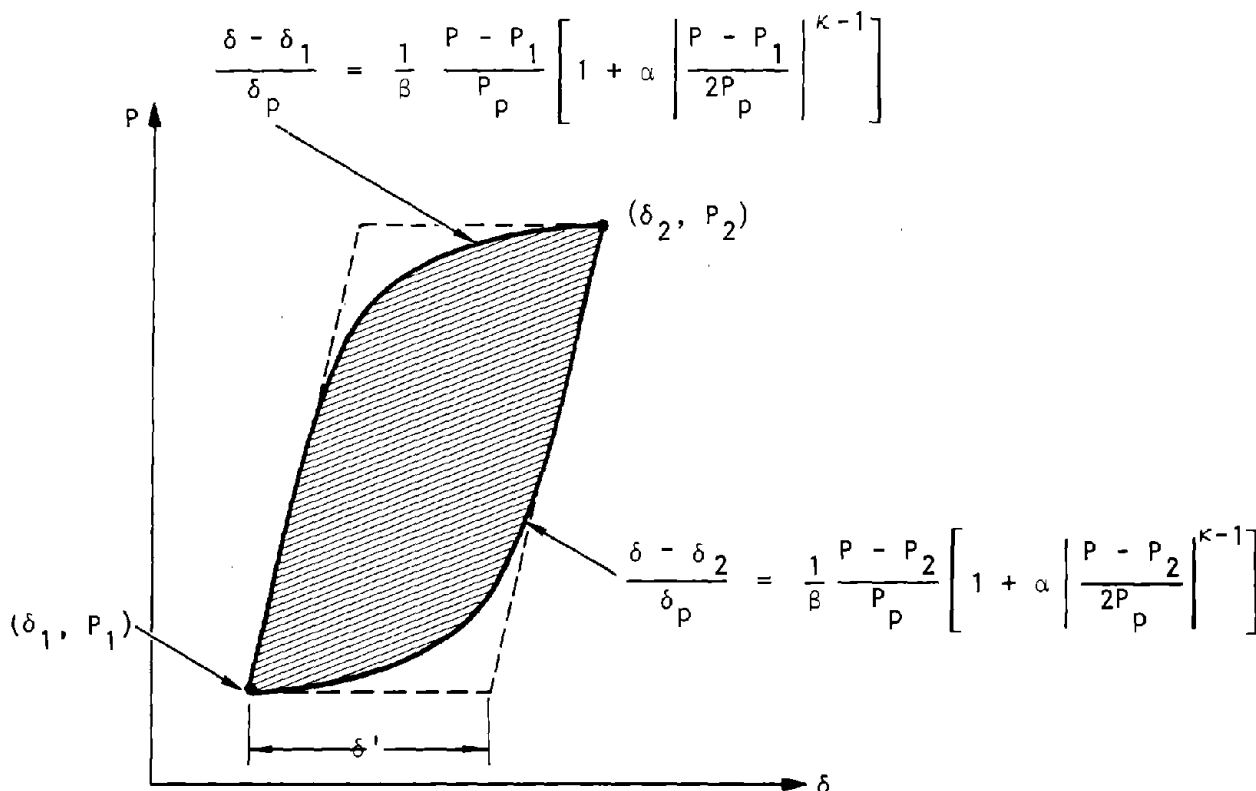


Figure 6-2. Hysteresis Loop (Popov-Pinkney, 1968)

f. The designer may be required to select from steels of different yield strengths. He may also be interested in the significance of the difference between the minimum and average value of the yield strength of a specified steel. (The elastic modulus is essentially the same for all steels.) Consider a cantilever beam with load P at free end (Popov-Pinkney, 1968) and first develop relationships for equal strength and equal stiffness.

(1) Two structures of equal strength: Both can support the same ultimate plastic load, but the elastic deflections corresponding to this load level will differ by the ratio of the yield strengths. Thus

$$P_{p2} = P_{p1}$$

$$\delta_{p1} = \frac{f_{s1}}{f_{s2}} \delta_{p2}$$

(2) Two structures of equal stiffness: These are structures for which $E_1 I_1 = E_2 I_2$; since the elastic modulus is the same for all steels, $I_1 = I_2$. The respective ultimate plastic loads differ by the ratio of the yield strengths, as do also the corresponding elastic deflections.

$$P_{p1} = \frac{f_{s1}}{f_{s2}} P_{p2}$$

$$\delta_{p1} = \frac{f_{s1}}{f_{s2}} \delta_{p2}$$

g. An example from Popov-Pinkney (1968) is reproduced here as figure 6-3. A comparison of load-deflection curves for A441 and A36 steel is shown using the Ramberg-Osgood curves. The hysteresis loops generated from these curves are used to make four comparisons in figure 6-4: (a) equal strength/equal load; (b) equal strength/equal deflection; (c) equal stiffness/equal load; and (d) equal stiffness/equal deflection. The following observations are made for this example. Performance of equal strength structures would be similar with somewhat larger deformations when A441 steel is used. For equal stiffness (members of identical cross section), and for a design that is dictated by the load capacity (case c), the ductility of the structure using A441 steel has not been fully developed. Larger loads (case d) would produce ductilities that correspond to the values experienced with the use of A36 steel. Similar conclusions, obvious to the designer, would have been reached if elastoplastic load-deflection relationships were used instead of the Ramberg-Osgood type. The example is given here, however, to emphasize the importance of using steel properties to their fullest advantage, depending on the specific application.

6-3. Shear strength of structural steel

a. The average stress at which an unreinforced web is fully yielded in pure shear is given by $f_s/\sqrt{3}$. Plastic bending strength of W beams is maintained until shear yielding occurs over the full effective

depth (ASCE, 1961). The static shear strength at yield may be expressed by:

$$V_u = \frac{f_s H_e t}{\sqrt{3}} = 0.55 f_s H t \quad (6-5)$$

where

H_e = Effective depth of web, distance between centroids of flanges $\approx 0.95 H$ (H is the full depth)

t = Web thickness

b. The effect of transverse shear forces is to reduce the full plastic moment. Denote the reduced plastic moment by M_{ps} . Theoretically, it is shown that

$$M_{ps} = M_p - \frac{9}{64} \left(\frac{V_s^2}{f_s} \right) \left(\frac{H_e^2}{Z} \right) \quad (6-6)$$

where

M_p = Plastic moment

V_s = Shear force corresponding to first yield in shear

H_e = Effective depth of beam web

f_s = Yield strength of steel

Z = Plastic section modulus

As an extreme condition, when shear produces full yielding of the web, and if it is assumed that the entire additional shear is taken by the flanges, using equations 6-5 and $V_s = V_u$ gives

$$M_{ps} = M_p - \frac{3 f_s t^2 H_e^4}{64 Z} \quad (6-7a)$$

or using the full depth H ,

$$M_{ps} = M_p - 0.038 f_s t^2 H^4 / Z \quad (6-7b)$$

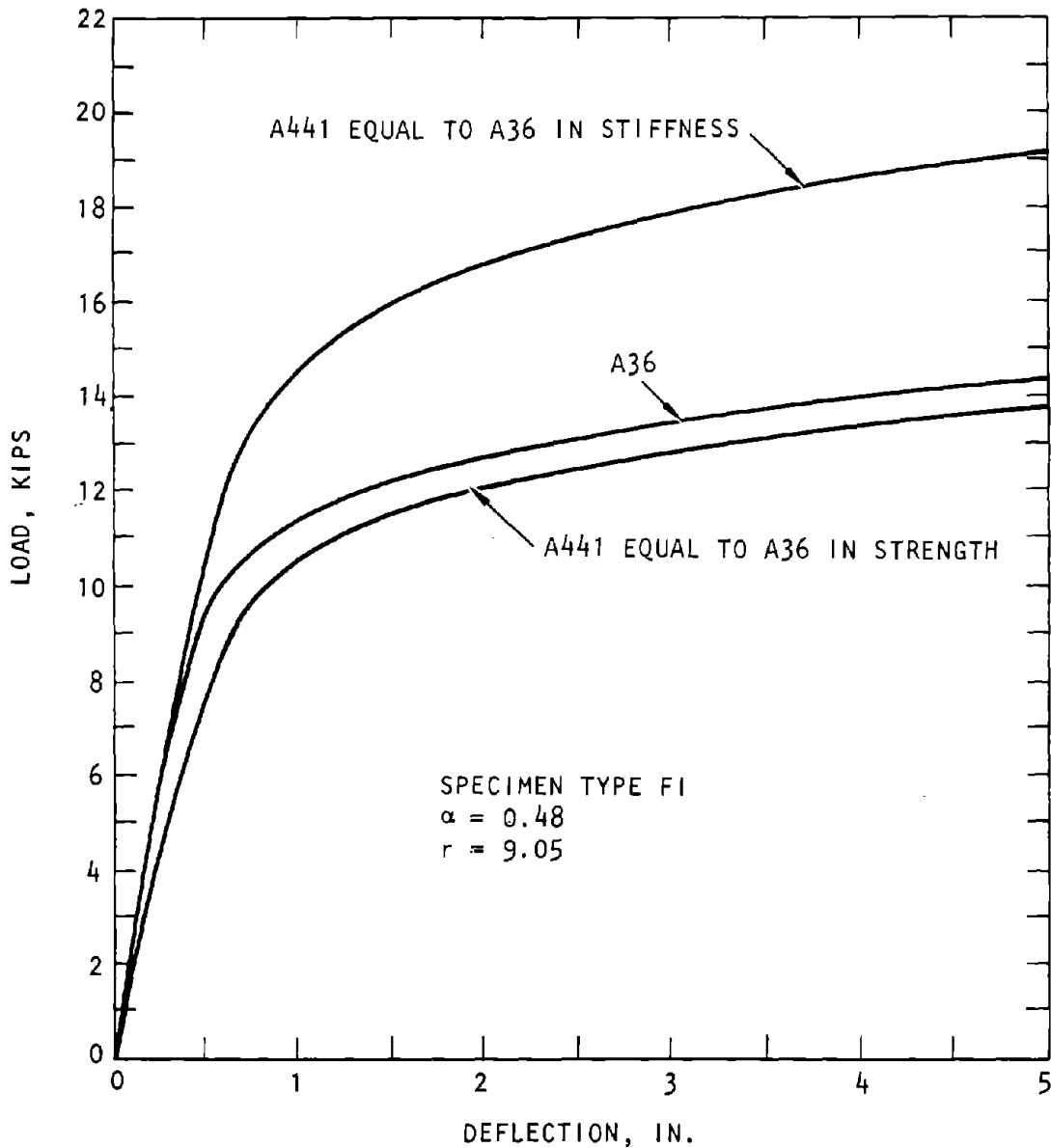
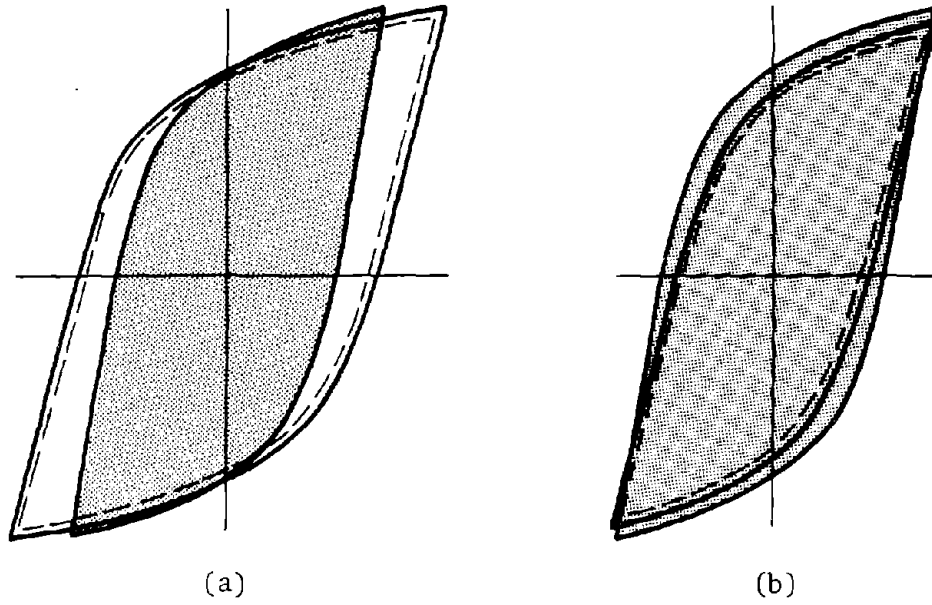
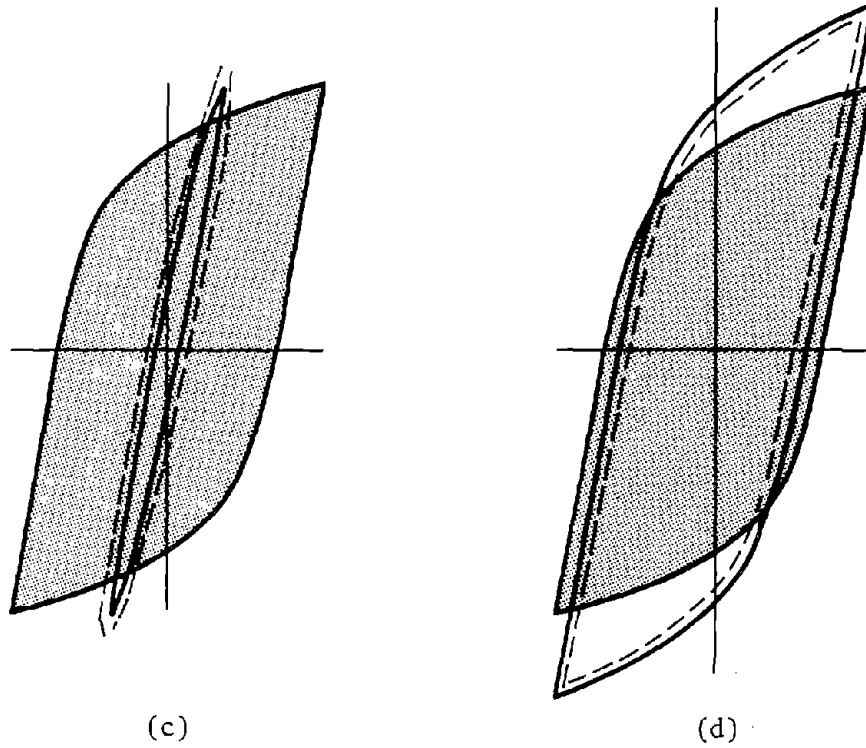


Figure 6-3. Comparison of Load Deflection Curves A-36 and A441 Steels (Popov-Pinkney, 1968)



EQUAL STRENGTH DESIGN



EQUAL STIFFNESS DESIGN

Figure 6-4. Comparison of Equal Strength and Equal Stiffness Designs (Popov-Pinkney, 1968)

These theoretical equations give conservative results because the implied reduction in moment capacity does not occur owing to strain hardening. It is recommended (ASCE, 1961) that, based on test results, no reduction of the plastic moment due to shear be made if the magnitude of the shear force at the ultimate load is less than V_u . More recent tests (Popov-Stephen, 1970) with cyclic loads show that in the immediate proximity of a rigid support a large portion of the shear is transferred from the web to the flanges and then to the support. Design practice neglects the shear transfer capacity of flanges. Considering all these variables, it is desirable to proportion W-sections so that $V_s < V_u$ when the full plastic moment M_p is developed and to consider M_p (without reduction) to be the flexural strength of the beam.

6-4. Combined flexural and axial loads on structural steel

a. In structures subjected to lateral loads imposed by a blast, the columns will be subjected to bending moments as well as axial loads, and they should be treated as beam-columns. The maximum allowable load for an axially loaded compression member for plastic design is given as

$$P_u = 1.7 A \sigma_a \tag{6-8}$$

where

- A = Gross area of member
- σ_a = Maximum allowable axial stress dependent on the slenderness ratio of the column

This relationship may also be used for dynamic loads. (See AISC Specification for the Design, Fabrication, and Erection of Structural Steel for Buildings, latest edition.)

b. Most compression members are also subjected to bending moments and, therefore, act as beam columns. If axially loaded members are sufficiently braced against buckling, the applied moments and axial forces will cause the structural element to go into the plastic range. Insufficient lateral bracing and a large difference between bending stiffnesses about the principal axes will cause the structural element to bend out of the plane of the applied moments and twist at the same time. For columns of intermediate slenderness ratio, this type of buckling takes place when parts of the column have yielded. Recommended spacing of the bracing to avoid this instability is given in AISC (1969) by the following expressions for critical spacing:

$$\frac{L_{cr}}{r} = \frac{1375}{F_y} + 25 \quad \text{when } +1.0 > \frac{M}{M_p} > -0.5$$

$$L_{cr} = \frac{1375 r}{F_y} \quad \text{when } -0.5 \geq \frac{M}{M_p} \geq -1.0$$

In which

- M = The lesser of the moments at the ends of the unbraced segment
- M/M_p = The end moment ratio (+ for reverse curvature, - for single curvature)

c. Width-thickness ratio specifications for single-web shapes and built-up sections are contained in AISC (1969); the proportions for minimum thickness of column shapes are shown in figure 6-5. For either flange, W/t_f should not exceed the following values.

F_y	W/t_f
36	17.0
42	16.0
45	14.8
50	14.0
55	13.2
60	12.6
65	12.0

For webs of members subject to plastic bending, H/t should not exceed the value given by the following expressions:

$$\frac{H}{t} = \frac{412}{\sqrt{F_y}} \left(1 - 1.4 \frac{P}{P_y} \right) \quad \text{when } \frac{P}{P_y} \leq 0.27$$

$$\frac{H}{t} = \frac{257}{\sqrt{F_y}} \quad \text{when } \frac{P}{P_y} > 0.27 \tag{6-9}$$

d. Members subject to combined axial load and bending moment should satisfy the following interaction formulas:

$$\frac{P}{P_u} + \frac{C_m M}{\left(1 - \frac{P}{P_e} \right) M_m} \leq 1.0 \tag{6-10}$$

$$\frac{P}{P_u} + \frac{M}{1.18 M_p} \leq 1.0; M \leq M_p \tag{6-11}$$

where

- M = Maximum applied moment
- P = Applied axial load
- $P_e = \frac{A \pi^2 E}{(KL/r)^2}$
- $C_m = 0.85$ for members in frames subject to sidesway
- $= 0.6 - 0.4 M_1/M_2$, but not less than 0.4 for members in frames braced against sidesway; where M_1/M_2 is ratio of smaller to larger end moments (+ for reverse curvature, - for single curvature)
- $= 0.85$ for members in frames braced against sidesway, subjected to

transverse loading between supports, and with ends restrained
 = 1.0 for members in frames braced against sidesway, subjected to transverse loading between supports, and with ends unrestrained

M_m = Maximum moment that can be resisted by the member in the absence of axial load

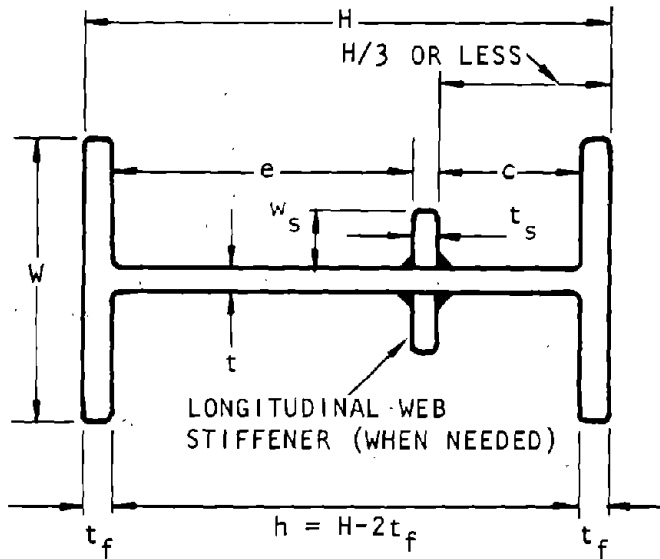


Figure 6-5. Typical Beam Section Reinforced to Prevent Web Buckling (COE, 1965)

For columns braced in the weak direction

$$M_m = M_p$$

For columns unbraced in the weak direction

$$M_m = \left[1.07 - \frac{(L/r_y) \sqrt{F_y}}{3,160} \right] M_p \leq M_p \quad (6-12)$$

e. In the plane of bending of columns which would develop a plastic hinge at ultimate loading, the slenderness ratio (L/r) shall not exceed C_c

$$C_c = \sqrt{\frac{2\pi^2 E}{F_y}} \quad (6-13)$$

The axial stress permitted on a compression member in the absence of bending moment is:

$$\sigma_a = \frac{1 - \frac{(KL/r)^2}{2 C_c^2}}{5/3 + \frac{3(KL/r)}{8 C_c} - \frac{(KL/r)^3}{8 C_c^3}} F_y \quad (6-14)$$

where

K = Effective length factor given in table 6-1 (from AISC Commentary, 1969)

Values of σ_a for various slenderness ratios may be obtained from tables in appendix A of the AISC specification 1969. Figures 6-6 and 6-7 show approximate interaction equations for wide-flange section.

6-5. Flexural and shear strength of reinforced concretes

a. Moment resistance under dynamic loads is obtained by using the dynamic strength for reinforcing steel and concrete in the formulas for static strength. The increase in strength of beams under dynamic loading may be obtained by using the increased strength of the separate materials. In order to achieve increased ductility, reinforced concrete beams should be doubly reinforced. The ductility ratio at failure, based on tests, is given by

$$\mu = \frac{\delta_u}{\delta_s} = \frac{0.1}{a_s - a_s'} \quad (6-15)$$

where

- μ = Ductility ratio
- δ_u = Collapse deflection
- δ_s = Maximum elastic deflection
- a_s = Tension steel reinforcement ratio
- a_s' = Compression steel reinforcement ratio

Shear failures should be avoided in order to permit full development of the flexural resistance. Beams should be designed with web reinforcement that develops the shears resulting from the ultimate moment capacities at the ends of the members. Because of lack of sufficient data on dynamic shear failure of beams, static strength values should be used for shear strength evaluation. The above considerations, combined with ultimate strength theory, are sufficient to evaluate the flexural and shear strength of reinforced concrete members. Textbooks on reinforced concrete design may, therefore, be used for the relationships of parameters that describe flexural and shear strength. With proper adjustments for the various capacity reduction factors (θ) and the dynamic strengths of materials, the CRSI Handbook (1978) may be used for the preliminary selection of member sizes. For ready reference, the basic flexural equations for rectangular sections are given below (see standard textbooks for Tee beams and other structural shapes). For flexure without axial load, the ultimate strength at the concrete section is assumed to be limited by yielding in the tensile steel and a strain in the outermost compressive fiber, ϵ'_u , equal to 0.003. The reinforcing steel in compression will have a strain:

$$\epsilon'_s = \epsilon'_u \left(\frac{c - d'}{c} \right) \quad (6-16)$$

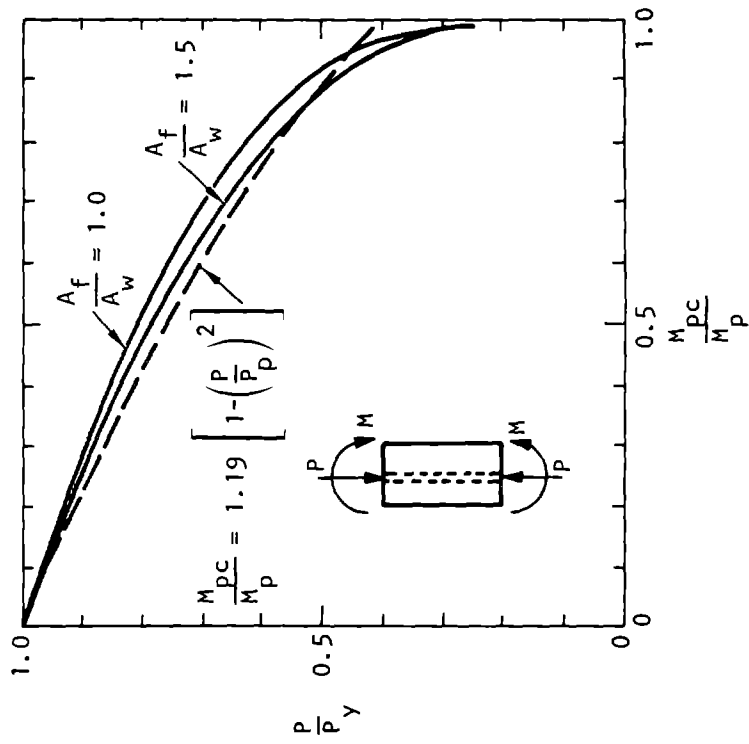


Figure 6-7. Approximate Interaction Equation for Wide-Flange Section (Weak Axis Bending, Short Column) (ASCE, 1961)

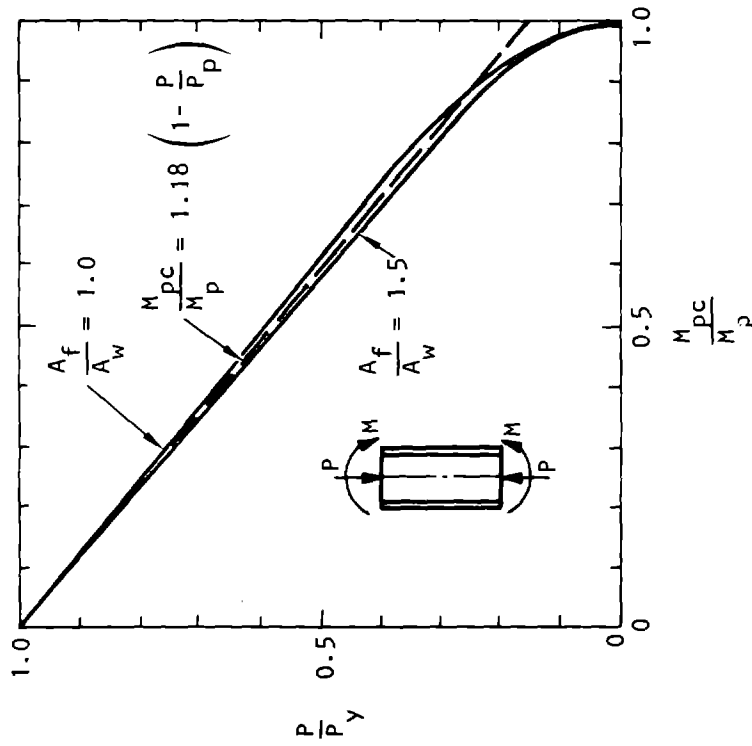


Figure 6-6. Approximate Interaction Equation for Wide-Flange Section (Strong Axis Bending, Short Column) (ASCE, 1961)

The compressive stress in the steel is given by

$$\begin{aligned}\sigma' &= E\varepsilon'_s = E\varepsilon'_u \left(\frac{c-d'}{c} \right) = 29 \times 10^6 \times 0.003 \left(\frac{c-d'}{c} \right) \\ &= 87,000 \left(1 - \frac{d'}{c/d} \right)\end{aligned}\quad (6-17)$$

where

c = Distance from compression surface of concrete to neutral axis

d = Distance from compression surface of concrete to centroid of tension reinforcement

d' = Distance from compression surface of concrete to centroid of compression reinforcement

Under special conditions, and only if demonstrated by tests, ε'_u may be taken to be larger than 0.003 for blast-loaded structures. This value should not, however, be assumed to be larger than 0.005.

b. The ultimate resisting moment of a rectangular section with tension reinforcement only and no axial load may be calculated by

$$M_u = Wd^2 a_s f_s \left(1 - 0.59 \frac{a_s f_s}{f'_c} \right) \quad (6-18)$$

where

M_u = Ultimate resisting moment

W = Width of section

d = Distance from compression surface of concrete to centroid of tension reinforcement

a_s = Tensile steel reinforcement ratio (A_s/Wd)

A_s = Area of tension reinforcement steel

f_s = Yield strength of reinforcement steel

f'_c = Compressive strength of concrete

To ensure a ductile response the reinforcement ratio, a_s , in equation 6-18 must not exceed that calculated by

$$a_s \leq \frac{55,500 k_1 f'_c}{f_s(87,000 + f_s)} \quad (6-19)$$

where, for unconfined numbers,

$$k_1 = 0.85 \text{ for } f'_c \leq 4000 \text{ psi}$$

$$= 0.85 - 0.05 \left(\frac{f'_c - 4000}{1000} \right) \text{ for } f'_c < 4000 \text{ psi}$$

The limitation of equation 6-19 is for a typical beam or slab with a depth that is small compared to the span. If the depth-to-span ratio of a slab is large and,

as a result, the out-of-plane loading stress approaches the flexural stress and the concrete is confined as it would be in a two-way slab, the strain that the concrete can sustain without crushing will be greater than the assumed ultimate strain of 0.003. In such a case, the limit imposed by equation 6-19 may be relaxed if supported by a special investigation based on an acceptable failure criterion such as Prager-Drucker criterion or other acceptable coulomb yield surfaces that can be adequately fitted to concrete triaxial test data. To use the confinement of the concrete to increase the allowable stress one must study the phasing of the triaxial stresses to make certain that the deviatoric stress remains within the failure envelope. This type of design refinement is not recommended for one-of-a-kind structures or where computer facilities are not available for determining the time-dependent parameters.

c. The ultimate resisting moment, M_u , of a rectangular section with both compression and tension reinforcement and no axial load may be calculated by

$$M_u = (A_s - A'_s) f_s \left(d - \frac{h}{2} \right) + A'_s f'_s (d - d') \quad (6-20)$$

where

A'_s = Area of compression steel reinforcement

h = Depth of rectangular stress block ($A_s - A'_s$) $f_s/0.85 f'_c W$

d' = Distance from compression, surface of concrete fiber to centroid of compression reinforcement

Equation 6-20 is valid only when the following expression is satisfied

$$a_s - a'_s \geq \frac{74,000 k_1 f'_c d'}{f_s d(87,000 - f_s)} \quad (6-21)$$

where

$$a'_s = A'_s/Wd$$

When $(a_s - a'_s)$ is less than the value given by equation 6-21 or when effects of compression steel are neglected, the calculated ultimate moment shall not exceed that given by equation 6-18. The quantity $(a_s - a'_s)$ shall not exceed the value of a_s given by equation 6-19. These formulas are valid for reinforcing steel strengths in a range allowed by ACI (1977). If yield strengths of 87 ksi or larger are used, the formulas give zero or negative results. This indicates that the compressive steel cannot yield without causing a strain in the concrete greater than 0.003 in. If the compressive-steel stress at the failure of a slab

is less than the yield stress, the formula for the ultimate moment should be changed to the following:

$$M_u = Wd^2 \left[a_s' (\sigma' - 0.85 f_c') (1 - d'/d) + 0.85 k_1 f_c' (c/d) (1 - k_1 c/2d) \right] \quad (6-22)$$

in which the compression stress in steel, σ' , is determined from

$$\sigma' = \frac{a_s'}{2a_s'} \left\{ \left[f_s + (87,000 + 0.85 f_c') \frac{a_s'}{a_s} \right] - \left(\left[f_s + (87,000 + 0.85 f_c') \frac{a_s'}{a_s} \right]^2 - 348,000 \frac{a_s'}{a_s} \left[f_s - 0.85 k_1 f_c' (d'/d)/a_s + 0.85 f_c' \frac{a_s'}{a_s} \right] \right)^{1/2} \right\}$$

and the depth from the compression surface of concrete to the neutral axis of a flexural section, c , is determined from

$$c = d' \left[\frac{87,000}{87,000 - \sigma'} \right]$$

The above equations are valid only when $\sigma' < f_s$. When $\sigma' \geq f_s$, equation 6-22 may still be used to determine M_u by substituting f_s for σ' and computing c with the following equation:

$$c = d \left[\frac{a_s f_s - a_s' (f_s - 0.85 f_c')}{0.85 k_1 f_c'} \right] \quad (6-23)$$

The maximum permissible values of a_s are determined as follows:

When $\Delta' = f_s$, $a_s - a_s' \leq 0.75 a_b$, when a_b , the steel ratio producing balanced conditions at ultimate strength, is

$$a_b \leq \frac{74,000 k_1 f_c'}{f_s (87,000 + f_s)} \quad (6-24)$$

where s is the stirrup spacing, A_v the stirrup area, and ℓ the horizontal projected length of the inclined crack. The shear capacity is then

$$S = \sigma_s W \ell + \frac{\ell}{s} A_v f_s$$

If the flexural reinforcement yields, the concrete shear-resisting part must be assumed to be inactive. According to ACI, the shear stress at cracking may be calculated by

$$\sigma_s = 1.9 \sqrt{f_c'} + 2500 \frac{a_s S d}{M_u} \leq 3.5 \sqrt{f_c'} \quad (6-25)$$

where a_s is the ratio of tension steel reinforcement area to concrete area, d is the distance from compression surface of concrete to centroid of tension reinforcement, M_u is the ultimate resisting moment, and Sd/M_u shall not be taken greater than 1.0. If the axial load is present, M_u is substituted in

$$M_m = M_u - P \left(\frac{4H - d}{8} \right)$$

where M_m is the modified ultimate moment due to presence of axial load, H is the overall thickness of member, and P is the axial load normal to section with shear loads, positive for compression. However, σ_s should satisfy

$$\sigma_s \leq 3.5 \sqrt{f_c' \left(1 + 0.002 \frac{P}{WH} \right)} \text{ psi}$$

instead of $3.5 \sqrt{f_c'}$.

$$\text{Then } a_s - a_s' \leq \frac{55,500 k_1 f_c'}{f_s (87,000 + f_s)}$$

when $\Delta' < f_s$, $a_s \leq 0.75 a_b / (1 - 0.75 \sigma' a_s' / f_s a_s)$, and

$$\sigma' / f_s = \left[(87,000 + f_s) / f_s \right] (1 - d'/d) - 1$$

When σ' / f_s exceeds unity, the compressive steel is at yield point stress and equation 6-22 applies.

d. The shear capacity of a section is expressed as

$$S = S_o + S_s$$

where S_o and S_s are the shear carried by the concrete and by the transverse reinforcement, respectively. The shear carried by the concrete is

$$S_o = \sigma_s W \ell$$

where σ_s is an average stress (the nominal shear stress) assumed to be uniform over the area $W \ell$ and is taken as the magnitude that causes the first diagonal crack. The shear force carried by vertical web reinforcement (stirrups) is

$$S = \frac{\ell}{s} A_v f_s$$

The static stress values are used to determine the allowable dynamic shear stress. This conservative approach is used for design because of the complexity and uncertainty of including all of the dynamic parameters influencing shear strength.

6-6. Combined flexural and axial loads on reinforced concrete

a. Columns with axial loads and bending moments can fail by yielding of the tension steel or by crushing of the concrete. Since the ultimate load in each case is determined by different stress conditions, design is facilitated by using a plot of axial load capacity vs. moment capacity. An example of such a plot is shown in figure 6-8. Equations to construct axial load-moment capacity design curves similar to figure 6-8 for any reinforced concrete column are available in standard textbooks. These formulas, however, do not account for the increased strengths due to dynamic loading. For ready reference and to illustrate procedures, given below is the ultimate strength of short rectangular members subject to combined bending and axial load and with bars in one or two faces, each parallel to the axis of bending. The following equations apply when h is not more than D and all of the reinforcement in any one face is located at approximately the same distance from the axis of bending.

$$P_u = 0.85 f'_c W h + A'_s f_s - A_s \sigma \tag{6-26}$$

where

P_u = Axial load capacity under combined axial load and bending

- h = Depth of equivalent rectangular stress block = $k_1 c$
- D = Overall depth of a rectangular section or diameter of a circular section
- W = Width of rectangular section
- c = Distance from compression surface of concrete to neutral axis
- σ = Calculated stress in tension steel

The balanced load, P_b , is computed using the following equation

$$P_b = f'_c W k_1 \frac{74,000 d}{(87,000 + f_s)} + f_s (A'_s - A_s) \tag{6-27}$$

The balanced moment, M_b , is computed by

$$M_b = f'_c W k_1 \frac{74,000 d}{(87,000 + f_s)} \left[d - d'' - \frac{43,500 d k_1}{(87,000 + f_s)} \right] + A'_s f_s (d - d' - d'') + A_s f_s d'' \tag{6-28}$$

where

d'' = Distance from plastic centroid to centroid of tension reinforcement,

$$d \left[1 - \frac{87,000}{(87,000 + f_s)} \right]$$

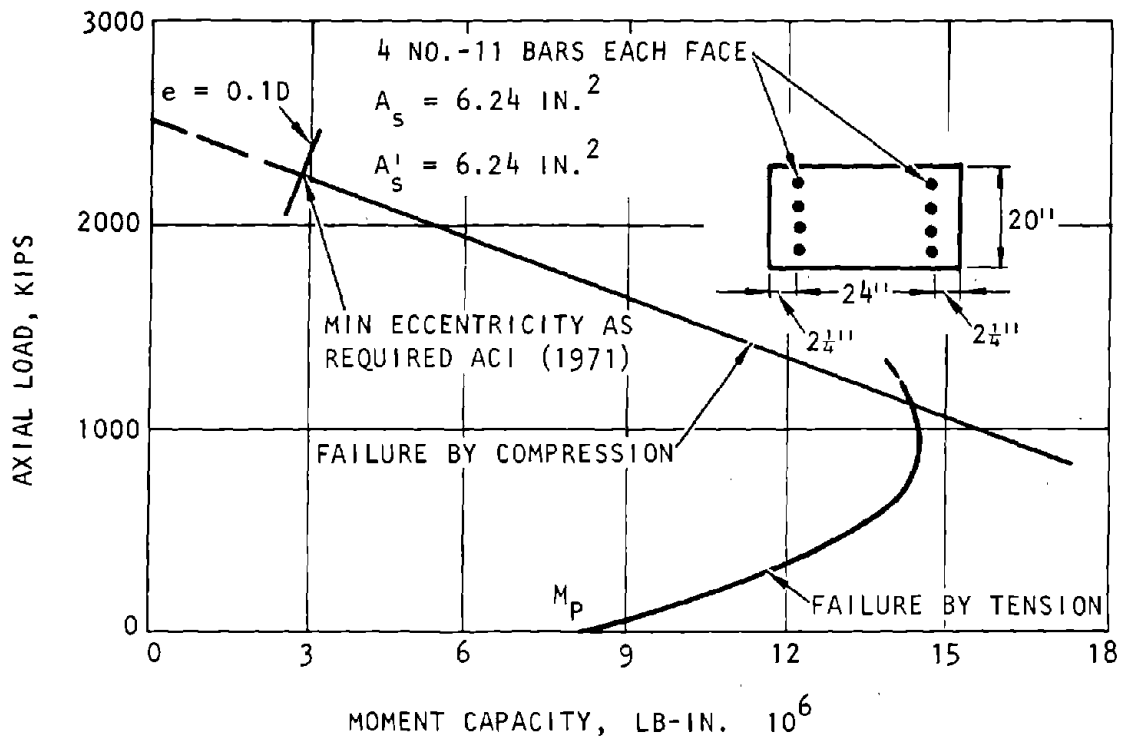


Figure 6-8. Axial-Load/Moment-Capacity Curve for Reinforced Concrete Columns (COE, 1965)

b. When the ultimate capacity of a member is controlled by tension ($P_u < P_b$) the ultimate strength will not exceed that computed by

$$P_u = 0.85 f'_c Wd \left[a'_s m' - a_s m + (1 - e'/d) + \left\{ (1 - e'/d)^2 + 2(e'/d)(a_s m - a'_s m') + 2 a_s m'(1 - d'/d) \right\}^{1/2} \right] \quad (6-29)$$

where

$$\begin{aligned} m &= f_s / 0.85 f'_c \\ m' &= m - 1 \\ e' &= \text{Eccentricity of axial load at end of member measured from the centroid of the tension reinforcement} \end{aligned}$$

For symmetrical reinforcement in two faces this reduces to

$$P_u = 0.85 f'_c Wd \left[-a_s + 1 - e'/d + \left\{ (1 - e'/d)^2 + 2 a_s m'(1 - d'/d) + 2 a_s e'/d \right\}^{1/2} \right] \quad (6-30)$$

With no compression reinforcement, equation 6-29 reduces to

$$P_u = 0.85 f'_c Wd \left[-a_s m + 1 - e'/d + \left\{ (1 - e'/d)^2 + \frac{2 e' a_s m}{d} \right\}^{1/2} \right] \quad (6-31)$$

c. When the ultimate capacity of a member is controlled by compression ($P_u > P_b$) the ultimate load is assumed to decrease linearly from P_o to P_b as the moment is increased from zero to M_b and

$$P_o = 0.85 f'_c (A - A_t) + A_t f_s \quad (6-32)$$

where

$$\begin{aligned} A &= \text{Gross area of section} \\ A_t &= \text{Total area of longitudinal reinforcement steel} \\ P_o &= \text{Ultimate axial load with no flexural moment} \end{aligned}$$

For this assumption the ultimate strength is given by equations 6-33 and 6-34.

$$P_u = \frac{P_o}{1 + [(P_o/P_b) - 1] e/e_b} \quad (6-33)$$

where

$$\begin{aligned} e &= \text{Eccentricity of axial load measured from plastic centroid} \\ e_b &= \text{Eccentricity of load } P_b \text{ measured from plastic centroid} \end{aligned}$$

$$P_u = P_o - (P_o - P_b) M_u/M_b \quad (6-34)$$

When P_u , P_o , P_b and M_b are either known or computed and $P_u > P_b$, the moment capacity, M_u , is found by

$$M_u = M_b \left(\frac{P_o - P_u}{P_o - P_b} \right) \quad (6-35)$$

Members subjected to a small compressive load ($P_u < 0.15 P_o$) may be designed for $M_u = P_u e$ using equation 6-18 or 6-20. The axial load capacities determined by all of the previous equations apply only to short members. If long members are required, their capacities should be reduced for the effects of length according to the requirements of the ACI Code.

6-7. Ultimate load for two-way slabs

a. *Square slab.* The ultimate uniform unit load that a square two-way slab can carry is expressed by the following formula:

$$U = \frac{24(M_1 + M_2)}{L^2} \quad (6-36)$$

where

$$\begin{aligned} L &= \text{Length of the side of the square slab} \\ M_1 &= \text{Positive yield moment per unit length} \\ M_2 &= \text{Negative yield moment per unit length} \end{aligned}$$

If the slab is simply supported, M_2 is zero. The yield moments, M_1 and M_2 , are computed using the methods previously described. Any inplane axial stresses will alter the yield moments and must be allowed for as described under "Combined Flexural and Axial Loads," (para. 6-6). Equation 6-36 is based on the Yield Line Theory, assuming diagonal yield lines as shown in figure 6-9.

b. *Rectangular slabs.* The ultimate uniform unit load that a rectangular two-way slab with edge moments can carry cannot be computed directly but must be solved by iteration as described below and shown in figure 6-10.

- Step 1. Select a value for "a."
- Step 2. Compute U_a by the formula:

$$U_a = \frac{6(M_1 + M_2)}{a^2}$$

- Step 3. Compute U_b by the formula:

$$U_b = \frac{4 L_2 (M_1 + M_3)}{L_1^2 \left(\frac{a}{3} + \frac{b}{2} \right)}$$

- Step 4. If U_a is not equal to U_b , go to Step 1 and select a new value for a and recompute. When the two values converge, the ultimate uniform load is determined.

The notations used above have the following meanings:

- U_a = Ultimate uniform unit load that trial segment A can support
- U_b = Ultimate uniform unit load that trial segment B can support

- M_1 = Positive yield moment
 - M_2 = Negative yield moment on short sides
 - M_3 = Negative yield moment on long sides
- A, B, a, b are identified in figure 6-10.

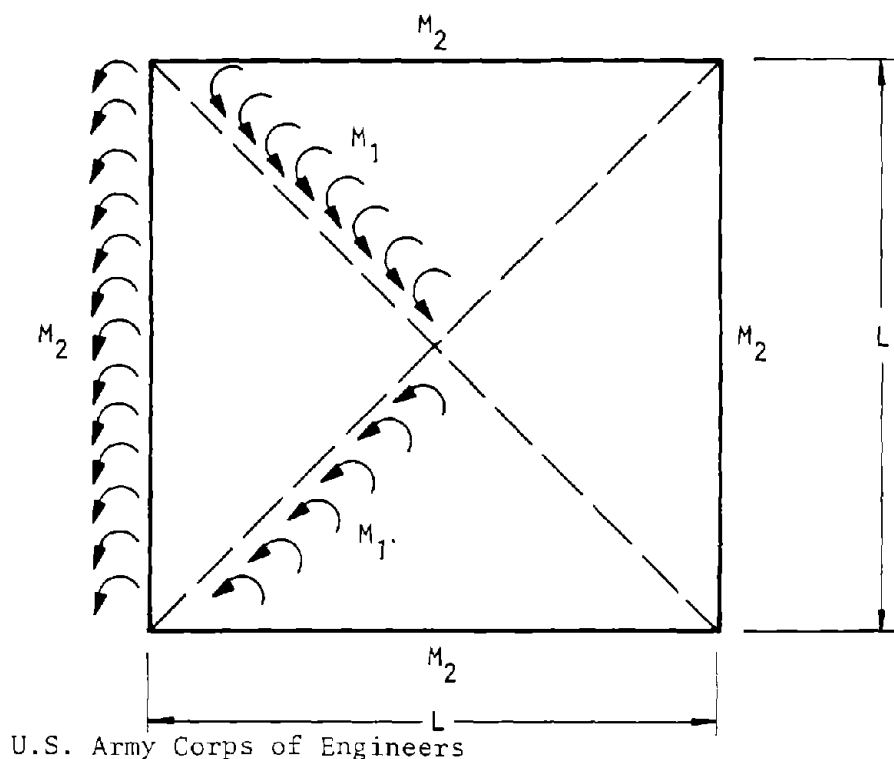


Figure 6-9. Yield Lines for a Square Slab

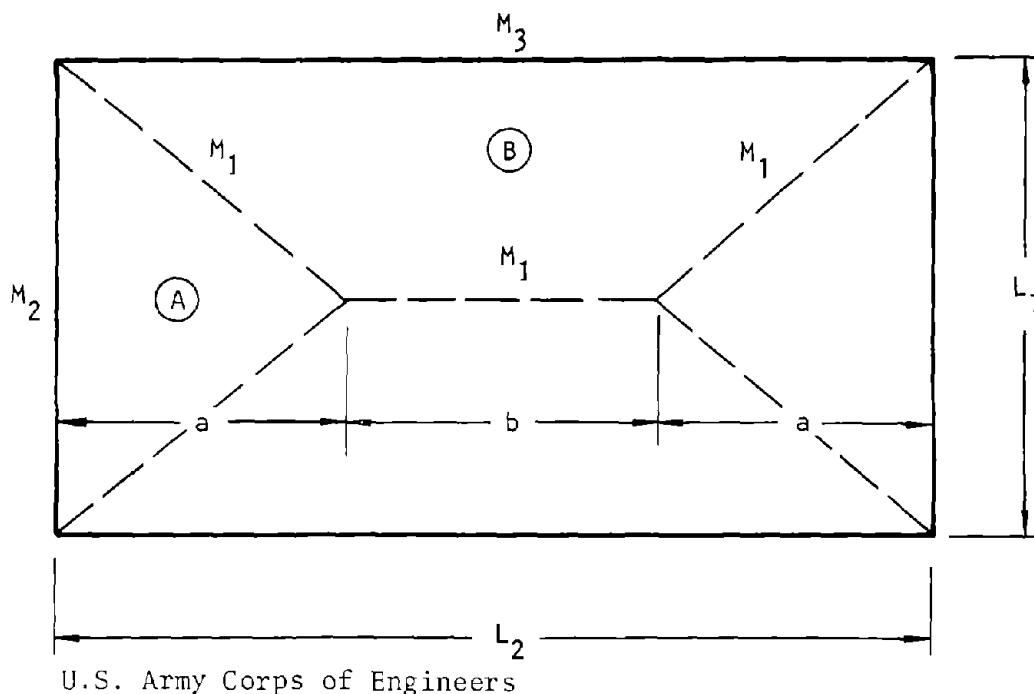


Figure 6-10. Yield Lines for a Rectangular Slab

c. *Strength of deep beams.* By definition, *deep beams* are beams with webs that are narrow and deep and the span to depth ratio is less than two or three. The conventional procedures used for design and analysis of normal reinforced concrete beams are not valid for determining the strength of deep beams. In the design of protective structures, especially above-ground construction, structural elements such as floor or roof slabs and walls are used to transmit lateral loads to the foundation. These slab and wall components are treated as deep beams and, depending on their orientation and function, are referred to as diaphragms (slabs) and structural walls (shear walls). They are usually stiffened and supported laterally along their edges by the intersecting floor, roof, and wall slabs. Portions of such intersecting slabs act as flanges to stiffen and strengthen the webs of the deep beams and should be so considered in the analysis of such beams. Under blast loading, deep beams are generally stressed by loads applied normal to their surfaces in addition to the deep beam loading. Because of their proportions both shear and moment stresses and strains must be included in determination of their strength and deformation. Procedures for design of deep beams acting as diaphragms or shear walls are described below. For a general discussion of the conventional, simply supported, and continuous deep beams and the reinforcing steel patterns recommended for various loading conditions, i.e., uniform concentrated, top or bottom application, etc., the reader is referred to standard textbooks (e.g. Park-Paulay, 1975) and available text reports on deep beams (e.g. Benjamin-Williams, 1957).

d. *Static shear loads.* Characteristic static load deflection curves obtained for structural walls are shown in figure 6-11. These curves were obtained from tests (Benjamin-Williams, 1957) of the structural walls of the type shown in figure 6-12. The walls are primarily shear-resisting elements. Tension and compression columns in the test represent the effect of the face walls or columns in a prototype structure, and normally resist axial loads induced by overturning reactions. The horizontal beam represents the effect of the roof slab. The wall panels were reinforced with equal percentages of vertical and horizontal steel bars uniformly distributed throughout the wall. Extra bars were placed in the columns and beam to simulate typical reinforcing for these elements. The structural wall deflection prior to the development of the initial tensile cracks is obtained by using simple bending and shear deformation equations. The deflection at first cracking, δ_c , for the cantilever shear wall shown in figure 6-12.

$$\delta_c = \frac{S_c H}{E_c} \left(\frac{H^2}{3I} + \frac{2.2}{LW} \right) \quad (6-37)$$

where the first term in the parentheses is a bending factor, the second term relates to shear, and where

S_c = Horizontal static load resistance of wall at first cracking

E_c = Modulus of elasticity of concrete

I = Moment of inertia about centroid of horizontal section through shear wall including frame but neglecting all reinforcement

L = Length of shear wall

W = Thickness of the shear wall

H = Height of shear wall

The shear wall deflection, δ_u , at which the ultimate resistance is reached is given by the relation:

$$\delta_u = 24 \left(\frac{H}{L} \right) \delta_c, \delta_u \geq \delta_c \quad (6-38)$$

When S_u is equal to or less than S_c , equation 6-38 has little significance. However, for all cases it is used as a design criterion to indicate the upper limit of deflection for which the shear wall may be designed. The above shear wall criteria are based upon tests in which the parameters were varied within the following limits:

- Column steel ratio 0.01 to 0.033
- Column steel adequately encased in concrete
- Concrete strength of 2000 to 4000 psi
- Length to height ratios of 0.9 to 3.0
- P/C ratios of 0 to 3.26 where C is the compression column influence factor computed as

$A_s f'_c \left[15 + 1.9 \left(\frac{L}{H} \right)^2 \right]$, lb and P is the panel strength taken as $f_{yp} t L$, lb

- f'_s of 42 to 52 ksi

- Shear wall steel ratios, $0 < a_s < 0.015$

e. *Dynamic shear loads.* Equations for structural wall capacity at first cracking of the concrete and at ultimate resistance are based on static tests. Dynamic capacities may be obtained by using dynamic strength values for the concrete and steel. The design equations are as follows: The horizontal dynamic load resistance of a shear wall at first cracking, S_{dc} , is given by

$$S_{dc} = 0.1 f'_c L W$$

where

f'_c = Ultimate concrete compressive strength

L = Wall panel length

W = Wall panel thickness

The horizontal ultimate dynamic resistance of a shear wall, S_{du} , is given by

$$\frac{S_{du}}{C_d} = \frac{0.1}{\frac{P_d}{C_d} + 0.1} + \frac{2.2 P_d}{C_d} \quad (6-39)$$

where

$$P_d = f_{ds} a_s W L$$

$$C_d = A'_s f'_c \left[15 + 1.9 \left(\frac{L}{H} \right)^2 \right]$$

f_{ds} = Dynamic yield strength of steel

a_s = Ratio of shear wall reinforcement in each direction (vertical and horizontal steel ratios are to be made equal)

A'_s = Area of column steel in compression side of wall

H = Wall panel height

The ratios C_d/S_{du} and P_d/S_{du} are plotted in figure 6-13 as functions of P_d/C_d . These values may be used in the design of the shear wall steel reinforcement and are obtained by using equation 6-32.

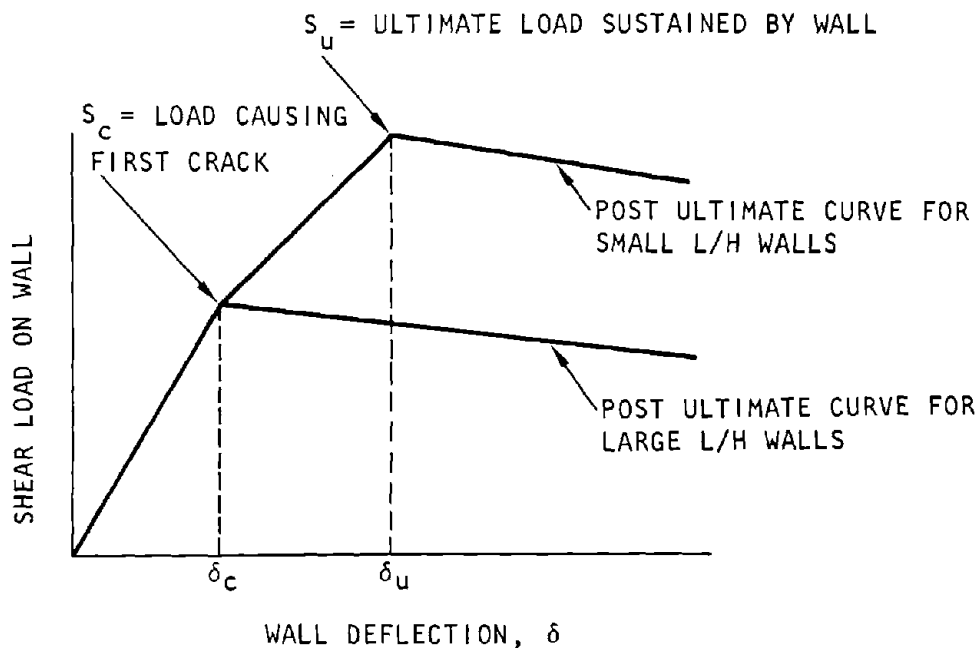


Figure 6-11. Characteristic Load-Deflection Curves for Structural Walls (COE, 1965)

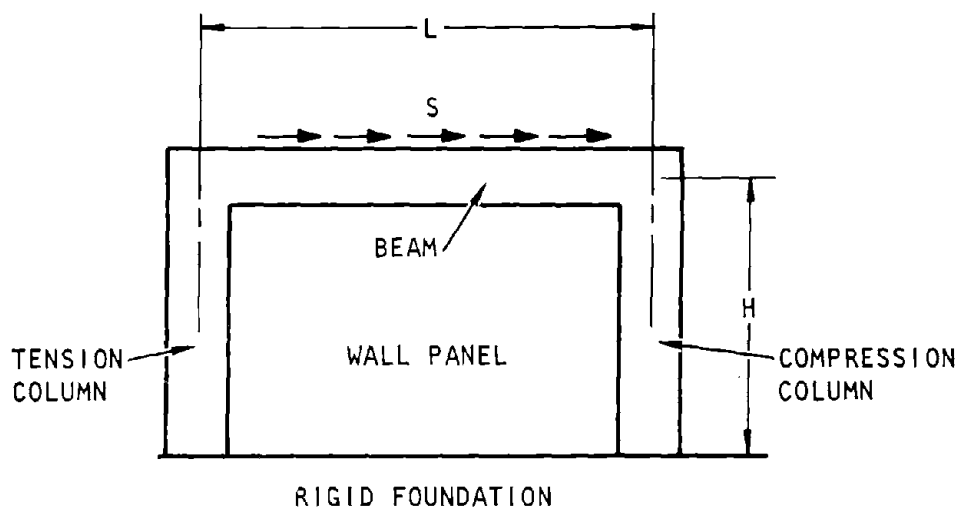


Figure 6-12. Structural Wall Test Model (COE, 1965)

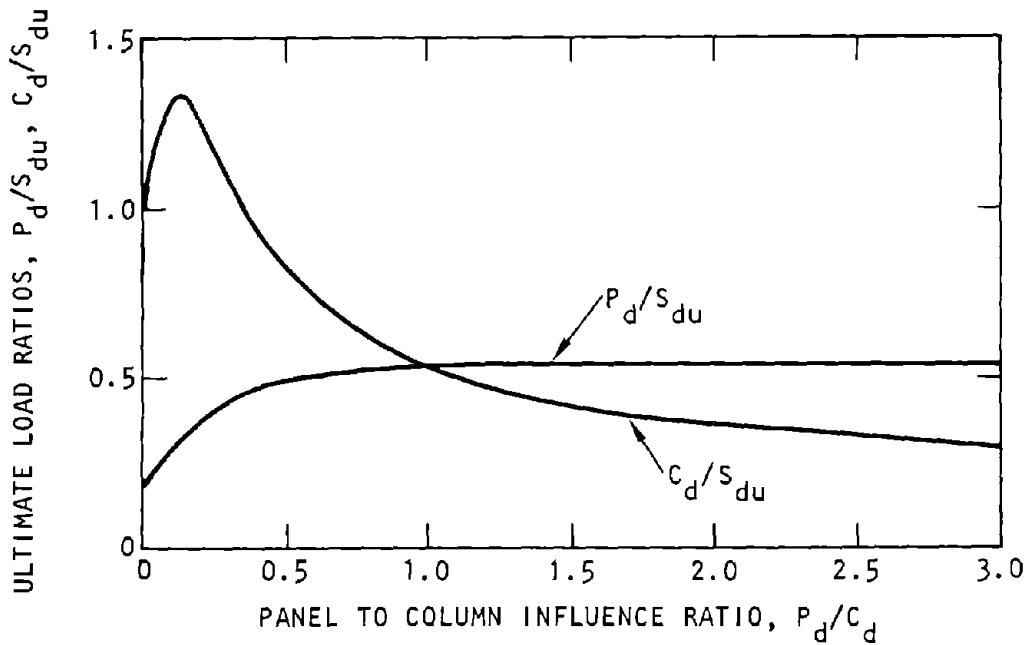


Figure 6-13. Dynamic Ultimate Load Ratios vs. Ratio of Panel Influence Factor to Column Influence Factor (COE, 1965)

f. *Combined shear and normal loads.* When structural walls are subjected to blast pressures normal to the plane of the wall at the same time that they are acting to resist shearing forces in the plane of the wall, the combined normal and shear load resistance at first cracking is defined by the straight line interaction equation

$$\frac{S'_c}{S_c} + \frac{N'_c}{N_c} \leq 1 \quad (6-40)$$

where

- S'_c = Applied shear load at first cracking under combined loading
 - S_c = Shear load resistance at first cracking with no normal load
 - N'_c = Total normal load at first cracking under combined loading
 - N_c = Total normal load resistance at first cracking with no shear load
- $$= \frac{0.1 f'_c L W^2}{6 H (0.07 - 0.04 \frac{H}{L})}$$
- L = Length of shear wall
 - H = Height of shear wall
 - W = Thickness of shear wall
 - f'_c = Static ultimate concrete compressive strength

The ultimate combined normal and shear load resistance is defined by the circular interaction equation

$$\left(\frac{S'_u}{S_u}\right)^2 + \left(\frac{N'_u}{N_u}\right)^2 \leq 1 \quad (6-41)$$

where

- S'_u = Ultimate applied shear load under combined loading
- S_u = Ultimate shear load resistance with no normal load
- N'_u = Normal load applied at yielding of reinforcement under combined loading
- N_u = Normal load resistance at yielding of reinforcement with no shear load

The value of N_u can be determined by use of the applicable equations for the bending strength of one- and two-way slabs. The wall deflection in the direction of the shear load under combined shear and normal load is not affected appreciably by the normal load and can be computed from equations 6-37 and 6-38.

g. *Structural walls with opening.* Structural walls that contain openings, such as those required for corridors and doorways, offer less resistance to shear loads than solid walls. These walls can be analyzed by treating them as a rigid frame, taking into consideration the deformations due to shear. The shear resistance of the portions of the wall between openings can then be determined by beam or deep-beam formulas depending on their dimensions.

6-8. Composite beam slabs

a. *Plastic bending strength.* Figure 6-14 shows a typical section through a concrete slab that is supported by steel beams and with shear connectors so designed that the beams and slab can be assumed to act together as a unit. Since the yielding of the steel beam controls the ductility, it is desirable that such yielding occur before the ultimate compressive capacity of the concrete slab is realized. The ultimate compressive strength of the concrete flange should,

therefore, be made at least twice the yield tensile strength of the steel beam. This will make the neutral plane of the composite beam lie within the concrete slab, and, if the concrete strength in tension is neglected, the ultimate stress distribution shown in figure 6-15 will be approached as plastic bending occurs. The plastic bending resistance is determined from

$$M_p = A f_{ds} \left(\frac{d}{2} + z \right) \quad (6-42)$$

where

$$z = W - \frac{A f_{ds}}{2 L f'_{dc}}$$

W = Thickness of concrete slab

H = Depth of steel beam

L = Width of concrete slab = spacing between beams, 1/2 the beam span, or the width of the steel beam flange + 8

times the thickness of the concrete slab, whichever is smallest

A = Area of steel beam

f_{ds} = Dynamic yield strength of structural steel beam

f'_{dc} = Dynamic compressive strength of concrete

The compressive strength of the total concrete flange and the tensile yield strength of the steel beam, assuming the dynamic strength values are developed under dynamic loading, are given by

$$\begin{aligned} C &= A_c f'_{dc} + A_s f_{ds} \\ T &= A f_{ds} \end{aligned} \quad (6-43)$$

where

A_c = Area of concrete slab

A_s = Area of reinforcing steel parallel to beam in width L

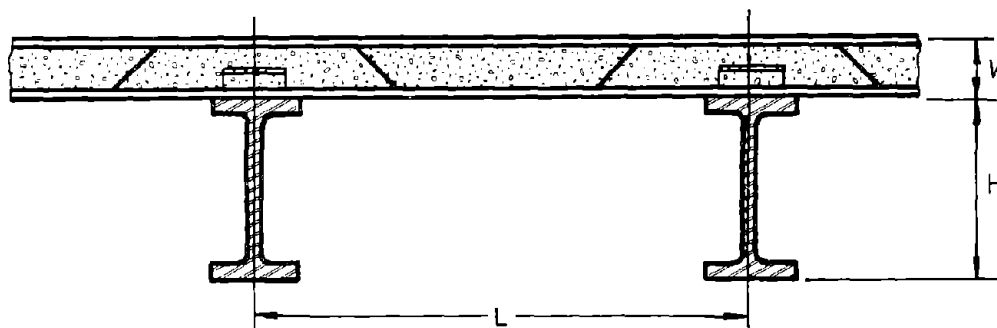


Figure 6-14. Composite Beam-Slab Section (COE, 1965)

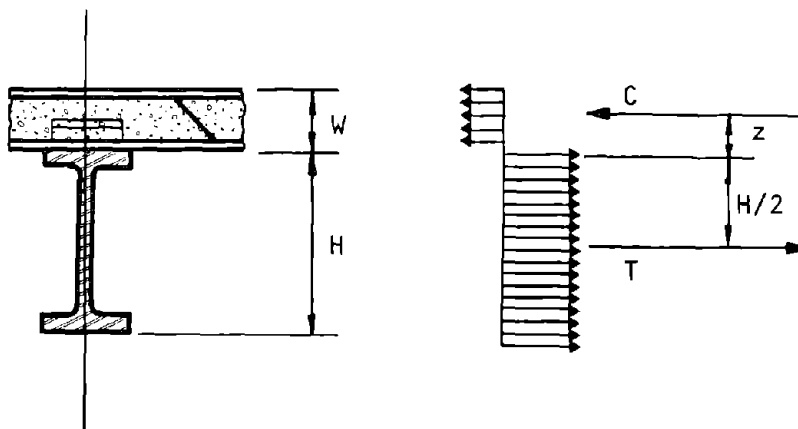


Figure 6-15. Plastic Stress Distribution in Composite Beam (COE, 1965)

b. *Strength of channel type shear connectors.* A channel type shear connector is illustrated in figure 6-16. The channel is rigidly welded to the top flange of the supporting wide-flange beam and the concrete transfers horizontal shear by pressure on the connector. The strength, Q , of such a shear connector developed during plastic distortion is (Viest et al.)

$$Q = \left(t_f + \frac{t_w}{2} \right) w \sqrt{f_{ds} f'_{dc}} \quad (6-44)$$

where

- w = Length of shear connector channel
- t_w = Web thickness of channel
- t_f = Maximum thickness of channel flange

The total number of shear connectors required between the points of zero and maximum moment is

$$n = \frac{A f_{ds}}{Q} \quad (6-45)$$

The required spacing of shear connectors is

$$s_c = Qd'/S \quad (6-46)$$

where

- S = Total shear at section considered
- d' = Distance between resultant tension and compression forces at section considered

Equation 6-46 is merely an alternate of equation 6-45 for obtaining the spacing of shear connectors. Equation 6-45 may be used to check the total number of connectors obtained by the use of equation 6-46. For purposes of calculating the required spacing of shear connectors, d' may be taken as $H/2 + 2W/3$. This approximation will give conservative spacing of shear connectors outside the region of plastic moment, but it is justified by the fact that exact computation of the moment arm is difficult because of the continuously changing stress distribution in the transition range between plastic and elastic sections. The spacing of the shear connectors will vary inversely in proportion to the vertical shear, S . For simply supported beams loaded at the center point, the shear is constant and therefore the spacing is constant. For uniformly loaded beams (fixed end or simply supported), the shear varies linearly and spacing of shear connectors along the beam is carried out exactly as in the design of stirrups in conventional reinforced concrete beam design. As shown in figure 6-16, the length, w , of a shear connector should not be more than the width of the beam minus 2 in. The height of the channel, d_c , should be greater than $W/2$ and also greater than $W - w/2$. The smallest channel section meeting these requirements will be the most economical section. It is recommended that for these shear connectors, the weld strength be taken as

60,000 psi times the throat area of the weld. The maximum shear stress intensity in the concrete on section a-a (fig. 6-16) is

$$v_m = \frac{\left(\frac{L - W}{L} \right) (A f_{ds}) \frac{S_m}{S_a}}{2 W L'} \quad (6-47)$$

where

- S_m = Maximum vertical shear in length, L'
- S_a = Average vertical shear in length, L'
- L' = Length between sections of zero and maximum moment being considered

This maximum shear stress must not exceed the allowable shear stress given by

$$v = 0.04 f'_c + (a_p + a_n) f_s$$

where

- a_p = Ratio of steel reinforcing placed parallel to the steel beam; A_s/LW
- a_n = Ratio of steel reinforcing placed perpendicular to the steel beam in excess of that required to carry the slab bending stresses
- f'_c = Static ultimate compression stress of concrete
- f_s = Yield stress of reinforcing steel

The concrete slab must be designed independently for bending and shear stresses resulting from its behavior as a slab or deep beam spanning between the steel beams.

6-9. Composite slabs with steel liners

a. *Introduction.* Structural slabs used as blast closures often consist of a steel plate overlaid with concrete and welded to a confining steel liner at the periphery of the concrete slab (fig. 6-17). Circular and rectangular shapes may be used. The steel plate provides bottom tensile reinforcing, electromagnetic radiation shielding, and protection against concrete spalling. The retaining ring provides an anchorage for the bottom plate (reinforcement), permits use of increased allowable concrete bearing and shear stresses because of confinement, and increases reliability of closure operation by prevention of spalls along the periphery of the closure.

b. *Ultimate load resistance of circular slabs.* Three equations relating closure material properties and dimensions to the maximum load-carrying capacity of the closure are presented below for flexure, shear, and bearing failure modes. The equations are based on the analyses of empirical relationships among test data combined with ultimate strength theory. Failure levels determined by these equations compare favorably with available test data (AA, 1977).

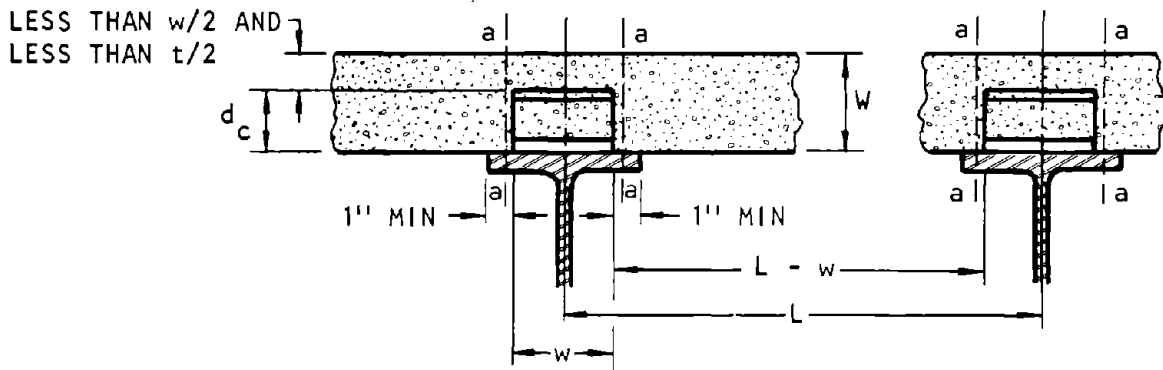
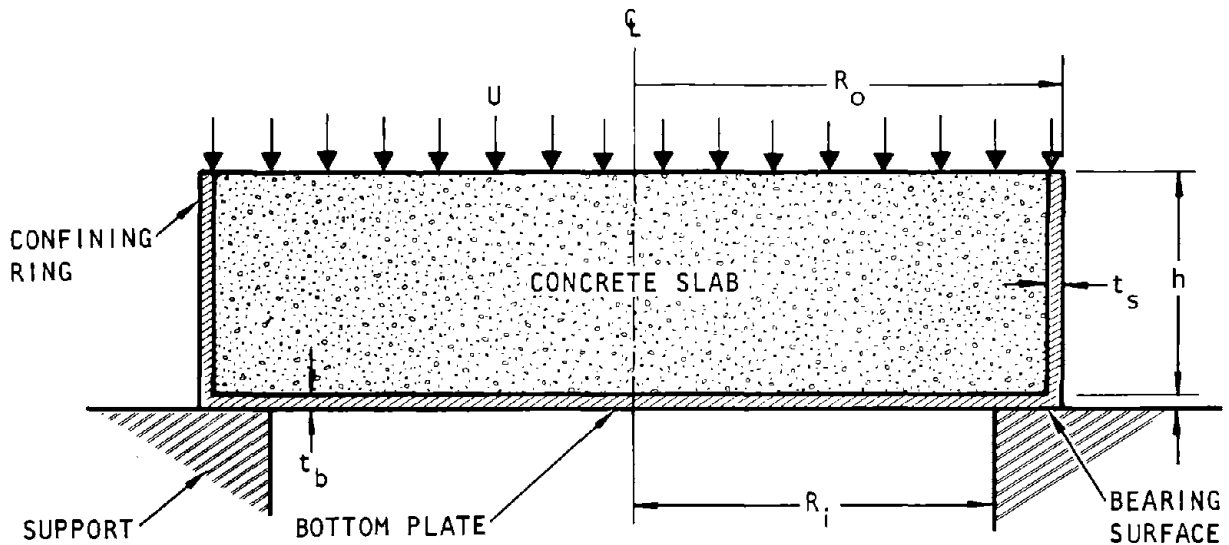


Figure 6-16. Dimensions of Channel Shear Connectors (COE, 1965)



U.S. Army Corps of Engineers

Figure 6-17. Composite Closure Configuration

c. *Flexural capacity.* The yield-line theory for ultimate strength design of concrete slabs is the basis for determining the flexural capacity of the composite closure design. However, the unique features of the concept also require consideration of the following factors when determining equilibrium forces acting on the slab segments:

- Confinement of concrete due to lateral forces imposed by periphery ring
- Influence of increased moment capacity due to horizontal thrust induced by friction at the support (bearing) area
- Effective span of closure as related to width of bearing surface

Based on the above considerations, Agbabian Associates (1977) derived the following quadratic equation for use in determining the flexural capacity, U , of a simply supported, circular, composite slab closure:

$$U^2 + \frac{4f'_c U}{\psi^2} \left[\frac{R'}{R} - \frac{2}{3} - \psi \left(\frac{h + (t_b/2)}{R} - \frac{P_1 + P_2}{f'_c} \right) \right]$$

$$- \frac{4f'_c{}^2}{\psi^2} \left[2 \left(\frac{h + (t_b/2)}{R} \right) \left(\frac{P_1 + P_2}{f'_c} \right) - \left(\frac{P_1 + P_2}{f'_c} \right)^2 - \frac{2e}{R} \frac{P_1}{f'_c} \right] = 0 \quad (6-48)$$

where

U = Ultimate uniform unit loading

$$P_1 = \begin{cases} \frac{t_s h f_s}{R^2} & \text{for thin ring } \left(t_s \leq \frac{R_o}{32} \right) \\ \frac{t_s h f_s}{4R^2} & \text{for thick ring } \left(t_s > \frac{R_o}{32} \right) \end{cases}$$

$$e = \begin{cases} \frac{h}{2} & \text{for thin ring} \\ \frac{h}{6} & \text{for thick ring} \end{cases}$$

$$P_2 = \frac{t_b f_s}{R}$$

- f'_c = Compressive strength of concrete
- ψ = Coefficient of friction at bearing surface
- R' = Radial distance from C_L to bearing reaction*
- R_o = Radial distance from C_L to outside surface of confining ring
- R = $R_o - t_s$
- h = Depth of concrete
- t_s = Thickness of steel confining ring
- t_b = Thickness of steel bottom plate
- f_s = Yield strength of steel

Equation 6-48 is based on the ultimate static load to which no safety factor has been applied. Appropriate enhancement factors may be applied to f'_c and f_s (para. 5-3c).

d. Limitation of flexural equation. When the forces contributing to lateral compression in the concrete at the periphery of the slab become large, the depth of the compression zone may exceed the depth of the slab. When this occurs, the limits of equation 6-48 are exceeded and the flexural capacity, U , of the composite closure should be computed by the following equation.

$$U \leq \frac{2}{\psi R} \left[f'_c (h - t_b) - \frac{f_s t_s h}{R} - f_s t_b \right] \quad (6-49)$$

e. Shear capacity. The ultimate shear capacity of a composite closure is governed by the shear strength and cross-section of the concrete slab as well as the influence of frictional forces at the bearing area and confining pressure from the steel ring. Based on the shear failure criterion given in the Air Force Manual for Design and Analysis of Hardened Structures, Crawford et al. (1974), and on work by Plamondon (1968) and Crist and Vaugh (1968), the ultimate shear capacity, U , of a composite closure slab can be taken as

$$U = 1.5 f_s \left(\frac{t_b}{R_i} \right) + 30 \sqrt{f'_c} \left(\frac{h}{R_i} \right) + 3 f_s \left(\frac{t_s}{R_i} \right) \left(\frac{h}{R_i} \right) \quad (6-50)$$

where

U = Ultimate uniform unit shear load

f. Bearing capacity. The bearing failure of a closure slab is characterized by the crushing of concrete above the bearing region. Agbabian Associates (1977) suggests a method for evaluating the bearing resistance of a composite closure design that considers the confining pressure imposed by the peripheral steel liner,

the shear strength of the concrete, the shear resistance of the steel bottom plate, and the friction between the uncrushed concrete slab and the steel confining ring. Utilizing this approach, the bearing capacity, U , of a circular composite closure is given by

$$U = f'_c \left\{ k \left(\frac{R_i}{R_o} \right) \left(\frac{t_b}{R_o} \right) + \frac{R^2 - R_i^2}{R_o^2} \left[1 + k \frac{t_s}{R} \tan^2 \left(45^\circ + \frac{\phi}{2} \right) \right] + 2 \psi_s k \frac{t_s}{R_o} \left[h - b \tan \left(45^\circ + \frac{\phi}{2} \right) \right] \right\} \quad (6-51)$$

where

- U = Ultimate uniform unit bearing load
- k = f_y/f'_c
- ψ = Coefficient of friction between the concrete and the steel ring (normally assumed as 0.6)
- b = $R = R_i$
- ϕ = Angle of internal friction of concrete. If not available from Mohr diagram, use $\phi \approx 40.0 (f'_c)^{0.13}$

g. Applicability of ultimate load resistance equations. The influence of confining stresses imposed by the periphery ring and the in-plane loads imposed at the closure edge attenuates as the span to depth ratio increases. It is recommended that the use of the equations for determining ultimate flexural, shear, and bearing capacity be limited to closures with span to depth ratios ≤ 6 . For ratios > 6 , the closures should be treated as two-way slabs.

6-10. Fiber-reinforced concrete

a. As in other structural materials, the strength of fiber-reinforced concrete can be defined in terms of an elastic limit stress (also called the first crack strength) and the ultimate strength. Fiber content, fiber geometry, and the distribution of the fibers have significant effects on the properties of fiber reinforced concrete, and the designer must select the actual properties he requires, then determine if a mix can be designed to satisfy those requirements. Publications of the American Concrete Institute (e.g., ACI, 1973 and 1974) provide guidelines, bounds on expected increase in strength, as well as detailed mechanical properties.

b. The load-deflection diagram of a fiber-reinforced concrete specimen loaded in flexure exhibits linearity up to the proportional (elastic) limit or point of first cracking. The load deflection curve beyond this point is nonlinear up to the maximum load, which defines the ultimate strength.

* R' may be assumed equal to R_i for very rigid supports. The resultant reaction force will vary from the edge ($R' = R_i$) to the center of the support ($R' = (R_i + R_o)/2$) as the stiffness of the support varies from rigid to very flexible.

c. One theory concerning the first crack strength of fiber-reinforced concrete states that material properties can be predicted from the individual properties of the matrix and the fibers. Up to the proportional limit, both the plain concrete and the fibers behave elastically. Increasing the volume of fibers increases the proportional limit approximately linearly. Researchers have observed that the effect of fibers on the first crack strength of concrete reinforced with up to 4% by volume and subjected to flexure, tension, or compression is small and linear. An approximation of the influence of fibers on the elastic properties of the composite concrete-fiber specimen can be estimated by

$$E_r = E_f V_f + E_c V_c$$

where E_r , E_f , and E_c are the moduli of elasticity for the composite, the fibers, and the concrete, respectively. V_f and V_c are the volume fractions of fiber and concrete. The equation is valid for composites with continuous fibers, elastic behavior of the materials, and no slippage between fibers and matrix. This relationship gives upper bound values because, due to possible debonding of the fibers, microcracking may occur before the proportional limit is reached. The theory discussed above is based on the assumption that the proportional limit depends on volume, orientation, and aspect ratio of the fibers.

d. The maximum loads, as indicated by the nonlinear load-deflection curve, is controlled primarily by fibers gradually pulling out and the stress of

the fiber. The decrease in load after ultimate is reached is much less for fiber reinforced concrete than for plain concrete and the total energy absorbed before complete failure is at least an order of magnitude higher. This provides a significant increase in ductility or toughness when compared to conventional concrete design. Up to an aspect ratio of 150, a linear relationship exists between aspect ratio and strength (aspect ratio is the fiber length divided by the equivalent diameter or thickness of the fiber). Based on this relationship, an expression for the ultimate strength is

$$f_r = C f_c V_c + F V_f L/D$$

where f_r and f_c are the stress values of the fiber-reinforced composite and the concrete matrix, respectively; L and D are length and diameter or thickness of the fiber; and C and F are constants that have to be obtained from test data for various types of fibers. The maximum value of C is unity and constant F depends on the bond strength between fibers and the matrix and on the randomness of the fibers.

e. Until more definitive data based on tests and field experience becomes available, any increase in strength resulting from the addition of fibers to the mix can be neglected during the design phase. The structures can be designed as if they were constructed from conventional reinforced concrete and any additional strength provided by the fibers can be utilized during the hardness verification phase of the program.

CHAPTER 7 NONDETERIORATING DESIGN DETAILS

7-1. Introduction

a. Protective construction incorporates special nondeteriorating design details in order to resist multiple attacks. These attacks may be sequenced from a multiple warhead with the arrival-time phasing of airblast and ground shock measured in milliseconds, or from several warheads delivered at intervals of seconds, minutes, or days. The combined effects of airblast and ground shock will depend on the phasing and direction of the loads and motions and on the location of the structural element within the parent system. If lateral loading is the predominating effect, the structural element may experience complete reversal of deformation due to the relative locations of structure and points of detonation (ground zero).

b. The structural elements must withstand repeated loading without jeopardizing PMMP. The principal objective is to develop the required ductility at connections in order to assure nondeteriorating behavior of structural elements. This section will emphasize considerations and procedures for designing connections. The design procedures are adapted primarily from cyclic loading tests performed to increase the data base for earthquake engineering. It is therefore necessary to use the appropriate provisions of earthquake-resistant design in order to avoid stiffness and strength degradation that would make a protective structure vulnerable to subsequent attacks.

7-2. Multiple loading of steel members

a. *Introduction.* Inelastic action occurs mostly at the joints of a structure since they are frequently located

at points of maximum shear and moment. In beam-to-column connections, inelastic behavior should be confined to the beam. Columns should remain elastic, except very short columns that can be allowed to yield without being loaded into the range of instability. Develop design details using equivalent static loads such that, at ultimate load, equilibrium conditions are satisfied within the assumptions of plastic behavior of the material.

b. *Welded and bolted connections.* The following guidelines have been substantiated by tests:

- Welds: Butt welds can develop the tensile yield stress of the parent metal on their minimum throat section and should be used for beam-column connections unless circumstances requiring use of fillet welds and/or bolted connections.
- Bolts: Bolted joints designed as moment connections should develop the full bending strength of the member.

c. *Types of connections.* Five types of connections were tested under cyclic loads (Popov-Pinkney, 1968). These are shown in figures 7-1 to 7-4. Under 5 cycles each at nominal $\pm 1/2$ percent controlled strain increments (approximately ± 1 in. of tip deflection) where there was no deflection due to workmanship, no significant deterioration was noted at loads that stressed the connection to the elastic limit. One specimen was subjected to 100 cycles with a tip deflection of about 2.6 times its maximum elastic deflection without showing significant deterioration. Loads of greater severity caused various failures: flange buckling, cracking in the plate at the end of the weld, or cracking in the flange at the outermost bolt line.

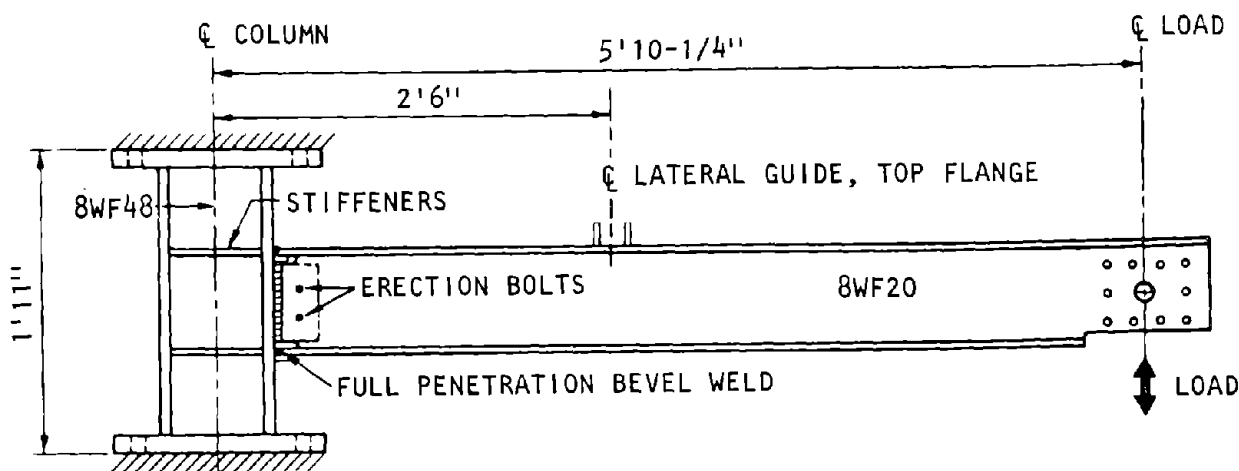


Figure 7-1. Beam-Column Connection, Type I, Detail Showing Test Device (Popov-Pinkney, 1968)

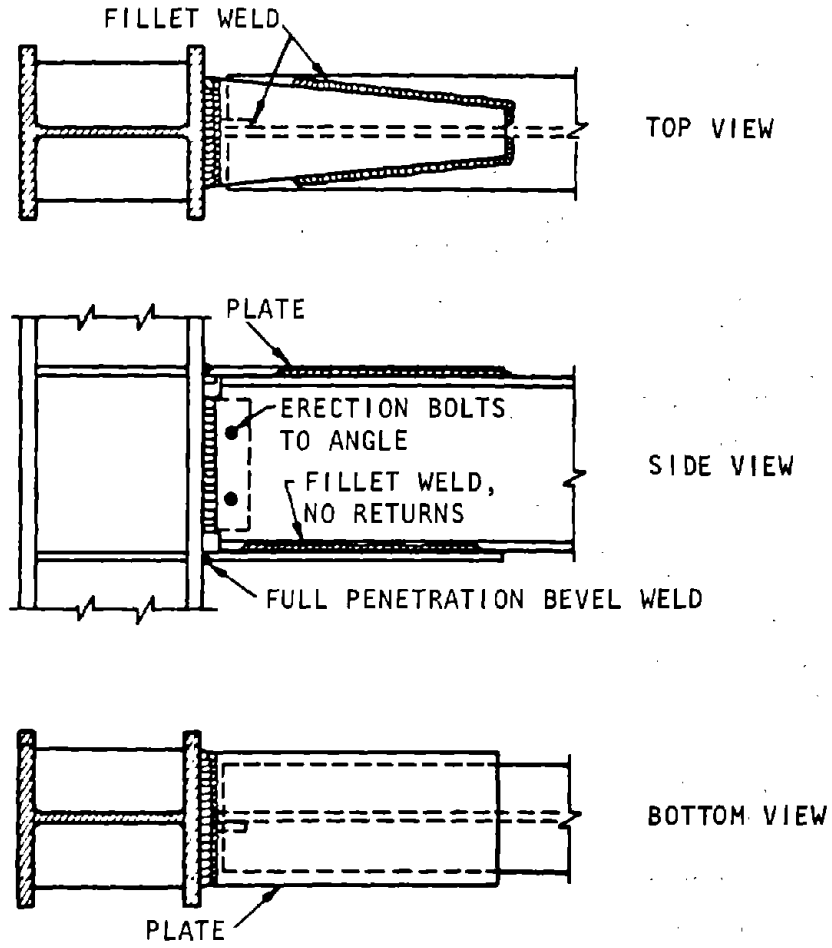


Figure 7-2. Alternative Beam-Column Connection, Type II (Popov-Pinkney, 1968)

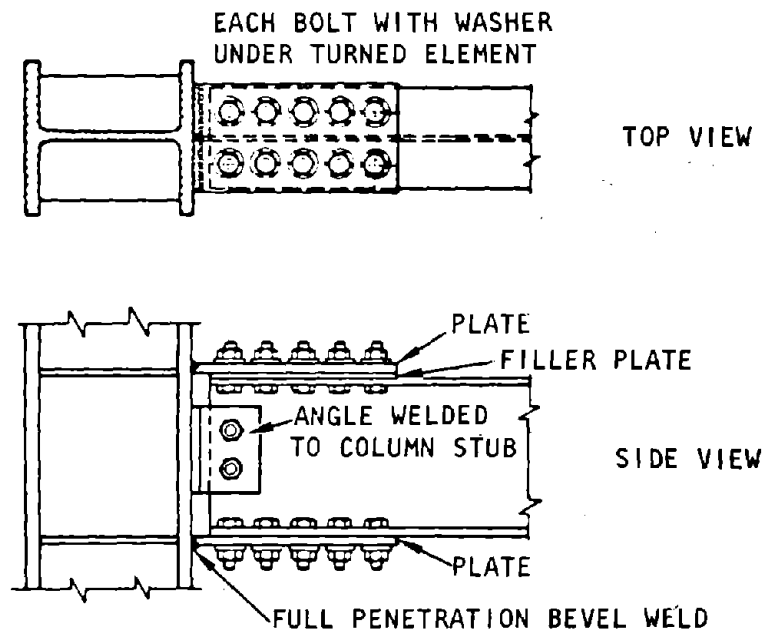


Figure 7-3. Alternative Beam-Column Connection, Type III (Popov-Pinkney, 1968)

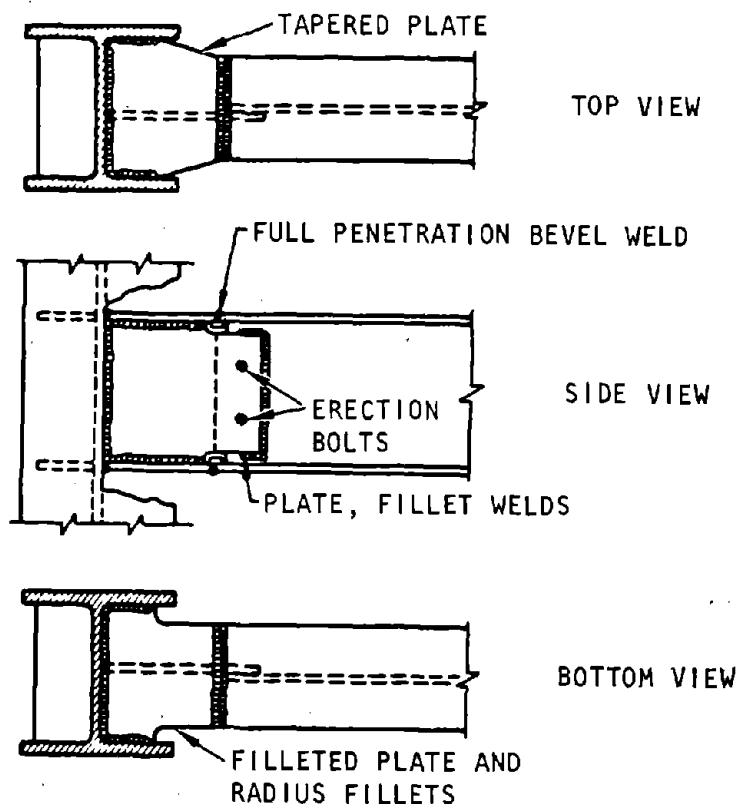


Figure 7-4. Alternative Beam-Column Connection, Type V (Popov-Pinkney, 1968)

d. *Load/deflection relationships.* When designing for multiple loading, take into account the hysteretic properties of the connection of the steel members. An equation based on the Ramberg-Osgood relationship defines the loading and unloading branches of the load-deflection diagram.

$$\frac{\delta}{\delta_p} = \frac{P}{P_p} \left[1 + \alpha \left| \frac{P}{P_p} \right|^{\kappa-1} \right] \quad (7-1)$$

where P and δ are load and deflection, P_p is the plastic load, and δ_p is the deflection at $P = P_p$. The α and κ are experimentally determined numbers. Average values for α and κ are 0.5 and 8, respectively.

e. *Hysteretic cycles.* Data for multiple loading may be obtained from cyclic tests or approximations based on cyclic tests. Unloading and reloading develop hysteretic cycles, shown in figure 7-5, that may be fitted by a curve of the Ramberg-Osgood form:

$$\frac{\delta - \delta_i}{\delta_p} = \frac{1}{\beta} \frac{P - P_i}{P_p} \left[1 + \alpha \left| \frac{P - P_i}{2P_p} \right|^{\kappa-1} \right] \quad (7-2)$$

where the subscript i refers to the point of last load reversal and β is the ratio of the slope of the unloading curve to the slope of the initial loading curve ($\beta = 1$ in most cases).

f. *Ductility factor.* The ductility factor μ has been defined as the ratio of total deformation to elastic deformation at yield. In multiple loading, this is not a cumulative damage indicator unless the recoverable deformation between loadings is accounted for. The residual plastic deformations of previous loadings, plus the deformation of the final loading, should be taken as the value of ductility that describes the ductile behavior of a multiple-loaded structural element. In figure 7-6, it is seen that the ductility ratios μ_1 , μ_2 , and μ_3 depend on the loading/unloading history.

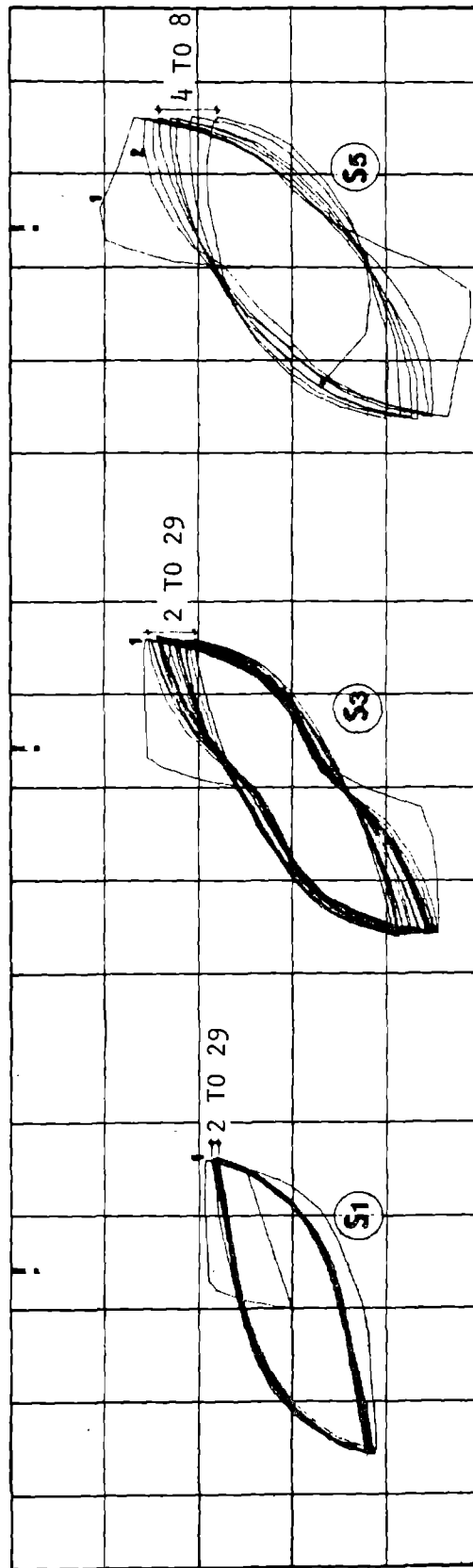


Figure 7-5. Flexural Hysteresis Loops for Reinforced Concrete (Parducci-Ferretti, 1973)

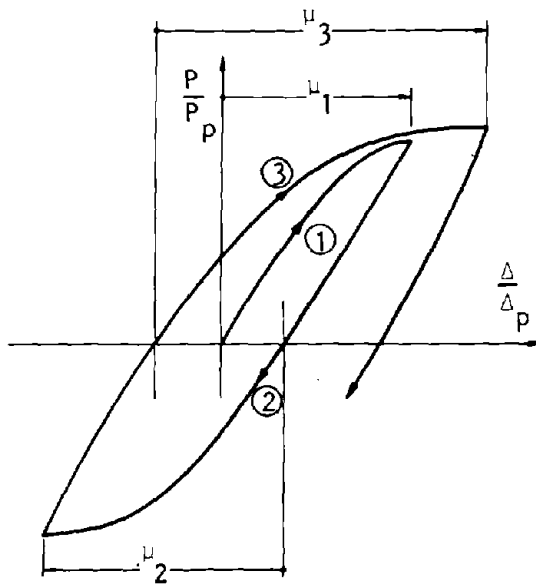


Figure 7-6. Definition of Ductility Factor μ (Popov-Pinkney, 1968)

7-3. Guidelines for connection details

a. *Introduction.* Suggested details (ASCE, 1961) will ensure that local buckling is prevented while the plastic moment capacity of the connection is developed under the applied loads. They are based on experimental data and engineering practice. For more detailed information, refer to ASCE 41 (1961) and AISC (1969, supp.). Presented below are guidelines and equations for designing connections between beams and column flanges, and for corners and haunches and different conformations.

b. *Unstiffened columns.* Column stiffeners are not needed adjacent to the beam compression flanges if

$$t_c \geq \frac{A_f}{t_f + 5 h_w} \tag{7-3}$$

where

- t_c = Column web thickness
- A_f = Area of one beam flange
- t_f = Beam flange thickness
- h_w = Column fillet depth, distance from flange face to end of fillet

Column stiffeners are not needed adjacent to the beam tension flanges if

$$t_c \geq 0.4 \sqrt{A_f} \tag{7-4}$$

where t_c = Column flange thickness

c. *Column stiffeners.* Column stiffeners at points of bearing of beam flanges should be proportioned to carry the excess of beam flange force over that which the column web and flange are able to carry. (Stiffeners should also be so proportioned that they do not buckle.)

d. *Shear stiffening in columns.* When unbalanced moments or external forces cause shear stresses in excess of the column web capacity, stiffening should be provided for the column. Such stiffening may take the form of diagonal stiffeners or web doubler plates.

e. *Straight corner connections.*

(1) *Web thickness required.*

$$t = \frac{\sqrt{3} M_p}{f_s H_p H_c} \tag{7-5}$$

where

- t = Required web thickness at beam column junction
- M_p = Plastic moment
- f_s = Yield stress
- H_b = Beam depth
- H_c = Column depth

(2) *Web stiffening.* If the web of a connection is too thin, it may be reinforced by doubler plates, or by diagonal stiffeners welded to the flanges and to the web. The area of a symmetrical pair of diagonal stiffeners should be

$$A_d = \frac{1}{\cos \theta} \left[\frac{M_p}{f_s H_b} - \frac{t_s H_c}{\sqrt{3}} \right] \tag{7-6}$$

in which

- θ = $\text{Tan}^{-1} (H_b/H_c)$, angle of diagonal stiffeners
- M_p = Plastic moment
- t_s = Stiffener thickness

f. *Taper haunches.* (1) *Lateral buckling.* The critical unbraced length of a compression flange that may be strained to the point of strain-hardening throughout its entire length without premature lateral buckling is conservatively estimated as:

$$L_c = 5.3 W \tag{7-7}$$

where W = Flange width

The critical unbraced length of a compression flange may be increased substantially by increasing the angle of taper or by increasing the thickness of the flanges.

(2) *Diagonal web stiffeners.* To resist an imbalance of inner flange forces and reinforce the web against undue shear deformation, a symmetrical pair of diagonal stiffeners may be provided having a total area:

$$A_d = \frac{A_r \cos(\Phi_r + \gamma) - A_c \sin \Phi_c}{\cos \theta} \tag{7-8}$$

where

- A_r = Area of inner flange of rafter haunch
- A_c = Area of inner flange of column haunch
- Φ_r = Angle of taper of rafter haunch
- Φ_c = Angle of taper of column haunch
- γ = Angle of inclination of rafter
- θ = Angle of slope of diagonal stiffener

Diagonal stiffeners should be welded to the web and to both flanges.

(3) *Transverse stiffeners.* Transverse stiffeners at the junctions of the tapered haunch and prismatic section serve to carry any imbalance of the inner flange force due to the sudden change in direction. Minimum size requirements will usually govern the thickness.

g. *Curves haunches.*

(1) *Required plastic modulus.* The plastic modulus at any point in the haunch must be adequate to resist the applied moment at that point. The web of the haunch should not be thinner than the web of the beam. The thickness of flange required to provide an adequate plastic modulus is given by

$$t_f = \frac{h_x - \sqrt{h_x^2 \frac{W}{W - t_s} - \frac{4 M_x}{f_s (W - t_s)}}}{2} \quad (7-9)$$

where

- h_x = Depth of haunch at section "x"
- M_x = Moment at section "x"

The depth of launch at section "x" is given by $h_x = H_b + 0.022 R$.

(2) *Lateral buckling.* The critical unbraced length of a curved compression flange strained to the point of strain-hardening without premature lateral buckling is conservatively estimated as

$$L_c = R\phi = 5.3 W \quad (7-10)$$

where ϕ = Central angle of curved flange ($45^\circ - \gamma/2$)
The critical unbraced length of a compression flange may be increased by increasing the thickness of the flanges.

(3) *Cross bending.* Cross bending occurs when radial components of the force in the curved flanges tend to bend the flange edges toward the web. The effect of cross bending on connection behavior will be negligible if

$$\frac{W^2}{2 R t_x} \leq 1 \quad (7-11)$$

(4) *Diagonal web stiffeners.* To reinforce the web against buckling due to radial compression in the curved inner flange, a symmetrical pair of diagonal stiffeners may be provided having a total area

$$A_d = 2 A_c \sin \left(22.5^\circ - \frac{\gamma}{4} \right) \quad (7-12)$$

where

- A_c = Area of inner flange
- γ = Angle of inclination of beam from horizontal

7-4. Multiple loading of reinforced-concrete members

a. *Introduction.* Stiffness and strength degradation in reinforced-concrete beams are a direct result of the cracking of the concrete and the subsequent yielding of the steel. Flexural cracks cause an instantaneous drop in the beam stiffness. Diagonal tension cracks further decrease the stiffness. Load reversals beyond the load level at which the diagonal tension cracks occurred have produced in experiments a set of diagonal cracks crossing the first set at approximately right angles. A yield plateau is then reached when the tension reinforcement starts to yield.

b. *Design considerations.* Flexural members with low shear exhibit high ductilities under load reversals, provided the compression reinforcement does not buckle. Since yielding of the tension reinforcement across cracks keeps these cracks open, the flexural capacity at high ductility depends on the state of stress in the steel. If cracks have developed on both sides of the neutral axis because of stress reversal, consider only the steel in obtaining the moment capacity of the cracked section. Use the formula

$$M_u = A_s f_s (d - d'); \text{ when } A_s = A'_s \quad (7-13)$$

where

- M_u = Moment capacity
- A_s = Area of rebar in tension
- A'_s = Area of rebar in compression
- f_s = Yield strength of reinforcing bars
- d = Distance from compression surface of concrete to centroid of tension reinforcement
- d' = Distance from compression surface of concrete to centroid of compression reinforcement

(1) Under multiple loading conditions, when the structural element has experienced load reversals, the shear resistance drops significantly. The shear capacity under these conditions may be significantly less than the ultimate shear capacity, s_u , taken as the total of the shear carried by the concrete and the shear resisted by web reinforcement. In order to avoid this deterioration in shear resisting capacity, increase the web reinforcement (number and size of stirrups) at critical sections where diagonal tension cracking is expected under load reversal.

(2) The effect of shear on stiffness degradation of flexural members is another factor to consider during multiple loading. Shear deformation further decreases both the loading and unloading stiffnesses of the member, which can be interpreted by evaluating the inelastic state of stress of the reinforced concrete member. The two general categories of inelastic behavior are stable and unstable.

(3) In the first category, hysteresis loops of plastic hinges are relatively stable with repeated loading (Parducci-Ferretti, 1973). These hysteresis loops demonstrate nearly uniform energy dissipation and load-carrying capacity from one load cycle to the next (fig. 7-5). Inelastic behavior can be accurately represented by steel yielding alternately in tension and compression.

(4) In the second category, plastic hinges are significantly affected by shear, resulting in unstable hysteresis loops that exhibit significant deterioration in stiffness and energy dissipation from one inelastic load cycle to the next (fig. 7-7). Loading for these members, carried across shear or diagonal tension cracks, produces crushing or grinding of the concrete from one load cycle to the next. This deteriorating behavior can be significantly reduced by placing reinforcing steel at angles across plastic hinges that have high shear during peak loading (figs. 7-8 and 7-9). This diagonal reinforcing steel, sometimes called "lacing," carries the shear load in tension or compression and eliminates the unrestrained movement across the diagonal shear cracks, causing concrete deterioration (Paulay, 1973; Popov et al., 1972). Instead of the concrete deteriorating, the steel bars yield; since steel yielding in tension and compression produces almost no deterioration, the resulting hysteretic behavior is relatively stable.

c. Design of reinforcing details. The reinforcing details required to produce flexural hysteretic behavior for beam-column connections, shear walls, and deep beams are given below. Particular attention should be given to secondary effects produced by these details, which can have an adverse effect on the inelastic response of the member.

d. Interior connections. At interior connections, with beams framing into the column on opposite faces, ultimate lateral loading usually produces yield moments in the same direction in beams (columns) on opposite faces of the column (beam). This loading condition produces tension yield stress in the reinforcing bar at one face of the column at the same instant that compression yield stress is developed in the same bar at the opposite column face. Very early in the inelastic history of the connection, bond fails around the longitudinal beam bar that is anchored in the column. In order to minimize the effect of bond failure in the anchored beam steel, the steel should be crossed as it goes through the column (fig. 7-10). With the beam

steel crossed in the column, the ultimate loads produced by lateral loading will tension the bottom steel of the left beam at the same time that the top steel of the right beam is tensioned to yield. Even if complete bond failure occurs around the crossed steel, yield stress will be developed in the longitudinal steel without movement of the bar. Constructing the connection on the diagonal as shown in figure 7-10 provides inelastic steel anchorage that is not affected by bond failure or concrete deterioration. The resulting hysteresis loops should be relatively stable with little change from one inelastic cycle to the next.

(2) Shear that the beam must carry near the column face will be increased. Since the top beam steel, which is bent down at the column face, and the bottom steel are stressed so that one is tensioned while the other is compressed, the shear force is additive. This additional shear, which is equal to $\sqrt{2} A_s' f_s$ for steel placed as shown in figure 7-10, should be carried by additional hoops in the beam near the column face with a total area equal to $\sqrt{2} A_s'$.

(3) The concrete on the inside face of the bent bar will be crushed. Excessive crushing can be avoided by considering the forces that are illustrated in figure 7-11. The total strength of concrete on the inside of the bend is equal to $0.85 f_c' \ell_b D$. This must exceed the steel bar force that is equal to $2A_b f_y \cos(90 - \theta/2)$, giving the equation:

$$\ell_b \geq 1.85 D \frac{f_s}{f_c'} \cos(90 - \theta/2) \tag{7-15}$$

where

- A_b = Rebar section area
- D = Rebar diameter
- f_c' = Concrete compressive strength
- ℓ_b = Required length for bend in rebar
- θ = Bend angle for diagonal rebar
- f_y = Yield strength of rebar

e. Secondary effects. Bending the beam steel diagonally through the column produces three secondary structural problems that must be considered in designing the connection and the beam.

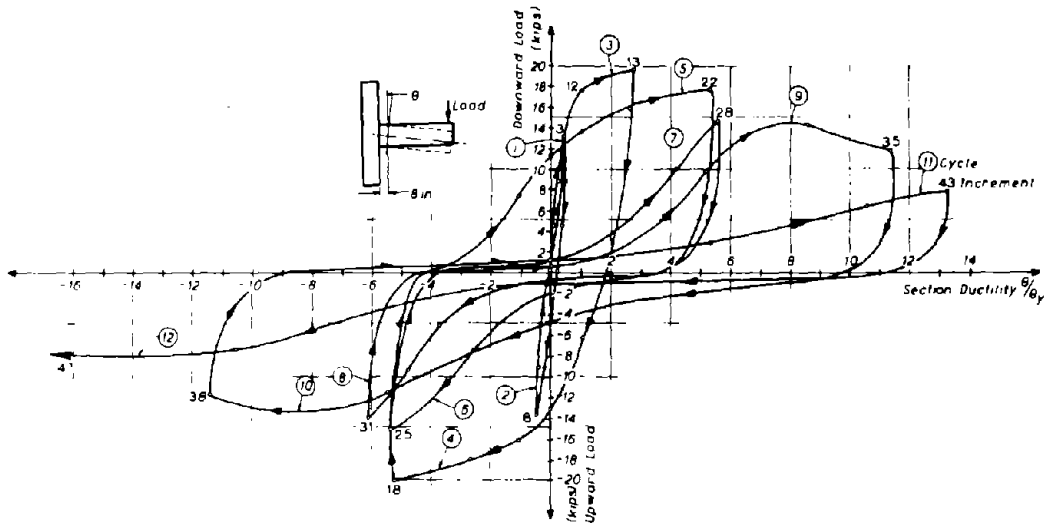
(1) If the column is narrower than the effective beam depth, the moment capacity will be reduced by:

$$\Delta M = \left(1 - \frac{\sqrt{2}}{2}\right) A_s' f_s (d - h/2) \tag{7-14}$$

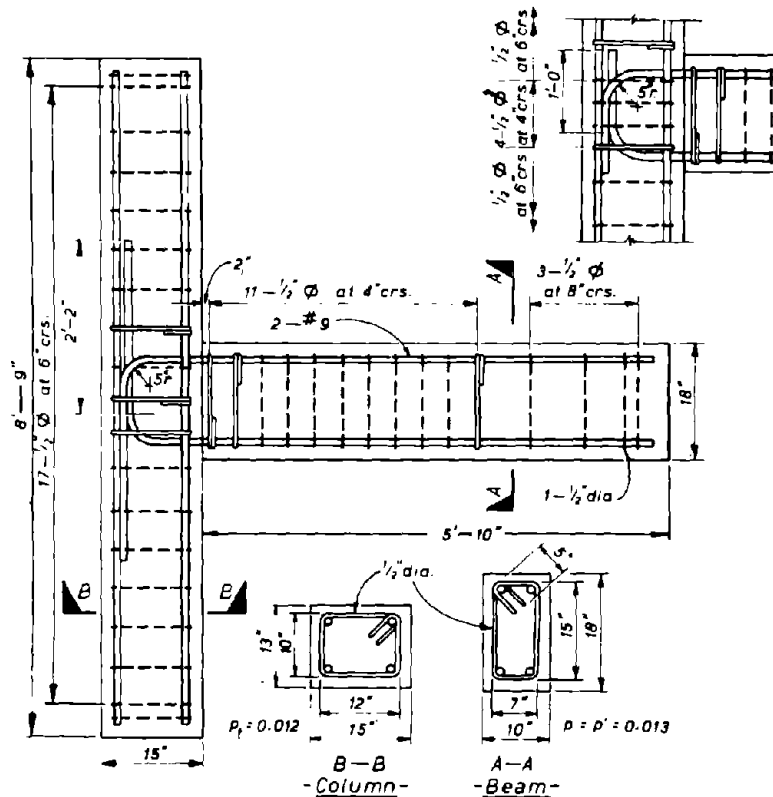
where

- ΔM = Reduction in moment capacity
- A_s' = Area of rebar in compression
- h = Depth of equivalent rectangular compression stress block
- d = Distance from compression surface of concrete to centroid of tension reinforcement

for each beam. (The change in moment arm should be small and can probably be ignored.)

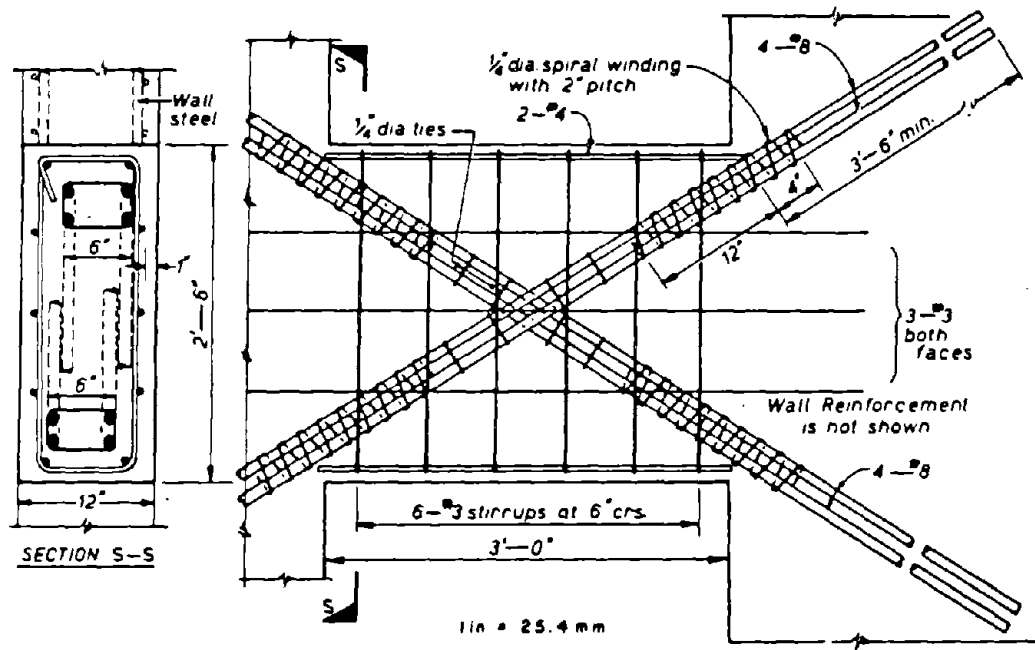


(a) Applied load vs. beam section ductility

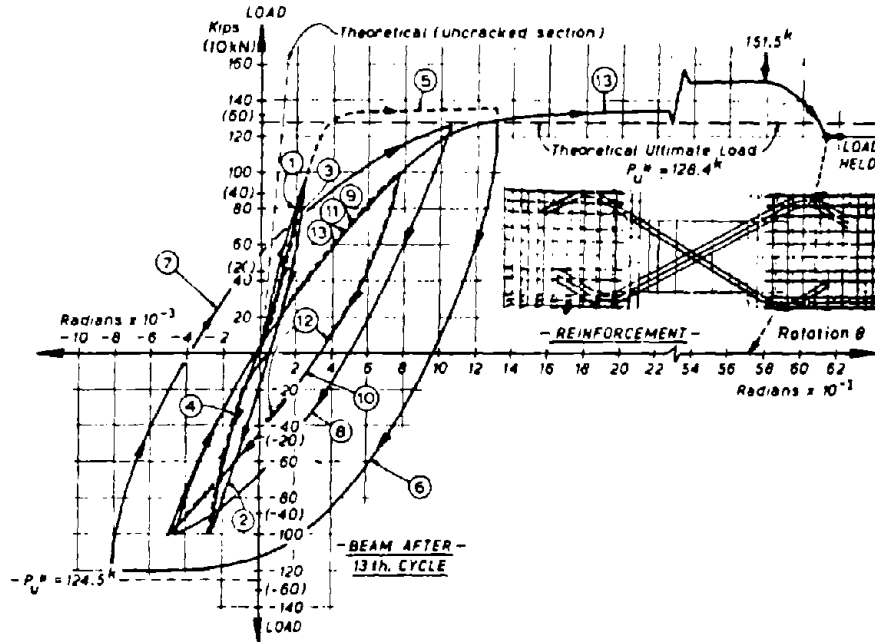


(b) Details of test units of Series 1

Figure 7-7. Shear Hysteresis Loops for Reinforced Concrete

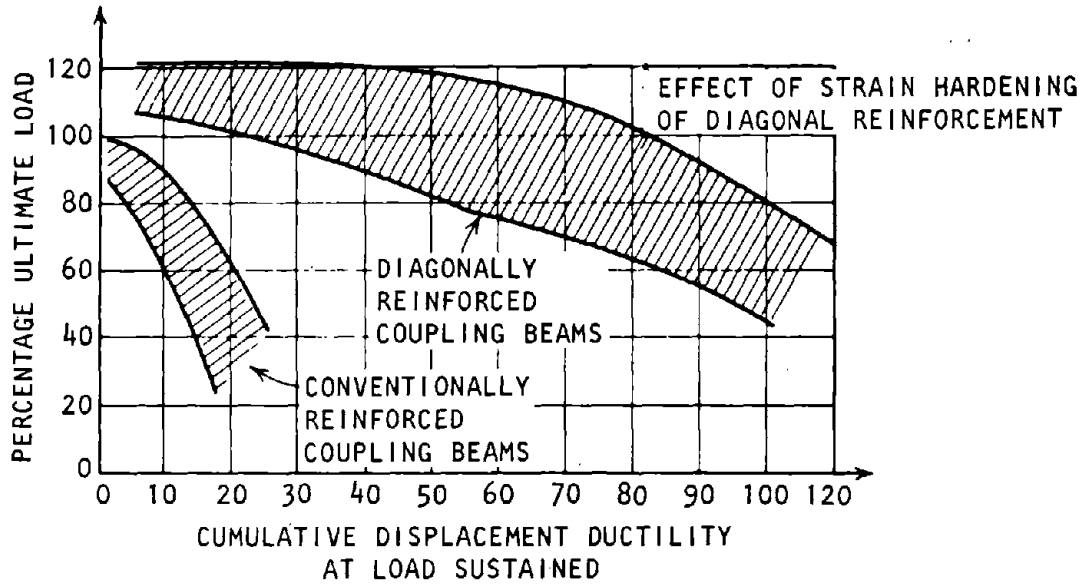


(a) Diagonally reinforced coupling beam



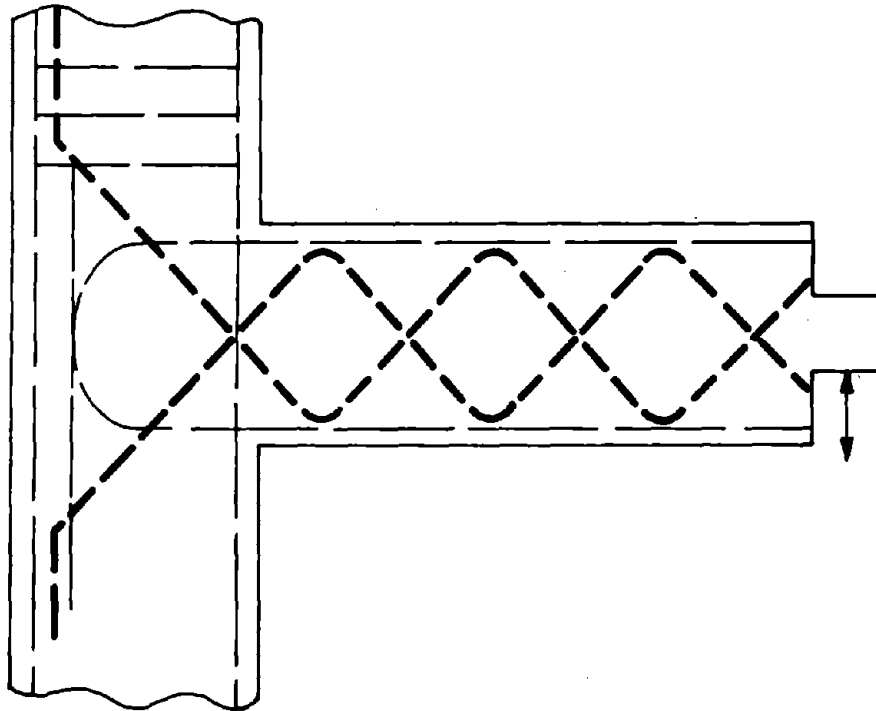
(b) Typical load rotation relationship for diagonally reinforced coupling beams

Figure 7-8. Diagonal Reinforcing for Plastic Hinges (Paulay, 1973)



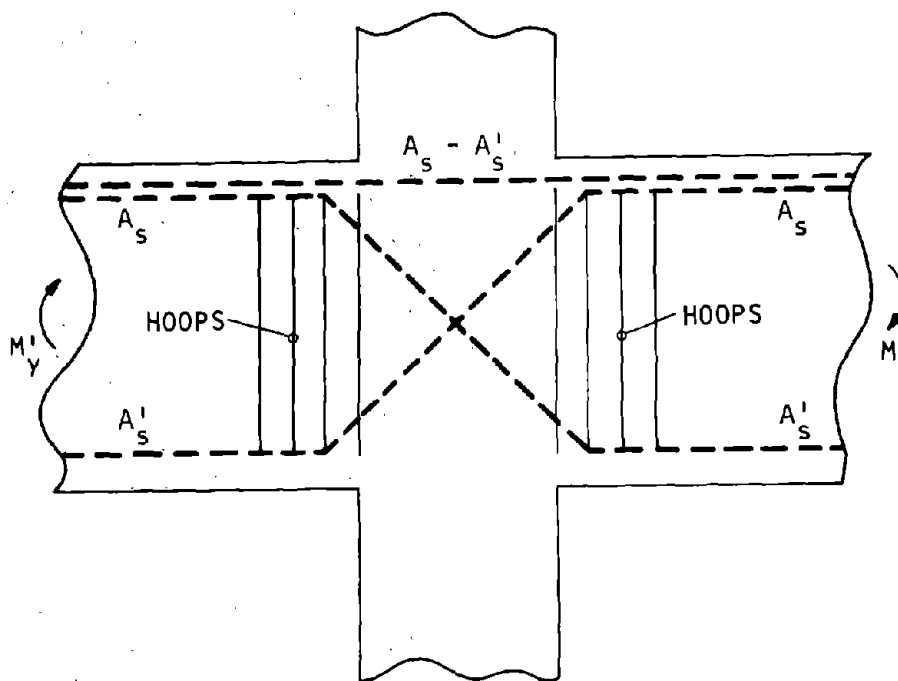
- (c) The range of cumulative ductilities sustained at observed load levels in deep coupling beams

Figure 7-8. (Concluded)



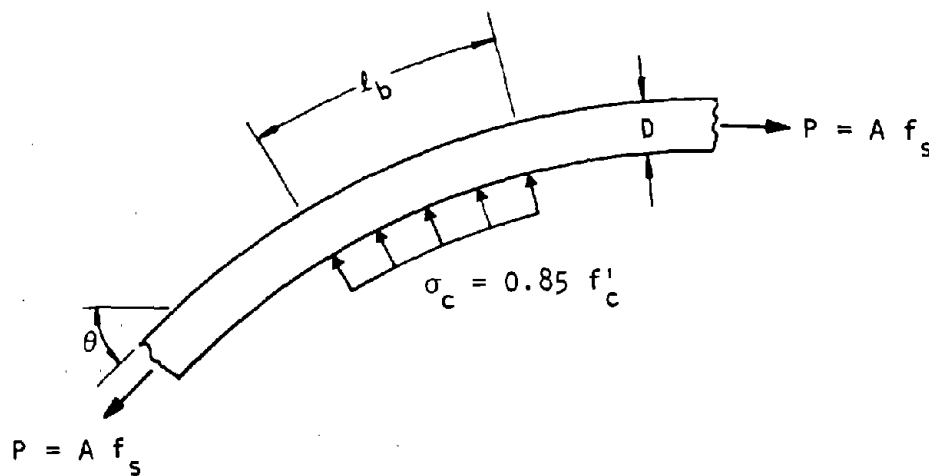
U.S. Army Corps of Engineers

Figure 7-9. Experimental Deep Beam with Additional Diagonal Reinforcement to Carry Shear



U.S. Army Corps of Engineers

Figure 7-10. Interior Connection with Diagonal Longitudinal Steel and Hoops for Additional Web Shear



U.S. Army Corps of Engineers

Figure 7-11. Concrete Crushing inside Curved Bar

If the concrete resistance is not adequate to resist the yielded steel bar, then l_b can be increased by increasing the radius of curvature for the bent bar, or stirrups can be used to help anchor the bent bar.

f. External connections. The second kind of connection that normally produces shear hysteresis loops because of concrete deterioration is the external connection made from one beam framing into an exterior column that extends to an upper story. Unlike interior connections, exterior connections do not have structural symmetry that can be used to provide mechanical anchorage for the longitudinal beam steel. Therefore, in constructing this kind of exterior

connection for inelastic loading, additional steel ΔA should be provided (fig. 7-12). Since the additional steel ΔA is on a diagonal, it is efficient for carrying internal forces across diagonal tension cracks. This steel will reduce movement across shear cracks, thereby reducing concrete deterioration. If the steel area ΔA is made equal to A'_s , the tensile stress in the bottom steel at ultimate positive moment will be reduced to $1/2 f_s$ and the top tensile stress at the ultimate negative moment will be reduced to $2/3 f_s$. Reducing the steel stress at the column face will force the plastic hinge away from the column into the beam where flexural hysteretic behavior can be expected.

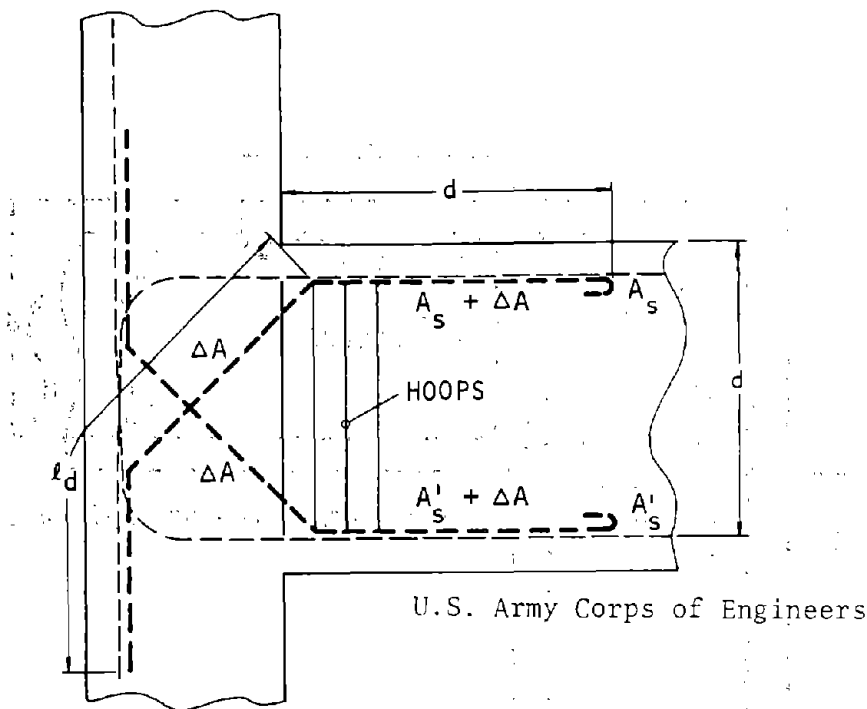


Figure 7-12. Exterior Connection with Additional Diagonal Steel and Hoops for Additional Web Shear

g. Secondary effects. The diagonal steel ΔA produces a higher ultimate moment capacity in the beam at the column face. This increased moment capacity must be considered in designing web reinforcement for the beam and in designing the column load capacity. Use equation 7-13, but reduce the stress from yield stress for exterior connections. To anchor the diagonal steel in the column, the required anchorage length (ℓ_d), measured from the column face, is computed in the same manner as the anchorage for the longitudinal beam steel. Anchorage of diagonal steel ΔA in the beam is a more difficult problem because the hinge will form adjacent to the terminated steel. This hinge location will cause concrete cracking that can reduce the effective anchorage. A solution to this problem is to anchor the steel in the beam at distance d and then terminate it with a standard hook.

h. L-shaped connections. A third kind of connection that produces the shear type of hysteretic behavior is the L-shaped connection made of one beam and one column. This corner connection also lacks structural symmetry and requires special mechanical anchorage in the region of plastic hinging. As with exterior T-shaped connections, diagonal steel should be used to force hinging away from the connection. The primary steel added to this connection is labeled ΔA in figure 7-13. If the diagonal steel ΔA has an area equal to the top beam steel A_s , then the longitudinal steel stress at the column face will be reduced to $f_y/2$ and the hinge will move from the column face into the beam.

i. Secondary effects. The increased yield moment capacity, increased beam shear at the column face,

and anchorage of diagonal steel ΔA are treated the same as for exterior T-shaped connections. An additional secondary design problem concerns positive moments that yield the bottom beam steel in tension. Because of the geometry of the connection, there is little chance for the concrete at the column face, in the region of the lower beam face, to carry the load developed by the yielding of the longitudinal steel in the beam. In this case, hoops labeled (B) in figure 7-14 should be provided at an angle of 45 deg with a total area of $\sqrt{2} A_s$.

j. Shear walls. Shear walls that are constructed in the traditional manner with longitudinal and lateral reinforcing steel respond to inelastic loading with a shear type of hysteretic loops. This hysteretic behavior can be changed to flexural hysteretic loops by placing the steel diagonally as shown in figure 7-8a. The forces that are produced by lateral loading are shown in figure 7-14. The shear wall is analyzed as a statically determinant structure with tension (T) and compression (C) equal to $2\sqrt{C}$ for a square shear wall, where S is the shear force. The total diagonal steel area is computed by dividing $2\sqrt{S}$ by the yield stress of steel and using half of the diagonal steel in each direction. In order for the diagonal compression steel to act as a column, the steel should be confined to respond as a ductile column. The details of anchoring both tension and compression diagonal steel are important because of the large forces involved.

k. Deep beams. Deep beams that are reinforced in the traditional manner with lateral and longitudinal steel respond to inelastic loading in a brittle manner with shear type hysteretic loops. This hysteretic

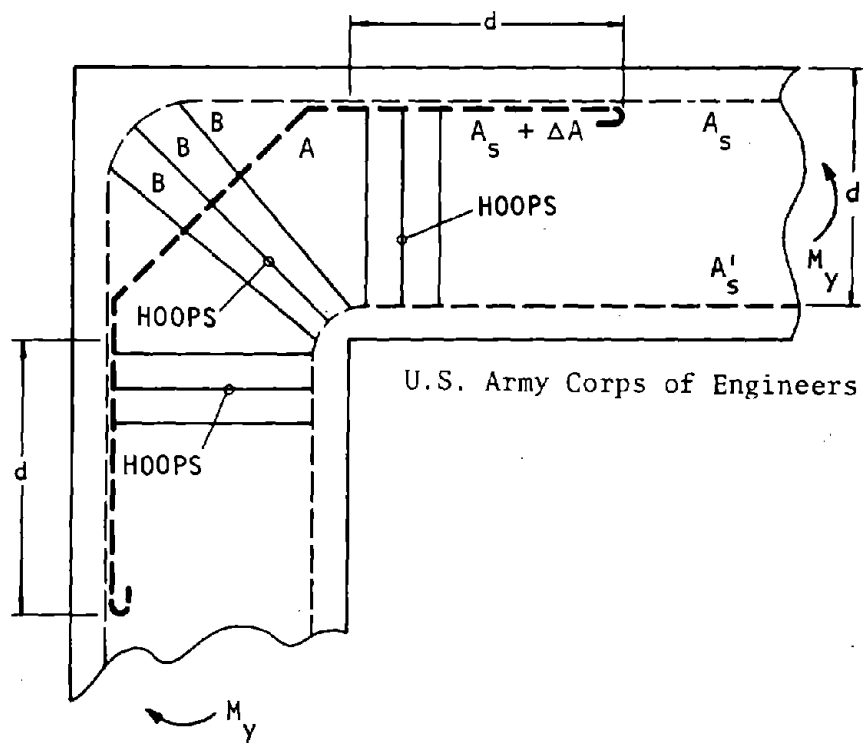
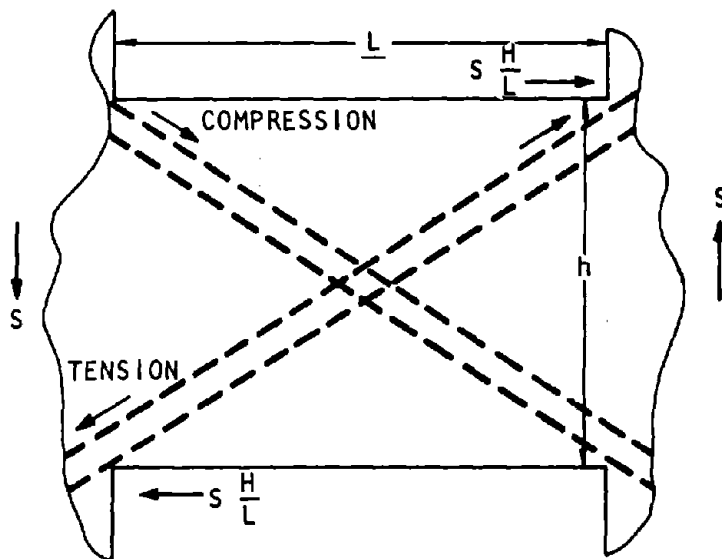


Figure 7-13. L-Shaped (Corner) Connection with Additional Diagonal Steel and Hoops

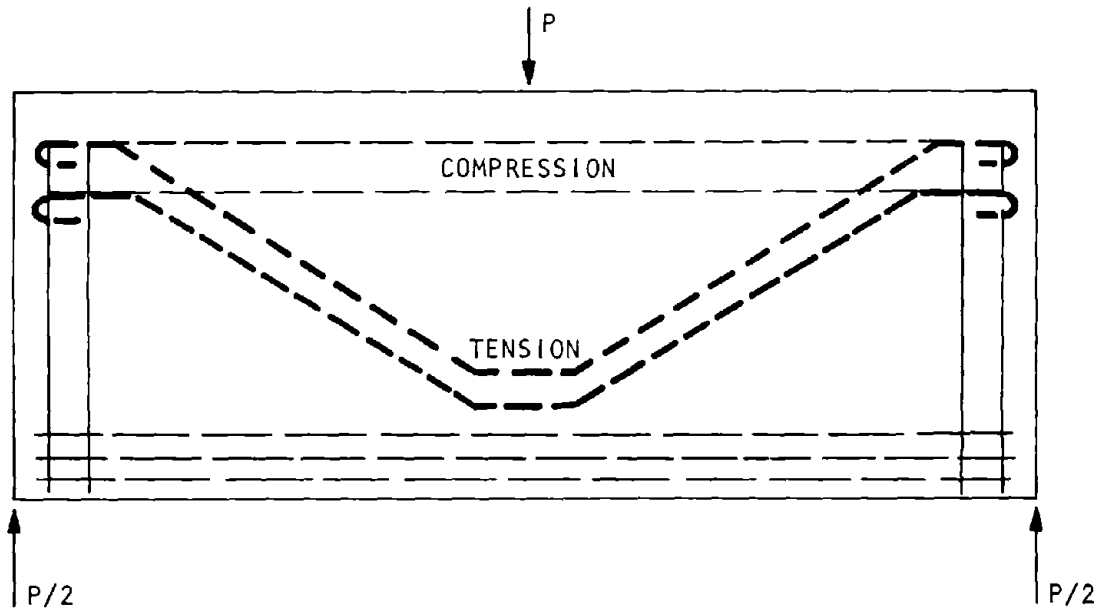


Forces used in designing shear wall
U.S. Army Corps of Engineers

Figure 7-14. Shear Wall Design for Protective Structures

behavior can be changed to flexural hysteresis loops by placing steel diagonally across shear and diagonal tension cracks (fig. 7-14). If the deep beam is constructed, as shown in figure 7-15, with diagonal steel in tension placed at 30 deg, then the total inelastic load in the steel will be equal to P, the applied external concentrated load. If the external load can be applied in the reversed direction, then diagonal steel should also be provided rotated 180 deg about the longitudinal axis.

l. *Secondary effects.* Adequate anchorage of the tension steel at the end of the beam should be provided. A ductile compression zone at the top of the beam adequate to carry $\sqrt{3/2}$ P load compression must also be provided. Collapse at ultimate load is likely to occur by lateral instability of the compression zone, making lateral support of this region a desirable condition.



U.S. Army Corps of Engineers

Figure 7-15. Diagonal Reinforcement for Deep Beam

CHAPTER 8

DYNAMIC STRUCTURAL ANALYSIS

8-1. Introduction

a. When designing structures to resist dynamic loads, approximation procedures are used. The design is validated by refined analyses. The refined analyses reduce the design uncertainties, demonstrate the sensitivity of the design to the various parameters, and provide directions for design modifications that improve structure performance. This approach allows for early decisions on the size and configuration of structural elements, in synthesizing the total structure, and in assuring compatibility with functional performance. The validation by refined analyses generally results in some design modifications that account for parameters overlooked in the approximation analyses. However, a well-executed design developed by approximation procedures seldom requires a basic change in design concept as a result of the refined analyses. This chapter discusses the approximation procedures to be used in the design process. These procedures apply equally to single loading as well as to multiple loading. Validation analyses are covered in chapter 9.

8-2. Reduction to a system with a few degrees of freedom

a. Impulsive loads, few modes. Structures possess many degrees of freedom. Structural elements, such as beams and slabs, having distributed mass, vibrate in an infinite number of modes. The participation of each mode depends on the load distribution along the member as well as the time variation of the load relative to the normal periods of vibration of the different modes. The periods of vibration depend on the stiffness, mass distribution, and support conditions of the element. The distortion of the structural element depends on the combined effect of the load and the modal shapes. In most structures subjected to impulsive loads, the excitation of only a few modes predominates. For approximation design procedure, a single mode may sometimes be considered sufficient to define the behavior of the structure. Such simplification, that is, expressing the structure response in terms of a single-degree-of-freedom (motion in one coordinate direction), is accepted design practice.

b. Single-degree-of-freedom methods. These simplified and rapid procedures determine the relationships among the peak dynamic force applied to a structure or structural element, the resistance of the element, and the ratio of the maximum deflection of the element to the yield deflection. Response charts of such relationships for both elastic and elastoplastic

systems are available. The charts usually assume undamped systems subjected to triangular or step pulse shapes with zero or finite rise times. Transformation factors have been developed that reduce many common structural elements to an *equivalent* single-degree-of-freedom system. The loading, mass, resistance, and stiffness of the real structure are multiplied by the corresponding transformation factors to obtain these parameters for the equivalent single-degree-of-freedom system.

c. Multi-degree-of-freedom methods. When it is necessary to represent a physical structure in its true spatial distribution of mass, stiffness, and strength and to excite the model through transient loadings to determine its response, a multi-degree-of-freedom analysis will be required. The structure is represented by a mathematical model consisting of either a series of springs and lumped masses, or by finite elements that divide the structure into subelements that in their assembled configuration represent the stiffness and mass properties of the modeled structure. The advantage of the finite element technique is direct readout of member stresses and motions. When spring/lumped-mass models are used, the gross motion of the structure is computed directly, but member stresses must then be computed by additional analyses.

d. Dynamic reactions. The approximations used in obtaining an equivalent single-degree-of-freedom system are generally good for one parameter; however, large errors may be introduced in obtaining other parameters. Equal displacement for the structural element and the corresponding single-degree-of-freedom system yields good results for bending moments but shear forces and dynamic reactions are not in acceptable agreement. In the single-degree-of-freedom system, the support reaction is always equal to the force in the spring. In the actual element, the distribution of the applied load and the inertial force along the element affect the dynamic reactions and the shear forces. To obtain dynamic reactions and shear forces, the actual element must be analyzed (chap. 9).

8-3. Resistance function and spring constant

a. Function of deflection. In the elastic range, the resistance of an element is a function of its displacement, $R = k\delta$, where k is the spring constant and is equal to the force required to cause a unit deflection, and δ is the deflection.

b. Types of resistance/deflection relationships. As an element is deflected by application of force, the

resistance/deflection relationship is altered. The simplest relationship is described by two ranges, elastic and plastic (fig. 8-1a). In other types of load and support conditions, more than two strain ranges are required to define the variation of R (fig. 8-1b). (A more general relationship is given by the Ramberg-Osgood equations, paragraphs 6-1d and 7-2d.)

c. *Equivalent spring constant.* With $R = k\delta$ and with equal displacements for both the equivalent system and the actual element, the equivalent spring constant is

$$k_E = K_R k = K_L k$$

where K_R and K_L are defined as resistance and load factors. They are equal because the support reaction in a single-degree-of-freedom system always equals the force in the spring.

8-4. Dynamic design factors

Dynamic design factors for equivalent single-degree-of-freedom systems are available based on resistance/deflection relations given in figure 8-2. The factors tabulated in tables 8-1 through 8-6 are

- K_L = Load factor
- K_M = Mass factor
- K_{LM} = Load-mass factor
- R_m = Maximum resistance of equivalent single-degree-of-freedom system when plastic moment is formed in flexural member
- k = Spring constant
- k_E = Effective spring constant (fig. 8-2)
- V = Dynamic reaction
- V_c = Dynamic column load

Notations for the use of tables 8-1 through 8-6 are given below:

NOTATION FOR DYNAMIC DESIGN FACTOR TABLES

- a = Short side of rectangular slab, ft
- b = Long side of rectangular slab, ft
- E = Modulus of elasticity, kips/sq in.
- I = Moment of inertia
- I_a = Average of gross and transformed moments of inertia (in two-way slabs, the average per unit width for short span)
- M_{pc} = Ultimate positive bending moment capacity per unit width at center of circular slab
- M_{ps} = Ultimate negative bending moment capacity per unit width at edge of circular slab
- M_p = Plastic resisting moment
- M_{Pm} = Plastic resisting moment at centerline of beam or slab, kip-ft

- M_{Pfa} = The component (in a plane perpendicular to edge a) of the total plastic bending moment capacity along the fracture line boundary of one area A, or the total positive plastic bending moment capacity for a section parallel to edge a, kip-ft
- M_{Pfb} = The component (in a plane perpendicular to edge b) of the total plastic bending moment capacity along the fracture line boundary of one area B, or the total positive plastic bending moment capacity for a section parallel to edge b, kip-ft
- M_{Ps} = Plastic resisting moment at support, kip-ft
- M_{Psa} = Total plastic bending moment capacity along edge a, kip-ft
- M_{Psb} = Total plastic bending moment capacity along edge b, kip-ft
- M_{Pmb}^o = Plastic positive bending moment capacity per unit width in short span, kip-ft/ft
- M_{Psa}^o = Plastic negative bending moment capacity per unit width at center of edge a for long span, kip-ft/ft
- M_{Psb}^o = Plastic negative bending moment capacity per unit width at center of edge b for short span, kip-ft/ft
- P = Total dynamic load on slab or beam, kips
- R = Total resistance of slab or beam, kips
- R_{mf} = Fictitious maximum resistance, kips (para. 8-4)
- V_A = Total dynamic reaction along one edge a, kips
- V_B = Total dynamic reaction along one edge b, kips

The load, mass, and load-mass factors are obtained from the following definitions:

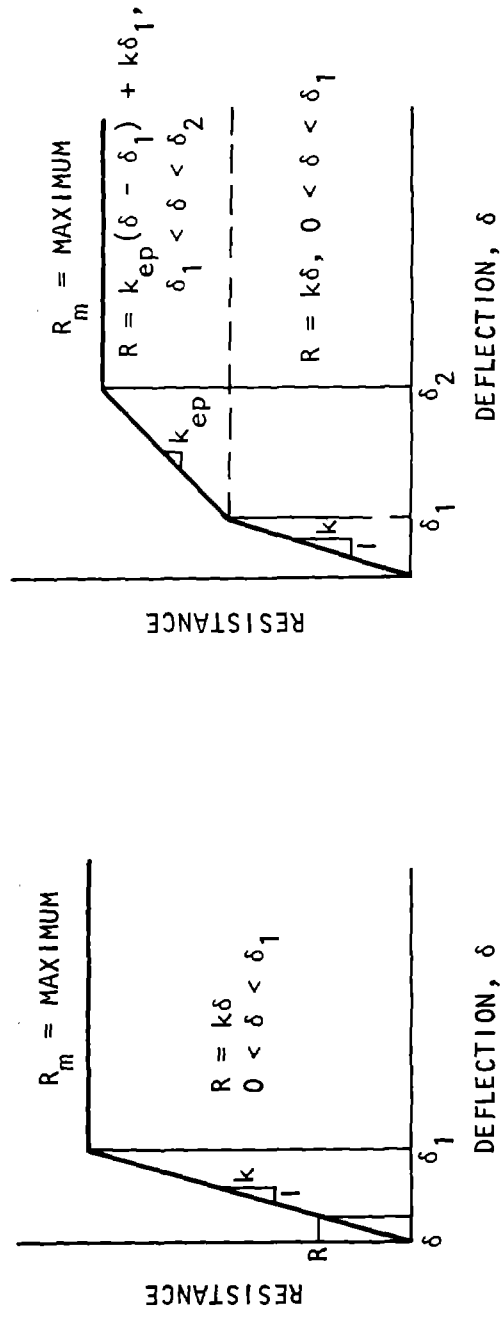
- K_L = Ratio of equivalent load on the single-degree-of-freedom system to actual load on the flexural member
- K_M = Ratio of equivalent mass of the single-degree-of-freedom system to total distributed mass of the flexural member
- $K_{LM} = K_M/K_L$

The period of the equivalent single-degree-of-freedom system is given by

$$T = 2\pi \sqrt{\frac{m_e}{k_E}} = 2\pi \sqrt{\frac{K_{LM}mL}{k}} \quad (8-1)$$

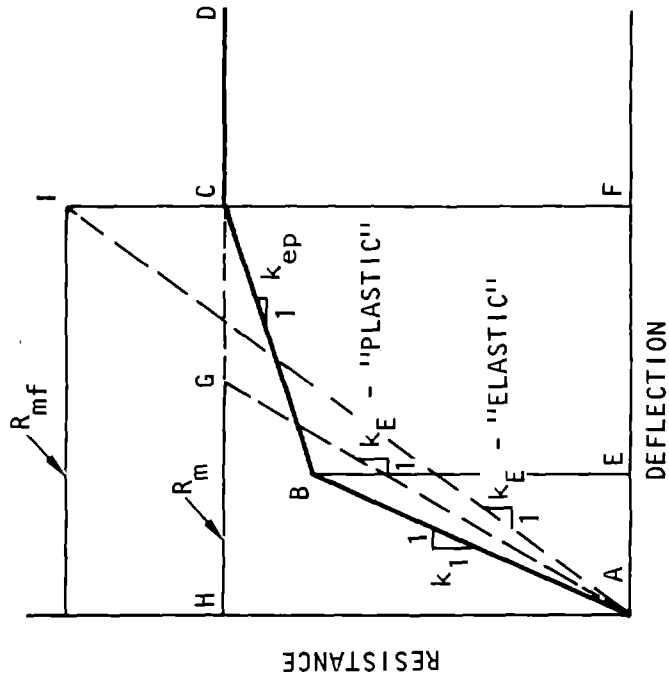
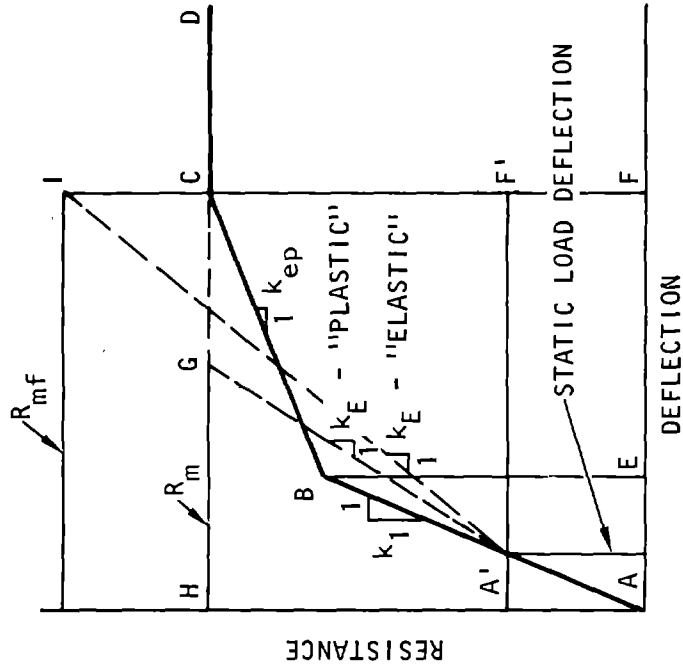
where

- m_e = Effective mass of structural element
- m = Mass per unit length
- L = Length of flexural member
- k = The load required to cause unit deflection of flexural member at midspan



(a) Simply-supported beam (b) Fixed-end beam

Figure 8-1. Resistance-Deflection Diagrams for Beams (COE, 1957)



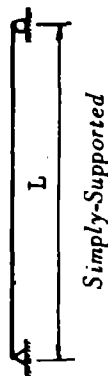
(a) Negligible static stresses in system

(b) Static stresses considered

Figure 8-2. General Resistance-Deflection Diagrams for Structural Elements (COE, 1957)

Table 8-1. Dynamic Design Factors: Beams and One-Way Slabs (COE, 1957; Biggs, 1964)

(a) Simply supported

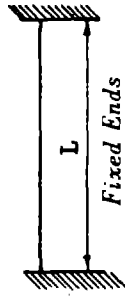


Loading Diagram	Strain Range	Load Factor K_L	Mass Factor K_M		Load-Mass Factor K_{LM}		Maximum Resistance R_m	Spring Constant k	Dynamic Reaction V
			Concentrated Mass *	Uniform Mass	Concentrated Mass *	Uniform Mass			
	Elastic	0.64		0.50		0.78	$\frac{8M_p}{L}$	$\frac{384EI}{5L^3}$	0.39 R+0.11P
	Plastic	0.50		0.33		0.66	$\frac{8M_p}{L}$	0	0.38R _m +0.12P
	Elastic	1	1.0	0.49	1.0	0.19	$\frac{4M_p}{L}$	$\frac{48EI}{L^3}$	0.78 R-0.28P
	Plastic	1	1.0	0.33	1.0	0.33	$\frac{4M_p}{L}$	0	0.75R _m -0.25P
	Elastic	0.87	0.76	0.52	0.87	0.60	$\frac{6M_p}{L}$	$\frac{56.4EI}{L^3}$	0.525R - 0.025F
	Plastic	1	1.0	0.56	1.0	0.56	$\frac{6M_p}{L}$	0	0.52R _{m} - 0.02F}

* Equal parts of the concentrated mass are lumped at each concentrated load.

Table 8-1. (Continued)

(b) Fixed ends



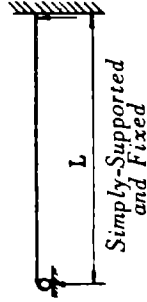
M_{Ps} = Ultimate moment capacity at support.
 M_{Pm} = Ultimate moment capacity at midspan

Loading Diagram	Strain Range	Load Factor K_L	Mass Factor K_M		Load-Mass Factor K_{LM}		Maximum Resistance R_m	Spring Constant k	Effective Spring Constant k_E		Dynamic Reaction V
			Concen-Uniform treated Mass*	Uniform Mass	Concen-Uniform treated Mass*	Uniform Mass			Elastic	Plastic	
	Elastic	0.53		0.41		0.77	$\frac{12M_{Ps}}{L}$	$\frac{384EI}{L^3}$	$\frac{264EI}{L^3}$	$\frac{307EI}{L^3}$	$0.36R + 0.14P$
	Elasto-Plastic	0.64		0.50		0.78	$\frac{8}{L}(M_{Ps} + M_{Pm})$	$\frac{384EI}{5L^3}$	$R_{mf} = \frac{22M_P}{L}$		$0.39R + 0.11P$
	Plastic	0.50		0.33		0.66	$\frac{8}{L}(M_{Ps} + M_{Pm})$	0			$0.38R_m + 0.12P$
	Elastic	1	1.0	0.37	1.0	0.37	$\frac{4}{L}(M_{Ps} + M_{Pm})$	$\frac{192EI}{L^3}$			$0.71R - 0.21P$
	Plastic	1	1.0	0.33	1.0	0.33	$\frac{4}{L}(M_{Ps} + M_{Pm})$	0			$0.75R_m - 0.25P$

* Concentrated mass is lumped at the concentrated load.

Table 8-1. (Concluded)

(c) Simply-supported and fixed



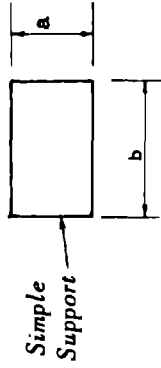
M_{ps} = Ultimate moment capacity at support
 M_{pm} = Ultimate moment capacity at midspan

Loading Diagram	Strain Range	Load Factor K_L	Mass Factor K_M		Load-Mass Factor K_{LM}		Spring Constant k	Effective Spring Constant k_E		Dynamic Reaction V
			Concen- trated Mass*	Uniform Mass	Concen- trated Mass*	Uniform Mass		Elastic	Plastic	
	Elastic	0.58		0.45	0.78	$185EI/L^3$	$\frac{153EI}{L^3}$	$\frac{160EI}{L^3}$	$V_1 = 0.26R + 0.12P$ $V_2 = 0.43R + 0.19P$ $V = 0.39R + 0.11F + M_{ps}/L$	
	Elasto- Plastic	0.64		0.50	0.78	$\frac{384EI}{5L^3}$	$\frac{11.6M_p}{L}$	$\frac{160EI}{L^3}$	$V = 0.38R_m + 0.12F + M_{ps}/L$	
	Plastic	0.50		0.33	0.66	0	$\frac{16M_{ps}}{3L}$	$\frac{6.63M_p}{L}$	$V_1 = 0.25R + 0.07F$ $V_2 = 0.54R + 0.14F$ $V = 0.78R - 0.28F + M_{ps}/L$	
	Elastic	1.0	1.0	0.43	0.43	$107EI/L^3$	$\frac{104EI}{L^3}$	$\frac{160EI}{L^3}$	$V = 0.75R_m - 0.25F + M_{ps}/L$	
	Elasto- Plastic	1.0	1.0	0.49	0.49	$48EI/L^3$	$\frac{2(M_{ps} + 2M_{pm})}{L}$	$\frac{160EI}{L^3}$	$V_1 = 0.17R + 0.17P$ $V_2 = 0.33R + 0.33P$ $V = 0.525R - 0.025F + M_{ps}/L$	
	Plastic	1.0	1.0	0.33	0.33	0	$\frac{2(M_{ps} + 2M_{pm})}{L}$	$\frac{9.52M_p}{L}$	$V = 0.52R_m - 0.02F + M_{ps}/L$	
	Elastic	0.81	0.67	0.45	0.55	$132EI/L^3$	$\frac{117.5EI}{L^3}$	$\frac{122EI}{L^3}$		
	Elasto- Plastic	0.87	0.76	0.52	0.60	$\frac{56EI}{L^3}$	$\frac{2(M_{ps} + 3M_{pm})}{L}$	$\frac{122EI}{L^3}$		
	Plastic	1.0	1.0	0.56	0.56	0	$\frac{2(M_{ps} + 3M_{pm})}{L}$	$\frac{9.52M_p}{L}$		

* Equal parts of the concentrated mass are lumped at each concentrated load.

Table 8-2. Dynamic Design Factors: Two-Way Slabs and Circular Slabs, Uniform Load (COE, 1957; Biggs, 1964)

(a) Simple supports, four sides

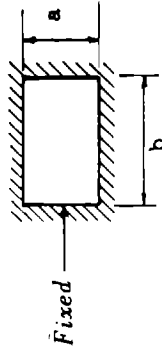


M_{Pfa}, M_{Pfb} = Total positive ultimate moment capacity along midspan section parallel to edges a and b, respectively

Strain Range	a/b	Load Factor K_L	Mass Factor K_M	Load-Factor K_{LM}	Maximum Resistance	Spring Constant k	Dynamic Reactions	
							V_A	V_B
Elastic	1.0	0.45	0.31	0.68	$\frac{12}{a}(M_{Pfa} + M_{Pfb})$	$252 EI/a^2$	0.07P+0.18R	0.07P+0.18R
	0.9	0.47	0.33	0.70	$\frac{1}{a}(12M_{Pfa} + 11M_{Pfb})$	$230 EI/a^2$	0.06P+0.16R	0.06P+0.16R
	0.8	0.49	0.35	0.71	$\frac{1}{a}(12M_{Pfa} + 10.3M_{Pfb})$	$212 EI/a^2$	0.06P+0.14R	0.06P+0.14R
	0.7	0.51	0.37	0.73	$\frac{1}{a}(12M_{Pfa} + 9.8M_{Pfb})$	$201 EI/a^2$	0.05P+0.13R	0.05P+0.13R
	0.6	0.53	0.39	0.74	$\frac{1}{a}(12M_{Pfa} + 9.3M_{Pfb})$	$197 EI/a^2$	0.04P+0.11R	0.04P+0.11R
	0.5	0.55	0.41	0.75	$\frac{1}{a}(12M_{Pfa} + 9.0M_{Pfb})$	$201 EI/a^2$	0.04P+0.09R	0.04P+0.09R
Plastic	1.0	0.33	0.17	0.51	$\frac{12}{a}(M_{Pfa} + M_{Pfb})$	0	0.09P+0.16R _m	0.09P+0.16R _m
	0.9	0.35	0.18	0.51	$\frac{1}{a}(12M_{Pfa} + 11M_{Pfb})$	0	0.08P+0.15R _m	0.08P+0.15R _m
	0.8	0.37	0.20	0.54	$\frac{1}{a}(12M_{Pfa} + 10.3M_{Pfb})$	0	0.07P+0.13R _m	0.07P+0.13R _m
	0.7	0.38	0.22	0.58	$\frac{1}{a}(12M_{Pfa} + 9.8M_{Pfb})$	0	0.06P+0.12R _m	0.06P+0.12R _m
	0.6	0.40	0.23	0.58	$\frac{1}{a}(12M_{Pfa} + 9.3M_{Pfb})$	0	0.05P+0.10R _m	0.05P+0.10R _m
	0.5	0.42	0.25	0.59	$\frac{1}{a}(12M_{Pfa} + 9.0M_{Pfb})$	0	0.04P+0.08R _m	0.04P+0.08R _m

Table 8-2. (Continued)

(b) Fixed four sides

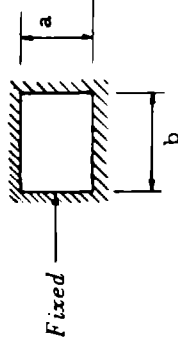


M_{Psa}, M_{Psb} = Total negative ultimate moment capacity along edges a and b , respectively

M_{Psa}^0, M_{Psb}^0 = Negative ultimate moment capacity per unit width at edges a and b , respectively

Strain Range	a/b	Load Factor K_L	Mass Factor K_M	Load-Mass Factor K_{LM}	Maximum Resistance	Spring Constant k	Dynamic Reactions	
							V_A	V_B
Elastic	1.0	0.33	0.21	0.63	$29.2M_{Psb}^0$	$810EI_a^2$	$0.10P + 0.15R$	$0.10P + 0.15R$
	0.9	0.34	0.23	0.68	$27.4M_{Psb}^0$	$743EI_a^2$	$0.09P + 0.14R$	$0.10P + 0.17R$
	0.8	0.36	0.25	0.69	$26.4M_{Psb}^0$	$705EI_a^2$	$0.08P + 0.12R$	$0.11P + 0.19R$
	0.7	0.38	0.27	0.71	$26.2M_{Psb}^0$	$692EI_a^2$	$0.07P + 0.11R$	$0.11P + 0.21R$
	0.6	0.41	0.29	0.71	$27.3M_{Psb}^0$	$724EI_a^2$	$0.06P + 0.09R$	$0.12P + 0.23R$
	0.5	0.43	0.31	0.72	$30.2M_{Psb}^0$	$806EI_a^2$	$0.05P + 0.08R$	$0.12P + 0.25R$
Elasto-Plastic	1.0	0.46	0.31	0.67	$\frac{1}{a} [12(M_{Pfa} + M_{Psa}) + 12(M_{Pfb} + M_{Psb})]$	$252EI_a^2$	$0.07P + 0.18R$	$0.07P + 0.13R$
	0.9	0.47	0.33	0.70	$\frac{1}{a} [12(M_{Pfa} + M_{Psa}) + 11(M_{Pfb} + M_{Psb})]$	$230EI_a^2$	$0.06P + 0.16R$	$0.08P + 0.20R$
	0.8	0.49	0.35	0.71	$\frac{1}{a} [12(M_{Pfa} + M_{Psa}) + 10.3(M_{Pfb} + M_{Psb})]$	$212EI_a^2$	$0.06P + 0.14R$	$0.08P + 0.22R$
	0.7	0.51	0.37	0.73	$\frac{1}{a} [12(M_{Pfa} + M_{Psa}) + 9.8(M_{Pfb} + M_{Psb})]$	$201EI_a^2$	$0.05P + 0.13R$	$0.08P + 0.24R$
	0.6	0.53	0.39	0.74	$\frac{1}{a} [12(M_{Pfa} + M_{Psa}) + 9.3(M_{Pfb} + M_{Psb})]$	$197EI_a^2$	$0.04P + 0.11R$	$0.09P + 0.26R$
0.5	0.55	0.41	0.75	$\frac{1}{a} [12(M_{Pfa} + M_{Psa}) + 9.0(M_{Pfb} + M_{Psb})]$	$201EI_a^2$	$0.04P + 0.09R$	$0.09P + 0.23R$	

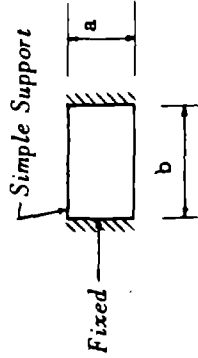
Table 8-2. (Continued)
(b) (Concluded)



Strain Range	a/b	Load Factor K_L	Mass Factor K_M	Load-Mass Factor K_{LM}	Maximum Resistance	Spring Constant k	Dynamic Reactions	
							V _A	V _B
Plastic	1.0	0.33	0.17	0.51	$\frac{1}{a} [12(M_{pfa} + M_{psa}) + 12(M_{pfb} + M_{psb})]$	0	$0.09P + 0.16R_m$	$0.09P + 0.16R_m$
	0.9	0.35	0.18	0.51	$\frac{1}{a} [12(M_{pfa} + M_{psa}) + 11(M_{pfb} + M_{psb})]$	0	$0.08P + 0.15R_m$	$0.09P + 0.18R_m$
	0.8	0.37	0.20	0.54	$\frac{1}{a} [12(M_{pfa} + M_{psa}) + 10.3(M_{pfb} + M_{psb})]$	0	$0.07P + 0.13R_m$	$0.10P + 0.20R_m$
	0.7	0.38	0.22	0.58	$\frac{1}{a} [12(M_{pfa} + M_{psa}) + 9.8(M_{pfb} + M_{psb})]$	0	$0.06P + 0.12R_m$	$0.10P + 0.22R_m$
	0.6	0.40	0.23	0.58	$\frac{1}{a} [12(M_{pfa} + M_{psa}) + 9.3(M_{pfb} + M_{psb})]$	0	$0.05P + 0.10R_m$	$0.10P + 0.25R_m$
	0.5	0.42	0.25	0.59	$\frac{1}{a} [12(M_{pfa} + M_{psa}) + 9.0(M_{pfb} + M_{psb})]$	0	$0.04P + 0.08R_m$	$0.11P + 0.27R_m$

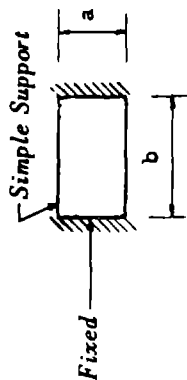
Table 8-2. (Continued)

(c) Simple supports, two long sides; fixed supports, two short sides



Strain Range	a/b	Load Factor K_L	Mass Factor K_M	Load-Mass Factor K_{LM}	Maximum Resistance	Spring Constant k	Dynamic Reactions	
							V_A	V_B
Elastic	1.0	0.39	0.26	0.67	$20.4 M_{Psa}^0$	$575 EI_a/a^2$	$0.09P+0.16R$	$0.07P+0.18R$
	0.9	0.41	0.28	0.68	$10.2 M_{Psa}^0 + \frac{11}{a} M_{Pfb}$	$476 EI_a/a^2$	$0.08P+0.14R$	$0.08P+0.20R$
	0.8	0.44	0.30	0.68	$10.2 M_{Psa}^0 + \frac{10.3}{a} M_{Pfb}$	$396 EI_a/a^2$	$0.08P+0.12R$	$0.08P+0.22R$
	0.7	0.46	0.33	0.72	$9.3 M_{Psa}^0 + \frac{9.7}{a} M_{Pfb}$	$328 EI_a/a^2$	$0.07P+0.11R$	$0.08P+0.24R$
	0.6	0.48	0.35	0.73	$8.5 M_{Psa}^0 + \frac{9.3}{a} M_{Pfb}$	$283 EI_a/a^2$	$0.06P+0.09R$	$0.09P+0.26R$
	0.5	0.51	0.37	0.73	$7.4 M_{Psa}^0 + \frac{9.0}{a} M_{Pfb}$	$243 EI_a/a^2$	$0.05P+0.08R$	$0.09P+0.28R$
Elasto-Plastic	1.0	0.46	0.31	0.67	$\frac{1}{a} [12(M_{Pfa} + M_{Psa}) + 12(M_{Pfb})]$	$271 EI_a/a^2$	$0.07P+0.18R$	$0.07P+0.18R$
	0.9	0.47	0.33	0.70	$\frac{1}{a} [12(M_{Pfa} + M_{Psa}) + 11(M_{Pfb})]$	$248 EI_a/a^2$	$0.06P+0.16R$	$0.08P+0.20R$
	0.8	0.49	0.35	0.71	$\frac{1}{a} [12(M_{Pfa} + M_{Psa}) + 10.3(M_{Pfb})]$	$228 EI_a/a^2$	$0.06P+0.14R$	$0.08P+0.22R$
	0.7	0.51	0.37	0.72	$\frac{1}{a} [12(M_{Pfa} + M_{Psa}) + 9.7(M_{Pfb})]$	$216 EI_a/a^2$	$0.05P+0.13R$	$0.08P+0.24R$
	0.6	0.53	0.37	0.70	$\frac{1}{a} [12(M_{Pfa} + M_{Psa}) + 9.3(M_{Pfb})]$	$212 EI_a/a^2$	$0.04P+0.11R$	$0.09P+0.26R$
	0.5	0.55	0.41	0.74	$\frac{1}{a} [12(M_{Pfa} + M_{Psa}) + 9.0(M_{Pfb})]$	$216 EI_a/a^2$	$0.04P+0.09R$	$0.09P+0.28R$

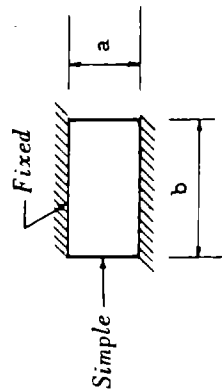
Table 8-2. (Continued)
(c) (Concluded)



Strain Range	a/b	Load Factor K_L	Mass Factor K_M	Load-Mass Factor K_{LM}	Maximum Resistance	Spring Constant k	Dynamic Reaction	
							V_A	V_B
Plastic	1.0	0.33	0.17	0.51	$\frac{1}{a} [12(M_{pfa} + M_{psa}) + 12 M_{pfb}]$	0	$0.09P + 0.16R_m$	$0.09P + 0.16R_m$
	0.9	0.35	0.18	0.51	$\frac{1}{a} [12(M_{pfa} + M_{psa}) + 11 M_{pfb}]$	0	$0.08P + 0.15R_m$	$0.09P + 0.18R_m$
	0.8	0.37	0.20	0.54	$\frac{1}{a} [12(M_{pfa} + M_{psa}) + 10.3 M_{pfb}]$	0	$0.07P + 0.13R_m$	$0.10P + 0.20R_m$
	0.7	0.38	0.22	0.58	$\frac{1}{a} [12(M_{pfa} + M_{psa}) + 9.7 M_{pfb}]$	0	$0.05P + 0.12R_m$	$0.10P + 0.22R_m$
	0.6	0.40	0.23	0.58	$\frac{1}{a} [12(M_{pfa} + M_{psa}) + 9.3 M_{pfb}]$	0	$0.05P + 0.10R_m$	$0.10P + 0.25R_m$
	0.5	0.42	0.25	0.59	$\frac{1}{a} [12(M_{pfa} + M_{psa}) + 9.0 M_{pfb}]$	0	$0.04P + 0.08R_m$	$0.11P + 0.27R_m$

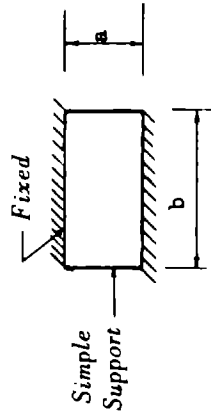
Table 8-2. (Continued)

(d) Simple supports, two short sides; fixed supports, two long sides



Strain Range	a/b	Load Factor K_L	Mass Factor K_M	Load-Mass Factor K_{LM}	Maximum Resistance	Spring Constant k	Dynamic Reactions	
							V_A	V_B
Elastic	1.0	0.39	0.26	0.67	$20.4 M_{Psb}^0$	$575 EI_a/a^2$	$0.07P+0.18R$	$C.09P+C.16R$
	0.9	0.40	0.28	0.70	$19.5 M_{Psb}^0$	$600 EI_a/a^2$	$0.06P+0.16R$	$0.10P+0.18R$
	0.8	0.42	0.29	0.69	$19.5 M_{Psb}^0$	$610 EI_a/a^2$	$0.06P+0.14R$	$0.11P+0.19R$
	0.7	0.43	0.31	0.71	$20.2 M_{Psb}^0$	$662 EI_a/a^2$	$0.05P+0.13R$	$0.11P+0.21R$
	0.6	0.45	0.33	0.73	$21.2 M_{Psb}^0$	$731 EI_a/a^2$	$0.04P+0.11R$	$0.12P+0.23R$
	0.5	0.47	0.34	0.72	$22.2 M_{Psb}^0$	$850 EI_a/a^2$	$0.04P+0.09R$	$0.12P+0.25R$
Elasto-Plastic	1.0	0.46	0.31	0.67	$\left[\frac{12M_{Pfa}}{a} + 12(M_{Psb} + M_{Pfb}) \right]$	$271 EI_a/a^2$	$0.07P+0.18R$	$0.07P+C.18R$
	0.9	0.47	0.33	0.70	$\left[\frac{12M_{Pfa}}{a} + 11(M_{Psb} + M_{Pfb}) \right]$	$248 EI_a/a^2$	$0.06P+0.16R$	$0.08P+C.20R$
	0.8	0.49	0.35	0.71	$\left[\frac{12M_{Pfa}}{a} + 10.3(M_{Psb} + M_{Pfb}) \right]$	$228 EI_a/a^2$	$0.06P+0.14R$	$0.08P+C.22R$
	0.7	0.51	0.37	0.73	$\left[\frac{12M_{Pfa}}{a} + 9.8(M_{Psb} + M_{Pfb}) \right]$	$216 EI_a/a^2$	$0.05P+C.13R$	$0.08P+C.24R$
	0.6	0.53	0.39	0.74	$\left[\frac{12M_{Pfa}}{a} + 9.3(M_{Psb} + M_{Pfb}) \right]$	$212 EI_a/a^2$	$0.04P+0.11R$	$0.09P+0.26R$
	0.5	0.55	0.41	0.74	$\left[\frac{12M_{Pfa}}{a} + 9.0(M_{Psb} + M_{Pfb}) \right]$	$216 EI_a/a^2$	$0.04P+0.09R$	$0.09P+0.26R$

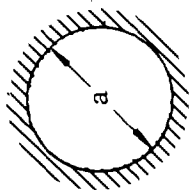
Table 8-2. (Continued)
(d) (Concluded)



Strain Range	a/b	Load Factor K_L	Mass Factor K_M	Load-Mass Factor K_{LM}	Maximum Resistance	Spring Constant k	Dynamic Reactions	
							V_A	V_B
Plastic	1.0	0.33	0.17	0.51	$\frac{1}{a} [12M_p f_a + 12(M_{psb} + M_{pfb})]$	0	$0.09P + 0.16R_m$	$0.09P + 0.16R_m$
	0.9	0.35	0.18	0.51	$\frac{1}{a} [12M_p f_a + 11(M_{psb} + M_{pfb})]$	0	$0.08P + 0.15R_m$	$0.09P + 0.18R_m$
	0.8	0.37	0.20	0.54	$\frac{1}{a} [12M_p f_a + 10.3(M_{psb} + M_{pfb})]$	0	$0.07P + 0.13R_m$	$0.10P + 0.20R_m$
	0.7	0.36	0.22	0.58	$\frac{1}{a} [12M_p f_a + 9.8(M_{psb} + M_{pfb})]$	0	$0.06P + 0.12R_m$	$0.10P + 0.22R_m$
	0.6	0.40	0.23	0.58	$\frac{1}{a} [12M_p f_a + 9.3(M_{psb} + M_{pfb})]$	0	$0.05P + 0.10R_m$	$0.10P + 0.25R_m$
	0.5	0.42	0.25	0.59	$\frac{1}{a} [12M_p f_a + 9.0(M_{psb} + M_{pfb})]$	0	$0.04P + 0.08R_m$	$0.11P + 0.27R_m$

Table 8-2. (Concluded)

(e) Circular slabs

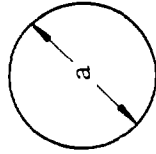


a = Diameter of slab

M_{pc} = Ultimate positive bending moment capacity per unit width at center of circular slab

M_{ps} = Ultimate negative bending moment capacity per unit width at edge of circular slab

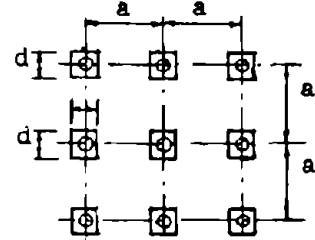
Fixed Edges



Simple Supports

Edge Condition	Strain Range	K_L	K_M	K_{LM}	Maximum Resistance	Spring Constant	Dynamic Reaction
Simple Supports	Elastic	0.46	0.30	0.65	$18.8 M_{pc}$	$\frac{216EI}{a^2}$	$0.28P + 0.72R$
	Plastic	0.33	0.17	0.52	$18.8 M_{pc}$	0	$0.36P + 0.64R_m$
Fixed Supports	Elastic	0.33	0.20	0.61	$25.1 M_{ps}$	$\frac{880EI}{a^2}$	$0.40P + 0.60R$
	Elastic-plastic	0.46	0.30	0.65	$18.3 (M_{pc} + M_{ps})$	$\frac{216EI}{a^2}$	$0.28P + 0.72R$
	Plastic	0.33	0.17	0.52	$18.8 (M_{pc} + M_{ps})$	0	$0.36P + 0.64R_m$

Table 8-3. Dynamic Design Factors for Flat Slabs: Square Interior Uniform Load (COE, 1957)



Strain Phase	d/a	Load Factor K_L	Mass Factor K_M	Load-Mass Factor K_{LM}	Spring Constant k (kips/ft)	Maximum Resistance R_m (kips)	Dynamic Column Load V_c (kips)
Elastic	0.05	8/15	0.34	0.64	$1.45EI_a/a^2$	$4.2 \Sigma M_P$	$0.16P + 0.84R + pd^2$
	0.10	8/15	0.34	0.64	$1.60EI_a/a^2$	$4.4 \Sigma M_P$	
	0.15	8/15	0.34	0.64	$1.75EI_a/a^2$	$4.6 \Sigma M_P$	
	0.20	8/15	0.34	0.64	$1.92EI_a/a^2$	$4.8 \Sigma M_P$	
	0.25	8/15	0.34	0.64	$2.10EI_a/a^2$	$5.0 \Sigma M_P$	
Plastic	0.05	1/2	7/24	7/12	0	$4.2 \Sigma M_P$	$0.11P + 0.86R_m + pd^2$
	0.10	1/2	7/24	7/12	0	$4.4 \Sigma M_P$	
	0.15	1/2	7/24	7/12	0	$4.6 \Sigma M_P$	
	0.20	1/2	7/24	7/12	0	$4.8 \Sigma M_P$	
	0.25	1/2	7/24	7/12	0	$5.0 \Sigma M_P$	

a = column spacing, ft.

E = compressive modulus of elasticity of concrete, kips/sq in.

I_a = average of gross and transformed moments of inertia per unit width, equal in both directions in. ⁴/ft.

P = total load on one slab panel, excluding capitals.

R = total resistance of one slab panel, excluding capitals.

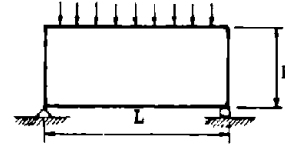
$$\Sigma M_P = M_{Pmp} + M_{Pmn} + M_{Pcp} + M_{Pcn} \quad (\text{Fig. 8-3})$$

Table 8-4. Dynamic Design Factors for Tee-Beams (COE, 1957)

		K_L	K_M	K_{LM}	k	R_m	M_{pos}	V_1	V_2
Fixed - Fixed	Triangular	0.72	0.60	0.83	Fig. 8-4	Fig. 8-5	Fig. 8-6	0.44R+0.06P	0.44R+0.06P
	Load & Mass	0.81	0.70	0.86	$60EI/L^3$	$\frac{6}{L}(M_{Ps}+M_{Pm})$		0.46R+0.04P	0.46R+0.04P
		0.67	0.50	0.75	0	$\frac{6}{L}(M_{Ps}+M_{Pm})$		0.44R+0.06P	0.44R+0.06P
Fixed - Fixed	Triangular	0.72	0.39	0.54	Fig. 8-4	Fig. 8-5	Fig. 8-6	0.48R+0.02P	0.48R+0.02P
	Load Uni-	0.81	0.50	0.62	$60EI/L^3$	$\frac{6}{L}(M_{Ps}+M_{Pm})$		0.52R-0.02P	0.52R-0.02P
	form Mass	0.67	0.33	0.50	0	$\frac{6}{L}(M_{Ps}+M_{Pm})$		0.50R	0.50R
Fixed - Fixed	Uniform	0.53	0.40	0.76	Fig. 8-4	Fig. 8-5	Fig. 8-6	0.36R+0.14P	0.36R+0.14P
	Load Uni-	0.64	0.50	0.78	$384EI/5L^3$	$\frac{8}{L}(M_{Ps}+M_{Pm})$		0.39R+0.11P	0.39R+0.11P
	form Mass	0.50	0.33	0.66	0	$\frac{8}{L}(M_{Ps}+M_{Pm})$		0.37R+0.13P	0.37R+0.13P
Fixed - Fixed	Triangular	0.59	0.67	1.14	Fig. 8-4	Fig. 8-5	Fig. 8-6	0.29R+0.05P	0.55R+0.11P
	Load & Mass	0.81	0.70	0.86	$60EI/L^3$	$\frac{3}{L}(2M_{Pm}+M_{Ps})$		0.46R+0.04P	0.46R+0.04P
		0.66	0.50	0.76	0	$\frac{3}{L}(2M_{Pm}+M_{Ps})$		0.44R+0.06P	0.44R+0.06P
Fixed - Fixed	Triangular	0.59	0.47	0.80	Fig. 8-4	Fig. 8-5	Fig. 8-6	0.25+0.09P	0.49R+0.17P
	Load Uni-	0.81	0.50	0.62	$60EI/L^3$	$\frac{3}{L}(2M_{Pm}+M_{Ps})$		0.52-0.02P	0.52R-0.02P
	form Mass	0.66	0.33	0.50	0	$\frac{3}{L}(2M_{Pm}+M_{Ps})$		0.50R	0.50R
Fixed - Fixed	Uniform	0.58	0.45	0.78	Fig. 8-4	Fig. 8-5	Fig. 8-6	0.26R+0.12P	0.43R+0.19P
	Load Uni-	0.64	0.50	0.78	$384EI/5L^3$	$\frac{4}{L}(2M_{Pm}+M_{Ps})$		0.39R+0.11P	0.39R+0.11P
	form Mass	0.50	0.33	0.66	0	$\frac{4}{L}(2M_{Pm}+M_{Ps})$		0.38R+0.12P	0.38R+0.12P

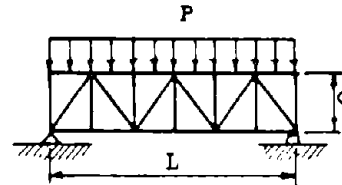
Table 8-5. Deep Beams: Uniform Load, Elastic Range (COE, 1957)

$$\frac{H}{L} > \frac{2}{5}$$



Support Condition	K_L	K_M	K_{LM}	Maximum Resistance, R_m		δ_b	δ_s	Dynamic Reaction
				Bending	Shear			
Fixed	0.53	0.41	0.77	$\frac{12M}{L}P$	$2V_u$	$\frac{L^3}{384E_c I_a}$	$\frac{L}{3E_c A_w}$	$V = 0.36R + 0.14P$
Simply-Supported	0.64	0.50	0.78	$\frac{8M}{L}P$	$2V_u$	$\frac{5L^3}{384E_c I_a}$	$\frac{L}{3E_c A_w}$	$V = 0.39R + 0.11P$
Simply-Supported and Fixed	0.58	0.45	0.78	$\frac{8M}{L}P$	$1.6V_u$	$\frac{L^3}{185E_c I_a}$	$\frac{15L}{148E_c A_w}$	$V_1 = 0.26R + 0.12P$ $V_2 = 0.43R + 0.19P$ (V_2 is at fixed end)

Table 8-6. Trusses: Simply Supported Uniform Load (COE, 1957)



Strain Range	Load Factor K_L	Mass Factor K_M	Load-Mass Factor K_{LM}	Spring Constant k	Dynamic Reactions
Elastic	0.64	0.50	0.78	$\frac{R_m E d}{C_t f_{dy} L^2}$	$V = 0.39R + 0.11P$
Plastic-Mid-span Yielding	0.50	0.33	0.66	0	$V = 0.38R_m + 0.12P$
Plastic-end Panel Yielding	1.0	1.0	1.0	0	$V = 0.39R_m + 0.11P + \frac{0.78P}{n}^*$

* N = Number of panels in truss

8-5. Dynamic design of structural elements

a. General procedures. In the design of any element, the essential steps after determining the dynamic load are as follows:

Step 1. Select dynamic design factors from tables 8-1 to 8-6 and figures 8-3 to 8-6.

Step 2. Select the maximum deflection criterion based on the permissible ductility factors (see *b* below).

Step 3. Determine the resistance required to satisfy the deflection criterion and select a member to provide the resistance. (See *c* below for relationship of resistance-load-ductility as a function of the natural periods of the single-degree-of-freedom system.)

Step 4. Detail the selected member to provide for end connections, shear strength, bond strength, variation in bending stresses, and rebound. (See *c* (3) below for rebound values.)

This approach is valid for elastic, elastoplastic, or plastic ranges of the structural deformation.

In Step 1 the equivalent single-degree-of-freedom system is defined.

In Step 2 the material properties and functional requirements of the structure determine the allowable maximum deflection.

In Step 3 the response of the single-degree-of-freedom is obtained; the load and the deflection are known; the required resistance is calculated.

In Step 4 the design process is completed.

b. Deflection criteria for elastoplastic design. Determine the amount of plastic deformation a structural system or element can experience and still be able to perform its function. The ductility ratio corresponding to collapse is defined as

$$\mu_c = \frac{\delta_c}{\delta_y}$$

where

δ_c = Maximum deflection at the point of collapse

δ_y = Deflection corresponding to initial yielding of the of structural element

If a design factor α , having a value less than 1.0 is introduced, the design maximum deflection is

$$\delta_m = \alpha \mu_c \delta_y$$

The value of α must be determined by considering the function and content of the structure, the sensitivity to dynamic loads, and the economics of construction. It is recommended that the value of α be taken between 1/2 and 1/3. The value of δ_c must be determined from a knowledge of the material properties and structure deformation characteristics. Some

results from test data are provided below for reinforced concrete and steel.

(1) Reinforced concrete.

(a) Concrete strength has little effect on the energy-absorbing capacity of beams failing initially in tension but does have an effect on the energy-absorbing capacity of beams failing in compression. The energy-absorption capacity is the area under the load-midspan deflection curve up to the deflection at maximum load-carrying capacity.

(b) The ductility of a beam is dependent on the percent of reinforcing steel.

(c) The compression reinforcement adds to the ductility of a beam. The addition of compression reinforcement enables a larger angle change to take place before the concrete crushes and thereby increases the deflection that the beam can undergo before collapse.

(d) To be most effective, the compression reinforcement must be well tied.

(e) For rectangular beams reinforced in tension only,

$$\mu_c = \frac{0.1}{a_s}$$

where a_s is the ratio of tension reinforcement area to the section area bd . A limiting value of μ_c is 50.

(f) For double-reinforced rectangular beams,

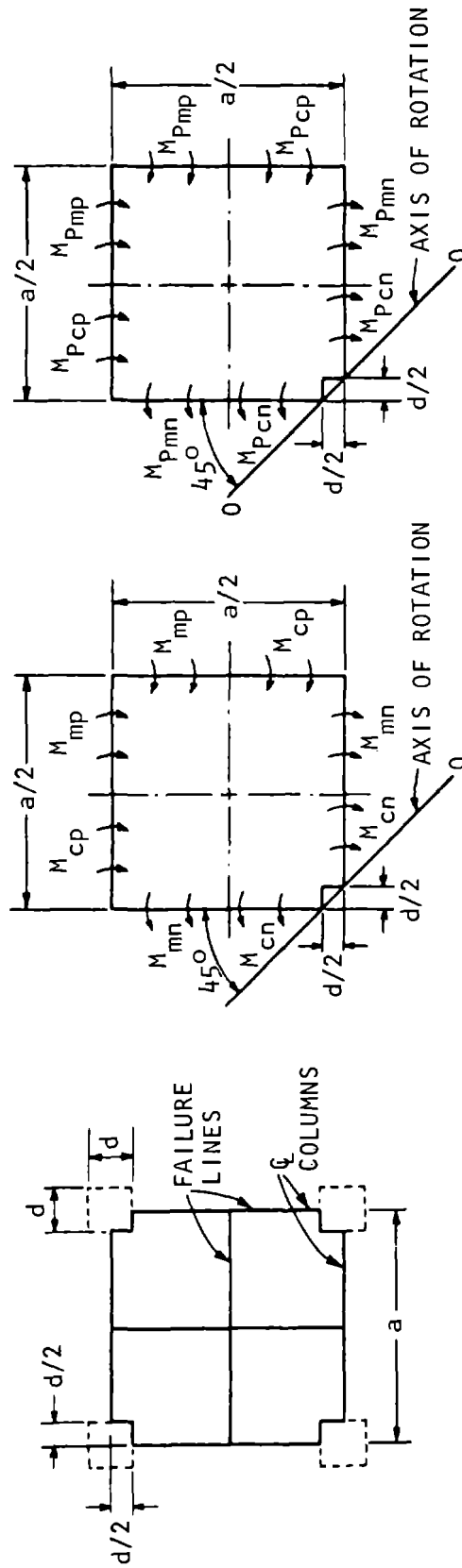
$$\mu_c = \frac{0.1}{a_s - a'_s}$$

where a_s and a'_s are respectively the ratios of tension and compression reinforcement areas to the section area bd . A limiting value of μ_c is 50 for the case in which $0 \leq a_s - a'_s < 0.002$.

(2) Steel.

(a) Experiments have shown that for W-beam sections, the average ductility ratio was 26 at failure for specimens loaded in the strong direction. In similar tests with superimposed axial load equal to three-fourths the ultimate lateral load, the ductility ratio was 8.1. The combination of axial load and lateral load on a beam reduces the elastic stiffness, decreases the maximum lateral load, decreases lateral load resistance after reaching maximum load, and decreases the ductility ratio, μ_c . Comparative tests of beams loaded in either the strong or weak directions indicated little difference in ductility ratio. These data are valid for laterally braced beam-columns.

(b) Welded frames tested to ultimate under vertical load with sidesway and lateral buckling prevented by special supports showed a range of ductility ratios from 6 to 16. The ratio of failure deflections to the span ranged from 0.036 to 0.068. The range of values resulted from varying the size of component elements.



(a) Assumed failure lines (b) Elastic condition (c) Plastic condition

Figure 8-3. Uniformly Loaded Square Interior Flat Slab, Assumed Maximum Moments and Failure Lines (COE, 1957)

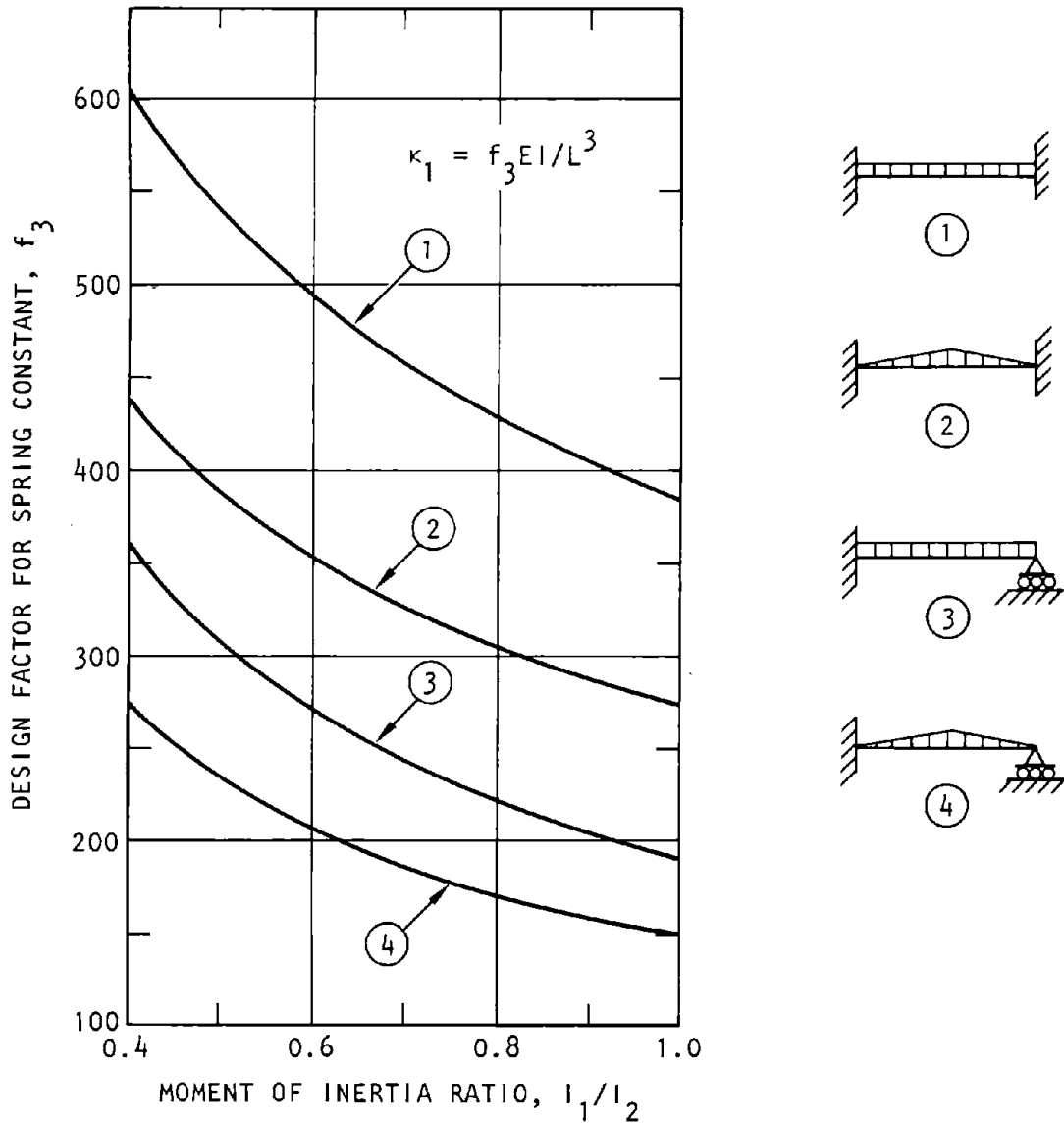


Figure 8-4. Tee-Beam Design Factor for Spring Constant (COE, 1957)

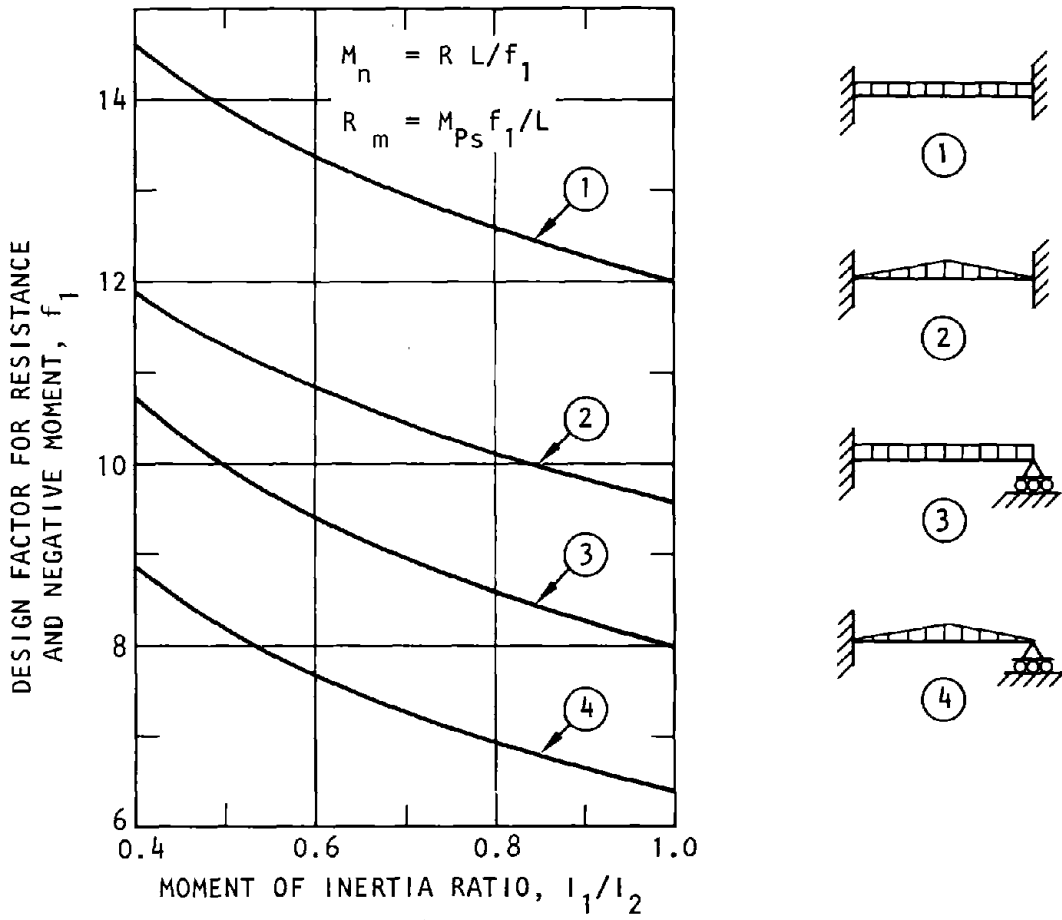


Figure 8-5. Tee-Beam Design Factor for Resistance and Negative Moment (COE, 1957)

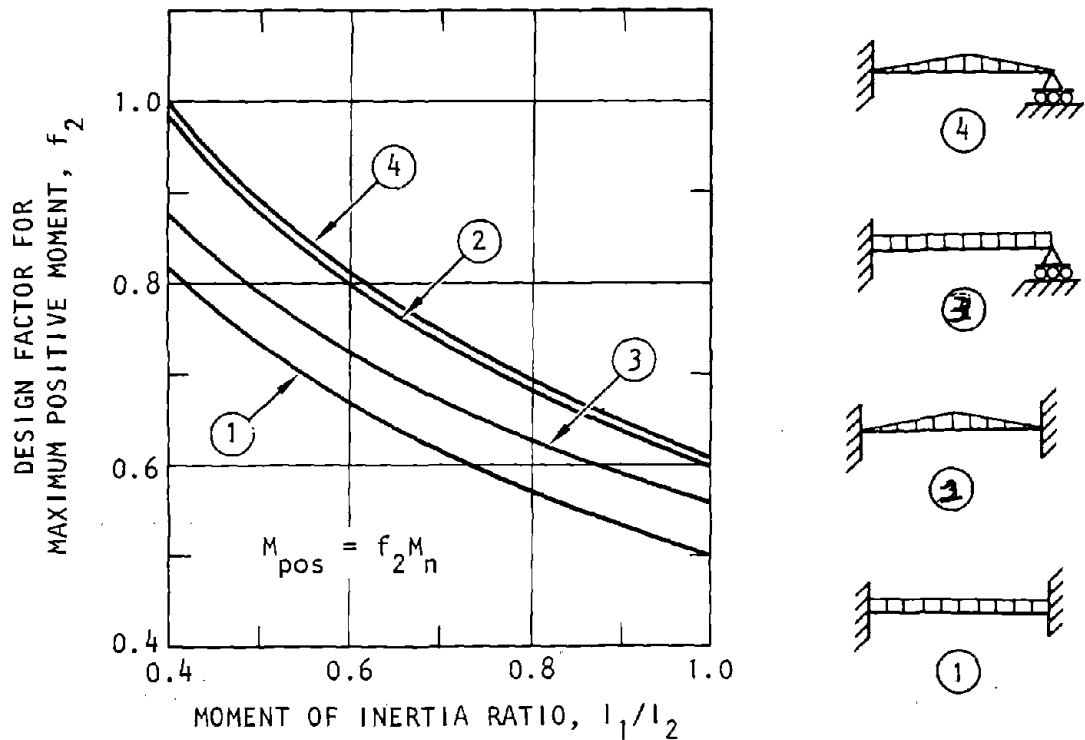


Figure 8-6. Tee-Beam Design Factor for Positive Moment (COE, 1957)

(3) Beam-columns. Combined blast and ground-shock loads often load structural elements as beam-columns. As a general rule, ductility ratios permissible for steel beam-columns where axial loads are more than half the ultimate lateral load should not exceed 1/3 the ductility ratios permissible for the same structural element if the axial load is not present.

(4) Composite section. Composite concrete and steel Tee-beams with channel shear connectors or Nelson studs subjected to a concentrated load at midspan produced an approximate ductility ratio of 8 and an approximate ultimate deflection ratio to span of 0.016. This latter ratio indicates the stiffness of composite beam construction.

(5) Summary. Table 8-7 is a summary of these test data. The designer should search the literature for failure data on structural elements that match as closely as possible the elements he is designing. Using the available data and the functional, loading-response, and economical considerations, he should select the appropriate value of α within the range recommended above. For example, whether a closure will be reopened or bypassed after a nuclear attack will make considerable difference in the selection of the value of α .

c. Elastoplastic response of single-degree-of-freedom systems.

(1) Flexure. The equivalent single-degree-of-freedom system is shown in figure 8-7. The combined effect of airblast and ground shock is given by $p(t) - m\ddot{y}$. The following additional terms are defined:

- μ = Ductility ratio, the quotient of the maximum design deflection displacement δ_m to the deflection δ_y corresponding to initial yielding of the structural element
- p_m = Peak magnitude of the force
- q_y = The effective force causing yielding of the element
- t_r = Rise time, the effective time required for the force to build up from zero to its maximum
- t_d = Effective duration, the time that the force is effective in causing initial deflection
- T = Natural period of vibration of the structural element

Figure 8-8 gives the appropriate relationships for a triangular loading, elastoplastic resistance assuming zero rise time, and zero damping. For a preliminary design, these relationships are most useful. The initial sizing of the structural element may be made (Step 3) by using this chart. It is necessary to validate the design with a more refined analysis. In combining airblast and ground shock, use the absolute sum of the maxima from the chart of figure 8-8, since the relationships shown in the figure do not account for the phasing of airblast and ground shock. The chart gives conservative results (1.5 to 2.0) because it neglects rise time and damping as well as phasing of the airblast and ground shock.

(2) Shear forces. Premature shear failure must be avoided and the structural element should be designed to reach its flexural resistance before shear failure occurs. Under blast and ground-shock forces,

Table 8-7. Summary of Test Data for Structural Elements (COE, 1957)

Test	Ductility Ratio* $\mu_c = \delta_c / \delta_y$	Ultimate Deflection to Span Ratio	References
Reinforced Concrete Beams	$0.1/a_s, \frac{0.1}{a_s - a'_s}$		Gaston et al., 1952
Steel Beam Lateral Load	26.4	0.097	Howland-Newmark, 1953
Steel Beams Lateral and Axial Load	8.1	0.025	Ibid.
Welded Frames Vertical Load	6 to 16	0.068 to 0.036	Ruzik et al., 1952
Composite Tee Beam	8	0.016	Viest et al., 1952

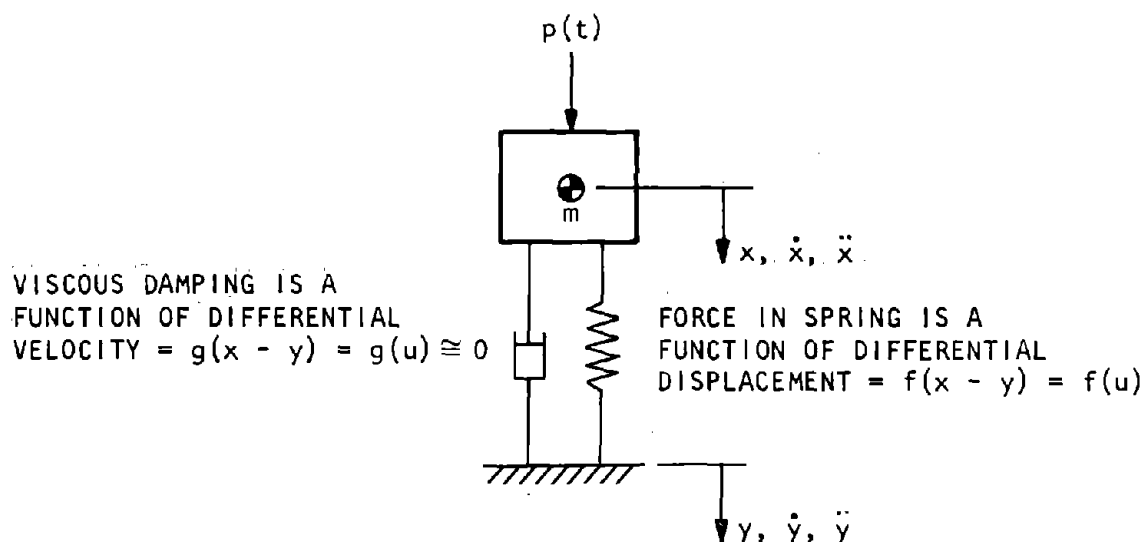
a_s = Ratio of area of tension reinforcement to the area of the concrete section

a'_s = Ratio of area of compressive reinforcement to the area of the concrete section

δ_c = Deflection at collapse

δ_y = Elastic limit deflection

*The ductility ratios presented in this table represent a summary of test results on beams and frames.



DIFFERENTIAL EQUATION OF MOTION:

$$m\ddot{u} + f(u) = p(t) - m\ddot{y}$$

$p(t)$ = FORCE ACTING ON MASS

m = MAGNITUDE OF MASS

x, \dot{x}, \ddot{x} = ABSOLUTE DISPLACEMENT, VELOCITY, AND ACCELERATION OF CENTROID OF MASS

y, \dot{y}, \ddot{y} = ABSOLUTE DISPLACEMENT, VELOCITY, AND ACCELERATION OF SUPPORT

u, \dot{u}, \ddot{u} = DISPLACEMENT, VELOCITY, AND ACCELERATION OF CENTROID OF MASS RELATIVE TO SUPPORT

Figure 8-7. Model and Notation for General Single-Degree-of-Freedom System (Merritt-Newmark, 1964)

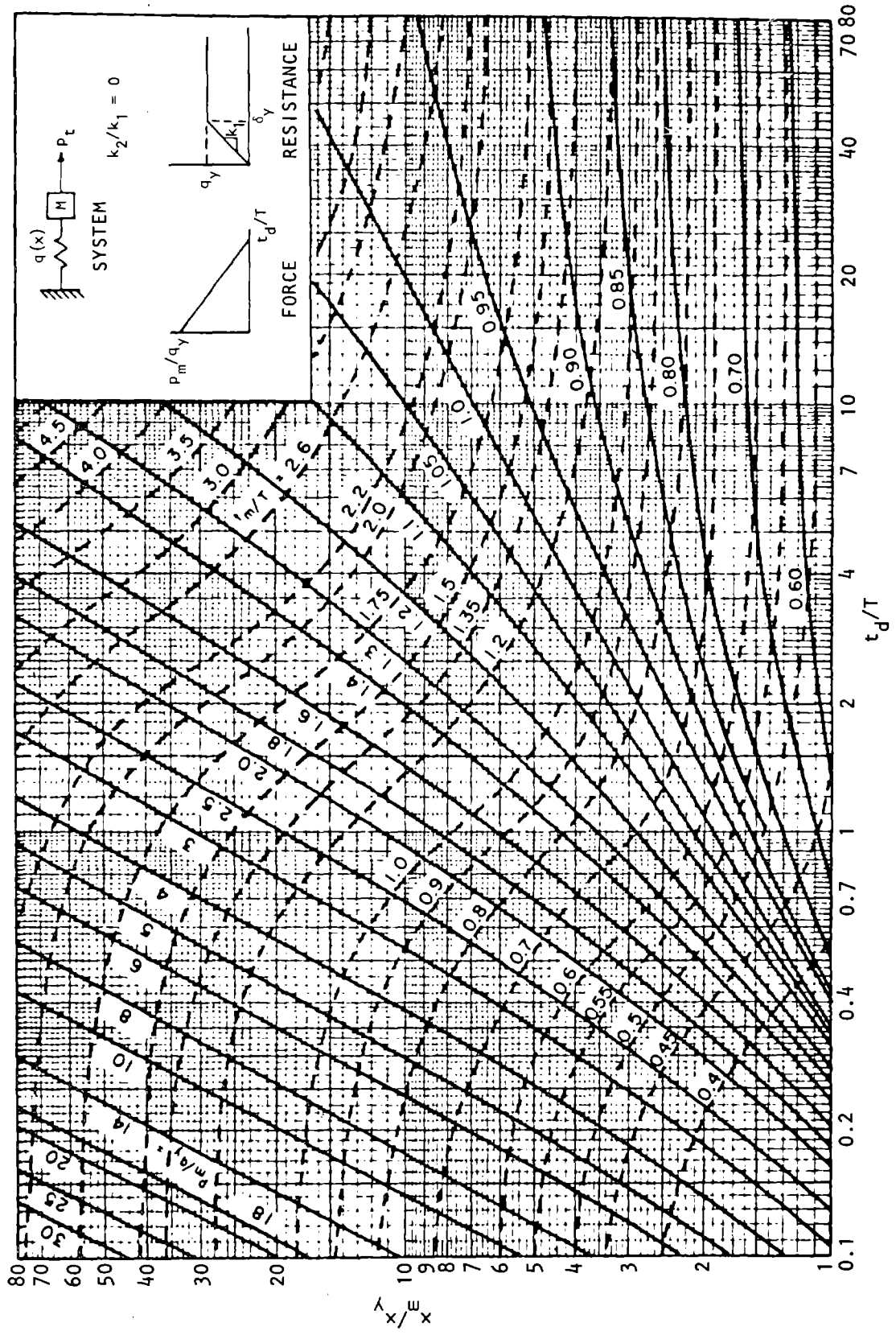


Figure 8-8. Maximum Response of Simple Spring Mass System to Initially Peaked Triangular Force Pulse (Merritt-Newmark, 1964)

a flexural member may experience shear stresses larger than if the same loads were applied statically. In Keenan (1976), dynamic increase factors (DIF) have been derived for shear forces. DIF is defined in the equation

$$DIF = \frac{S_d}{S_s} \quad (8-2)$$

where S_d and S_s are dynamic and static shear, respectively, at the same point in the beam or slab. Approximate solutions (Keenan, 1976) are as follows (fig. 8-9):

(a) Elastic case for $0 < t < t_y$, where t_y is time to reach dynamic yield deflection.

$$p_t = p_m \left(1 - \frac{t}{t_d}\right) \quad \text{Triangular load}$$

$$S_s = \frac{R_u L}{2} \left(1 - \frac{2z}{L}\right) \quad \text{Maximum static shear at distance } z$$

$$\delta_t = C \delta z (L^3 - 2Lz^2 + z^3) \quad \text{Deflected shape}$$

From the free-body diagram of figure 8-9b, the dynamic shear at each support is

$$S_d \left(\frac{61L}{192}\right) - M - p_t \frac{L}{2} \left(\frac{61L}{192} - \frac{L}{4}\right) = 0$$

Since the midspan moment, $M = RL^2/8$ for a uniform resistance R ,

$$S_d = 0.3934RL + 0.1065p_t L$$

From equation 8-2, using $S_s = \frac{R_u L}{2}$ at $z = 0$,

$$DIF = 0.7868 \frac{\delta}{\delta_E} + 0.2131 \frac{P_m}{R_u} \left(1 - \frac{t}{t_d}\right)$$

The terms in the above equations are defined in figure 8-9.

(b) Plastic Range $\delta > \delta_y$. A plastic hinge is assumed to be formed at midspan. The deflected shape and the inertia force distributions are linear. From the free-body diagram of figure 8-9c, the dynamic shear at each support is

$$S_d(0,t) = 0.375R_u L + 0.125p_t L$$

and

$$DIF = 0.750 + 0.250 \frac{P_m}{R_u} \left(1 - \frac{t}{t_d}\right)$$

This last equation is used in the construction of the design chart shown in figure 8-10, assuming undamped systems. Use of the chart is as follows. Enter the chart with known values of the time ratio, td/T , and read the value of DIF_m (td = load duration, T = fundamental period). The corresponding maximum dynamic shear at a distance z from the supports is approximately

$$S_{dm} = DIF_m \left[\frac{R_u L}{2} \left(1 - \frac{2z}{L}\right) \right]$$

where R_u is the dynamic ultimate flexural resistance (psi or other units of force per unit area).

$$R_u = \frac{8M_p}{L^2} \quad \text{Simple-simple beam}$$

$$R_u = \frac{8}{L^2} (M_n + M_p) \quad \text{Clamped-clamped beam}$$

$$R_u = \frac{2M_n}{L^2} \quad \text{Clamped-free slab}$$

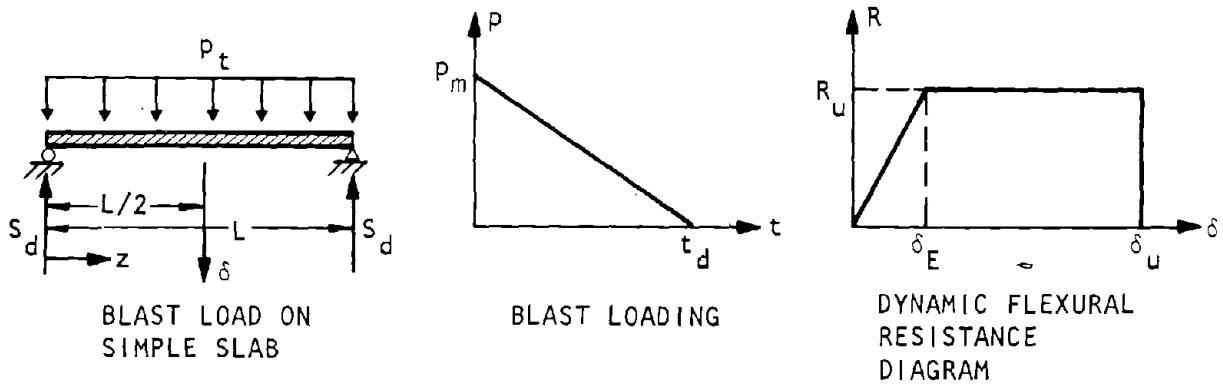
$$R_u \cong \frac{4}{L^2} (M_n + 2M_p) \quad \text{Simple-clamped beam}$$

The terms are defined in figures 8-9 and 8-10.

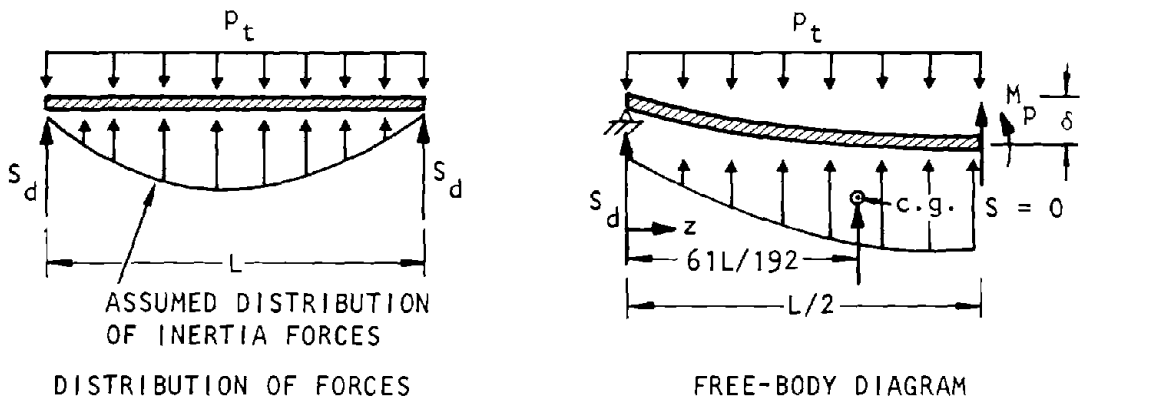
(3) Rebound. Rebound as a result of strain energy stored in the structural element is an important consideration for the design of connections, closure hinges and latches, and negative reinforcement for flexural members. For loads of long duration the rebound is normally less than the primary displacement. As a limiting case, for short duration loads, the rebound approaches the primary displacement. Figure 8-11 gives the relationships for the elastic rebound of undamped systems.

8-6. Analysis of complex structures

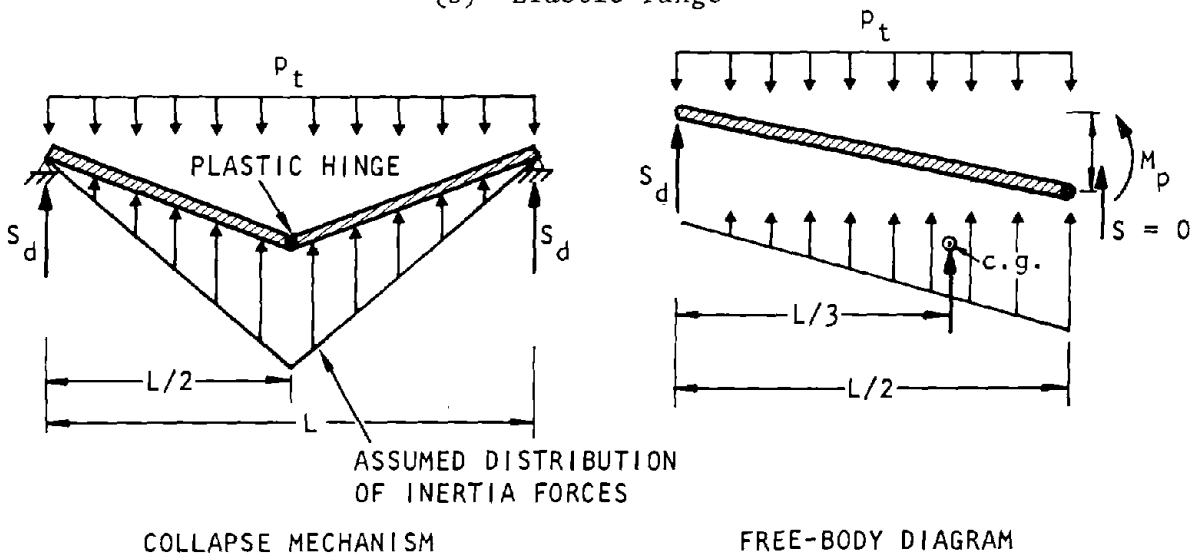
a. Use numerical procedures for complex structures requiring more refined analyses than those described in the earlier parts of this section. Special knowledge of mathematical modeling and computer programs will be required. Before a more complex analysis is undertaken, the principal elements of the structure should still be sized either by using equivalent static loads or by the simple procedures described earlier. If validation analyses and design procedures are not formally separated, the designer may wish to exercise his judgment as to whether the complex analyses are justified for design optimization while the design is in progress. In such a case, any one of several validation analysis methods may be used for finalizing design by using an iterative procedure. Mathematical techniques are found in textbooks. Computer code descriptions must be reviewed by the designer to make a selection of his approach (see appendix C



(a) Simple slab subjected to uniform blast load



(b) Elastic range



(c) Plastic range

Figure 8-9. Forces and Reactions on a Simple Slab Subjected to Uniform Blast Load (Keenan, 1976)

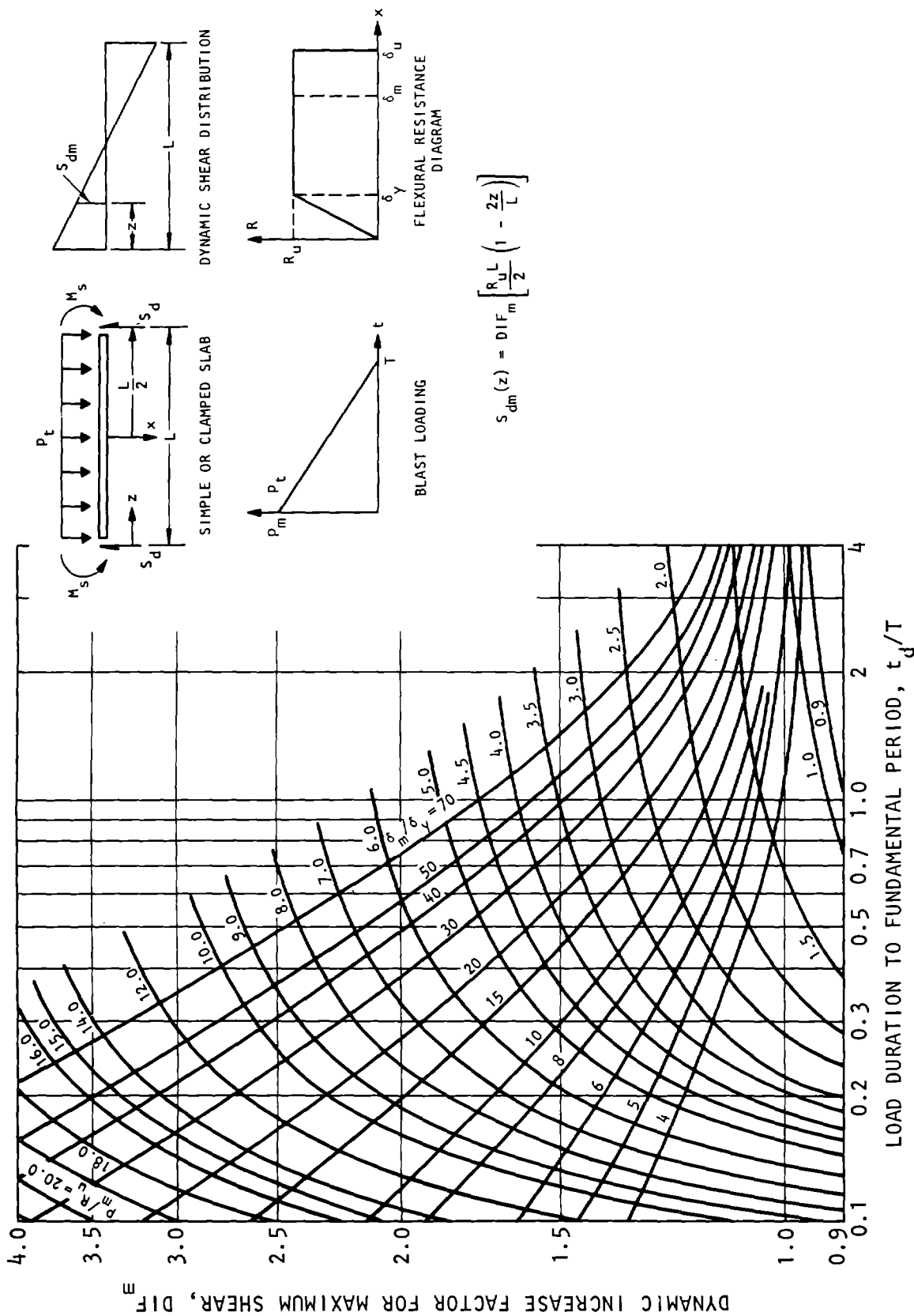


Figure 8-10. Design Chart for Maximum Dynamic Shear in a One-Way Slab (Adapted from Keenan, 1976)

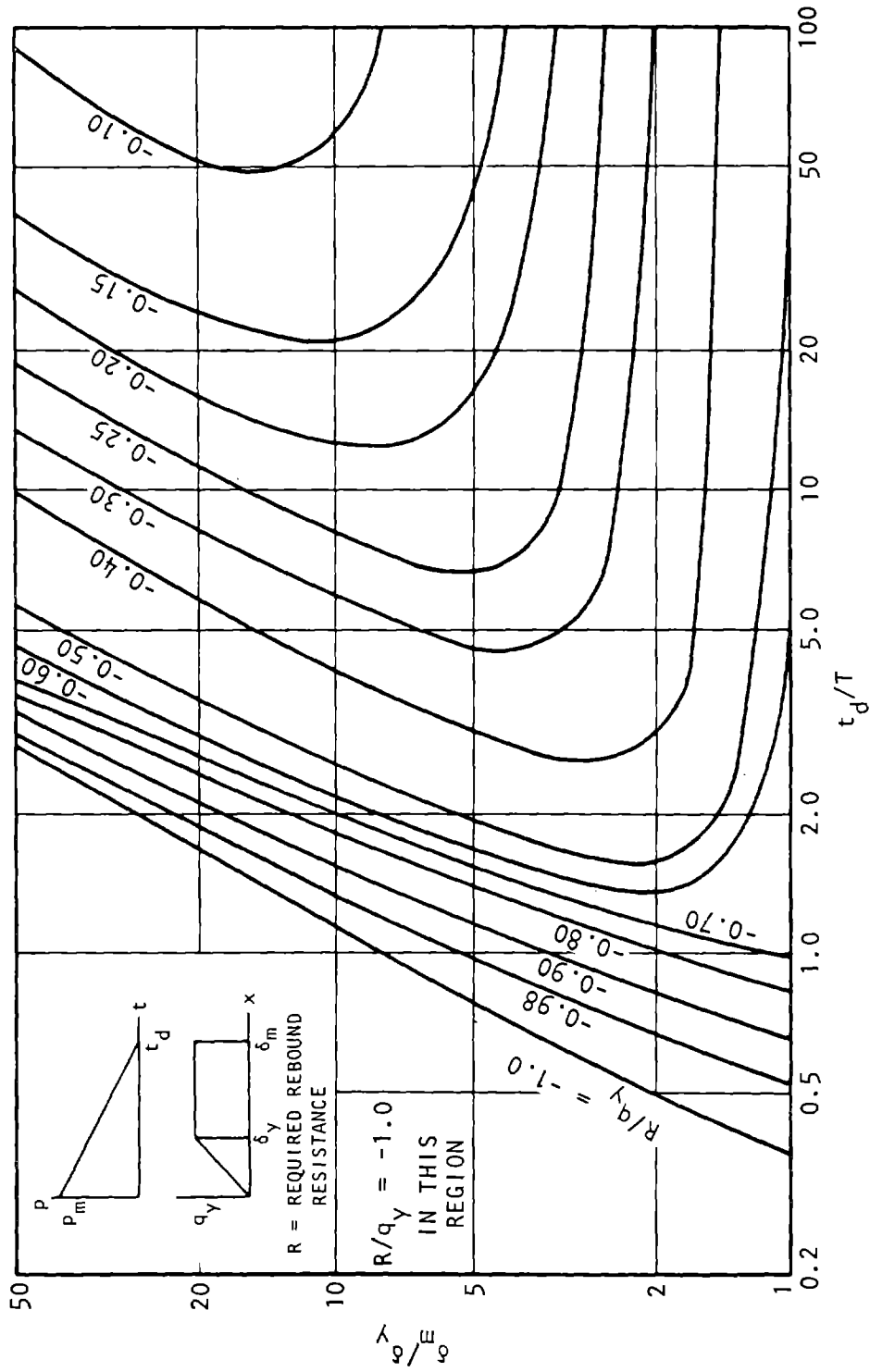


Figure 8-11. Design Chart for Elastic Rebound (Merritt-Newmark, 1964)

for a list of some available codes). Such analyses are usually made by the finite element method, described in chapter 9. Brief statements of the types of analyses follow. Refer to chapter 9 for detailed procedures.

b. Elastic Analysis.

(1) Equivalent static analysis. Static analyses use the matrix displacement method of linear structural analysis. This method involves the solution of a set of simultaneous linear equations relating to the unknown generalized joint displacement components to the known unbalanced generalized force components at each joint.

(2) Frequencies and mode shapes. As in the case of the single-degree-of-freedom system discussed earlier, the designer must choose the general deformation patterns of the mode shapes he desires and must prescribe a set of force patterns whose resulting deformations include such mode shapes.

(3) Shock response spectral analysis. A desired number of frequencies and mode shapes are first computed. Spectral amplitudes of the structure response at each modal frequency of the structure are obtained using an input response spectrum. These amplitudes for each mode are obtained by multiplying the corresponding value of the input response spectrum by an appropriate magnification factor that is dependent on the characteristic shape of the structure for the mode considered. The root sum square of the individual spectral response amplitudes at each point in the structure provides a reasonable estimate of the peak response at that point. Maximum joint displacements and the maximum element stresses, forces, and moments corresponding to all the desired natural frequencies of the structure are also obtained. The combined response of the structure in all its desired natural modes is obtained by the root sum square of the joint displacements and element stresses, forces, and moments.

(4) Dynamic response by normal mode method. The dynamic response of a structure subjected to airblast and ground shock may also be computed by the normal mode method using time-dependent inputs. A delay time may be specified for the force in order to treat moving blast loads.

(5) Dynamic response by step-by-step method. This method computes the dynamic response of a linearly elastic structure to time-dependent forcing

functions, time-dependent boundary displacement functions, and ground motion. A delay time may also be specified for the loading in order to simulate the moving airblast. The dynamic response is obtained by integrating the equations of motion directly with respect to time. The solution includes the relative and absolute displacements, velocities, and accelerations at selected time intervals. Time histories of the stress components for the selected elements are obtained. Response spectra are also obtainable from these results.

c. Nonlinear response by step-by-step method. The response is obtained by a step-by-step integration of the equations of motion. Since the stiffness matrix for the structure is displacement dependent, the equations of motion are written in an incremental form and integrated in time with an equilibrium check. The stiffness matrix is updated at selected intervals. The nonlinear elements may have any arbitrary material property as discussed in chapter 5.

(1) The nonlinear response of the structure is analyzed to determine where and when the formation of plastic hinges will occur or the ultimate capacity of the member exceeded. This analysis is facilitated by a first step in which the linear response of the structure due to the specified input is obtained. This preliminary analysis is intended to provide the information regarding the points where the plastic hinges are expected to form.

(2) Having obtained information about the joints where plastic hinges may develop from the above analysis, a new structure model for nonlinear analysis is prepared. This model includes, in addition to the elastic elements, nonlinear elements where plastic hinge formations are expected.

(3) It is possible that the nonlinear response of the structure may indicate some additional joints where plastic hinges may form. In such a case it may be necessary to revise the structure model and repeat the analysis. In many cases, however, the engineer should be able to select the locations of these hinges on the basis of the results from the linear analysis by introducing nonlinear elements at a place where the response moment is close to the yield point moment.

(4) This two-step method is more cost effective than starting the response analysis using nonlinear elements throughout the structure.

CHAPTER 9

NUMERICAL METHODS FOR STRUCTURE DESIGN VERIFICATION

9-1. Introduction

This section describes numerical methods used to verify the design of soil/structure systems and structural elements. It also explains the operation of structural computer codes and the preparation of input data. There is a large number of general-purpose and special-purpose structural computer codes that may be used for design verification analyses of hardened structures. These codes are based on the use of finite elements, and their information has evolved from matrix methods of algebra. The principles of matrix methods of structural analysis and types of finite elements that are commonly used are presented in appendix B for ready reference. A compilation of most of the currently available codes with a summary of their main features is given in appendix C. Some of these codes were not designed for hardened structures, but their characteristics make them suitable for such applications. Others have been specifically prepared for the analysis of hardened soil/structure systems and structural elements. The discussion that follows, although generally pertaining to SAP IV, applicable to most finite element computer codes.

9-2. Static analysis

a. External loads. The external loads are the concentrated forces and moments that are applied to the structure directly at the joints or nodal points. The forces at a joint must be resolved into components in the global coordinate directions. Several different load conditions, each consisting of a different set of joint loads, can be considered for a given structure.

b. Body forces. The body forces consist of gravity loads, thermal loads, normal pressures, and fixed-end forces and moments. The effects of the body forces (any linear combination of loads) can be considered separately or in combination with the external loads.

c. Gravity loads. Gravity loads must be in the direction of global coordinates. Once mass of materials in each specified element has been calculated, the gravity load is treated as though equally distributed among nodal points.

d. Thermal loads. Different elements may have different temperatures to approximate the spatial distribution of the temperature. To include thermal effects of an element in the analysis, the element temperature and the coefficient of thermal expansion are provided. Equivalent fixed-end forces and moments may be used to account for thermal effects in beam elements.

e. Pressure loads and fixed-end forces. The pressure loads can be specified only for axisymmetric solid and

three-dimensional solid elements. The pressure loads are always assumed to act normal to a surface. For each beam element, fixed-end forces and moments can be specified to account for any loading on the beam between the joints.

f. Solution technique. Static structural problems may be solved by using the matrix displacement method of linear structural analysis. This method involves the solution of a set of simultaneous linear equations relating to unknown generalized joint displacement components to the known unbalanced generalized force components at each joint. In matrix notation, the governing equations are:

$$[K]\{U\} = \{P\} \quad (9-1)$$

where

- {U} = Vector of unknown displacements
- {P} = Vector of unbalanced joint loads
- [K] = Global stiffness matrix generated from the individual element stiffness properties

When several load conditions are considered at one time, {U} and {P} in equation 9-1 become matrices whose columns correspond to different load conditions. The order of the [K] matrix is equal to the total DOF of the structure. A modified Gaussian elimination technique is used to solve equation 9-1. This involves a reduction of the equations to transform the [K] matrix to an upper triangular matrix. A back substitution procedure is applied to the resulting equations to solve for the unknown displacements {U}.

g. Input data. The input for static analysis consists of the joint, element, and load descriptions. The joint description consists of the joint restraints and the joint coordinates, both in a Cartesian global coordinate system. The element consists of the element number, the joints comprising the element, the body force information, and the material and geometric properties of the element. The input loading information consists of the joint loads for each load case. In addition, certain other controlling variables, such as the total number of joints, must be identified.

h. Output data. The output for static analysis consists of an echo printing of input data, the nodal point displacements, and the element stresses. For each joint where certain DOF are restrained, zero values will be indicated for the corresponding displacement components. Element stresses are printed out separately for the elements in each group. For a truss element the output consists of the axial stress and the axial force in the bar. For a three-dimensional beam

element, six components (one axial and two shear forces, one twisting and two bending moments) are output. For the membrane, axisymmetric solid, and three-dimensional solid elements, the output consists of three, four, and six stress components, respectively, in addition to the principal stresses and their orientation. For the shell and plate element, the output consists of three stress components and three moment components.

i. Computer run times. The computer run time required to solve a given static structural problem depends on many variables such as the type of computer, number of joints, and number of elements. A significant part of the total run time is generally required for solving equation 9-1. The total time required to solve these simultaneous equations is proportional to the product of the total DOF of the structure and the square of the bandwidth. The total run time can be expressed as

$$t = k_1 + k_2NM^2 + \sum_{i=1}^7 c_i(NEL)_i \quad (9-2)$$

and

$$M = NBAND + NL$$

where

- k_1, k_2, c_i = Constants that depend on the computer used
- N = Total DOF of the structure
- $NBAND$ = Bandwidth of the global stiffness matrix
- NL = Number of different load cases
- $(NEL)_i$ = Number of elements of Type i
- i = 1, 2, 3, 4, 5, 6, or 7 denoting truss, beam, membrane, axisymmetric solid, three-dimensional solid, shell and plate, or boundary spring element, respectively

For a given computer, the user can establish the constants k_1 , k_2 , and c_i by timing several example problems.

9-3. Response spectrum

a. Input data. The input consists of ground-shock accelerations in the form of an acceleration spectrum in the X, Y, or Z direction. This input spectrum is specified in terms of periods and the corresponding spectral acceleration values; the range of these periods should cover all natural frequencies considered in the analysis. The input spectrum should account for any structural damping.

b. Output data. The output consists of the maximum joint displacements and the maximum element stresses, forces, and moments corresponding to all the desired natural frequencies of the structure. The combined response of the structure in all its desired

natural modes is obtained by outputting the root mean square joint displacements and element stresses, forces, and moments.

c. Method of analysis. The engineer must specify the number of frequencies to be considered in the analysis and the method to be used to extract the mode shapes and frequencies. If the Rayleigh-Ritz method is indicated, a sufficient number of static load conditions should also be provided. The computation gives spectral amplitudes of the structure response at each modal frequency of the structure. These amplitudes for each mode are obtained by multiplying the corresponding value of the input response spectrum by an appropriate magnification factor. This factor is dependent on the characteristic shape of the structure for the mode considered. The root mean square of the individual spectral response amplitudes at each point in the structure provides a reasonable estimate of the peak response at that point. The theoretical basis for computing the spectral amplitudes is as follows. The equations of motion for a three-dimensional structure subjected to ground motions in three coordinate directions are

$$[M]\{\ddot{u}_a\} + [C]\{\dot{u}_r\} + [K]\{u_r\} = 0 \quad (9-3)$$

where

$$\{\ddot{u}_a\} = \begin{bmatrix} \ddot{u}_{xa} \\ \ddot{u}_{ya} \\ \ddot{u}_{za} \\ \ddot{\theta}_{xa} \\ \ddot{\theta}_{ya} \\ \ddot{\theta}_{za} \end{bmatrix} = \begin{bmatrix} \ddot{u}_{xg} \\ \ddot{u}_{yg} \\ \ddot{u}_{zg} \\ 0 \\ 0 \\ 0 \end{bmatrix} + \begin{bmatrix} \ddot{u}_{xr} \\ \ddot{u}_{yr} \\ \ddot{u}_{zr} \\ \ddot{\theta}_{xr} \\ \ddot{\theta}_{yr} \\ \ddot{\theta}_{zr} \end{bmatrix} = \{\ddot{u}_g\} + \{\ddot{u}_r\} \quad (9-4)$$

and

- $[M]$ = Mass matrix
- $[C]$ = Damping matrix
- $[K]$ = Stiffness matrix
- $\{\ddot{u}\}, \{\dot{u}\}, \{u\}$ = Acceleration, velocity, displacement vectors

in which the subscripts a, g, and r denote absolute, input ground and relative motions, respectively. Equation 9-3 can be rewritten as

$$[M]\{\ddot{u}_r\} + [C]\{\dot{u}_r\} + [K]\{u_r\} = \{P\} \quad (9-5)$$

where

$$P = -[M]\{\ddot{u}_g\} = - \begin{bmatrix} M_x \ddot{u}_{xg} \\ M_y \ddot{u}_{yg} \\ M_z \ddot{u}_{zg} \\ 0 \\ 0 \\ 0 \end{bmatrix} \quad (9-6)$$

The displacements of the structure are now expressed in terms of the mode shapes $[\Phi]$

$$\{u_r\} = [\Phi] \{R\} \quad (9-7)$$

and

$$\begin{aligned} \{\dot{u}_r\} &= [\Phi] \{\dot{R}\} \\ \{\ddot{u}_r\} &= [\Phi] \{\ddot{R}\} \end{aligned} \quad (9-8)$$

where $\{R\}$ represents the modal amplitudes. The substitution of equations 9-7 and 9-8 into equation 9-5 yields

$$[M][\Phi]\{\ddot{R}\} + [C][\Phi]\{\dot{R}\} + [K][\Phi]\{R\} = \{P\} \quad (9-9)$$

Premultiplication of equation 9-9 by $[\Phi^T]$ and the use of the orthonormal properties $[\Phi]$ produces a set of decoupled second order differential equations of the form

$$\{\ddot{R}\} + [D]\{\dot{R}\} + [\omega^2]\{R\} = \{F\} \quad (9-10)$$

where

$$\begin{aligned} [D] &= [\Phi^T][C][\Phi] \\ &= [2\lambda\omega] \end{aligned} \quad (9-11)$$

and

$$\begin{aligned} \{F\} &= [\Phi^T]\{P\} \\ &= \{F_x\} + \{F_y\} + \{F_z\} \end{aligned} \quad (9-12)$$

in which

$$\begin{aligned} \{F_x\} &= -[\Phi_x]^T [M_x] \{\ddot{u}_{xg}\} \\ \{F_y\} &= -[\Phi_y]^T [M_y] \{\ddot{u}_{yg}\} \\ \{F_z\} &= -[\Phi_z]^T [M_z] \{\ddot{u}_{zg}\} \end{aligned} \quad (9-13)$$

It should be noted here that equation 9-11 involves an assumption on the type of damping. A typical expression of equation 9-10 for the n th mode is of the form

$$\ddot{A}_n + 2\lambda\omega_n \dot{A}_n + \omega_n^2 A_n = F_{nx} + F_{ny} + F_{nz} \quad (9-14)$$

Now, by definition the spectral displacement is the maximum displacement of a unit mass system subjected to ground accelerations governed by the equation (Newmark-Rosenblueth, 1971)

$$\ddot{v} + 2\lambda\omega \dot{v} + \omega^2 v = \ddot{u}_g(t) \quad (9-15)$$

For a given frequency, damping, and ground motion history, this spectral displacement has been

calculated as $S(\omega)$. Therefore, for the three-dimensional structure subjected to an acceleration in the X-direction, the maximum response of the n th mode will be

$$R_{nx}(\max) = \{\Phi_{nx}\}^T [M_x] S_x(\omega_n) \quad (9-16)$$

Or the true three-dimensional maximum displacement of the structure subjected to a ground acceleration in the X-direction for the n th mode is

$$u_{nx}(\max) = \{\Phi_n\} R_{nx}(\max) \quad (9-17)$$

It should be noted here that all components of displacements may exist in a given mode even though this type of loading is in only one direction. Similarly, for ground accelerations in the Y- and Z-directions

$$\begin{aligned} u_{ny}(\max) &= \{\Phi_n\} R_{ny}(\max) \\ u_{nz}(\max) &= \{\Phi_n\} R_{nz}(\max) \end{aligned} \quad (9-18)$$

where

$$\begin{aligned} R_{ny}(\max) &= \{\Phi_{ny}\}^T [M_y] S_y(\omega_n) \\ R_{nz}(\max) &= \{\Phi_{nz}\}^T [M_z] S_z(\omega_n) \end{aligned} \quad (9-19)$$

Having obtained the maximum displacements in each mode, the stresses corresponding to the maximum displacements are computed. As an estimation of the maximum displacements and stresses of the structure, the root mean squares of the maximum total modal values are computed.

9-4. Dynamic response by normal mode method

a. Input data. The dynamic response of a structure subjected to ground motion and time-dependent forcing functions may be obtained by the normal mode method. The input consists of ground motion in the form of translational acceleration histories in three global directions (X, Y, or Z). The dynamic loading on the structure consists of load and moment histories applied at any joint of the structure. The ground motion and the dynamic loading inputs are specified by a set of time functions defined at discrete time points. Linear interpolation is used within the program to evaluate intermediate points. The force applied at any joint of the structure is then described by a scalar multiplier and one of the time functions. A delay time may also be specified for the force in order to treat moving loads such as blast loads. Provision is made to input the initial modal displacements and velocities to account for the case when the system does not start from rest. The structural damping is specified through the modal damping fractions. The input also includes

the joint and component numbers for which displacement, velocity, or acceleration time histories are required. Similarly, the element and stress component numbers for which stress time histories are required are also input.

b. Output data. The output may consist of relative and absolute time histories of displacement, velocity, and acceleration components at selected joints. Time histories of stress components for selected elements in the structure are also printed out. The output for each time history is followed by the maximum value and the time corresponding to this maximum value.

c. Method of analysis. The dynamic response of a structural system due to time-dependent loads and ground motion is obtained by approximating the displacement response of the structure by a linear combination of a number of lower mode shapes of the system. The number of the mode shapes that are considered in the analysis depends upon the integration time step specified by the engineer. It is desirable in computer codes that all the higher modes whose periods are less than five times the integration time step be deleted automatically. The decoupled second order differential equations of motion for each mode may be integrated numerically by the linear acceleration method. The structural damping is included in the form of modal damping fractions, which may have different values for different modes. The finite element formulation leads to the following equations of motion of a structural system subjected to ground motion and time-varying loads.

$$[M]\{\ddot{u}_r\} + [C]\{\dot{u}_r\} + [K]\{u_r\} = \{F\} \quad (9-20)$$

where

$$\begin{aligned} \{F\} &= \{P\} - [M]\{\ddot{u}_g\} \\ \{P\} &= \text{Applied force vector} \end{aligned} \quad (9-21)$$

and other symbols are as previously defined. The displacements of the structure are now approximated by a linear combination of the mode shapes $[\Phi]$.

$$\{u_r\} = [\Phi]\{R\} \quad (9-22)$$

and

$$\begin{aligned} \{\dot{u}\} &= [\Phi]\{\dot{R}\} \\ \{\ddot{u}\} &= [\Phi]\{\ddot{R}\} \end{aligned} \quad (9-23)$$

where $\{R\}$, $\{\dot{R}\}$ and $\{\ddot{R}\}$ represent the modal displacement, velocity, and acceleration amplitudes, respectively. Substitution of equations 9-21 and 9-23 into equation 9-20 and premultiplication of the resulting equation by $[\Phi]^T$ yields

$$\{\ddot{R}\} + [D]\{\dot{R}\} + [\omega^2]\{R\} = \{F'\} \quad (9-24)$$

where

$$\begin{aligned} [D] &= [\Phi]^T[C][\Phi] \\ \{F'\} &= [\Phi]^T\{F\} \end{aligned} \quad (9-25)$$

In arriving at equation 9-24, the orthonormal properties of $[\Phi]$, are utilized. To simplify equation 9-24 further, an assumption on the type of damping in the structure is usually made. Specifically, the damping matrix $[C]$ is assumed to have the properties to make $[D]$ a diagonal matrix whose elements are related to the modal damping fraction, i.e.,

$$[D] = [2\lambda\omega] \quad (9-26)$$

where λ_n is the damping ratio as a fraction of critical damping associated with the n th mode. As a result of the assumption in equation 9-25, equation 9-24 reduces to a set of "uncoupled," second order, ordinary differential equations and is given by

$$\{\ddot{R}\} + [2\lambda\omega]\{\dot{R}\} + \omega^2\{R\} = \{F'\} \quad (9-27)$$

The above equations may be integrated numerically step by step using the linear acceleration method to yield the modal amplitudes, $\{R\}$, $\{\dot{R}\}$ and $\{\ddot{R}\}$. The actual displacements, velocities, and accelerations for each time step are the calculated from equations 9-22 and 9-23. Finally, element stresses are computed from the actual displacements. Note that response motions obtained as above are relative to the fixed points of the structure. To obtain absolute motions, the program must add ground motions, if any, to the relative motions.

9-5. Dynamic response by direct integration method

a. Input data. The dynamic response of a linearly elastic structure to time-dependent forcing functions, displacement functions, and ground motions may be obtained by integrating the equations of motion directly with respect to time. The input consists of the time histories of applied forces and prescribed boundary displacements, data defining the absorbent boundary, time histories of ground acceleration in the x, y, and z directions, damping constants, and integration parameters.

b. Output data. The output will consist of the displacements, velocities, and accelerations of unconstrained degrees of freedom at specified intervals, as well as stress time histories. If a restart option is exercised, the program generates a data tape containing all the pertinent information to continue the solution at a later time.

c. *Method of analysis.* A step-by-step method of integration of the matrix equation of motion to compute the response of the structure to arbitrary time-dependent forces, displacements, or ground accelerations has been developed by Wilson et al. (1973). This integration scheme is unconditionally stable and therefore places no restriction on selection of the time step. However, the engineer must select and provide a time step that may be based on the cut-off frequency of the system and the characteristics of the input disturbance or the finite element mesh size. The choice of the integration time step also affects the level of the damping that is introduced into the system (Wilson et al., 1973). An option to vary the integration time step may also be provided in the program, which can be used to optimize the solution time. This method should include a restart capability to terminate a problem solution at any point and then to continue the solution at a later time. The input ground motion is in the form of ground accelerations in the direction of the three global axes (X, Y, and Z). The dynamic loading and boundary displacements consist of the time-dependent loads and displacements applied to the translational and rotational degrees of freedom. A delay time may also be specified for the loading in order to simulate the moving loads such as the blast loads.

d. *Step-by-step method of integration.* For a structural system composed of finite elements, the matrix equations of motion to be integrated in time are

$$[M]\{\ddot{u}\} = [C]\{\dot{u}\} + [K]\{u\} = \{P\} \quad (9-28)$$

The accelerations are assumed to vary linearly within a time interval $\tau = \theta\Delta t$ where Δt is the time step and θ is a constant ≥ 1 which may take the values between 1.43 and 2.7 for unconditional stability. It should be noted here that the integration procedure with $\theta = 2.0$ corresponds to the modified acceleration method due to Wilson (1968). Equation 9-28 satisfied at time $t + \tau$ gives

$$[M]\{\ddot{u}\}_{t+\tau} + [C]\{\dot{u}\}_{t+\tau} + [K]\{u\}_{t+\tau} = \{P\}_{t+\tau} \quad (9-29)$$

From the linear acceleration assumption, the following expressions for $\{\ddot{u}\}_{t+\tau}$ and $\{\dot{u}\}_{t+\tau}$ in terms of the variables at time t and $\{u\}_{t+\tau}$ are established:

$$\begin{aligned} \{\ddot{u}\}_{t+\tau} &= \frac{6}{\tau^2} \{u\}_{t+\tau} - \{a\}_t \\ \{\dot{u}\}_{t+\tau} &= \frac{3}{\tau} \{u\}_{t+\tau} - \{b\}_t \end{aligned} \quad (9-30)$$

where $\{a\}_t$ and $\{b\}_t$ are computed from the known values of the state variables at time t

$$\{a\}_t = \frac{6}{\tau^2} \{u\}_t + \frac{6}{\tau} \{\dot{u}\}_t + 2 \{\ddot{u}\}_t$$

$$\{b\}_t = \frac{3}{\tau} \{u\}_t + 2 \{\dot{u}\}_t + \frac{\tau}{2} \{\ddot{u}\}_t \quad (9-31)$$

From equations 9-29 and 9-30 the following equation for the evaluation of $\{u\}_{t+\tau}$ can be established

$$[\bar{K}]\{u\}_{t+\tau} = \{\bar{P}\}_{t+\tau} \quad (9-32)$$

where the effective stiffness matrix $[\bar{K}]$ is independent of time and the effective load vector $\{\bar{P}\}$ is a function of load at time $t + \tau$ and of known values at time t . They are given by

$$[\bar{K}] = [K] + \frac{3}{\tau} [C] + \frac{6}{\tau^2} [M]$$

$$\{\bar{P}\}_{t+\tau} = \{P\}_{t+\tau} + [M]\{a\}_t + [C]\{b\}_t \quad (9-33)$$

By substituting the $\{u\}_{t+\tau}$ into equation 9-30 the values of the accelerations and velocities at this time are also known. Then the value of these variables at the desired time $t + \Delta t$ can be determined from the following equations:

$$\begin{aligned} \{\ddot{u}\}_{t+\Delta t} &= (1 - \frac{1}{\theta}) \{\ddot{u}\}_t + \frac{1}{\theta} \{\ddot{u}\}_{t+\tau} \\ \{\dot{u}\}_{t+\Delta t} &= \{\dot{u}\}_t + \frac{\Delta t}{2} (\{\dot{u}\}_t + \{\dot{u}\}_{t+\tau}) \\ \{u\}_{t+\Delta t} &= \{u\}_t + \Delta t \{\dot{u}\}_t + \frac{\Delta t^2}{6} (2\{\ddot{u}\}_t + \{\ddot{u}\}_{t+\tau}) \end{aligned} \quad (9-34)$$

The procedure is repeated for the next time step until the solution advances to the specified point in time. For linear systems, the effective stiffness matrix need be formed only once. However, if the time step of integration is altered, the effective stiffness matrix will have to be reformulated.

e. *Damping.* The damping matrix $[C]$ is assumed to have the following general form

$$[C] = \alpha [M] + \beta [K] + [C_a] \quad (9-35)$$

where α and β are constant and $[C_a]$ is a matrix containing the dashpot coefficients. The first two terms on the right-hand side of equation 9-35 represent uniform damping while the last term indicates localized viscous damping. The choice of the damping constants α and β depends entirely on the type of the problem. In general, the critical damping ratio for each mode λ_n (if the frequencies and mode shapes are defined) is related to α and β through the following relation

$$\lambda_n = \frac{\alpha}{2\omega_n} + \frac{\beta\omega_n}{2} \quad (9-36)$$

where ω_n is the frequency of the n th mode. Some damping is also introduced into the system by the integration scheme that depends on the θ and Δt . A certain degree of engineering judgment is therefore required in the selection of the constants α , β , and θ and the time step Δt . The details of the level of the damping introduced into the system by the integration scheme are given by Wilson et al. (1973). For the special case of the ground motion analysis, the accelerations, velocities, and displacements computed from the above method are relative values. The loading functions $\{P\}$, in this case, have the following form

$$\{P\} = [M] \left(\{1_x\} \ddot{u}_{gx} + \{1_y\} \ddot{u}_{gy} + \{1_z\} \ddot{u}_{gz} \right) \quad (9-37)$$

where \ddot{u}_{gx} , \ddot{u}_{gy} , and \ddot{u}_{gz} are the components of the ground accelerations in x, y, and z directions and $\{1_x\}$, $\{1_y\}$, and $\{1_z\}$ are vectors that have the value of one at degrees of freedom corresponding to x, y, and z, respectively, and zeros for the rest of the degrees of freedom.

f. Kinematic boundary conditions. the given displacement boundary conditions are first transformed into forced boundary conditions. This is achieved by attaching fictitious springs with large spring constants to the prescribed degrees of freedom and applying a force to produce the desired displacement. This procedure only affects the above time integration scheme in the solution of equation 9-32. To improve the accuracy of the method in the process of back substitution, the displacements of the prescribed degrees of freedom are set equal to the specified displacements.

g. Absorbent-boundary technique. When the structure to be analyzed extends indefinitely in one or more directions, a finite element representation of the structure must necessarily be of finite dimensions. This truncation of space creates an artificial boundary in the finite element mode; therefore, reflections from the fictitious boundary intermingle with the real response of the structure and introduce undefined errors in the solution. One remedy to the problem is to make the finite element grid so large that reflections do not reach the points of interest during the time of interest. But for many problems where the time of interest is relatively large, this is not practical. An absorbent-boundary technique due to Lysmer and Kuhlemeyer (1969) may be incorporated into the program for the purpose of preventing unwanted reflections from a boundary by providing a set of three dashpots with appropriate properties at each nodal point on the boundary. It is assumed that the set of fictitious dashpots are attached to the boundary nodal points. Let D_p and D_s represent the dashpot constants perpendicular to the boundary surface and in the plane of the boundary surface, respec-

tively. The values of D_p and D_s are given by the following relations:

$$\begin{aligned} D_p &= \rho a V_p \\ D_s &= \rho a V_s \end{aligned} \quad (9-38)$$

where a is the tributary surface area of the nodal point, ρ is the mass density, and V_p and V_s are the dilational and distortional wave velocities. This method is known to produce accurate results for one-dimensional wave propagation problems. In two- and three-dimensional problems, the method is approximate and the efficiency in transmitting the energy depends on the angle of incident waves with respect to the boundary. For problems in which the major portion of the incident waves are perpendicular to the boundary, the method is expected to produce reasonably accurate results.

9-6. Nonlinear dynamic analysis

a. Input data. The dynamic response of a structural system consisting of any combination of linear elements and nonlinear elements to time-dependent forces, boundary displacements, and ground motions is computed by integrating the equations of motion directly with respect to time. The input is similar to the linear dynamic option described in paragraph 9-5a. In addition, the nonlinear material properties and element descriptions for the nonlinear elements are required.

b. Output data. The output is similar to the previous option described in paragraph 9-5b.

c. Method of analysis. Here an incremental form of step-by-step method of time integration of equations of motion is used to compute the response of a structural system consisting of a combination of linear elements and nonlinear elements. This incremental step-by-step method, due to Wilson et al. (1973) is considered to be very accurate since it satisfies the equilibrium at the end of each time step. The stiffness matrix in this case is displacement dependent, and, therefore, is updated at selected intervals. The other features of this option are similar to the linear step-by-step analysis option described in paragraph 9-5.

d. Step-by-step method of integration. For the nonlinear systems, the matrix equations of motion are written in an incremental form, but the expression of total equilibrium is preserved:

$$\begin{aligned} [M] \{\ddot{u}\}_{t+\tau} + [C]_t \{\Delta \dot{u}\}_t + [K]_t \{\Delta u\}_t \\ = \{P\}_{t+\tau} - \{F^d\}_t - \{F^e\}_t \end{aligned} \quad (9-39)$$

where

$$\begin{aligned}
 \{\ddot{u}\}_t &= \text{Acceleration vector at time } t \\
 \{\Delta \dot{u}\}_t &= \{\dot{u}\}_{t+\tau} - \{\dot{u}\}_t = \text{Increment of velocity vector} \\
 \{\Delta u\}_t &= \{u\}_{t+\tau} - \{u\}_t = \text{Increment of displacement vector} \\
 \{F^d\}_t &= \text{Internal resisting force vector due to damping} \\
 \{F^e\}_t &= \text{Internal resisting force vector due to stresses} \\
 \tau &= \theta \Delta t
 \end{aligned}$$

From the linear acceleration assumption, $\{\ddot{u}\}_{t+\tau}$ and $\{\Delta \dot{u}\}_t$ can be expressed in terms of known quantities and $\{\Delta u\}_t$ as

$$\begin{aligned}
 \{\ddot{u}\}_{t+\tau} &= 6/\tau^2 \{\Delta u\}_t - 6/\tau \{\dot{u}\}_t - 2\{\ddot{u}\}_t \\
 \{\Delta \dot{u}\}_t &= 3/\tau \{\Delta u\}_t - 3\{\dot{u}\}_t - \tau/2 \{\ddot{u}\}_t
 \end{aligned} \quad (9-40)$$

Substitution of equation 9-40 into equation 9-39 results in the following equation that can be solved to obtain $\{\Delta \bar{u}\}_t$:

$$[\bar{K}]_t \{\Delta \bar{u}\}_t = \{\bar{P}\}_{t+\tau} \quad (9-41)$$

Where the effective stiffness matrix $[\bar{K}]_t$ and the effective load vector $\{\bar{P}\}_{t+\tau}$ are given by

$$\begin{aligned}
 [\bar{K}]_t &= [K]_t + 3/\tau [C] + 6/\tau^2 [M] \\
 \{\bar{P}\}_{t+\tau} &= \{P\}_{t+\tau} - \{F^e\}_t - \{F^d\}_t \\
 &\quad + (3\{\dot{u}\}_t + \tau/2 \{\ddot{u}\}_t) [C]_t \\
 &\quad + (6/\tau \{\dot{u}\}_t + 2\{\ddot{u}\}_t) [M]
 \end{aligned} \quad (9-42)$$

Equation 9-41 can be solved to obtain $\{\Delta \bar{u}\}_t$. Note that in general the effective stiffness matrix $[\bar{K}]_t$ is dependent on the displacements at time t due to the material nonlinearity. But for weak nonlinear problems, it is not necessary to reform the stiffness matrix after every step. Finally, the displacements, velocities, and accelerations at time $t + \Delta t$ can be calculated by the following expressions:

$$\begin{aligned}
 \{\ddot{u}\}_{t+\Delta t} &= \frac{6}{\theta^2} \{\Delta \bar{u}\}_t - \frac{6}{\theta} \{\dot{u}\}_t + (1 - \frac{3}{\theta}) \{\ddot{u}\}_t \\
 \{\dot{u}\}_{t+\Delta t} &= \{\dot{u}\}_t + \frac{\Delta t}{2} (\{\ddot{u}\}_t + \{\ddot{u}\}_{t+\Delta t}) \\
 \{u\}_{t+\Delta t} &= \{u\}_t + \Delta t \{\dot{u}\}_t + \frac{\Delta t^2}{6} (2\{\ddot{u}\}_t + \{\ddot{u}\}_{t+\Delta t})
 \end{aligned} \quad (9-43)$$

The procedure is repeated for few time steps while keeping the effective stiffness matrix $[K]_t$ constant. The effective stiffness matrix is reformulated at every few steps and the whole procedure is repeated. The other features of this option such as the kinematic boundary conditions, absorbent-boundary technique, and the damping matrix are described in paragraphs 9-5. A comparison of the different methods of dynamic analyses are provided in table 9-1.

9-7. Modeling techniques

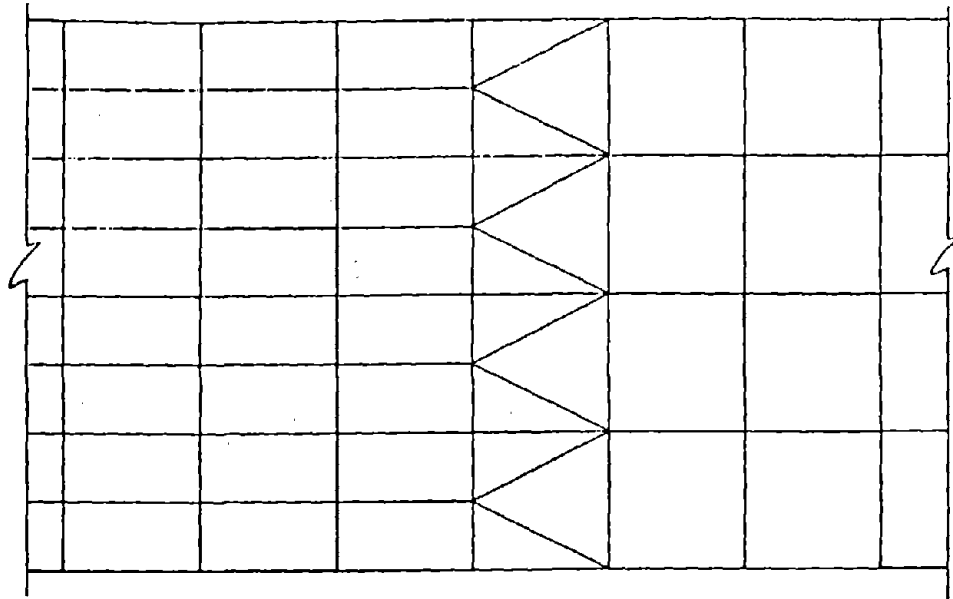
a. Meshing techniques when a soil/structure or structural system is idealized by the different types of finite elements, best results will be obtained if the elements are as regular in shape as possible. Membrane, axisymmetric, solid, and shell and plate elements should be as close to a square as possible. Long rectangles should be avoided where possible. For best results the three-dimensional elements should be either cubes or rectangular bricks. Usually, triangular elements are used only in the transition region from a coarse mesh to a fine mesh or vice versa, as shown in figure 9-1a. The mesh shown in figure 9-1b presents a possible alternate scheme that completely avoids the use of triangular elements. Whenever a composite structure is modeled by a number of different elements, care must be exercised in connecting the degrees of freedom (DOF) at a joint that interfaces two or more different types of elements. For example, when one end of a three-dimensional beam element connects to a node of a three-dimensional solid element, the beam element is not capable of transferring the three moment components to the solid element and the beam element will be free of any joint moments at the connection. This situation can be remedied by various artifices. Consider, for example a structural problem in which the response of a tower embedded firmly in the ground and subjected to airblast and dead loads is desired. For this case, it is assumed that the ground can be represented by the membrane elements while the tower is best represented by beam elements. If the mesh shown in figure 9-2a is used for this purpose, the tower becomes unstable as joint 23 acts as a hinge. One way to remedy the above situation is to introduce two fictitious beam elements considerably stiffer than the other beam elements, as shown in figure 9-2b. It should be noted here that most computer programs available (appendix C) have preprocessors for generating and displaying finite element meshes. A separate graphic grid generator is available at WES (Tracy, 1977).

b. Meshing of nonlinear elements. To demonstrate the use of nonlinear elements, the nonlinear response of a building frame is considered. The building is shown in figure 9-3. The nonlinear response of the

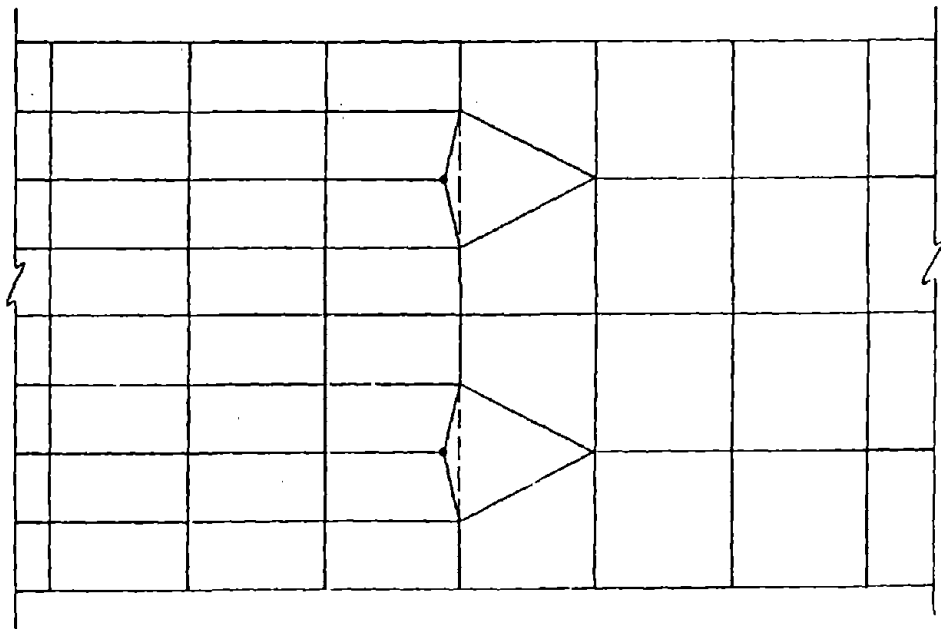
Table 9-1. Comparison of Different Methods of Dynamic Analysis

No.	Item to be Compared	Modal Analysis Methods			Direct Integration Method
		Response Spectrum Method	Time-History Method		
1	Major Computational Effort Involved	Extract mode shapes and frequencies.	Extract mode shapes and frequencies.		Triangularization and back substitution.
2	Total Cost of Computations	Most economical. Cost is essentially independent of the duration of the input record.	Computational effort increases with the duration of the input record.		Most expensive. Cost is directly proportional to the duration of the input record.
3	Input for Analysis	Design spectrum.	A time history is to be generated if the input is a design spectrum.		A time history to envelop design spectrum.
4	Multidirectional Input	Responses from the individual analyses must be combined in some manner.	Can be accounted for in one operation by simultaneously applying time histories for horizontal and vertical input motions.		Can be accounted for in one operation by simultaneously applying time histories for horizontal and vertical input motions.
5	Type of Analyses	Only linear analyses are possible.	Only linear analyses are possible.		Linear and nonlinear analyses are possible.
6	Energy Absorbing Boundary Using Dampers	Not possible.	Not possible.		Can be used effectively to simulate infinite extent of soil media.
7	Form of Damping	Modal damping ratios can directly be used. The damping matrix must be such that the equations are decoupled under appropriate transformation.	Modal damping ratios can directly be used. The damping matrix must be such that the equations are decoupled under appropriate transformation.		Damping matrix must be constructed from the given modal damping ratios using an available method. Also the form of the damping matrix is not restricted. Rayleigh type damping, when used, conserves computer storage.
8	Different Damping in Different Parts of the System	Cannot be handled directly. An approximate procedure must be used to estimate effective damping ratios.	Cannot be handled directly. An approximate procedure must be used to estimate effective damping ratios.		Can be handled directly if a damping matrix can be provided for each part.
9	Accuracy of Solution	Depends on the number of modes considered. The maximum modal responses are combined in some approximate way.	Depends on the number of modes considered in the analysis. Desired level of accuracy can generally be obtained.		Desired accuracy can be obtained, in general, by adjusting the integration time step.

U.S. Army Corps of Engineers



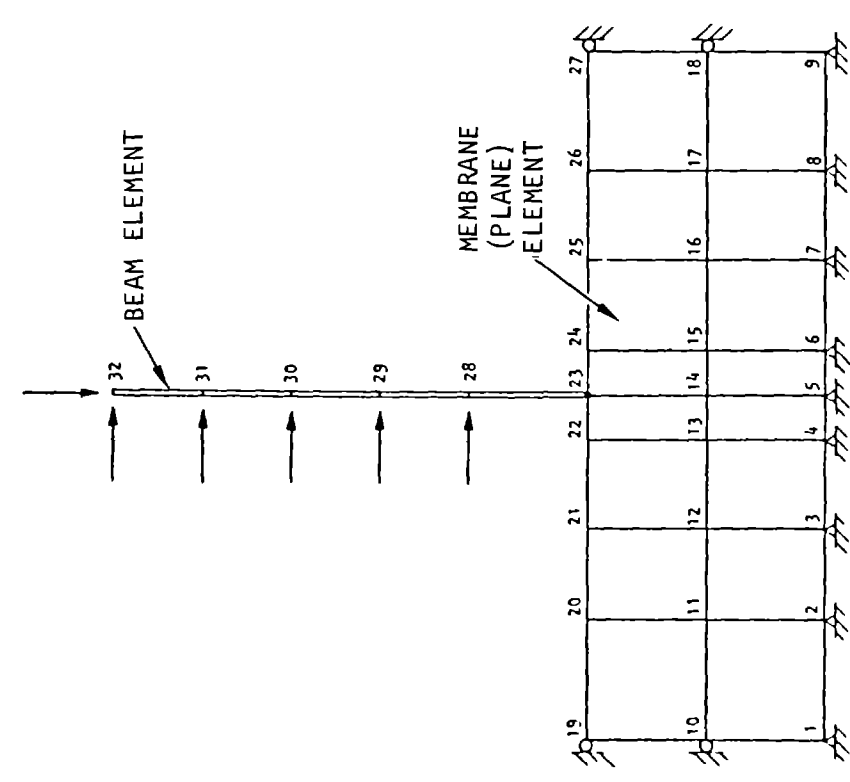
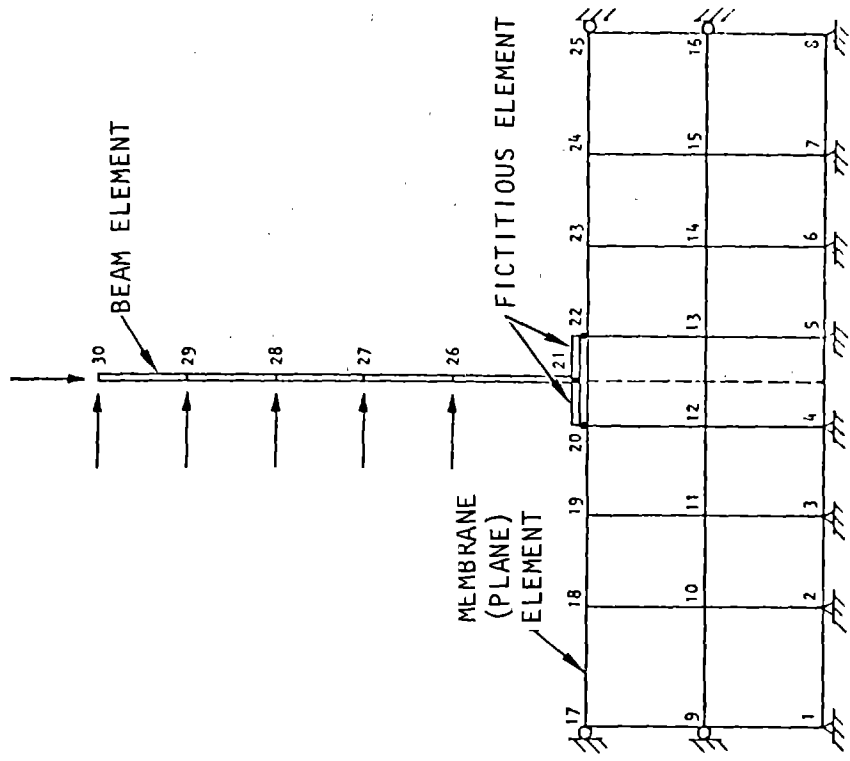
(a) Transition from a fine mesh to a coarse mesh using triangular elements



(b) Transition from a fine mesh to a coarse mesh using quadrilaterals only

U.S. Army Corps of Engineers

Figure 9-1. Meshing Techniques



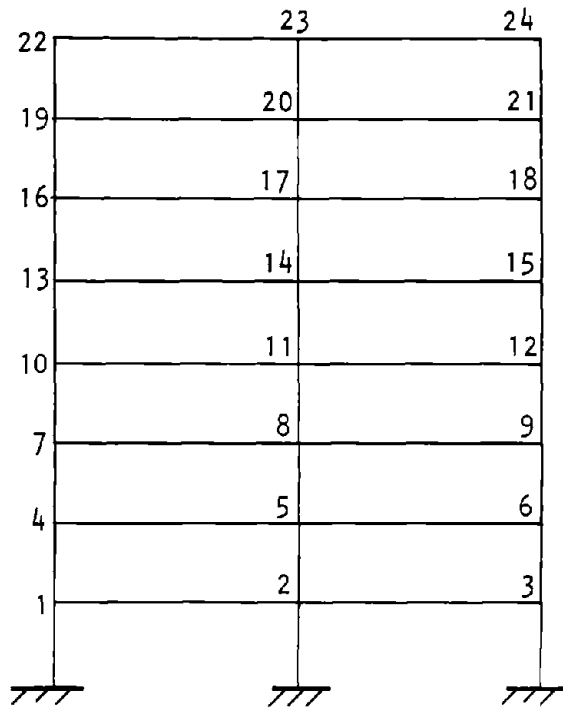
(a) Incorrect model of the tower and the ground
 U.S. Army Corps of Engineers

(b) Correct model of the tower and the ground

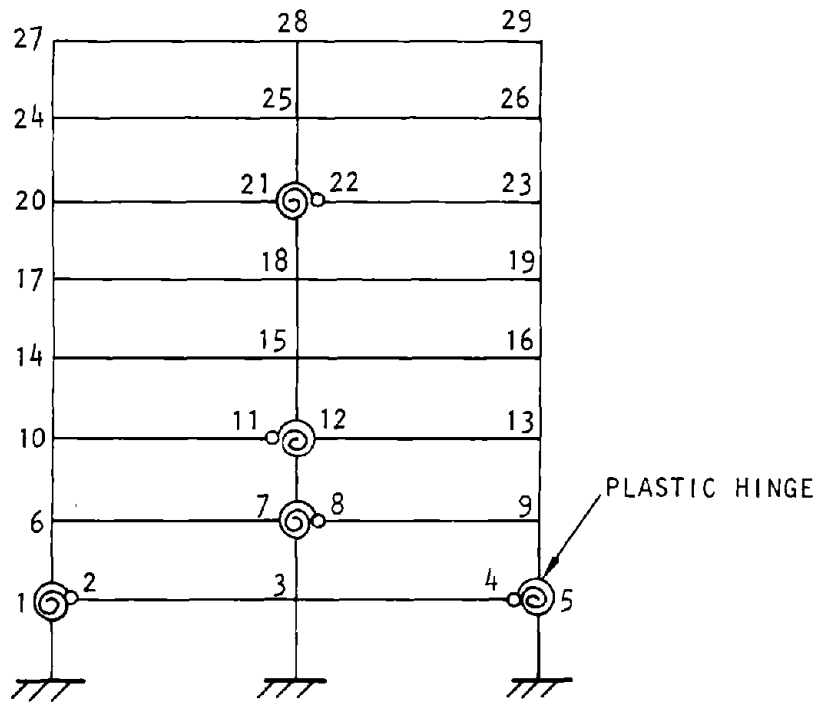
Figure 9-2. Modeling Techniques

building will be due mainly to the formation of plastic hinges at some key joints. A plastic hinge will result whenever the response moment values exceed the yield point moment of a member. The first step in the analysis is to obtain the linear response of the building due to the specified input. The building model as shown in figure 9-3a consists of elastic beam elements only. This preliminary analysis is intended to provide the information regarding the points where the plastic hinges are expected to form. Having obtained information about the joints where plastic hinges may develop from the above analysis, a new building model for nonlinear analysis is prepared. This model is shown in figure 9-3b. In addition to the elastic beam elements, the model includes nonlinear

moment springs to simulate plastic hinge formations. For each original node where a hinge forms, an additional node whose translational DOF are slaved to the original node is introduced. The moment spring is then connected to the rotational DOF of the two joints. It is possible that the nonlinear response of the buildings (fig. 9-3b) may indicate some additional joints where plastic hinges may form. In such a case it may be necessary to revise the building model and repeat the analysis. In many cases, however, the engineer should be able to select the locations of these hinges on the basis of the results from the linear analysis by introducing a nonlinear moment spring at a place where the response moment is close to the yield point moment.



(a) Building model for linear analysis



(b) Building model for nonlinear analysis

U.S. Army Corps of Engineers

Figure 9-3. Building Models

CHAPTER 10 ABOVEGROUND STRUCTURES

10-1. General

a. An aboveground structure is exposed to all nuclear weapon effects and must be designed to protect materiel and personnel from these environments. The facility design is normally dictated by airblast loadings, although nuclear radiation shielding requirements will sometimes control the thickness of structural elements. The cost of hardening aboveground structures increases rapidly if the specified hardness level cannot be met by structural configuration alone. There are also limitations on feasibility. If the structure can perform its functions underground, consider this alternative for attenuating the nuclear-weapon-effects environment.

b. In general, the airblast effects will govern the design of aboveground structures. The adequacy of the structure under the secondary weapon effects of nuclear radiation, ground shock, fireball, thermal radiation, ejecta/debris impact and depth, dust erosion, and firestorm can then be determined and modifications made as required. Free-field nuclear weapon phenomena are delineated in TM 5-858-2. The translation of the free-field phenomena into loads acting on aboveground structures will be developed in this chapter.

10-2. Resistance/geometry selection

The following resistance/geometry concepts, listed in order from least to greatest inherent hardness, are rational candidates for aboveground structures:

- Rigid frame
- Shear wall
- Arch
- Dome

Rigid frame and shear wall are best suited for multistoried facilities, whereas arch and dome construction are best suited for single story, relatively compact facilities. Rigid frame and shear-wall structures require blast-resistant exterior walls and roof to carry the blast loads to the frame and shear walls and as a result become progressively more inefficient imitators of arch and dome construction as the hardness level increases. The choice of resistance/geometry will, in general, ultimately be based on cost effectiveness.

10-3. Construction material selection

Reinforced-concrete construction has been found to be cost effective in the past. Steel and composite construction should also be considered, particularly for relatively small structures. See chapter 6.

10-4. Design for airblast

a. Airblast loads. Aboveground structures will be subjected to the direct effects of airblast as well as to the movements of the ground beneath and around the structure. External loads imposed by the airblast are assumed to be independent of structure motions; external loads from ground shock must be determined by considering structure/medium interaction. The airblast loading on exposed structure surfaces is a function of the free-field overpressure and dynamic pressure; the size, shape, and orientation of the surface; and the location and orientation of other surfaces in the vicinity. Overpressure, reflected pressure, and dynamic pressure must be considered. The size and shape of the structure and the character of the airblast pulse will determine the relative importance of these three components. For large structures subjected to short-duration blast waves, the net loading due to reflected pressures will probably be more important than that due to the dynamic pressure. As the structure becomes smaller or the blast-wave duration becomes larger, the net loading due to overpressure on front and rear surfaces becomes of less importance than the dynamic or drag loading.

b. Overpressure. The shock wave from the sudden release of energy in a nuclear explosion is called a "blast wave" and is characterized by a sudden increase in pressure which immediately begins to decay, as shown in figure 10-1. As the front of the blast wave travels across the terrain, the transient pressure in excess of the ambient is defined as the "overpressure." The peak overpressure is the maximum value of the overpressure at a given location. Its magnitude and its variation with time are functions primarily of the weapon yield, the height of burst, and the distance from the burst. Quantitative values for all parameters describing the airblast pulse are presented for combinations of weapon yield, range from burst point, and height of burst in TM 5-858-2.

c. Reflected pressure. Whenever the blast wave strikes a surface, reflection causes an increase in the peak overpressure. This reflection is caused when the moving air changes direction and momentum as a result of striking the surface. The ratio of reflected overpressure to incident pressure is called the "reflection factor." The reflection factor varies with both the peak overpressure of the incident wave and the angle at which the blast wave strikes the surface. Highest reflection factors occur at a zero angle of incidence, i.e., a surface normal to the direction of propagation of the blast wave. Figure 10-2 gives reflection factors

for an angle of incidence equal to zero. Figure 10-3 shows the effect of the angle of incidence on reflection factors for a wide range of overpressure levels.

d. *Dynamic pressure.* Dynamic pressures on structures are proportional to the mean density of the air particles and to the square of the peak wind velocity behind the shock front. Drag forces are associated with these strong transient winds behind the shock front. In particular, some structure geometries are described as "drag sensitive" because they are quickly enveloped by the blast wave and translatory forces are primarily a result of drag forces acting on the structure. These drag forces are a function of the size and shape of the structure and the peak value of the dynamic pressure. Quantitative data defining the parameters of dynamic pressure loadings on structures are presented in TM 5-858-2.

e. *Drag and lift forces.* The dynamic pressure is related to the pressure acting on the structure by shape factors called "drag coefficients." These coefficients are affected by many variables, including dynamic pressure level; temperature; body size, shape, and surface texture; and orientation to other subjects. Since dynamic pressure is constantly changing behind the shock front, the drag coefficient is also subject to change. In most cases, however, this change is neglected and the drag coefficient corresponding to flow conditions near the shock front is used. The total drag force acting on an object is given by

$$F_D = C_D q A_p \tag{10-1}$$

where

- C_D = Drag coefficient for structural element
- q = Dynamic pressure

A_p = Projected area of structural element on a plane perpendicular to the air flow

Figure 10-4 gives values of C_D as a function of peak overpressure for four structural shapes.

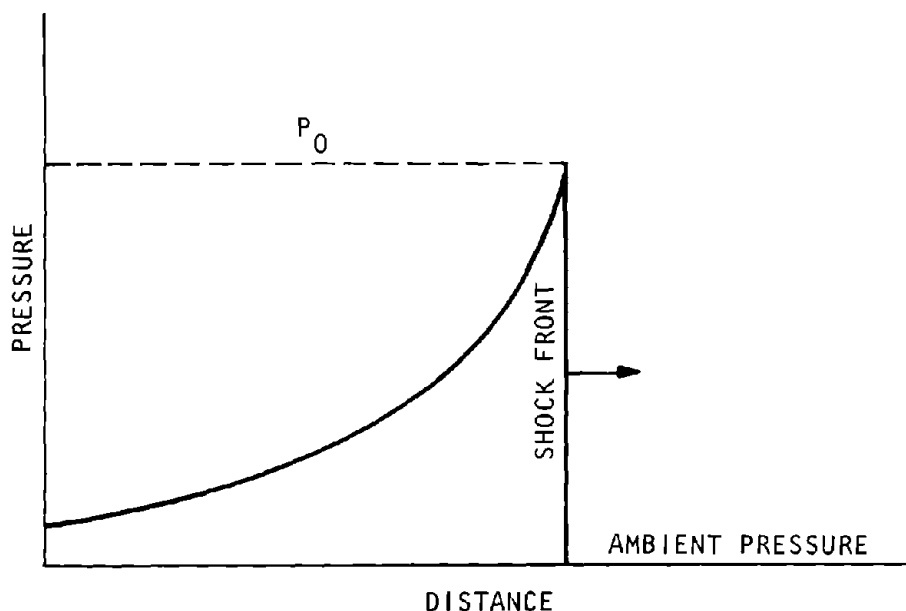
(1) Curve (a) of figure 10-4 applies to a plate of infinite length oriented normal to the free-field air flow. Since the effects of length in the direction of air flow are minor for Mach numbers greater than about 0.5, this curve can be applied to objects of rectangular cross section and great length at right angles to the direction of free-field air flow.

(2) Curve (b) applies to a disk oriented normal to the direction of free-field air flow. It can also be applied to an object with a plane front face normal to the shock front and a length in the direction of the shock front of the same order of magnitude as the minimum front-face dimension. Coefficients from this curve become unreliable if the ratio of front-face dimensions varies greatly from 1. In these cases, the proper drag coefficient lies between curves (a) and (b).

(3) Curve (c) applies to a long cylinder with its axis in the plane of the shock front. This curve will give conservative values when applied to a semicylindrical object on a plane surface.

(4) Curve (d) applies to a sphere. It will give conservative values when used to evaluate drag forces on a dome on a plane surface. This curve may also be used to establish a lower bound for the loading on a short cylinder with its axis in the plane of the shock front.

(5) The coefficients from figure 10-4, used in equation 10-1, yield the *total* drag force on a structural element and not the pressures on individual surfaces. Figure 10-5 can be used to determine the average drag pressure on surfaces oriented normal



U.S. Army Corps of Engineers

Figure 10-1. Variation of Pressure in a Blast Wave

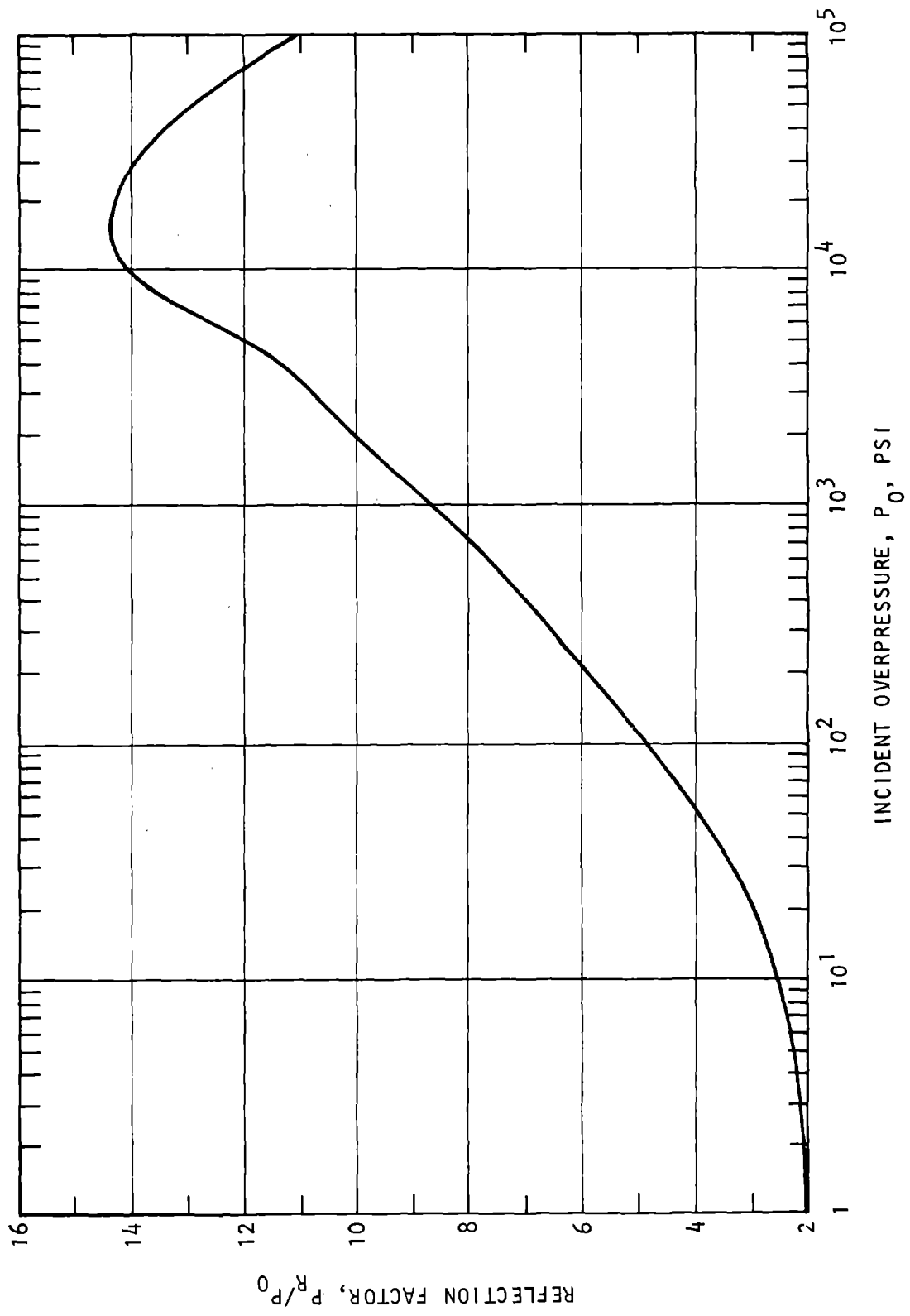


Figure 10-2. Normal Reflection Factor in Sea Level Air vs. Incident Overpressure (Brode, 1970)

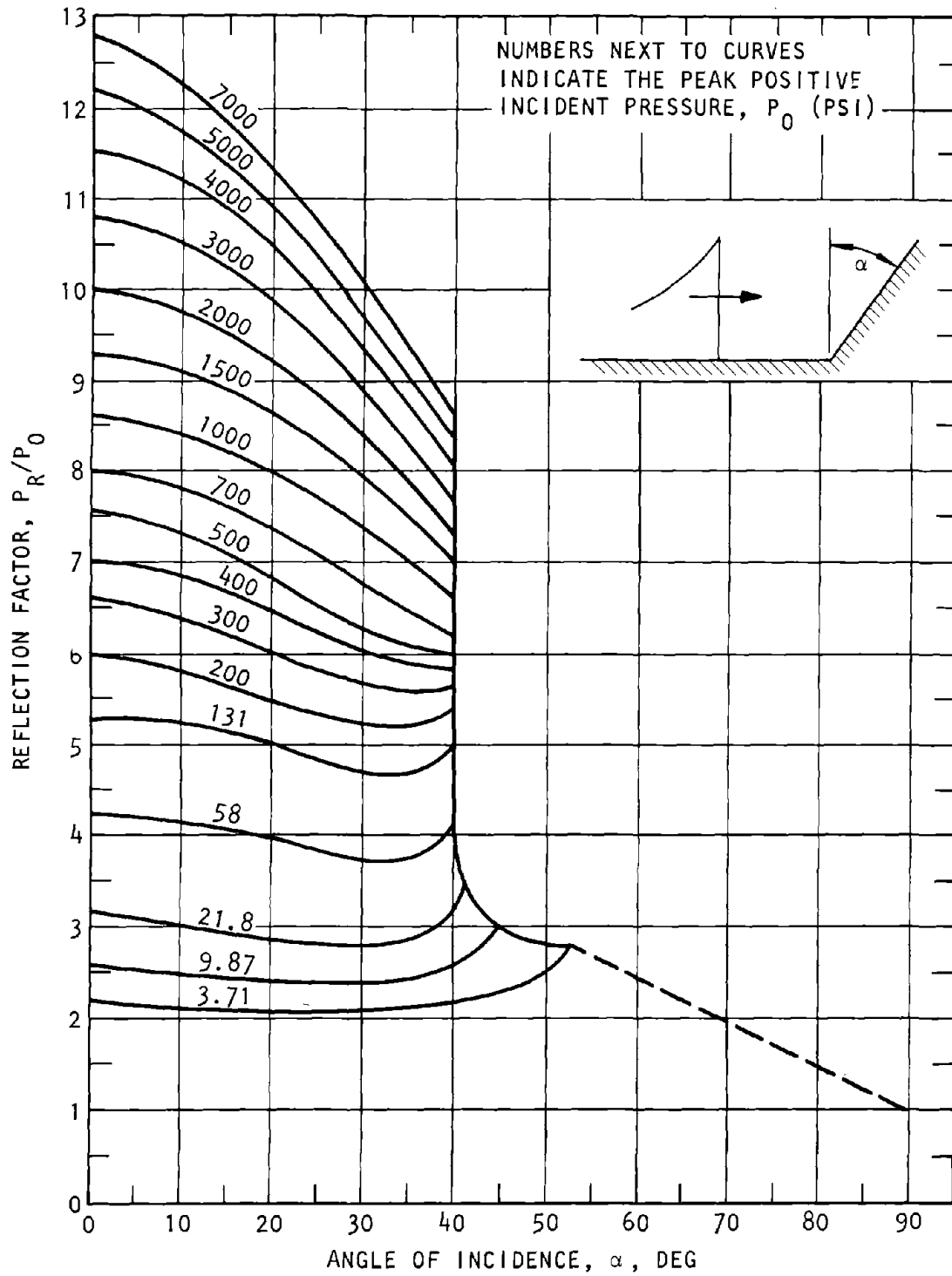
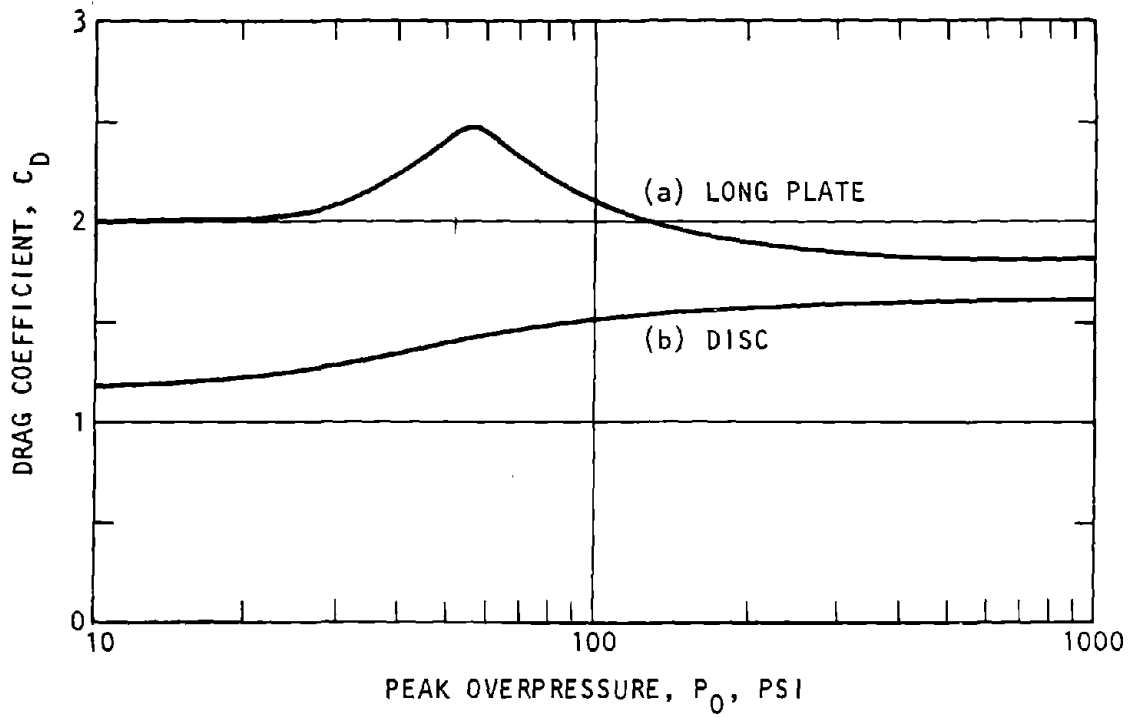
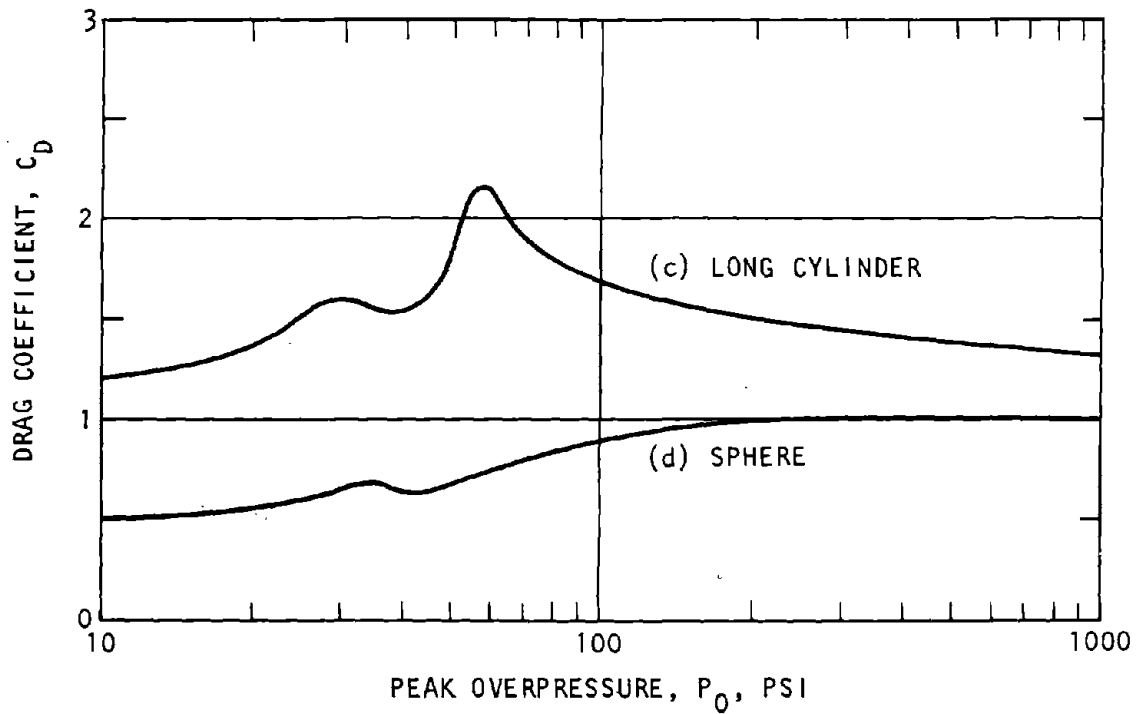


Figure 10-3. Reflected Pressure Coefficient vs. Angle of Incidence (A/N/AF, 1969)

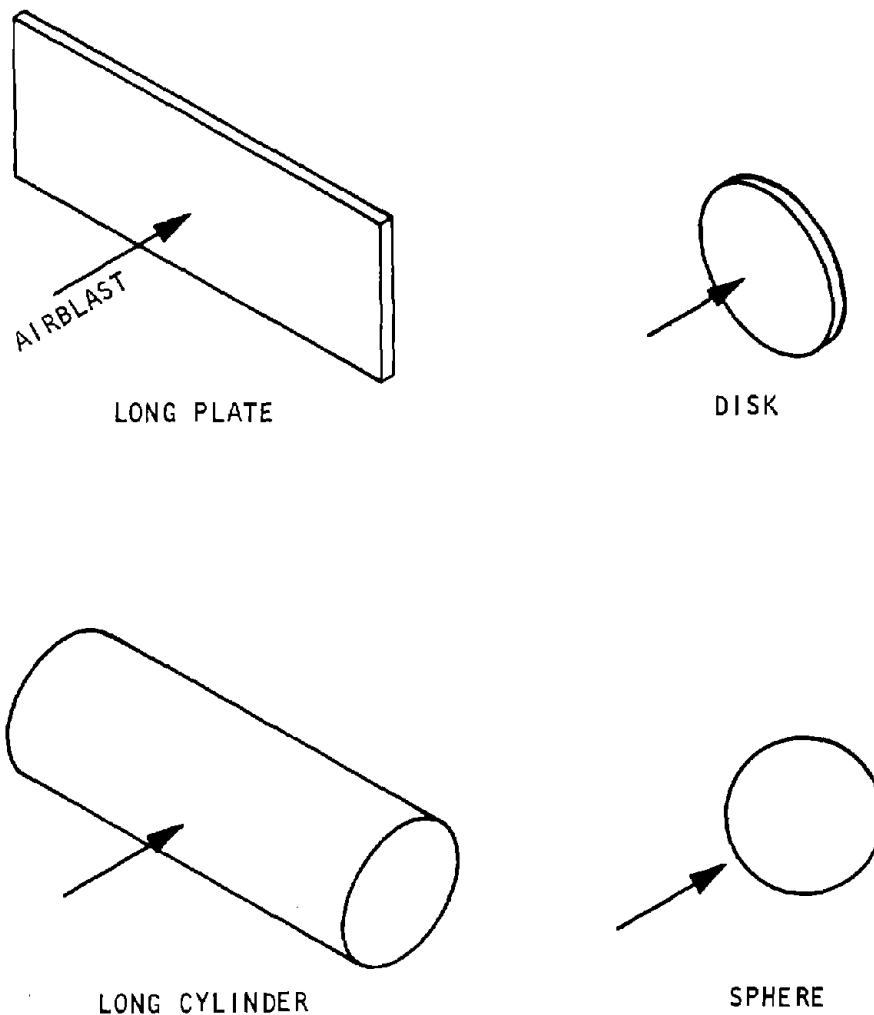


(a) Drag coefficients for long plate and disk



(b) Drag coefficients for long cylinder and sphere

Figure 10-4. Object Drag Coefficients (Newmark-Haltiwanger, 1962)



(c) Orientation of objects

Figure 10-4. (Concluded)

to the direction of the shock front. Note that the coefficient for rear surfaces is negative. The rear surface coefficient can also be used to determine the average drag pressure on the side and top surfaces of a structure. Figure 10-6 gives average drag coefficients for a sloping surface exposed to head-on dynamic pressure as a function of overpressure. The total drag force F_S on a surface due to the drag pressure is given by

$$F_S = C_S q A \quad (10-2)$$

where A is the total area of the surface. The coefficient C_S is obtained from figures 10-5 and 10-6.

(6) Tables 10-1 and 10-2 provide drag coefficients for structural shapes and rectangular bodies at low flow velocities and can be considered applicable at peak overpressures less than 20 psi. However, these

tables provide approximate values for pressures above 20 psi. C_L in table 10-1 is a lift coefficient, used to determine the drag force in a direction perpendicular to the direction of the shock front. Note that this lift force must be considered for any unsymmetrical shape.

(7) Except for figure 10-6, the drag coefficients for flat surfaces, given in figures 10-4 and 10-5 and tables 10-1 and 10-2, are applicable only when the surface is normal to the direction of flow of the free-field dynamic pressure. They are, however, conservative for other angles of incidence. Figure 10-7 shows the effect of the angle of inclination and length-to-width ratio on C_D , C_L , and the location of the center of pressure for flat plates. Since the data presented in figure 10-7 were obtained at low-pressure levels, they can only provide a rough estimate of the effect of orientation on drag coefficients at higher pressure levels.

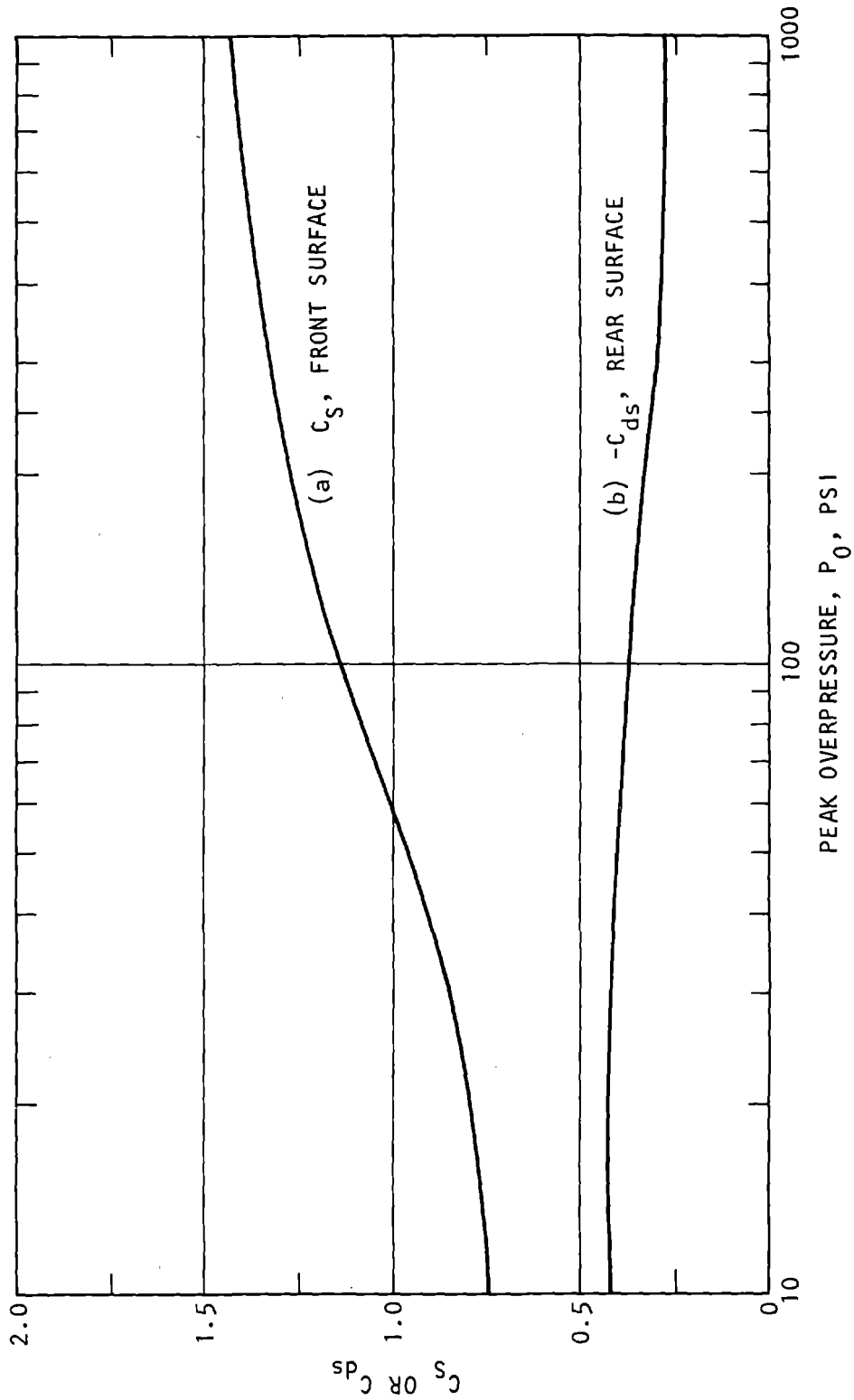
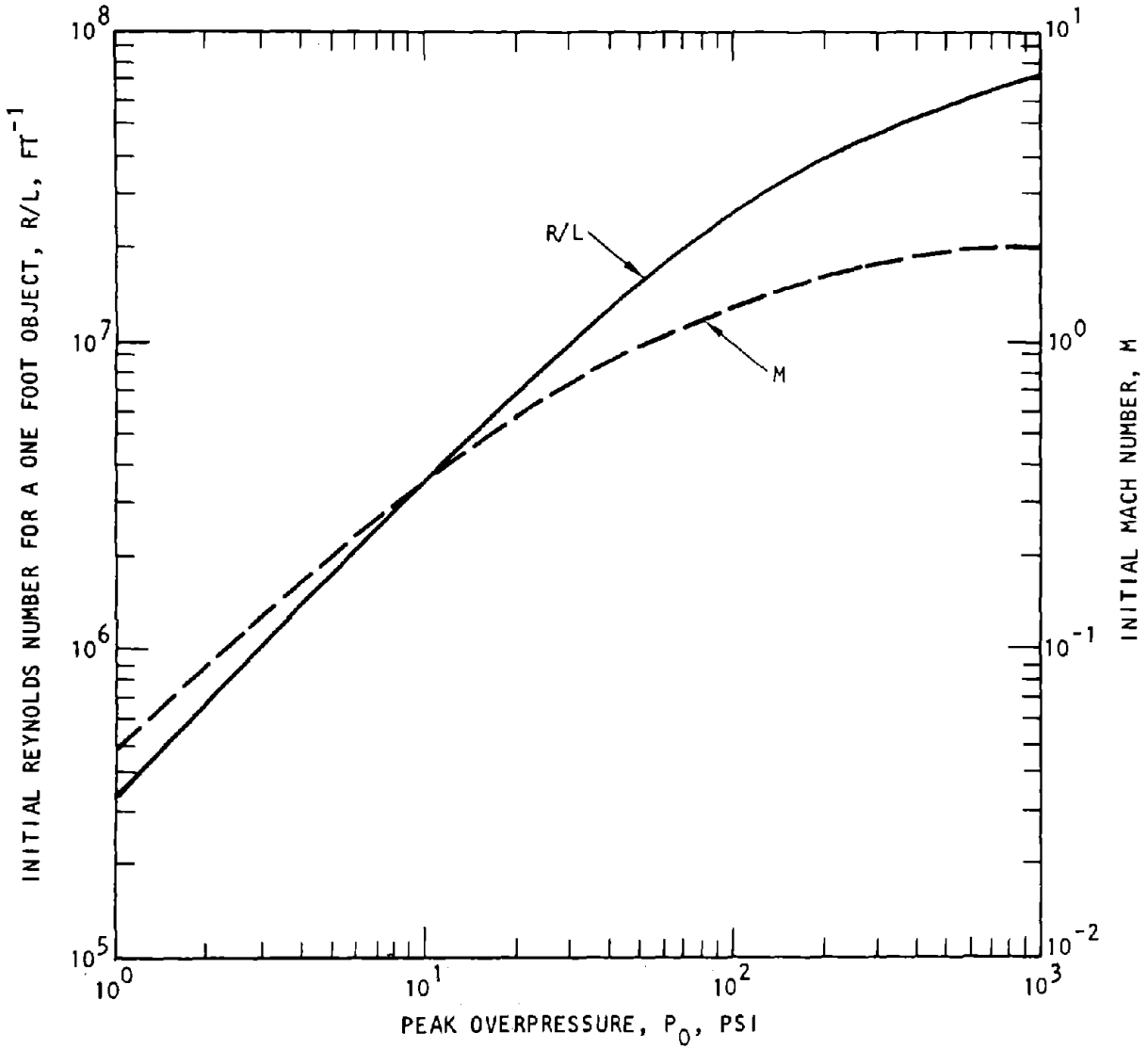
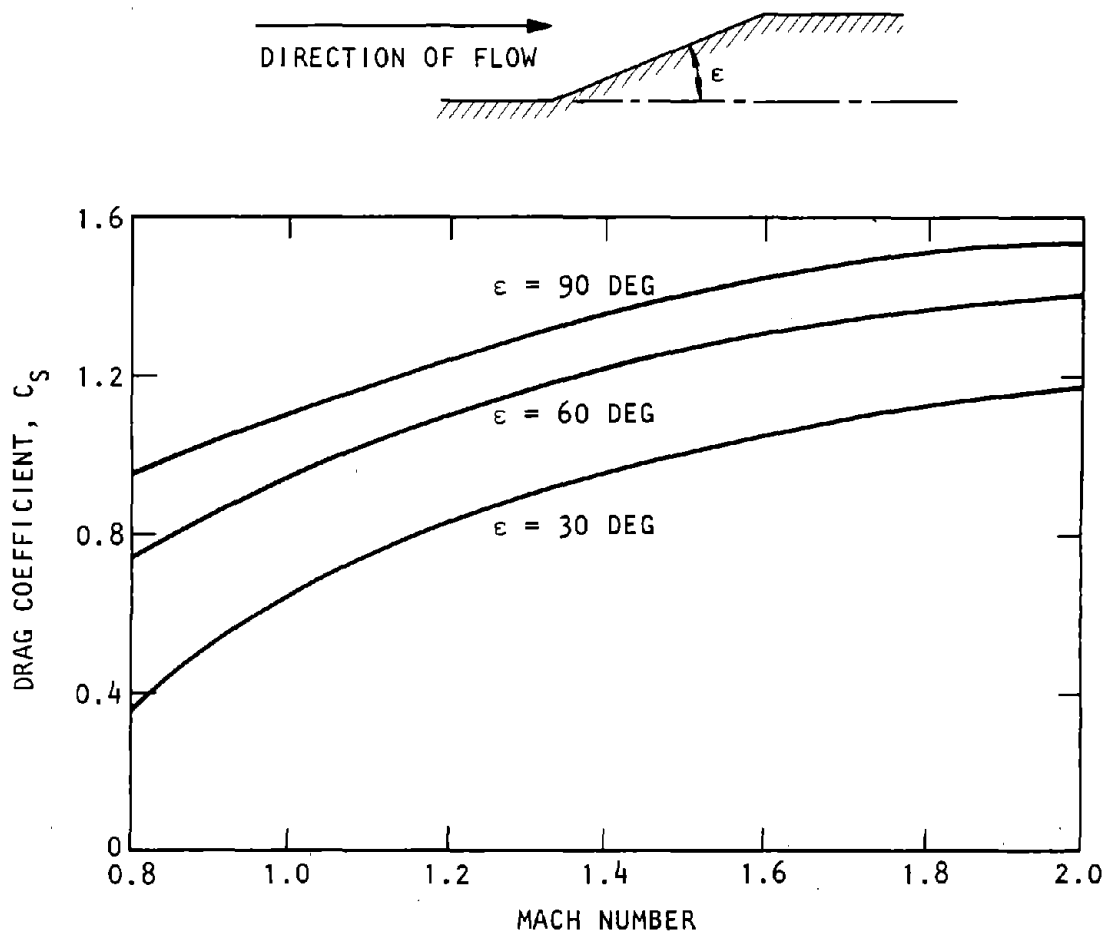


Figure 10-5. Surface Drag Coefficients (Newmark-Haltiwanger, 1962)



(a)

Figure 10-6. Average Drag Coefficient C_D on Front Face of a Wedge (Crawford et al., 1974)



(b)

Figure 10-6. (Concluded)

f. Loads on rectangular structures. As the shock front of an ideal blast wave propagating perpendicular to the ground encounters the front face (side facing the point of detonation) of a closed rectangular structure, it is reflected to some higher value that is a function of the peak incident overpressure and the orientation of the front face to the shock front. The blast wave then bends around the structure, subjecting first the sides and roof and finally the rear face to pressures equal to the incident overpressure (fig. 10-8). At the same time, these surfaces are also subjected to drag pressures, which are a function of the dynamic pressure and drag coefficient for the surface. The total pressure on any face is the algebraic sum of the overpressure or the reflected pressure and the drag pressure, acting on the face at any instant of time. The loading on the front, rear, and roof surfaces

of completely closed rectangular structures must be considered separately.

g. Front face loading. An idealized representation of the load acting on the front face of a rectangular structure is shown in figure 10-9a. The maximum pressure, P_R , is taken equal to the peak reflected pressure on the face. The rise to peak overpressure is accomplished in a finite time; however, the maximum intensity of reflected pressure and the time variance for the reflected pressure before it attains its maximum value are uncertain.

(1) If the rise time, t_r , exceeds the stagnation time, t_s , there is no reflection process, and the front-face pressure is equal to the sum of the overpressure and the dynamic pressure time histories. As shown in figure 10-9a, the stagnation time is the time required for the peak reflected pressure on the front face

TM 5-858-3

to decay to a value equal to the sum of the overpressure and the drag pressure:

$$P = P_o + C_S q \quad (10-3)$$

where

- P = Overpressure as a function of time
- C_S = Drag coefficient for front surface
- q = Dynamic pressure as a function of time

The stagnation time may be taken as

$$t_s = \frac{3d_s}{V} \quad (10-4)$$

where

- d_s = Least distance from stagnation point on front face to edge of structural element
- V = Shock front velocity (TM 5-858-2)

The stagnation point on the front face is defined to be that point at which no lateral flow occurs. For an aboveground rectangular structure with its foundation flush with the ground surface, the quantity d_s is equal to the height of the structure or half its width, whichever is less.

(2) If the rise time is less than t_s given by equation 10-4 but greater than zero, it is conservative to take the peak reflected pressure equal to that for a

Table 10-1. Drag and Lift Coefficients for Structural Shapes of Infinite Length at Low Overpressures (Less than 20 psi) (Newmark-Haltiwanger, 1962)




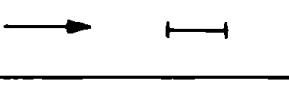
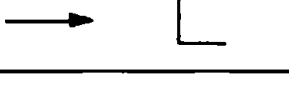


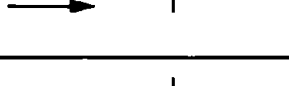
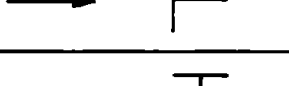
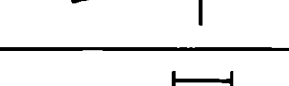
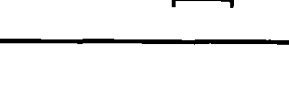
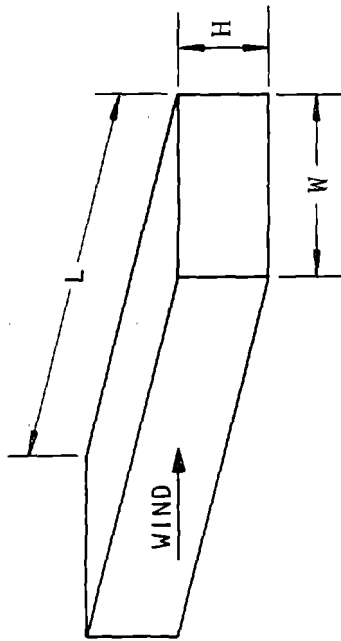
Profile and Wind Direction	C _D	C _L
	2.03	0
	1.96 2.01	0
	2.04	0
	1.81	0
	2.00	0.3
	1.83	2.07
	1.99	-0.09
	1.62	-0.48
	2.01	0
	1.99	-1.99
	2.19	0

Table 10-2. Drag Coefficients for Rectangular Bodies at Low Overpressures (Less than 20 psi) (Neumark-Haltiwanger, 1962)



DRAG COEFFICIENT FOR NORMAL INCIDENCE ON FRONT FACE

L/H	Flat Plate										Flat Plate on Ground			Parallel-epiped		
	1.0	2.0	5.0	10.0	20.0	40.0	∞	1.0	10.0	∞	∞	∞	∞	∞	∞	∞
W/H	0	0	0	0	0	0	0	0	0	0	0	0	0	0.1	1.0	6.0
Front Face, C _S	0.76							0.60	0.72							
Rear Face, C _S	0.36							1.38	0.38							
C _D for Total Drag	1.12	1.19	1.20	1.23	1.42	1.66	1.98	1.10	1.20	1.20	1.20	1.20	1.20	1.95	2.03	0.90

rise time of zero. For a vertical surface, the variation of reflected pressure prior to its maximum value can usually be taken with little error to be linear from zero to maximum in a time equal to the rise time of the overpressure pulse.

(3) The idealized reflected pressure loading shown in figure 10-9a is considered a reasonable approximation of the average load on the front face. After the reflected pressure effects have vanished, the load on

the front face is equal to the overpressure plus the drag pressure, as indicated in the figure.

h. Sloped-front-face loading. If the front face of the structure slopes upward from the ground surface, the blast wave does not impinge on all elements of the wall surface at the same time; rather, the wave front traverses the wall in a finite time equal to the horizontal projection of the wall divided by the shock front velocity. Figure 10-9a still characterizes such

$$F_D = C_D HLq$$

$$F_L = C_L HLq$$

$$\text{MOMENT ARM} = C_e H$$

LENGTH, L
 WIDTH, H
 DYNAMIC PRESSURE, q

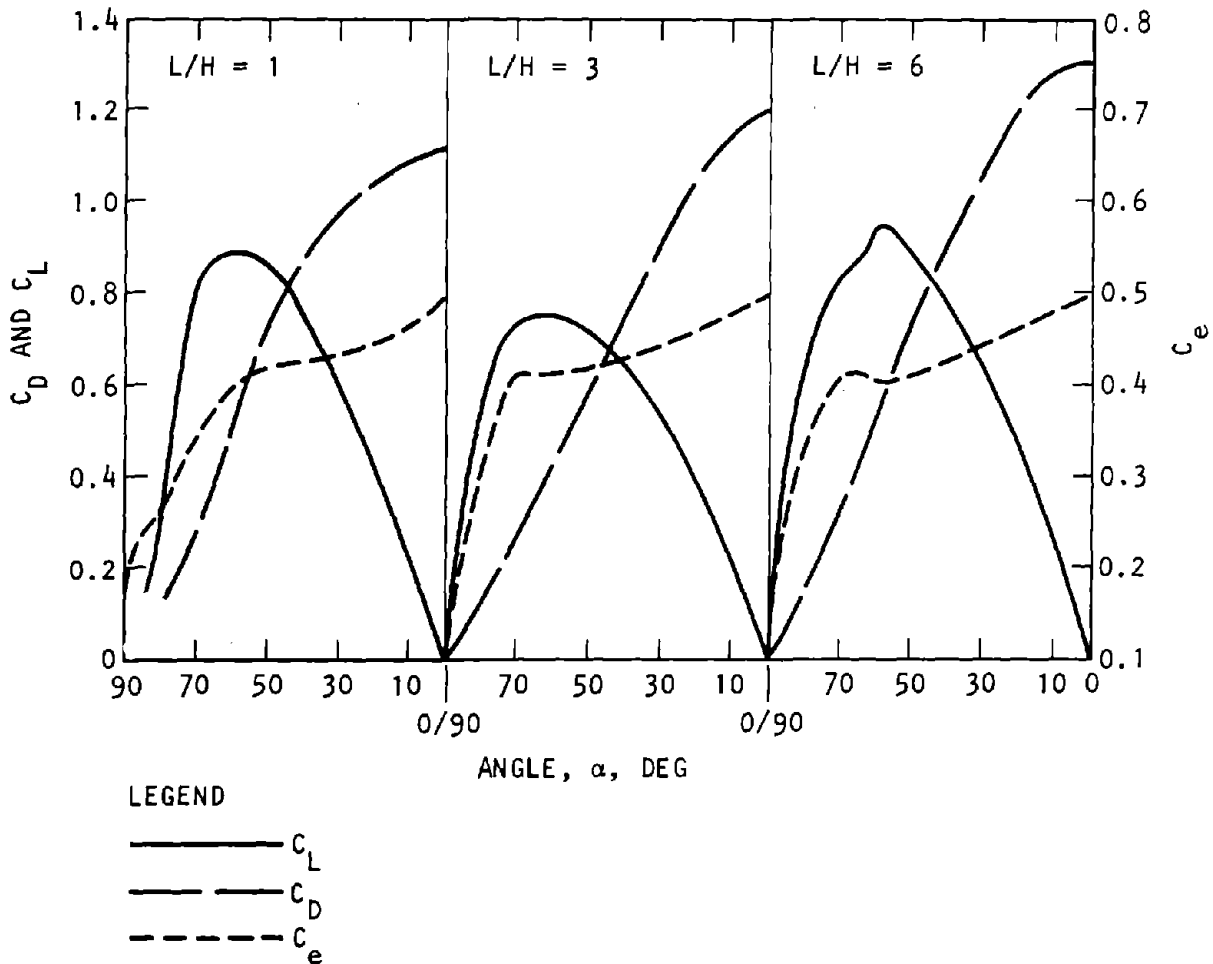
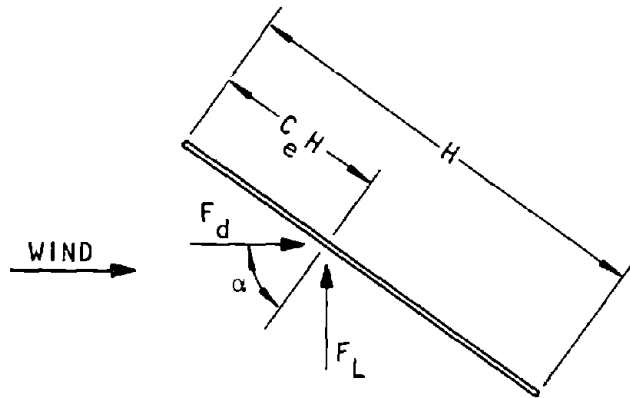


Figure 10-7. Effects of Inclination and Length on Flat Plate Drag Force at Low Overpressures (Less than 20 psi) (Newmark-Haltiwanger, 1962)

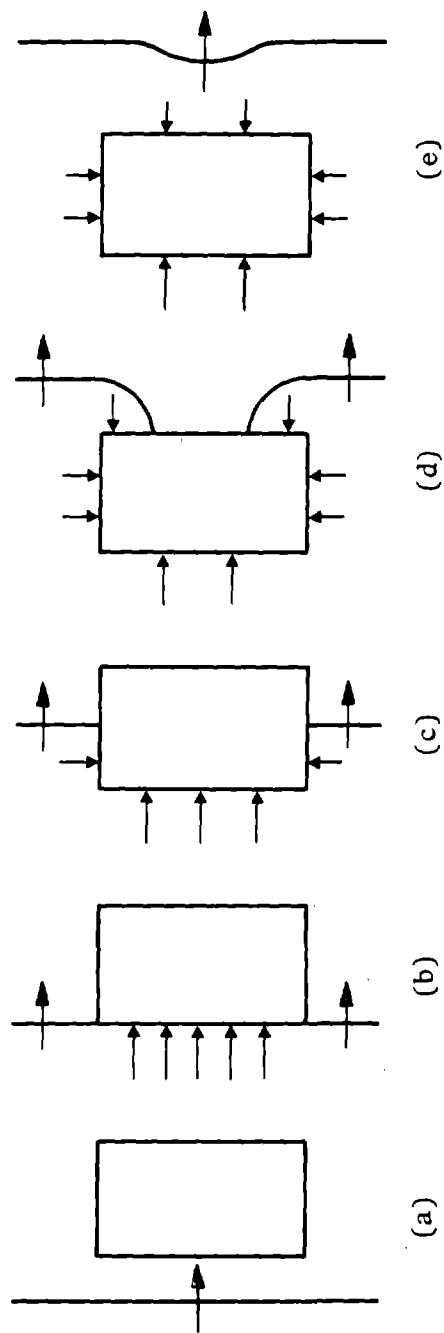
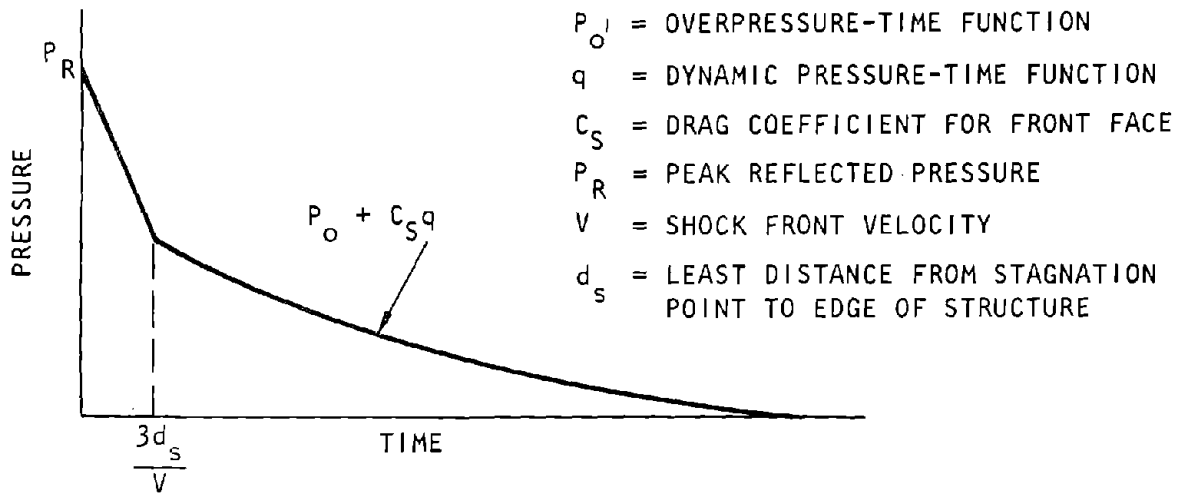
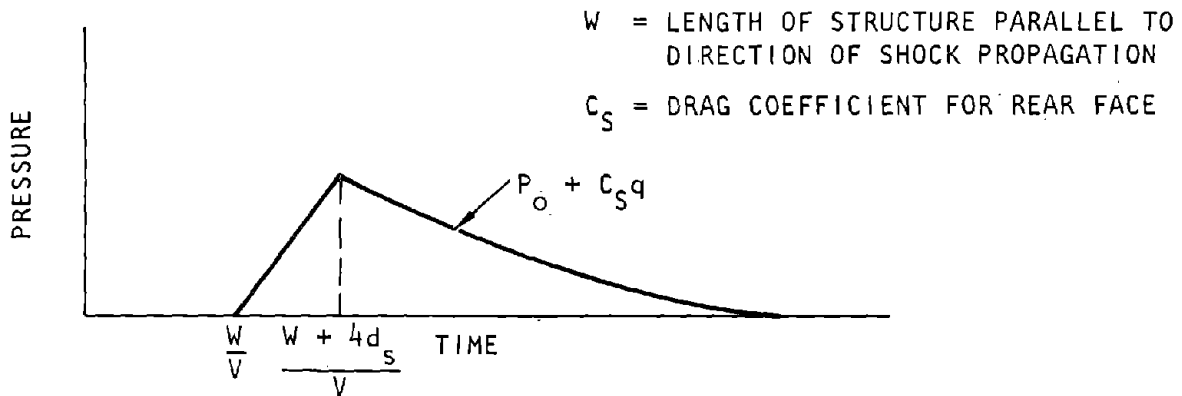


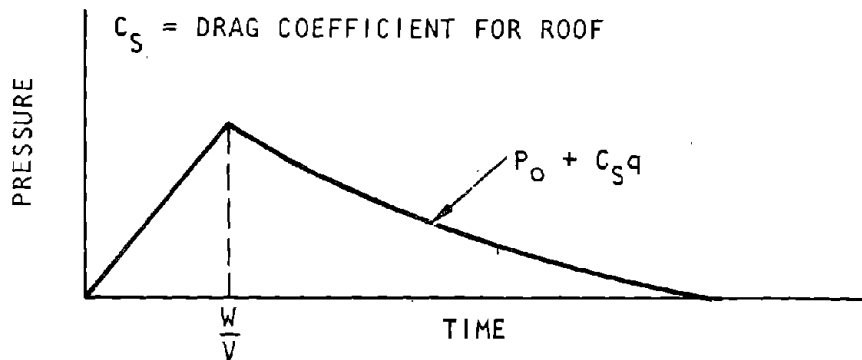
Figure 10-8. Stages in the Diffraction of a Blast Wave by a Structure without Openings (Plan view) (Glasstone, 1962)



(a) Front wall loading



(b) Rear wall loading



(c) Roof and side-wall loading

Figure 10-9. Loading on Aboveground, Closed, Rectangular Structure (Newmark, Halmiwanger, 1962)

a loading; the rise time to maximum reflected pressure may be taken to be equal to the transit time of the shock pulse across the inclined surface plus the rise time of the overpressure pulse. Similarly, a linear decay from peak reflected pressure to the condition of equation 10-3 in a time interval equal to $3d_s/V$ may be used. Dimension d_s is taken equal to the shortest distance from the stagnation point to the edge of the surface measured on the wall rather than along its vertical projection. Note that the reflection factor and the drag coefficient vary with the slope of the inclined surface.

i. Rear-face loading. The loading on the rear face of an above-ground closed rectangular structure is shown in figure 10-9b. No pressure is felt on the rear face until the shock front reaches that point. Pressure begins to build up on the back face at a time equal to the length of the structure in the direction of shock propagation divided by the velocity of shock propagation. After the rear face has become completely engulfed in the blast, the pressure reaches a maximum value equal to the side-on overpressure minus the drag pressure, which acts as a suction at the rear face. Since the overpressure pulse does not impinge on the rear face, there is no reflected pressure. The pressure on the rear face is assumed to build up linearly in a time equal to d_s/V or the rise time of the overpressure pulse, whichever is greater. d_s and V are defined in the same manner as for the front face. The linear variation of pressure with time assumed for this build-up period is only an approximation; its actual variation is uncertain.

(1) For large-yield weapons and structures of normal proportions, ignore the variation in free-field conditions between the front and rear faces of the structure.

(2) For smaller yields and long structures, give some consideration to the decrease in free-field overpressure and dynamic pressure, consistent with an increase in range from ground zero equal to the length of the structure in the direction of shock propagation.

j. Roof and side-wall loading. As the blast wave passes over the structure, the roof and side-wall loading at any time is equal to the overpressure minus a negative drag pressure, or suction. This negative drag pressure is a function of the dynamic pressure and the drag coefficient, both of which vary with the overpressure level. The real loading is a complex function of both the location on the roof surface and the time-dependent variation of the overpressure. Since a finite time is required for the shock wave to traverse the roof of the structure, the average time to maximum pressure will be greater than the rise time of the overpressure pulse. The roof/side-wall loading shown in figure 10-9c is considered average. It rises linearly from zero to a maximum value in a time equal to the transit time of the shock front across

the roof plus the rise time of the overpressure pulse. In most cases the rise time of the overpressure pulse is small compared to the transit time and can be neglected. If the roof structure consists of separate panels supported on walls or columns, compute only the transit time along the panel in the direction of shock propagation rather than the entire length of the roof. Side-wall loading is equivalent to the roof loading.

k. Net horizontal loading. The net horizontal loading between the front and rear faces of an above-ground structure will tend to cause the structure to slide and overturn. This differential in loading is obtained as a function of time by taking the difference between the front and rear face loadings at each instant of time. Figure 10-10 is a graphic representation of the net horizontal loading on a structure.

l. Blast wave approaching along the arch axis. Consider an arch structure with blast-resistant end walls. The structure will be enveloped in an essentially uniform external force traveling axially along the arch. The magnitude of this load is the free air overpressure (fig. 10-11) on a strip of differential width measured along the arch axis. The compressive loading as a function of time is (fig. 10-11c):

$$P = P_0(1 - t/t_d) e^{-t/t_d} \quad (10-5)$$

where

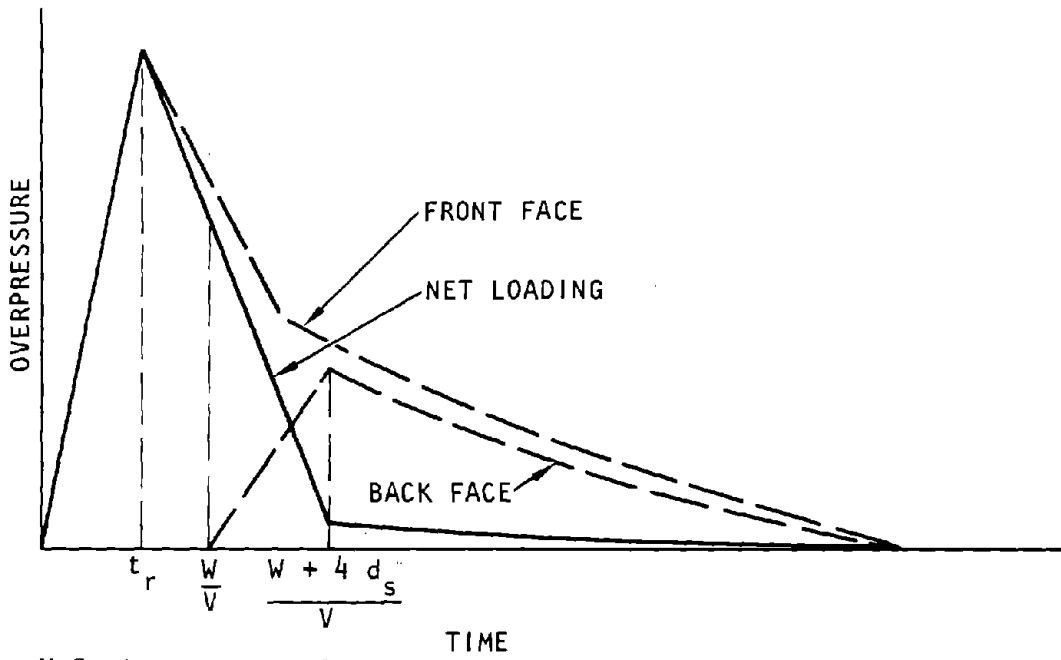
- P = Uniform compressive force applied radially
- P_0 = Maximum incident overpressure
- t = Time measured from the instant the blast wave reaches the strip of differential width being considered
- t_d = Time duration of the positive phase of the incident blast wave

For a strip of finite width W , the average compressive load on the element will reach a maximum at the instant that the blast wave just passes over the entire width of the strip, and its magnitude will be the value of the incident overpressure acting at the center of the strip. A linear variation of overpressure over the distance W may be assumed if the time required for the blast wave to traverse this distance is small compared to the duration of the blast wave (less than about $0.1 t_0$). The time to reach maximum compressive loading is

$$t_r = W/V \quad (10-6)$$

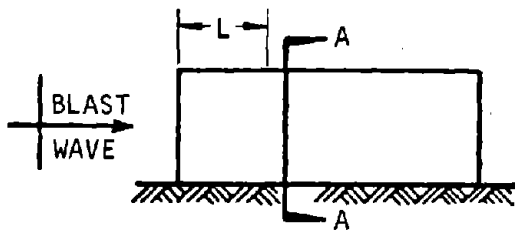
where V is the shock front velocity. The intensity of this compressive loading after time t_r is (fig. 10-11d):

$$P = P_0 \left(1 - \frac{t - 1/2 t_r}{t_d} \right) e^{-(t - 1/2 t_r)/t_d} \quad (10-7)$$



U.S. Army Corps of Engineers

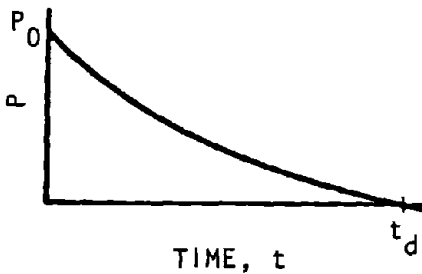
Figure 10-10. Net Horizontal Loading on a Structure in the Shock Direction



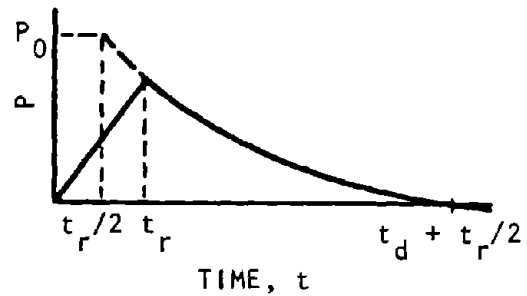
(a) Orientation of blast wave and structure



(b) Section A-A



(c) Loading on a ring of differential width along the arch axis



(d) Loading on a ring of finite width

Figure 10-11. Loading on a Circular Arch Element for Axially Approaching Blast Wave (COE, 1960b)

m. Blast wave approaching normal to the arch axis. The pressures on the "windward" and "leeward" sides of the arch will differ, each varying with time. Higher reflected pressures will act on the lower, more nearly vertical part of the arch near the support on the "windward" side. The pressure on the leeward (or far) side will be relatively low until the blast wave traveling over the arch strikes the ground on the far side of the structure. However, the overpressures on the far side of the arch are never greater than the incident overpressure.

(1) After the shock wave travels over the arch, the pressures begin to equalize over the entire surface. Within a period of about five or six times the shock-transit time, the structure will be in a region of uniform overpressure.

(2) In the earlier stages of loading the arch will be subjected to unbalanced forces causing lateral movement of the crown, and inward deflection on the windward side and an outward deflection on the leeward side (fig. 10-12). The unbalanced loading has two components: (1) symmetrical or "compression mode" loading, and (2) antisymmetrical or "deflection mode" loading. An approximation procedure may be used. It may be assumed that the overpressure at any time *t* can be expressed by an average value for the windward side and another average value for the leeward side. Let these two average values be designated by P_n and P_f respectively. An equivalent set of symmetrical and antisymmetrical loadings, designated as the compression mode loading P_c and the deflection mode loading P_d , respectively, are defined as follows:

$$P_c = 0.5(P_n + P_f)$$

$$P_d = 0.5(P_n - P_f) \tag{10-8}$$

Consider as an example a semicircular arch loaded as shown in figure 10-13a. This is an approximate description of the actual variation of the loading of the arch. A further approximation is made by averaging the arch loadings illustrated in figure 10-13a as indicated below.

For the near side,

$$P_n = \frac{1}{3} \left(\frac{33}{2} + 32 + 25 + \frac{14}{2} \right) = 26.8 \text{ psi}$$

For the far side,

$$P_f = \frac{1}{3} \left(\frac{14}{2} + 5 + 0 + \frac{0}{2} \right) = 4.0 \text{ psi}$$

These loadings are illustrated in figure 10-13b. Equation 10-8 is now applied to this averaged loading system to obtain the two modal loadings, yielding

$$P_c = 0.5(26.8 + 4.0) = 15.4 \text{ psi}$$

$$P_d = 0.5(26.8 - 4.0) = 11.4 \text{ psi}$$

These modal loadings are illustrated in figures 10-13c and d. Note that the superposition of the compression mode loading of figure 10-13c on the deflection mode loading of figure 10-13d yields the averaged loading of figure 10-13b, which is assumed equivalent to the blast loading of figure 10-13a. These approximate overpressures are suitable for design purposes. Their pressure/time relations for any point on the arch can also be determined, as shown in figure 10-14.

(3) The time scale is given in terms of the transit time t_s , the time required for the shock front to pass over the span of the arch. To determine the magnitude

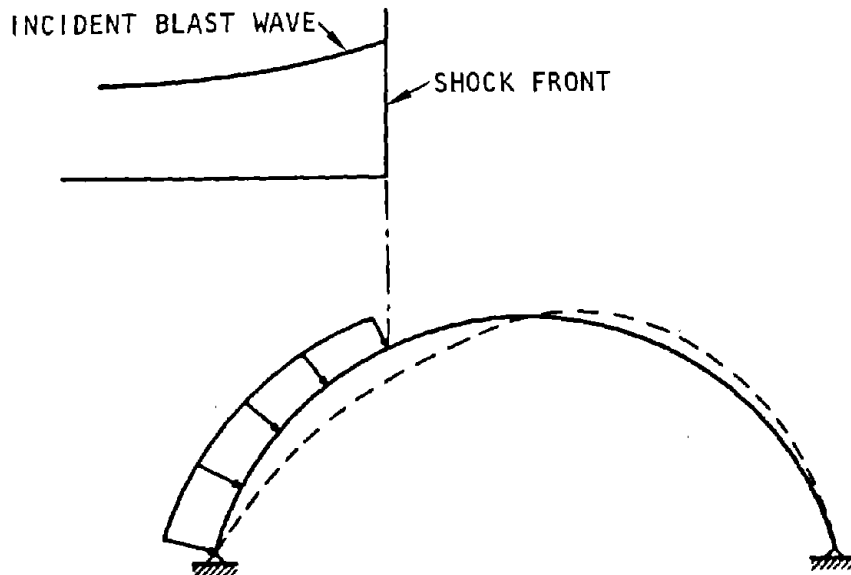


Figure 10-12. Deflected Shape of Arch During Early Stages of Blast Loading Normal to Arch Axis (COE, 1960b)

of the compression mode loadings at times in excess of $2.5 t_t$, the incident overpressure curve as a function of time is plotted with its origin at time $t_t/2$, the time the shock front reaches the crown of the arch.

(4) Both components are equal for values of t less than the time required for the shock front to reach the crown of the arch. The deflection mode overpressure drops linearly from a maximum value of P_0 to the drag pressure produced by the incident overpressure existing at time $t = 2.5 t_t$, multiplied by the drag coefficient C_D . The drag coefficient C_D is taken equal to one-half the average of the local drag coefficients on the windward side, minus one-half the average of the local drag coefficients on the leeward side. The drag pressure is given by the approximate relation

$$\text{Drag pressure} = 0.022 P_0^2 \tag{10-9}$$

where P_0 is the incident overpressure at time $t - t_t/2$. The deflection mode overpressures may become negative when the average loading on the leeward side of the arch exceeds that on the windward side.

However, the negative values are not usually large and do not last very long.

n. Blast wave approaching at an angle to the arch axis. When the blast wave approaches the structure at an angle, the determination of the forces imposed on the arch is difficult. The direction of loading that produces critical response may be taken as either normal to the arch axis or parallel to it. Consider both of these conditions in designing the structure.

o. Loads on dome structures. Two components of loading are considered similar to loads on arch structures: (1) symmetrical or "compression mode" loading, and (2) antisymmetrical or "deflection mode" loading. One modal response of each type should be considered for preliminary design.

(1) Determine the modal loadings by using the average intensities of blast pressure over the windward and leeward halves of the dome. The average intensity over each half of the dome is obtained from the individual load/time curves for several points on the surface of the dome. Consider the dome shown in figure 10-15. Determine the average overpressures on the windward and leeward sides of the dome by

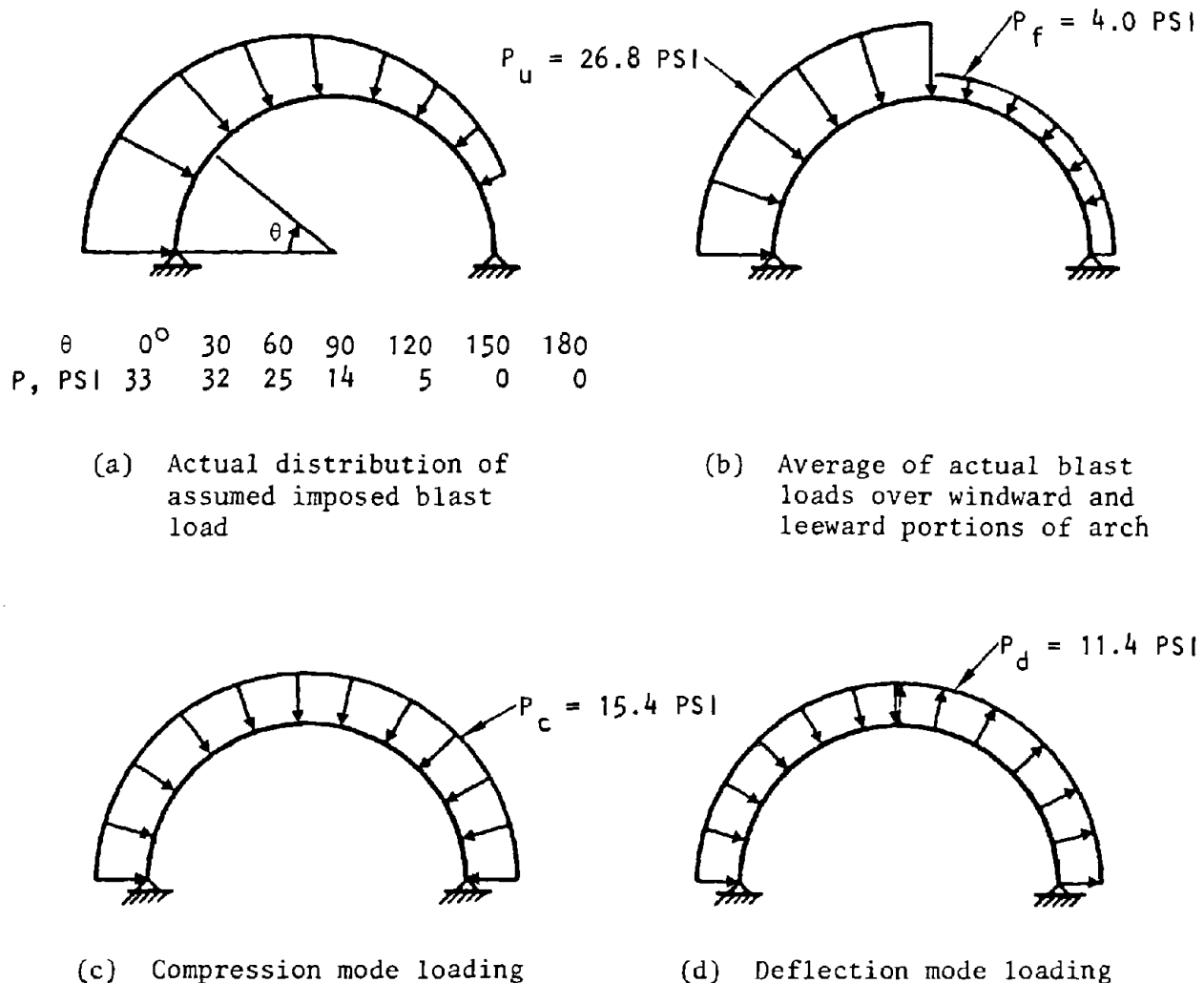


Figure 10-13. Approximate Modal Loadings from Imposed Blast Loadings (COE, 1960b)

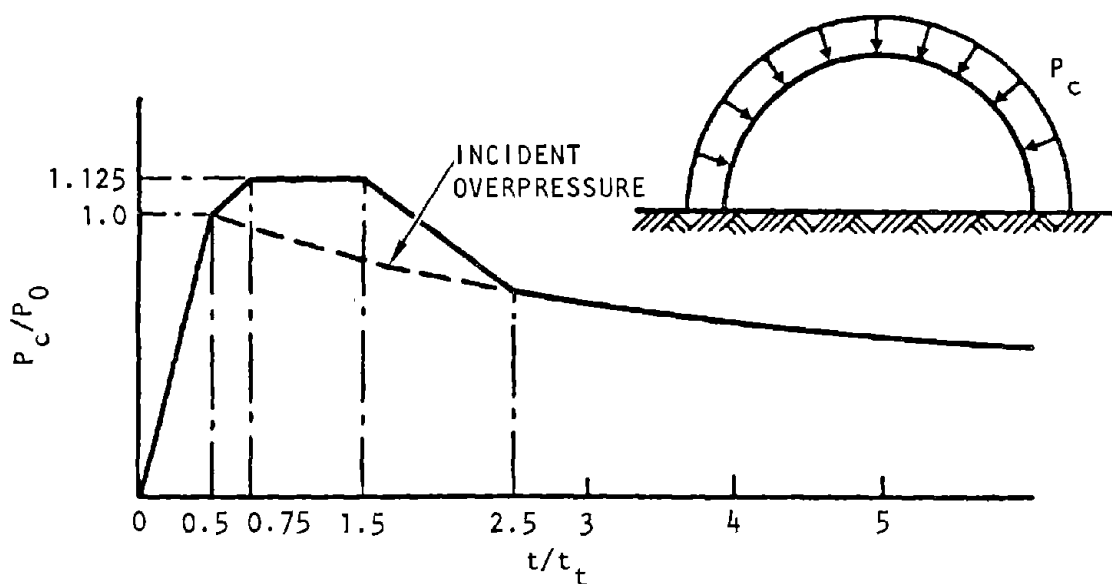
averaging the overpressures existing in meridional strips for different β angles. It is suggested that load/time curves for a hemispherical dome be determined for α values of 15 deg, 45 deg, 75 deg, 105 deg, 135 deg, and 165 deg, on meridional strips having β values of 22.5 deg, 67.5 deg, 112.5 deg, and 157.5 deg. Because of rotational symmetry, the load/time curves for points having β values of 22.5 deg and 67.5 deg will be the same as those for corresponding points having β values of 157.5 deg and 112.5 deg, respectively. The average pressure/time curve of the windward side of the dome can be obtained by an arithmetical averaging of intensities on the windward side. The average pressure curve for the leeward side is similarly obtained.

(2) Obtain the compression and deflection mode loadings by the same method as outlined for arch structures. Denoting the average pressure on the windward side of the dome by P_n and that on the leeward side by P_f , the compression and deflection mode loadings are given by the relations:

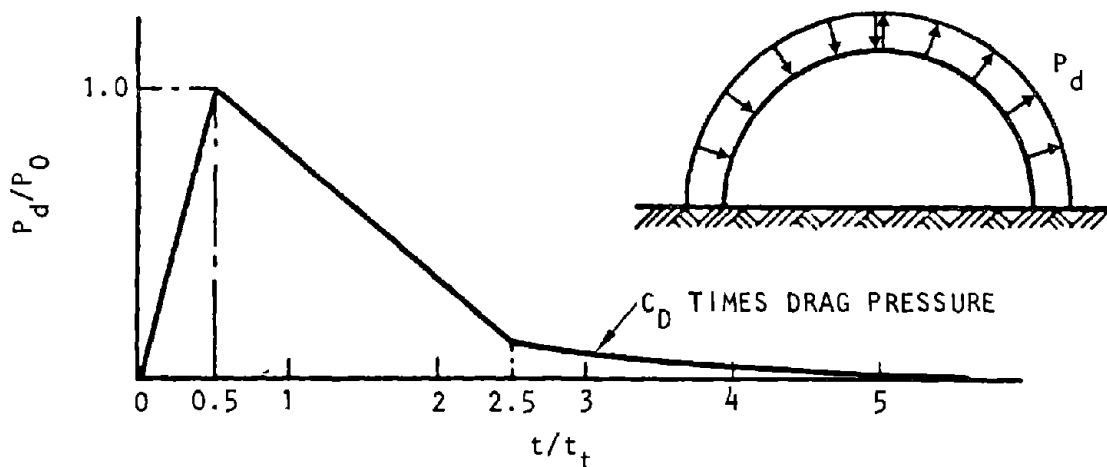
$$P_c = 0.5 (P_n + P_f)$$

$$P_d = 0.5 (P_n - P_f) \tag{10-10}$$

For design purposes, the maximum values of P_c and P_d are of primary interest, therefore, the curves of load/time for various points on the dome need only be computed for a duration of time equal to about



(a) Compression mode loadings



(b) Deflection mode loadings

Figure 10-14. Approximate Modal Loadings (COE, 1960b)

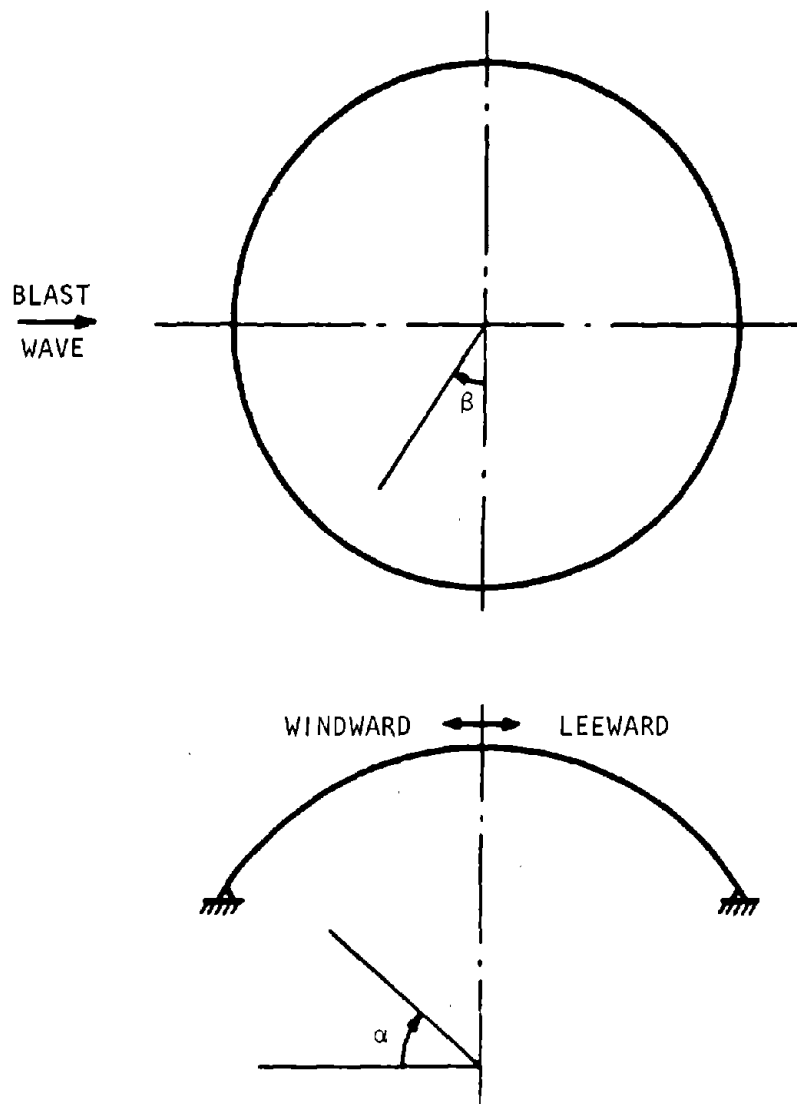


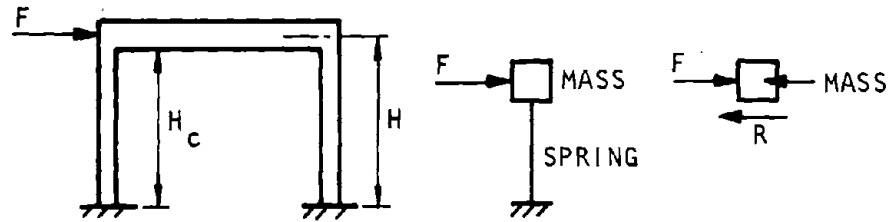
Figure 10-15. Plan and Sectional Views of a Typical Dome (COE, 1960b)

twice the transit time of the shock wave over the dome.

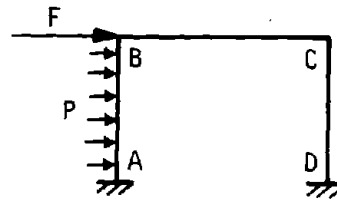
10-5. Frame structures under blast loads

a. Framing arrangements. The blast-resistant designs of frame buildings make no radical departures from conventional framing arrangements. It is generally preferred to make the exterior columns independent of the exterior walls. The walls are often designed to span vertically between the wall footing and the roof slab so that the lateral motion of the frame will be less. This arrangement precludes designing the column to act as a beam spanning between the foundation and the girder. The equivalent SDOF dynamic system for the single-story frame is

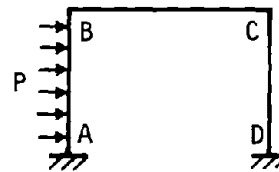
a concentrated mass supported by a massless spring having the lateral resistance properties of the columns (fig. 10-16a). If the exterior walls are designed to act as two-way panels or one-way panels spanning horizontally between columns, columns should be capable of resisting directly applied transverse loads in addition to resisting the lateral motion of the frame. In figure 10-16b, two edges of the panel load the columns directly and the other edges transmit load to the roof and the foundation. The portion of the load transmitted to the roof is indicated by *F*. The column loading *P* is assumed to be uniformly distributed. The sketch in figure 10-16c represents a frame building with the exterior wall framed horizontally. In this case there is no concentrated load, *F*.



(a) Single-story frame and equivalent dynamic system



(b) Columns subjected to directly applied lateral loads from two-way wall panels



(c) Columns subjected to directly applied lateral loads from wall panels spanning horizontally

U.S. Army Corps of Engineers

Figure 10-16. Single-Story Frame Model and Column Load Conditions

b. Shear and moment resistance of columns. Each column resists the lateral motion of the frame through the action of shear forces and bending moments in the columns, as indicated in figure 10-17. The shear resistance in terms of the column bending moments and the axial load is:

$$R_s = \frac{M_T + M_B - P_a \delta}{H_c} \quad (10-11)$$

where

H_c = Clear height of the column as shown in figure 10-16a

M_T, M_B = Top and bottom clear height end moments

P = Axial load on the column

δ = Lateral deflection of the top end of the column

In the plastic range the top and bottom moments are assumed to be equal to a maximum moment M_d so that

$$R_s = R_m = \frac{2M_d - P_d \delta}{H_c} \quad (10-12)$$

The value of M_d to be used in equation 10-12 is a variable, dependent on the direct stress (chap. 6). If

there is no direct stress, M_d can be replaced by M_p giving

$$R_m = \frac{2M_p}{H_c} \quad (10-13)$$

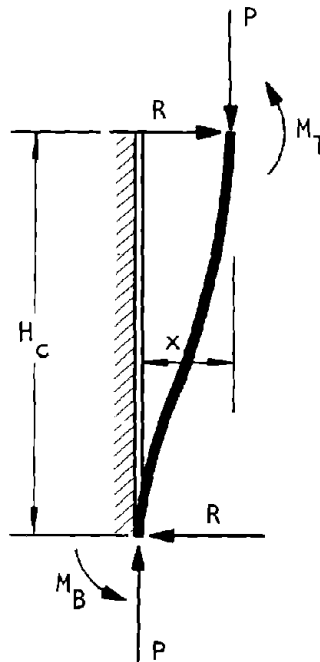
In equations 10-11 and 10-12, R_s is a function of M , P , δ , and H_c . In a given design, two of the four factors are known: H_c is a constant and P_a is of known variation with time. The remaining two terms are related: i.e., for a given column, M is a function of δ and P_a , so that the variation of M and then R may be determined from the variation of δ and P_a . For a frame with infinitely rigid girders (e.g., k for girder ten times or more greater than that of the column),

up to the elastic limit, the spring constant, k , for one column is

$$k = \frac{12EI}{H_c^3} \quad (10-14)$$

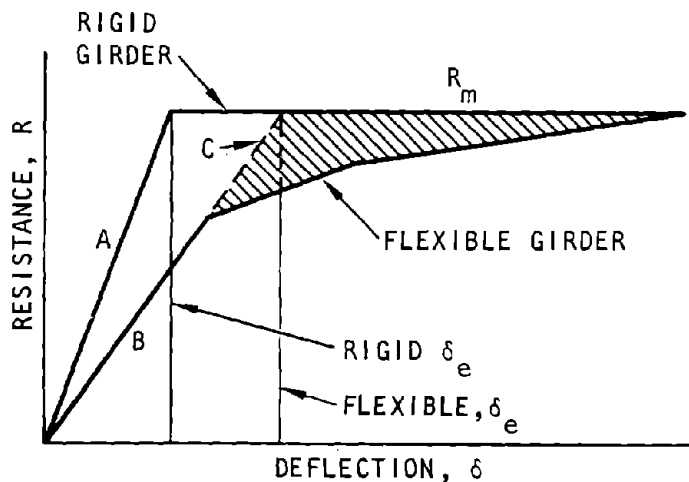
To obtain the maximum elastic displacement δ_e defined by figure 10-18, it is necessary to obtain the maximum or plastic resistance R_m and divide by k . For a complete frame with n columns from equation 10-14,

$$k = n \frac{12EI}{H_c^3} \quad (10-15)$$



U.S. Army Corps of Engineers

Figure 10-17. Shear Resistance and Bending Moments in a Column Subjected to Lateral Displacement and Vertical Load



U.S. Army Corps of Engineers

Figure 10-18. Effect of Girder Flexibility on Resistance-Deflection Diagram of Multibay Frames

and from equation 10-13, neglecting the entire effect of direct stress,

$$R_m = n \frac{2M_p}{H_c} \quad (10-16)$$

so that

$$\delta_e = \frac{R_m}{k} = \frac{M_p h^3}{6EIh_c} \quad (10-17)$$

Equations 10-15 and 10-16 apply only when all the columns of the story are identical in strength and stiffness. If this condition is not true, the equations are modified as follows:

$$k = \frac{12E\Sigma I}{H^3} \quad (10-18)$$

$$R_m = \frac{2\Sigma M_p}{H_c} \quad (10-19)$$

where

$$\begin{aligned} \Sigma I &= \text{Sum of } I \text{ values for all columns in the} \\ &\text{story} \\ \Sigma M_p &= \text{Sum of plastic column moments in the} \\ &\text{story} \end{aligned}$$

For the case in which the direct stress is considered important, the maximum resistance from equation 10-13 becomes

$$R_m = \frac{2M_d n - P_a \delta}{H_c} \quad (10-20)$$

and the maximum elastic displacement from equation 10-17 becomes

$$\delta_e = \frac{M_d H^3}{6EIH_c} - \frac{P_a \delta H^3}{12EIh_c} \quad (10-21)$$

where M_d is a function of P_a (see below). Use equation 10-20 in numerical analyses where the effect of P_a and δ can be introduced. For preliminary design purposes, where it is desirable to account for the approximate effect of P_a in order to simplify the computations, base the design on

$$R_m = \frac{2M_d n}{H_c} \quad (10-22)$$

c. The effect of direct stress on column resistance. The value of M_d to be used in equations 10-20 and 10-21 is variable dependent upon the direct stress.

The relationship is different for steel and reinforced concrete. A reinforced-concrete section carrying both direct stress and bending moment has a higher moment-carrying capacity for a limited but important range of axial loads than the same section carrying only bending moment. However, a structural steel section carrying both direct stress and bending moment has a lower moment-carrying capacity than the same section carrying only bending moment.

(1) The increased bending strength that results from axial stress in the columns should be introduced in the preliminary design of reinforced-concrete frames. If this effect is neglected, the preliminary design is generally very conservative. When the direct stress effect is introduced, a more reasonable column size can be determined.

(2) For steel columns the effect of direct stress on bending strength is much less important than it is for concrete columns; in many cases reasonable results are obtained by neglecting the effect of direct stress in the preliminary design of the column—especially when the axial stresses are low compared with the bending stresses ($f_a < 0.15f_p$). However, the effect of direct stress is usually considered in making the numerical analysis to verify the preliminary design. Column buckling under combined axial load and bending must be prevented in order to maintain the lateral resistance of the frame. The allowable axial load used in the interaction formula is based on $\frac{KL}{r}$ which is a buckling consideration.

d. The effect of girder flexibility on column resistance. In the preliminary design of the columns, the frame response is determined under the assumption that the joint rotations are negligible. If the girders are designed to act in the elastic range (*g* below), the resulting error is not large. If all the columns in a story have the same section and are of equal height, this assumption results in equal moments at the top and bottom of all columns and a linear variation of resistance with displacement up to the plastic resistance. If the assumption of infinitely stiff girders is not made, the resistance-deflection diagram for a given frame may be determined by a conventional moment distribution analysis in which a translation of the joints (side sway) is considered.

(1) Neglecting the flexibility of the girders results in an over-estimate of the energy-absorption capacity of the frame. Consequently, the displacement of the structure and the required resistance of the columns are underestimated. It is not desirable to incorporate the flexibility effects into the preliminary design procedure. Recognize that the designs obtained by the preliminary design method are slightly unconservative, and make allowance for this difference. Include this flexibility effect when the preliminary design is checked by a numerical integration procedure.

(2) The recommended procedure for approximating the effect of girder flexibility for use in the numerical integration analysis of single-story structures is described below. Figure 10-18 presents a resistance-deflection diagram for a typical multicolumn frame subject to lateral load only. Line A represents the resistance for infinite girder stiffness. With infinite girder stiffness, plastic hinges would develop simultaneously at both ends of all columns. If the actual girder flexibility is considered, the hinges would be found to develop successively as indicated by Line B. The recommended resistance diagram is Line C, an extension of the initial slope of Line B to the intersection with the line of maximum resistance. The shaded area represents the error introduced. Use of Line C will result in the calculated deflections being less than the true deflection, but the error is generally very small (under 10 percent). To obtain the effective spring constant k for girder flexibility, determine the slope of Line C by imposing an arbitrary lateral deflection on the frame and calculating the resistance corresponding to this deflection. The ratio of the resistance to the displacement is $k = R/\delta$.

e. Effect of lateral deflection on column resistance. The resistance is subject to reduction by the combined effect of the lateral deflection and the axial column loads (eq. 10-11). In single-story frames this effect is small; it is neglected in the preliminary design procedures but included in the final numerical analysis.

f. Design of columns. In the preliminary design of steel columns the frame girders are assumed to be perfectly rigid, and the axial load in the columns is neglected so that the required moments, the spring constant, and the limiting elastic deflection of the columns can be obtained from equations 10-15 and 10-17. From equation 10-16

$$M_P = \frac{R_m H_c}{2n} \quad (10-23)$$

The cross section required to provide the plastic bending moment resistance M_P is determined from data for steel columns.

(1) The preliminary design procedure for reinforced concrete columns is different from that for steel because allowances are made for the effect of direct stress on the bending resistance of the column. After solving for the required M_d from equation 10-22, determine the dimensions of the cross section. Since M_d is a function of P_a , use the time average of the total axial load P_a for the time interval estimated to be the plastic phase. From the equations in chapter 6 for eccentrically loaded columns, a cross section is selected that will provide the necessary M_d at the average P_a . Compute k and δ_e . For both steel and concrete, $k = 12EI_n/H^3$. However, from equation 10-17

$$\delta_e = \frac{M_P H^3}{6EI H_c} \quad \text{for steel}$$

$$\delta_e = \frac{M_d H^3}{6EI H_c} \quad \text{for concrete} \quad (10-24)$$

Use these parameters in the remainder of the design procedure without modification by any load or mass factors, because the single-story frame is considered to be directly replaceable by an SDOF system. Complete the preliminary design in accordance with the steps in chapter 6.

(2) After the girder is designed, verify the preliminary column design using a step-by-step numerical integration procedure. The more exact numerical analysis includes all the factors that have been neglected in order to simplify the preliminary procedure: the effect of girder flexibility, of vertical load eccentricity, of direct stress, and of the dynamic response of the wall and roof elements on the lateral and vertical load/time curves. As discussed in *c* above, simplify the procedure by using the average column axial loads instead of considering the individual columns separately. Determine the effect of girder flexibility as indicated in *d* above.

g. Design of roof girders. The design of roof girders in building frames for blast loads is complicated by the time variation of the lateral and vertical blast loads and the difference in time required for the different girders to reach maximum stress. In general, the maximum frame moments due to the vertical loads develop before those due to the lateral loads. Conventional static loads must be considered in addition to the blast loads. In a building with openings it is possible to have internal pressures of such magnitude as to develop net upward forces on the roof girders.

(1) To obtain the maximum lateral stiffness for the building frame, design the roof girders in frames to act elastically. To simplify design procedures, consider continuous-span beams as single-span elements with restraints (fig. 10-19). It is recommended that single-span frame girders such as A be designed elastically to carry vertical loads as simply supported beams. Exterior girders such as B should be designed elastically to carry vertical loads as beams fixed at the first interior support and pinned at the exterior support. Interior girders such as C should be designed elastically to carry the vertical loads as beams fixed at both ends. In order to develop the maximum lateral resistance of the frame, design the girders so that the plastic hinges form in the columns. The bending strength of the girders at any point must equal the moment at that point due to static and dynamic vertical loads, plus the moment due to lateral motion. The latter is computed by applying to the girder the full plastic hinge moments of all the columns

simultaneously. This approach is conservative because it assumes that all the maximum moments develop at the same time.

(2) When frame girders are subjected to blast loading, the critical girder in a symmetrical multibay frame is the front girder and the critical section is at the first interior support. At this section the frame moment in the girder should be a fraction of the column maximum moment M_d . For a two-bay frame, use $1/2 M_d$; for a three-bay frame, use $2/3 M_d$; and for a four-bay frame, use $5/8 M_d$.

h. Multistory frame buildings without wall participation. The motion of each floor of a multistory frame building is dependent on its associated mass, the external force at the floor level, the force transmitted downward by the columns above, and the resistance to motion provided by the columns above and below. Represent the equivalent dynamic system (fig. 10-20) by a series of concentrated masses, one for each floor, separated by massless springs having the resistance properties of the columns.

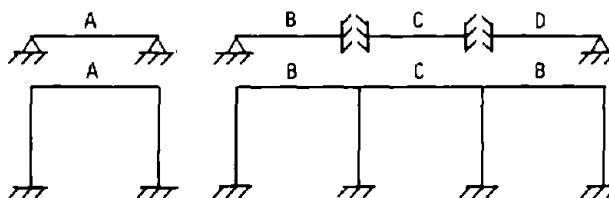
(1) *Columns.* From equation 10-11, it is seen that the combined effect of the lateral deflection and the vertical column loads reduces the resistance of a frame building. In single-story frames, this effect is small and may be neglected in the preliminary design procedure. In the preliminary design of multistory

buildings, however, the effect of deflection on the resistance must be included.

(2) *Roof Girders.* The discussion in *g* above covering the behavior and design of roof girders is directly applicable to multistory frame buildings.

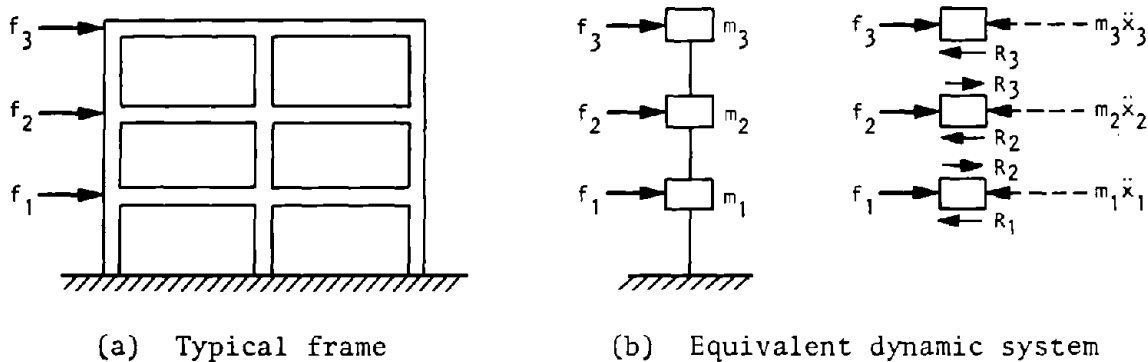
(3) *Floor Girders.* In windowless multistory buildings, the floor girders are subject to both conventional static vertical loads and to the dynamic frame loads resulting from the lateral distortion. However, in buildings with openings that are covered by frangible materials, floor girders may be subject to essentially the same loading conditions as roof girders. It is important to note that floor girders must be capable of withstanding the combined effect of the end moments in both columns adjacent to the girder, as well as the vertical load moment. Unless the girders in multistory frames are absolutely rigid, the shear in a story is affected by the relative deflection in that story. It is also affected by the relative deflection of all other stories, but this is of secondary importance and may be neglected. To obtain the spring constant k for a given story of a multistory building, the following approximation procedure may be used:

- (a) Apply the full plastic hinge moments of the columns above and below to each girder.
- (b) Determine the rotation of the girder at each joint (e.g., by the Moment Area Method).



U.S. Army Corps of Engineers

Figure 10-19. Single-Span Support Assumptions for Design of Frame Girders



(a) Typical frame

(b) Equivalent dynamic system

Figure 10-20. Multistory Frame Building and the Equivalent Dynamic System (COE, 1960a)

(c) Considering a particular story, take $R_m = \Sigma M_d / H_c$, and $k = R_m / \delta_r$; the spring constant is given by

$$k = \frac{(\Sigma M_d)12E(\Sigma I)}{[H^2 (\Sigma M_d) + 6EH(\Sigma I\theta)]H_c}$$

where

- ΣI = Sum of all the column moments of inertia in the story
- $\Sigma I\theta$ = Sum of $I\theta$ products for each end of each column
- $\Sigma \theta$ = Joint rotation as determined in step b
- δ_r = Limiting elastic relative floor displacement

This procedure is based on the assumption that all columns develop end hinges simultaneously. The error involved is minor because the effect of girder flexibility is of secondary importance.

i. Multistory frame buildings with participating walls. If the walls of multistory buildings are constructed to be continuous over the full height of the structure, they will assist the frame in resisting lateral blast loads. In a multistory blast-resistant building the exterior walls may be assumed to be continuous over the full height of the building but hinged at the supporting floors, so that the floor-to-wall continuity is not considered a factor in determining the lateral resistance. Figure 10-21 shows the equivalent dynamic system.

10-6. Shear wall structures

a. Structure arrangement. Shear walls transfer lateral loads to the foundation through both bending and shearing action. They are inherently strong, will resist large lateral forces, and will result in a more economical structure for blast resistance than will rigid-frame construction. Columns are usually provided between the shear walls to carry the vertical

loads, including blast loads on the roof. The columns in shear-wall structures are not subject to the same degree of bending from the lateral loads as are those in rigid-frame structures, and can therefore be of smaller cross section than in a comparable rigid-frame building.

(1) A blast load applied to the front wall of a shear wall structure, as shown in figure 10-22, is transmitted through the roof and floor slabs to the shear walls and thus to the foundation. The front wall of the structure spans vertically between the foundation, the floor, and the roof slab. The upper floor and roof slabs act as deep beams, and in turn transmit the front wall reactions to the shear walls.

(2) Subjected to the same blast load as shown in figure 10-22, the roof and floor slabs act as the webs of W-shaped or channel-shaped deep beams with portions of the front and rear walls acting as the flanges. In these deep beams the shear distribution is essentially uniform over the depth of the web. Hence the assumption is made that the horizontal roof and floor slab reactions are uniformly distributed along the shear walls. Horizontal blast loads applied to the back walls of the structure are carried in a similar manner through the roof and floor slabs to the shear walls.

(3) Under a horizontal blast load shear walls are designed for plastic behavior and may be considered vertical cantilever beams, supported at the base and loaded with horizontal loads at each floor level. Vertical loads are caused by the blast forces on the roof slab. In addition, vertical shearing forces are developed along the front and back edges of each shear wall due to the unbalanced forces between the roof and foundation on both the front and back walls (fig. 10-23). The front and back walls act integrally with the shear wall in resisting bending. A flange width of one-sixth of the shear wall height each side of the web should be used if the front and back walls are designed for plastic behavior in vertical bending between floors.

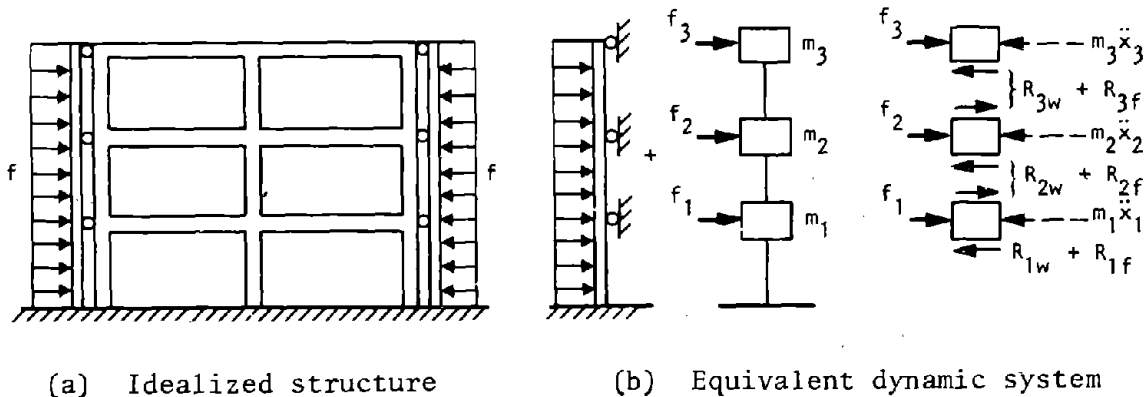


Figure 10-21. Multistory Frame Building with Participating Walls and the Equivalent Dynamic System (COE, 1960a)

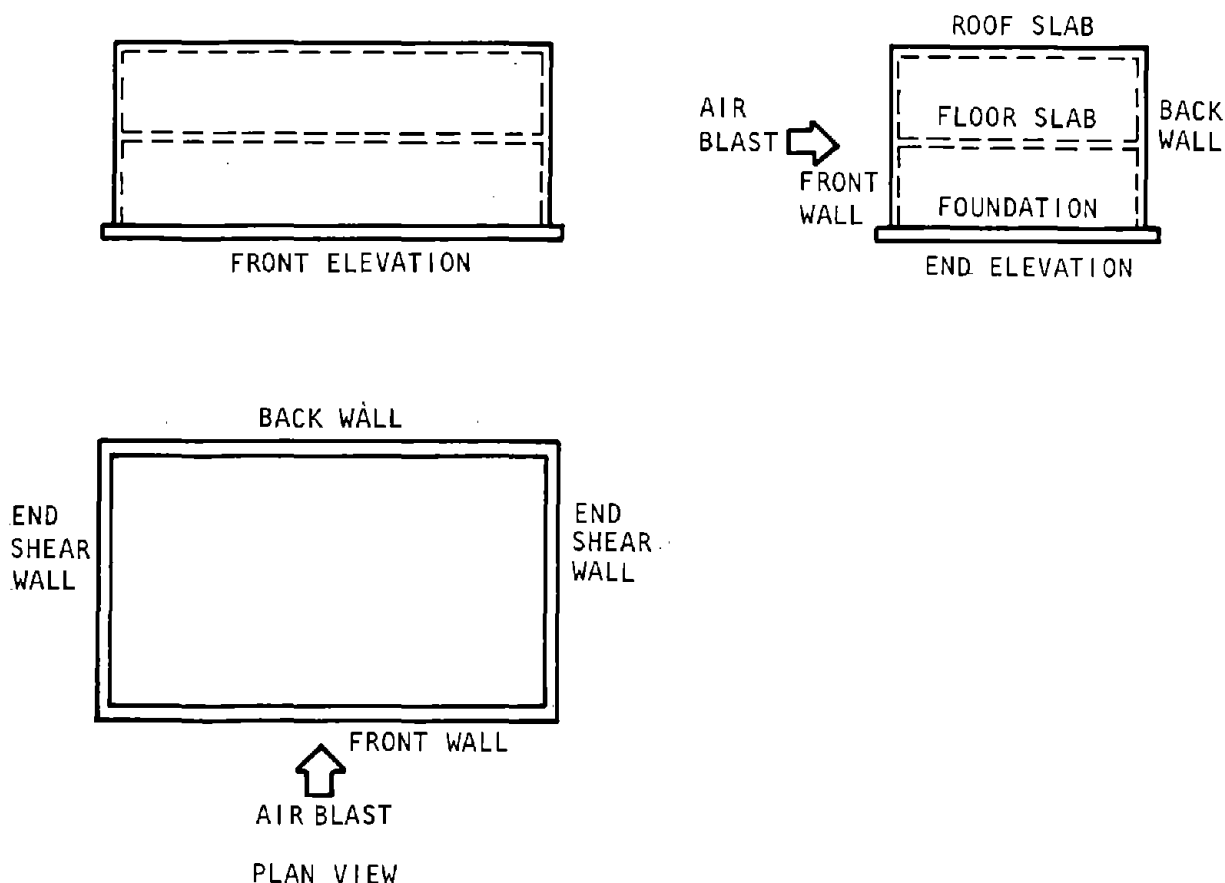


Figure 10-22. Simple Shear Wall Structure (COE, 1958)

(4) A shear wall structure may have steel roof framing as illustrated in figure 10-24. Steel roof trusses carry the vertical loads; horizontal trusses carry the lateral blast forces to the shear walls.

(5) A structure with interior shear walls is illustrated in figure 10-25. Interior shear walls usually contain openings for corridors and doorways. The corridor walls may or may not be structural walls. The resistance to lateral deflection of a shear wall with openings is determined by a rigid frame analysis using both shear and moment deformations. The presence of integral corridor walls, which may act as flanges, should be taken into account in the final design. However, the effective flange width should be determined according to the procedures for T-beams in the ACI Building Code (1977).

(6) The distribution of lateral loads to shear walls by roof and floor slabs acting as horizontal deep beams is an indeterminate problem dependent upon the stiffness of the floor slab and the relative stiffness of the walls. One approach is to assume that the roof and floor slabs are rigid plates and to divide the load among the shear walls in proportion to their relative stiffnesses. This procedure implies equal deflection of all walls in the absence of torsion.

(7) If the shear wall arrangement is not symmetrical, torsional stresses will be developed in the plane of the floor and roof slabs. These torsional stresses are distributed to all the walls that support the roof and floor, and the more rigid walls will carry the large share of the torsion. For this case the assumption should be made that the torsional stresses are carried by the walls that are normal to the shear walls, because of the plastic deformations that the shear walls may undergo as compared to the small elastic deformations of the other walls. An asymmetrical structure having a number of shear walls with various stiffnesses may be analyzed by the methods described by the Portland Cement Institute, 1955, using the center of mass and the center of rigidity as is done in seismic design.

b. Resistance of shear walls. The resistance function of a shear wall is an expression relating its lateral deformation to the resistance that the wall develops towards that deformation. The idealized resistance function of a simple one-story shear wall is illustrated in figure 10-26.

(1) The total wall deflection includes both moment and shear deformations. Portions of the front and back walls act as flanges on the shear wall web

and will affect the moment deformation, but only the shear wall web section contributes to the shear deformation. The steel in the wall may be proportioned so that $R_c = R_u$ and hence $k_2 = 0$. Resistance functions for this case are given below (COE, 1958) for a single two-story shear wall (fig. 10-27). For other cases an equivalent average resistance function with $R_u = R_c$ may be substituted.

Case 1:	$R_1 = k_{11}y_1 = k_{12}d_2$	$ R_1 \leq (R_1)_c$
	$R_2 = k_{21}y_1 + k_{22}d_2$	$ R_2 \leq (R_2)_c$
Case 2:	$R_1 = C_1 + k'_{11}d_1$	$ R_1 \leq (R_1)_c$
	$R_2 = (R_2)_c$	$ R_2 = (R_2)_c$
Case 3:	$R_1 = (R_1)_c$	$ R_1 = (R_1)_c$
	$R_2 = C_2 + k'_{22}(x_2 - x_1)$	$ R_2 \leq (R_2)_c$

k_{ij} (where $i=1, 2$ and $j = 1, 2$) = wall resistance in i th story developed by unit lateral deflection of top of j th story wall

k_{11} = Wall resistance in first story developed by unit lateral deflection of top of first-story wall

d_i = Lateral deflection of top of i th story wall

R_i = Lateral resistance developed in i th story wall

$(R_i)_c$ = Lateral resistance of i th story wall at which initial cracking occurs

As the maximum resistance $R_u = R_c$ is reached in any story, the resistance functions are altered to reflect the plastic stress condition (no further increase in moment and shear stresses) in that particular story wall under further deformation.

(2) In general, the shear wall problem is not as simple as illustrated in figure 10-26 and 10-27. Many shear wall structures have longitudinal corridors that require openings in the shear walls (fig. 10-28). The maximum lateral resistance of each story is determined by the strength of the individual shear-wall components. The parts of the wall and foundation that join the two portions of the shear wall are made strong enough so that the initial cracking will occur in the shear wall panels on each side of the openings, thus developing the full strength of the shear wall.

c. Sliding and overturning. Shear walls are very stiff structural elements, and their behavior is greatly affected by the inertial forces caused by small sliding and overturning tendencies. In preliminary design, consider the rigid body sliding and overturning. In the final design, make a combined dynamic, sliding, and overturning analysis. Numerical procedures will be required to perform these analyses. The basic relationships are given below (COE, 1958).

d. Rigid body sliding and overturning. When the externally applied lateral blast load exceeds the lateral resistance available from the combined action of friction on the bottom of the foundation and passive pressure on the rear faces of the footings, the building will move in the direction of the blast. The structure must displace against the soil in order to develop passive pressure. The magnitude of the resistance as a function of displacement is not known. It is therefore recommended that the resistance-displacement diagram assumed for the passive pressure be pure plastic. The increase in passive pressure resulting

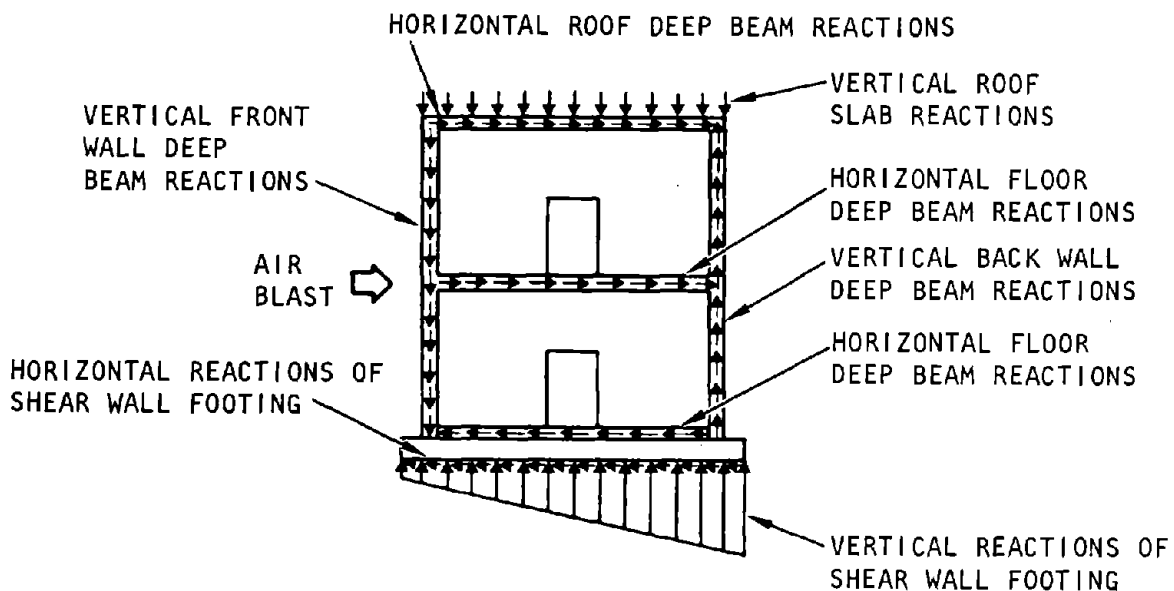


Figure 10-23. Forces Acting on Shear Wall (COE, 1958)

from blast pressure resulting on the ground surface behind the building should be included by treating it as a surcharge on the ground surface.

(1) The total vertical force exerted by the footings on the soil at any time is equal to the weight of the structure plus the blast load on all exposed horizontal elements such as the roof and footing projections and the vertical component of the inertial force resulting from the rotation of the building. If the angular acceleration of the structure is upward at the front footing the inertial force would be downward on the front footing and upward on the rear footing, and vice versa. The vertical motion of the structure as a whole is assumed to be small; hence the corresponding vertical inertial forces are ignored. The vertical dynamic reactions on the footings are obtained from the vertical reactions of the roof slab and girders upon the columns and walls. For the dynamic overturning and sliding analyses the vertical reactions are generally obtained for the average roof overpressure acting over the entire roof area simultaneously.

(2) For structures located on soil, the structure is considered to rotate about the centroidal axis through the base of the footings; sliding and overturning are analyzed simultaneously. Figure 10-29 illustrates the forces acting upon the structure as a rigid body. The

structure rotates about the centroidal axis through the point "0" at the base of the footings. The angular acceleration of the structure about this axis is given by:

$$\alpha_o = \frac{M_o - F_o \bar{y}}{I_o - m \bar{y}^2} \tag{10-26}$$

where

- α_o = Angular acceleration of structure about axis of rotation
- ω_o = Angular velocity of structure about axis of rotation (fig. 10-29)
- θ_o = Angular displacement of structure about axis of rotation (fig. 10-29)
- M_o = Moment of all external forces about axis of rotation
- F_o = Summation of all external horizontal forces applied to the structure including foundation reactions
- \bar{y} = Vertical distance from axis of rotation to centroid of total moving mass, m
- I_o = Mass moment of inertia of structure about axis of rotation
- m = Total moving mass of structure and earth enclosed between footings

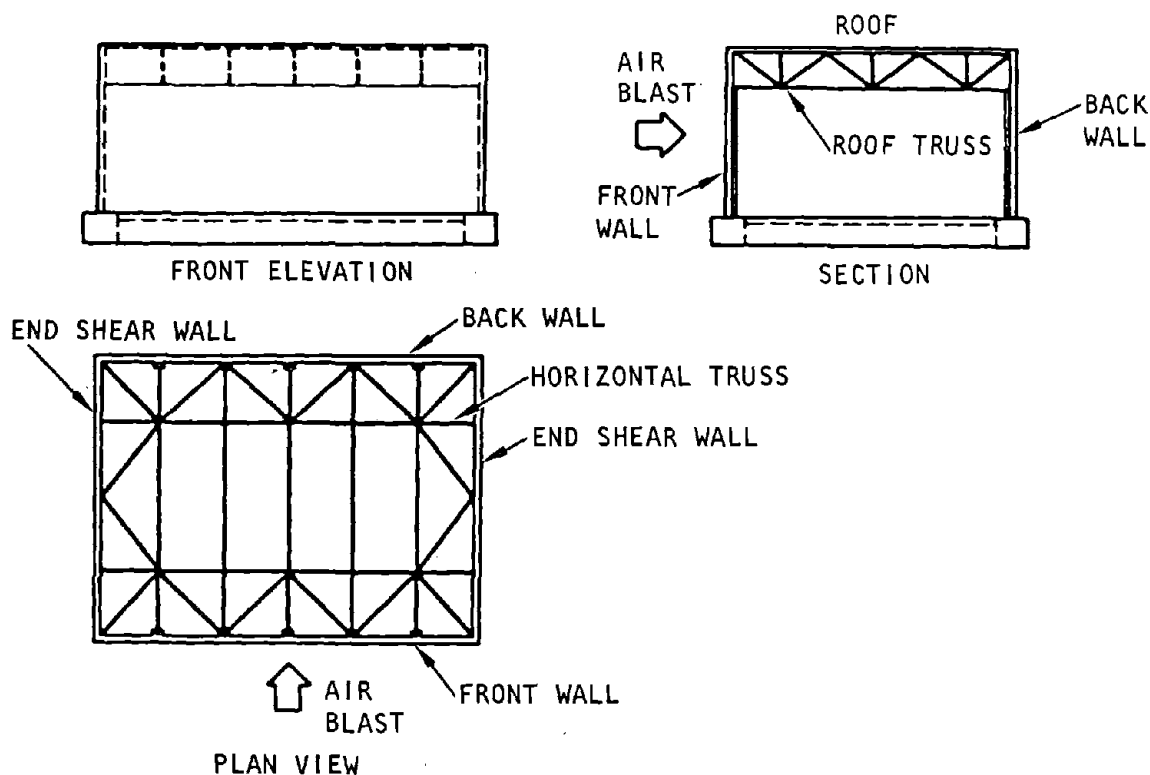


Figure 10-24. Shear Wall Structures with Steel Framing (COE, 1958)

- m_T = Mass of structure considered to rotate as well as translate
- \bar{y}_r = Vertical distance from axis of rotation to centroid of rotating mass, m_T

The rotational stiffness B of a rigid rectangular foundation on soil is expressed by:

$$B = \frac{E_s}{4} cd^2 \quad (10-27)$$

where

- c, d = Dimensions of foundation where c is parallel to the axis of rotation
- E_s = Effective constrained modulus of elasticity of the soil to a depth (below the bottom of the footing) of twice the shortest plan dimension of the footing

The horizontal acceleration of the centroidal axis is given by

$$\ddot{x}_o = \frac{F_o}{m} - \alpha_o \bar{y} \quad (10-28)$$

where

- \ddot{x}_o = Horizontal acceleration of axis of rotation
- v_o = Horizontal velocity of axis of rotation
- x_o = Horizontal displacement of axis of rotation

The force components necessary for the computation of the total force F_o and the total moment M_o are illustrated in figure 10-29 for a symmetrical structure. The computation of the sliding and rotation of the structure as a function of time is accomplished by concurrent numerical integrations of equations 10-26 and 10-28. If the structure does not slide or stops sliding ($v_o = 0$) at some point in the analysis, equation 10-26 must be revised to the following form

$$\alpha_o = \frac{M_o}{I_o} \quad (10-29)$$

For the case of no sliding, only the solution by numerical integration of equation 10-29 is necessary.

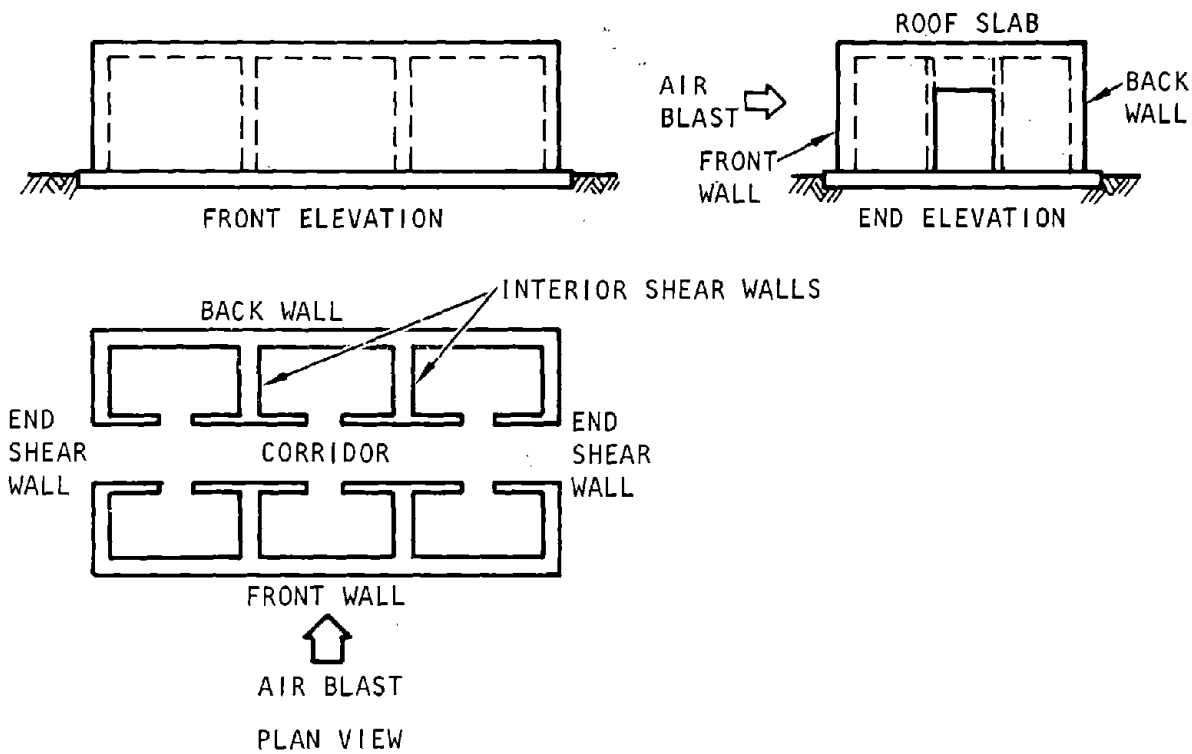


Figure 10-25. Shear Wall Structure with Interior Shear Wall (COE, 1958)

When the structure does not slide, the velocity v_o of the axis of rotation is equal to zero and the acceleration \ddot{x}_o is equal to zero. Setting equation 10-28 equal to zero the following sliding criterion is obtained:

$$\left. \begin{array}{l} \text{Sliding occurs when } F_o > m\bar{y}\alpha_o \\ \text{When } v_o = 0 \text{ and } F_o \text{ is not greater than } m\bar{y}\alpha_o, \\ \text{then } F_o = m\bar{y}\alpha_o \end{array} \right\} \quad (10-30)$$

The value thus obtained for F_o , the summation of all external horizontal forces applied to the structure—including the foundation reactions—may be used to

determine the magnitude of the horizontal foundation reaction developed when the structure does not slide. These reactions are necessary to compute the value of M_o for the solution of equation 10-29.

e. *Simultaneous dynamic sliding and overturning.* Simultaneous dynamic sliding and overturning analysis includes the horizontal deformation of the shear walls in addition to rigid body modes of behavior. The forces acting upon a two-story structure are illustrated in figure 10-30. In a manner similar to that for the rigid body analysis, the structure is assumed to rotate about point "0," the centroidal axis at the base of the footings. The angular acceleration

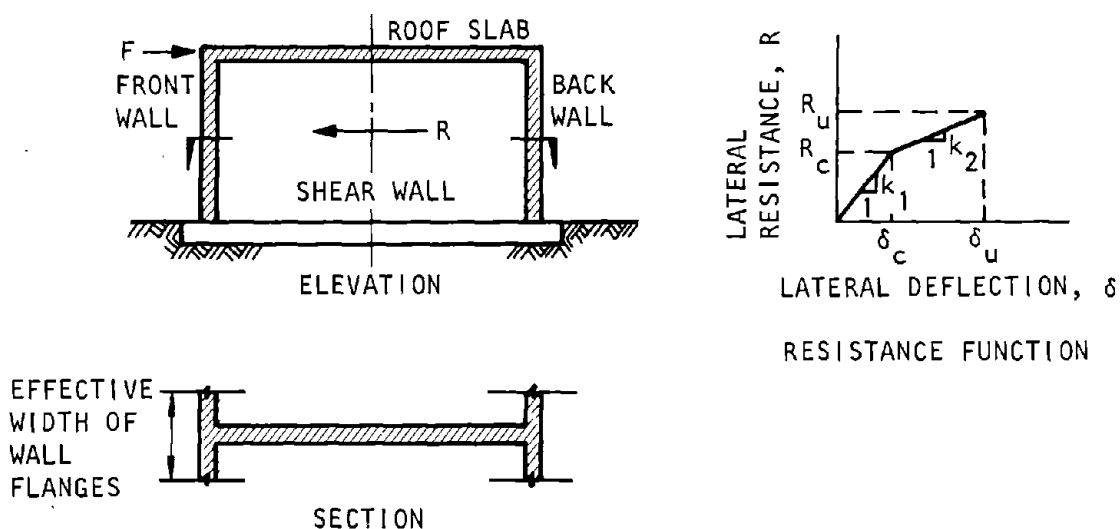


Figure 10-26. Idealized Resistance Function for a One-Story Shear Wall (COE, 1958)

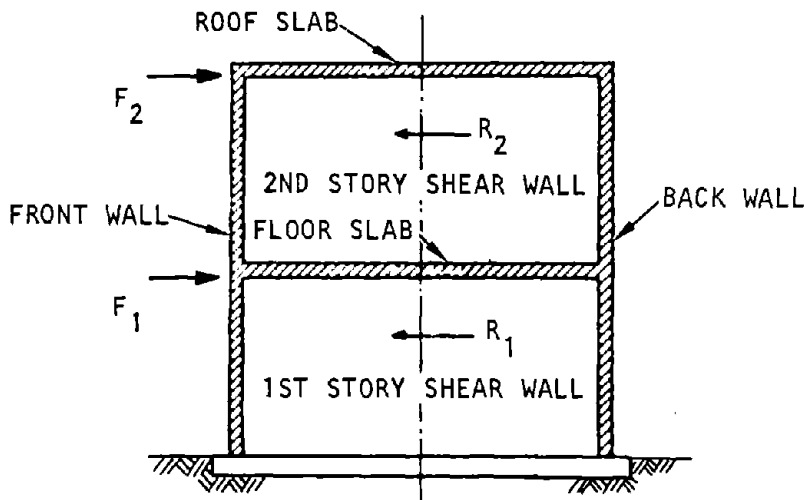


Figure 10-27. Two-Story Shear Wall (COE, 1958)

of the structure about this axis is given for a structure of n-stories by:

$$\alpha_o = \frac{M_o - (F_1 - R_1)y_1 - (F_2 - R_2)y_2 - (F_3 - R_3)y_3 \dots - (F_n - R_n)y_n}{I_o - m_1y_1^2 - m_2y_2^2 - m_3y_3^2 \dots - m_ny_n^2} \quad (10-31)$$

where

- α_o = Angular acceleration of structure about axis of rotation of structure
- M_o = Moment of all external forces about axis of rotation
- $F_i(i = 1,2\dots n)$ = Summation of all external horizontal forces applied to mass m_i , including foundation reactions
- $R_i(i = 1,2\dots n)$ = Horizontal resistance developed by structure at location of mass m_i due to internal structural deformation

I_o = Mass moment of inertia of structure about axis of rotation

The horizontal acceleration of the axis of rotation is given by:

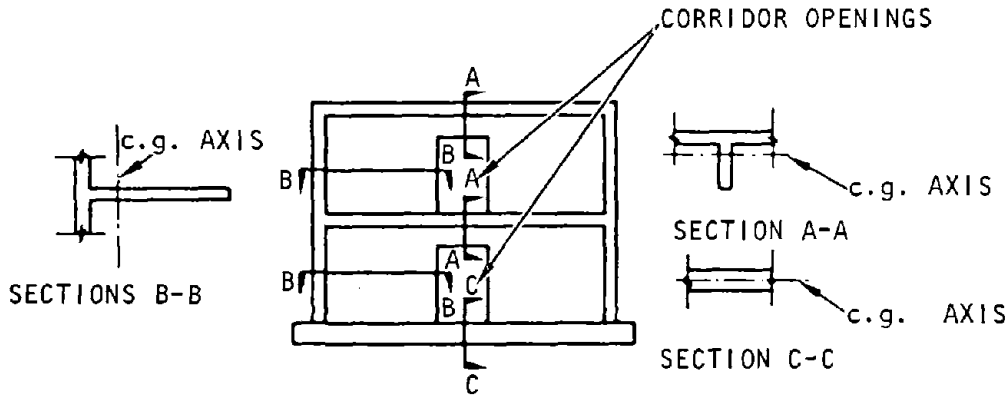
$$\ddot{x}_o = \frac{(F_1 - R_1)}{m_1} - \alpha_o y_1 \quad (10-32)$$

The relative horizontal accelerations of the shear walls are given by:

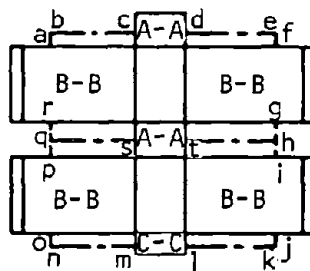
$$\ddot{x}_i = \frac{(F_i - R_i)}{m_i} - (\ddot{x}_o + \alpha_o y_i) \quad (10-33)$$

where

- $\ddot{x}_i(i = 2,3\dots n)$ = Horizontal acceleration of the mass at floor level "i" with respect to the acceleration caused by the rigid body sliding and overturning about axis "0"
- $\dot{x}_i(i = 2,3\dots n)$ = Horizontal velocity of the mass at floor level "i" with



(a) Shear wall with openings



FRAME HAS INFINITE I AND A OVER REGIONS ab, bc, de, ef, ETC.
 FRAME HAS FINITE I AND A IN SECTS A-A, B-B, AND C-C.

(b) Equivalent frame

Figure 10-28. Shear Wall with Openings and Equivalent Frame (COE, 1958)

respect to the velocity caused by the rigid body sliding and overturning about axis "0"

$x_i (i = 2, 3, \dots, n) =$ Horizontal displacement of the mass at floor level "i" with respect to the displacement caused by the rigid body sliding and overturning about axis "0"

The force components used for the computation of the forces F_i and the moment M_o are shown for a symmetrical structure in figure 10-30. The computation of the shear wall displacements and the sliding and rotation is accomplished by a numerical integration of equations 10-31, 10-32, and 10-33. The deflections must all be computed simultaneously. If the structure does not slide or stops sliding ($\dot{x}_o = 0$) at some point in the analysis, equation 10-31 becomes:

$$\alpha_o = \frac{M_o - (F_2 - R_2)y_2 - (F_3 - R_3)y_3 - \dots - (F_n - R_n)y_n}{I_o - m_2y_2^2 - m_3y_3^2 - \dots - m_ny_n^2} \tag{10-34}$$

For the case of no sliding, only the solution by numerical integration of equations 10-33 and 10-34 is necessary. When the structure does not slide, the velocity v_o of the axis of rotation "0" is equal to zero and the acceleration \ddot{x}_o is equal to zero. Setting equation 10-32 equal to zero, the following criteria are obtained:

Sliding occurs when $(F_1 - R_1) > m_1y_1\alpha_o$
 When $v_o = 0$ and $(F_1 - R_1)$ is not greater than $m_1y_1\alpha_o$, then $(F_1 - R_1) = m_1y_1\alpha_o$

Care must be taken in the computation of I_o , the mass moment of inertia of the structure about the axis of rotation "0." Because of the manner of construction of the structure, it is often desirable to assume that some portion of the structure (such as the shear walls, front and back walls, and the edges of the roof supported by the walls) rotate as well as translate, whereas other portions (isolated footings and the columns and the roof supported by them) translate without rotating. The computation of I_o is thus the determination of the polar moment of inertia about

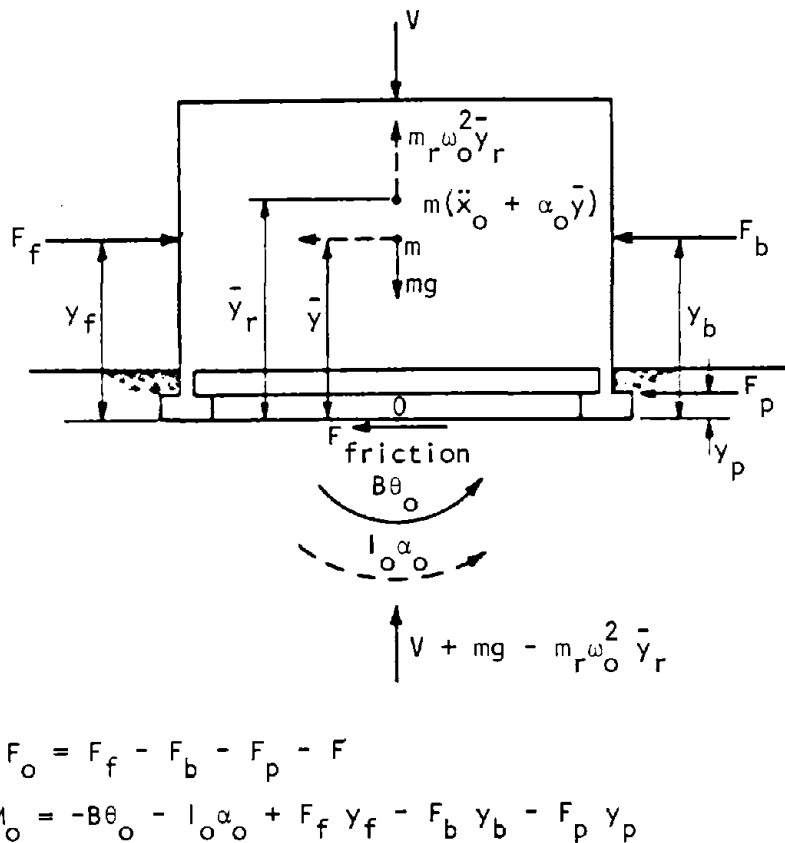


Figure 10-29. Forces Acting upon Structure as a Rigid Body (COE, 1958)

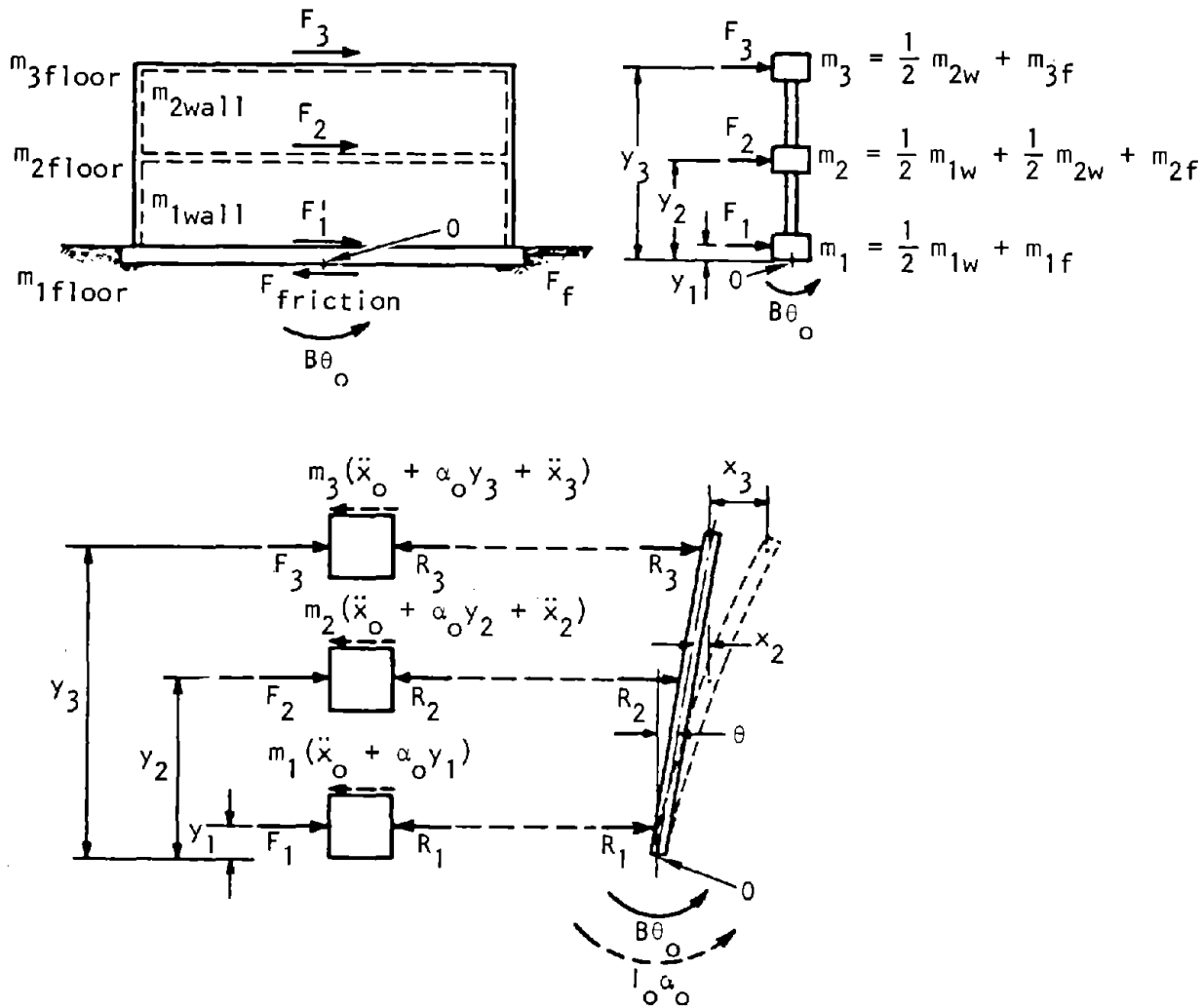


Figure 10-30. Force Acting upon Two-Story Structure (COE, 1958)

“0” of those masses that rotate and translate and the moment of inertia about a horizontal plane through “0” of those masses that only translate.

10-7. Arches

a. Types of arch structures. A barrel arch of reinforced concrete and concrete slabs supported by steel or concrete arched ribs are examples of arch structures.

(1) The presence of end or intermediate walls or stiffening ribs in a long structure will supply rigidity to an arch and increase its resistance to lateral loads. This increase rigidity will manifest itself when the spacing of these stiffeners is fairly small. End walls influence the structural response of the arch when the spacing of the walls is equal to or less than $0.75 \sqrt{Rh}$, where R is the radius of the arch and h is its thickness. If the intermediate diaphragms or stiffeners are added, their effectiveness only becomes apparent when their spacing is less than $1.50 \sqrt{Rh}$. This latter spacing is based on the assumption that complete fixity exists at the junction of the stiffener and

the arch. Disregarding the effects of the end walls and intermediate stiffeners on the arch will yield a conservative design.

(2) The response of an arch structure is obtained from estimates of frequencies of vibration of the structure in the compression and deflection modes, the yield resistance, and the ductility ratio of maximum allowable deflection to the yield deflection. Assume an idealized elastoplastic resistance. Determine the natural period using a stiffness corresponding to that associated with the yield resistance divided by the yield deflection. In a fixed-end structure, use a stiffness corresponding to the resistance after plastic hinges have formed at several points, including the incipient final plastic hinge that leads to collapse.

b. Response to compression mode loading. In the compression mode, the arch is very stiff and the natural period is consequently very short. For a circular arch with pinned ends and of constant cross section, the lowest natural frequency is one for which the arch vibrates in the shape shown by the dashed

curve of figure 10-31. The natural period of vibration, in seconds, for this mode of vibration is given by:

$$T = \frac{2\pi L^2}{C_1} \sqrt{\frac{m}{EI}} \quad (10-35)$$

where

- L = Span of the arch
- m = Mass per unit length of circumference of arch
- E = Modulus of elasticity
- I = Moment of inertia of the arch cross section

$$C_1 = 4 \sin^2 \frac{\theta}{2} \sqrt{0.820 \left(\frac{R}{r}\right)^2 + \left(\frac{\pi^2}{\theta^2} - 1\right)^2} \quad (10-36)$$

where R is the radius of the arch, θ is the angle in radian formed by two normals to the surface at the arch support lying on the same meridional plane, and r is the radius of gyration of the cross section. For a circular arch with fixed ends and of constant cross section, the lowest natural frequency is one for which the arch vibrates in the shape shown by the dotted curve of figure 10-32. In this case the period is given by

$$T = 2\pi \frac{L^2}{C_2} \sqrt{\frac{m}{EI}} \quad (10-37)$$

where

$$C_2 = 4 \sin^2 \frac{\theta}{2} \sqrt{\frac{2}{3} \left(\frac{R}{r}\right)^2 + \left(\frac{\pi^2}{\theta^2} - 1\right)^2} \quad (10-38)$$

Consider the arch illustrated in figure 10-33. Using the geometric properties shown and taking $E = 3 \times 10^6$ lb/in² from equation 10-37, the natural period will be equal to 0.015 sec. This short period is of the order of the rise time to peak of the overpressure as it traverses the arch. As the rise time of the imposed compression mode loading approaches the natural period of the structure, the dynamic load factor approaches unity. The stresses produced are, therefore, essentially those that would be produced by the same load applied statically. Note that the loading in the compression mode should not exceed the yield resistance of the structure (ductility factor $\mu \leq 1$). Since the variation of axial stress in the compression mode is approximately uniform over finite lengths of the arch, allowing the stresses to reach their dynamic yield values will result in the formation of plastic hinges that extend over a finite length of the arch rather than at localized points. This will result in a "softening" of the arch and a correspondingly large increase in deflections.

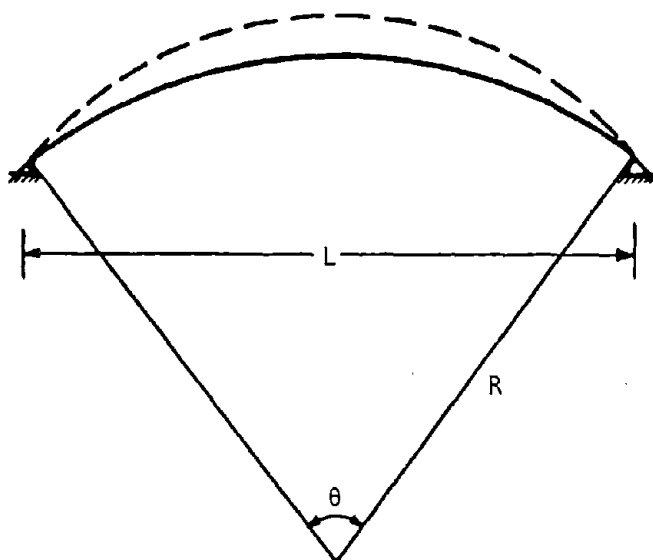


Figure 10-31. Vibrational Shape Associated with the Lowest Natural Frequency of a Two-Hinged Arch in the Compression Mode (COE, 1960b)

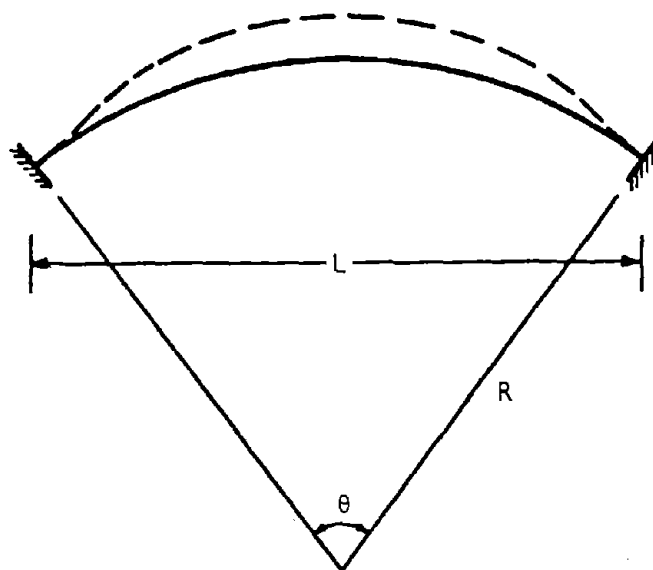
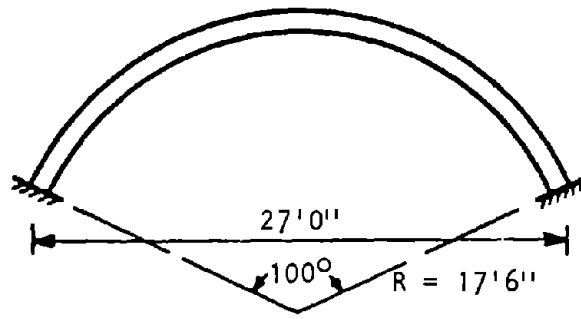


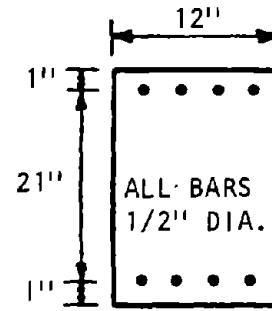
Figure 10-32. Vibrational Shape Associated with Lowest Natural Frequency of a Fixed-End Arch in the Compression Mode (COE, 1960b)

c. Response to deflection mode loading. In the deflection mode the structure is relatively flexible as compared to its behavior in the compression mode. The dotted curve of figure 10-34 shows the vibrational shape of the circular arch with pinned ends and of constant cross section. The natural period of vibration is given by:

$$T = \frac{2\pi L^2}{C_3} \sqrt{\frac{m}{EI}} \quad (10-39)$$



(a) Elevation of arch



(b) Typical cross section of arch

Figure 10-33. Sample Arch (COE, 1960b)

where C_3 is plotted in figure 10-35. For a circular arch with fixed ends and of constant cross section, the vibrational shape is shown by the dotted curve of figure 10-36. The natural period of vibration is given by:

$$T = \frac{2\pi L^2}{C_4} \sqrt{\frac{m}{EI}} \quad (10-40)$$

where C_4 is plotted in figure 10-37. Equation 10-39 is based on the assumption that the primary behavior in this mode is in flexure with a consequent neglect of axial deformation. Except for very flat arches, θ less than about 50 deg, the accuracy of these relations is good. Because the natural period of vibration is long compared with the duration of the deflection mode loading, the load on the structure may be assumed to be an equivalent rectangular pulse of the same area as the applied load. Figure 10-14 gives a representative loading curve. Figure 10-38 illustrates the deflection curve of the arch showing that the maximum deflections occur at the quarter points. The response of the arch is obtained by the following approximate procedure. Let the impulse be defined as

$$Q = P_i T_i \quad (10-41)$$

where T_i is arbitrarily chosen and is suitably small. The localized resistance diagram is shown in figure 10-39.

$$\frac{(P_i T_i)^2}{2m_e} = R_u \left(\delta_m - \frac{\delta_e}{2} \right) \quad (10-42)$$

where

- m_e = Effective mass of the structure
- R_u = Yield resistance
- δ_m, δ_e = Maximum permissible deflection and yield deflection, respectively

The effective mass m_e is related to the period of the structure:

$$T = 2\pi \sqrt{\frac{m_e \delta_e}{R_u}} \quad (10-43)$$

Combining the two preceding relations yields the equation

$$\frac{P_i}{R_u} (2\pi T_i / T) = \sqrt{2 \frac{\delta_m}{\delta_e} - 1} \quad (10-44)$$

This relation is theoretically correct only if T_i approaches zero, but it is adequate for T_i as large as 0.2 T. The total impulse per unit area normal to the arch surface for the deflection mode loading is approximately

$$Q = (1.25 \text{ to } 1.50) P_o t_t \quad (10-45)$$

where

- P_o = Peak overpressure
- t_t = Transit time

The yield resistance is, therefore:

$$R_u = \frac{2\pi}{T} (1.5 P_o t_t) \frac{1}{\sqrt{2 \frac{\delta_m}{\delta_e} - 1}} \quad (10-46)$$

Equation 10-44 can be used to find either the desired resistance R_u , the impulse $P_i T_i$ that will just produce a certain deflection, or the ductility factor defined as the ratio of the maximum to yield deflections δ_m / δ_e when the other quantities are given. Because of the freedom of choice of T_i , equation 10-44 is essentially only a relation between P_i / R_u and δ_m / δ_e and the values are plotted in figure 10-40 for a value of

$T_i = (1/2\pi) T$. The approximate time to reach the maximum deflection t_m is given by:

$$t_m/T = 0.091 + (P_i/R_u)(T_i/T) \tag{10-47}$$

or for $T_i = (1/2\pi) T$

$$T_m/T = 0.091 + 0.159 (P_i/R_u) \tag{10-48}$$

Equation 10-47 is also plotted in figure 10-40.

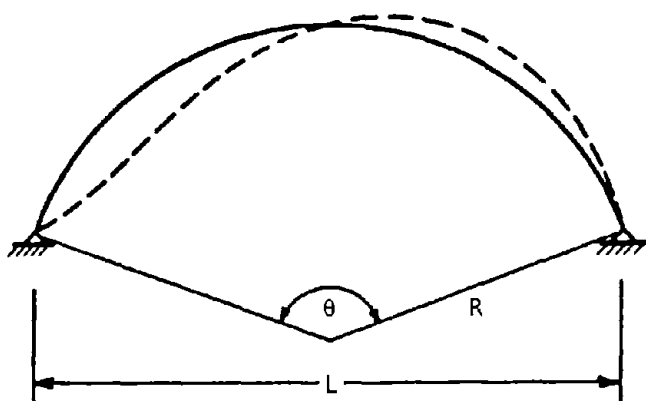


Figure 10-34. Vibrational Shape Associated with Lowest Natural Frequency of a Two-Hinged Arch in the Deflection Mode (COE, 1960b)

d. *Buckling effects.* The susceptibility of the arch to buckling under the compression mode loadings will have an effect on the deflection under deflection mode loadings. A uniformly distributed pressure may cause buckling of the arch into shapes shown by the dotted lines of figures 10-41 and 10-42. This tendency to buckle will increase the deflections as computed under deflection mode loadings. For a two-hinged arch, the uniform pressure that produces buckling is given by:

$$P_B = \frac{EI}{R^3} \left(\frac{4\pi^2}{\theta^2} - 1 \right) \tag{10-49}$$

For a fixed-end arch the uniform pressure that produces buckling is:

$$P_B = \frac{EI}{R^3} (k^2 - 1) \tag{10-50}$$

where k is defined by the relation

$$k \tan \frac{\theta}{2} \cot \frac{k\theta}{2} = 1 \tag{10-51}$$

Figure 10-43 is a plot of k as a function of θ . If we designate by δ_m the deflection in the deflection mode

when there is no buckling load, and by δ'_m the deflection when there is a compressive force tending to produce buckling, the relation between these two deflections is given by

$$\frac{\delta'_m}{\delta_m} = \frac{\delta_m/\delta_m}{\delta_m/\delta_e} = \frac{1}{1 - P_c/P_B} \tag{10-52}$$

where P_c is the compressive mode loading. This relation is strictly applicable only for elastic behavior. Under dynamic conditions, the strength of the arch would be higher than under static conditions since it takes time for the arch to buckle. Equation 10-51 can be used as an approximation. For P_c , use the average value of the compression mode loading over the time to reach maximum deflection in the deflection mode.

e. *Blast wave traveling along the arch axis.* When a blast wave approaches normal to the end wall of the structure, the loading on any ring is approximately instantaneous. Considering elastic behavior, since the duration of the load is long and the natural period of vibration of the structure is short, the dynamic load factor approaches two, that is, the stresses produced are twice those that would be produced by the same load applied statically. The resistance to this type of loading is primarily by means of direct stress in the arch. This axial stress, approximately constant over the length of the arch, will develop plastic zones, rather than plastic hinges, over those portions of the arch at which the stress is approximately equal to the dynamic yield strength of the material. This condition, if allowed to develop, will result in either large deflections of the arch or instability, neither of which can be tolerated. Both of these conditions may be considered as failure or collapse conditions. Thus, for an arch loaded by a blast wave traveling axially along the structure, the response should be confined to elastic action only. The adequacy of the structure against buckling should be checked by means of equation 10-49 or 10-50.

10-8. Domes

a. *Types of dome structures.* Blast-resistant dome structures are designed to have surfaces that are monolithic. Ribs or other supporting elements are not very effective in resisting the external loads. They are generally reinforced along their support by a ring beam that resists the thrust of the dome by tension in the ring. The dome should be designed to resist the applied blast loads by elastic action only.

b. *Structural response to compression mode loading.* In the compression mode, the dome is very stiff and the period of vibration is consequently very short. For

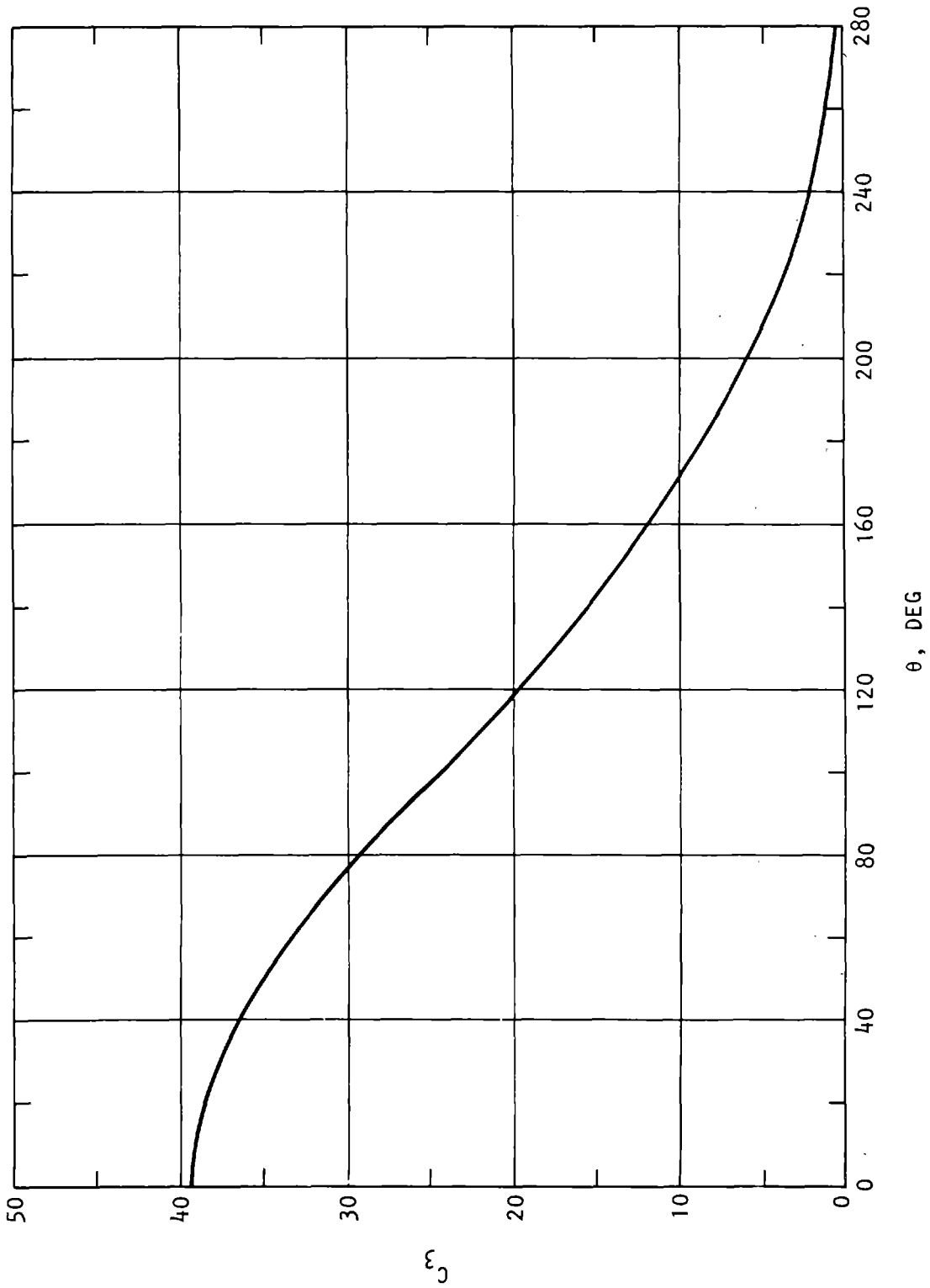


Figure 10-35. Vibration Parameter C_3 as a Function of the Central Angle θ for a Two-Hinged Arch in the Deflection Mode (COE, 1960b)

a complete spherical shell of constant thickness, the period T in seconds is:

$$T = 2\pi \sqrt{\frac{mR^2(1-\nu)}{2Eh}} \quad (10-53)$$

where

- m = Mass per unit surface area of the dome
- R = Radius of the dome
- ν = Poisson's ratio
- E = Modulus of elasticity
- h = Dome thickness

The period of a structural dome is different from that given by equation 10-53 because the shell structures are not completely spherical and are also influenced by the support conditions. The exact relation for the period of a dome that is not completely spherical is not important, since it is seen from equation 10-53 that the period is very short. The modal loadings to which a dome is subjected have rise times of the same order of magnitude as the transit time of the shock wave over the structure. The ratio of the rise time to the period is large and the stresses that are produced by this dynamic loading are the same as those that would be produced by the peak value of the compression mode loading applied statically.

c. Structural response to deflection mode loading. The dome resists deflection mode loadings by developing internal forces in the plane of the surface. Resistance to this antisymmetrical loading is accomplished primarily by axial deformation rather than by bending of the dome. The period under this type of loading is therefore likely to be of the same order of magnitude as that under the compression mode loadings. Recognizing that the period is short, the exact value is not important. The rise time of the deflection mode loading is of the same order of magnitude as the transit time of the shock wave. Therefore, the stresses produced by the dynamic loading are the same as those obtained by the peak deflection mode loading applied statically.

d. Combined response of structure to modal loadings. The sum of the maximum intensities of stress due to dead weight loading and compression and deflection mode loadings should not exceed 0.8 of the dynamic yield strength of the concrete, in keeping with the approximations involved in the determination of the applied dynamic loads. In the case of reinforced-concrete domes, reinforcement should be provided in both the meridional and latitudinal planes.

e. Buckling of structure. The critical uniform radial pressure causing buckling of a complete sphere is

given by the relation

$$P_B = \frac{2Eh^2}{R^2\sqrt{3(1-\nu^2)}} \quad (10-54)$$

where the quantities are as defined in equation 10-53. Experimental results show that domes usually buckle under loads approximately 1/3 to 1/4 that given by equation 10-54. Since the dome will require time to buckle under dynamic loads, the compression mode loadings may approach the critical buckling pressure much more closely than would be the case if the same load were applied statically. For preliminary designs the peak value of the compression mode loading should not exceed 1/3 the critical pressure given by equation 10-54.

f. Spread footings. Aboveground structures tend to slide laterally and rotate under blast loading. Figure 10-44 shows the sources of lateral resistance on spread-footing foundations.

(1) The sliding of structures is resisted by passive pressure on the rear vertical faces of the foundations and by friction between the soil and the foundation. In structures on pile foundations, lateral movement of the foundation is resisted by lateral shearing and bending forces in the piles and by the passive pressure on pile caps. Batter piles resist lateral loads with a component of their axial force and provide a more rigid structure. Batter piles may be required for large horizontal forces or for weak overburden. Where practical, caissons are a good alternative to vertical and batter piles for resisting sliding of structures.

(2) Horizontal blast loads tend to overturn structures, thus causing unequal distribution of foundation pressure. This unequal distribution of pressure in general causes a reduction in the available frictional resistance at the front of the structures is generally small. This lack of sufficient frictional resistance at the base of footings for the walls and columns near the front of structures makes it necessary to utilize the lateral resistance furnished by the passive pressure on the back of these footings, or to provide footing struts or floor slab diaphragms connected to the rear footings where the bearing pressures are high and large friction forces can be developed. The passive pressure on the rear vertical face of rear wall footings is also much higher than for the front wall footings, due to the effect of the blast pressure on the ground surface at the rear of the structure.

(3) In the case of shear-wall buildings with interior columns carrying large vertical loads but not lateral loads, the large column loads permit development of large frictional forces which may be utilized to resist the total lateral loads. The column footings may be tied to the shear walls by horizontal floor slab/deep beams, or a mat foundation may be used.

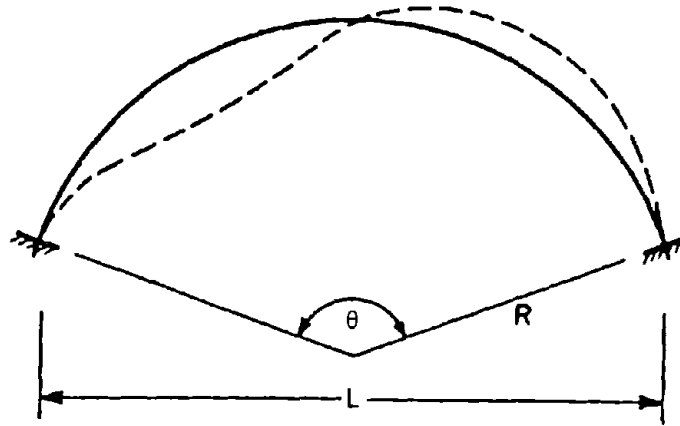


Figure 10-36. Vibrational Shape Associated with Lowest Natural Frequency of a Fixed-End Arch in the Deflection Mode (COE, 1960b)

(4) For structures that resist horizontal blast loading through rigid frame action, maximum restraint against rotation at the bottoms of the frame columns will require that individual footings be rather large by conventional standards. In most cases continuous footings or mat foundations may be more advantageous.

(5) In the case of interior or front wall footings, the resistance available due to passive pressure is a function of the depth to the surface of the soil and the weight of the soil enclosed between the footings. The maximum resistance that the soil enclosed between the footings can provide is the lesser of (a) the resistance due to passive pressure of the soil, or (b) the frictional resistance approximated by the product of the coefficient of friction and the weight of the soil between footings. Wherever backfill is necessary in the construction of the footing, it is recommended that compacted sand and gravel be used so that the frictional resistance may be a maximum. For the development of maximum frictional resistance it is preferable to pour foundations against undisturbed soil. The passive pressure on the rear face of the foundation is increased by the blast pressure acting on the ground surface at the rear of the structure. The blast pressure on the ground also causes soil pressures to develop on the front face and top surface of the front footings. The pressure on the top of the footings at the front of the building due to the blast pressure on the ground surface is a very important source of resistance to overturning.

(6) For design purposes: If friction equal to or greater than the net lateral force can be developed, the lateral motion of the foundation may be assumed to be negligible; and if friction alone is not great enough but if friction plus passive pressure equal to or greater than the net lateral force can be developed, the footing motion should be considered. For

preliminary design, this may be assumed to be limited to about 4 percent of the footing depth.

(7) The resistance available from passive pressure at any time should be made equal to, or greater than, twice the difference between the total lateral load on the footing and the available friction.

(8) In many foundation designs it will be found uneconomical to prevent lateral motion of the structure by providing friction and passive pressures to resist the total lateral dynamic reactions on the footings. In these cases a dynamic analysis should be performed to determine the magnitude of the footing motion.

g. Pile foundations. In pile foundations the piles may be used to resist uplift forces resulting from blast and the lateral forces may be resisted by either vertical or batter piles.

(1) The vertical load on any pile of a group under the action of the vertical load and the lateral loads should not exceed the dynamic bearing capacity of the pile. Assuming the foundation cap to be rigid and that batter piles are provided to carry the lateral forces, the axial force in any pile may be computed by the following formula:

$$\text{Vertical force per pile} = C \left(\frac{V}{N} \pm \frac{Mx_1}{\sum x^2} \right) \quad (10-55)$$

where

C = 1.0 for vertical piles and $\cos^2 \beta$ for batter piles, and β is the angle of inclination of the pile with the vertical.

V = Total vertical force on piles.

N = Weighted number of piles in group, where vertical piles are weighted with the factor 1.0 and batter piles are weighted with the factor $\cos^2 \beta$.

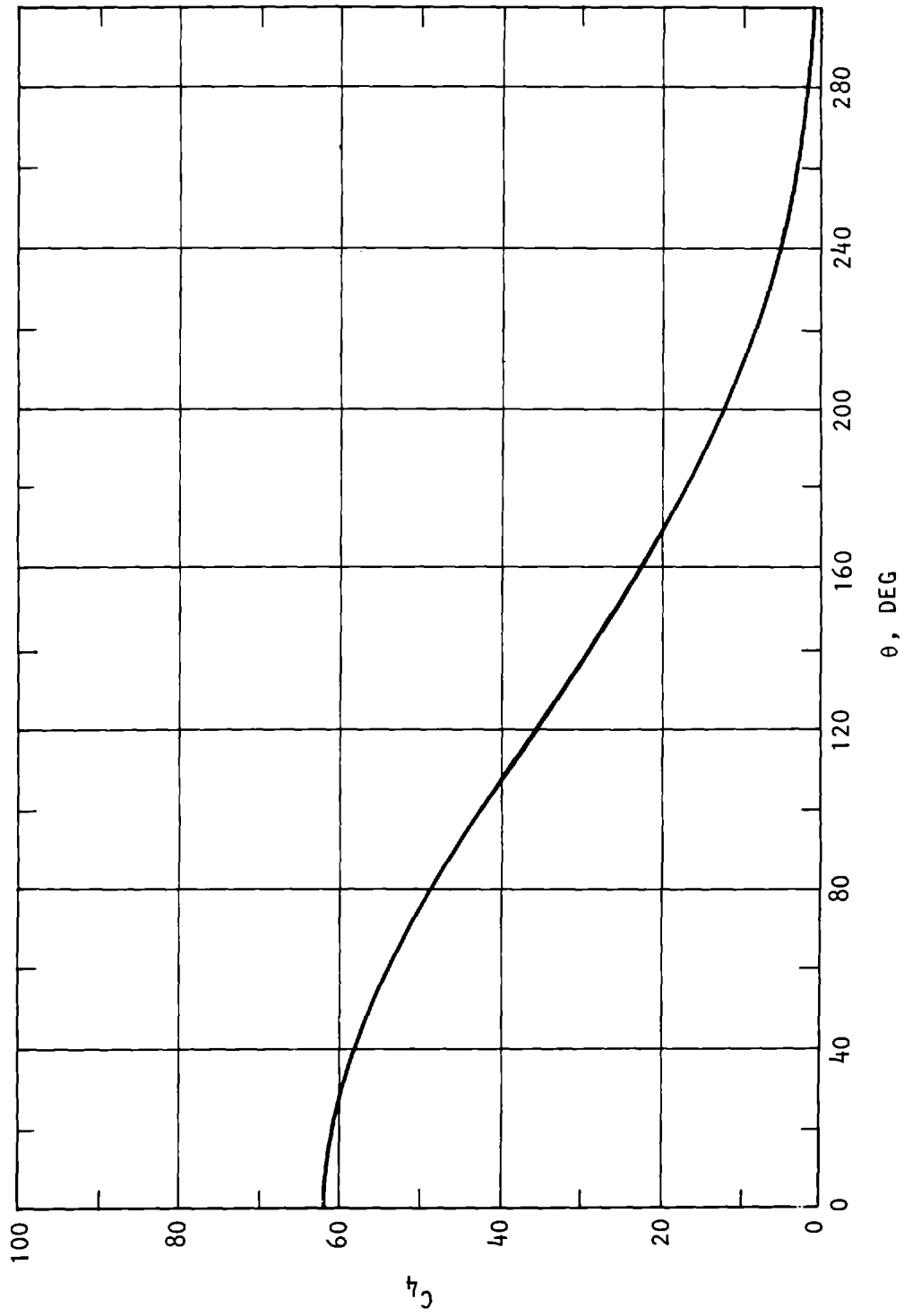


Figure 10-37. Vibrational Parameter C_4 as a Function of the Central Angle θ for a Fixed-End Arch in the Deflection Mode (COE, 1960b)

- M = Moment of forces on piles about their centroidal axis.
- x = Distance of any pile from the centroidal axis, multiplied by the proper weighting factor.
- x_1 = Distance of the pile in question from the centroidal axis.

In this equation the piles are considered to be capable of resisting uplift forces. Normally, an uplift force sufficient to cause tension failure of a pile cannot be developed at the top of the pile before the pile will pull away from the pile cap. This type of failure should be prevented in blast-resistant structures by increasing the length of pile embedment in the concrete pile cap or by other anchoring methods for pile caps.

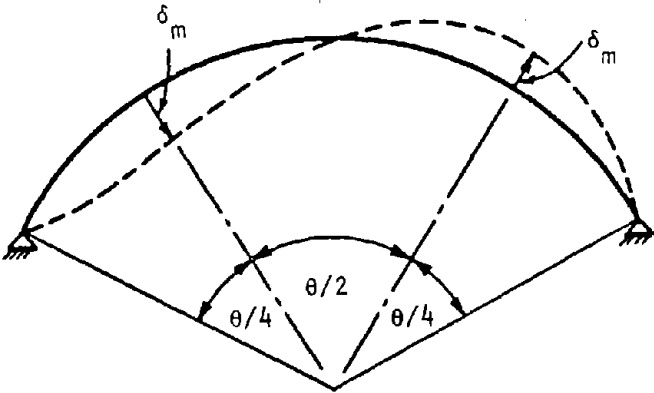


Figure 10-38. Location and Direction of Maximum Deflections of an Arch Subjected to Deflection Mode Loadings (COE, 1960b)

(2) Piles in clay have pulling resistance approximately equal to the resistance to further penetration. Piles in sand have pulling resistance approximately equal to one-half the resistance to further penetration.

(3) The effect of dynamic loading on the load capacity of the pile should be tested at the site wherever possible.

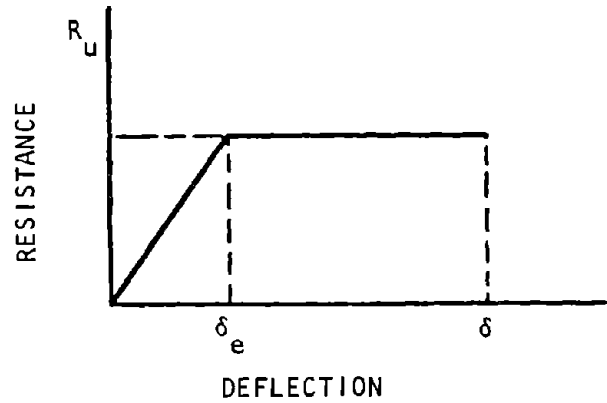


Figure 10-39. Idealized Resistance Function (COE, 1960b)

(4) Pile foundations should be designed so that the lateral load is resisted by the combination of batter piles and passive resistance on the footing or walls. The resistance-deformation relationship of these two systems may not permit the assumption of simultaneous action in many cases; however, if one type of resistance is exceeded, a small deformation of the structure will allow the excess to be carried by the other type of action.

(5) The spacing of piles should be determined on the same basis used for conventional pile foundations (see TM 5-818-1 and EM 1110-2-2906.

h. Design requirements of pile foundations. The design of foundations for aboveground structures should meet the following requirements:

- The lateral motion of the foundation should be limited to predetermined amounts without affecting their usefulness.
- The entire structure must be stable against overturning. In general, only very small rotations are permissible.
- The vertical bearing pressure resulting from the combined effect of all vertical loads and overturning moments should not exceed the dynamic design bearing capacity of the soil underlying the foundation.
- The foundation elements should be proportioned to withstand the loads results from the maximum soil pressures.

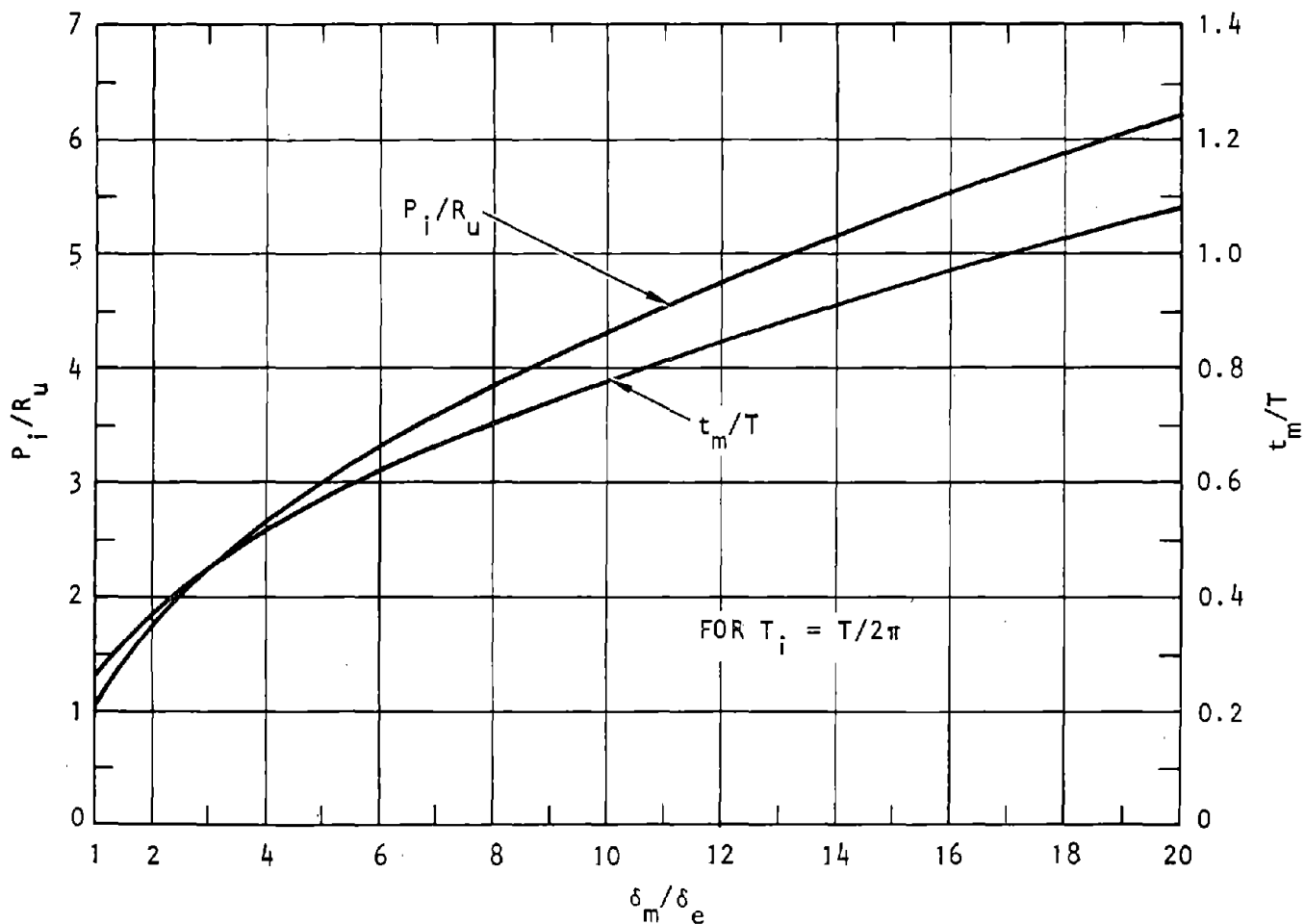


Figure 10-40. Relative Values of Parameters in the Deflection Mode (COE, 1960b)

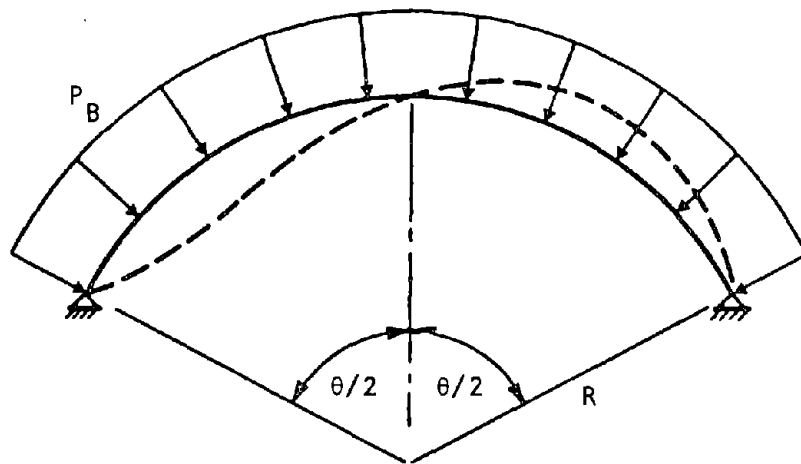


Figure 10-41. Buckled Shape and Distribution of Critical Pressures for a Two-Hinged Arch (COE, 1960b)

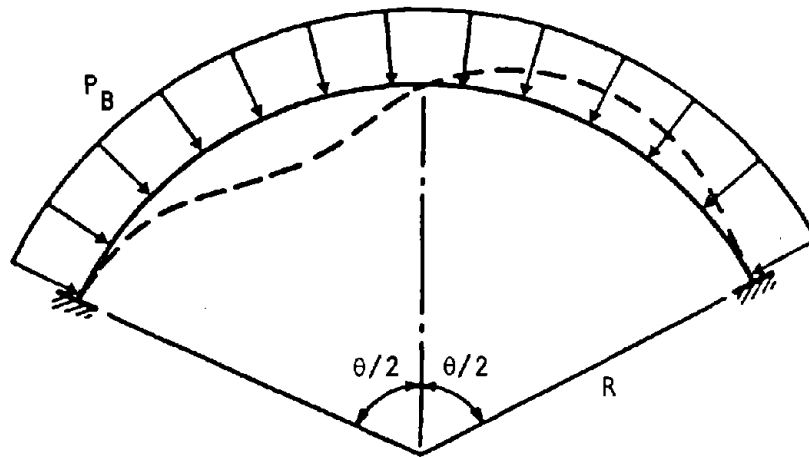


Figure 10-42. Buckled Shape and Distribution of Critical Pressure for a Fixed-End Arch (COE, 1960b)

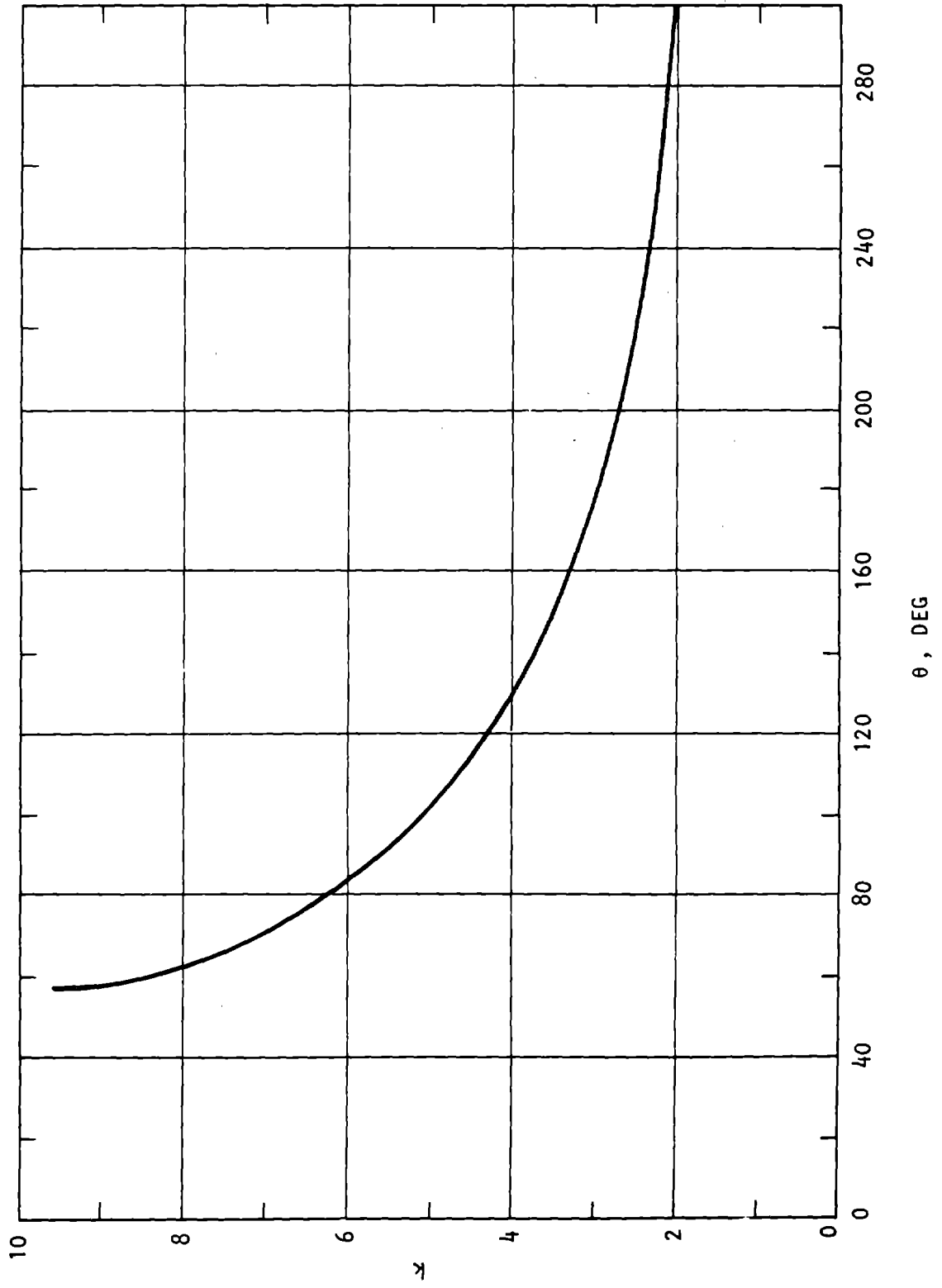
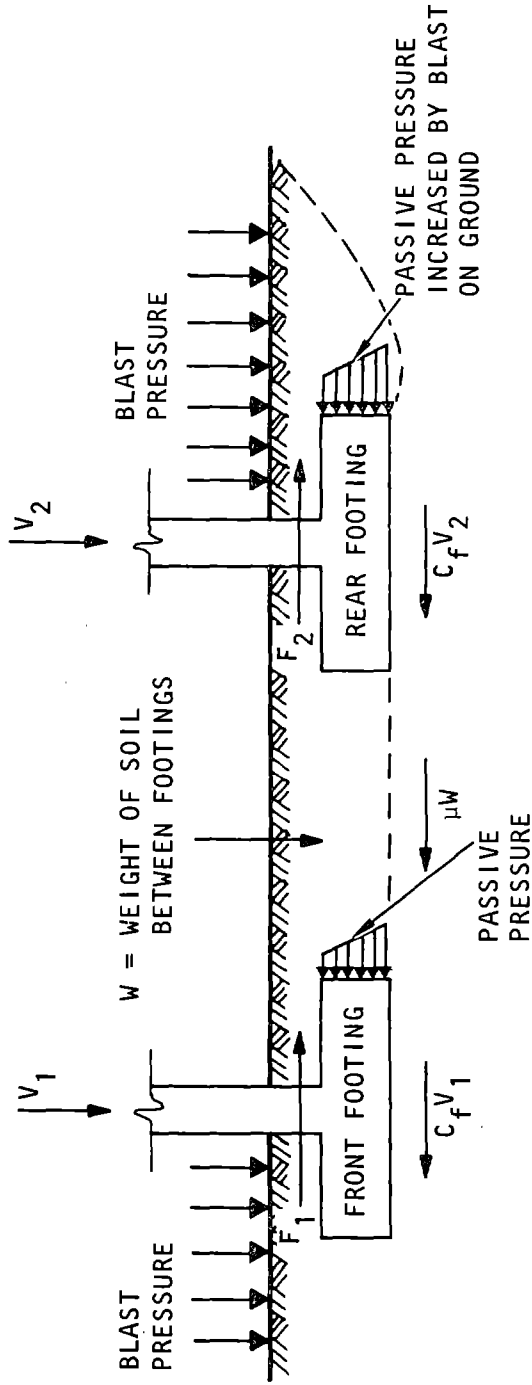
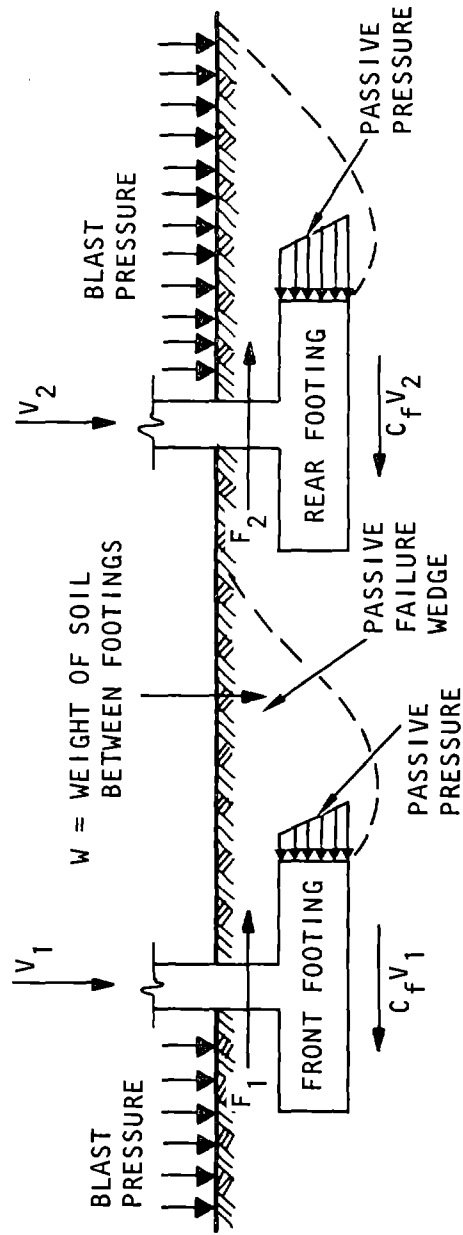


Figure 10-43. Buckling Parameter k as a Function of the Central Angle θ for a Fixed-End Arch (COE, 1960b)



(a) Case I: $C_f W <$ potential passive pressure behind front footing



(b) Case II: Passive pressure behind footing $< C_f W$

Figure 10-44. Sources of Lateral Resistance on Spread-Footing Foundations (COE, 1957)

CHAPTER 11

FLUSH, PARTIALLY BURIED, AND SHALLOW-BURIED STRUCTURES

11-1. Design threats

Design threats for shallow-buried structures are airblast, ground shock, and ejecta impact. In general, unless there are limitations on the length of umbilicals to the ground surface, specify the structure placement at a depth that eliminates the other nuclear weapon effects (e.g. radiation) as controlling design criteria. When the warheads have quite small CEPs (see Appendix D) and the structures are to be designed for very high overpressures, consider placing the structure in rock or selecting a monolithic structural configuration that may experience large displacements as a rigid body but will only allow tolerable deformations of the structural elements. Design the umbilical and internal connections and the mountings for structure contents of monolithic structures to allow for relative displacements from weapon effects (TM 5-858-4). The ground-shock environment for shallow-buried structures is obtained from basic relationships given in TM 5-858-2. Such data should be interpreted in terms of the geological and soil properties at the site. Define airblast-induced and crater-induced ground-shock transmission by wave-attenuation principles.

11-2. Site properties

a. The typical site profile for shallow-buried protective structures is stratified soil. Equivalent homogeneous properties may be assumed only if the variation in soil characteristics is gradual. Figure 11-1, a soil profile obtained at an actual site, shows very sharp differences in soil stiffness, which must be accounted for in determining the soil/structure interaction.

b. In soils with high cohesive strengths, vertical cuts may be stable. In most cases, however, the completed excavation must be back-filled and the properties of the backfill material must be included as part of the total soil definition.

c. The position of the water table in the soil is critical. Numerous design and construction problems are avoided if the structure is placed above the water table. The principal design problem is an increase in the static loads from relatively low lateral pressures in dry soil to hydrostatic pressures in saturated soil. The principal construction problem is the need for effective waterproofing during the useful life of the structure.

d. Seasonal variations of the water table such as that caused by irrigation or rainy seasons should be investigated. Also possible future construction of dams or canals could cause the water table to vary. The critical condition should be used for design.

11-3. Structure/medium interaction

a. General. Underground structures experience stresses that are transmitted through the surrounding medium. As the pressure waves propagate through the soil or rock medium and approach the structure, the free-field motions will be modified because of differences in the material properties of the structure and the medium. The change in free-field motions due to the presence of a structure is termed structure/medium interaction or soil/structure interaction. The three effects of importance are the arching of the soil, the interface reflections at the structure/medium interface, and the stress concentration factors due to the presence of the structure.

(1) Shallow-buried structures are exposed to ground shock induced by airblast waves that are usually out of phase with crater-induced ground shock. The coupled effect of the two ground shocks (and for partially buried structures, the additional effect of the air slap) constitutes a complex interaction problem. Interaction causes important effects on any structure that does not match the displaced medium in mass or stiffness. Interaction occurs whether the structure is hollow or solid; rigid or flexible; or fully buried, partially buried, or resting on the ground surface. It occurs whether the structure or free-field medium or both are loaded.

(2) It is necessary to select and size structural elements by preliminary design methods and to verify or modify the design by analysis. To perform a structure/medium interaction analysis the following important parameters of a mathematical model must be determined:

- Airblast loads
- Free-field medium loading: spatial time history
- Medium layering and material properties
- Medium/structure interface: transmission properties
- Structure: geometric and material properties
- Structure contents: location and geometric and material properties

(3) For design purposes, the air overpressure loading may be assumed to be uniformly distributed over a large area on the ground surface surrounding the underground structure. It may further be assumed that the pressure wave propagates vertically downward with the wave front parallel to the ground surface.

(4) The following additional assumptions are acceptable, if the surrounding medium has gradually varying properties. (For a medium such as the one shown in figure 11-1, numerical procedures (e.g., the

SAGA program identified in table C-1 of appendix C) must be used to obtain the stresses and deformations of the structure.)

(a) The soil may be considered to have uniform properties satisfying the Coulomb-Mohr failure criterion. This criterion states that the resistance to failure on the slip planes in the soil is given by the relationship:

$$\tau_u = C + P_n \tan \phi \quad (11-1)$$

where

- τ_u = Ultimate shearing resistance of the soil
- C = Soil cohesion

ϕ = Soil's angle of internal friction

P_n = Pressure normal to surface

(b) Slip planes in the soil between the ground surface and the structural element, as shown in figure 11-2, define the surfaces where the shear resistance of the soil has been reached. Experiments have shown that pressures required for failure of structural elements are several times greater than those predicted by theory. The designer should recognize that for a dense granular material, initial slip is accompanied by an increase in volume whereas simple theoretical approaches assume that the plastic flow of the soil occurs at constant volume.

DEPTH, FT	MATERIAL DESCRIPTION	LAYER NUMBER	REFRACTION SEISMIC VELOCITY, FT/SEC	ESTIMATED ARRIVAL TIME OF WAVE FRONT, SEC
0				0
5	DRY CLAY	1	1,600	
8.77				0.0055
10	WET CLAY	2	4,300	
16.24				0.0072
20.44	LIMESTONE	3	18,000	
25	INTER-BEDDED LIMESTONE AND SHALE	4	8,500	
30				0.0075
32.84				0.0089
35.24	LIMESTONE	5	8,500	
40	SHALE	6	6,000	
41.64				0.0103
45.24	COAL	7	2,800	
50	SHALE	8	7,000	
51.74				0.0115
55	LIMESTONE	9	10,900	
60.84				0.0125
60				0.0133

Figure 11-1. Free-Field Geological Profile of Representative Site Obtained from Borings and Seismic Surveys (Lee-Agbabian, 1976)

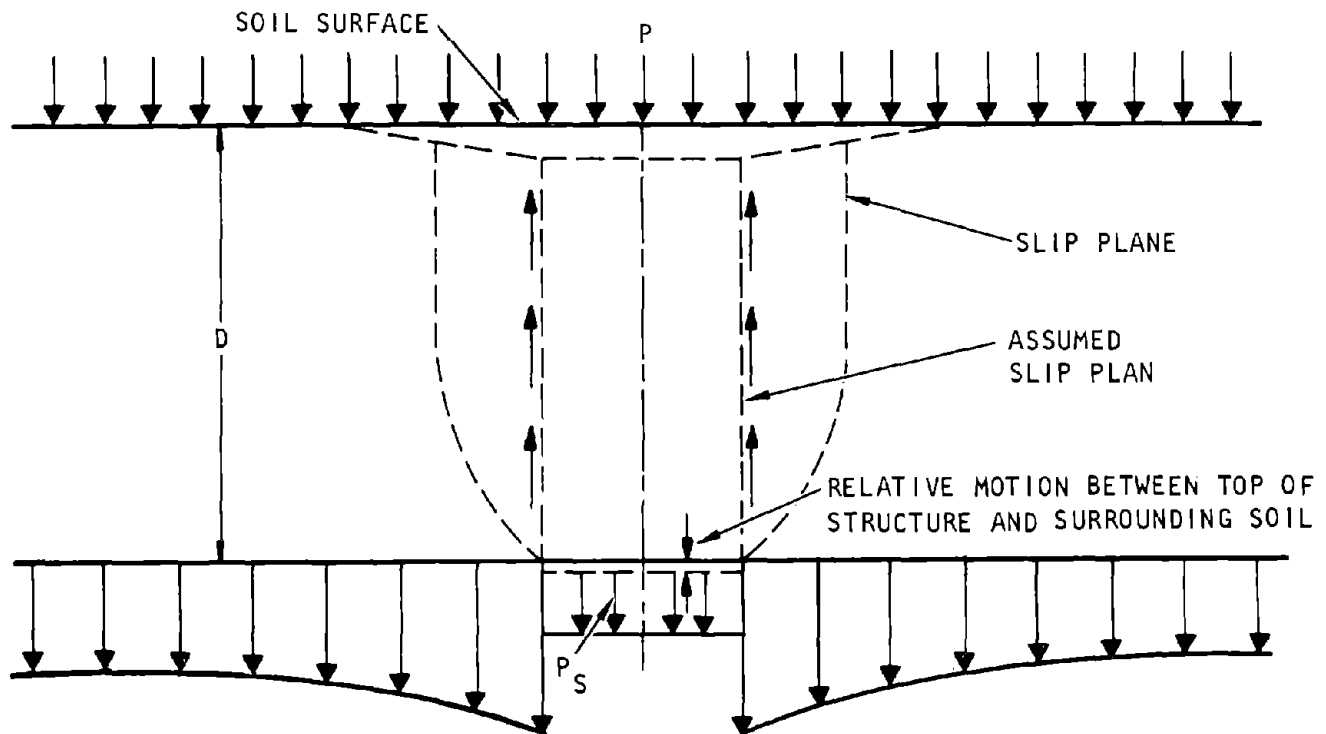


Figure 11-2. Soil Failure as a Result of Downward Motion of a Flexible Structure (Wiehle, 1964)

(c) The attenuation in pressure due to arching is strongly influenced by the angle of friction ϕ . Better agreement with experiments is obtained if it is assumed that the angle of friction ϕ increases with the depth-to-span ratio. It has been suggested that the variation of ϕ with depth may be represented by the ratio of ϕ_z/ϕ , where ϕ_z is the angle of friction at depth (Mosburg-Talda, 1966). This ratio varies from 1.0 for structures placed at the ground surface where there is small lateral constraint, to 1.5 for a depth of burial equal to the width of the structure. At greater depths the value of ϕ_z/ϕ is assumed to remain approximately 1.5.

(5) Formulas given in this section may be used for preliminary design. They are either based on static load conditions that are considered good approximations for dynamic loads or on idealized mathematical models (one-dimensional, elastic or elastoplastic, simple span, etc.) that give relatively simple solutions for dynamic loads. The effect of soil arching, which strongly influences the pressures that reach the structure, is of primary consideration in these formulas.

(6) Three methods of analysis are discussed below: finite element, discrete interactor, and closed form. (The finite-difference analysis technique, although essentially equivalent to finite element analysis, has not been widely used by structural engineers.)

b. Analytical methods

(1) **Finite Element.** In the finite element method the medium in the vicinity of the structures is represented as separate elements that, when taken

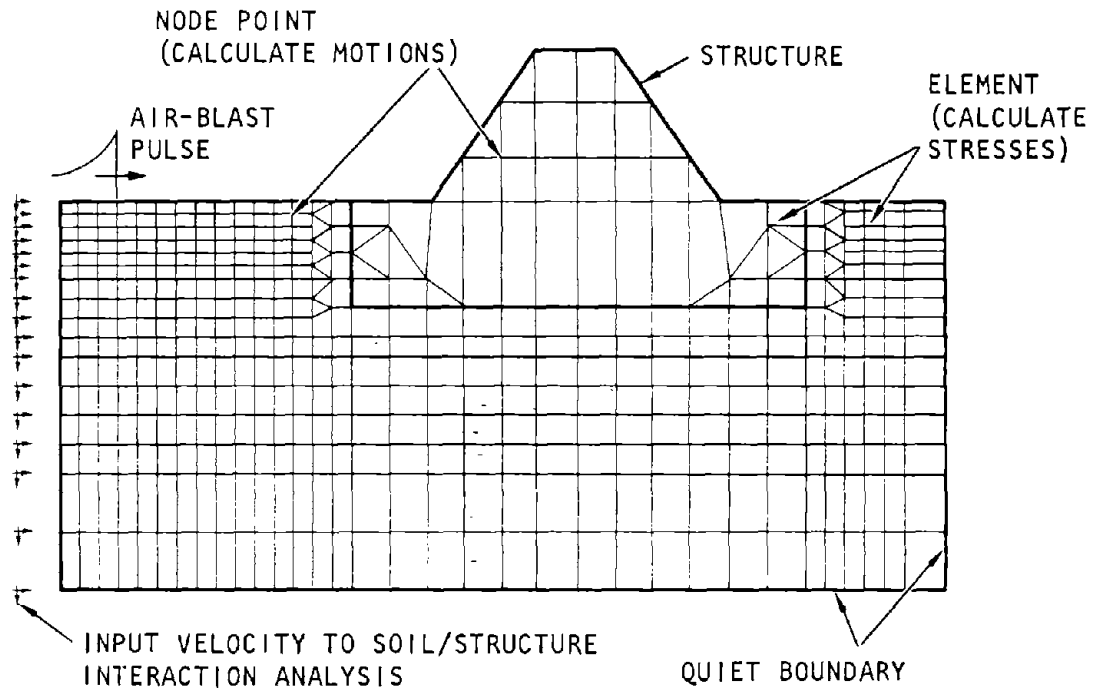
collectively, mathematically approximate the behavior of a continuum. Complicated geometries, layered media, nonlinear materials, and arbitrary loading conditions can be modeled with a finite element grid. An example is shown in figure 11-3a. Free-field loading is applied to the outer edge of the grid; the inner edge of the media grid is connected in an appropriate manner to a finite element model of the structure. The airstream is applied vertically as a traveling pressure wave to the top surface of the grid. With this method, special nonreflecting conditions (a "quiet boundary") must be used on the bottom and right hand boundaries to prevent signals from artificially reflecting back toward the structure. The primary advantage of a finite element model is that realistic variations in medium and structure properties can be provided. The structural/medium mass is properly distributed and the interaction between the structure and medium is an inherent consideration of the model. The finite-element approach models all interaction phenomena within the accuracy of the material and geometric modeling used. Some finite-element computer programs permit sliding at the medium/structure interface as well as debonding and rebonding of the structure. However, debonding and rebonding capabilities are still being perfected.

(2) **Discrete Interactors.** In the discrete interactor method, individual interactors are attached in an appropriate manner to the structure boundary as illustrated in figure 11-3b. The outer end of the interactor is driven by the free-field response. Various interactor models that have been used are shown in

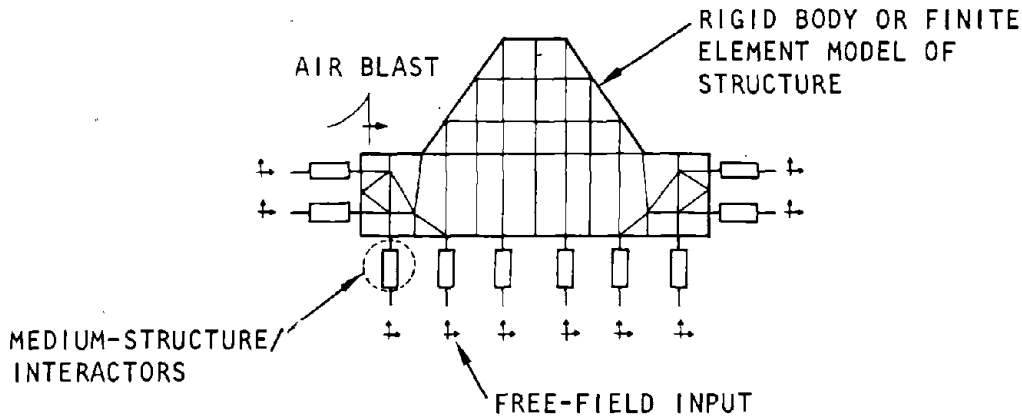
the figure. The constitutive relationships for these interactors can be made as complex or simple as required. Springs are used to estimate stresses dependent on relative displacement; dashpots are used for those dependent on velocity between the free-field and the structure. The spring constant selected for determining normal forces must introduce the stiffness of the soil column normal to the structure. The dashpot element provides for internal damping of the soil and for the energy lost by geometric dispersion of the pressure wave. The force due to free-field medium stress is applied to the structure directly. The shear

spring element represents the shear resistance of the soil layer at the interface of the soil and the structure. Another factor that must be considered is the soil mass that moves with the structure. This is frequently neglected or an arbitrary amount is added to the mass of the structure (Richart et al., 1970). The accuracy of the discrete interactor method depends on the constitutive relationships used for the interactors.

(3) Closed Form. Closed-form solutions are available for simplified representations of structure geometry and stiffness, medium properties, and



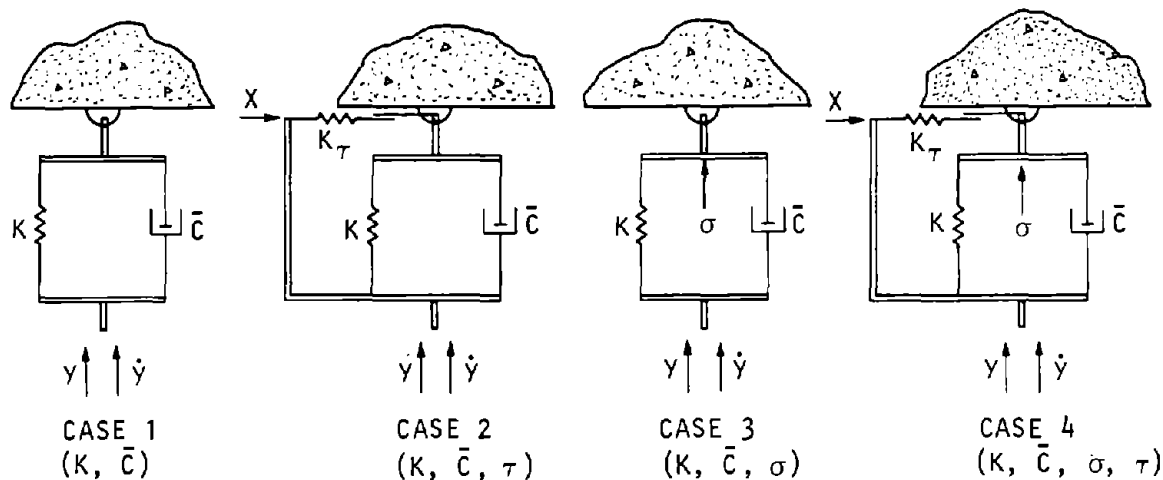
(a) Finite element approach



(b) Discrete interactor approach

U.S. Army Corps of Engineers

Figure 11-3. Medium/Structure Interaction



- y, x FREE-FIELD NORMAL AND TANGENTIAL DISPLACEMENT INPUT
- \dot{y} FREE-FIELD NORMAL VELOCITY INPUT
- σ FREE-FIELD STRESS (NORMAL)
- K SPRING CONSTANT--NORMAL FORCES (RELATIVE DISPLACEMENT COEFFICIENT)
- \bar{C} DAMPING CONSTANT (RELATIVE VELOCITY COEFFICIENT)
- τ SHEAR STRESS MODELED BY INTERACTOR
- K_{τ} SPRING CONSTANT--SHEAR FORCES

(b) Discrete interactor approach (CONCLUDED)

Figure 11-3. (Concluded)

loading conditions. These solutions are quite useful for preliminary design but usually not for final design and design verification. Also, closed-form solutions applicable to the variety of structure configurations considered are limited. Some of these solutions form the basis of the preliminary design formulas given in this chapter.

c. *Arching.* Structure/medium interaction in buried structures is affected by arching in the following ways:

(1) If the stiffnesses of the structure and surrounding medium are identical, then both the structure and the medium will deform the same amount. No arching stress will develop.

(2) If the structure is more compressible than the surrounding soil or rock medium, then the structure will deform more than the surrounding medium. This will cause shear stresses to mobilize within the medium along the planes of relative displacement. The shear stresses will act in a direction to reduce the stress in the vicinity of the structure to a level

below that of the free-field stress. The phenomenon of reduction in applied stress due to the flexibility of the structure is termed "active arching."

(3) If the stiffness of the buried structure exceeds that of the surrounding medium, the medium will deform more than the buried structure. The mobilized shear stresses in the soil now act in a direction that increases the stress in the vicinity of the structure to a level above that in the free field. The phenomenon of increased pressures applied by the medium to the structure because of the relative rigidity of the structure is termed "passive arching."

(4) If the ratio of the rise time of the free-field pressure pulse, t_r , to the characteristic period of the structure/medium system, T , is very small, then the structure will not have time to deform prior to application of the full free-field pressure, and a reduction in applied loads due to active arching will not occur. If, on the other hand, this ratio is large, then the structure will experience reduced loadings. This indicates that arching effects are most important

when the applied loadings approach a static condition; if dynamic loading effects are important, then active arching of the structure/medium system will be reduced.

(5) The amount of arching that occurs is a function of the amount of displacement of the part of the structure on which the pressure acts.

(6) For arching in cohesive soils the following guidelines, based on experimental data, are given:

- Active and passive arching can be developed in a cohesive soil.
- Structure behavior is governed principally by its stiffness relative to the stiffness of the soil. The limiting load on the structure is, however, sometimes governed by the bearing capacity of the soil beneath the structure.
- Most of the arching action takes place within one diameter above the structure.
- For structure stiffnesses greater than that of the soil, the stiffness of the soil beneath the structure dominates the behavior.
- The amount of active arching decreases when creep occurs; however, cohesive soils appear capable of sustaining arching for long periods of time.

d. Effects of backpacking. A concept for reducing the transmission of shock loadings to buried protective structures is the encasement of the structure in a crushable energy-absorbing material. Typical backpacking materials have been discussed in paragraph 5-6. The effects of backpacking on the response of protective structures may be summarized as follows:

- The pressure transmitted to the structure is dependent on the yield stress of the backpacking material.
- Both velocities and accelerations of the structure are attenuated.
- Backpacking does not offer particular advantages in controlling the peak structure displacements.

e. Effect of moisture. A completely saturated soil will propagate stresses with little attenuation. See paragraph 5-10d for the effect of pore pressures on soil properties.

f. Effect of relative motions. The finite transit time of the load along the structure will cause motions relative to the soil. The structure will experience distortions due to unsymmetrical or nonuniform loading during the transit time of the airblast.

(1) Figure 11-4a shows shear forces developing along the soil/structure interface as the wave front moves parallel to the longitudinal axis of a structure (pipe, cable, tunnel). Axial forces in the structure are obtained by a summation of the shear stresses.

(2) Figure 11-4b shows how relative vertical motions can develop in a structure. At point A on the structure the stress wave in the soil has progressed

to a point below the structure; for all points on the structure to the right of B the stress wave has not reached the structure. Point A tends to deflect downward an amount compatible with the strain induced in the soil below the structure. At time t , the deflection at B is zero. If the structure is flexible, it will deflect with the surrounding medium. It must, however, possess sufficient strength to resist the loads associated with this relative motion.

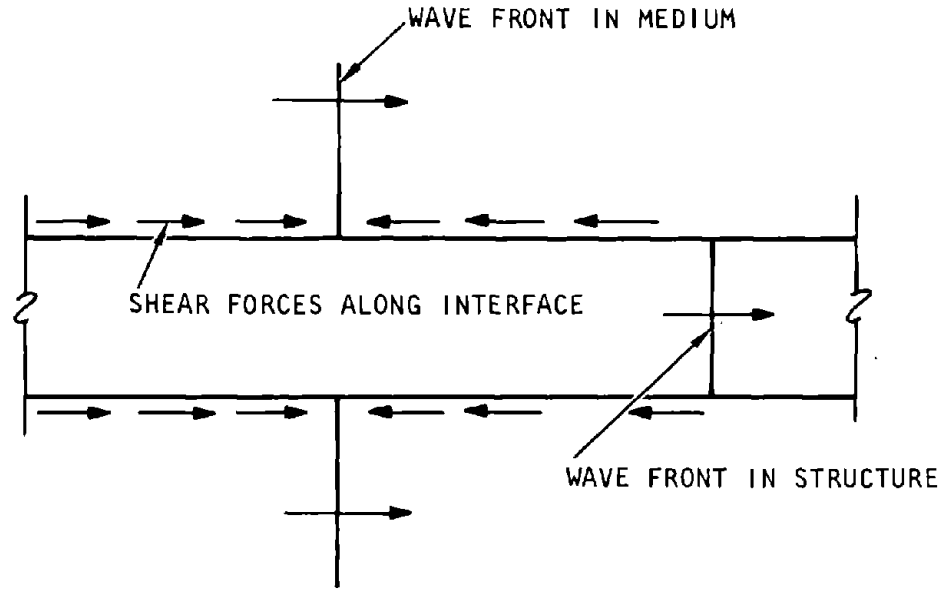
g. Effect of dynamic loads. The pressure transmitted to the structure is influenced by the ratio of soil depth to structure width and the relative stiffness of soil and structure, as in the case of static loading. In general, however, the pressure reaching the structure is higher for dynamic loading than for a static loading of the same overpressure. When the overpressure is applied slowly, the soil is compacted and the relative density increases, resulting in more arching action. During dynamic loading, the relative density will not increase as much as in the static case; hence more pressure will be transmitted to the structure.

(1) A blast pressure with a very sharp rise time will reach the structure without any arching through the soil because arching is initiated as a result of the deformation of the structure. The peak load will arrive at the structure before the structure has had an opportunity to deform. If the rise time is slow, the structure begins to deform as it is loaded and arching in the soil above takes place. Arching estimated by static analysis must therefore be reduced for dynamic effects.

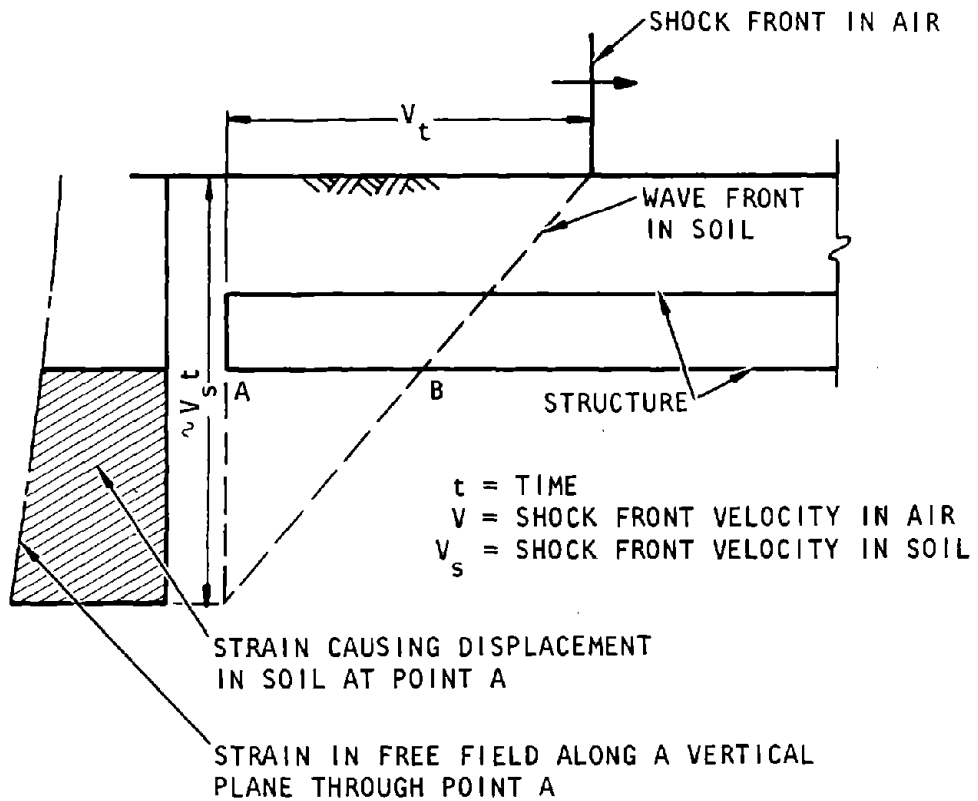
(2) If the ratio of rise time to the structure's natural period is equal to or larger than unity, arching effects may be taken approximately equal to those obtained for the static case. No arching should be assumed, for design purposes, if this ratio is equal to or less than 0.20. For intermediate values, a linear interpolation may be used.

11-4. Loads on earth-mounded structures

a. Effect of earth mounding. Aboveground or partially buried structures may be earth mounded to reduce the effect of antisymmetrical loading of the structure as the blast wave transits the structure. The effect of the forces reaching the structure is reduced because (a) the drag pressures are attenuated due to the streamlining effect of the earth mound, and (b) the shear resistance of the surrounding soil mass provides partial resistance to the surface blast pressures. Figure 11-5 shows the reflected and drag pressures as a function of the angle that the earth mound makes with the ground surface. The figure shows the pressure/time relationship for the windward side. On the leeward side, pressure reflection does not take place; only the side-on overpressure, corresponding to $\alpha = 0$ deg, reduced by the drag pressure, is present.



(a) Effect of relative motion between soil and structure



(b) Conditions producing lateral motion of medium relative to structure axis

Figure 11-4. Effects of Shock Wave Propagating along Longitudinal Axis of Structure (Merritt-Neumark, 1964)

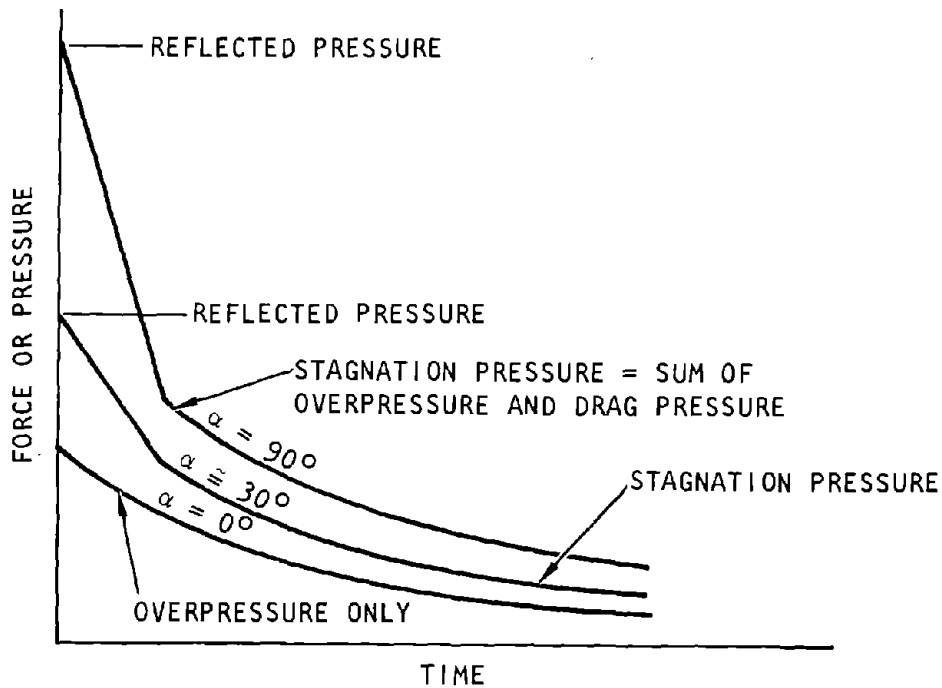
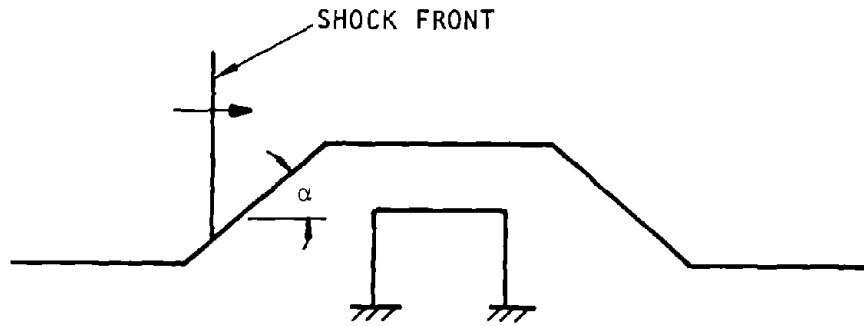


Figure 11-5. Pressures Acting on Windward Face of Soil Mounded over a Structure (Merritt-Newmark, 1964)

b. *Configurations.* Recommended earth cover configurations are shown in figure 11-6. In Region A, the maximum slope permitted is 1 to 2; elsewhere no limitations apply except that cover must be no less than minimum shown. The minimum is to stabilize the structure and reduce reflections while additional cover in Region A is not required for structural purposes but may be needed for radiation protection. For design purposes, the effect of unsymmetrical loading may be neglected if the recommended proportions are maintained. Numerical methods of soil/structure interaction must be used to determine the forces acting on the mounded structure if less than the recommended minimum cover is used. As an approximation, however, a linear interpolation may be made between the forces acting on the completely exposed and fully buried structures (Merritt-Newmark, 1964).

11-5. Loads on silos and vertical shafts

a. *Stresses in vertical cylinder during passage of airblast.* Airblast overpressures propagating on the ground surface induce ground shock that deforms a vertical shaft or silo radially in compressive and flexural modes, and laterally as a vertical cantilever (fig. 11-7). A general expression may be written (Costantino et al., 1964):

$$\sigma_r = \sigma_o + k(w_o - w) + c(\dot{w}_o - \dot{w}) \tag{11-2}$$

where

- σ_r = Radial stress applied to cylinder, a function of the circumferential angle θ and depth z.
- θ = Circumferential angle of cylinder

- σ_o = Free-field radial stress that would act on the vertical cylinder if it deformed with the free field
- k = Factor of proportionality relating relative radial displacement to load (foundation modulus)
- w_o = Free-field radial displacement
- w = Radial displacement of cylinder
- c = Factor of proportionality relating relative radial velocity to load (damping coefficient)
- \dot{w}_o = Free-field radial velocity
- \dot{w} = Radial velocity of cylinder

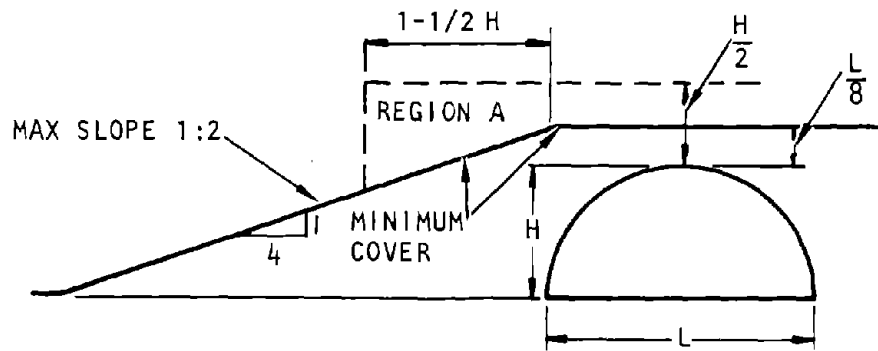
Note that σ_r is not constant around the cylinder because it includes compressional and flexural modes of stress. Solutions to equation 11-2 depend on the definition of w , k , and c . At a given depth, it is of the form

$$\sigma_r = \sum_{n=0}^N \sigma_n \cos n\theta$$

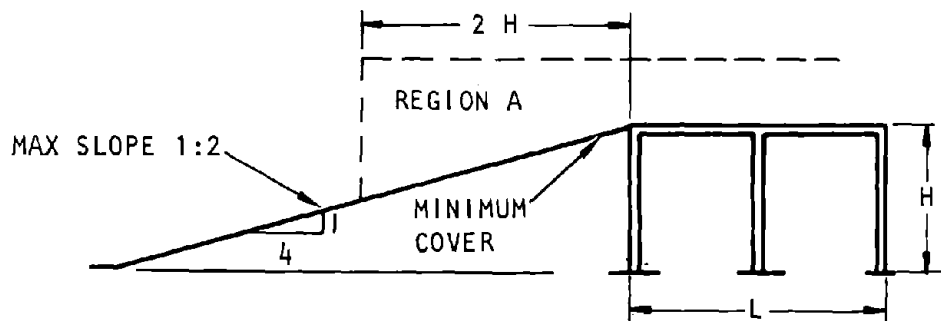
where N represents the total number of response modes. The force acting on the vertical cylinder can be determined by a computer solution, accounting for time variations at discrete locations along the vertical cylinder.

(1) The cantilever deformation effect may be separately considered by assuming the vertical cylinder to be rigid. For this case w may be replaced by the centerline displacement of the vertical cylinder. The force-per-unit length of the vertical cylinder will then depend on the relative displacements and velocities in the direction of the airblast propagation.

(2) Numerical solutions may be obtained as an extension of the "discrete interactors" method described in paragraph 11-3b(2). Values must be assigned to k and c and the displacement and velocity functions must be defined from ground-shock-propagation theory. Solutions for some special cases are discussed by Costantino et al. (1964). However, because of its complexity, this method should be used for design verification and simpler methods must be used for preliminary design.



(a) Arch or dome



(b) Rectangular structure

Figure 11-6. Minimum Cover for Fully-Buried Condition (Merritt-Newmark, 1964)

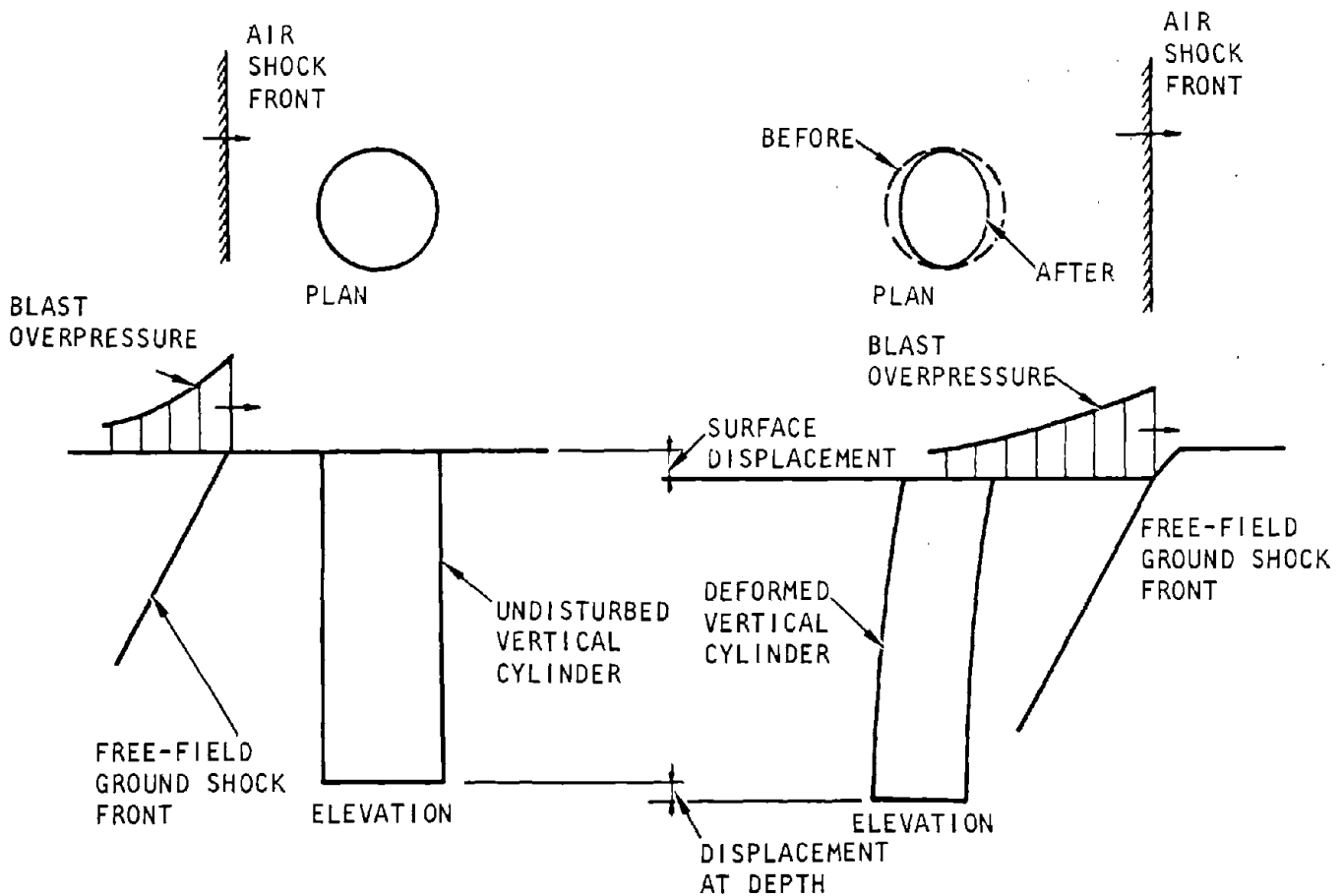


Figure 11-7. Deformation of a Vertical Cylinder (Costantino et al., 1964)

(b) *Horizontal static pressures.* Figure 11-8 shows the horizontal dead load pressure on a vertical shaft or silo as a function of depth. The pressure curve is given by

$$\frac{P_z}{P_\infty} = \frac{z/R}{z/R + 2.5} \quad (11-3)$$

where P_z is the pressure at depth z , P_∞ is the pressure at infinite depth, and R is the structure radius. For practical purposes the pressure P_z may be taken equal to P_∞ at z/R ratios in excess of 20. P_∞ is a function of the angle of friction of the soil, the soil density, and the silo radius, and it is given by the curve of figure 11-9 (not to be used for $\phi < 25$ deg). Hydrostatic pressures must be added to the value of P_z at depths below the water table. Airblast pressure loads must be superimposed on the dead load from lateral soil pressures. For preliminary design, an equivalent static pressure may be assumed, and the soil may be considered an elastic medium. The horizontal pressure due to the airblast on a relatively rigid vertical cylinder will be

$$P_{ax} = \frac{\nu P_{az}}{1 - \nu} \quad (11-4)$$

where

- ν = Poisson's ratio of medium
- P_{az} = Vertical component of airblast pressure at depth z

The reduction of lateral pressure due to the flexibility of the vertical cylinder is accounted for by the reduction factor $\frac{N}{N+1}$. The reduced lateral pressure P_r on a flexible vertical cylinder due to airblast is then:

$$P_r = \frac{NP_{ax}}{N+1} = \frac{N\nu P_{az}}{(N+1)(1-\nu)} \quad (11-5)$$

where

- $N = \left(1 + \nu\right) \frac{E_\ell W_\ell}{E_s R}$
- E_ℓ, E_s = Moduli of elasticity of vertical cylindrical structure and surrounding soil
- W_ℓ = Cylinder thickness
- R = Silo or shaft radius

The total radial pressure P_H on the vertical cylinder is the sum of the radial pressures P_z and P_r , where P_r is the airblast-induced radial pressure, reduced by structure flexibility.

$$P_H = P_z + P_r = \frac{P_\infty z/R}{z/R + 2.5} + \frac{NP_{ax}}{N + 1} \quad (11-6)$$

Note that the airblast pressures, P_{az} and P_{ax} , attenuate as a function of depth. Attenuation estimates may be made from wave propagation theory. For large-yield weapons and for structures at shallow depth, this attenuation may be neglected during preliminary design.

c. *Nonuniformity of circumferential pressure.* An equivalent static load may be assumed for

preliminary design purposes. The deformation of a vertical shaft or silo near the ground surface may be defined simply by a compressive and a flexural mode. The compressive stresses are obtained from the lateral pressure P_H . The circumferential flexure in the structure may be approximately defined by assuming it to be oval in a sinusoidal shape. The equation for the moment due to a sinusoidal unbalanced load distribution is

$$M = 1/3 P_e R^3$$

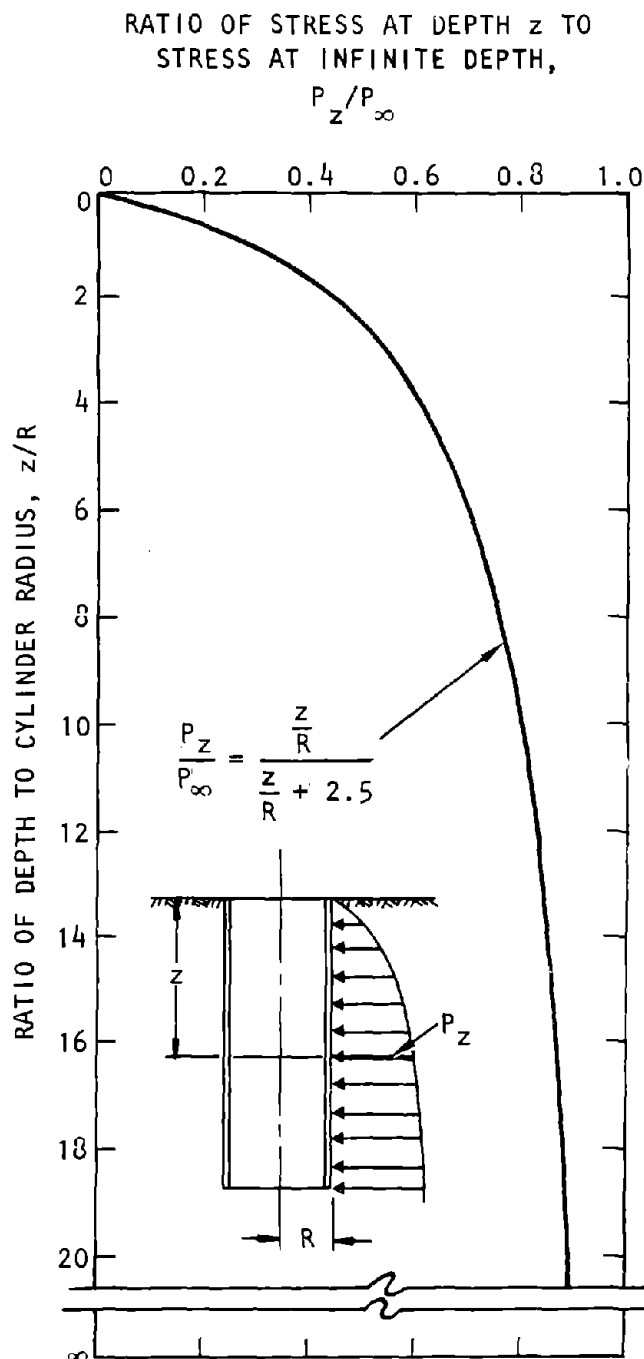


Figure 11-8. Horizontal Static Stress Distribution against Vertical Cylinder (Merritt-Newmark, 1964)

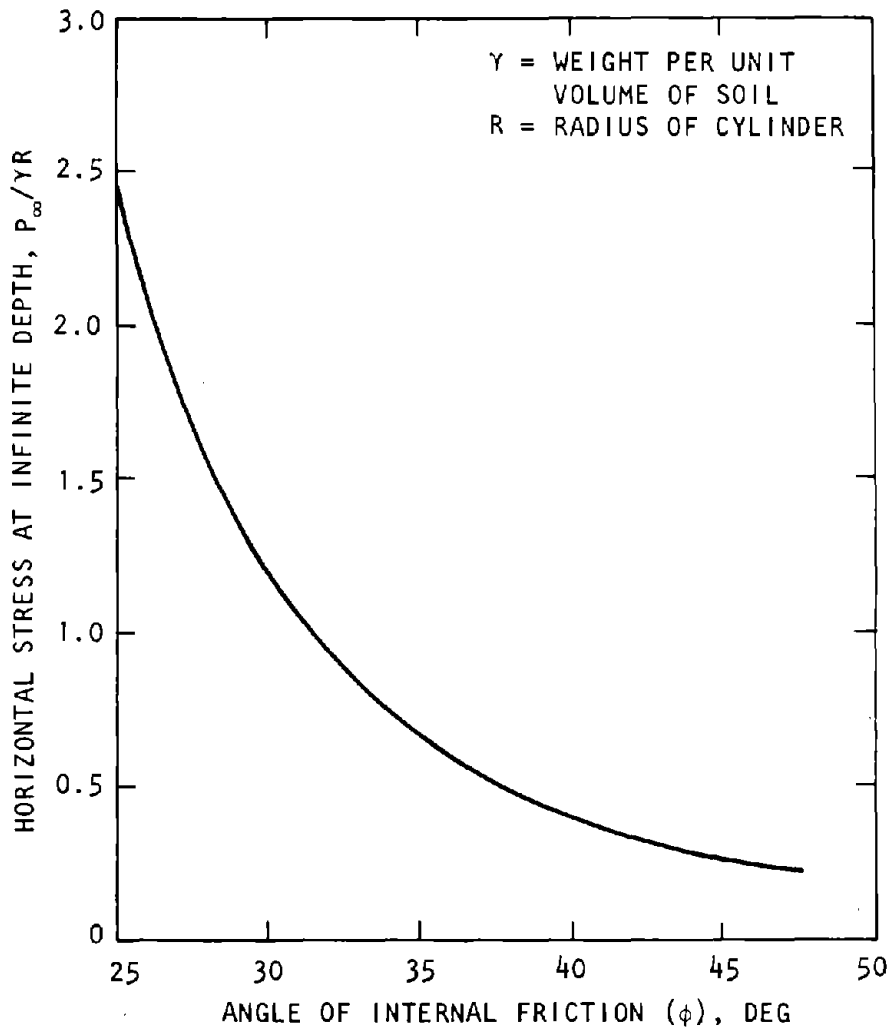


Figure 11-9. Magnitude of Horizontal Static Stress on Cylinder at Infinite Depth (Merritt-Newmark, 1964)

where

P_e = Amplitude of the unbalanced loading, taken at about 10% of the lateral force P_H , disregarding the hydrostatic pressure

d. *Downdrag forces.* Frictional forces at the interface of the vertical cylinder and the soil resist relative vertical motions due to different stiffnesses of structure and medium. These are sometimes called "downdrag" forces. For design purposes, allowance may be made for the disturbance of the soil near the vertical cylinder by assuming the angle of friction is 5 deg less than the in situ soil. The downdrag forces may be expressed as

$$P_v = P_H \tan (\phi - 5) \leq \tau_m \quad (11-7)$$

where

ϕ = Angle of internal friction of the soil
 τ_m = Shearing strength of the disturbed soil near the vertical cylinder

For silos, it is important to determine the direction of relative motion. The following is recommended for preliminary design (Merritt-Newmark, 1964):

- Assume reversal of shear force direction at about mid-depth.
- The summation of shear forces to the point of shear reversal is taken as the maximum downdrag force.
- Add these downdrag forces to airblast forces applied directly to the roof of the silo to obtain maximum vertical forces.

e. *Nonlinear effects of multilayered soil.* Numerical procedures using nonlinear soil properties are needed for vertical cylinders in stratified soil. The example of a silo in the soil profile of figure 11-1 is shown in figure 11-10 (Lee-Agabian, 1976). The entire structure is embedded in the soil with a closure flush with the ground surface. An airblast overpressure applied on the roof and surrounding soil will cause relative motions between the vertical structure and the soil. Using a finite-element axisymmetric representation

of the soil/structure system, the equations of motion at the nodal point masses are given by

$$M\ddot{u}_t + K_{t-\Delta t}du_t = P_t - F_{t-\Delta t} \quad (11-8)$$

where

- M = Nodal point masses
- \ddot{u}_t = Nodal point accelerations at time t
- $K_{t-\Delta t}$ = Stiffness at time t-Δt

- du_t = Generalized incremental displacements between time t - Δt and t
- $F_{t-\Delta t}$ = Internal resisting forces at time t - Δt
- P_t = External loads at time t

A step-by-step integration of these equations will give the deformations of the vertical structure, the in situ

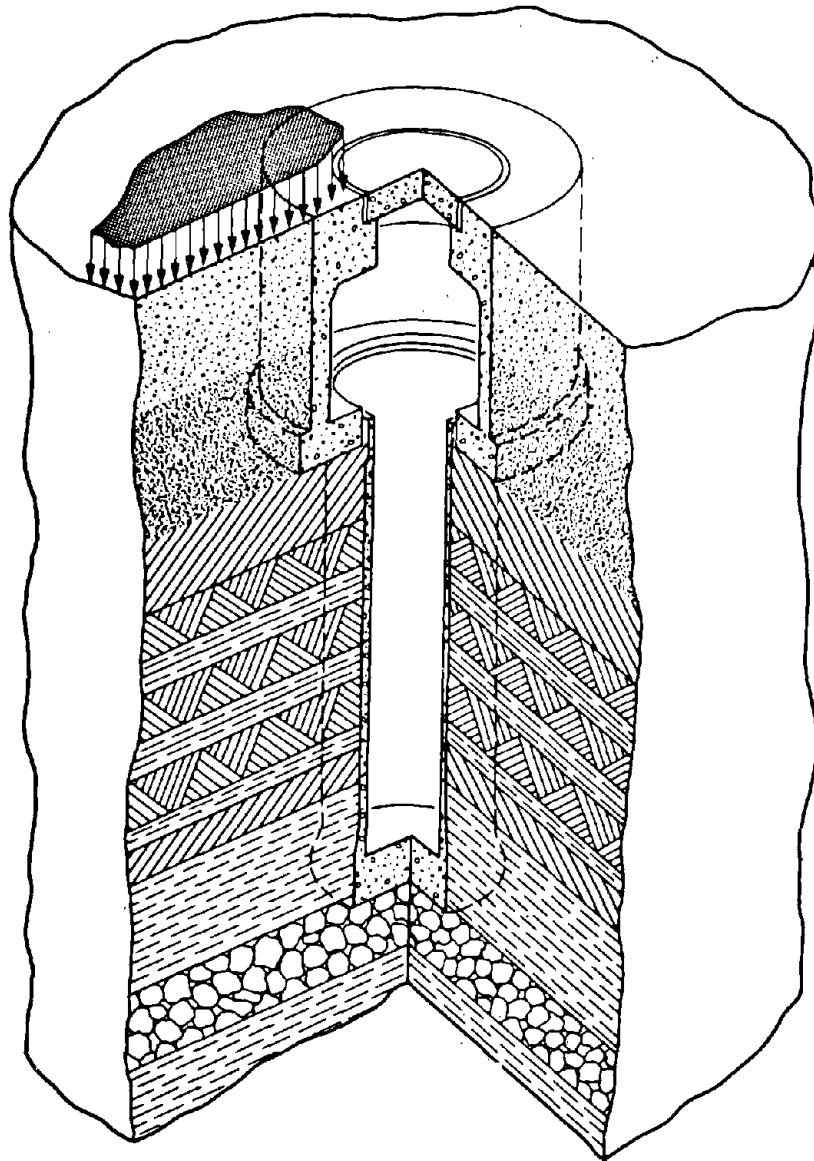


Figure 11-10. Site of Underground Reinforced-Concrete Structure Subjected to Overhead Blast Loading (Lee-Agabian, 1976)

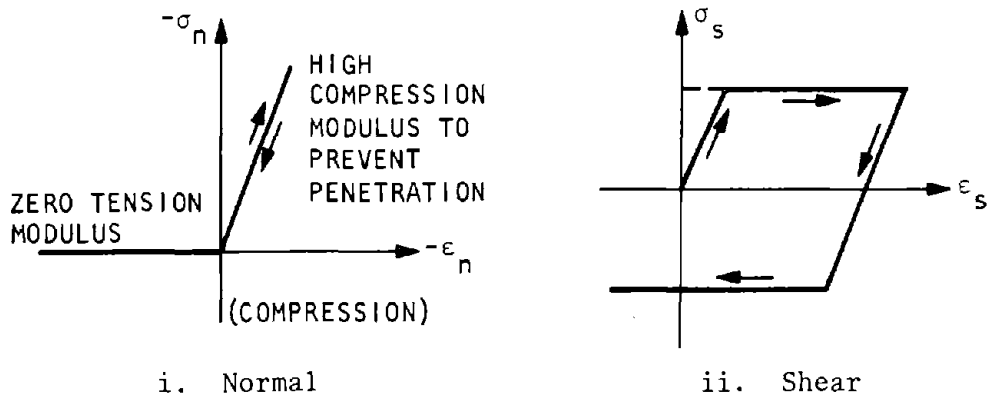
soil, and the backfill at various times during the application of the airblast. The elements representing the soil near the structure should have properties limiting the downdrag forces to the shear resistance. In figure 11-11 simplified nonlinear properties for interface slip elements are shown. This type of analysis of dynamic response is necessary to verify the preliminary design. An iteration procedure is followed if design modifications are made. Because of the availability of such refined verification procedures, the methods used in preliminary design may be kept quite simple.

11-6. Loads on shallow-buried structures

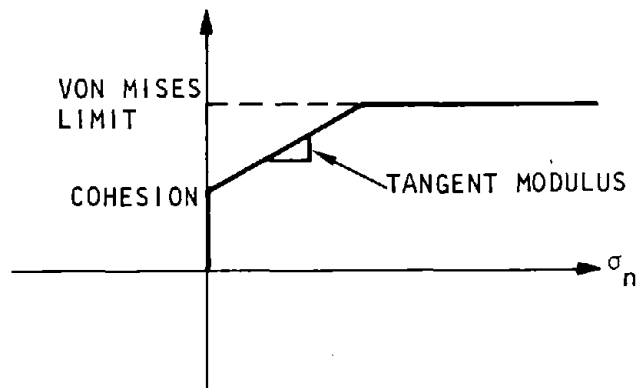
a. *Rectangular or box structures.* Failure of the soil/structure system takes place when the roof of the structure fails as a result of a downward movement of the mass of soil directly above the structure.

b. *Static loads.* Figure 11-12 shows the deflection of a slab and the forces acting on it and on the soil prism above (Allgood, 1964). The free-body diagram gives the relationship:

$$(P - P_S) W + \gamma DW = 2\tau_f D \tag{11-9}$$



(a) Stress/strain curves for a slip element



(b) Modified Mohr-Coulomb criterion for maximum shear stress in the slip material

Figure 11-11. Simplified Nonlinear Properties (Lee-Agabian, 1976)

where

- P = Surface pressure
- P_S = Average pressure on slab
- γ = Soil density
- W = Width of slab
- D = Depth of soil above the structure
- τ_f = Failure shear stress = C + k_oσ_v
- tan φ
- C = Soil cohesion coefficient
- k_o = Coefficient of lateral pressure at rest
- σ_v = Vertical stress in soil
- φ = Angle of internal friction

Letting σ_v = P for shallow-buried structures gives

$$\frac{P}{W} = \frac{1 - P_S/P}{2k_o \tan \phi + (2C - \gamma W)/P} \quad (11-10)$$

The percent of loading carried by arching is

$$100 \psi_a = 100(P - P_S)/P$$

$$= \frac{100D}{W} \left[2k_o \tan \phi + (2C - \gamma W)/P \right] \quad (11-12)$$

where ψ_a is the fraction of airblast load carried by arching. The slab deflection that corresponds to maximum possible arching for a given D/W is obtained by substituting the stress/strain condition at incipient shear failure τ_f = ε_fG = (δ_f/D)G, where G is the shear modulus of the soil.

$$\delta_f = \frac{W}{2G} \left[P - P_S \right] + \frac{\gamma DW}{2G} \quad (11-13)$$

or

$$\delta_f = \frac{PD}{2G} \left[2k_o \tan \phi + (2C - \gamma W)/P \right] + \frac{\gamma DW}{2G} \quad (11-14)$$

The above expressions apply for D < the depth of cover D_a required for all of the surface load to be carried by arching. D_a is obtained by setting P_S = 0 in equation 11-10:

$$D_a = \frac{W}{2k_o \tan \phi + (2C - \gamma W)/P} \quad (11-15)$$

c. *Dynamic loads.* The soil/structure system in this case (fig. 11-13a) is the same as for the static case except that the inertia forces are included (Van Horn, 1964). The applied surface overpressure (fig. 11-13b) may be approximated by the triangular pulse

$$P_t = P_o(1 - t/t_d) \quad (11-15)$$

as shown in figure 11-13c. Several cases will be considered.

(1) Let t_m be the time when the maximum value of the displacement is reached. This may occur either at 0 ≤ t_m ≤ t_d or at t_m ≥ t_d. The following two equations define the relationship between the peak overpressure and an equivalent uniform static pressure. For the first case when 0 ≤ t_m ≤ t_d,

$$\left(\frac{r}{t_d}\right)^2 = \frac{4}{3} \frac{\Gamma}{\Lambda} \left(1 - \frac{\Lambda}{\Gamma}\right)^3; \quad 1 \leq \frac{\Gamma}{\Lambda} \leq 2 \quad (11-16)$$

For the second case when t_m ≥ t_d,

$$\left(\frac{r}{t_d}\right)^2 = \frac{1}{4} \left(\frac{\Gamma}{\Lambda}\right)^2 - \frac{1}{3} \left(\frac{\Gamma}{\Lambda}\right); \quad 2 \leq \frac{\Gamma}{\Lambda} \quad (11-17)$$

where Γ and Λ are functions of peak overpressure and uniform static pressure, and r is a parameter.

The terms in the above expressions are defined as follows:

- r = $\sqrt{\frac{2Q\delta_m}{R}}$
- Γ = P_O/γL_S
- Λ = P_u/γL_S
- δ_m = Maximum deflection
- P_O = Peak overpressure
- γ = Soil density
- L_S = Length parameter, area divided by semiperimeter
- P_u = Uniform static air pressure

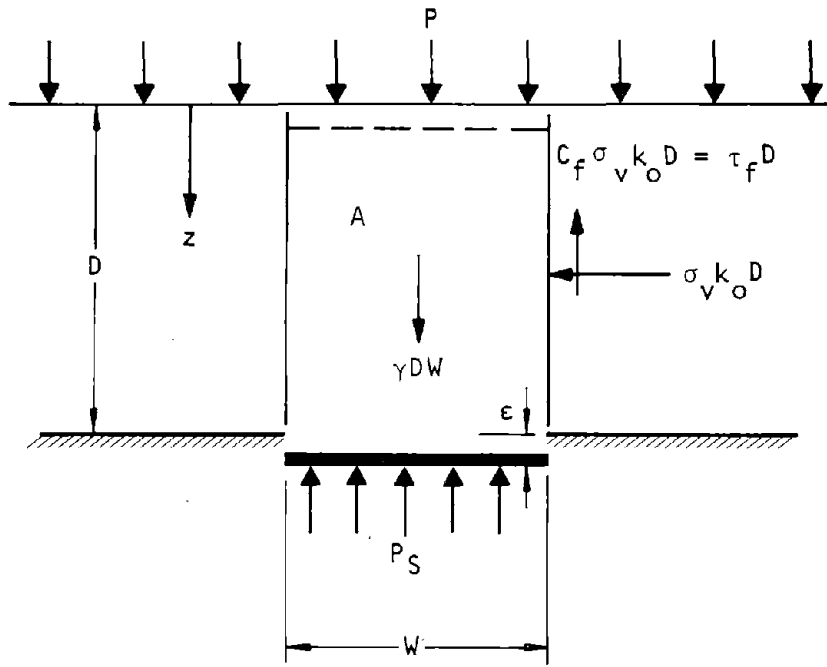
Q is a parameter whose value will be defined later for each case. It is important to note that Γ/Λ is the ratio of the peak overpressure to the static air pressure. The values of Γ, Λ, and Q depend on the configuration of the soil/structure system. They are specifically dependent on the relative motions between the soil prism above the structure and the adjacent soil. Their values for different cases, given in (4) below, are therefore related to the relative motions that are described in the following chapter.

(2) In figure 11-14 the following soil and structure motions are shown:

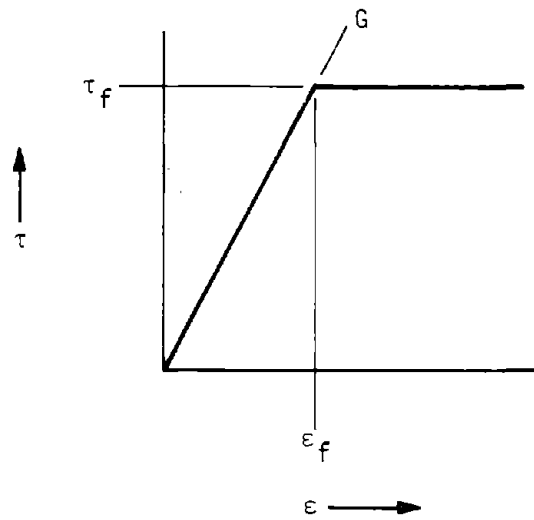
- S_g = Settlement of the natural ground surface adjacent to structure
- S_m = Deformation of the fill material adjacent to the structure
- S_f = Settlement of the base of the structure
- δ_s = Deflection of the top of the structure with respect to the base

The settlement ratio r_s is defined as

$$r_s = \frac{(S_m + S_g) - (S_f + \delta_s)}{S_m} \quad (11-18)$$

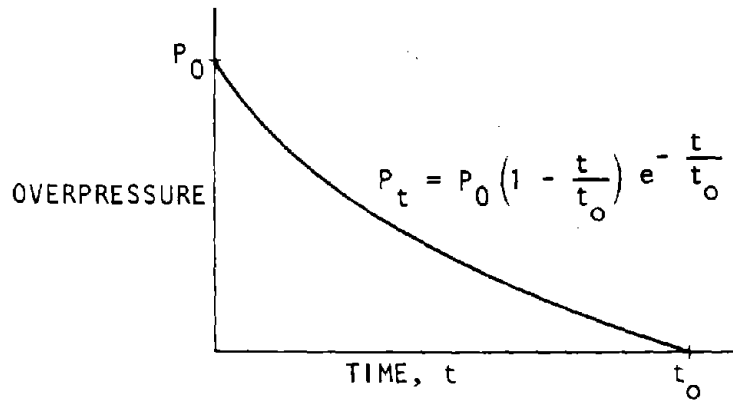


(a) Soil-slab

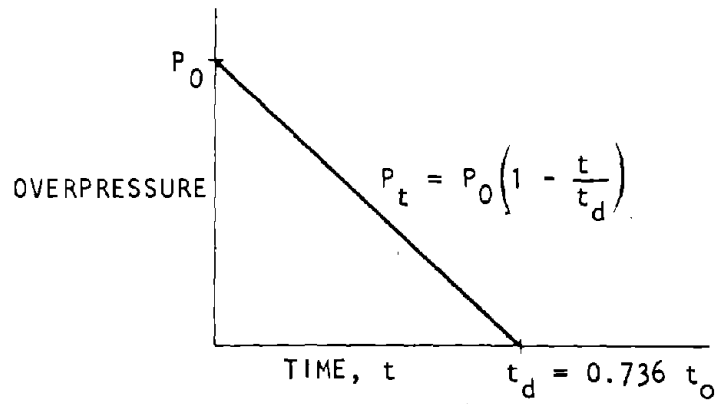


(b) Elastoplastic soil defining τ_f

Figure 11-12. Static Loads on Shallow-Buried Slab (Allgood, 1964)



(a) Actual overpressure-time relationship on ground surface



(b) Assumed overpressure-time relationship on ground surface

Figure 11-13. Dynamic Loads on Shallow-Buried Rectangular Structure (Van Horn, 1964)

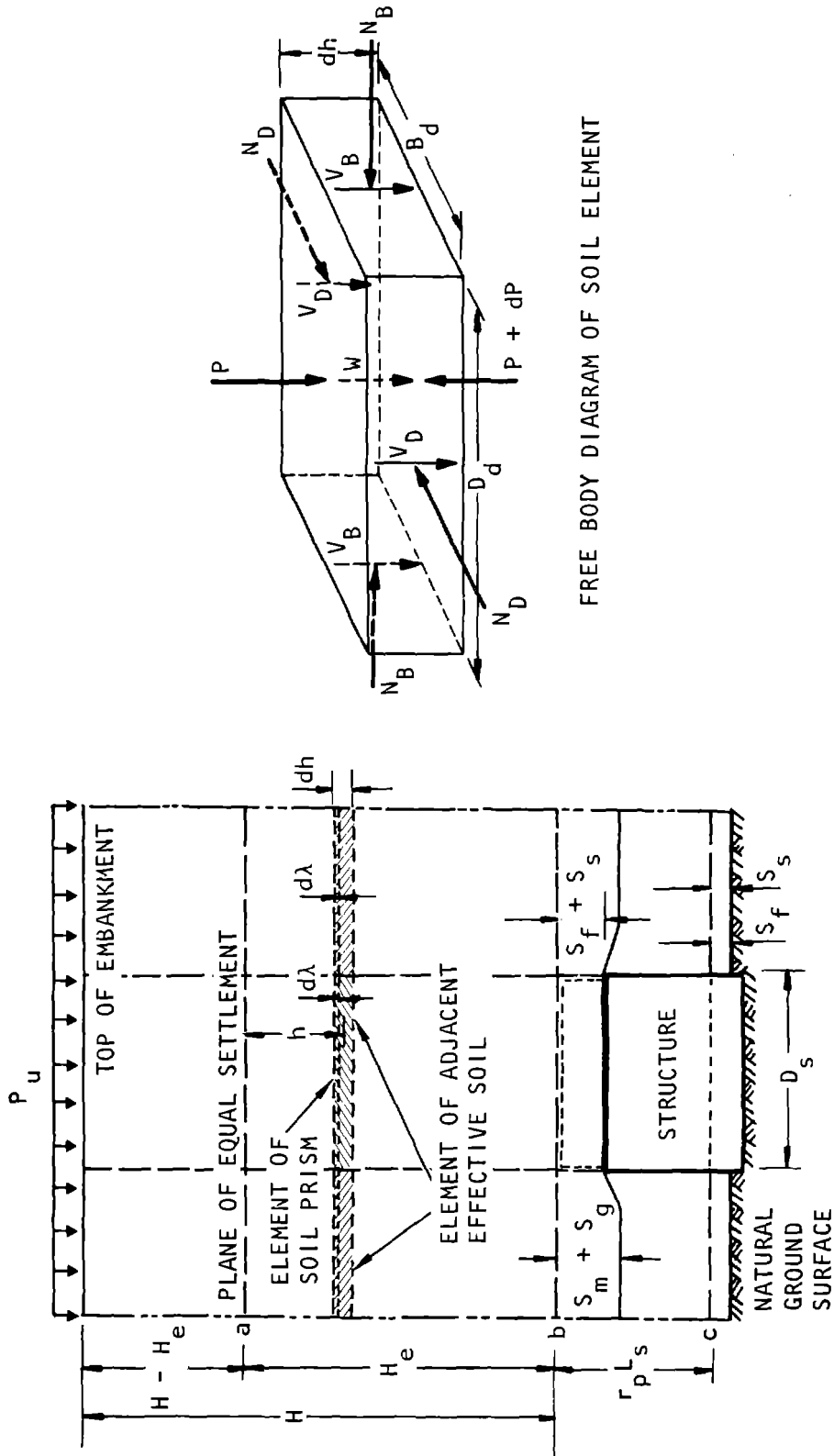


Figure 11-14. Settlements that Affect Loads on Structures (Van Horn, 1964)

For a positive value of r_s , the load on the structure is greater than the weight of the soil prism because shearing forces act downward, below the plane of equal settlement at the vertical interface of the soil prism and the adjacent soil.

(3) The load on the structure is less than the weight of the soil if r_s is negative, the direction of the shearing forces at the interface of prism and adjacent soil being reversed. This behavior of the soil/structure system determines the arching effect of the soil that modifies the load due to blast overpressure. The blast pressure reaching the roof of the structure is strongly influenced by the positive or negative sign of r_s .

(4) Cases of Interest for Shallow-Buried Structures.

Case 1. The value of r_s is negative. Shearing forces on the soil prism above the structure are upward. Arching effect of the soil reduces the pressures on the roof of the structure.

$$\Gamma_1 = \frac{P_0}{\gamma L_s} \tag{11-19}$$

$$\Lambda_1 = \frac{P_S}{\gamma L_s} \left\{ e^{2k_o \tan \phi \frac{D}{L_s}} + \left(\frac{2C}{\gamma L_s} - 1 \right) \left(e^{\frac{2k_o \tan \phi \frac{D}{L_s} - 1}{2k_o \tan \phi}} \right) \right\} \tag{11-20}$$

$$Q_1 = \frac{1}{2g k_o \tan \phi} \left\{ e^{2k_o \tan \phi \frac{D}{L_s} - 1} \right\} \tag{11-21}$$

where terms not previously defined are

- P_S = Vertical pressure in soil prism at top of structure
- k_o = Lateral pressure coefficient
- D = Depth of soil above top of structure
- L_s = $WL/(W+L)$, length parameter, area of structure roof divided by semiperimeter (L is length of structure)
- g = Gravitational acceleration

Case 2. The value of r_s is positive. Shearing forces on the soil prism above the structure are downward. Arching effect of the soil increases pressures on the roof of the structure.

$$\Gamma_2 = \frac{P_0}{\gamma L_s} \tag{11-22}$$

$$\Lambda_2 = \frac{P_S}{\gamma L_s} \left\{ e^{-2k_o \tan \phi \frac{D}{L_s}} + \left(\frac{2C}{\gamma L_s} + 1 \right) \left(e^{\frac{-2k_o \tan \phi \frac{D}{L_s} - 1}{2k_o \tan \phi}} \right) \right\} \tag{11-23}$$

$$Q_2 = -\frac{1}{2g k_o \tan \phi} \left\{ e^{-2k_o \tan \phi \frac{D}{L_s} - 1} \right\} \tag{11-24}$$

Case 3. A trench with vertically cut walls whose width is larger than the width of the structure. In this case r_s is negative but the shear planes are assumed to coincide with the vertical cuts of the trench. Equations 11-19, 11-20, and 11-21 apply except L_s is replaced by L_t , the length parameter for the trench. $L_t = W_t L / (W_t + L)$ where W_t is the width of the trench and, as before, L is the characteristic length of the shallow-buried structure. Other cases include structures that are partially embedded below ground surface and earth mounded. Values for Γ , Λ , and Q for such cases are given by Van Horn (1964).

d. Design by iteration (Van Horn, 1964). In figure 11-15 the relationship of the ratio Γ/Λ to $(r/t_d)^2$ is given. This figure or equations 11-16 and 11-17 may be used when designing by an iterative procedure. These are the steps:

1. Using equations 11-19 or 11-22 and from the known values of P_0 , γ , and L_s , obtain Γ .
2. Assume a value of Γ/Λ and compute R .
3. Determine P_S from equations 11-20 or 11-23 and computed value of Λ .
4. Using P_S as the applied pressure, design the slab and calculate the deflection δ_s of the slab corresponding to P_S .
5. Using values of δ_s , Λ , and Q , obtain $r = \sqrt{2Q\delta_s/\Lambda}$.
6. Using the computed values of r and the given value of t_d , obtain $(r/t_d)^2$ and select the corresponding value of Γ/Λ from equations 11-16 and 11-17 or figure 11-15.
7. Repeat the iteration if the originally assumed value of Γ/Λ and its final value do not agree by starting again with the average of the two values.

The iteration does not require a knowledge of the magnitude of r_s , the relative motion. It is only important to determine whether it has a positive or negative sign in order to obtain the direction of arching, resulting in an increase or decrease of the pressure P_S reaching the structure as compared with the peak surface overpressure P_0 .

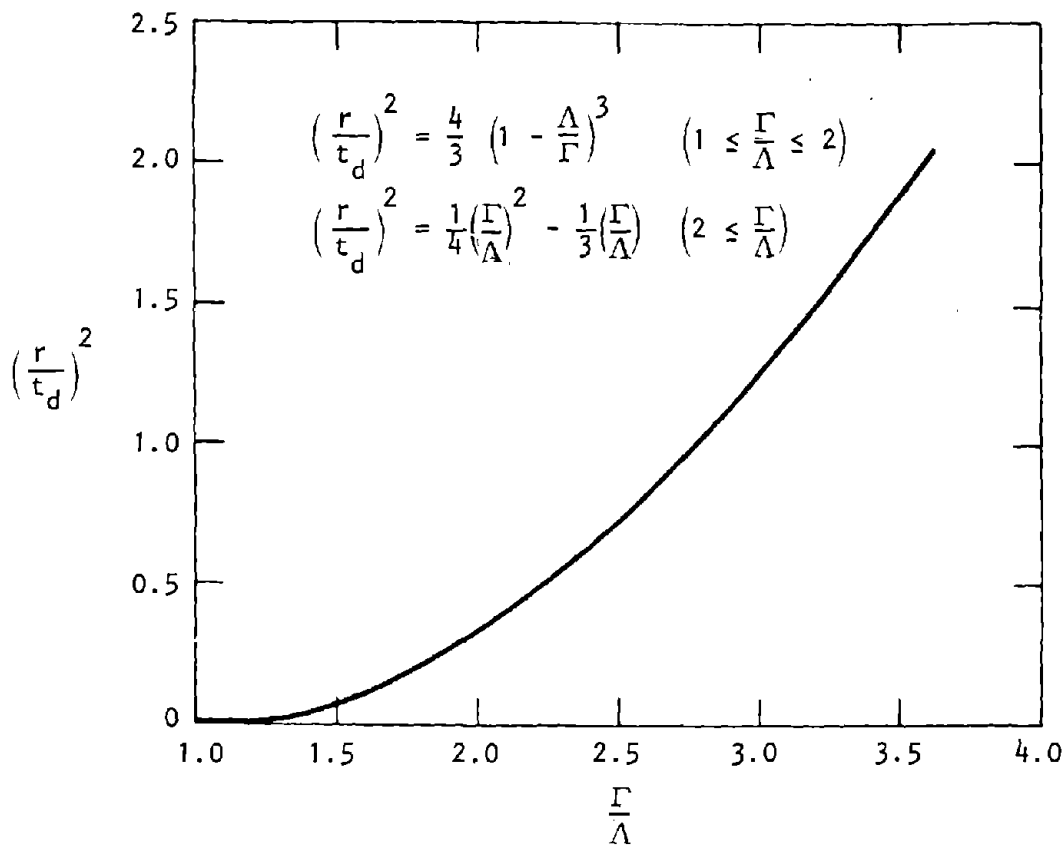


Figure 11-15. Relationship Between $(r/t_d)^2$ and Γ/Λ (Van Horn, 1964)

e. *Static loads on tunnels and conduits.* Applied load, cylinder diameter, and soil modulus govern the deflection of a shallow-buried thin cylinder. For thick cylinders, the effect of the shell stiffness also becomes significant. An equation for deflection, known as the Iowa Formula, is given by Spangler (1960):

$$\delta = k_\delta \frac{k_b P_s R^3}{EI + 0.061 E_s R^3} \quad (11-25)$$

where

- δ = Horizontal or vertical deflection of cylinder, in.
- k_δ = Deflection lag factor
- k_b = Bedding constant (a function of bedding angle α , from fig. 11-16)
- P_s = Vertical load on cylinder per unit length, lb/in.
- R = Cylinder radius, in.
- E = Cylinder modulus of elasticity, psi
- I = Cylinder section moment of inertia, in.⁴/in.
- E_s = Soil modulus of elasticity, psi

The loading assumptions that are the basis for the Iowa Formula are shown in figure 11-16. The normal range of values for the deflection lag factor k_δ suggested for design purposes is from 1.25 to 1.50. The bedding angle α is one-half the angle subtended by the cylinder in contact with the cylinder bedding. The relationship between the bedding constant k_b and bedding angle is as follows (Spangler, 1960);

Bedding Angle, α , deg	0	15	22½	30
	45	60	90	
Bedding Constant, k_b	0.110	0.108	0.105	0.102
	0.096	0.090	0.083	

A value of $E_s = 700$ psi is recommended for design if the sidefill is compacted to 90% or more of Proctor density for two cylinder diameters on each side of the cylinder. The deflection of the structure, δ , will determine the arching effect of the soil above the cylinder. The equations for box structures (eqs. 11-9 and 11-10) may be used to obtain the surface overpressure P corresponding to P_s by replacing D in these equations

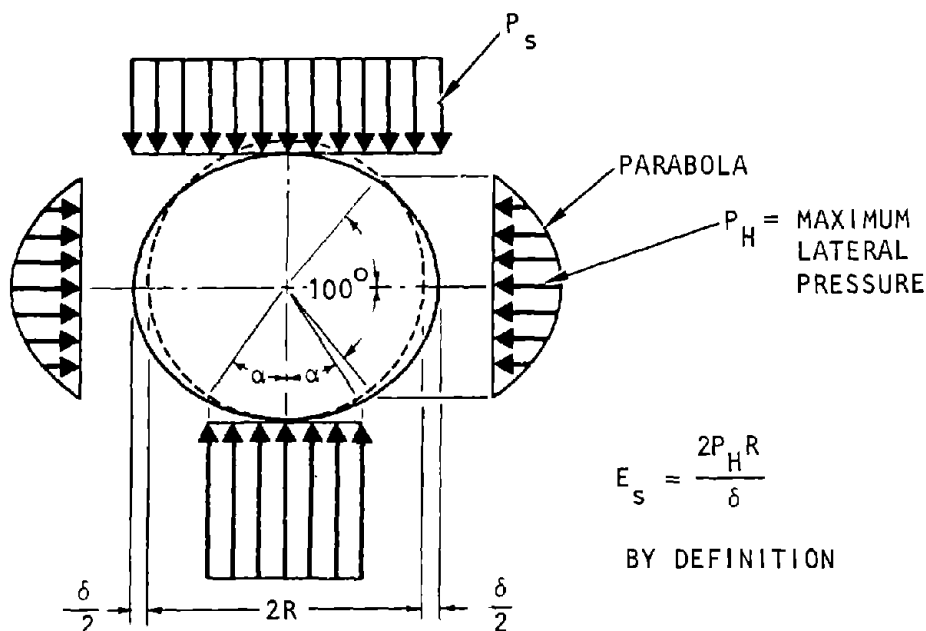


Figure 11-16. Loading Assumptions for Iowa Formula (Spangler, 1960)

with $R + D_o$, where R is cylinder radius and D_o is soil cover above the crown; and by replacing W with $2R$.

f. Dynamic loads on tunnels and conduits. The equations developed for box structures (eqs. 11-15 through 11-24) may also be assumed applicable for cylindrical structures. D in these equations is replaced by $R + D_o$, where D_o is soil cover above the crown; and W is replaced by $2R$.

(1) Buckling of Cylinders. Buckling of a symmetric soil-tube configuration is given by

$$P_c = 2k_a \sqrt{\frac{K_s EI}{R^3}} \tag{11-26}$$

where

- K_s = Modulus of vertical soil reaction
- EI = Stiffness of cylinder wall
- R = Radius of cylinder
- k_a = Arching factor of soil

The modulus of vertical soil reaction K_s depends on the ring geometry and the soil properties. Thus, K_s is affected by the pressure itself and the arching condition in the soil. Approximate results are obtained by setting $k_a = 1.5$ for stiff soil and $k_a = 1.0$ for compressible soil. An approximate value for K_s is

$$K_s = \frac{0.75 E_s [1 - (R_i/R_o)^2]}{(1 + \nu) [1 + (R_i/R_o)^2(1 - 2\nu)]} \tag{11-27}$$

where

- ν = Poisson's ratio for the soil
- E_s = Constrained modulus of the soil
- R_i = Inside radius of the tube
- R_o = Outside radius of equivalent thick soil ring, which may be roughly assumed to be equal to the outside radius of the tube plus the thickness of soil cover above the crown of the tube

(2) Nonsymmetrical Load on Cylinders. The sliding wedge concept of soil failure is shown in figure 11-17. This type of soil deformation takes into account loads from earth-moving equipment during construction. This concept may be applied for preliminary design of shallow-buried cylinders subjected to unsymmetrical static loads. However, very conservative results will be obtained for the transient unsymmetrical airblast loading, as the wave transits the structure. The airblast is not stationary and it takes less time for the airblast to traverse the diameter of the cylinder than for the second wedge to move up in the configuration of the unsymmetrical deformation shown in the figure. Nevertheless, this is a method that may be used for estimating the upper bound of the flexural stresses in a moment-resistant cylindrical structure.

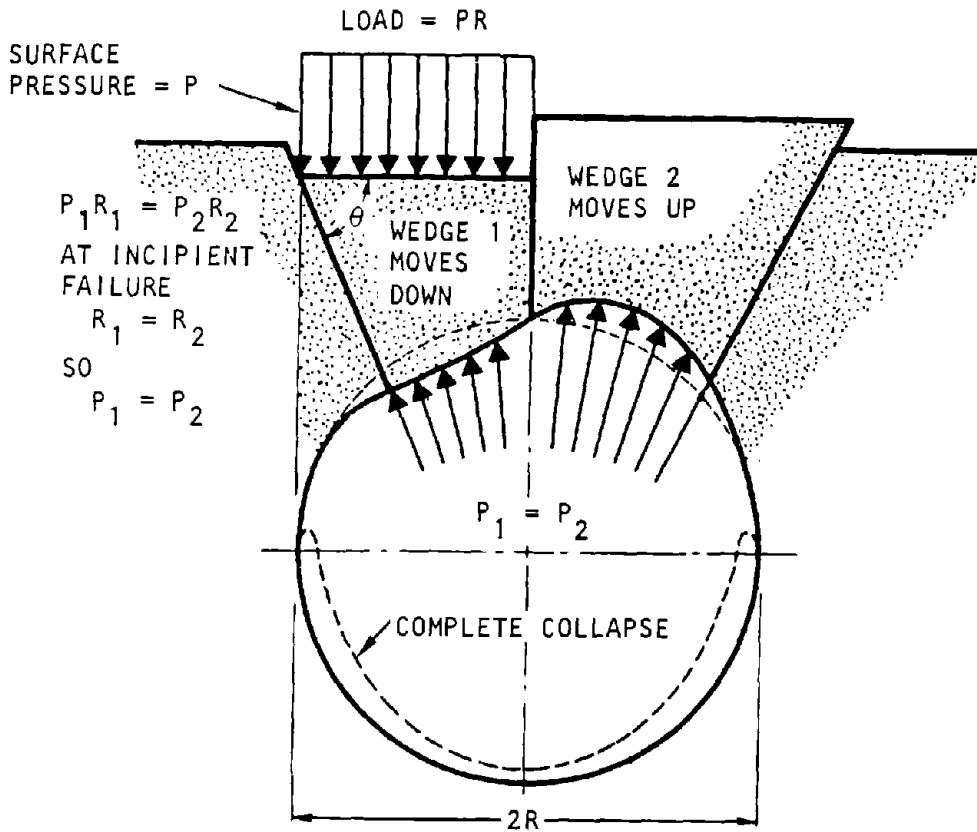


Figure 11-17. Sliding Wedge Theory of Failure of Buried Flexible Conduit Due to Surface Pressure P above Half of Cylindrical Conduit (Watkins, 1964)

g. Arches and domes. The “arching” or relief of pressure due to the deformation of an arch or a dome is less than in flat roofed structures because of the greater stiffness an arch or dome structure has as compared with a slab. Note that relief of pressure will also occur if the structure moves as a rigid body due to footing settlements resulting from high-bearing pressures or when the footing pushes the soil into the enclosed space within the structure. Calculation procedures for arching effects are similar to the method used for tunnels and conduits, once the structure settlement is determined.

11-7. Design of shallow-buried structures

a. Design requirements. The attenuated pressures obtained at the level of the buried structural element are applied as dynamic loads, and the design of the element is carried out by an iteration procedure, since dynamic arching is strongly dependent on the deflection of the structure. Primary effects to consider are:

- Flexure and shear in roofs of rectangular structures

- Combined direct stress, flexure, and shear in walls of rectangular structures
- Direct stress in interior walls and columns of rectangular structures
- Direct stress and flexure in shells of arches and domes
- Direct stress and flexure in vertical cylindrical structures

b. Design methods for rectangular structures. The design of roof walls and interior walls and columns of rectangular structures is carried out by relating their resisting capacities to limiting ductility factors and using the methods of chapter 8.

c. Design methods for tube, arch, and dome structures. Tube, arch, and dome structures require the determination of reaction forces that are more complex than for walls and slabs of rectangular structures. Tubes that are short relative to their diameter (i.e., its length is less than five times its diameter) should include the effect of the end walls on the overall stiffness of the structure (chap. 10). Arches or

cylindrical structures, such as tunnels, may be designed by considering the transverse section in a soil medium under plane strain. Dome structures may be designed by selecting a thickness equal to one-half that of an arch. Two methods of designing these structures are described below.

(1) Method 1. An approximate procedure for preliminary design is as follows:

- a. Assume potential active and passive failure planes of the soil.
- b. Apply the overpressure on the soil above the structure treating the soil within the planes of failure and the structure as a free-body diagram.
- c. Estimate arching effects in the soil from the guidelines of paragraph 11-3.
- d. Design the structure for compressive and flexural forces applying overpressures reduced by the arching action.

Equivalent loads based on simple distributions along the arc of an arch are shown in figure 11-18. The first component is a uniform compressive force. The second is a flexural component. The flexural component is greatly diminished after the airblast front passes over the arch. For design purposes the maximum value of this latter loading may be assumed to be one-half the total compressive pressure, P_n . This condition corresponds to the case when the blast is passing the crown of the arch. These two conditions are assumed for design:

- The arch is fully loaded with a uniform pressure P_n after the blast front passes the structure (fig. 11-18a).
- The arch is loaded with a uniform pressure of $1/2 P_n$ plus the unsymmetrical pressure of $1/2 P_n$ when the blast load passes the crown of the arch (fig. 11-18b).

Expressions for these cases are as follows (COE, 1960b):

Compression Mode Loading (Two-Hinged Arch)

$$\begin{aligned} V_a &= V_b = P_n R \sin k_a \\ H_a &= H_b = P_n R \cos k_a \\ T &= P_n R \\ \beta &= \text{One-half the central angle of the arch} \end{aligned} \tag{11-28}$$

where V_a, V_b , are vertical reactions at the hinges, H_a and H_b are the horizontal reactions, T is the thrust, and P_n is the radial pressure.

Deflection Mode Loading (Two-Hinged Arch)

$$V_a = V_b = \frac{P_n R}{\sin \beta} \left[\sin \frac{\beta}{2} \sin \frac{3}{2} \beta - \sin^2 \frac{\beta}{2} \right]$$

$$H_a = H_b = P_n R [1 - \cos \beta]$$

$$\begin{aligned} M_\theta &= V_a \left\{ R \left(\sin \beta - \left[\sin \beta - \theta \right] \right) \right\} \\ &+ H_a \left\{ R (\cos [\beta - \theta]) \right. \\ &\left. - \cos \beta \right\} - P_n (2R^2) \sin^2 \frac{\theta}{2} \end{aligned}$$

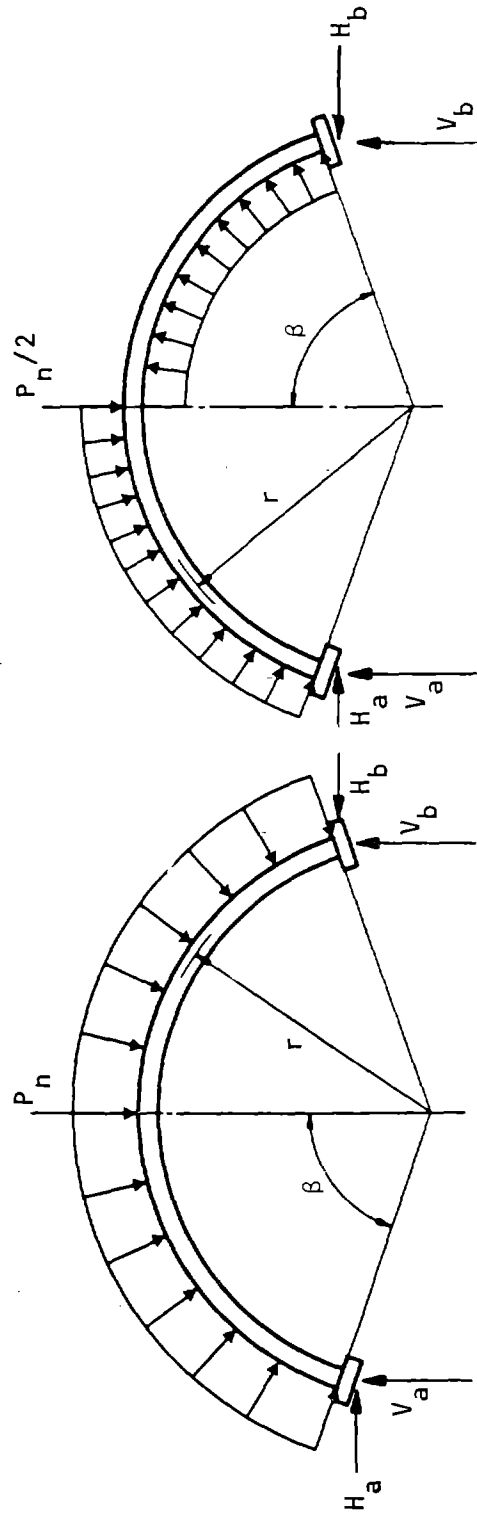
$$\begin{aligned} S_\theta &= V_a \cos (\beta - \theta) + H_a \sin (\beta - \theta) \\ &- P_n (2R) \sin \frac{\theta}{2} \cos \frac{\theta}{2} \end{aligned} \tag{11-29}$$

where

- M_θ = Bending moment at any point on the arch defined by the central angles, θ , to the nearest support
- S_θ = Shear at the same point as M_θ

Equations for end conditions other than hinged are obtained from the laws of statics together with the appropriate compatibility conditions.

(2) Method 2. For this method it is assumed that the vertical component of loading is equal to the static overpressure applied directly over the structure, after including the effect of arching. The horizontal load component is $K P_o$, where K is a fraction of the vertical load P_o . In the limiting case when $K = 1$, the loading is hydrostatic. Tests have shown that K is not a constant during the application of the blast load (Flathau-Meyer, 1966). As bending of the arch occurs the arch deflects outward and the resistance of the soil forces the arch into the compression mode. An average value for K should be selected based on the flexibility of the structure and the soil characteristics. The least conservative value is $K = 1$, because under hydrostatic pressures, the structure is under uniform compression. Figure 11-19, 11-20, and 11-21 give values of thrust, shear, and moment for a two-hinged arch and various values of K (Flathau et al., 1962). The overpressure P_o is the value of the airblast pressure that reaches the arch at the level of its crown. The effect of the soil cover must be added as an additional surcharge. It is noted that, as explained in paragraph 11-3g, the arching effect is minimal for a short duration load, whereas static loads (dead loads of soil cover) will induce a stronger arching in the soil. These differences must be taken into account when combining the effect of soil dead load and overpressure. For arches whose soil cover is equal to or less than one-half the radius of the arch, the arching effect may be neglected and the pressures resulting from soil dead load may be assumed to be as shown



(a) Uniform compression loading

(b) Flexural loading

U.S. Army Corps of Engineers

Figure 11-18. Simple Equivalent Loads for Arch Design

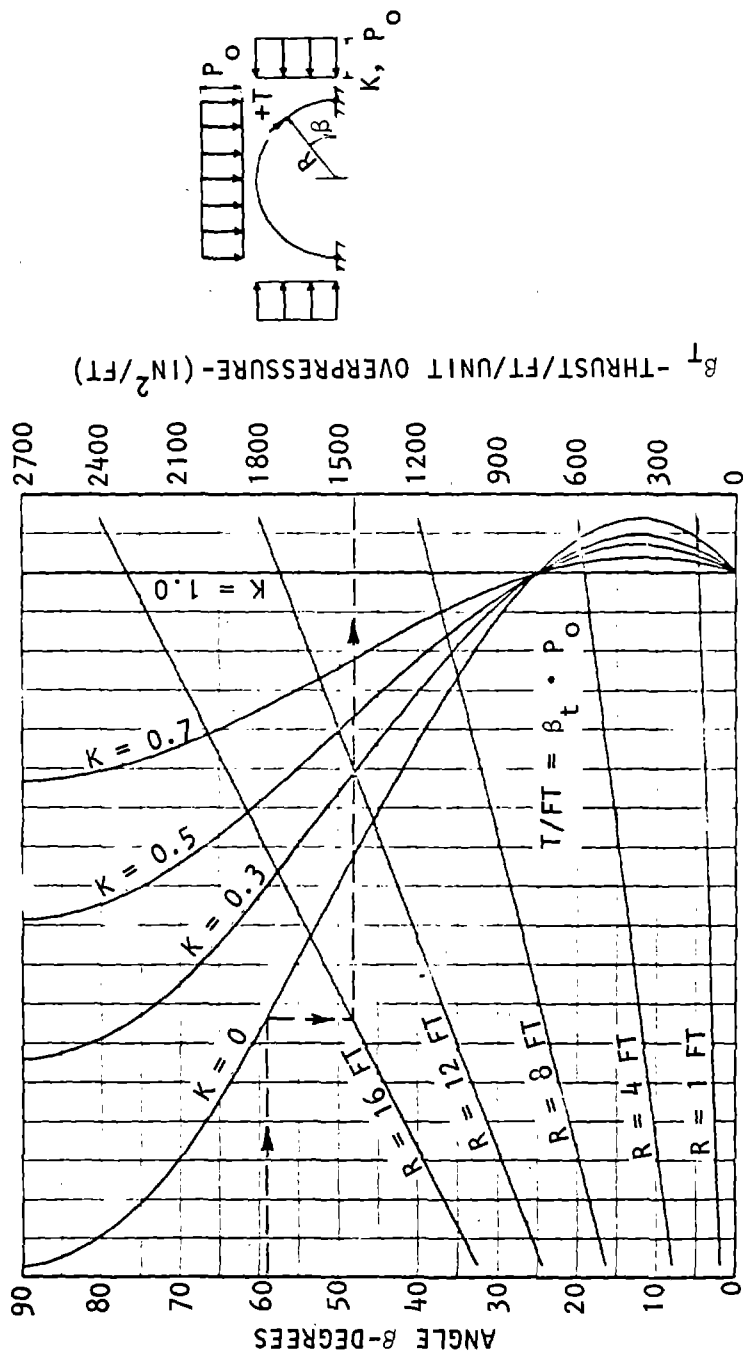


Figure 11-19. Thrust (T) Due to Ground-Surface Overpressure (P_0) for a Hinged Arch (Flathau et al., 1962)

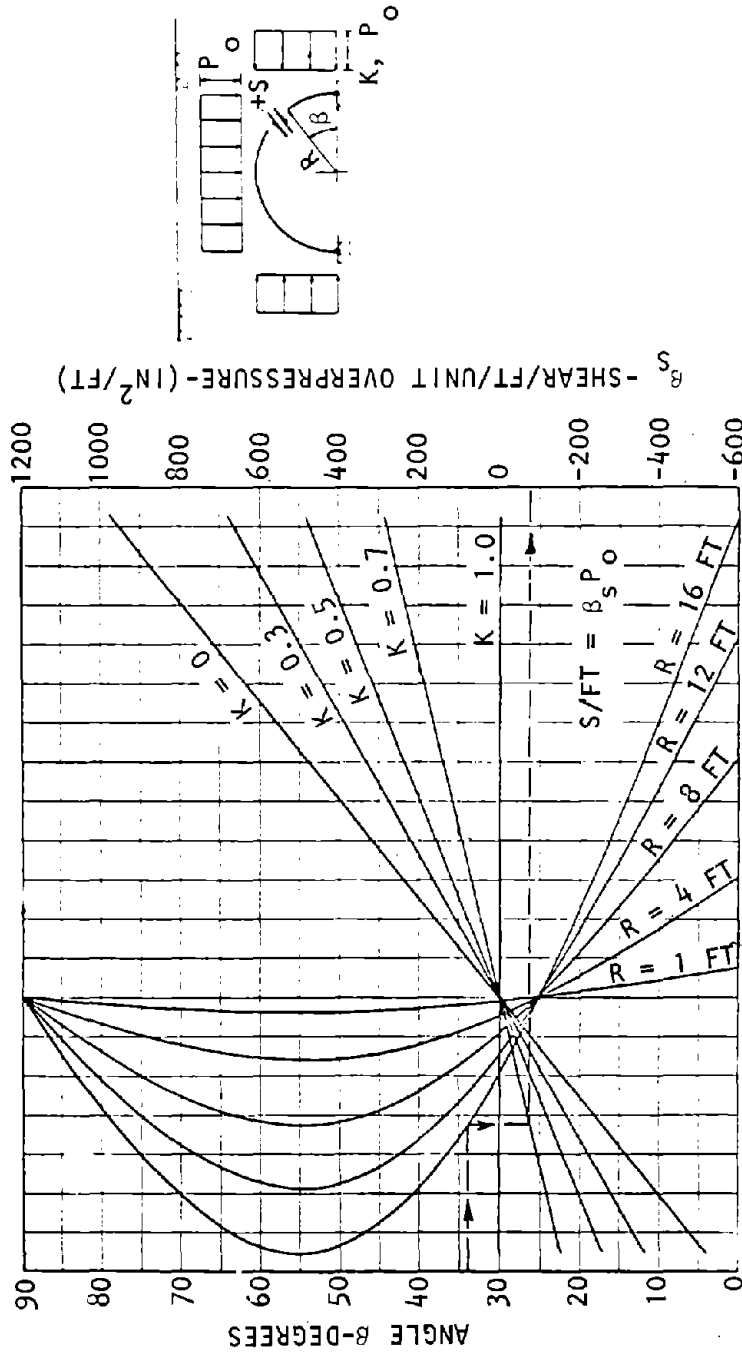


Figure 11-20. Shear (S) Due to Ground-Surface-Air Overpressure (P₀) for a Hinged Arch (Flathau et al., 1962)

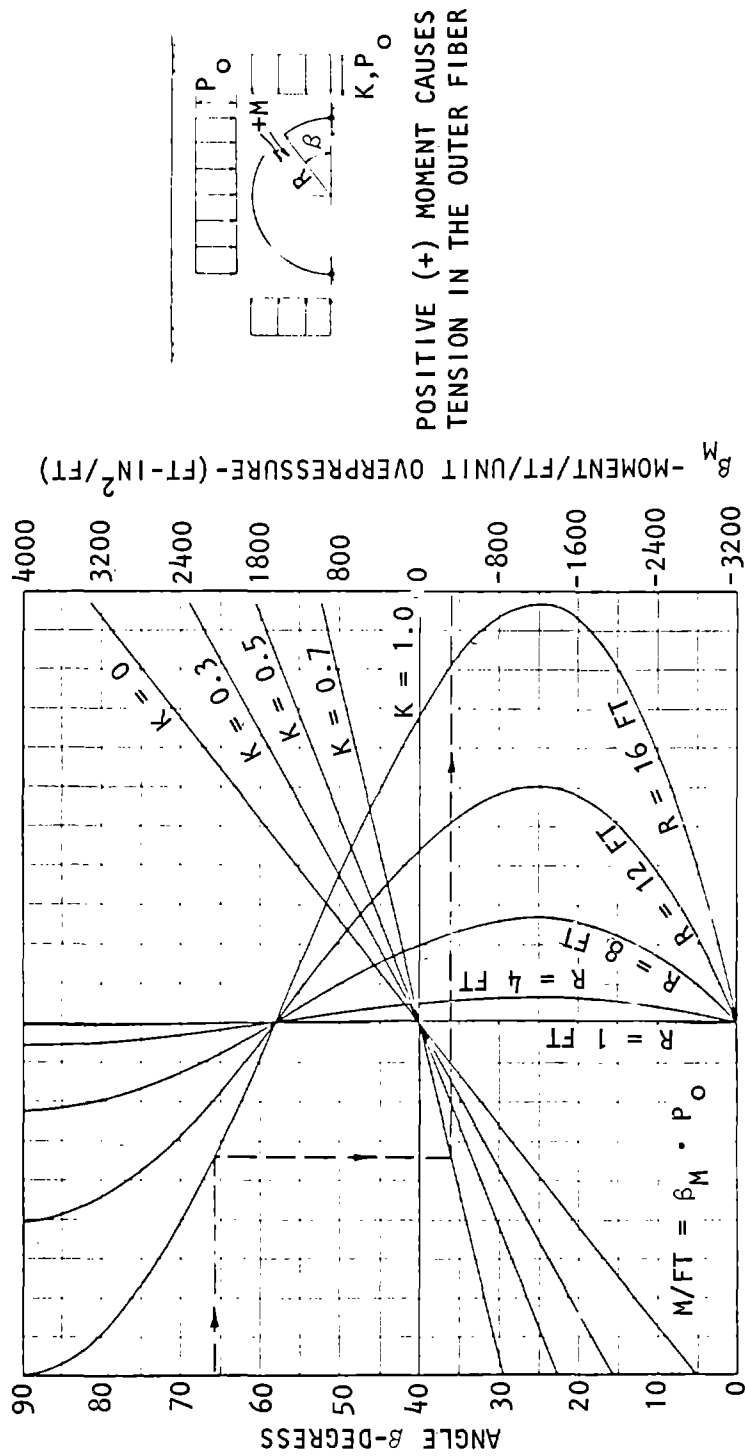


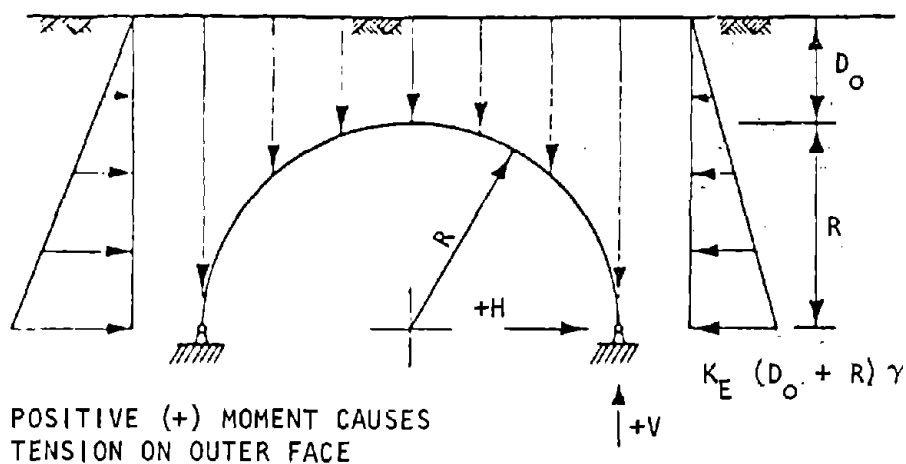
Figure 11-21. Moment (M) Due to Ground-Surface-Air Overpressure (P_O) for a Hinged Arch Flathau et al., 1962)

in figure 11-22. For the specific case of the soil cover, $D_o = 1/2 R$. The thrusts, shears, and moments are given in figures 11-23, 11-24, and 11-25 (Flathau et al., 1962).

11-8. Analysis for design verification

Final design must be verified by soil/structure interaction analysis. This approach is necessary because without such an analysis, the designer can rely only on engineering judgment for determining the potential planes of failure in the soil. Soil/structure interaction analyses may be carried out by considering a plane stress wave traversing the structure. Best results are obtained by numerical procedures using nonlinear properties of the soil. The idealization of the soil/structure system led to the formulas of the earlier subsections. For tractable solutions the pro-

pagating airblast was replaced by a blast pressure uniformly loading a large area above the structure. Numerical methods (finite element) are not restricted by these idealizations (chap. 9). For example, in figure 11-26 are shown the deformations of a multispan structure as the blast propagates from left to right. The distorted shape of the structure is a direct result of the interaction of the structure and the surrounding medium. Numerical values of deformations are included in this example only to illustrate the type of results obtained by such an analysis. The effect of arching, stress concentrations, or reflections, if any, that modify the loading on the structure are implicitly included in the calculations. The distorted shape of the structure permits the designer to calculate the stresses in various sections of the structure. These stress calculations, of course, may be included in the computer solution.



- b = UNIT WIDTH OF SECTION, FT
- D_o = DEPTH OF EARTH COVER OVER ARCH CROWN, FT
- K_E = HORIZONTAL LOAD FACTOR FOR EARTH LOAD
- R = RADIUS TO CENTERLINE OF ARCH, FT
- γ = UNIT WEIGHT OF SOIL, LB/FT³

Figure 11-22. Springing Line Reactions from Dead Loads for a Two-Hinged Arch (Flathau et al., 1962)

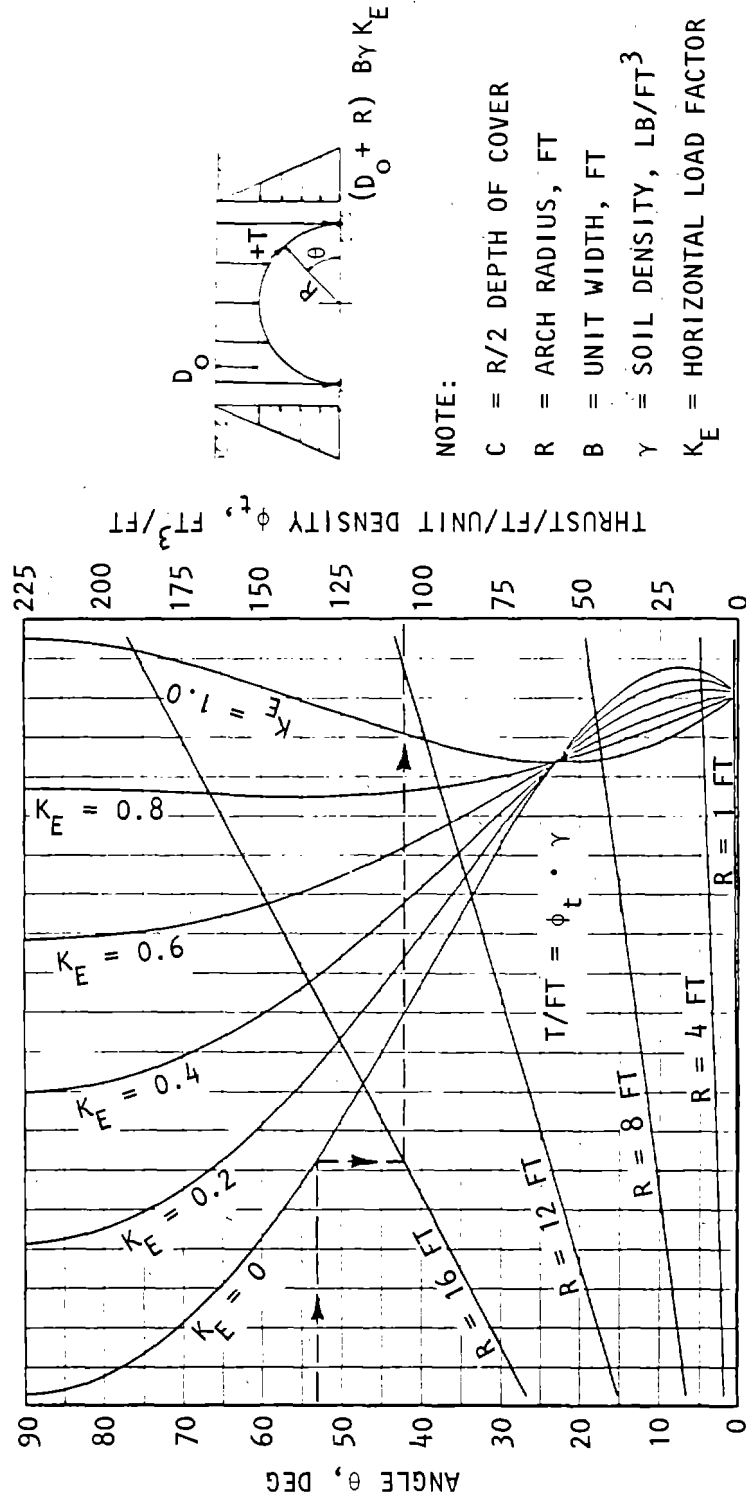


Figure 11-23. Thrust (T) Due to Earth Loads for a Hinged Arch (Flathau et al., 1962)

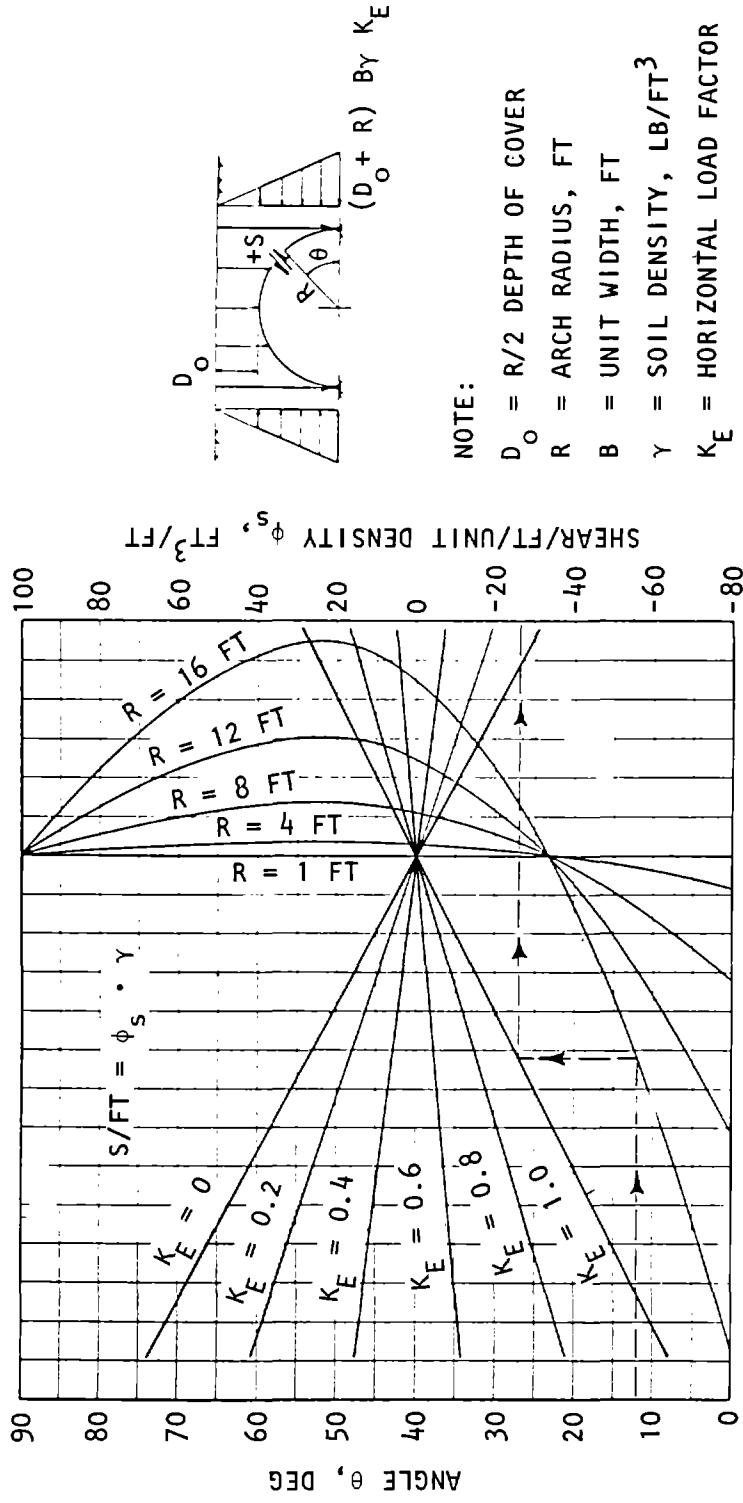


Figure 11-24. Shear (S) Due to Earth Loads for a Hinged Arch (Flathau et al., 1962)

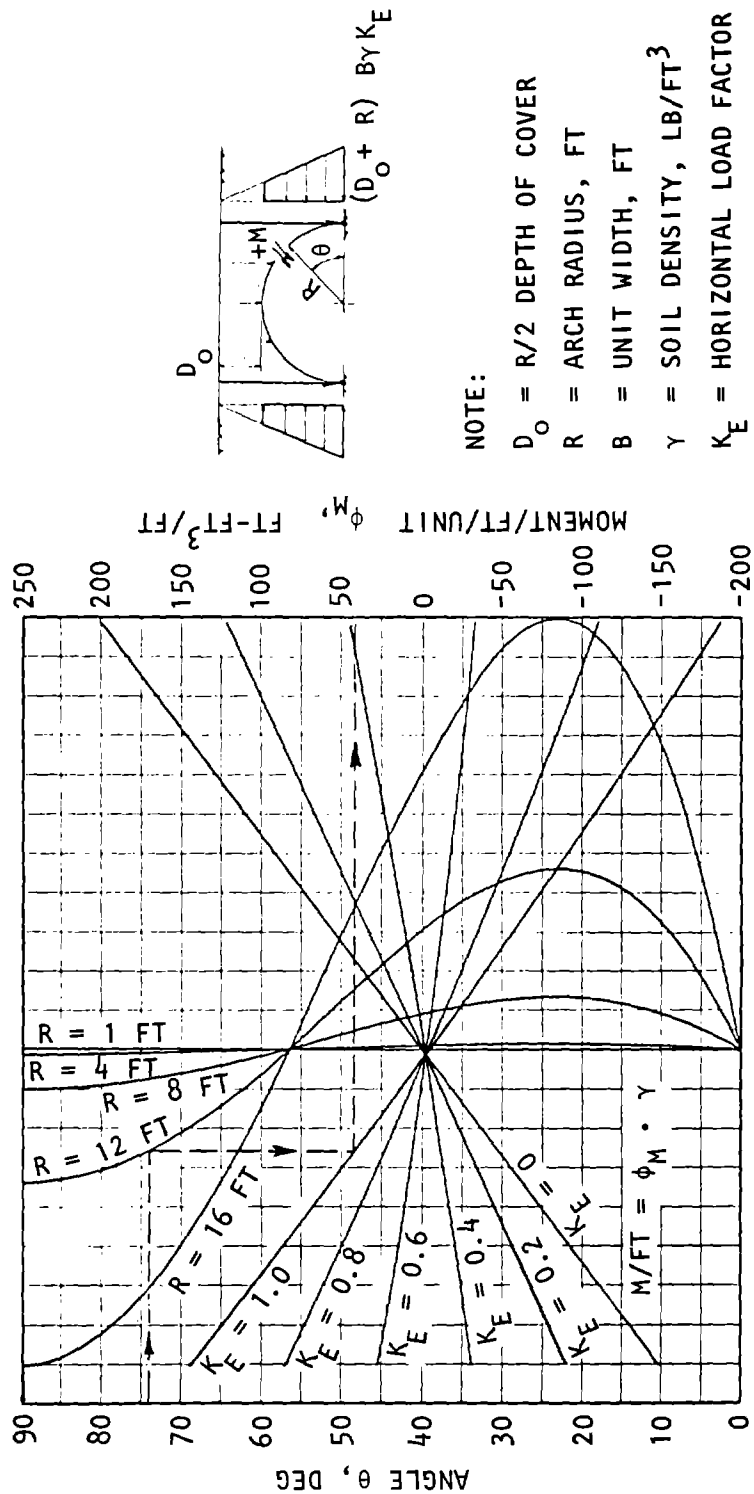
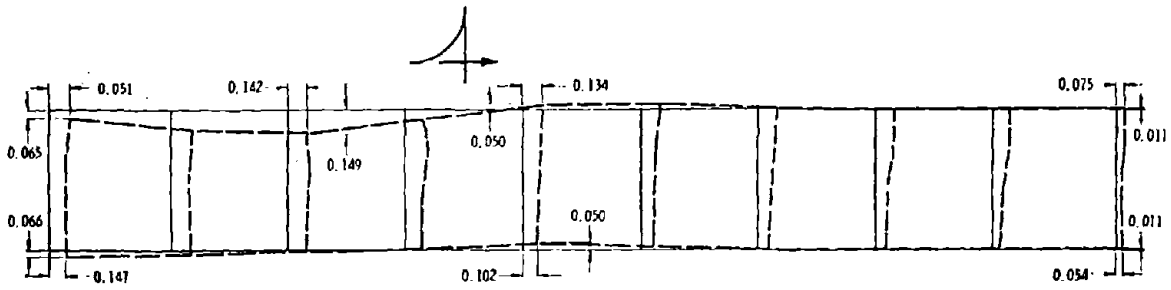
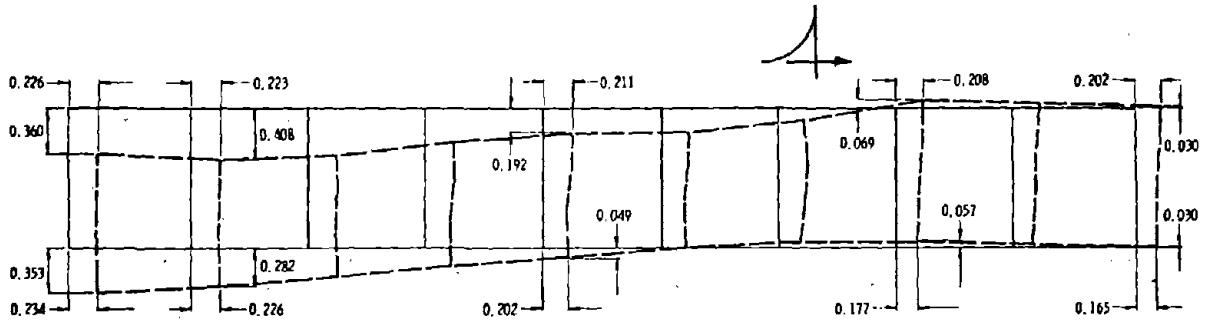


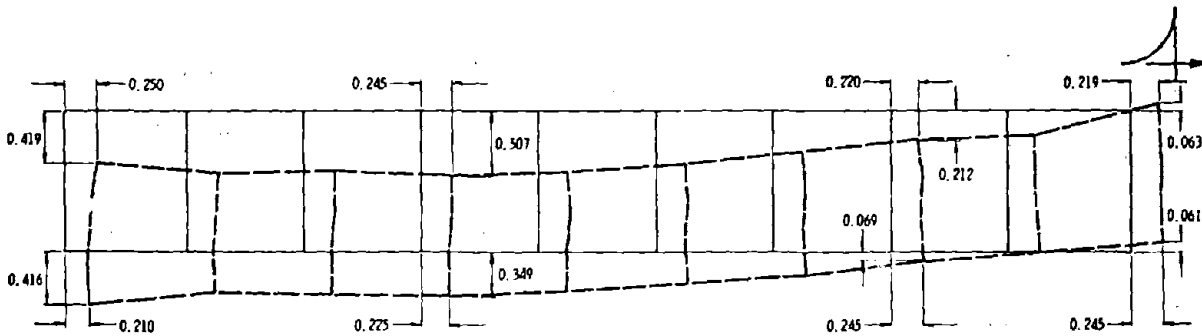
Figure 11-25. Moment (M) Due to Earth Loads for a Hinged Arch (Flathau et al., 1962)



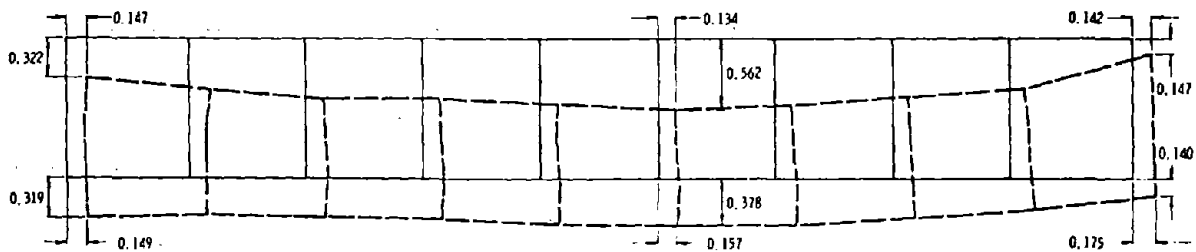
(a) $t = 0.20$ sec



(b) $t = 0.25$ sec

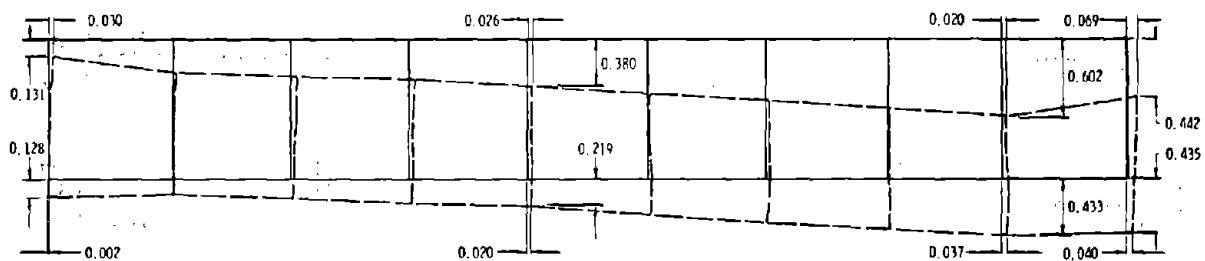


(c) $t = 0.30$ sec

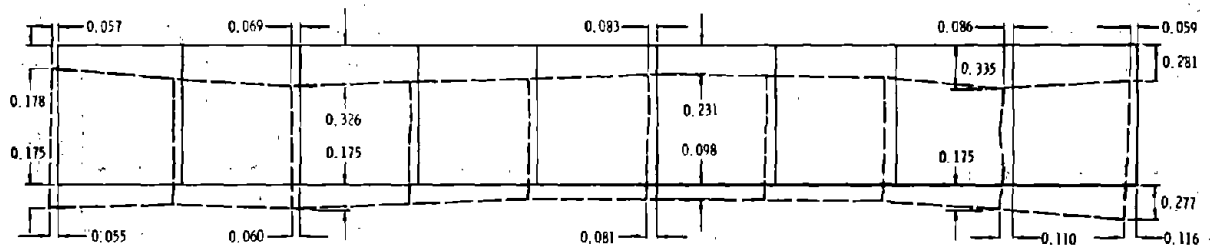


(d) $t = 0.35$ sec

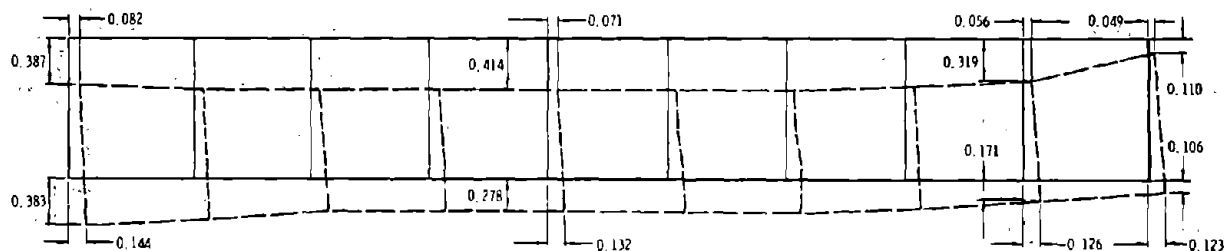
Figure 11-26. Illustrative Example of Time-Dependent Deformed Shapes of Buried Structure (AJA, 1971)



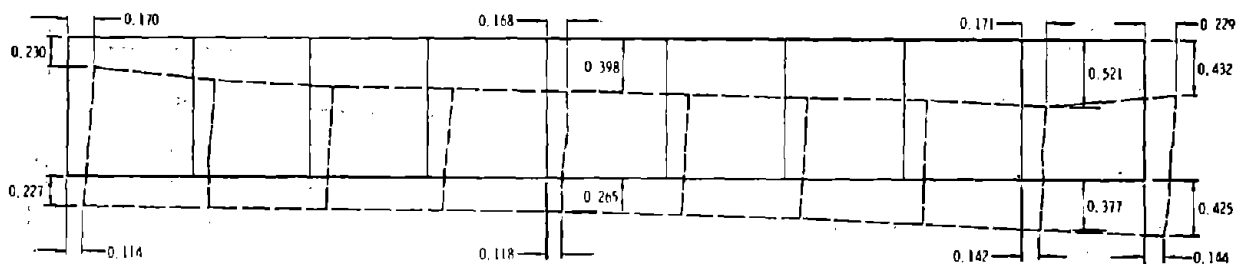
(e) $t = 0.40$ sec



(f) $t = 0.50$ sec



(g) $t = 0.60$ sec



(h) $t = 0.70$ sec

Figure 11-26. Illustrative Example of Time-Dependent Deformed Shapes of Buried Structure (AJA, 1971)—Continued

CHAPTER 12

DEEP-BURIED STRUCTURES

12-1. Introduction

a. A facility is said to be deep-buried, or deep-based, if it is buried deeply enough in the earth that the prime-mission materiel/personnel will physically survive when weapons of the anticipated threat are delivered with great accuracy and detonated overhead. Burial depths could range from as shallow as several tenths of a kilometer to as deep as three kilometers, depending principally on the site geology, the size and number of weapons composing the threat, and the duplication and dispersion of prime-mission materiel/personnel. Because of high temperatures (>35°C) and large in situ stresses, construction at greater depths is generally impractical on the scale of interest.*

b. The adaptability of systems to deep burial depends principally upon the requirements for trans-attack/postattack message communications and physical access to the ground-surface region and beyond. Undoubtedly, some combination of deception, duplication, dispersion, nomadization, hardening, and reconstitution would have to be used for the system's mission-critical umbilicals. For the system's deep-buried components, only hardening may be required.

c. The deep-buried components would be housed within a complex (or dispersed complexes) of shafts, boreholes, tunnels, and cavities. These complexes would be buried deeply enough to place them outside the crater rupture zone and beyond the reach of killing levels of ground-shock motion and stress. The survivable rock openings would need to be specially sized, configured, oriented, and reinforced. Survivable spheroidal or cylindrical cavities up to a few tens of meters in diameter would be used. Massive reinforced-concrete liners up to a few meters in thickness might be installed to reinforce openings. Minimum-diameter, reinforced boreholes and passages would provide survivable connections between cavities.

d. In general the threat for a deep-buried system would be specified with enough options to allow the designers to synthesize the system from a number of worst-case designs. A host of small-yield weapons, tens of large-yield weapons, or perhaps several superyield weapons, all delivered with great accuracy, would typify the threat for a deep-buried system.

e. The suitability of a candidate site from the standpoint of system survivability must be examined simultaneously from three viewpoints: threat, weapon effects, and protective-facilities-subsystem response.

Since the very site properties that reduce weapon-effect environments may also allow for threat escalation and degrade the performance capabilities of protective facilities-subsystems, it is important that these counteracting effects be simultaneously taken into account when comparative site evaluation is performed. Unfortunately, past site-evaluation (beneficial siting) studies have been too narrow in thrust to indicate reliably what generic site—soft rock, soft rock over hard rock, or hard rock—would be desirable from the standpoint of survivability.

f. The burial depth must satisfy survivability requirements, constructibility, and any constraints on construction cost and schedule. Siting at the shallowest feasible depth is not necessarily effective, since ground shock continues to decrease with depth and thus diminishes hardening requirements and costs. On the other hand, construction risks, costs, and schedules all increase with further increase in depth. Clearly, the optimal burial depth must be determined by tradeoffs of depth-dependent risks, costs, and schedules of concepts that can survive the threat options.

g. This section treats only the designing of ground-shock resistant rock openings that house the deep-buried components. The designing of a ground-shock survivable shaft, borehole, tunnel, or cavity comprises the interrelated determination of:

- Distance to Adjacent Openings (para. 12-2)
- Geometry/Orientation (para. 12-3)
- Absolute Size (para. 12-4)
- Reinforcement (para. 12-5)
- Excavation Method (para. 12-6)

12-2. Distance to adjacent openings

Separate the rock openings sufficiently to reduce mutual interaction to an acceptable level. As a minimum, separate the openings, center to center, a distance equal to the sum of their diameters. If one of the openings is subject to collapse, increase the separation distance so that the loosening of the rock mass is negligible within the interaction zone of the surviving opening. Minimize the number of intersections of hardened rock openings. Use a 90-deg intersection where intersection is unavoidable.

12-3. Geometry/orientation

a. Candidates. For rock openings, (boreholes, shafts, tunnels, cavities) that must survive, use one of the following geometries/orientations (it is assumed that

*For some soft-rock sites, construction may be impractical at depths as shallow as one kilometer.

the ground surface on which the attacking weapons will be detonated is more or less horizontal):

- Vertical circular cylinders
- Horizontal circular cylinders
- Horizontal elliptical cylinders, major axis vertical
- Spheres
- Prolate spheroids, axis of rotation vertical

Use the spherical and spheroidal geometries either as end caps to the cylindrical geometries or as discrete openings themselves. The horseshoe and rectangular geometries used for conventional rock openings are not suitable for hardened openings.

b. *Selection criteria.* Select the optimum geometry/orientation by tradeoff and compromise of the following conflicting criteria:

- Maximize usability
- Maximize constructability, considering safety, risks, costs, and schedule
- Minimize concentration of *in situ* and ground-shock-induced stress in the rock (*c* below)
- Minimize product of the rock-opening radius of curvature and the free-field ground-shock acceleration (*c* (1) below)

c. *Minimize concentration of stress.* The severity of material failure of the rock surrounding the rock opening will be reduced as the concentrations of free-field overburden (in situ) and ground-shock stress adjacent to the opening are reduced. For purposes of selecting the rock-opening geometry/orientation, use the peak compressive and tensile tangential stresses at the edge of the opening as the measure of stress concentration. Assume:

- The rock as a continuum, without planes of weakness, that exhibits linear-elastic behavior
- No relief of overburden stress concentration
- Static application of the peak ground-shock stress

(1) Vertical circular cylinder. The elastostatic tangential (horizontal) stress at the edge of a vertical, circular cylindrical opening is

$$\sigma_t = \sigma_{gs0} \cos^N \beta [2K_{gs} + (1 - K_{gs})(1 - 2 \cos 2\theta) \sin^2 \beta] + 2 K_{ob} \sigma_{ob} \quad (12-1)$$

where

- K_{gs} = Ratio of transverse to radial ground-shock stress at the wave front
- K_{ob} = Ratio of horizontal to vertical overburden (in situ) stress
- N = Rate of ground shock attenuation with distance, i.e., r^N (para. 9-2, TM 5-858-2)
- β = Burst standoff angle defined in figure 12-1
- θ = Angle defined in figure 12-1

σ_{gs0} = Peak radial (vertical) ground-shock stress at the depth of the opening for $\beta = 0$

σ_{ob} = Vertical overburden (in situ) stress at the depth of the opening

Compressive stresses are positive.

(2) Horizontal circular cylinder. The elastostatic tangential (hoop) stress at the edge of a horizontal circular cylindrical opening is

$$\sigma_t = \sigma_{ob} [(1 + K_{ob}) + 2(1 - K_{ob}) \cos 2\theta] + \sigma_{gs0} \cos^N \beta [(1 + K_{gs}) + 2(1 - K_{gs}) \cos 2(\theta + \beta)] \quad (12-2)$$

where θ is the angle defined in figure 12-2 and the remaining symbols are as previously defined in (1) above and in figure 12-1.

(3) Horizontal elliptical cylinders. The elastostatic tangential (hoop) stress at the edge of a horizontal elliptical cylindrical opening with major vertical axis is (Greenspan, 1944):

$$\sigma_t = \frac{2 S_y h/w + (S_y - S_x)(h/w)^2 - (1 + h/w)^2 \sin^2 \theta + S_{xy} (1 + h/w)^2 \sin^2 \theta}{\sin^2 \theta + (h/w)^2 \cos^2 \theta} \quad (12-3)$$

where

- h = Opening height
- w = Opening width
- θ = Angle defining the target location for stress calculation as shown in figure 12-2
- S_x = Horizontal component of free-field stress
 $= 0.5 \sigma_{gs0} \cos^N \beta [1 + K_{gs} - (1 - K_{gs}) \cos 2\beta] + K_{ob} \sigma_{ob}$ (12-4)
- S_y = Vertical component of free-field stress
 $= 0.5 \sigma_{gs0} \cos^N \beta [1 + K_{gs} + (1 - K_{gs}) \cos 2\beta] + \sigma_{ob}$ (12-5)
- S_{xy} = Shear component of free-field stress
 $= 0.5 \sigma_{gs0} \cos^N \beta [1 - K_{gs}] \sin 2\beta$ (12-6)

and the remaining symbols are as defined in (1) above and in figure 12-1.

(4) Sphere. The elastostatic tangential stress at the edge of a spherical opening is

$$\sigma_t = \sigma_{ob} \frac{-(3 + 15\nu) + 27 K_{ob} + 30(1 - K_{ob}) \cos^2 \theta}{14 - 10\nu} + \sigma_{gs0} \cos^N \beta \frac{-(3 + 15\nu) + 24 K_{gs} + 30(1 - K_{gs}) \cos^2(\theta + \beta)}{14 - 10\nu} \quad (12-7)$$

where

θ = Angle defined in figure 12-2.

ν = Poisson's ratio of the rock

and the remaining symbols are as previously defined in (1) above and in figure 12-1.

(5) Prolate spheroid. The elastostatic tangential stress at the edge of a prolate spheroidal opening with vertical axis of rotation can be approximated by the stress obtained from equation 12-3 multiplied by the ratio of the stress from equation 12-7 to the stress from equation 12-2.

d. *Minimize product of the rock-opening radius of curvature and the free-field ground-shock acceleration.* The likelihood of spallation and loss of structural integrity of the rock-opening walls will be reduced as the product of the opening radius of curvature and the free-field ground-shock acceleration is reduced. Use the following form of this product for purposes of rock-opening geometry/orientation selection:

$$\frac{1}{a} \int R A_n da \quad (12-8)$$

where

A_n = Component of free-field acceleration normal to opening wall

R = Opening radius of curvature

a = Surface area of opening

12-4. Absolute size

a. *Determinants.* The hardness of a rock opening can be size dependent. Absolute size effects arise from:

- Free-field stress gradient (b below)
- Macroscopic planes-of-weakness spacing (c below)
- Material variability (d below)

b. *Free-field stress gradient.* The relationship between free-field ground-shock stress gradient and absolute opening size can be understood by examining the simple, linearly varying, biaxial stress field shown in figure 12-3a. Assume that the stress gradient corresponds to the linear rise of a ground-shock stress pulse traveling with velocity C , rise time t_r , and peak stress σ_{max} , all at range r . Then the difference between the free-field stress at r and at $r - R$ will be

$$\Delta\sigma = \frac{R'}{t_r \cdot C} \cdot \sigma_{max} \quad (12-9)$$

Assume further that radius R' corresponds to the smallest radius from r at which the free-field stress is, for all practical purposes, not disturbed by the presence of an opening at r . The normal free-field stress on a circle of radius R' , centered at r , can be broken down into the Fourier series:

$$\sigma(\theta)|_{R'} = \sum_{n=0}^3 \sigma_n \cos n\theta \quad (12-10)$$

which includes only the $n = 0, 1, 2,$ and 3 terms indicated in figure 12-3b.

(1) These load components can be treated as quasi-static loads to be resisted by the rock in the interaction zone and by any reinforcement in the opening. It is seen that the familiar quasi-static uniform ($n = 0$) and ovaling/pure-shear ($n = 2$) components of free-field load are not affected by the stress gradient, but that the rigid body ($n = 1$) and second bending ($n = 3$) components are. Since R' is proportional to the size of the opening, an absolute-size effect exists for the rigid body ($n = 1$) and second bending ($n = 3$) components. Of course, an absolute-size effect occurs for the $n = 1, 2, 3, 4, 5, 6...$ components that arise when the ground-shock pulse initially engulfs the opening.

(2) Use the information from above to determine if the free-field stress gradient effect is significant. (In general, this effect will be insignificant.) If the effect is found to be significant, use the above information to provide preliminary design requirements and then verify the requirements using more elaborate mathematical simulations.

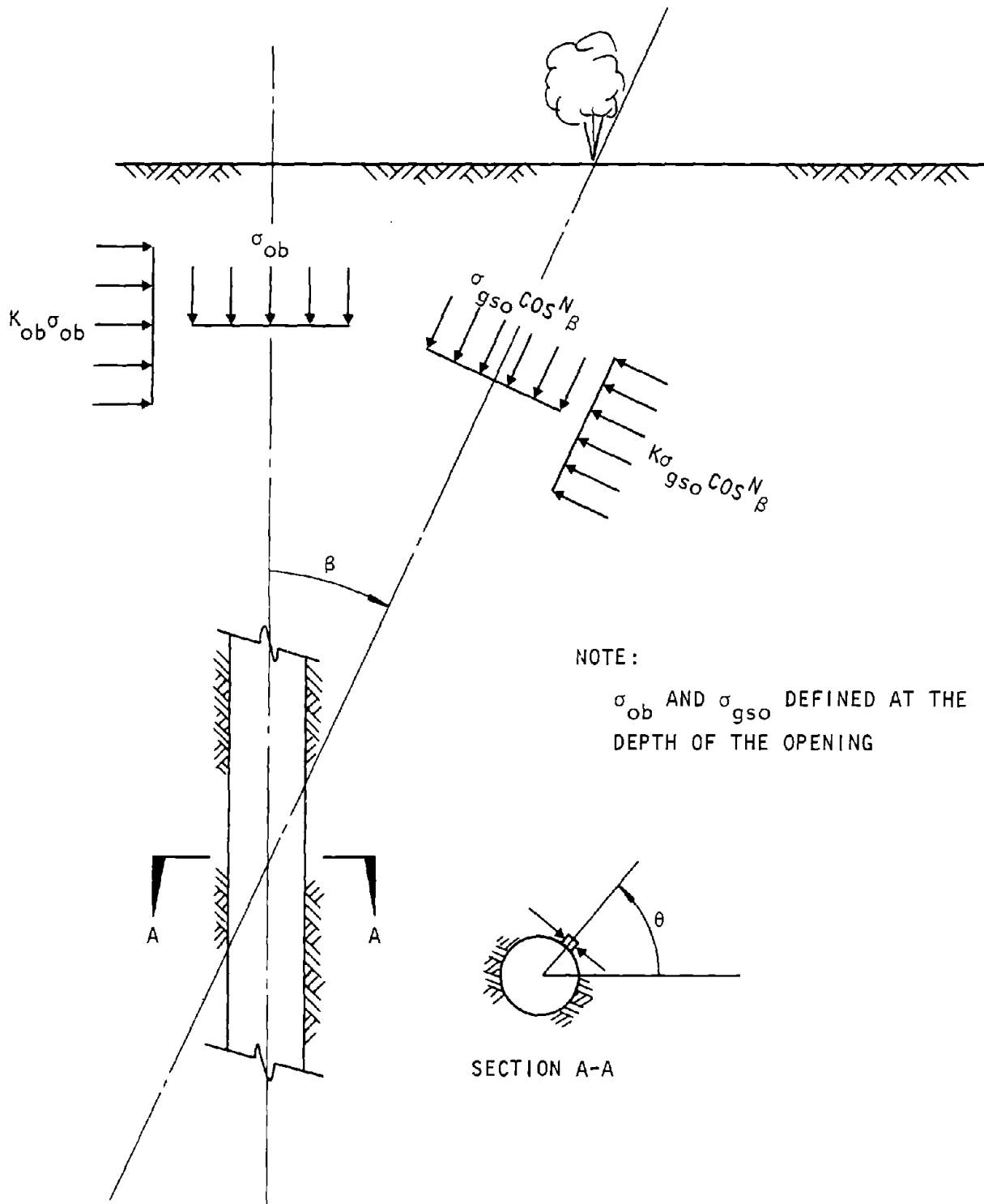
(c) *Spacing of macroscopic planes of weakness.* The relative sizes of the spaces between more or less regular arrays of joints in the rock and the lateral dimensions of an opening (or its interaction zone) can alter the effective strength and stiffness of the rock. In general, the harder the rock, the greater the influence of the joints. Use the material properties obtained from small intact samples of rock when the opening dimensions are small compared to the joint spacing, since the rock appears as a monolithic mass to the opening. Use the material properties obtained from a sample containing a large number of joints when the opening dimensions are large compared to the joint spacing. Use continuum models with the appropriate material properties at those two extremes, since there is no size effect.

(1) In the middle range, where the opening cross section spans a few joint-defined blocks, *continuum* models based on either the intact (microscopic) properties or gross (macroscopic) properties fail to describe the behavior of the opening. Use elaborate mathematical simulations to calculate the response of opening for this middle range. However, continuum modeling with the strength-reductions shown in figure 12-4 can be used for purposes of preliminary design in this middle range (Hendron-Aiyer, 1972).

(2) As the ratio of opening diameter to joint spacing increases, failure becomes progressively more likely until, finally, collapse occurs under gravity loading alone. Estimate the gravity-collapse-threshold ratio of opening diameter to joint spacing (B/S) using the collapse of free-standing, unreinforced masonry construction under gravity load (Heyman, 1966):

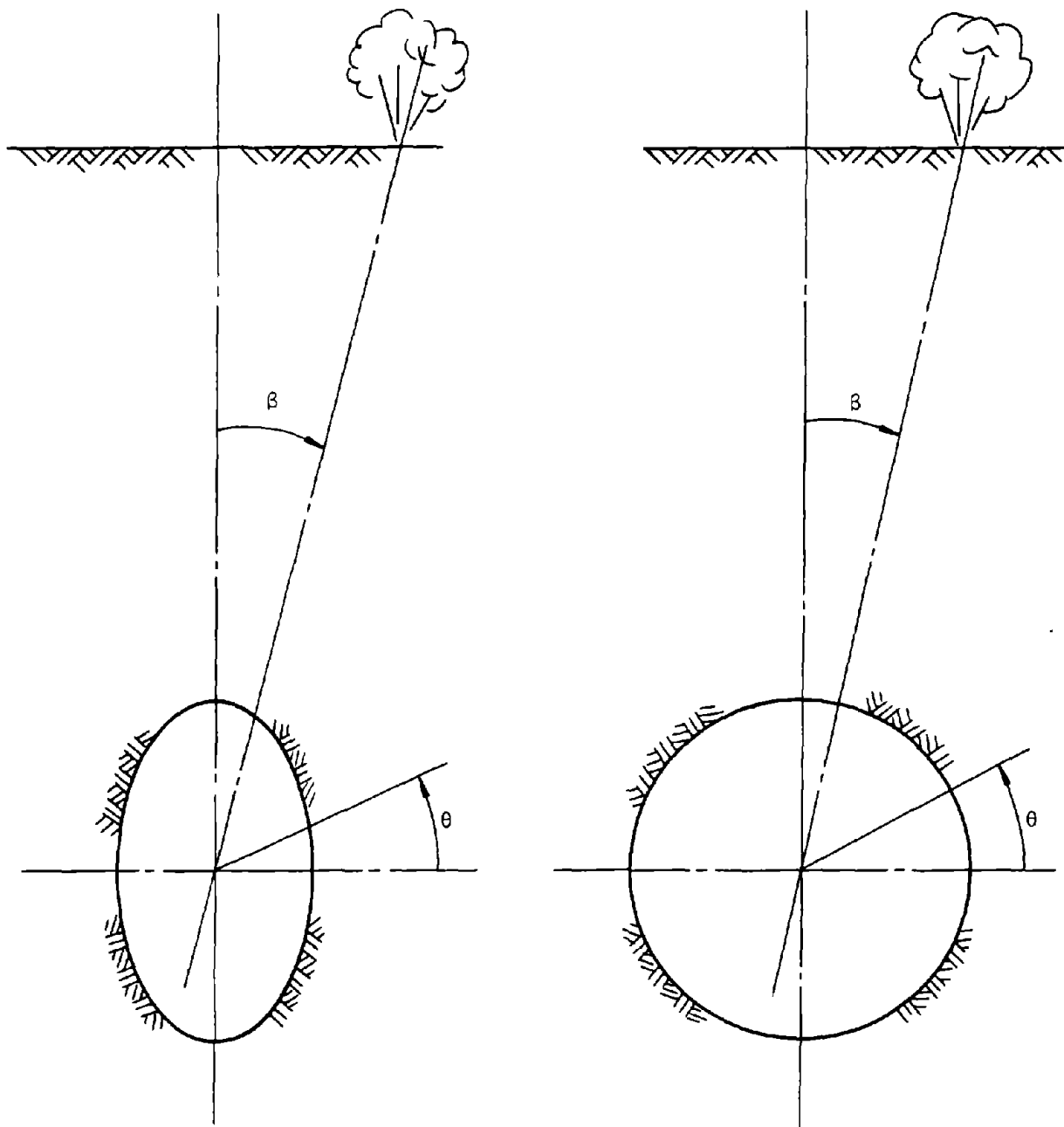
Horizontal circular cylindrical opening: $B/S \simeq 20$

Spherical cavity: $B/S \simeq 40$ (12-11)



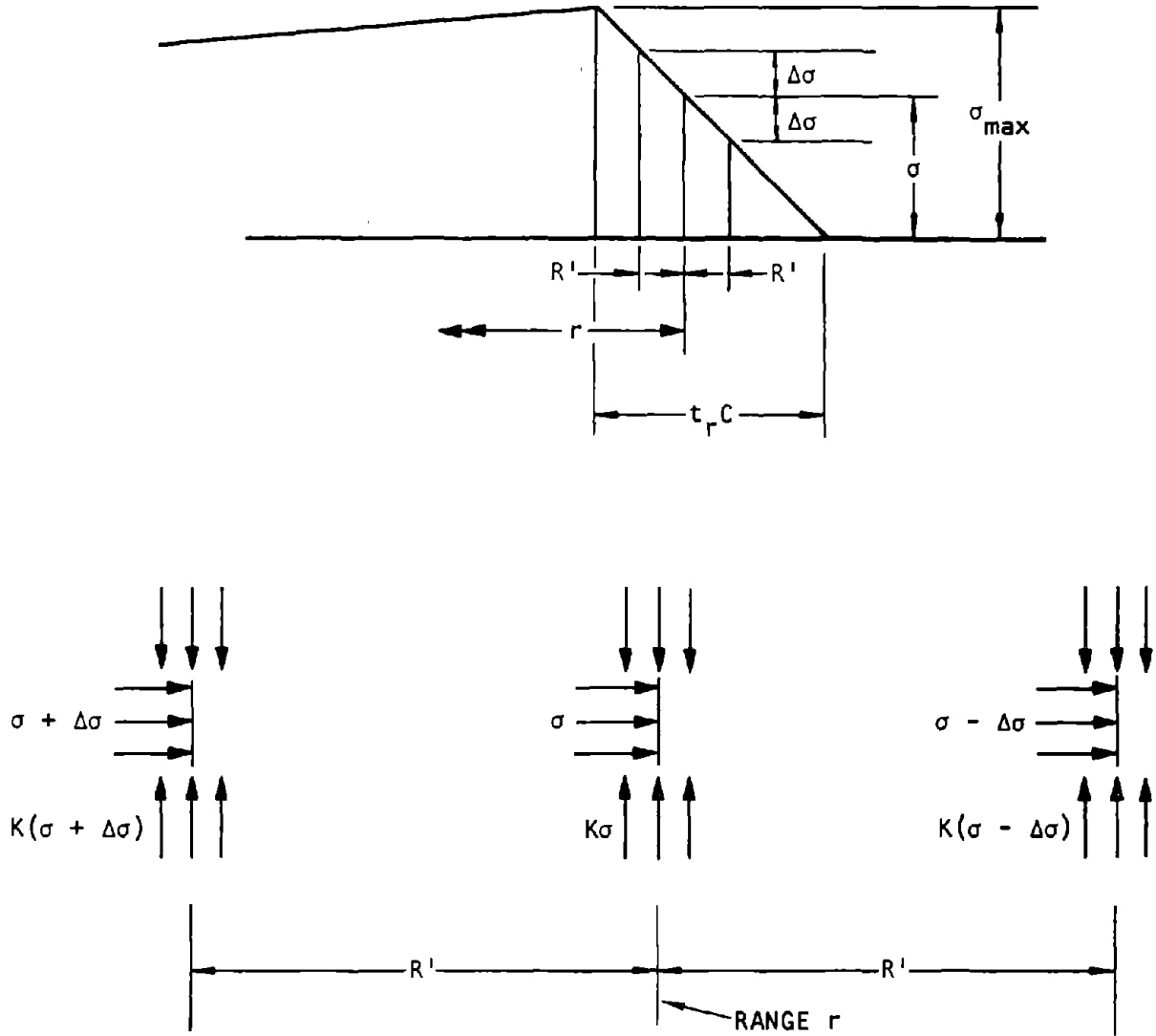
U.S. Army Corps of Engineers

Figure 12-1. Vertical, Circular, Cylindrical Opening Subjected to Ground Shock and Overburden Stresses



U.S. Army Corps of Engineers

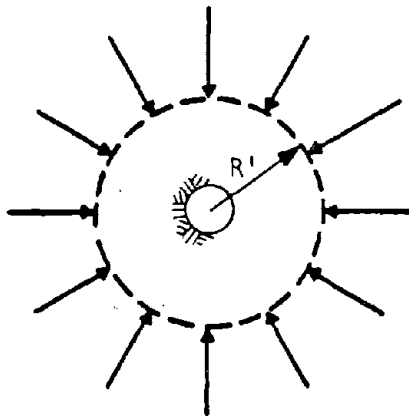
Figure 12-2. Definition of Angle θ for Three Types of Openings: (1) Horizontal Circular and Elliptical Cylinders (2) Spheres, and (3) Prolate Spheroids



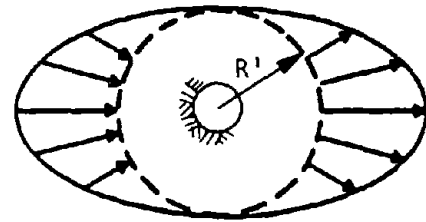
(a) Stress gradient

U.S. Army Corps of Engineers

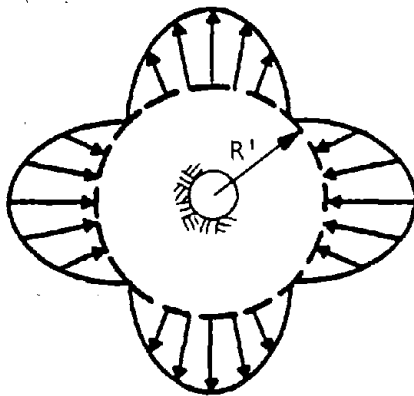
Figure 12-3. Quasi-Static Components of Free-Field Ground Shock



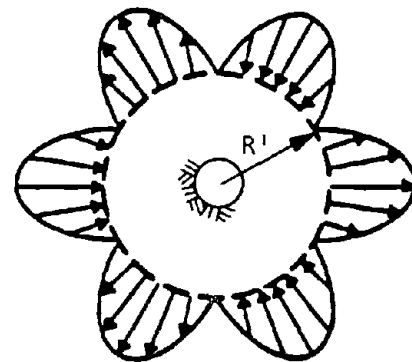
UNIFORM: $\sigma \frac{1 + K}{2}$



RIGID BODY: $\Delta\sigma \frac{3 + 4}{4} \cos \theta$



OVALING: $\sigma \frac{1 - K}{2} \cos 2\theta$



BENDING: $\Delta\sigma \frac{1 - K}{4} \cos 3\theta$

(b) Stress components

Figure 12-3. (Concluded)

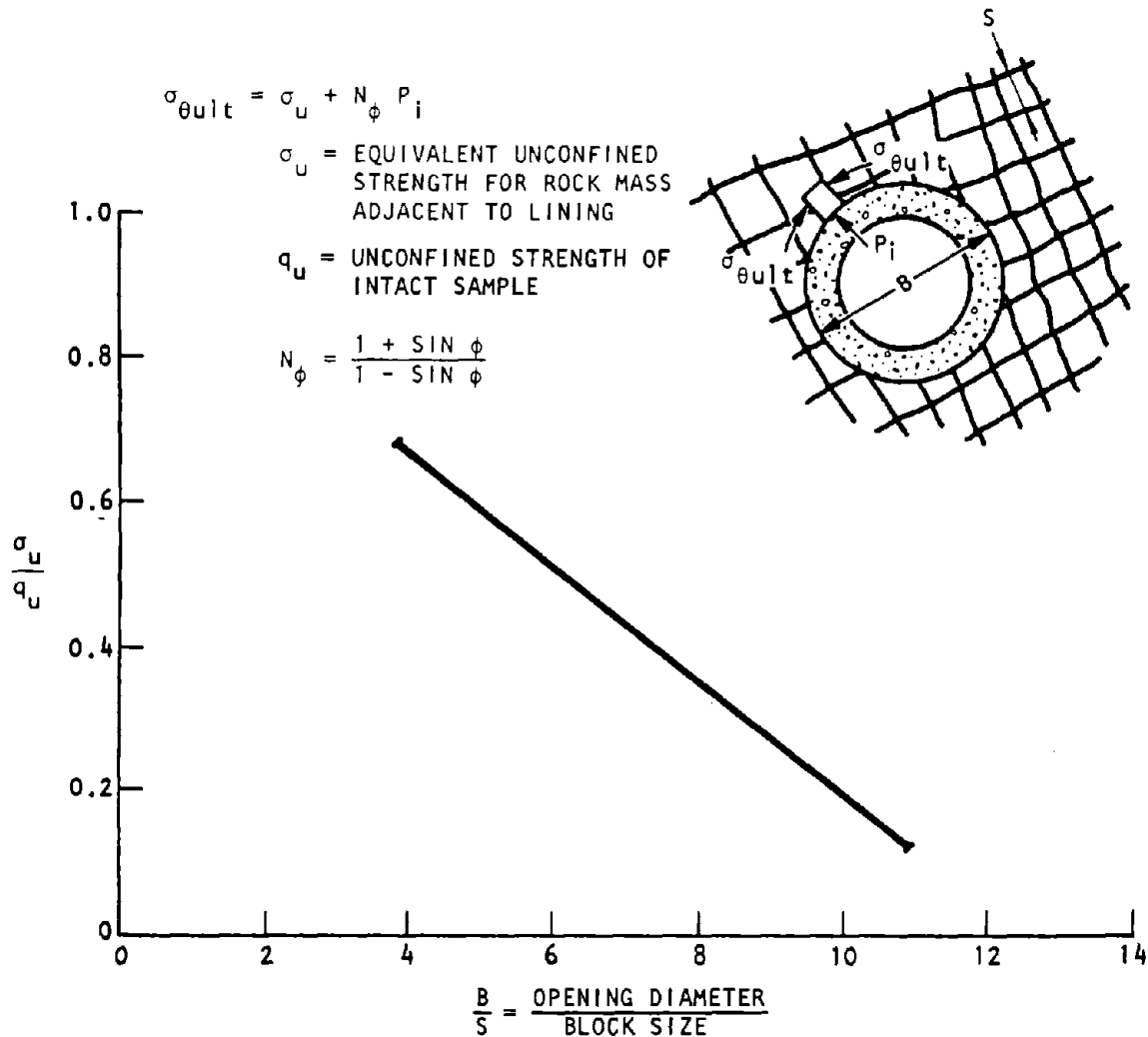


Figure 12-4. Ratio of in situ Strength to Laboratory Strength as a Function of Opening Diameter to Joint Spacing (Hendron-Aiyer, 1972)

d. *Material variability.* Absolute size may also influence rock-opening performance through the natural variability (or homogeneity) of the rock. The larger the opening, the larger the interaction zone and the more likely that strength and stiffness variability will be found. Estimate the variability of the rock properties within the interaction zone by use of appropriate statistical sampling and testing of either the interaction zone rock or another volume of rock. Introduce these variabilities into your mathematical simulations. In the event variabilities are large and well defined, explicitly model them.

12-5. Reinforcement

a. *Failure modes.* Rock openings will usually have to be reinforced. What constitutes failure and what the reinforcement must do to prevent failure are functions of the severity of the ground-shock environment and the strengths of the rock and the reinforcement. The HARD HAT and PILE DRIVER underground nuclear test events at the Nevada Test Site, in conjunction with the Hard Rock Silo Development

(HRSD) test program at Cedar City, Utah, have provided information on the failure mechanisms of lined and unlined openings in rock. What has become vividly clear after studying these tests is that, ignoring simple spallation, two distinct types of ground-shock-induced failure of a rock opening are possible: Material failure and mechanical failure. These two generic types can be viewed as four failure modes:

- Swelling of the opening's walls from material failure of the surrounding rock
- Swelling of the opening's walls from mechanical failure of the surrounding rock
- Loss of structural integrity (large-scale mechanical failure) of the opening's wall
- Spallation of the opening's walls due to the tensile reflection of the ground-shock wave front

b. *Material failure.* Material failure is characterized by yielding, flow, and swelling of the rock within the interaction zone to such an extent that there is a permanent reduction in opening volume. This type of failure can occur only when the *in situ* yield strength of the intact rock is exceeded and when mechanical

failure is precluded. Material failure was dramatically exhibited in the highly stressed close-in drifts of PILE DRIVER (Distefano et al, 1970).

c. Mechanical failure. Mechanical failure, on the other hand, is characterized by relative movement along macroscopic planes of weakness (joints, fractures, partings, and separations) lying within the interaction zone. Mechanical failure actually begins with the development of the opening during excavation, where it is manifested as a general loosening of the rock adjacent to the opening. During ground-shock loading, the loosening effect is increased and appears, under the best of conditions, as a swelling of the opening walls. Various degrees of mechanical failure were in evidence in the more remote drifts, tunnels, and shafts of PILE DRIVER and in the HRSD test events.

(1) Loss of opening wall structural integrity can be triggered by the expulsion of unkeyed blocks of rock into the opening resulting from (a) the enhanced (or reduced) acceleration on the head-on (or back) face of the opening, relative to the free-field, during rapid changes in acceleration such as during initial engulfment, and (b) the tendency for tensile circumferential straining, i.e., unkeying action, at the head-on and back faces. Depending upon the circumstances, the expulsion of rock blocks may or may not lead to further loss of structural integrity. Evidence of this mechanism was found in the PILE DRIVER and the HRSD test event ROCKTEST II. In PILE DRIVER, a rock block (roughly 0.6 by 1.2 by 2.4m) was expelled from the newly excavated, unreinforced extension of the main access shaft during the event (Distefano et al., 1970). At this range the estimated free-field stress was 7000 N/cm² and the acceleration level was 20g. In ROCKTEST II, a large rock block (roughly 1.2 by 1.2 by 2.4m) was expelled from the wall of a previously tested cavity located in an adjacent test bed (HANDEC II) by the ROCKTEST II generated ground shock (AJA, 1970). It is estimated that a free-field acceleration of 10 to 20g existed at the range of this opening.

(2) These are two examples of the expulsion-triggering mechanism without further loss of structural integrity. Whether this mechanism was responsible for the more serious mechanical failures seen in PILE DRIVER and ROCKTEST II cannot presently be answered. Other triggering mechanisms are, of course, possible.

(3) The loss of structural integrity becomes significantly more imminent with each attack because of progressive degradation of the shear resistance of the planes of weakness with each attack. This fact was driven home by the report that the unlined access tunnels of HARD HAT "were severely damaged by the PILE DRIVER detonation, and large quantities of rock fell into the openings" (Distefano

et al., 1970). The PILE DRIVER acceleration environment, less severe than the previous HARD HAT environment, is estimated to have been 20 to 100g at various points along the HARD HAT access tunnels.

d. Reinforcement selection. Opening reinforcement will not be required, provided:

- Either spallation does not occur, or its effect is not critical, or spallation protection is provided around the housed component itself, e.g., an equipment canopy.
- Either joint spacing is larger than the opening cross-sectional dimensions or opening collapse can be tolerated.
- Either material failure does not occur, or the accumulated inelastic deformations are functionally tolerable for the number of bursts expected. (This suggests that oversizing the opening cross-sectional dimensions might prove to be an effective means of accommodating material failures.)

If any one of these conditions is not met, opening reinforcement will be required; in general, opening reinforcement will be required.

(1) Reinforcement concepts for deep-buried rock openings are listed in table 12-1. To date, attention has been directed almost exclusively to the development of rock-bolt and liner reinforcement.

(2) The technical effectiveness of rock-bolt and liner reinforcement is determined more by the mix and relative severity of mechanical and material failure of the rock opening than by a threshold intensity (or range) of ground-shock environment.

(3) Rock bolts (with wire mesh) are virtually ineffective in preventing or controlling material failure and cannot effectively be designed to accommodate material failure. In the absence of material failure, however, rock bolts can be effective in preventing or controlling spallation and controlling mechanical failure, provided that bolt anchorage can be maintained for multiple bursts. Bolt lengths of one-half to one times the opening diameter will be required. Bolt spacing will be determined by the joint spacing and pull-out capacity of the bolt.

e. Reinforced concrete liners. Integral reinforced concrete liners are virtually ineffective in preventing or controlling material failure of hard rock due to their limited load and strain capacities. Highly reinforced (ductile) liners are effective in preventing spallation and mechanical failure of the opening.

f. Steel liners. Built-up or massive monocoque steel liners are effective in preventing or controlling material or mechanical failure.

g. Backpacker liner. Backpacker liners are virtually ineffective in preventing or controlling material failure, but can easily accommodate mechanical failure. The backpacker concrete liner

Table 12-1. Reinforcement Concepts for Rock Openings

Strengthen Interaction-Zone Rock

Hard rock
 Grout joints
 Cement joints
 Soft rock
 Freeze
 Impregnate

Weaken Interaction-Zone Rock

Reduce hard rock to rubble

Support Opening Wall

Gas
 Liquid
 Backfill
 Ice
 Sand
 Foam
 Elastomer
 Rubble
 Rock bolts
 Liner
 Integral
 Continuous
 Articulated
 Backpacking
 Continuous
 Articulated

U.S. Army Corps of Engineers

can be used effectively to prevent or control mechanical failure, provided the backpacking is relatively stiff.

h. Selection criteria. Select the optimum reinforcement concept by tradeoff of hardness, constructibility, and costs

12-6. Design procedures for opening reinforcement

a. Preliminary design to prevent/accommodate material failure. Preliminary design procedures (Britt, 1977) are presented for the reinforcement of circular cylindrical cavities. Extrapolation to openings with noncircular cross-section is possible by judicious comparison of elastic stress concentration factors. In some cases, these procedures will also be adequate for final design; however, in general, elaborate mathematical simulations will be required to support final design.

(1) First, design the reinforcement to withstand a material failure of the rock. Use the design procedure provided below, or a similar procedure. As appropriate, account for the absolute size of the opening (para. 12-4).

(2) For cases where the opening diameter is not small compared to the joint spacing, determine the adequacy of the reinforcement evolved to resist material failure of the opening. Use the procedure presented in paragraph 12-6 below or a similar procedure. Modify the reinforcement design as required.

b. Background. Drake and Britt (1976) have extended static procedures of Newmark (1969) and Hendron and Aiyer (1972) to accommodate dynamic loads. The salient features of this dynamic design method are summarized here in charts suitable for preliminary design of deep underground structures in rock (figs. 12-5 to 12-30) from Britt (1977).

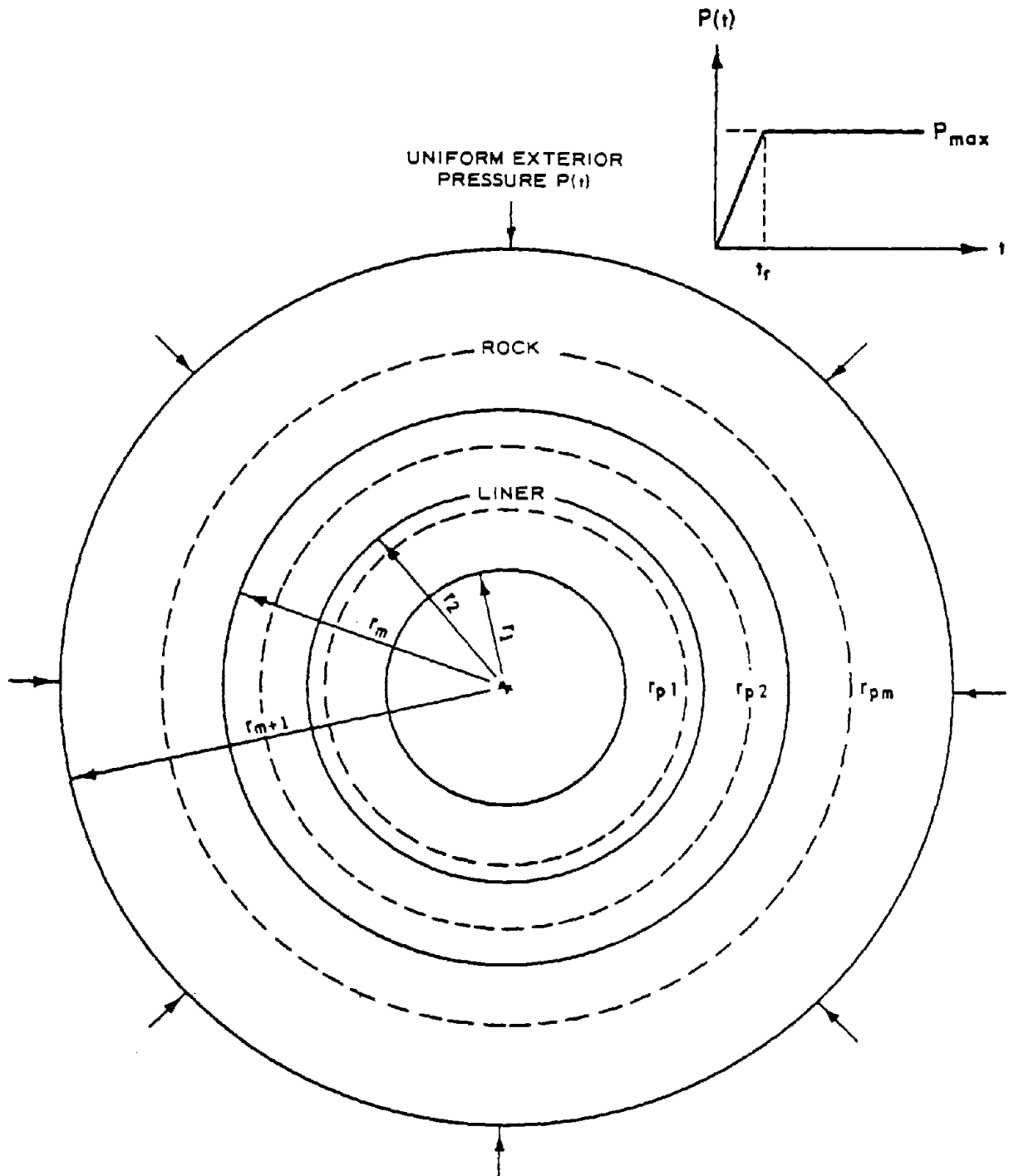


Figure 12-5. Geometry of Rock/Liner System (Britt, 1977)

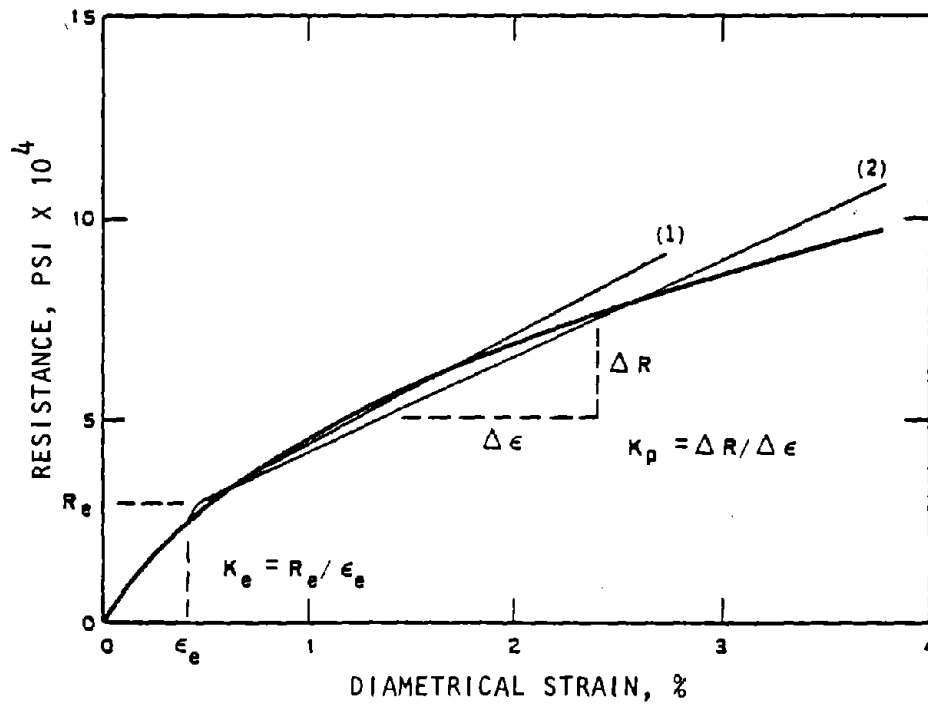
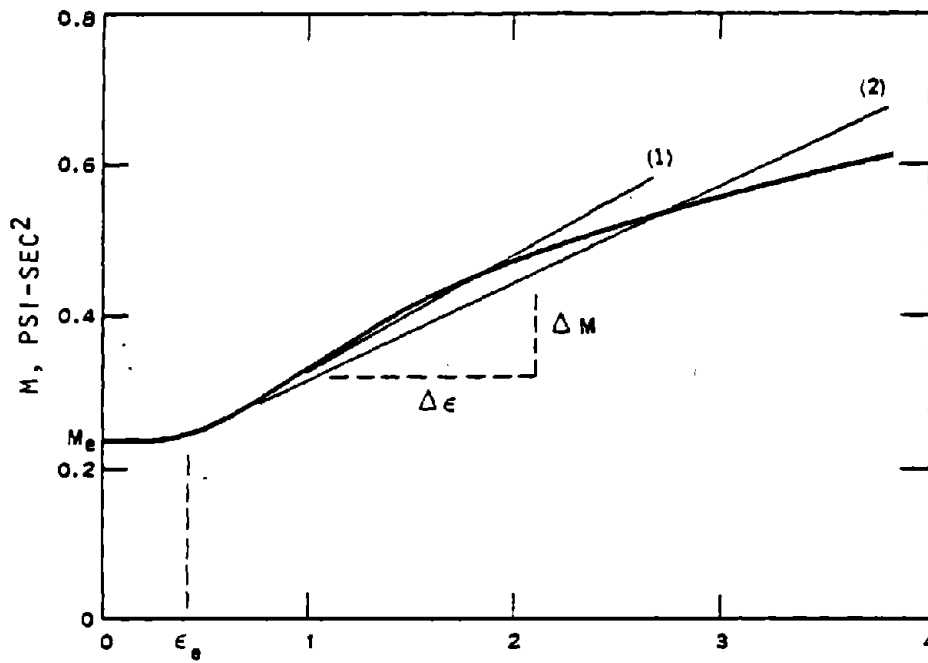


Figure 12-6. Examples of Bilinear Fits to Effective Resistance and Mass Functions (Britt, 1977)

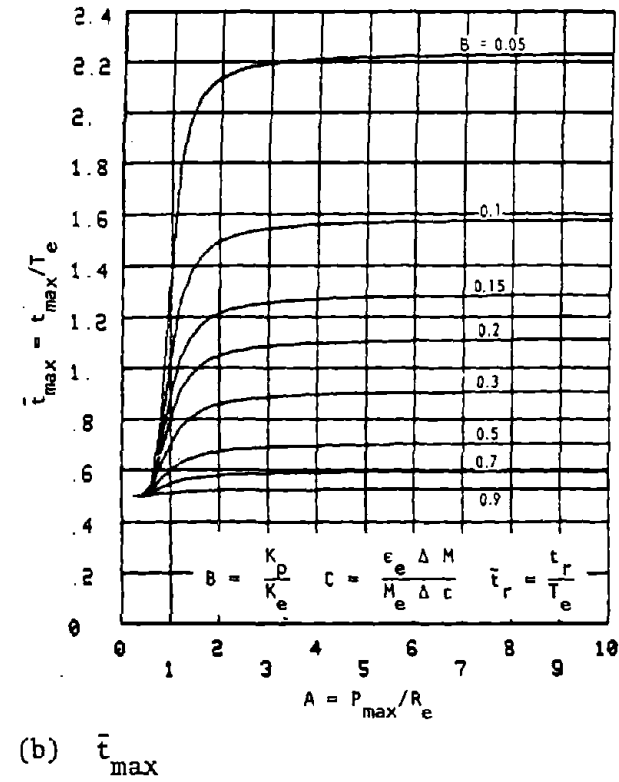
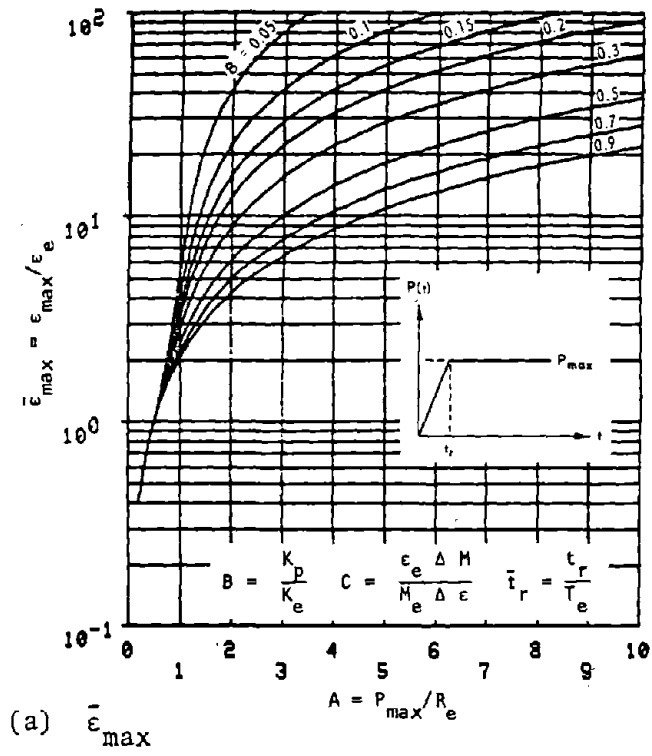
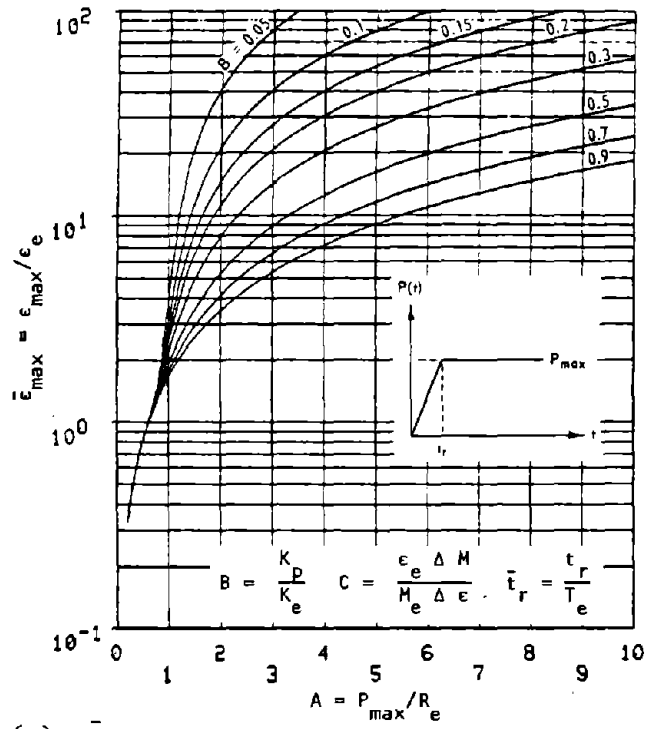
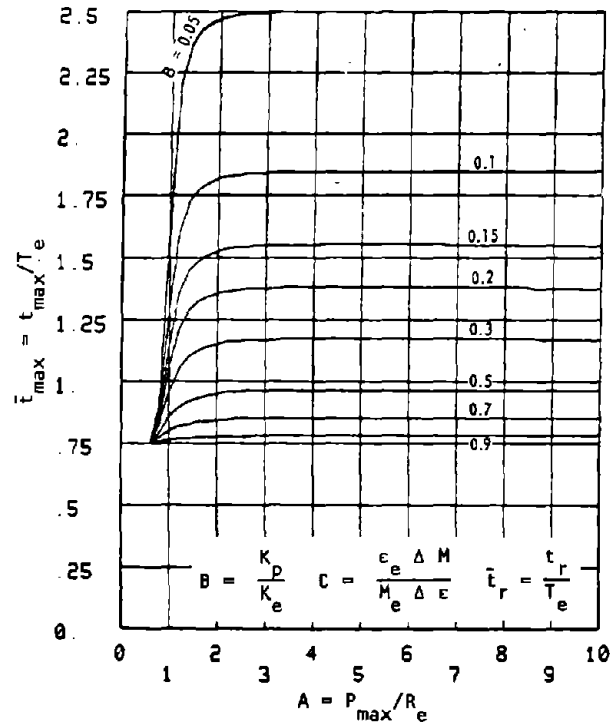


Figure 12-7. Curves for Tunnel-Liner Systems, $C = 0$ and $\bar{t}_r = 0$ (Britt, 1977)

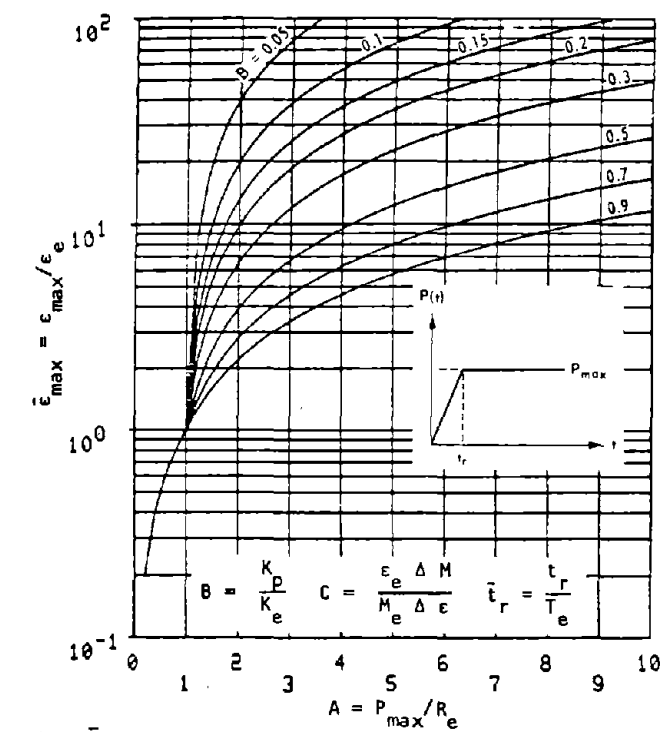


(a) $\bar{\epsilon}_{max}$

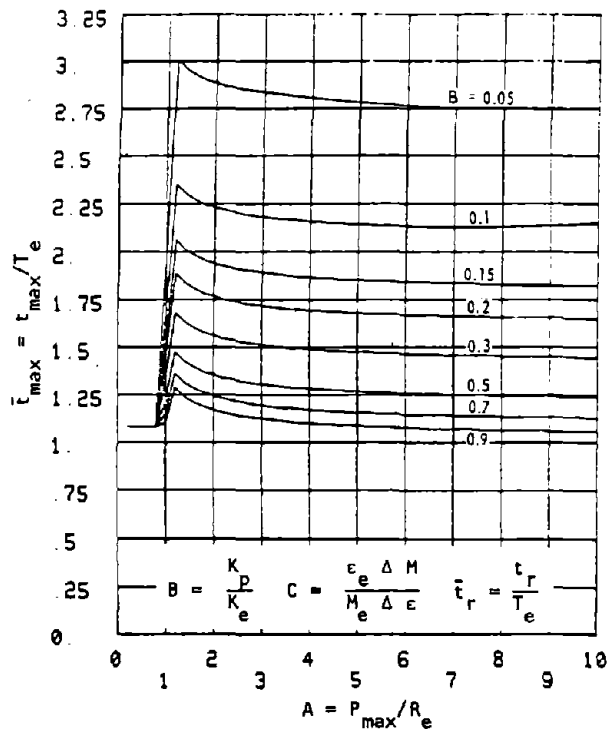


(b) \bar{t}_{max}

Figure 12-8. Curves for Tunnel-Liner Systems, $C = 0$ and $\bar{t}_r = 0.5$ (Britt, 1977)



(a) $\bar{\epsilon}_{max}$



(b) \bar{t}_{max}

Figure 12-9. Curves for Tunnel-Liner Systems, $C = 0$ and $\bar{t}_r = 1$ (Britt, 1977)

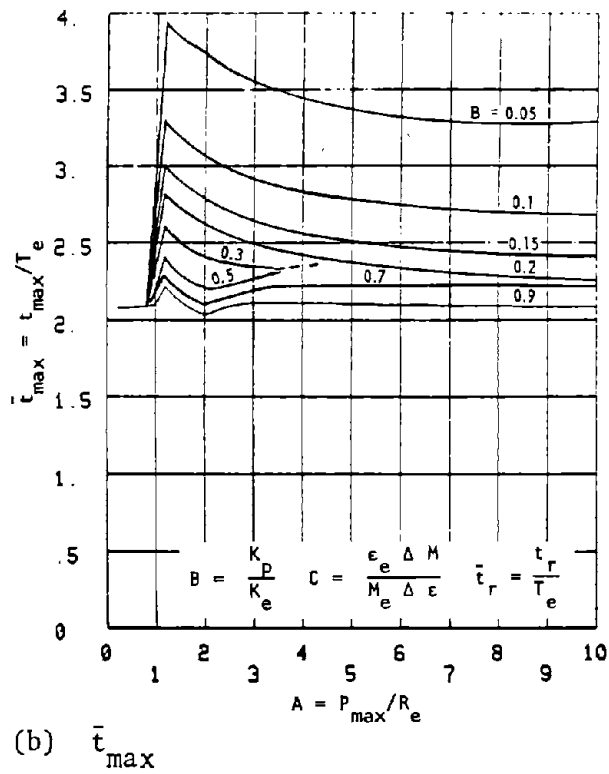
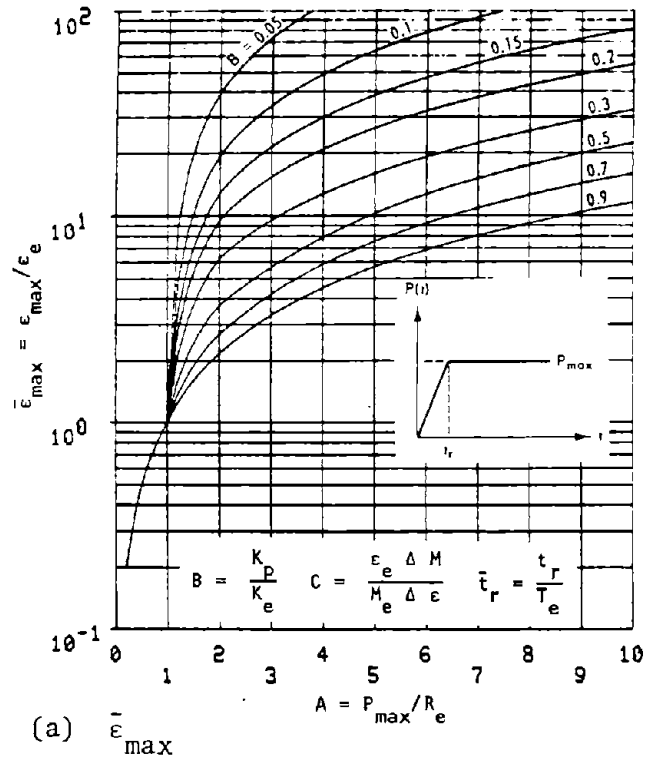


Figure 12-10. Curves for Tunnel-Liner Systems, $C = 0$ and $\bar{t}_r = 2$ (Britt, 1977)

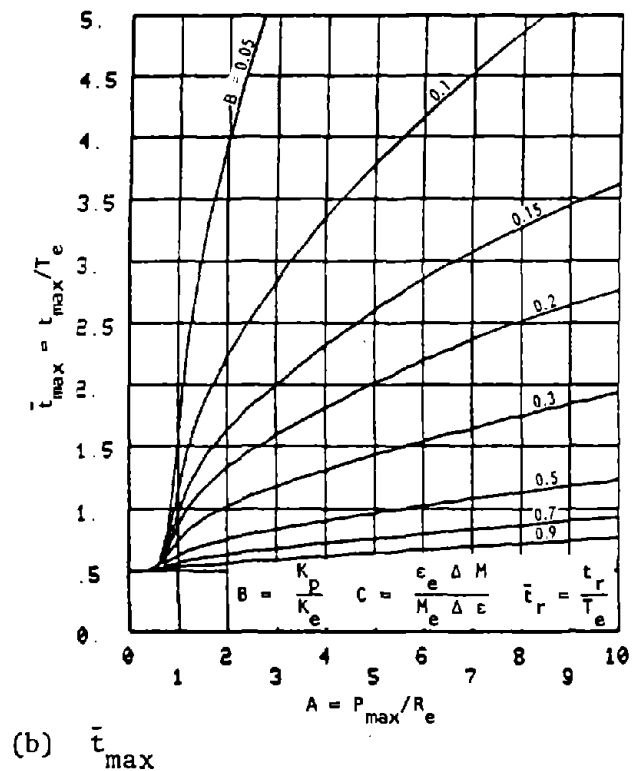
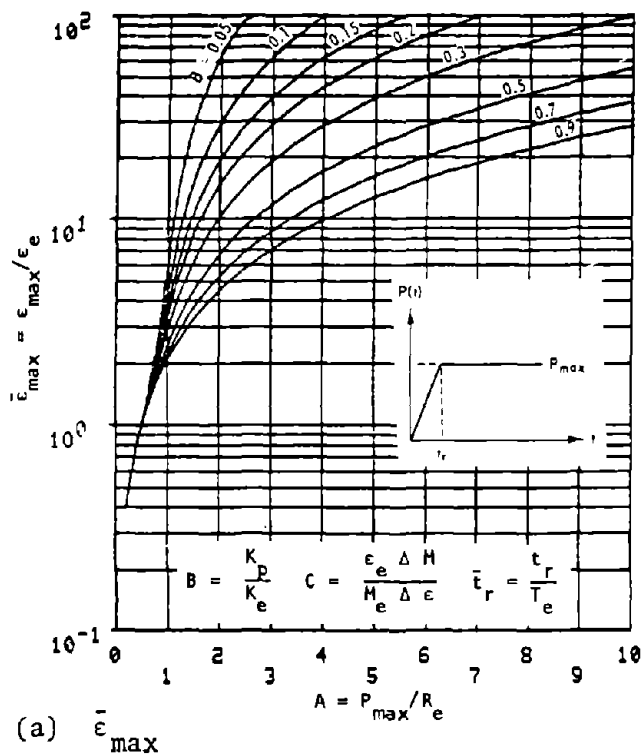
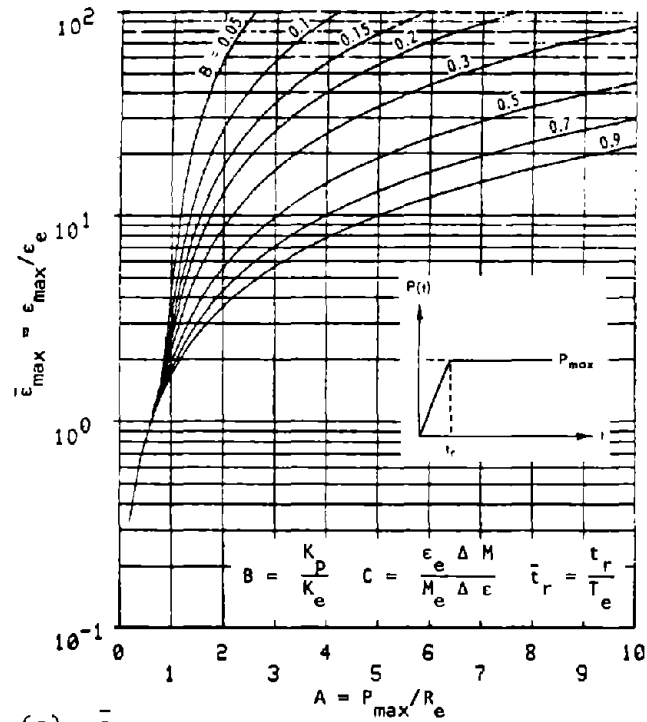
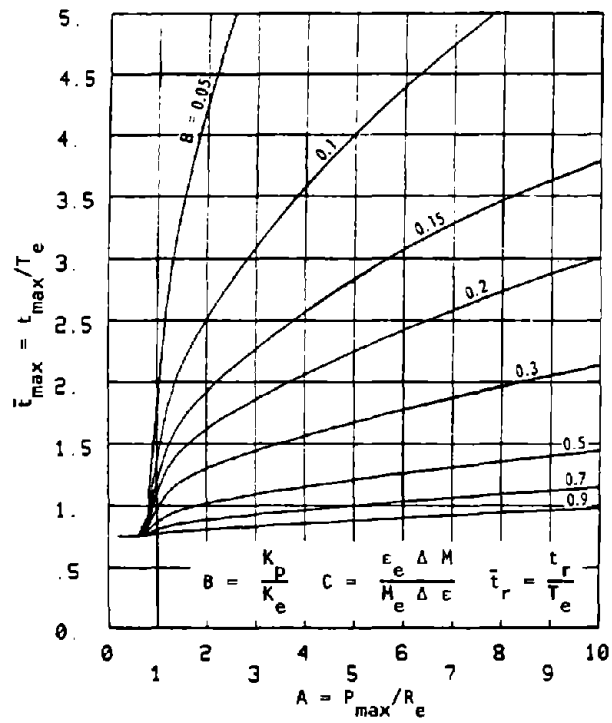


Figure 12-11. Curves for Tunnel-Liner Systems, $C = 0.1$ and $\bar{t}_r = 0$ (Britt, 1977)

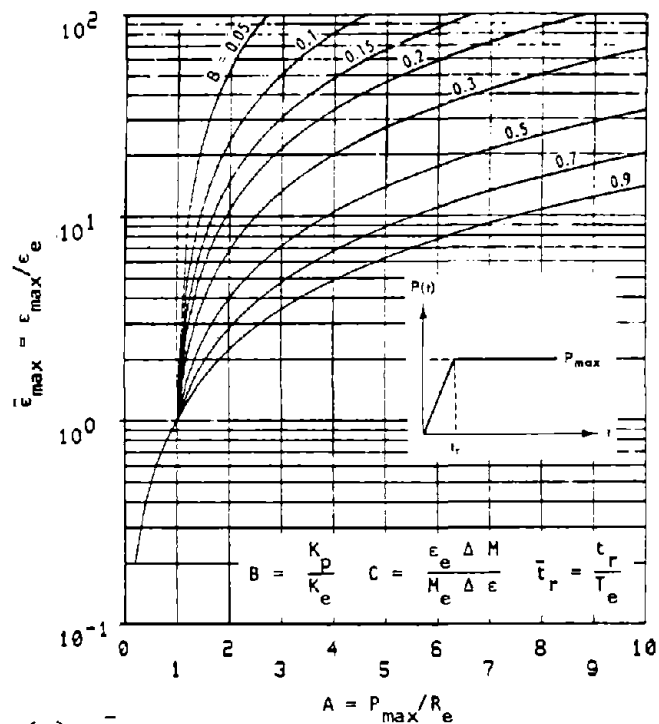


(a) $\bar{\epsilon}_{max}$

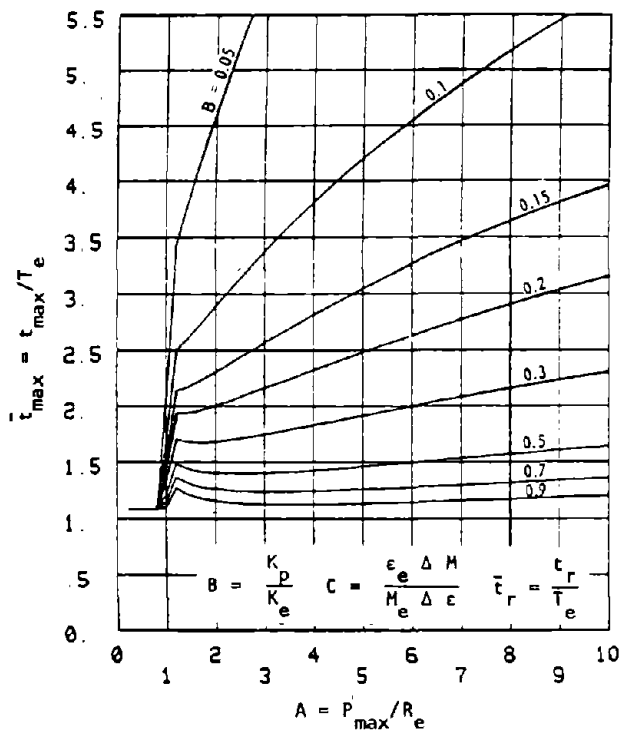


(b) \bar{t}_{max}

Figure 12-12. Curves for Tunnel-Liner Systems, $C = 0.1$ and $\bar{t}_r = 0.5$ (Britt, 1977)



(a) $\bar{\epsilon}_{max}$



(b) \bar{t}_{max}

Figure 12-13. Curves for Tunnel-Liner Systems, $C = 0.1$ and $\bar{t}_r = 1$ (Britt, 1977)

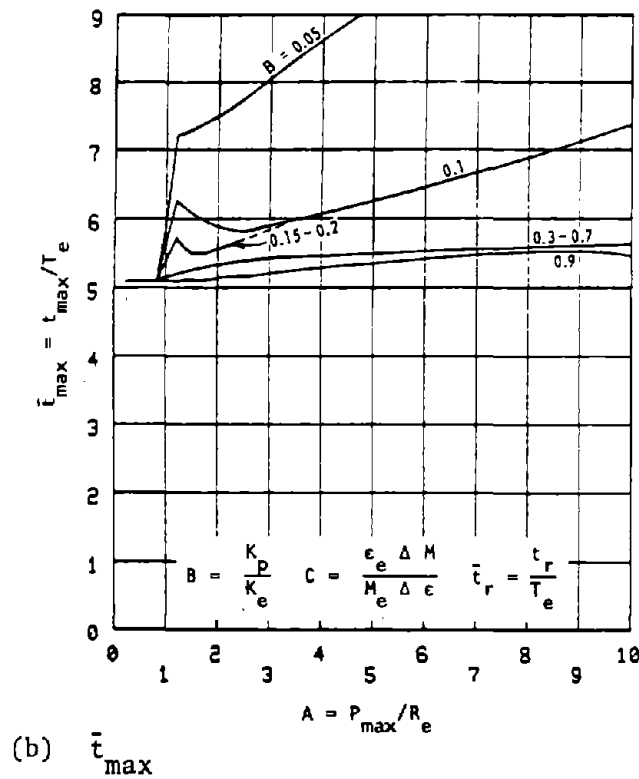
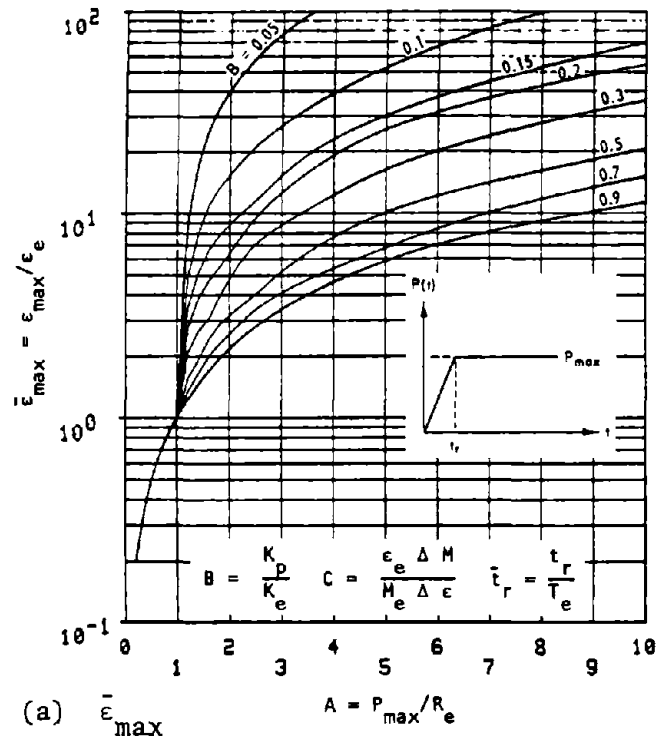
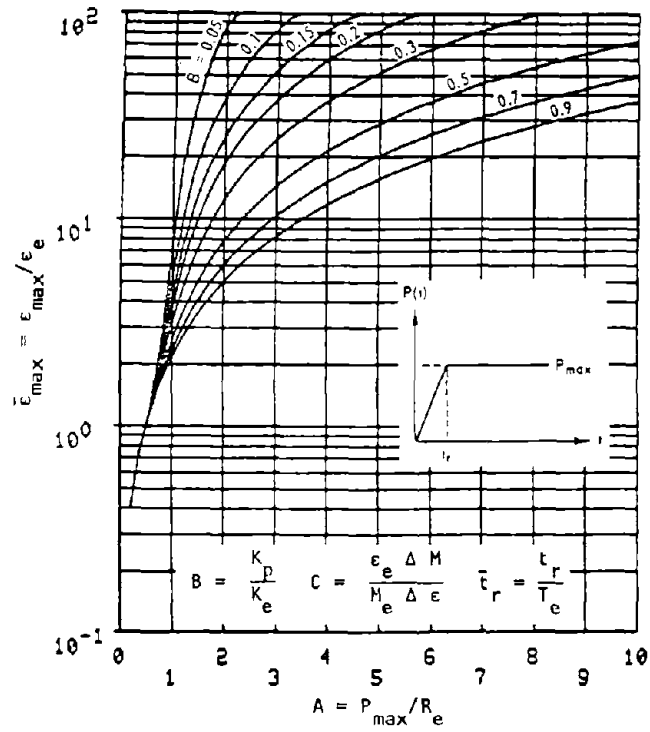
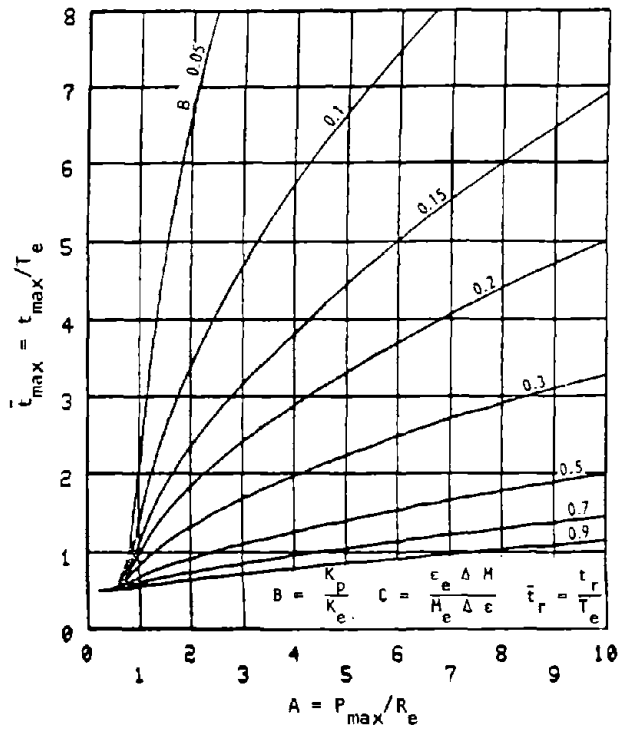


Figure 12-14. Curves for Tunnel-Liner Systems, $C = 0.1$ and $\bar{t}_r = 5$ (Britt, 1977)

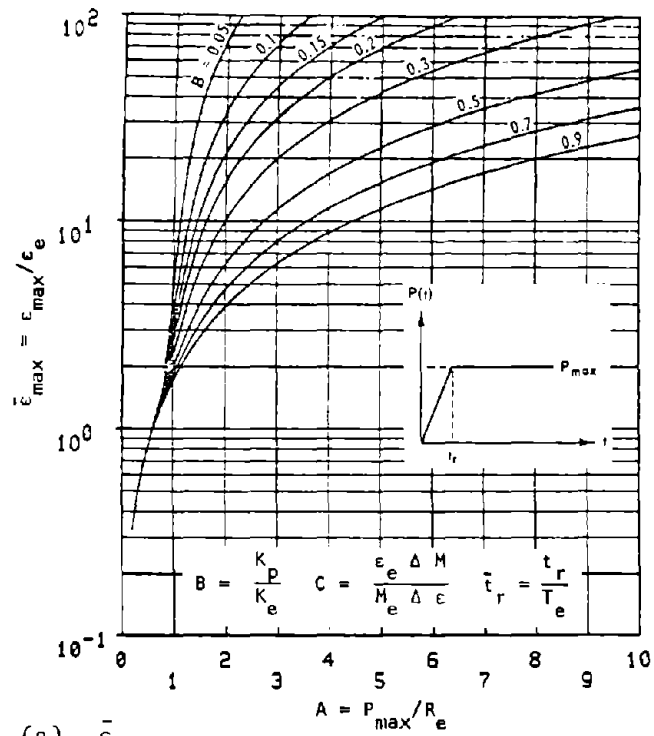


(a) $\bar{\epsilon}_{max}$

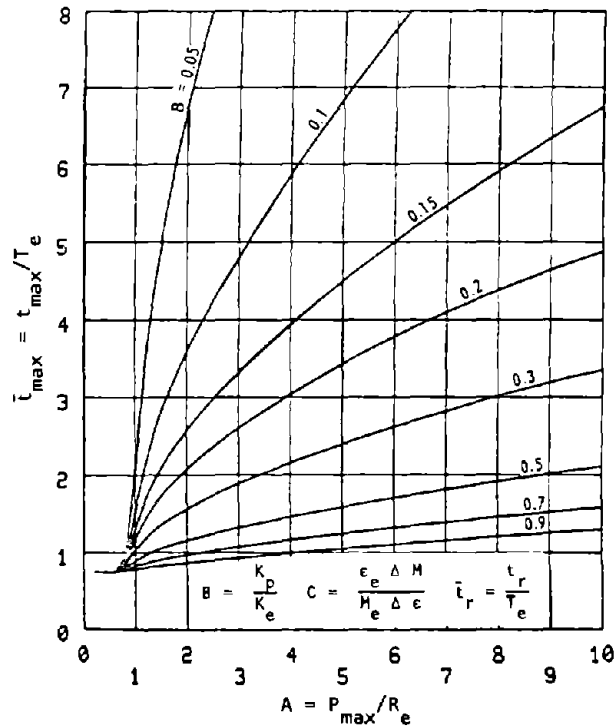


(b) \bar{t}_{max}

Figure 12-15. Curves for Tunnel-Liner Systems, $C = 0.3$ and $\bar{t}_r = 0$ (Britt, 1977)

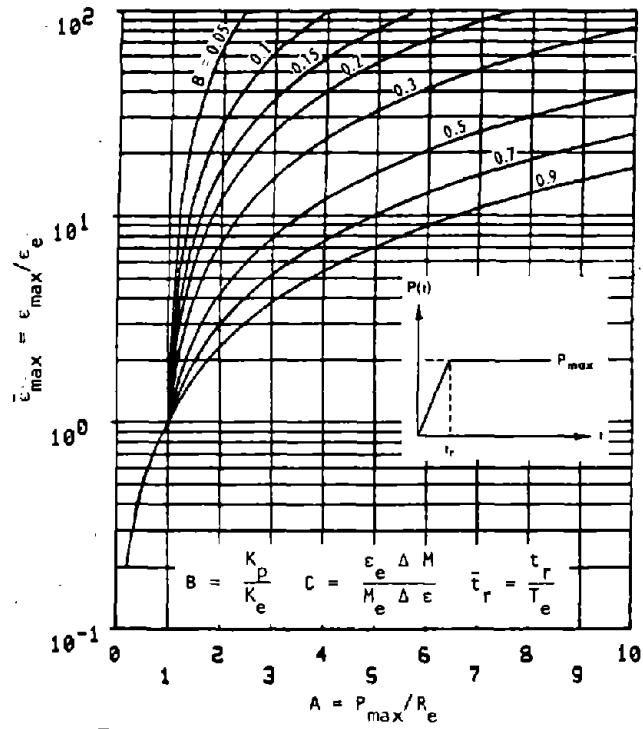


(a) $\bar{\epsilon}_{max}$

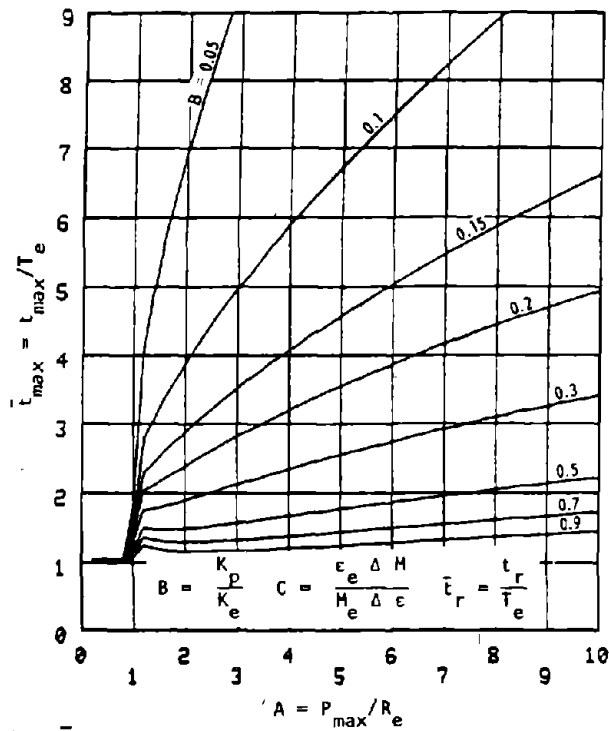


(b) \bar{t}_{max}

Figure 12-16. Curves for Tunnel-Liner Systems, $C = 0.3$ and $\bar{t}_r = 0.5$ (Britt, 1977)

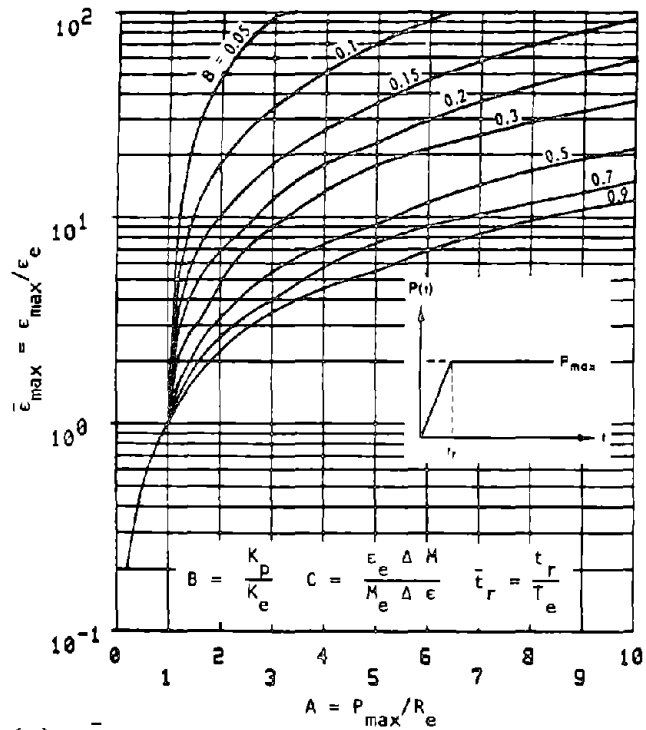


(a) $\bar{\epsilon}_{max}$

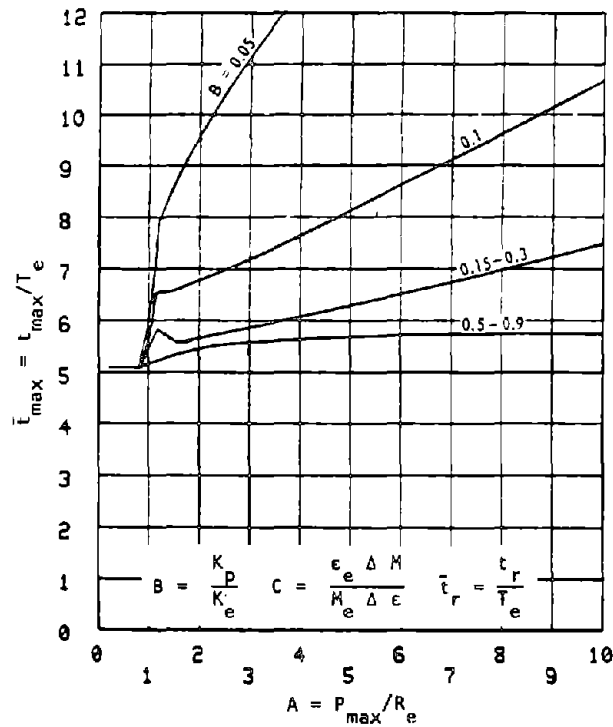


(b) \bar{t}_{max}

Figure 12-17. Curves for Tunnel-Liner Systems, $C = 0.3$ and $\bar{t}_r = 1$ (Britt, 1977)

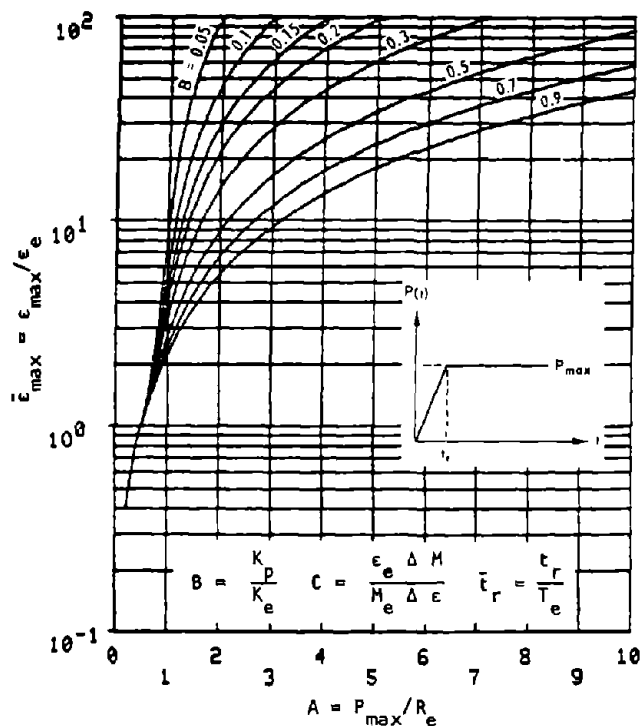


(a) $\bar{\epsilon}_{max}$

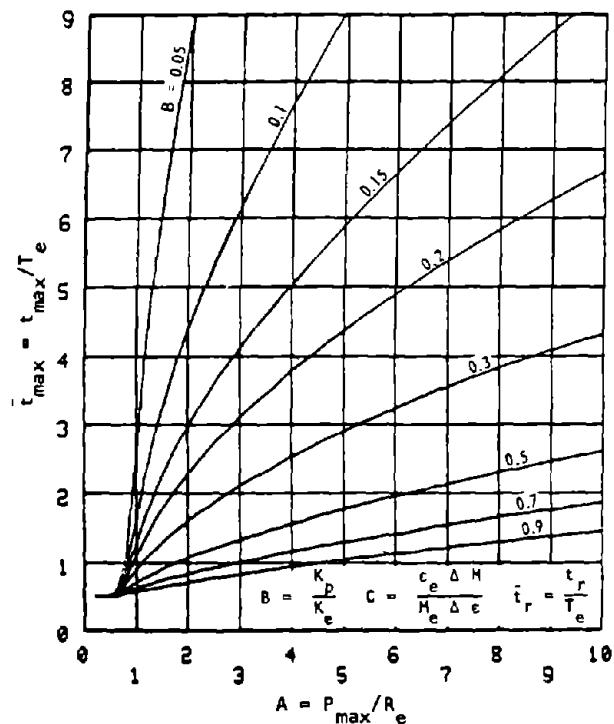


(b) \bar{t}_{max}

Figure 12-18. Curves for Tunnel-Liner Systems, $C = 0.3$ and $\bar{t}_r = 5$ (Britt, 1977)

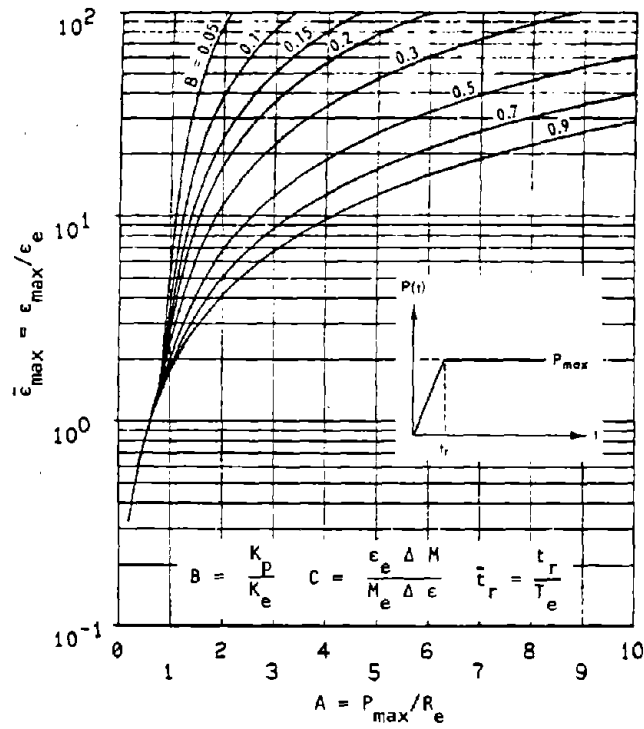


(a) $\bar{\epsilon}_{max}$

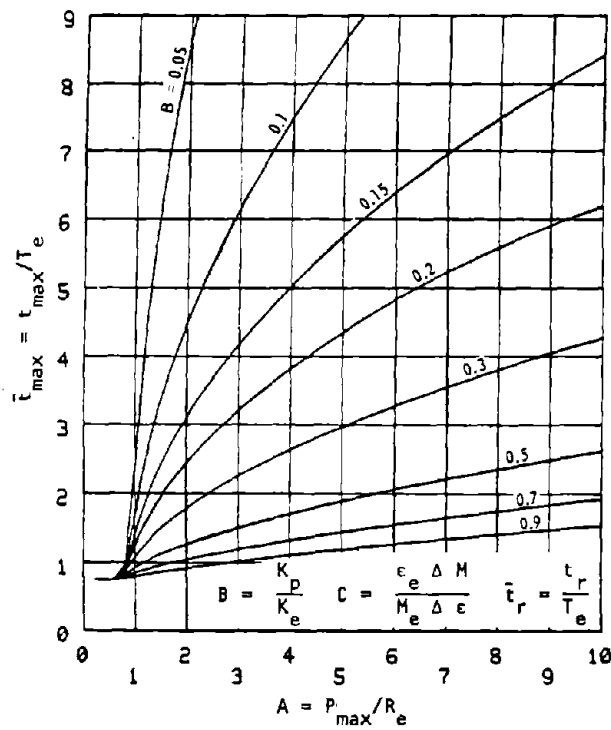


(b) \bar{t}_{max}

Figure 12-19. Curves for Tunnel-Liner Systems, $C = 0.5$ and $\bar{t}_r = 0$ (Britt, 1977)

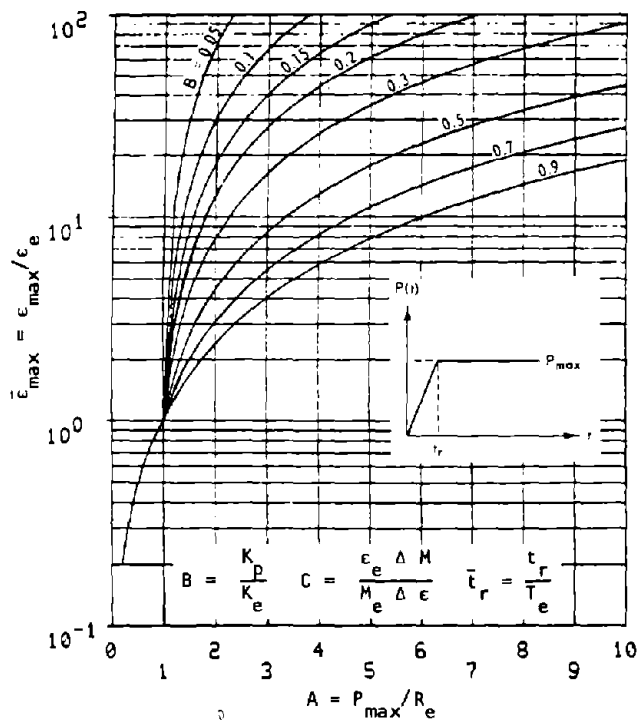


(a) $\bar{\epsilon}_{max}$

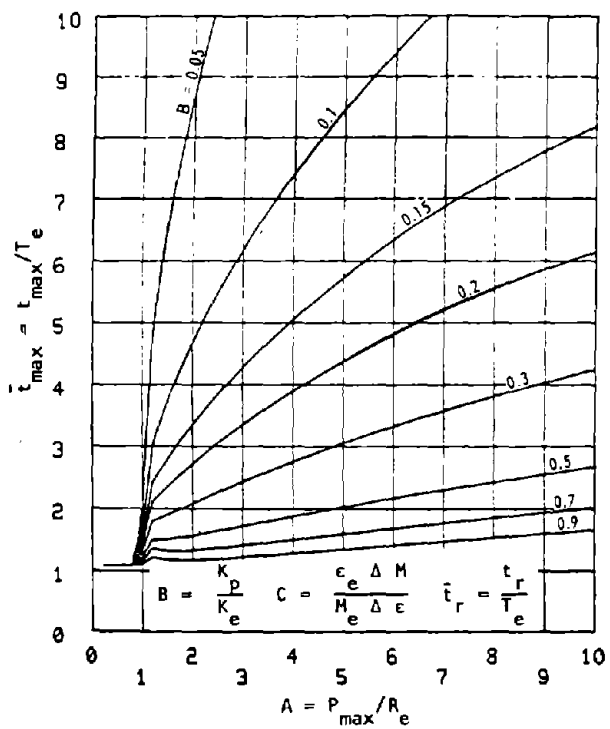


(b) \bar{t}_{max}

Figure 12-20. Curves for Tunnel-Liner Systems, $C = 0.5$ and $\bar{t}_r = 0.5$ (Britt, 1977)

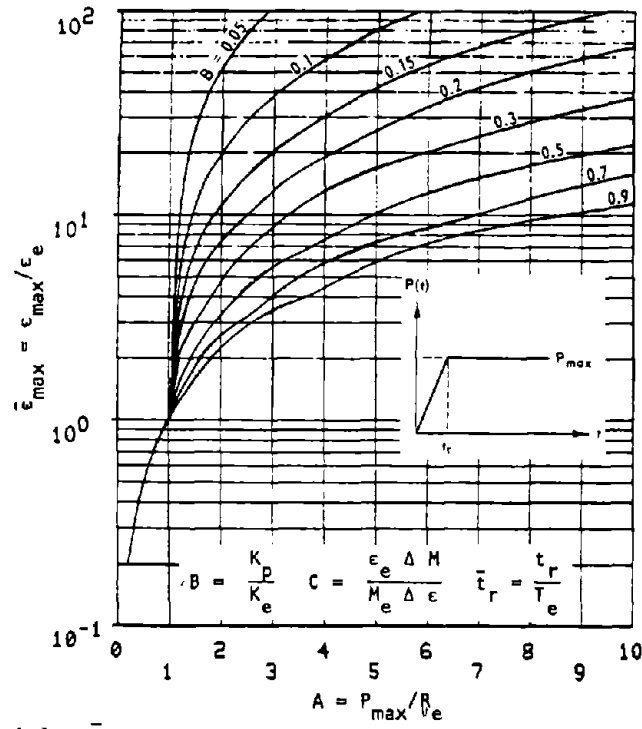


(a) $\bar{\epsilon}_{\max}$

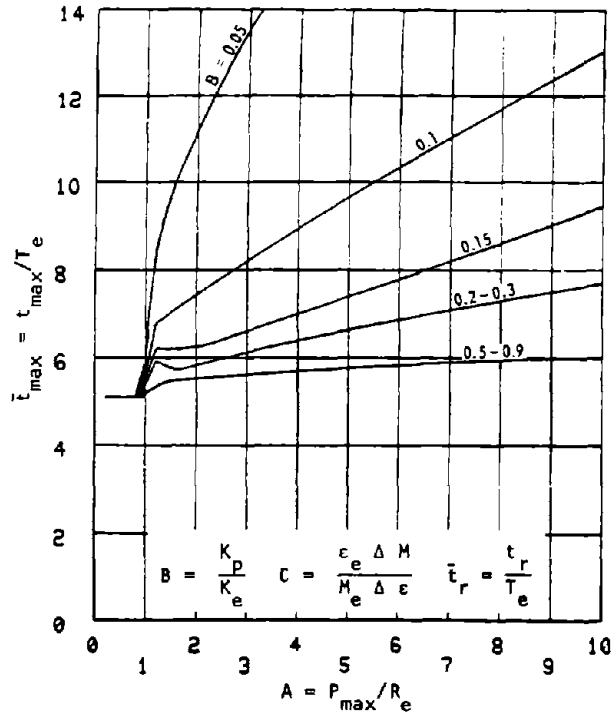


(b) \bar{t}_{\max}

Figure 12-21. Curves for Tunnel-Liner Systems, $C = 0.5$ and $\bar{t}_r = 1$ (Britt, 1977)

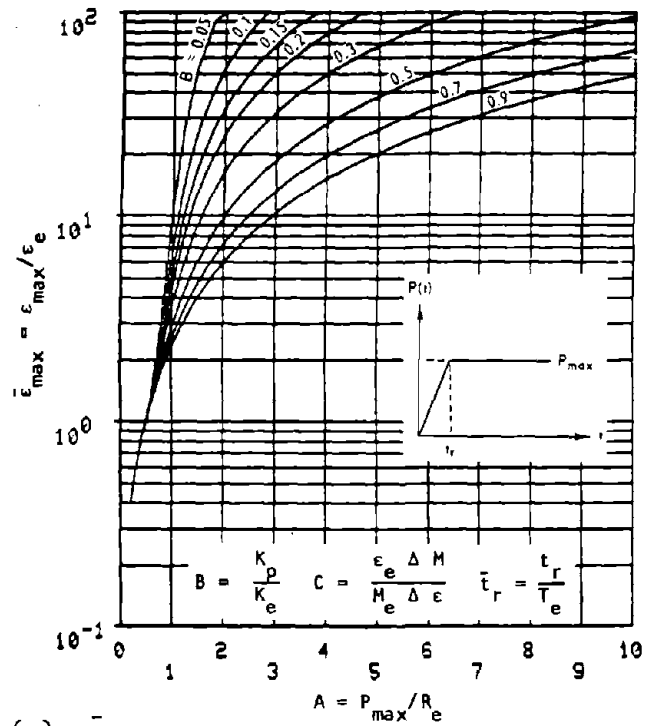


(a) $\bar{\epsilon}_{\max}$

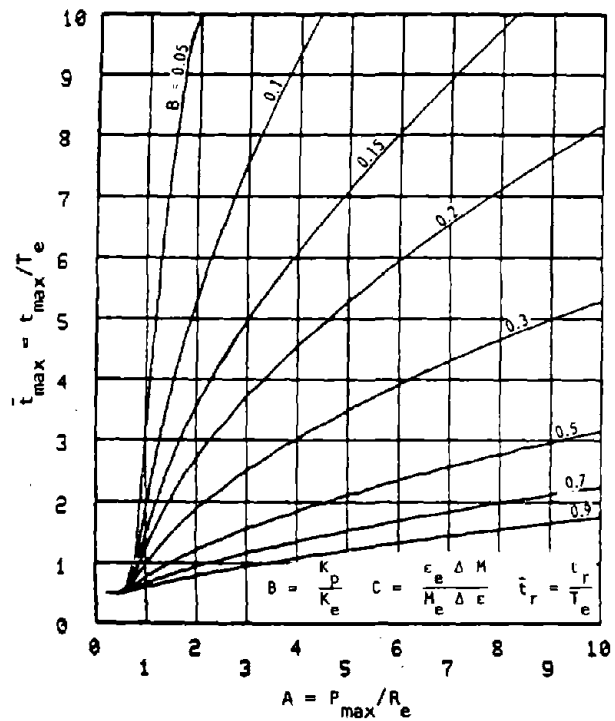


(b) \bar{t}_{\max}

Figure 12-22. Curves for Tunnel-Liner Systems, $C = 0.5$ and $\bar{t}_r = 5$ (Britt, 1977)

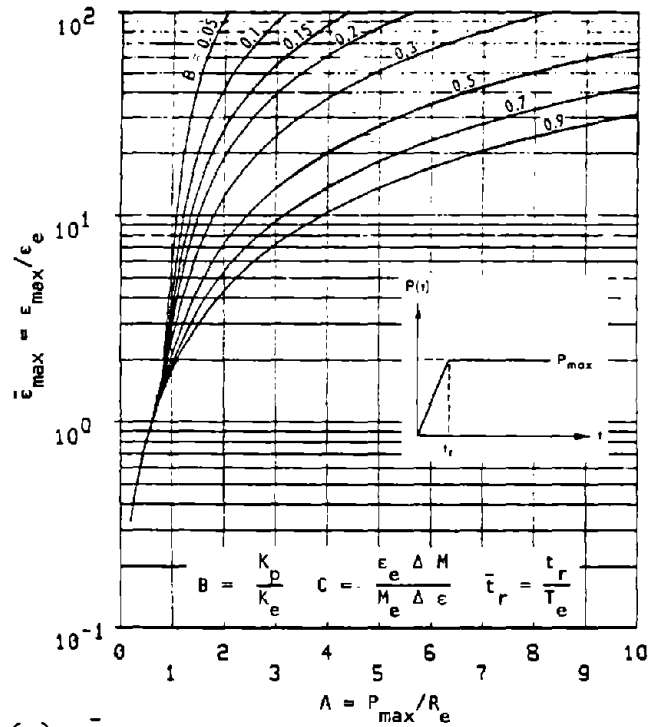


(a) $\bar{\epsilon}_{max}$

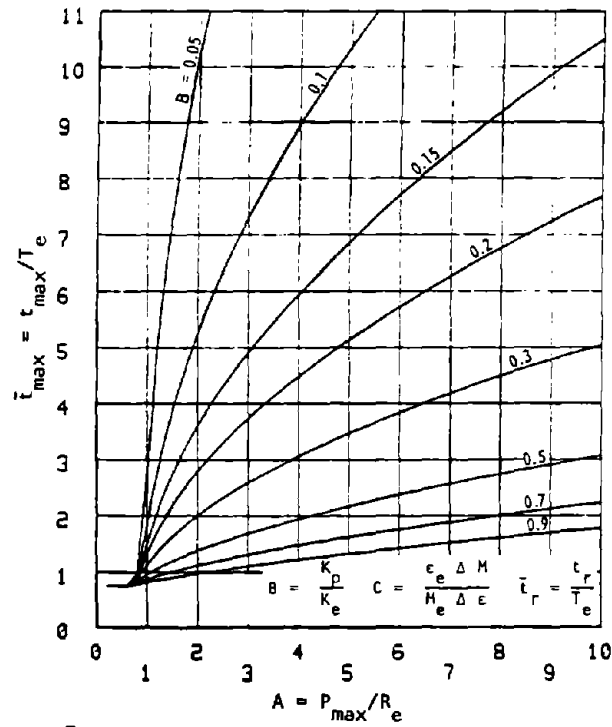


(b) \bar{t}_{max}

Figure 12-23. Curves for Tunnel-Liner Systems, $C = 0.7$ and $\bar{t}_r = 0$ (Britt, 1977)

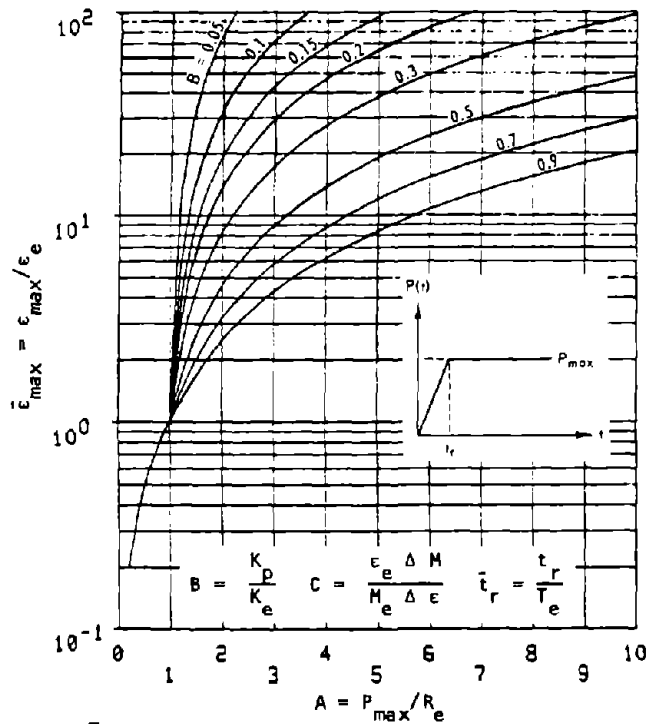


(a) $\bar{\epsilon}_{max}$

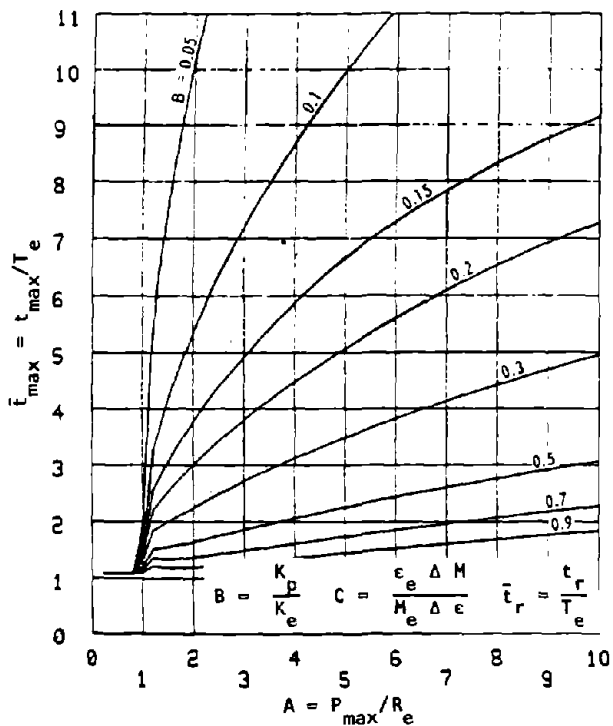


(b) \bar{t}_{max}

Figure 12-24. Curves for Tunnel-Liner Systems, $C = 0.7$ and $\bar{t}_r = 0.5$ (Britt, 1977)

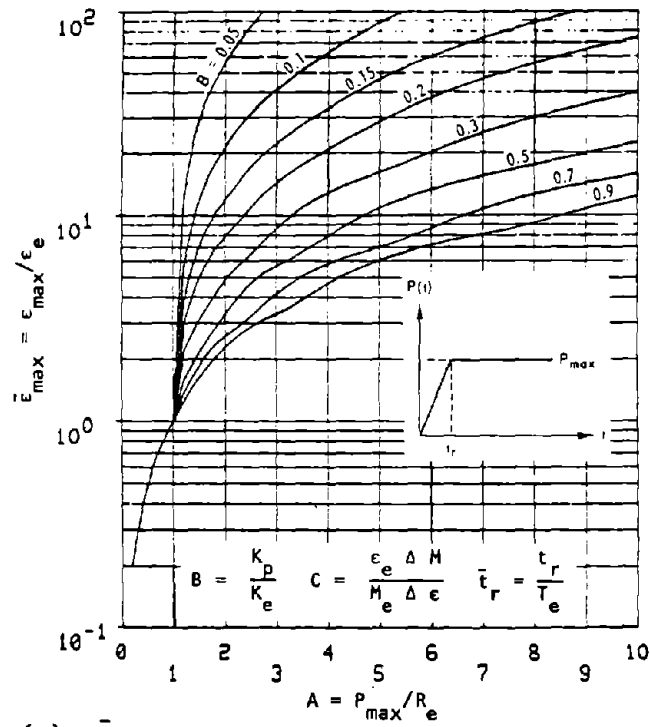


(a) $\bar{\epsilon}_{max}$

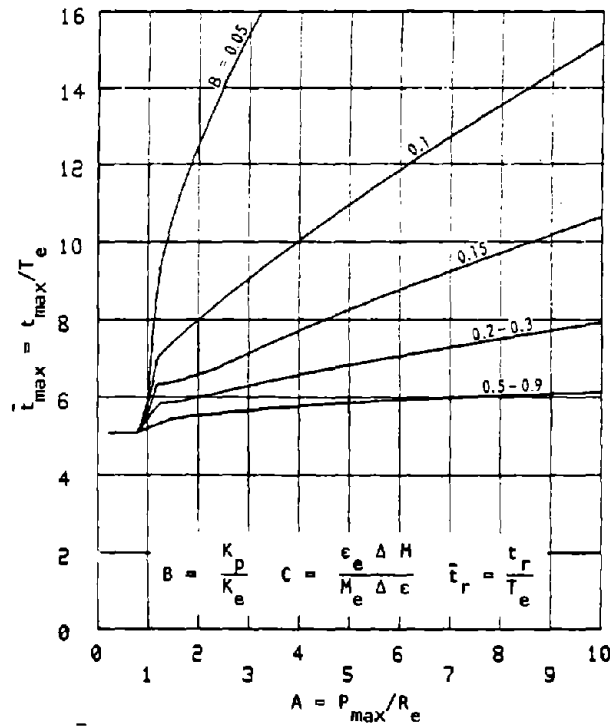


(b) \bar{t}_{max}

Figure 12-25. Curves for Tunnel-Liner Systems, $C = 0.7$ and $\bar{t}_r = 1$ (Britt, 1977)

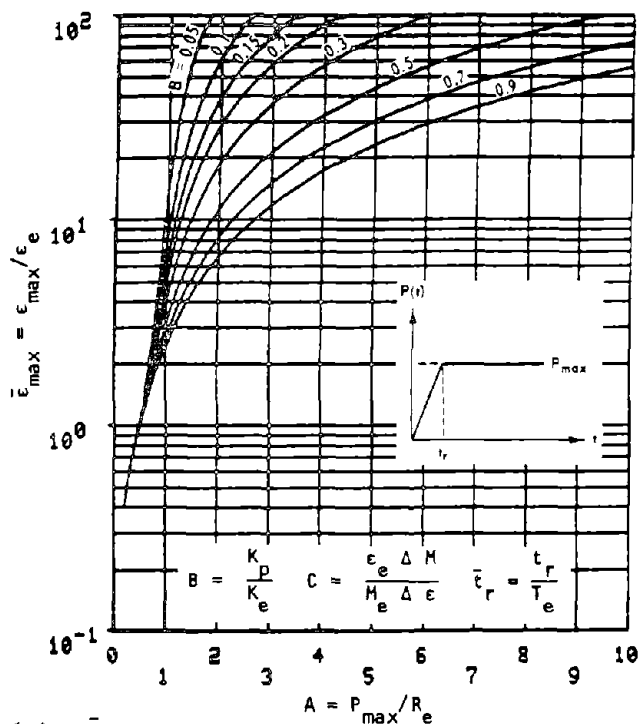


(a) $\bar{\epsilon}_{max}$

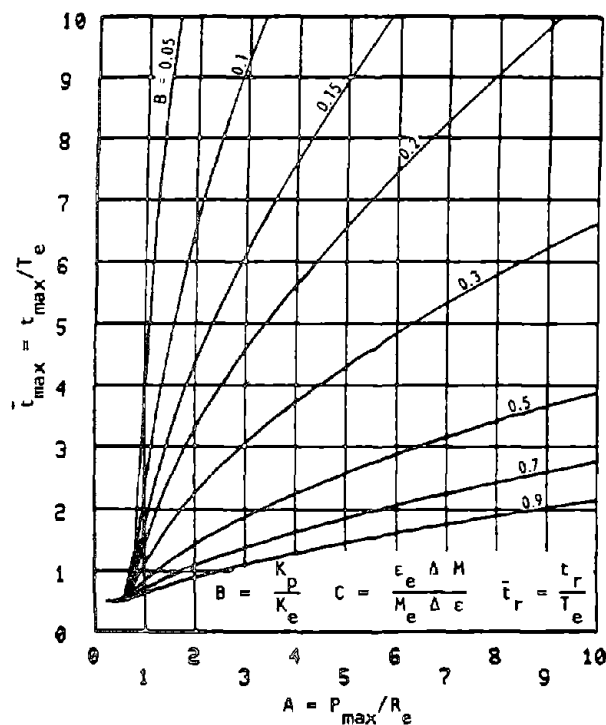


(b) \bar{t}_{max}

Figure 12-26. Curves for Tunnel-Liner Systems, $C = 0.7$ and $\bar{t}_r = 5$ (Britt, 1977)

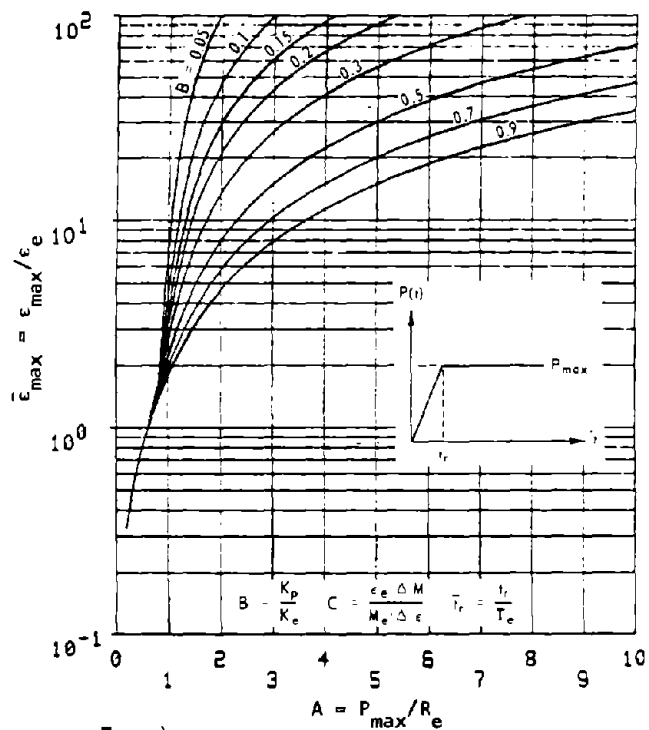


(a) $\bar{\epsilon}_{max}$

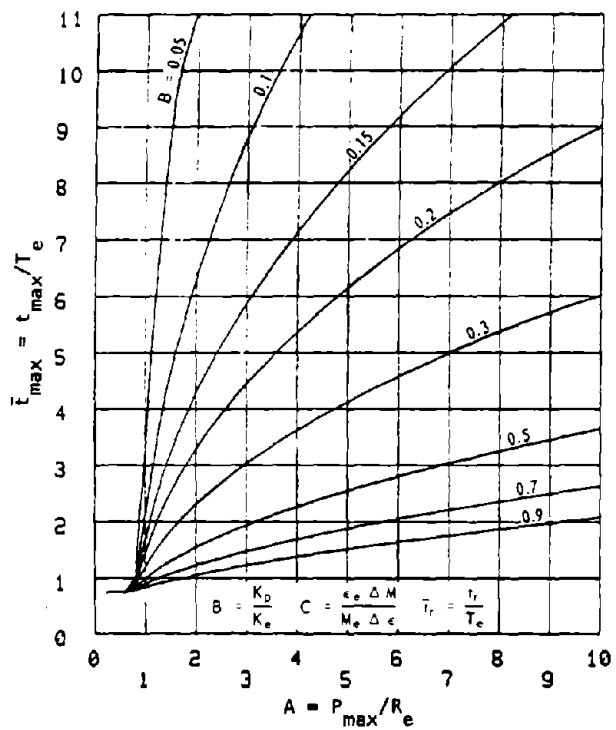


(b) \bar{t}_{max}

Figure 12-27. Curves for Tunnel-Liner Systems, $C = 1$ and $\bar{t}_r = 0$ (Britt, 1977)



(a) $\bar{\epsilon}_{max}$



(b) \bar{t}_{max}

Figure 12-28. Curves for Tunnel-Liner Systems, $C = 1$ and $\bar{t}_r = 0.5$ (Britt, 1977)

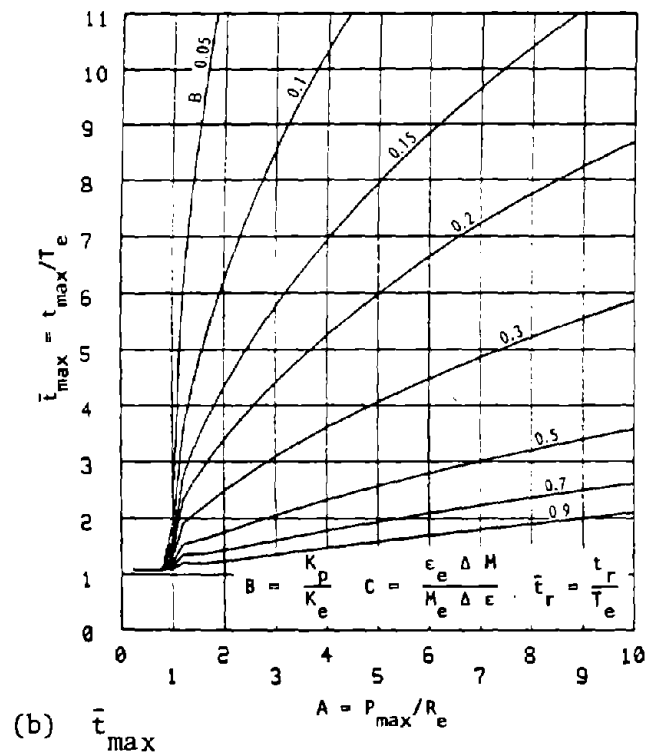
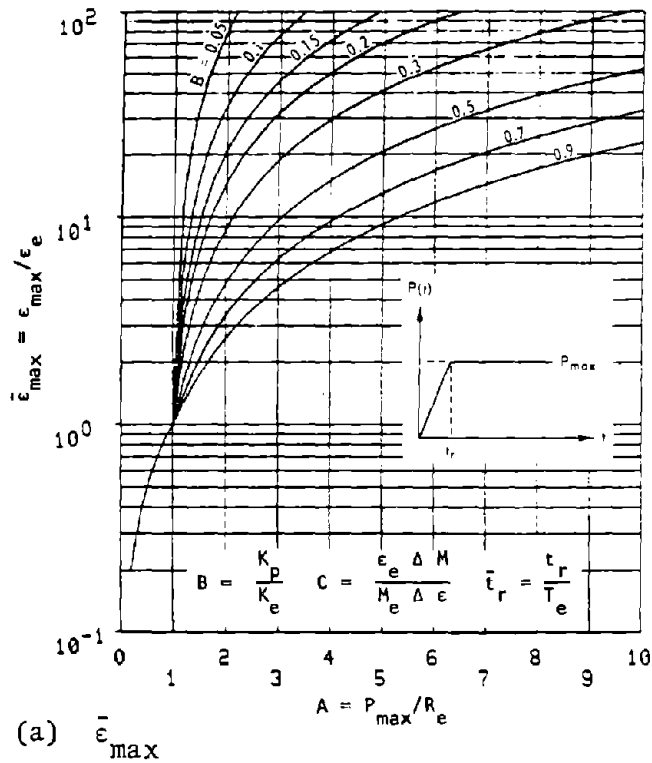


Figure 12-29. Curves for Tunnel-Liner Systems, $C = 1$ and $\bar{t}_r = 1$ (Britt, 1977)

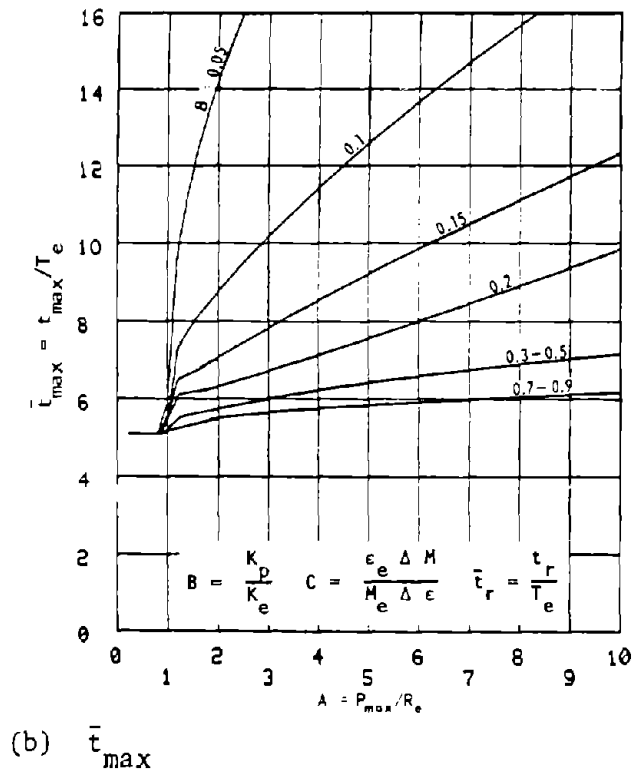
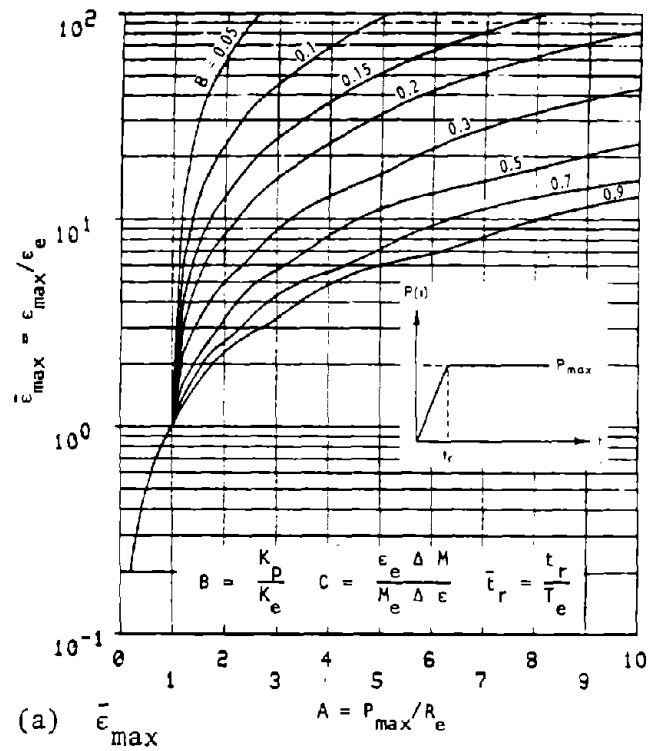


Figure 12-30. Curves for Tunnel-Liner Systems, $C = 1$ and $\bar{t}_r = 5$ (Britt, 1977)

c. *Applications and limitations of the design charts.* The design charts are applicable to the preliminary design of cylindrical lined tunnels in rock subjected to the long-duration ground-shock loadings produced by nuclear weapons. The theoretical model consists of multilayered concentric cylinders of elastoplastic materials with a time-dependent, axially symmetric load representing the free-field stress applied to the exterior boundary. Each element in the cross-section is assumed incompressible and its yield governed by a Mohr-Coulomb failure criterion. A first-order correction factor is given to account for compressibility of the materials.

(1) The following conditions should be approximated before using the design charts:

- The structure is composed of concentric cylinders of circular cross section as shown in figure 12-5.
- The yielding of the structure and surrounding rock is governed by the Mohr-Coulomb failure criterion.
- The expected deformation (especially compaction) of liner and rock is small.
- The ultimate loading of the structure is nearly axisymmetric.
- The duration of the loading is at least 5 to 10 times the response and engulfment times of the structure.

(2) For example, use of the charts appears to be appropriate for design of cylindrical tunnels with concrete and steel liners sited in hard rock such as granite. But the charts will provide only a conservative lower bound estimate of the response of structures located in weak, highly compactible rocks such as tuff.

d. *Problem formulation.* Solutions of the theoretical model are cast in the form normally used in structural dynamics:

$$M \frac{d^2\epsilon}{dt^2} = P(t) - R(\epsilon) \tag{12-12}$$

where

- M = Effective mass (mass/length)
- ϵ = Diametrical strain (positive inward)
- t = Time
- P(t) = External load (positive in compression)
- R(ϵ) = Internal load-resistance

Definitions of the effective mass and load-resistance functions are given in the next paragraph.

e. *Application of the analysis to obtain design charts.* For the purposes of design charts, the equation of motion (eq. 12-12) and its solutions are put into a dimensionless form. The effective resistance and mass are approximated with bilinear functions of normalized strain. Further, since the time t_{max} at which the maximum strain ϵ_{max} occurs for most prac-

tical hardened tunnel-liner structures subjected to nuclear ground shock is small compared with the duration of the loading pulse or free-field stress, P(t) is adequately approximated by a ramp fronted step load with rise time t_r , as shown in figure 12-5. This load is a good approximation in most cases if the duration of the triangular pulse describing the ground shock stress is 5 to 10 times t_{max} . The equation of motion (eq. 12-12) is put into dimensionless form using the following elastic parameters:

- ϵ_e = Elastic limit or maximum elastic strain
- K_e = Effective elastic stiffness
- R_e = $K_e \epsilon_e$ = Maximum elastic resistance
- M_e = Effective mass (mass/length) in elastic deformation
- $T_e = 2\pi \sqrt{\frac{M_e}{K_e}}$ = Effective elastic period

The dimensionless variables are then

$$\bar{\epsilon} = \frac{\epsilon}{\epsilon_e} \tag{12-13}$$

$$\bar{t} = \frac{t}{T_e} \tag{12-14}$$

$$\bar{t}_r = \frac{t_r}{T_e} \tag{12-15}$$

$$A = \frac{P_{max}}{R_e} \tag{12-16}$$

$$\bar{R}(\bar{\epsilon}) = \frac{R(\epsilon)}{R_e} \tag{12-17}$$

$$\bar{M}(\bar{\epsilon}) = \frac{M}{M_e} \tag{12-18}$$

where P_{max} is the peak value of P(t). Equation 12-12 becomes

$$\frac{\bar{M}(\bar{\epsilon})}{(2\pi)^2} \frac{d^2\bar{\epsilon}}{d\bar{t}^2} = \begin{cases} A\bar{t}/\bar{t}_r - \bar{R}(\bar{\epsilon}) & \text{for } 0 \leq \bar{t} < \bar{t}_r \\ A - \bar{R}(\bar{\epsilon}) & \text{for } \bar{t} \geq \bar{t}_r \end{cases} \tag{12-19}$$

where $\bar{R}(\bar{\epsilon})$ and $\bar{M}(\bar{\epsilon})$ are expressed as the bilinear functions

$$\bar{R}(\bar{\epsilon}) = \begin{cases} \bar{\epsilon} & \text{for } \bar{\epsilon} \leq 1 \\ 1 + B(\bar{\epsilon} - 1) & \text{for } \bar{\epsilon} > 1 \end{cases} \tag{12-20}$$

$$\bar{M}(\bar{\epsilon}) = \begin{cases} 1 & \text{for } \bar{\epsilon} \leq 1 \\ 1 - C(\bar{\epsilon} - 1) & \text{for } \bar{\epsilon} > 1 \end{cases} \tag{12-21}$$

and

$$B = \frac{K_p}{K_e} \quad (12-22)$$

$$K_p = \frac{\Delta R}{\Delta \epsilon} \text{ for } \epsilon > \epsilon_e \text{ (i.e., } \bar{\epsilon} > 1) \quad (12-23)$$

$$C = \frac{\epsilon_e}{M_e} \frac{\Delta M}{\Delta \epsilon} \text{ for } \epsilon > \epsilon_e \text{ (i.e., } \bar{\epsilon} > 1) \quad (12-24)$$

Examples of bilinear fits to $R(\epsilon)$ and $M(\epsilon)$ curves are shown in figure 12-6. The 1-lines are better approximations for $\epsilon < 2$ percent, but the 2-lines would be used if strains up to 4 or 5 percent were of interest. The charts, figures 12-7 to 12-30, summarize the maximum values of the normalized strain $\bar{\epsilon}_{\max} = \epsilon_{\max}/\epsilon_e$, and dimensionless time $\bar{t}_{\max} = t_{\max}/T_e$, at which $\bar{\epsilon}_{\max}$ occurs for the parameters A, B, and C. Note that A is a measure of the magnitude of the applied load or free-field stress, B is a measure of the stiffness of the rock-liner structure in plastic deformation, and C is a measure of the change in effective mass or density as the structure yields. The determination of B and C and the elastic normalizing parameters from material properties is discussed in the next paragraph.

f. Determining chart parameters from material properties. The geometry of the rock-liner system is shown in figure 12-5. The number of concentric material layers of the system is denoted by m . Generally, the liner is represented by $m-1$ layers and the rock by the single m th layer. Each material denoted by the subscript i is described by the properties density ρ_i , shear modulus G_i , cohesion q_i , the angle of internal friction ϕ_i , and Poisson's ratio ν_i . In some cases the unconfined compressive strength σ_u may be known instead of q . These parameters are related by

$$q = \sigma_u \frac{1 - \sin \phi}{2 \cos \phi} \quad (12-25)$$

Also, Young's modulus E is often given rather than G . Values of G are obtained from E and ν using

$$G = \frac{E}{2(1 + \nu)} \quad (12-26)$$

In Drake and Britt's model (1976) each material layer yields from its inner boundary r_i outward. When a material layer is partially plastic and partially elastic, the radius r_{pi} denotes the boundary between the interior plastic region and the exterior elastic region. These boundaries are denoted by dashed lines in figure 12-5. A material layer is entirely elastic when $r_{pi} = r_i$. The layer is completely plastic when $r_{pi} = r_{i+1}$ which is the outer boundary of the layer.

The effective resistance and mass functions $R(\epsilon)$ and $M(\epsilon)$ can be determined when the values of r_{pi} are known. Drake and Britt give a relation for r_{pi} involving acceleration or inertial terms. If the design level of maximum diametrical strain is not much larger than about 2 to 5 percent, the inertial terms in r_{pi} can be neglected. A relatively simple equation for r_{pi}/r_i as a function of diametrical strain ϵ at the interior $r = r_i$ of the liner is

$$\frac{r_{pi}}{r_i} = \left[\frac{4G_i \epsilon \left(\frac{r_1}{r_i}\right)^2}{n_i (Y_{i-1} + K_{i-1} \epsilon) + 2q_i \sqrt{n_i + 1}} \right]^{1/(n_i + 2)} \quad (12-27)$$

where

$$n_i = \frac{2 \sin \phi_i}{1 - \sin \phi_i} \quad (12-28)$$

the effective plastic resistance of layer i is

$$Y_i = Y_{i-1} \left(\frac{r_{pi}}{r_i}\right)^{n_i} + \frac{2q_i \sqrt{n_i + 1}}{n_i} \left[\left(\frac{r_{pi}}{r_i}\right)^{n_i} - 1 \right] \quad (12-29)$$

and the effective elastic stiffness is

$$K_i = K_{i-1} \left(\frac{r_{pi}}{r_i}\right)^{n_i} + 2G_i \left(\frac{r_1}{r_i}\right)^2 \left[1 - \left(\frac{r_i}{r_{pi}}\right)^2 \right] \quad (12-30)$$

where $Y_0 = 0$ and $K_0 = 0$. In the case $n_i = 0$, (or $\phi_i = 0$),

$$\lim_{n_i \rightarrow 0} \frac{1}{n_i} \left[\left(\frac{r_{pi}}{r_i}\right)^{n_i} - 1 \right] = \ln \left(\frac{r_{pi}}{r_i}\right) \quad (12-31)$$

Whenever equation 12-27 gives a value of r_{pi}/r_i greater than r_{i+1}/r_i , the layer is completely plastic and $r_{pi}/r_i = r_{i+1}/r_i$ must be used. To calculate r_{pi}/r_i , begin at $i = 1$, the inside boundary of the liner. In this case Y_{i-1} and K_{i-1} are zero. Then with r_{p1}/r_1 known, Y_1 and K_1 can be calculated and hence also r_{p2}/r_2 . Continuing this process out to the rock ($i = m$) surrounding the liner, all the Y_i and K_i can be determined. In the equations for Y_i and K_i , the outside rock boundary r_{m+1} should be taken as ∞ in the case of nuclear ground-shock loading. The total resistance function $R(\epsilon)$ is given by

$$R(\epsilon) = K_m \epsilon + Y_m \quad (12-32)$$

where Y_m is zero if the liner and rock are elastic. The effective mass is obtained from

$$M = r_1^2 \sum_{j=1}^m \left\{ \frac{\rho_j}{n_j} \left[\left(\frac{r_{pj}}{r_j} \right)^{n_j} - 1 \right] \right\}_{k=j+1}^m \left(\frac{r_{pk}}{r_k} \right)^{n_k} + \rho_j \ln \left(\frac{r_{j+1}}{r_{pj}} \right) \quad (12-33)$$

Here we cannot let $r_{m+1} \rightarrow \infty$ since M would be ∞ also. Parametric studies have shown that an appropriate value of r_{m+1} to use in calculating M is $r_{m+1} \approx 3r_m$. Equations 12-32 and 12-33 supply the effective resistance and mass functions needed in determining the parameters B and C of the charts. To obtain B and C from $R(\epsilon)$ and $M(\epsilon)$, the elastic normalizing constant must first be computed from the relations

$$K_e = \sum_{j=1}^m 2G_j \left[\left(\frac{r_1}{r_j} \right)^2 - \left(\frac{r_1}{r_{j+1}} \right)^2 \right] \quad (12-34)$$

where $r_{m+1} \rightarrow \infty$ and $r_1/r_{m+1} \rightarrow 0$.

$$M_e = r_1^2 \sum_{j=1}^m \rho_j \ln \left(\frac{r_{j+1}}{r_j} \right) \quad (12-35)$$

where $r_{m+1} \approx 3r_m$. If the inner layer of the liner fails first, then the elastic limit is

$$\epsilon_e = \frac{q_1 \sqrt{n_1 + 1}}{2G_1} \quad (12-36)$$

Using equations 12-22, 12-24, and 12-27 through 12-36, values of B and C can be calculated. In practice one may not use ϵ_e as given in equation 12-36 but rather must fit "best" bilinear curves to $R(\epsilon)$ and $M(\epsilon)$. In this way effective values of K_e , M_e , ϵ_e , and R_e are obtained. Usually, plotting a few points of the $R(\epsilon)$ and $M(\epsilon)$ curves is adequate to allow one to draw accurate visual fits to the curves. Static resistance-strain curves, $R(\epsilon)$, can also be obtained using the charts of Newmark (1970) and Hendron and Aiyer (1972).

g. A first-order compressibility correction. The equations described above and the charts of $\bar{\epsilon}_{\max}$ and \bar{t}_{\max} (fig. 12-7 through 12-30) are for incompressible media. The first-order correction factor given in Drake and Britt (1976) may be used to approximately account for the compressibility of the liner and surrounding rock. The corrected normalized maximum

strain, $\bar{\epsilon}_{\max}^c$, is related to the incompressible value $\bar{\epsilon}_{\max}$ through

$$\bar{\epsilon}_{\max}^c = 2(1 - \nu)\bar{\epsilon}_{\max} \quad (12-37)$$

where ν is an average of the Poisson's ratios of the liner and rock. For common rock and liner materials, ν ranges from about 0.2 to 0.3 and $2(1 - \nu) = 1.5$ is adequate for most preliminary design calculations.

*h. Example applications of the charts.** To illustrate the use of the design charts, consider the following steel and concrete liner sited in a relatively weak granite. The inner liner is 1.5-in.-thick steel with an inside diameter of 48 in. The steel and the granite are separated by 11 in. of concrete. The radii r_i defined in figure 12-5 are then

$$\begin{aligned} r_1 &= 24 \text{ in. I.D.} \\ r_2 &= 25.5 \text{ in. I.D. plus thickness of steel} \\ r_3 &= 36.5 \text{ in. I.D. plus thickness of steel plus concrete} \end{aligned}$$

For the resistance calculation, take the outside rock radius to be $r_4 = \infty$ so that $1/r_4 = 0$. For the effective mass calculation use $r_4 = 3r_3$. For properties of materials use the quantities listed below.

Steel:

$$\begin{aligned} \rho_1 &= 7.5 \times 10^{-4} \text{ psi-sec}^2/\text{in.}^2 \\ G_1 &= 12 \times 10^6 \text{ psi} \\ q_1 &= 27,500 \text{ psi} \\ \phi_1 &= 0 \text{ deg} \\ \nu_1 &= 0.27 \\ \sigma_{u2} &= 55,000 \text{ psi} \end{aligned}$$

Concrete:

$$\begin{aligned} \rho_2 &= 2.25 \times 10^{-4} \text{ psi-sec}^2/\text{in.}^2 \\ G_2 &= 2.13 \times 10^6 \text{ psi} \\ q_2 &= 2,000 \text{ psi} \\ \phi_2 &= 37 \text{ deg} \\ \nu_2 &= 0.25 \\ \sigma_{u1} &= 8,000 \text{ psi} \end{aligned}$$

Granite:

$$\begin{aligned} \rho_3 &= 2.5 \times 10^{-4} \text{ psi-sec}^2/\text{in.}^2 \\ G_3 &= 4 \times 10^6 \text{ psi} \\ q_3 &= 2,900 \text{ psi} \\ \phi_3 &= 30 \text{ deg} \\ \nu_3 &= 0.25 \\ \sigma_{u3} &= 10,000 \text{ psi} \end{aligned}$$

(1) First determine the effective elastic stiffness K_e , effective mass M_e , and elastic limit ϵ_e using equations 12-34, 12-35, and 12-36. Expanding the summation in equation 12-34 for three material layers, obtain

*The units of density were chosen to be consistent with P_{\max} in psi and r_i in inches. To convert unit weight in lb/ft³ to density in psi-sec²/in² divide by 667,000. To convert density in kg/m³ to density in psi-sec²/in² multiply by 9.36×10^{-8} .

$$K_e = 2 \left\{ G_1 \left[\left(\frac{r_1}{r_1} \right)^2 - \left(\frac{r_1}{r_2} \right)^2 \right] + G_2 \left[\left(\frac{r_1}{r_2} \right)^2 - \left(\frac{r_1}{r_3} \right)^2 \right] + G_3 \left(\frac{r_1}{r_3} \right)^2 \right\}$$

where $r_1/r_4 \approx r_1/\infty = 0$. Substituting the numerical values of the parameters yields

$$K_e = 2 \left\{ 12 \times 10^6 \left[1 - \left(\frac{24}{25.5} \right)^2 \right] + 2.13 \times 10^6 \left[\left(\frac{24}{25.5} \right)^2 - \left(\frac{24}{36.5} \right)^2 \right] + 4 \times 10^6 \left(\frac{24}{36.5} \right)^2 \right\} = 8.13 \times 10^6 \text{ psi}$$

Similarly, $M_e = 0.231 \text{ psi-sec}^2$ is obtained from equation 12-35. Using equation 12-28, the value $n_1 = 0$ is obtained, and from equation 12-36 $\epsilon_e = 0.00115$.

(2) To determine resistance points in the region of plastic deformation ($\epsilon > \epsilon_e$), use equations 12-27 through 12-33. From equation 12-28 calculate $n_1 = 0$, $n_2 = 3.02$, and $n_3 = 2.00$. Next, using equation 12-27 determine the ratios of the plastic boundaries r_{pi} to the inside radii r_i starting at $i = 1$ and working up to $i = 3$. Calculate for $\epsilon = 0.01$. When $i = 1$, $Y_{i-1} = Y_0 = 0$, $K_{i-1} = K_0 = 0$; hence,

$$\frac{r_{p1}}{r_1} = \left(\frac{4G_1\epsilon}{2q_1\sqrt{n_1+1}} \right)^{1/n_1+2} = \left[\frac{4(12 \times 10^6)(0.01)}{2(27,500)\sqrt{0+1}} \right]^{1/0+2} = 2.95$$

But $r_2/r_1 = 1.0625$. This means that the steel layer is completely plastic, and hence, $r_{p1}/r_1 = r_2/r_1 = 1.0625$ must be used for $\epsilon = 0.01$ and larger strains.

(3) Y_1 and K_1 can now be evaluated using equations 12-29, 12-30, and 12-31. Equation 12-31 applies because $n_1 = 0$. Since $Y_0 = 0$ and $K_0 = 0$, the equations reduce to

$$Y_1 = 2q_1\sqrt{n_1+1} \ln \frac{r_{p1}}{r_1} = 2q_1 \ln \frac{r_2}{r_1} = 3334 \text{ psi}$$

and

$$K_1 = 2G_1 \left(\frac{r_1}{r_2} \right)^2 \left[1 - \left(\frac{r_2}{r_{p1}} \right)^2 \right] = 2G_1 \left(\frac{r_1}{r_2} \right)^2 \left[1 - \left(\frac{r_2}{r_2} \right)^2 \right] = 0 \text{ psi}$$

These values of Y_1 and K_1 do not change for increasing strain ϵ since the plastic boundary r_{p1} has reached its maximum value.

(4) All information needed to calculate r_{p2}/r_2 from equation 12-27 is now available, and the result is $r_{p2}/r_2 = 1.33$ and $r_{p2} = 33.9$ in. Thus, at the strain $\epsilon = 0.01$ the concrete layer is about half plastic and half elastic. For $i = 2$, equations 12-29 and 12-30 become

$$Y_2 = Y_1 \left(\frac{r_{p2}}{r_2} \right)^{n_2} + \frac{2q_2\sqrt{n_2+1}}{n_2} \left[\left(\frac{r_{p2}}{r_2} \right)^{n_2} - 1 \right] = 11,520 \text{ psi}$$

and

$$K_2 = K_1 \left(\frac{r_{p2}}{r_2} \right)^{n_2} + 2G_2 \left[\left(\frac{r_1}{r_{p2}} \right)^2 - \left(\frac{r_1}{r_3} \right)^2 \right] = 2.93 \times 10^5 \text{ psi}$$

These values of Y_2 and K_2 can be substituted into equation 12-27 to obtain $r_{p3}/r_3 = 1.15$ and $r_{p3} = 42.0$ in. For $i = 3$, equations 12-29 and 12-30 become, with $r_4 = \infty$ and $r_1/r_4 = 0$,

$$Y_3 = Y_2 \left(\frac{r_{p3}}{r_3} \right)^{n_3} + \frac{2q_3\sqrt{n_3+1}}{n_3} \left[\left(\frac{r_{p3}}{r_3} \right)^{n_3} - 1 \right] = 16,900 \text{ psi}$$

and

$$K_3 = K_2 \left(\frac{r_{p3}}{r_3} \right)^{n_3} + 2G_3 \left(\frac{r_1}{r_{p3}} \right)^2 = 3.00 \times 10^6 \text{ psi}$$

For the present example the number m of material layers is 3. Thus equation 12-32 for the total resistance of the liner-rock system becomes

$$R(\epsilon) = K_3\epsilon + Y_3$$

Substituting the values of K_3 and Y_3 above and $\epsilon = 0.01$ yields $R(0.01) = 47,000$ psi, which is plotted on the lower graph of figure 12-6. From equations 12-33 and 12-31 the effective mass M is calculated:

$$M = r_1^2 \left\{ \left[e_1 \ln \left(\frac{r_{p1}}{r_1} \right) \left(\frac{r_{p2}}{r_2} \right)^{n_2} + \frac{e_2}{n_2} \left[\left(\frac{r_{p2}}{r_2} \right)^{n_2} - 1 \right] \right] \left(\frac{r_{p3}}{r_3} \right)^{n_3} + \frac{e_3}{n_3} \left[\left(\frac{r_{p3}}{r_3} \right)^{n_3} - 1 \right] + e_1 \ln \left(\frac{r_2}{r_{p1}} \right) + e_2 \ln \left(\frac{r_3}{r_{p2}} \right) + e_3 \ln \left(\frac{r_4}{r_{p3}} \right) \right\}$$

$$M(0.01) = 0.33 \text{ psi-sec}^2$$

where the value $r_4 = 3r_3$ has been used as suggested previously.

(5) Using the same procedure as for $\epsilon = 0.01$, additional points at $\epsilon = 0.005, 0.02, \text{ and } 0.03$ were calculated and plotted, along with the elastic values, in figure 12-6. Smooth curves were then drawn through these points and the bilinear fits denoted (1) and (2) were visually produced.

(6) From previous experience with similar structures it was determined that the liner in the example could safely take about 2 percent strain without buckling. This figure was then taken as the design criterion for the structure. To apply the dynamic design charts, the bilinear fits ((1) in figure 12-6), which are good up to 2 to 2.5 percent, should be used. From these curves the effective elastic limit is $\epsilon_e = 0.004$, the effective elastic stiffness is $K_e = 7.5 \times 10^6$ psi, and the effective elastic period is $T_e = 2\pi\sqrt{M_e/K_e} = 1.1$ msec. These values of ϵ_e and K_e should be used instead of the results obtained earlier from equations 12-34 and 12-36. The effective maximum elastic resistance from the fit (1) is then $R_e = 30,000$ psi, the effective plastic stiffness is $K_p = \Delta R/\Delta \epsilon \approx 2.5 \times 10^6$ psi, and the slope of the M curve in plastic deformation is $\Delta M/\Delta \epsilon \approx 15$. The chart parameters B and C are then obtained from equations 12-22 and 12-24.

$$B = \frac{K_p}{K_e} \approx \frac{2.5 \times 10^6}{7.5 \times 10^6} \approx 0.33$$

$$C = \frac{\epsilon_e}{M_e} \frac{\Delta M}{\Delta \epsilon} = \frac{0.004}{0.213} 15 \approx 0.26$$

The $B = 0.3$ curve of figure 12-15a and b should be used to obtain $\bar{\epsilon}_{\max} = \epsilon_{\max}/\epsilon_e$ and $\bar{t}_{\max} = t_{\max}/T_e$. For a peak free-field stress $P_{\max} = 43,500$ psi (3 kilobars), $A = P_{\max}/R_e = 43,500/30,000 = 1.45$. For $\bar{t}_r = 0$ figure 12-15a gives $\bar{\epsilon}_{\max} \approx 7$ and figure 12-15b gives $\bar{t}_{\max} \approx 1.1$. Hence, $\epsilon_{\max} = \epsilon_e \bar{\epsilon}_{\max} \approx 0.004 \times 7 = 0.028$ or 2.8 percent and $t_{\max} = T_e \bar{t}_{\max} \approx 1.1 \text{ msec} \times 1.1 \approx 1.2$ msec. Using the average value of Poisson's ratio $\nu = 0.25$, equation 12-37 gives a compressibility correction factor of 1.5 and a corrected maximum strain of $\epsilon_{\max}^c = 4.2$ percent. Thus, for a suddenly applied load ($\bar{t}_r = 0$) and $P_{\max} = 43,500$ psi, the dynamic strain is more than double the 2 percent design level of maximum strain that has been assumed for the structure. Figures 12-16 through 12-18 would be used to determine the structural response if $P(t)$ had a nonzero rise time. In figure 12-17 for $\bar{t}_r = 5$ the response is essentially quasi-static. These charts show that for the present example the maximum static strain is less than half the dynamic strain produced by a suddenly applied load. At the lower stress level $P_{\max} = 29,000$ psi (2 kilobars), $A = 0.97$. With $\bar{t}_r = 0$ the charts give values of $\bar{\epsilon}_{\max} \approx 3$ and $\bar{t}_{\max} \approx 0.8$ which yield $\epsilon_{\max} \approx 1.2$ percent and $t_{\max} \approx 0.9$ msec. Using $\nu = 0.25$, the corrected maximum strain is $\epsilon_{\max}^c \approx 1.8$ percent, which is within the design level.

i. Design charts. The maximum dynamic response of cylindrical underground structures subjected to the long-duration ground-shock loading of nuclear explosions is summarized in figures 12-7 through 12-30. The maximum normalized diametrical strain $\bar{\epsilon}_{\max} = \epsilon_{\max}/\epsilon_e$ and the dimensionless time of maximum strain $\bar{t}_{\max} = t_{\max}/T_e$ are given in the charts for the characteristic parameters A, B, C, and \bar{t}_r where:

- $T_e = 2\pi\sqrt{M_e/K_e}$ = Effective elastic period
- $A = P_{\max}/R_e$ = Dimensionless maximum applied load
- $B = K_p/K_e$ = Dimensionless plastic stiffness
- $C = (\epsilon_e/M_e)(\Delta M/\Delta \epsilon)$ = Dimensionless rate of change of effective mass in plastic deformation
- $\bar{t}_r = t_r/T_e$ = Normalized rise time of applied load

The material properties needed to determine the chart parameters are illustrated in figure 12-6; an example using the charts is given in *h* above. Charts are included in this appendix for normalized rise times ranging from $\bar{t}_r = 0$ for a suddenly applied load to $\bar{t}_r = 2$ or 5 where the structural response is essentially quasi-static. On the figures for $\bar{t}_r = 2$ or 5, some of the \bar{t}_{\max} curves for the larger values of B have been smoothed to produce readable "average" curves, which deviate from the original ones by less than about one fourth.

j. Preliminary design requirements to prevent mechanical failure. (Bagge, 1972). The opening reinforcement must prevent loss of structural integrity (gross mechanical failure) under ground shock when the ratio of opening diameter to joint spacing is not small compared to unity. This section presents upper bound design requirements for reinforcement that will prevent loss of structural integrity (assuming no material failure) of a circular cylindrical opening under dynamic ground-shock loading perpendicular to the opening axis. These requirements can also be used for cylindrical openings with noncircular cross sections—provided the deviation from circularity is not severe—by use of an equivalent circular opening, and for extrapolation to noncylindrical openings. When the direction of ground-shock propagation is not perpendicular to the opening axis, the component of the free-field ground shock acceleration that is perpendicular to the opening axis should be used. Three types of opening reinforcement are considered: integral liner, backpacked liner, and rock bolts.

(1) Consider the two cases shown in figure 12-31. Imagine that the planes of weakness cannot sustain tensile stresses and that the blocks of rock do not support one another through wedging action. For the first example (fig. 12-31a), which is the free field without the openings, there will be little tendency for relative movement between the cavity core and either of the regions containing planes of weakness. In the second example, however, there will be a marked tendency for relative movement of the shadow region into the

opening during initial engulfment and the illuminated region into the opening, as the free-field ground-shock velocity begins to decay from its positive peak. It is this marked tendency for relative movement of the rock into the opening that, if left unchecked by opening reinforcement, could cause loss of structural integrity of the opening.

(2) To establish theoretical conditions for the opening's loss of structural integrity, it is necessary to postulate that unwedged blocks of rock exist in the shadow or illuminated regions of the opening. The three simple patterns of planes of weakness in figure 12-32 demonstrate the reasonableness of this postulation. A single set of planes of weakness does not create a condition for critical mechanical failure (fig. 12-32a). For a set of nonorthogonal planes (fig. 12-32b), unwedged blocks of rock are presented when the direction of ground-shock propagation is parallel to the long diagonal of the formed blocks. Figure 12-32c shows that unwedged blocks of rock are presented for orthogonal joint planes wherever the direction of ground-shock propagation is parallel to a diagonal of the formed blocks. A critical condition also exists for the orthogonal set of planes whenever the direction of ground-shock propagation is parallel to a set of relatively compressible planes of weakness. Since multiple sets of planes of weakness are almost always encountered in practice, it is realistic to postulate that unwedged blocks of rock exist in the shadow and illuminated regions of the opening. The following assumption has therefore been made regarding planes of weakness:

The entire interaction zone of the cavity is cut by several sets of planes of weakness of negligible tensile strength in such a fashion that (1) the characteristic dimensions of the blocks of rock are small compared to the cavity diameter and (2) the blocks of rock are not mutually supported by wedging action.

(3) The postulation that the planes of weakness have negligible strength is quite reasonable for multiple-burst threats.

(4) It should be pointed out that the reinforcement design requirements presented below are linearly dependent upon (1) the increment of the free-field ground shock acceleration occurring over a period of two engulfment times and (2) the magnitude of the opening's radius.

(5) The following inputs are assumed to be known:

- Free-field ground shock stress, velocity, and acceleration histories
- The stress ratio K behind the ground shock wave front
- The effective propagation velocity C of the ground shock
- The weight density γ of the rock

- The opening's radius R

(6) The following procedure can be used to determine the design parameters for an integral liner, a backpacked liner, or rock bolts:

Step a. Calculate the engulfment time of the opening: $t_e = 2R/C$.

Step b. Divide the free-field ground shock acceleration history into a succession of constant acceleration steps of duration $2t_e$, as illustrated in figure 12-33a.

Step c. Construct an incremental free-field acceleration history as shown in figures 12-33b and c. Assume that this history is an envelope history of peak response for use in the state-of-stress equations derived for the reinforcement.

Step d. Select trial values of the reinforcement design parameters:

- (1) Integral liner: h, E, γ_ℓ
- (2) Backpacked liner: $h, E, \gamma_\ell, h_{bp}, E_{bp}, \gamma$
- (3) Rock bolts: $A_{rb}, S, L, E_{rb}, \gamma_{rb}, \mu$

Step e. Calculate the state of stress in the reinforcement using the applicable set of equations (given below) with the envelope δA history constructed in step c.

Step f. Calculate the quasi-static stress history of the reinforcement that arises from the normal interaction of the reinforcement with the free-field ground shock.

Step g. Add the stress histories calculated in steps e and f.

Step h. Compare the peak stresses found in step g to the allowable resistance of the reinforcement. (If the stresses arising from the rigid-body acceleration of the reinforcement itself are not negligible compared to those in steps f and g, then they must also be taken under consideration. Also, the buckling resistance of liners must be considered.)

Step i. Reiterate steps d through h until an acceptable state of stress is obtained.

k. Sample application. An integral liner of thickness h , radius R , Young's modulus E , and weight density γ_ℓ is used to reinforce the opening (fig. 12-34). The following assumptions are made:

- The liner thickness is small compared to the liner opening radius ($R/h \geq 5$).
- The liner responds elastically.
- The liner responds in two uncoupled modes corresponding to the uniform and ovaling components of loading.
- The periods of vibration of the liner are taken as the breathing (T_0) and ovaling (T_2) periods of vibration of the free-standing liner under radial loading:

$$T_0 = 2\pi \sqrt{\frac{\gamma_\ell R^2}{Eg}}, \quad T_2 = 2\pi \sqrt{\frac{\gamma_\ell R^2}{Eg}} \cdot \sqrt{\frac{5}{3} \left(\frac{R}{h}\right)^2} \quad (12-38)$$

- Peak response is taken as the sum of the peak response in each mode without regard to phasing. The peak state of stress in the liner (required effective dynamic resistance) is:

Fully Welded Rock/Liner Interface (σ'_{rr} and $\sigma'_{r\theta}$)

$$N = R^2 \gamma \delta A (1 + K) DLF_0$$

$$M = -0.5 R^3 \gamma \delta A (1 - K) \cos 2\theta DLF_2$$

$$\sigma_N = \frac{N}{h} = R \frac{R}{h} \gamma \delta A (1 + K) DLF_0$$

$$\sigma_M = \frac{6M}{h^2} = \pm 3R \left(\frac{R}{h}\right)^2 \gamma \delta A (1 - K) \cos 2\theta DLF_2$$

$$\sigma_{NM} = \sigma_N + \sigma_M = R \frac{R}{h} \gamma \delta A \left[(1 + K) DLF_0 \pm 3 \frac{R}{h} (1 - K) \cos 2\theta DLF_2 \right]$$

Full-Slip Rock/Liner Interface (σ'_{rr} only)

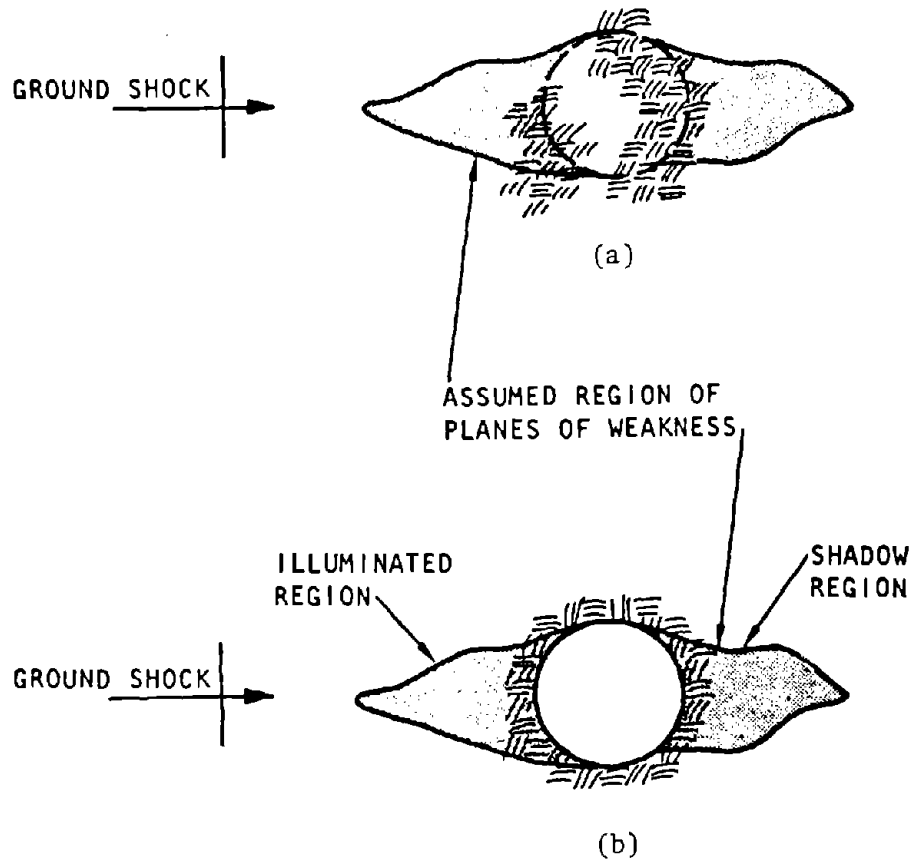
$$N = R^2 \gamma \delta A (1 + K) DLF_0$$

$$M = -\frac{1}{3} R^3 \gamma \delta A (1 - K) \cos 2\theta DLF_2$$

$$\sigma_N = R \frac{R}{h} \gamma \delta A (1 + K) DLF_0$$

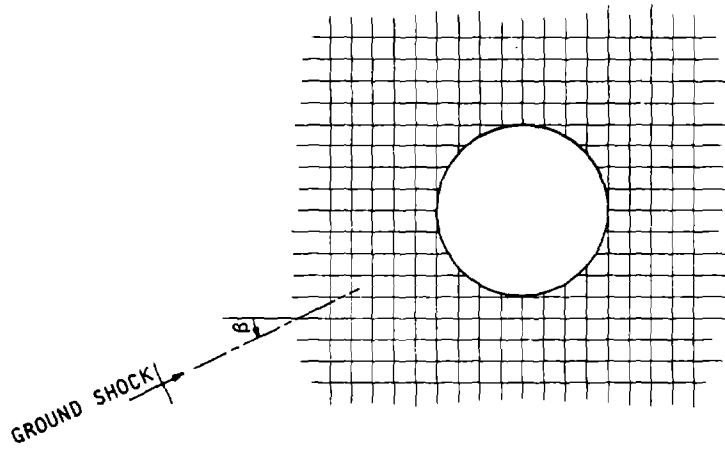
$$\sigma_M = -2R \left(\frac{R}{h}\right)^2 \gamma \delta A (1 - K) \cos 2\theta DLF_2$$

$$\sigma_{NM} = R \frac{R}{h} \gamma \delta A \left[(1 + K) DLF_0 \pm 4 \frac{R}{h} (1 - K) \cos 2\theta DLF_2 \right]$$

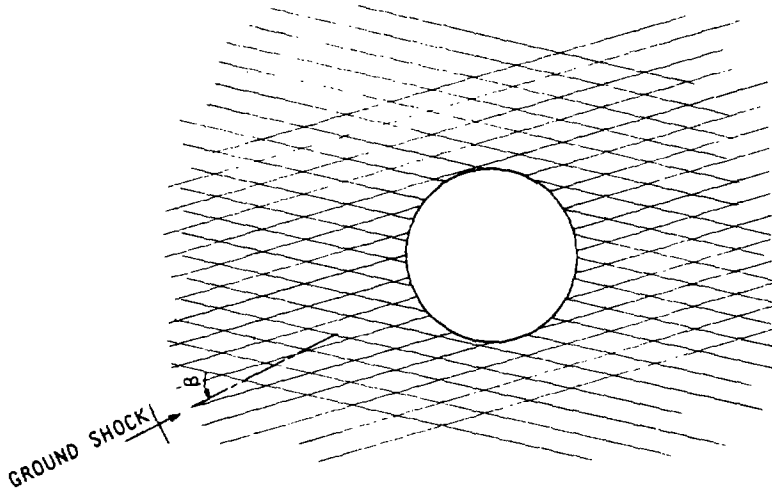


U.S. Army Corps of Engineers

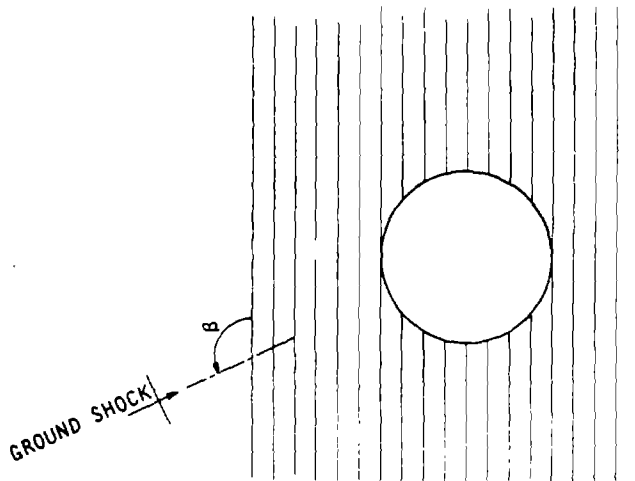
Figure 12-31. Mechanical Failure of a Rock Cavity



(c) Orthogonal set

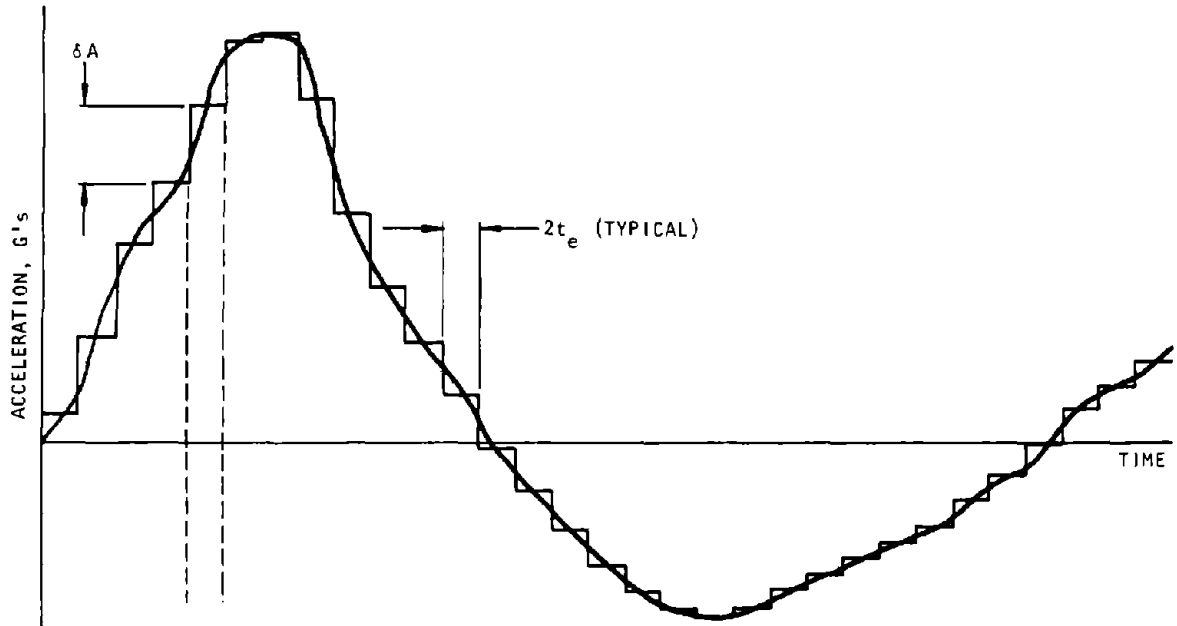


(b) Nonorthogonal set



(a) Single set
U.S. Army Corps of Engineers

Figure 12-32. Three Patterns of Planes of Weakness



(a) Free-field acceleration history



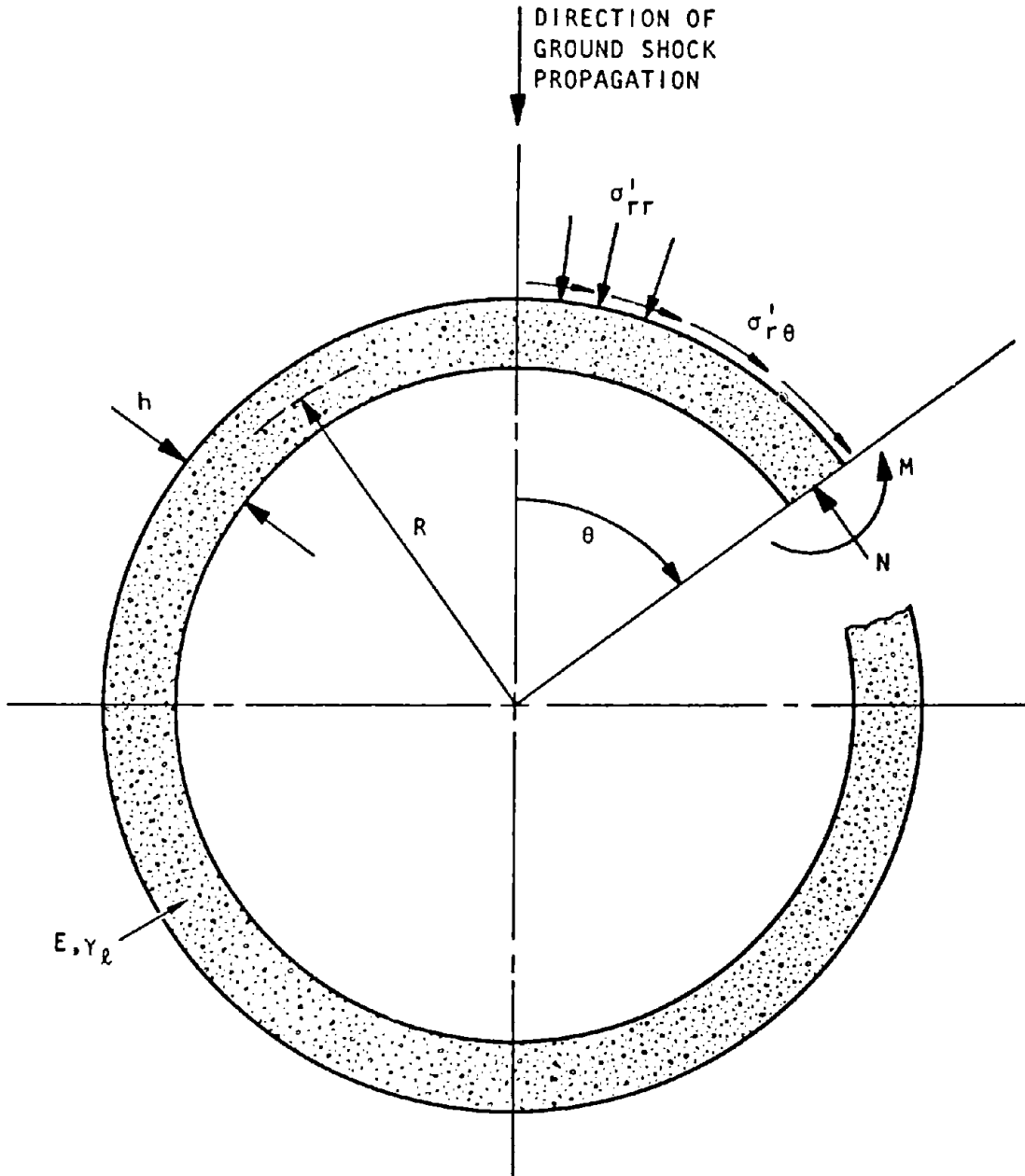
(b) Critical increments in free-field acceleration



(c) Incremental free-field acceleration history

U.S. Army Corps of Engineers

Figure 12-33. Construction of Incremental Free-Field Acceleration History



U.S. Army Corps of Engineers

Figure 12-34. Liner Reinforcement

where

$$DLF_0 = \frac{\pi t_d/T_0}{1 + \frac{2.2(t_d/T_0)^2}{1 + 1.4 t_d/T_0}}$$

$$DLF_2 = \frac{\pi t_d/T_2}{1 + \frac{2.2(t_d/T_2)^2}{1 + 1.4 t_d/T_2}}$$

$$\frac{t_d}{T_0} = \frac{2}{\pi C} \sqrt{\frac{Eg}{\gamma_\ell}}$$

$$\frac{t_d}{T_2} = \frac{1.55 h}{\pi C R} \sqrt{\frac{Eg}{\gamma_\ell}}$$

$$t_d = 2t_e = 4R/C$$

(1) A layer of backpacking material of thickness h_{bp} , effective modulus of elasticity E_{bp} , and weight density γ_{bp} —is placed between the cavity wall and the liner considered above. The following assumptions are made:

- The liner and backpacking thicknesses are small compared to the liner (opening) radius ($R/h \geq 5$, $R/h_{bp} \geq 5$).
- The liner and backpacking respond elastically.
- The rock/backpacking interface does not transmit shear stresses, i.e., the interface is a full-slip interface.
- It is sufficient that only the radial restraining stresses are reacted by the liner and backpacking.
- The effect of the backpacking is accounted for by treating the backpacking as a massless radial spring element of stiffness

$$k_{bp} = \frac{E_{bp}}{h_{bp}}$$

in series with the liner flexibility, and by adding all backpacking mass to the liner.

- The modified liner responds in two uncoupled modes corresponding to the uniform and ovaling components of loading.
- The periods of vibration of the modified liner are taken as the following variations of equations 12-38.

$$T'_0 = 2\pi \sqrt{\frac{\gamma_\ell R^2}{Eg}} \sqrt{\left(1 + \frac{m_{bp}}{m}\right) \left(1 + \frac{k_o}{k_{bp}}\right)}$$

$$T'_2 = 2\pi \sqrt{\frac{\gamma_\ell R^2}{Eg}} \sqrt{\left(\frac{5R}{3h}\right)^2} \sqrt{\left(1 + \frac{m_{bp}}{m}\right) \left(1 + \frac{k_2}{k_{bp}}\right)}$$

where

$$k_o = \frac{Eh}{R^2}$$

$$k_2 = \frac{3 Eh^3}{4 R^4}$$

$$m = h\gamma_\ell$$

$$m_{bp} = h_{bp}\gamma_{bp}$$

- Peak response is taken as the sum of the peak response in each mode without regard to phasing. The peak state of radial stress in the backpacking (required effective dynamic resistance) is:

$$\sigma_{bp} = R\gamma \delta A[(1 + K)DLF'_0 + (1 - K) \cos 2\theta DLF'_2]$$

where

$$DLF'_0 = \frac{\pi t_d/T'_0}{1 + \frac{2.2(t_d/T'_0)^2}{1 + 1.4 t_d/T'_0}}$$

$$DLF'_2 = \frac{\pi t_d/T'_2}{1 + \frac{2.2(t_d/T'_2)^2}{1 + 1.4 t_d/T'_2}}$$

$$\frac{t_d}{T'_0} = \frac{2}{\pi C} \sqrt{\frac{Eg}{\gamma_\ell}} \sqrt{\frac{1}{\left(1 + \frac{h_{bp} \gamma_{bp}}{h \gamma_\ell}\right) \left(1 + \frac{E}{E_{bp}} \frac{h}{R} \frac{h_{bp}}{R}\right)}}$$

$$\frac{t_d}{T'_2} = \frac{1.55 h}{\pi C R} \sqrt{\frac{Eg}{\gamma_\ell}} \sqrt{\frac{1}{\left(1 + \frac{h_{bp} \gamma_{bp}}{h \gamma_\ell}\right) \left(1 + \frac{3}{4} \frac{E}{E_{bp}} \left(\frac{h}{R}\right)^3 \frac{h_{bp}}{R}\right)}}$$

The peak state of stress in the liner (required effective dynamic resistance) is:

$$N = R^2\gamma \delta A(1 + K)DLF'_0$$

$$M = -\frac{1}{3} R^3\gamma \delta A(1 - K) \cos 2\theta DLF'_2$$

$$\sigma_N = R \frac{R}{h} \gamma \delta A(1 + K)DLF'_0$$

$$\sigma_M = -2R \left(\frac{R}{h}\right)^2 \gamma \delta A(1 - K) \cos 2\theta DLF'_2$$

$$\sigma_{NM} = R \frac{R}{h} \gamma \delta A [(1 + K) DLF'_0 \pm 4 \frac{R}{h} (1 - K) \cos 2\theta DLF'_2]$$

(2) Radially positioned rock bolts of cross-sectional area A_{rb} , weight density γ_{rb} , effective modulus of elasticity E_{rb} , and spacing s (each way) are used to reinforce the cavity wall. The following assumptions are made:

- It is sufficient that only the radial stress loading is carried by the bolts.
- The bolts are anchored into the free field at a distance L from the cavity wall.
- The bolts are allowed to respond inelastically.
- The bolt material is modeled as an elastic-perfectly plastic material.
- The period of vibration of a bolt is taken as

$$T_{rb} = 2L \sqrt{\frac{\gamma_{rb}}{E_{rb}g}}$$

The pretensioning stress required in the bolt to effect no resistance at the face of the opening is:

$$\sigma_{rb} = R \gamma \delta A \frac{S^2}{A_{rb}} [1 + K + (1 - K) \cos 2\theta] DLF_{rb}$$

where

$$DLF_{rb} = \frac{\pi t_d / T_{rb}}{\sqrt{2\mu - 1} + \frac{4.4(t_d / T_{rb})^2 (2\mu - 1) / 2\mu}{1 + 1.4 t_d / T_{rb}}}$$

$$\frac{t_d}{T_{rb}} = \frac{2R}{LC} \sqrt{\frac{E_{rb}g}{\gamma_{rb}}}$$

μ = Ductility ratio, i.e., the ratio of maximum response strain in the rock bolt to the effective yield strain of the rock bolt

The length of the rock bolt must satisfy some minimum-length criterion. Just what this minimum length should be is not at all clear. However, judging from the load durations involved, it would appear that the rock bolt must have a length of $4R$, where zero resistance is required at the cavity wall. It may be tentatively assumed that it is sufficient to provide a rock bolt length of $2R$, with full resistance over the entire length.

12-7. Excavation method.

The method used to excavate a rock opening has a significant impact on the ground-shock hardness of a minimally reinforced rock opening. The drill-and-blast method degrades both the strength and stiffness of the adjacent rock by loosening existing joints and by fracturing. Hardness is thus degraded for minimally reinforced openings. Specify boring whenever possible for minimally reinforced openings, since boring causes almost no degradation of the adjacent rock.

APPENDIX A PROBABLISTIC DESIGN OF HARDENED STRUCTURES UNDER UNCERTAINTIES

A-1. General

a. The survivability requirements for a facility are defined by specifying a minimum probability for the facility's physical survival under a nuclear-weapon attack and for retaining its physical integrity during the specified endurance period (see TM 5-858-1, para. 4-4). Uncertainties underlie all steps of the design process for meeting this requirement and must be estimated in order to achieve a prescribed survivability goal.

b. TM 5-858-1 describes survivability models for weapon-threat scenarios and uncertainties in threat definition. Weapon-effect data and calculation of uncertainties of each effect are provided in TM 5-858-2. Systematic approaches for estimating uncertainties as a basis of hardness verification are presented in TM 5-858-6. Methods for estimating uncertainties and probabilistic design of structures are given in this appendix.

c. Uncertainties exist in input loads/displacements, geometry, and material properties. Resistance capacities are influenced by all three parameters. Loads will influence resisting capacities if there is coupling; for example, the moment-resisting capacity of a beam column depends on the axial load. Uncertainties also result from approximations in mathematical models. Construction-control techniques and tolerances also introduce uncertainties.

d. Methods for estimating the probability of survival or failure of a structure under applied loads are described in the literature (e.g., Ang Cornell, 1974). In this appendix a brief summary of the theory is given, followed by examples for determining uncertainties in load input, material properties, approximations for analysis, and construction tolerances.

A-2. Analytical basis for survival (failure) estimates

a. Let S denote the largest combined load or load effect (e.g., internal moment, stress) that is applied on a structural component during its lifetime. Consider S as a random variable with density function $f_S(s)$. Let the corresponding strength of the component, denoted by R , be a random variable with density function $f_R(r)$. For a given component, the functions $f_S(s)$ and $f_R(r)$ may appear as in figure A-1. For the purpose of the present study, assume that R and S are statistically independent.

b. The failure of the component is defined by the event $R < S$; therefore, the failure probability is obtained as:

$$P_f = P(R < S) = \int_0^{\infty} P(R < S | S = s) f_S(s) ds$$

$$= \int_0^{\infty} F_R(s) f_S(s) ds \quad (A-1)$$

where

$$F_R(s) = \int_0^s f_R(r) dr \quad (A-2)$$

is the cumulative distribution function of R evaluated at $r = s$.

c. Equation A-1 is solved if the functions $f_S(s)$ and $f_R(r)$ are known. For most practical cases, however, obtaining these functions is extremely difficult or impossible. For example, since S is the sum of load effects from many sources (e.g., dead loads, live loads, airblast, ground shock), the evaluation of $f_S(s)$ requires a full knowledge of the stochastic laws and the corresponding correlations for each load source.

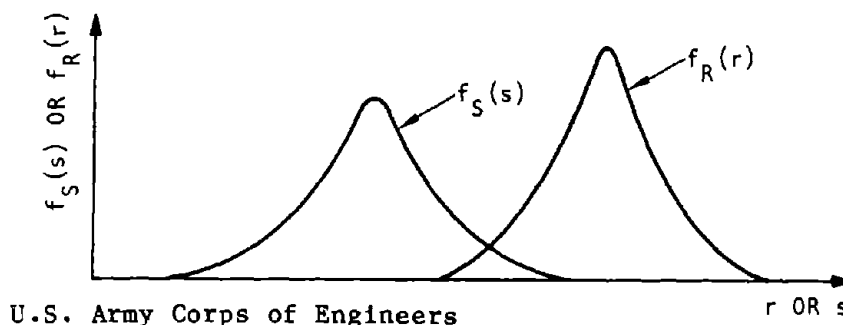


Figure A-1. Load and Resistance Probability Density Functions

Likewise, the evaluation of $f_R(r)$ requires the knowledge of the probability distribution for material properties and behaviors, and even construction practices. Therefore, an accurate evaluation of equation A-1 is impossible; nevertheless, if mean values and standard deviations of variables are known, an approximate evaluation of the probability of failure, P_f , is possible by prescribing physically reasonable distributions for R and S. Even though this method will not yield the actual failure risk, the nominal failure risk obtained can be used as a relative measure of the underlying risk, thus allowing for comparison of various designs or structures.

d. Failure probability can be expressed with the following alternative formulation. Consider R-S to be the random variable. Failure will occur when this random variable has a negative value. Therefore, P_f can be obtained as

$$P_f = P(R - S < 0) \\ = F_{R-S}(0) \tag{A-3}$$

where $F_{R-S}(0)$ is the cumulative distribution function of R-S evaluated at zero. Since R-S can have both positive and negative values, a normal distribution is reasonable and can be prescribed. Let \bar{R} and \bar{S} be the means and σ_R and σ_S be the standard deviations of R and S, respectively. Using first-order linear approximations (Ang-Cornell, 1974), evaluate the mean and standard deviation of R-S as follows:

$$R-S \cong \bar{R} - \bar{S} \tag{A-4}$$

$$\sigma_{R-S} \cong \sqrt{\sigma_R^2 + \sigma_S^2} \tag{A-5}$$

Then equation A-3 gives

$$P_f = 1 - \phi \left(\frac{\bar{R} - \bar{S}}{\sqrt{\sigma_R^2 + \sigma_S^2}} \right) \tag{A-6}$$

where ϕ denotes the value of the standard normal probability. Finding the required mean resistance, \bar{R} , from equation A-6 gives

$$\bar{R} = \bar{S} + \phi^{-1}(1 - P_f) \sqrt{\sigma_R^2 + \sigma_S^2} \\ = \bar{S} + \beta \sqrt{\sigma_R^2 + \sigma_S^2} \tag{A-7}$$

where $\beta = \phi^{-1}(1 - P_f)$ is the value of the standard normal variate at the cumulative probability $(1 - P_f)$, which represents the survival probability. This parameter, therefore, can be regarded as a consistent measure of survivability.

e. With the normal distribution assumed for the performance function (R-S), the values of β for various levels of failure probability are:

Probability of Failure	β
10^{-1}	1.28
10^{-2}	2.33
10^{-3}	3.09
10^{-4}	3.72
10^{-5}	4.25
10^{-6}	4.75
10^{-7}	5.20
10^{-8}	5.61

f. The value of β for design should be determined on the basis of cost-benefit trade-off studies. For large β the initial cost of construction is high; however, future losses due to damage are unlikely. On the other hand, for small β the initial cost is low, but future losses due to damage are more probable. An optimum value of β should be obtained from economic considerations. If such studies cannot be carried out, a value of β should be determined through calibration with other existing structures which require the same level of reliability; i.e., first evaluate β for an existing structure, then use that value to design a new structure. In practical design situations, required values of β are specified by codes or by the systems engineers.

A-3. Reliability-based design factors

a. Equation A-7 can be used to obtain safety, load, and strength factors associated with a desired level of reliability. In the following sections the cases of one and of multiple loads are discussed.

b. Consider the case of one load. The variabilities due to R and S may be separated. Let

$$\sqrt{\sigma_R^2 + \sigma_S^2} = \alpha(\sigma_R + \sigma_S) \tag{A-8}$$

where

$$\alpha = \frac{\sqrt{\sigma_R^2 + \sigma_S^2}}{\sigma_R + \sigma_S}$$

has a value between 0.707 and 1.00; and generally $\alpha = 0.75$ can be assumed. Using equation A-8 in A-7 obtains

$$\bar{R} = \bar{S} + 0.75\beta(\sigma_R + \sigma_S) \tag{A-9}$$

Therefore,

$$\bar{R} - 0.75\beta\sigma_R = \bar{S} + 0.75\beta\sigma_S \tag{A-10}$$

or

$$(1 - 0.75\beta\Omega_R) \bar{R} = (1 + 0.75\beta\Omega_S) \bar{S} \tag{A-11}$$

where $\Omega_R = \sigma_R/\bar{R}$ and $\Omega_S = \sigma_S/\bar{S}$ are the coefficients of variation. From the above derivation the strength and load factors, ψ and δ , respectively, associated with the reliability index β , are obtained as

$$\psi = 1 - 0.75 \beta \Omega_R \quad (A-12)$$

$$\delta = 1 + 0.75 \beta \Omega_S \quad (A-13)$$

Note that these factors must be applied to the *mean* values of resistance and load, respectively, as indicated in equation A-11. Corresponding to equation A-11, a safety factor, γ , for reliability index β is obtained as

$$\gamma = \frac{1 + 0.75 \beta \Omega_S}{1 - 0.75 \beta \Omega_R} \quad (A-14)$$

This factor should be applied to the mean load to obtain the required mean resistance.

c. Equations A-12 to A-14 show that the design factors ψ , δ , and γ are all dependent on the required reliability through the parameter β . It is also observed that these factors are related to the uncertainties in resistance and load through the coefficients of variation Ω_R and Ω_S . For practical design situations, evaluate Ω_R and Ω_S and determine the design factors for any required value of β from equations A-12, A-13, and A-14. Based on these values, determine the required mean resistance either from

$$\psi \bar{R} = \bar{S} \quad (A-15)$$

or from

$$\bar{R} = \gamma \bar{S} \quad (A-16)$$

d. When multiple loads S_1, S_2, \dots, S_n are acting, let

$$S = S_1 + S_2 + \dots + S_n \quad (A-17)$$

with $\bar{S} = \bar{S}_1 + \bar{S}_2 + \dots + \bar{S}_n$ and

$$\sigma_S = \sqrt{\sigma_{S_1}^2 + \sigma_{S_2}^2 + \dots + \sigma_{S_n}^2} \quad (A-18)$$

where S_i and σ_{S_i} are the mean and standard deviation of S_i . Now let

$$\alpha_s = \frac{\sqrt{\sigma_{S_1}^2 + \sigma_{S_2}^2 + \dots + \sigma_{S_n}^2}}{\sigma_{S_1} + \sigma_{S_2} + \dots + \sigma_{S_n}} \quad (A-19)$$

Then using equation A-10

$$\begin{aligned} \bar{R} - 0.75 \beta \sigma_R = \bar{S}_1 + \bar{S}_2 + \dots + \bar{S}_n \\ + 0.75 \beta \alpha_s (\sigma_{S_1} + \sigma_{S_2} + \dots + \sigma_{S_n}) \end{aligned} \quad (A-20)$$

or

$$(1 - 0.75 \beta \Omega_R) \bar{R} = \sum_{i=1}^n \left(1 + 0.75 \beta \alpha_s \Omega_{S_i} \right) \bar{S}_i \quad (A-21)$$

where Ω_{S_i} is the coefficient of variation of S_i . From this equation the load factor for S_i is obtained as

$$\delta_i = 1 + 0.75 \beta \alpha_s \Omega_{S_i} \quad (A-22)$$

Note that strength and safety factors remain the same as given in equations A-12 and A-14, respectively. For the multiple load case, therefore, equation A-15 modifies to

$$\psi \bar{R} = \sum_{i=1}^n \delta_i \bar{S}_i \quad (A-23)$$

where δ_i is evaluated as in equation A-22.

A-4. Bias and estimating errors

a. In A-2 above, S was defined as the combined load or load effect, and R as the resistance of the structural element. For example, in designing for the tension reinforcement of a reinforced concrete beam, S is the acting moment at the critical section and R is the ultimate moment capacity. Both of these random variables are generally functions of other variables. For example, S is a function of each applied load (e.g., dead load, live load, air-blast, ground shock); R is a function of material strength and dimensions. In practice, distributions of S and R are usually not available and must be obtained in terms of distributions of function variables. Such derivations are often too complicated; thus, approximate methods are required. For the purpose of generality consider Z as representing either R or S . Let Z be a function of random variable X_1, X_2, \dots, X_n , i.e.,

$$Z = g(X_1, X_2, \dots, X_n) \quad (A-24)$$

where X_i may represent such variables as loads, dimensions, and material strengths; and $g(\cdot)$ represents the relation of Z to X_i . On the basis of first-order approximations (Ang Tang, 1975), the mean and coefficient of variation of Z are obtained as

$$\bar{Z} \cong g(\bar{X}_1, \bar{X}_2, \dots, \bar{X}_n) \quad (A-25)$$

and

$$\begin{aligned} \Omega_Z^2 \cong \Omega_g^2 + \sum_{i=1}^n \frac{\bar{X}_i^2}{\bar{Z}^2} \left(\frac{\partial g}{\partial X_i} \right)_0^2 \Omega_{X_i}^2 \\ + \sum_{i \neq j}^n \sum_{j=1}^n \frac{\bar{X}_i \bar{X}_j}{\bar{Z}^2} \left(\frac{\partial g}{\partial X_i} \frac{\partial y^g}{\partial X_j} \right)_0 \rho_{ij} \Omega_{X_i} \Omega_{X_j} \end{aligned} \quad (A-26)$$

where \bar{X}_i is the mean of X_i obtained from unbiased data, Ω_{X_i} is the coefficient of variation of X_i including the inherent randomness as well as estimation errors; i.e.,

$$\Omega_{X_i} = \sqrt{\delta_{X_i}^2 + \Delta_{X_i}^2} \quad (A-27)$$

where Ω_g is the coefficient of variation associated with the variability as well as modeling errors of the function $g(\cdot)$, and ρ_{ij} denotes the correlation between X_i and X_j . The subscript "o" implies that the partial derivatives $\partial g/\partial X_i$ are to be evaluated at the mean values, \bar{X}_i .

b. When statistical data are biased, \bar{X}_i must be replaced by $\bar{N}_{X_i} \bar{X}_i$, where \bar{N}_X represents the bias factor. Also, when the function $g(\cdot)$ is biased, i.e., either systematically underestimated or overestimated, a bias factor, \bar{N}_g , must be included in equation A-25. Thus, for each X_i four values must be determined, i.e.:

- Mean of sample, \bar{X}_i
- Bias factor, \bar{N}_{X_i}
- Inherent randomness, σ_X
- Estimation error, Δ_X

Also, for the function $g(\cdot)$ both the bias factor, \bar{N}_g , and the modeling error, Ω_g , must be determined.

c. Some examples are given in paragraph A-5 below for illustration only. The designer must select an appropriate data base for each function, either

from existing test data or from simulated experiments specifically designed for the structure that is being designed.

E-5. Uncertainties in ground-shock waveforms

a. The shape of the ground-shock waveform is difficult to predict. It is therefore necessary to determine whether elements responding to ground shock are sensitive to waveform. Designers often synthesize a simple, linearly or exponentially decaying wave and an oscillatory wave (fig. A-2). Certain ground-shock parameters are defined in advance. For the decay wave type, these are: (1) rise time to peak positive particle velocity, (2) positive and negative phase durations, and (3) peak positive and negative velocity amplitudes. For the oscillatory wave type, the ground-shock parameters are: (1) the number of cycles, and (2) the period and peak velocity of each cycle.

b. Twenty-nine wave shapes are considered here that use various amplitude ratios, duration ratios, and phasing of the two types of velocity waveforms

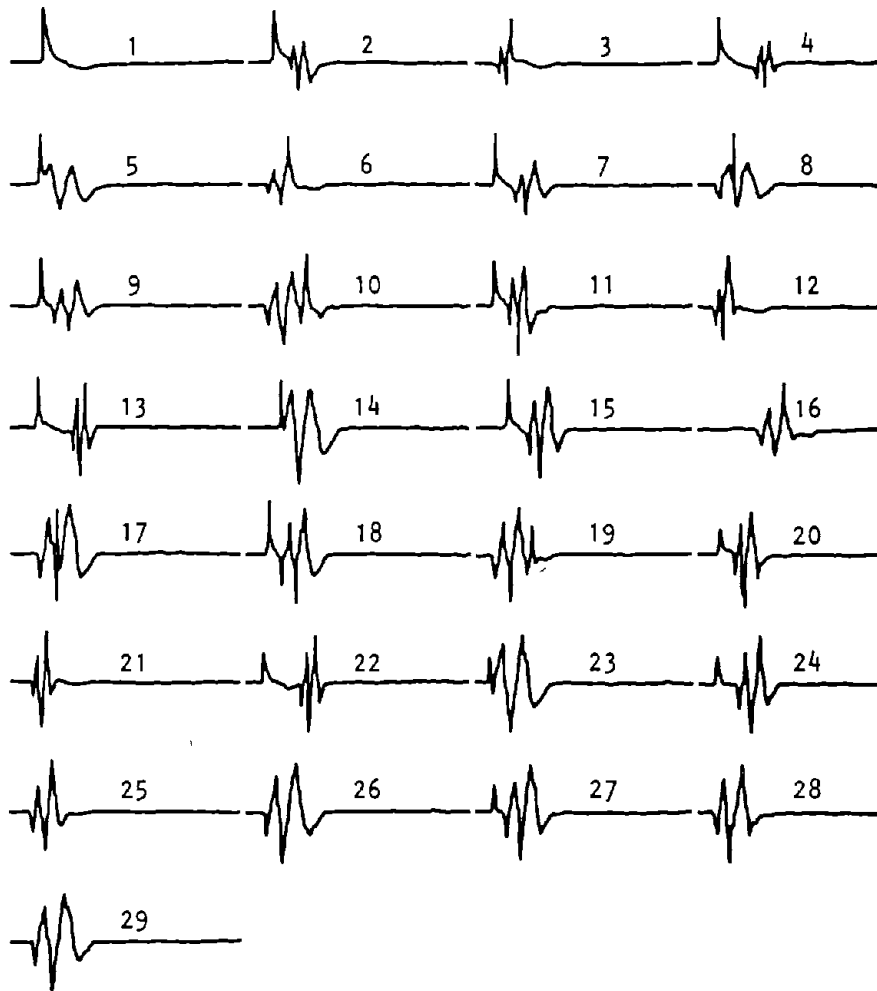


Figure A-2. Velocity Waveforms Used as Inputs (Ralph M. Parsons Co., 1962)

tabulated in table A-1. These wave shapes have been patterned after data obtained from five nuclear experiments and are given in figure A-2 (Parsons, 1962). The responses of undamped linear single-degree-of-freedom (SDOF) Systems to these inputs are given in figure A-3.

c. The curves of figure A-3 give the response of an SDOF system in terms of the ratio of a pseudo-velocity, ωx_m , to the peak input velocity V_m . This is

a standard way of representing ground-motion spectra.

d. Peak relative displacements and peak absolute accelerations are obtained, respectively, from the relationships

$$x_m = \text{Pseudo-velocity divided by } \omega$$

$$G_m = \text{Pseudo-velocity multiplied by } \omega/g$$

Table A-1. Key to Wave Shape Combinations of Figure A-2 (Ralph M. Parsons, Co., 1962)

Amplitude Ratio		Duration Ratio		Phasing	
	<u>Type I:Type II</u>		<u>Type I:Type II</u>		
A ₁	2:1	A ₂	2:1	A ₃	
B ₁	1:1	B ₂	1:1	B ₃	
C ₁	1:2	C ₂	1:2	C ₃	
Shape No.	Combination	Shape No.	Combination	Shape No.	Combination
1	Type I	13	B ₁ B ₂ C ₃	25	C ₁ B ₂ C ₃
2	A ₁ A ₃ A ₃	14	B ₁ B ₂ A ₃	26	C ₁ C ₂ A ₃
3		15		27	B ₃
4		16		28	C ₃
5	A ₁ B ₂ A ₃	17	B ₁ C ₂ A ₃	29	Type II
6		18			
7		19			
8	A ₁ C ₂ A ₃	20			
9		21			
10		22			
11	B ₁ A ₂ A ₃	23			
12		24			

In Type B₃ and C₃ the shorter duration type is always centered on the beginning or end, respectively, of the longer duration. Thus, in A₂B₃ Type II starts first and is half over before Type I begins (see shapes 3, 12, or 21 on fig. A-2). In C₂B₃, on the other hand, Type I starts first and is half over before Type II begins (see shapes 9, 18, or 27 on fig. A-2).

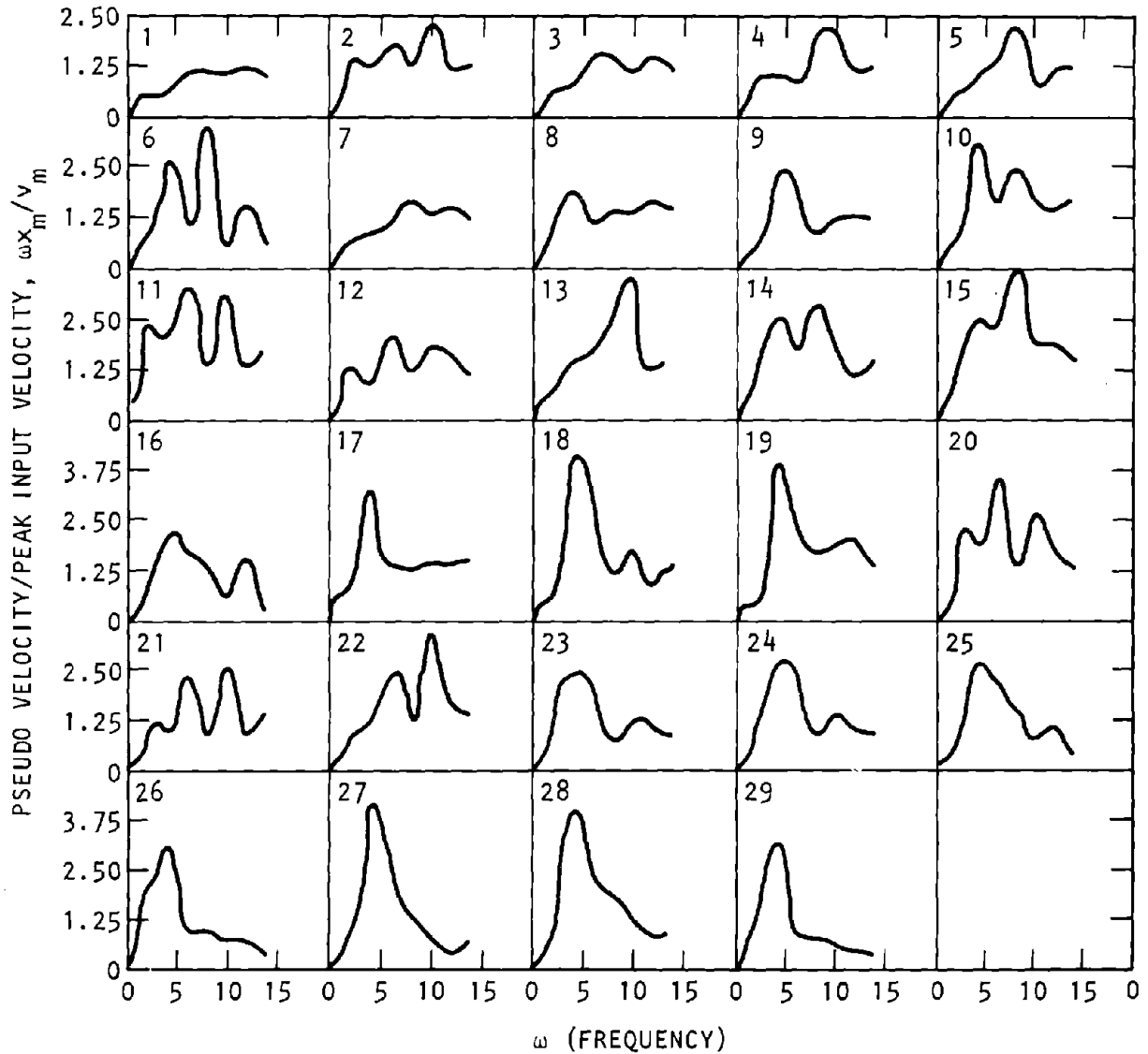


Figure A-3. Responses of Undamped Linear SDOF Systems (Ralph M. Parsons Co., 1962)

The actual maximum relative velocity \dot{x}_{max} is different from the pseudo-velocity except in the special case of a sinusoidal function:

$$x = x_m \sin(\omega t + \phi) \tag{A-28}$$

where $|\dot{x}|_{max}$ is exactly equal to ωx_m .

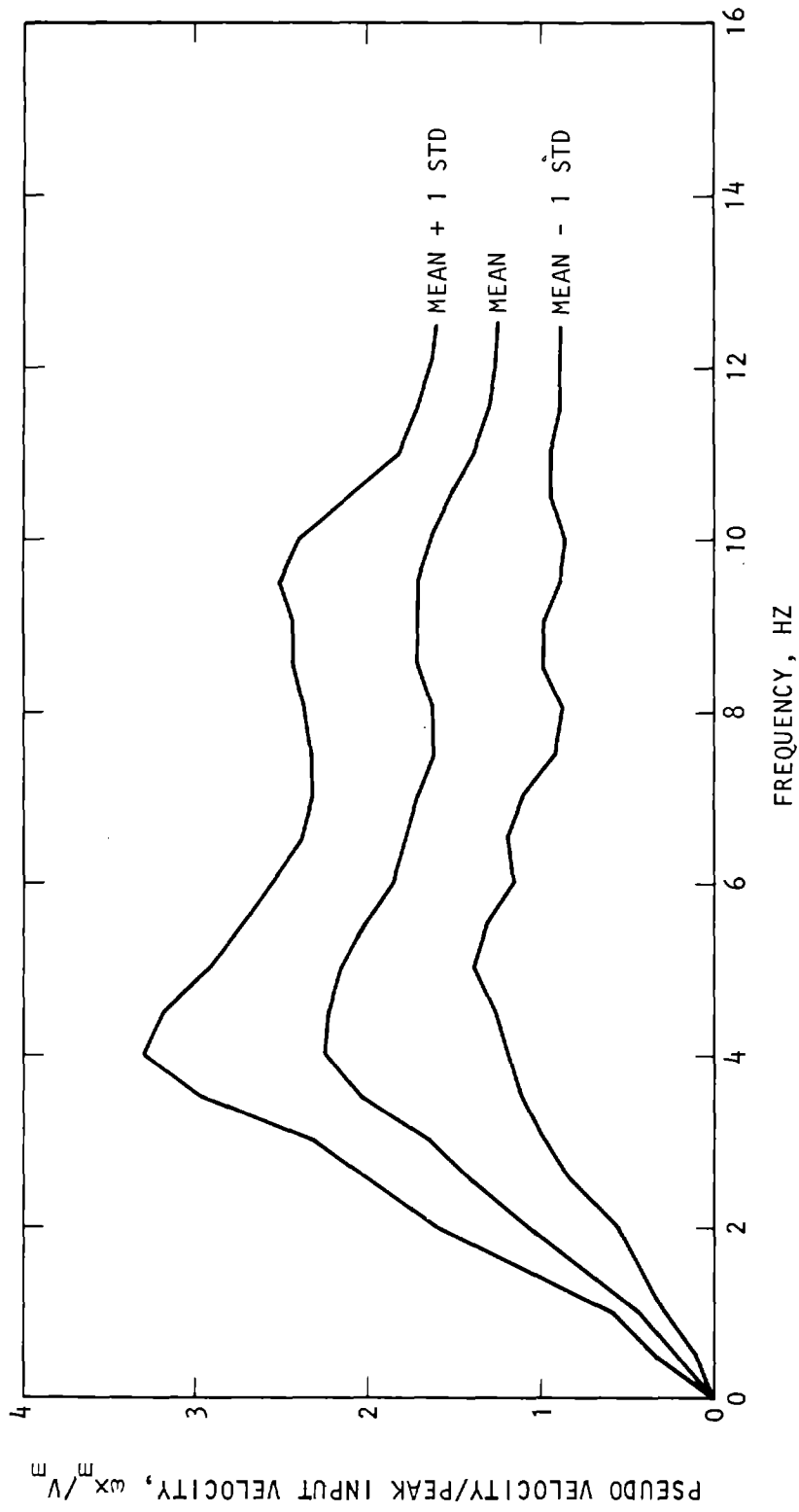
e. For an SDOF system of a given frequency there are 29 peak velocity response values. The mean value and the COV (coefficient of variation) obtained from these 29 values have some statistical significance

(Table A-2). Plots of the mean values and the COVs as a function of frequency are used as a general design tool, and are given in figures A-4 and A-5.

f. Note that when mean and COV values are obtained, the ensemble should be well specified. If the ensemble of the 29 waveforms is an ensemble of actual waveforms (i.e., measured during explosions), then the mean and COV relate to the actual response of an SDOF system. However, if the 29 records are synthesized for design purposes, the mean and COV will be meaningful only if similar to the total population of actual waveforms (i.e., have the same number from each type of wave).

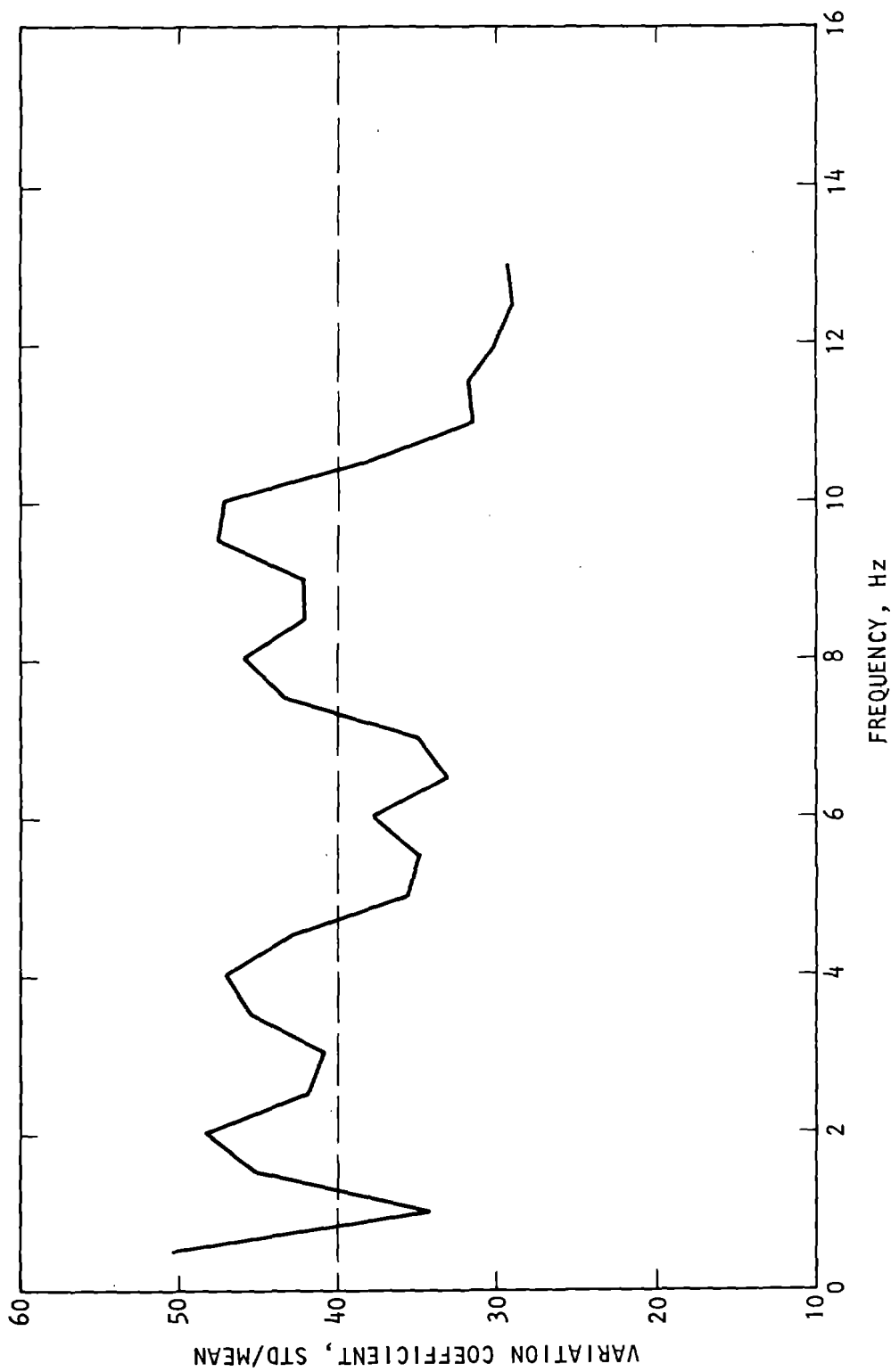
Table A-2. Coefficient of variation in design Parameters (Gallo-Ang, 1976)

Parameter X	Predicted Mean, \bar{X}	Basic Variability δ_X	Prediction COV, Δ_X	Total COV, Ω_X
f_y (Nominal 40 ksi)	47.7 ksi	0.09	0.12	0.150
f_y (Nominal 60 ksi)	64.0 ksi	0.07	0.12	0.139
f'_c (Nominal 3 ksi)	3.5 ksi	0.12	0.18	0.216
f'_c (Nominal 4 ksi)	4.7 ksi	0.12	0.18	0.216
A_s		0.02	0.03	0.036
b		0.04	0.02	0.045
d		0.07	0.05	0.086
$k_1 k_3$	0.72	0.12	0.05	0.130
η	0.59	0.05	0.00	0.050



U.S. Army Corps of Engineers

Figure A-4. Mean and Standard Deviation Values for 29 Waveforms



U.S. Army Corps of Engineers

Figure A-5. Variation Coefficient as a Function of Frequency for 29 Waveforms

A-6. Errors in use of mathematical models

a. In the design of structures the following simplifying assumptions are often made:

- Material behavior is elastoplastic.
- Wave input is triangular.
- Damping is negligible.
- The structural element behaves as an SDOF system.

These assumptions give the so-called equivalent dynamic system. Equivalence is obtained by finding a correspondence at all times between the displacement, velocity, and acceleration of the SDOF system and the governing dimension of the actual structures. Also, the external work must equal the sum of the kinetic and strain energies for both the equivalent system and the actual structure. There is often a bias in the development of an equivalent system; the bias often can be determined by comparing the mathematical model with exact solutions.

b. An example of modeling equivalence is given below (para. A-7) for a simply supported, uniformly loaded beam. Expressions similar to those below can also be obtained for the fixed-end beam as well as for various load and support conditions for beams, slabs, and other structural elements. With the load, mass, and resistance factors known, a structural element may be analyzed as an SDOF system to obtain its response under dynamic load.

A-7. Simply supported, uniformly loaded beam

a. *Equivalent SDOF.* The equivalent spring/mass systems for the approximate models are given in figure A-6 (COE, 1957) and are described below for elastic range and plastic range. Mathematical symbols are those found in the AISC Standard Handbook.

b. *Elastic Range.* For the model during the elastic stage, determine load, mass, and resistance as follows:

(1) *Load factor.* The deflected shape of the beam under dynamic loading is considered to be the same as that for static loading. For the simple supported beam

$$y = \frac{p(t)x}{24EI} (L^3 - 2Lx^2 + x^3) \tag{A-29}$$

with the mid-span deflection equal to

$$y_c = \frac{5L^4}{384EI} \cdot p(t) \tag{A-30}$$

The deflection of the equivalent SDOF system, y_e , at any time is taken equal to the mid-span deflection of the actual beam y_c , i.e. $y_e = y_c$.

$$\text{From } W_a = W_e \tag{A-31}$$

where

$$W_a = \text{Work done on the beam at any time} = \int_0^L \frac{1}{2} y p(t) dx$$

$$W_e = \text{Work done on the equivalent SDOF system} = \frac{1}{2} P_e(t) y_e$$

obtain K_L , the ratio of equivalent load to actual load:

$$K_L = \frac{P_e(t)}{p(t)L} = \frac{16}{25} \tag{A-32}$$

where $P_e(t)$ = Equivalent load on the SDOF system

(2) *Mass Factor.* From the relationship for kinetic energies, $(KE)_a = (KE)_e$, obtain

$$\int_0^L \frac{1}{2} m \dot{y}^2 dx = \frac{1}{2} M_e \dot{y}_e^2 \tag{A-33}$$

where M_e is the equivalent mass of the SDOF system. Then K_m the mass factor is

$$K_m = \frac{M_e}{mL} = \frac{1}{2} \tag{A-34}$$

(3) *Resistance Factor.* From $y_c = 5pL^4/384EI$, $R = ky_c$ for the actual beam, and $R_e = k_e y_e$ for the equivalent SDOF system, since

$y_e = y_c$, then

$$\frac{R_e}{R} = \frac{k_e}{k} \tag{A-35}$$

k is the load required to cause unit deflection of the beam at mid-span; hence

$$k = \frac{384EI}{5L^3} \tag{A-36}$$

k_e is obtained by equating the strain energy of the deflected shape of the beam to that of the equivalent system.

$$\int_0^L \frac{EI}{2} (y'')^2 dx = \frac{1}{2} k_e y_e^2 = \frac{1}{2} k_e y^2 \tag{A-37}$$

where y'' is the second derivative with respect to x of the beam deflection equation. Integrating this expression gives

$$\frac{k_e}{k} = \frac{16}{25} \tag{A-38}$$

the same ratio as the load factor.

(4) *Natural Period.* The natural period of the equivalent system is usually obtained by considering

the stiffness of beam and spring equal and obtaining a load-mass factor $K_{LM} = K_M/K_L$, then

$$T = 2\pi\sqrt{\frac{M_3}{k_e}} = 2\pi\sqrt{\frac{K_{LM}mL}{k}} \quad (A-39)$$

c. *Plastic range.* A linear deflection curve is assumed after a plastic hinge is developed at the mid-span. Then $y = y_c \frac{2x}{L}$ and $y_e = y_c$. By equating the expressions for work done, we obtain the load factor

$$K_L = \frac{P_e(t)}{p(t)L} = \frac{1}{2} \quad (A-40)$$

Equating the expressions for the kinetic energy, the mass factor $K_m = \frac{M_e}{mL} = \frac{1}{3}$. Strain energies for beam and equivalent system are equated as follows. Strain energy of the beam

$$(SE)_a = 2M_c\theta_c \quad (A-41)$$

where

$$\begin{aligned} M_c &= R L/8 \\ \theta_c &= 2y_c/L \end{aligned}$$

For the equivalent system, $(SE)_e = R_e y_e$, since $y_c = y_e$

$$R_e y_c = \frac{R y_c}{2} \quad (A-42)$$

and

$$\frac{R_e}{R} = 1/2 \quad (A-43)$$

The resistance factor for the plastic range is 1/2, compared to 16/25 for the elastic (eq. A-38).

d. *Comparison with exact solutions.* The equivalent SDOF described above is approximate because of two assumptions: (1) the static deflection shape is used instead of the modal shape, and (2) higher modes are neglected. Exact solutions for undamped elastic systems were compared with solutions by the approximation method; figure A-7 reproduced from COE (1957) shows the maximum possible errors in using an equivalent SDOF system. The loading in this case is triangular with time. It is seen that the exact solution gives higher values for shear at the supports, mid-span moments, and mid-span deflections. In figure A-8 a similar comparison is made for a fixed-end beam under a uniform triangular load. The errors in maximum moments and shears are known in this example. The equivalent SDOF model gives results on the unconservative side. Unless such explicit comparisons are made between models and exact solutions, the designer should allow for errors in

mathematical modeling by including an estimated uncertainty when determining the load and capacity factors for the structural element. Note that the errors in these examples were all one-sided. A bias factor must therefore be used to account for such errors.

A-8. Uncertainties in resisting capacity of reinforced concrete elements

a. *General.* There are uncertainties in the properties of reinforced concrete sections that will influence the accuracy of equations for moment and shear resistance as given in chapter 6. These uncertainties, adopted from Gallo-Ang (1976), are delineated below.

b. *Uncertainties in moment resistance.* The moment capacity of reinforced concrete elements that fail through yielding of the tension reinforcement is expressed as:

$$M_u = \left[C_c \left(1 - C_c \frac{\eta}{f'_c b d} \right) \right] d + C_s (d - d') - p \left(\frac{d - d'}{2} \right) \quad (A-44)$$

where

$$\begin{aligned} C_c &= P + T_s - C_s \\ T_s &= A_s f_y \\ C_s &= A'_s \left[c f_y - k_3 f'_c \right] \end{aligned}$$

The constants k_3 and $\eta (= k_2/k_1 k_3)$ depend on the assumed concrete stress block distribution with $k_3 \cong 0.85$, $\eta \cong 0.59$, and

$$c \cong \frac{\bar{f}'_s}{\bar{f}_y} \quad (A-45)$$

Other symbols are conventional ACI notation. The COV of M_u is obtained from the variations of its component variables using the methods described in paragraph A-4 above. Figure A-9 gives the uncertainties in M_u for three sets of conditions (Gallo-Ang, 1976). In the figures, \bar{q} and \bar{q}' are the mean values of A_s/bd and A'_s/bd , respectively. \bar{P} and \bar{P}_B are the mean values of the axial load and the balanced axial load.

c. *Uncertainties in shear resistance.* Consider the possibility that shear failure will occur before the ultimate moment capacity of the member is exceeded. The shear capacity is

$$V_u = V_c + V_s \quad (A-46)$$

where V_c is the shear carried by the concrete and V_s is the shear carried by the transverse reinforcement. Using ACI notation

$$V_u = v_c b d + \frac{d}{s} A_v f_y \quad (A-47)$$

where

$$v_c = 1.9\sqrt{f'_c} + 2500\rho \frac{Vd}{M - P\left(\frac{h}{2} - \frac{d}{8}\right)} \quad (A-48)$$

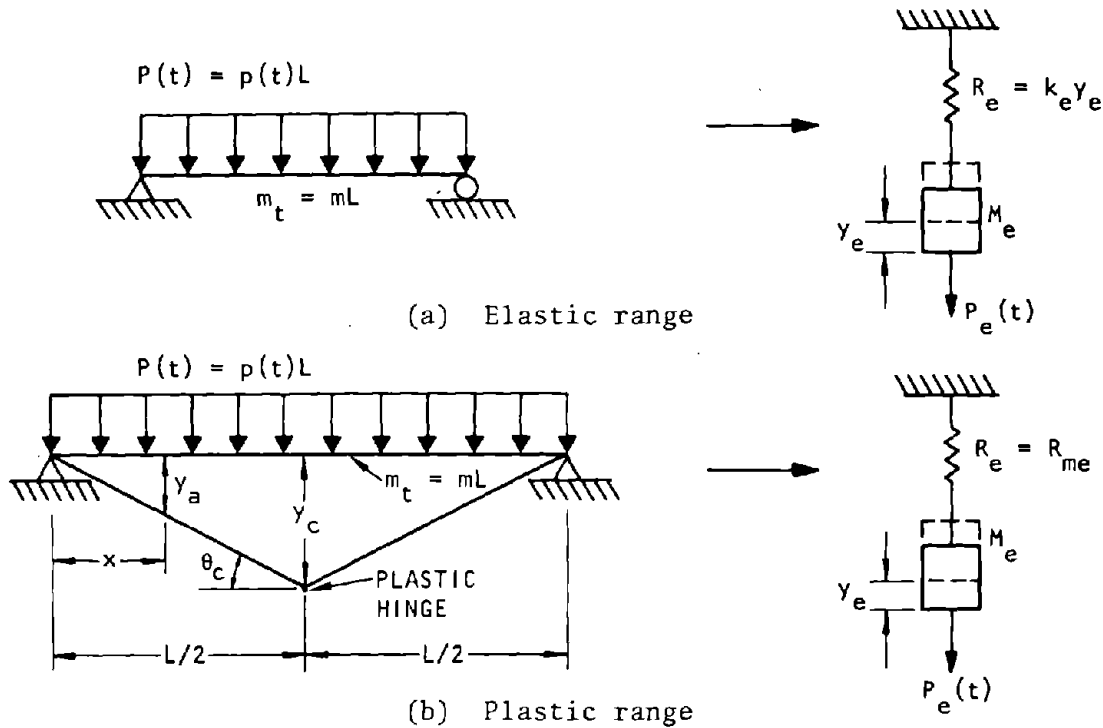
$$\leq 3.5\sqrt{f'_c} \sqrt{1 + 0.002 \frac{P}{bh}} \quad (A-49)$$

is an expression for the shear cracking stress in concrete. The COV for v_c is given (Gallo-Ang, 1976) as

$$\Omega_{v_c} = \frac{1}{v_c} \left[\left[\frac{1.9\sqrt{f'_c}}{2} \right]^2 \Omega_{f'_c}^2 + (2500 \bar{\rho} \left(\frac{V}{M_m} \right) d)^2 \left(\Omega_{A_s}^2 + \Omega_b^2 + \Omega_{V/M_m}^2 \right) \right]^{1/2} \quad (A-50)$$

when equation A-48 governs, and as

$$\Omega_{v_c} = \frac{1}{2} \left[\Omega_{f'_c}^2 + \left\{ \frac{0.002P/bh}{1 + 0.002P/bh} \right\}^2 \left(\Omega_P^2 + \Omega_b^2 + \Omega_h^2 \right) \right]^{1/2}$$



Strain Range	Load Factor K_L	Mass Factor K_M	Load-Mass Factor K_{LM}	Maximum Resistance R_m	Spring Constant k	Dynamic Reaction V
S.S. Beam						
Elastic Range	0.64	0.50	0.78	$\frac{8M_P}{L}$	$\frac{384EI}{5L^3}$	$0.39 R + 0.11P$
Plastic Range	0.50	0.33	0.66	$\frac{8M_P}{L}$	0	$0.38 R_m + 0.12P$
Fixed-End Beam						
Elastic Range	0.53	0.41	0.77	$\frac{12M_{Ps}}{L}$	$\frac{384EI}{L^3}$	$0.36 R + 0.14P$
Elasto-Plastic Range	0.64	0.50	0.78	$\frac{8}{L}(M_{Ps} + M_{Pm})$	$\frac{384EI}{5L^3}$	$0.39 R + 0.11P$
Plastic Range	0.50	0.33	0.66	$\frac{8}{L}(M_{Ps} + M_{Pm})$	0	$0.38 R_m + 0.12P$

Figure A-6. Two Examples of Dynamic Design Factors for Equivalent SDOF Systems (COE, 1957).

when

$$v_c = 3.5 \sqrt{f'_c} \sqrt{1 + 0.002 \frac{P}{bh}}$$

Figure A-10 gives the COV for v_c and V_u . The total COV of V_u is given as a function of r_s , where

$$r_s = \frac{\bar{v}_c \bar{b} \bar{d}}{\frac{\bar{d}}{s} \bar{A}_v \bar{f}_y} \quad (A-52)$$

in which s is stirrup spacing. Figure A-10c is based on the expression

$$\begin{aligned} \Omega_{V_u}^2 = & \Omega_d^2 + \left[\frac{r_s}{r_s + 1} \right]^2 \left[\Omega_{V_c}^2 + (1 - c) \Omega_b^2 \right] \\ & + \left[\frac{1}{r_s + 1} \right]^2 \left[\Omega_s^2 + \Omega_{A_v}^2 + \Omega_{f_y}^2 \right] \end{aligned} \quad (A-53)$$

where

$$c = 2 - \left(\frac{3.8 \sqrt{f'_c}}{\bar{v}_c} \right) \quad \text{or} \quad \frac{0.002 \bar{P} / \bar{b} \bar{h}}{1 + 0.002 \bar{P} / \bar{b} \bar{h}}$$

depending on whether equation A-48 or A-49 is used to calculate v_c . The bias and prediction error associated with evaluation of v_c and V_u are given in Gallo-Ang (1976). For v_c , a bias factor of 0.96 to 1.29, depending on the amount of reinforcement and the axial load, is specified. The uncertainty due to prediction error is estimated to be about 16%. For the total shear capacity, v_u , the bias factor and the prediction error are estimated to be 1.14 and 16% for $p=0$, and 1.23 and 11% for $P>0$, respectively.

d. Uncertainties in stiffness. The stiffness EI of a beam at yield is given by

$$EI = \frac{M_y}{\phi_y} \quad (A-54)$$

where ϕ_y is the curvature at yield. Test data from experiments performed by a large number of investigators are summarized in table A-3 (Gallo-Ang, 1976), giving the prediction uncertainty. In addition to the prediction uncertainty Δ_x (tabulated values), the coefficient of variation, δ_x , of EI must also be known. This is estimated to be about 0.20 for most reinforced concrete members. The COV is stiffness, therefore, for the first set of tests given in table A-3 is

$$\Omega_{EI} = \sqrt{(0.20)^2 + (0.20)^2} = 0.28 \quad (A-55)$$

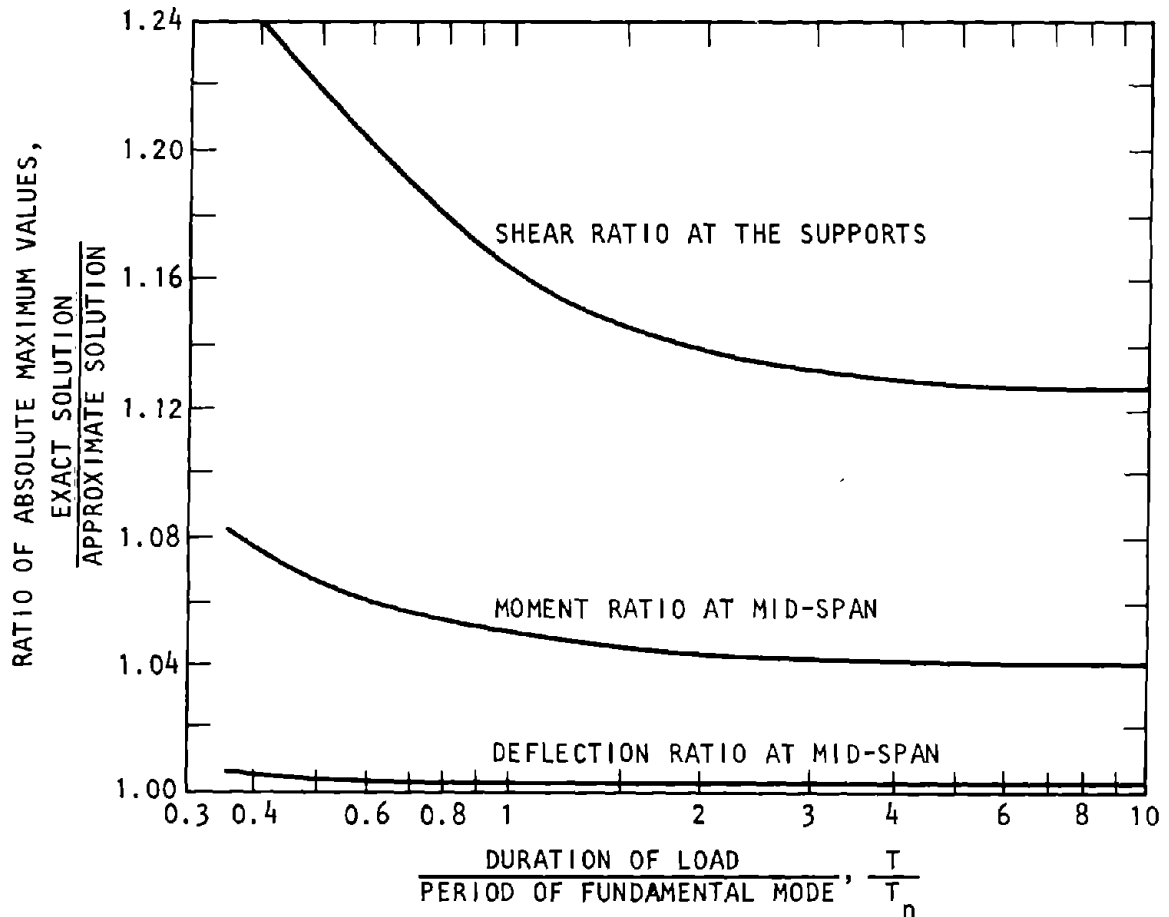


Figure A-7. Maximum Possible Errors in Using an Equivalent SDOF System. Simply Supported Beam Subjected to a Linearly Decaying Uniform Load. (COE, 1957)

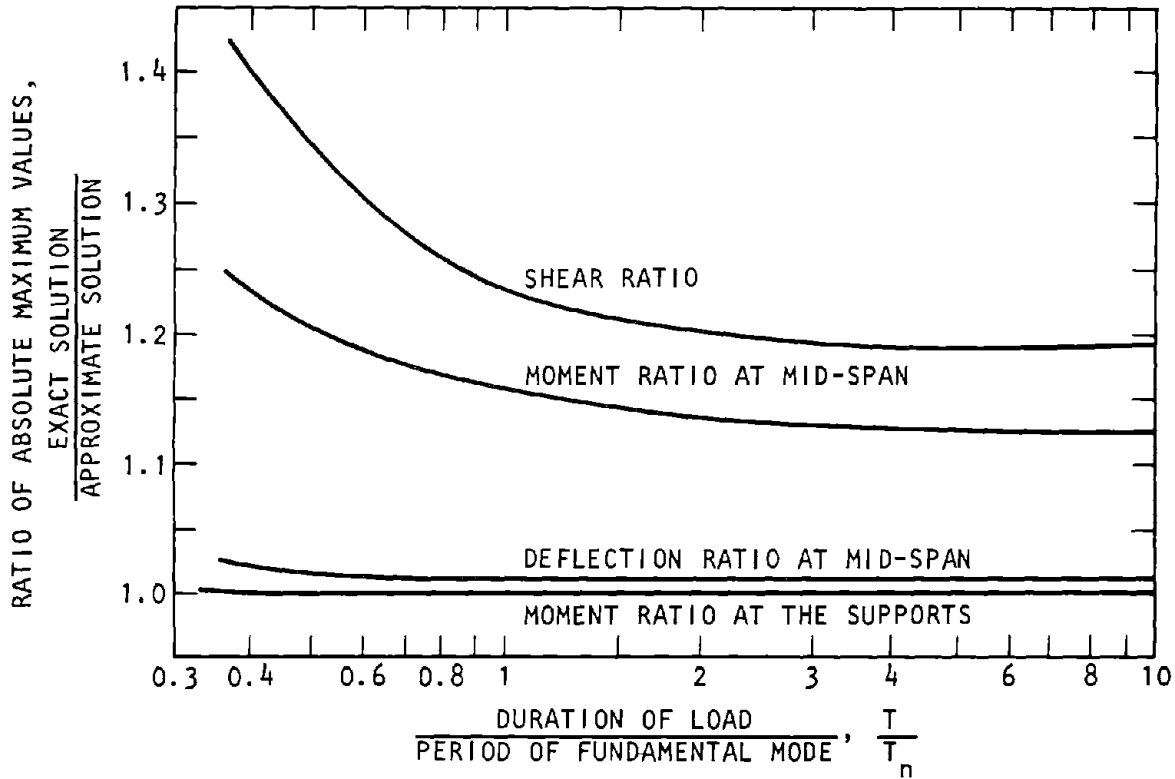


Figure A-8. Maximum Possible Errors in Using an Equivalent SDOF System. Fixed-End Beam Subjected to a Linearly Decaying Uniform Load.

Figure A-11 gives COVs in stiffness for symmetrically reinforced columns.

e. *Uncertainties in beam-column interaction.* Ellingwood (1977) has investigated the uncertainties in the estimate of the resistance of a reinforced concrete beam column. Resistance at fixed eccentricity is given by

$$R = \left[p^2 + \left(\frac{M}{h} \right)^2 \right]^{1/2} \quad (A-56)$$

if thrust and moment increase in proportion until the ultimate strength is reached. For this case $M = Pe$ where e is the eccentricity, and e/h is the eccentricity ratio ($h =$ depth of beam). In addition to the uncertainties of material properties, dimensions, and analysis assumptions discussed earlier, Ellingwood has concluded that good concrete quality control appears essential when e/h is small. At large e/h , bar placement is the key parameter.

A-9. Tolerance in reinforced concrete construction

a. Tight tolerances increase construction costs; loose or no tolerances can adversely affect structure function and/or safety. Tolerances actually obtained in concrete construction are much larger than commonly expected (Birkeland et al., 1971). In hardened reinforced-concrete structures, where heavier steel reinforcement is used, specified construction

tolerances are more difficult to achieve, unless construction control is very meticulously exercised. Designers and constructors should arrive at a mutual understanding of how tolerances should be considered in design, controlled during construction, or enforced by inspection.

b. As guidelines for dimensional tolerances consider the following:

(1) Recognize that published specifications for concrete tolerances will probably be difficult to achieve. Tolerances that the constructor considers unusually severe or unrealistic will increase the construction cost with no guarantee that they will be achieved. Assume that a realistic tolerance for most concrete dimensions on surfaces is ± 1 in.

(2) Select design concepts that will accommodate realistically obtainable tolerances. Consider the impact on design if the specified tolerances are not met and how these out-of-specification variations can be accommodated.

(3) Scale the drawings so that the constructor can easily identify critical dimensions and the inspector can measure them directly.

(4) Select construction concepts that will directly control critical dimensions.

c. As guidelines for placement of reinforcing bars consider the following:

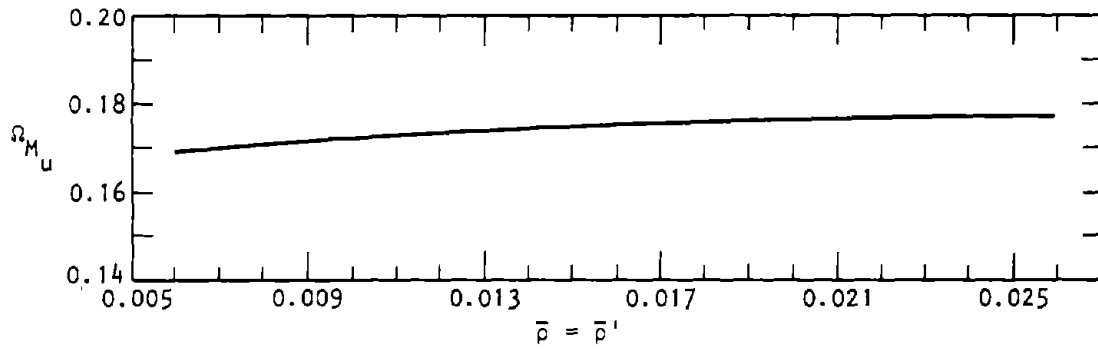
(1) Bar placement errors in concrete columns can result in excessive concrete cover over the exterior

bars, which causes decreased column capacities, especially for high eccentricities of loading (Drysdale, 1975). Calculations based on actual location of column reinforcing in more than 230 existing columns indicated strength reductions of greater than 15% in some instances, with a mean reduction of 5 percent (a bias factor of 0.95) and a coefficient of variation of 3 percent.

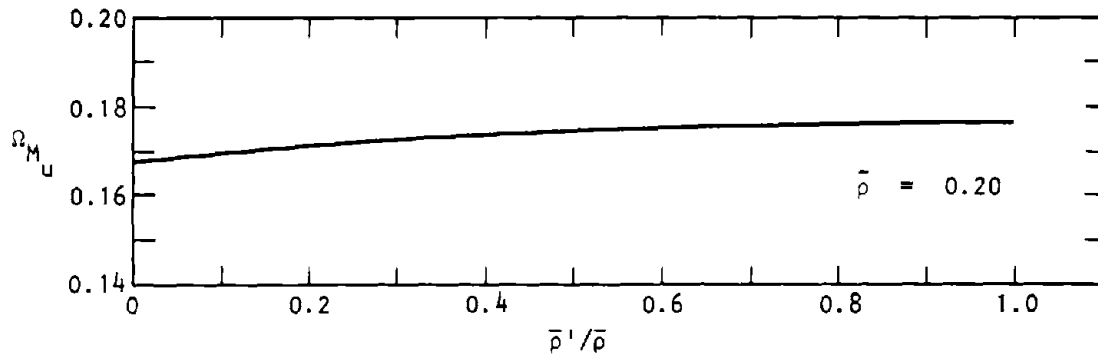
(2) Mean ultimate bending capacity may be reduced. The combined effect of variability in bar placement and beam dimensions was statistically evaluated for more than 250 cast-in-place reinforced

concrete beams and joints (Connolly and Brown, 1976) showing a mean reduction of 4% in ultimate bending moment capacity (a bias factor of 0.96).

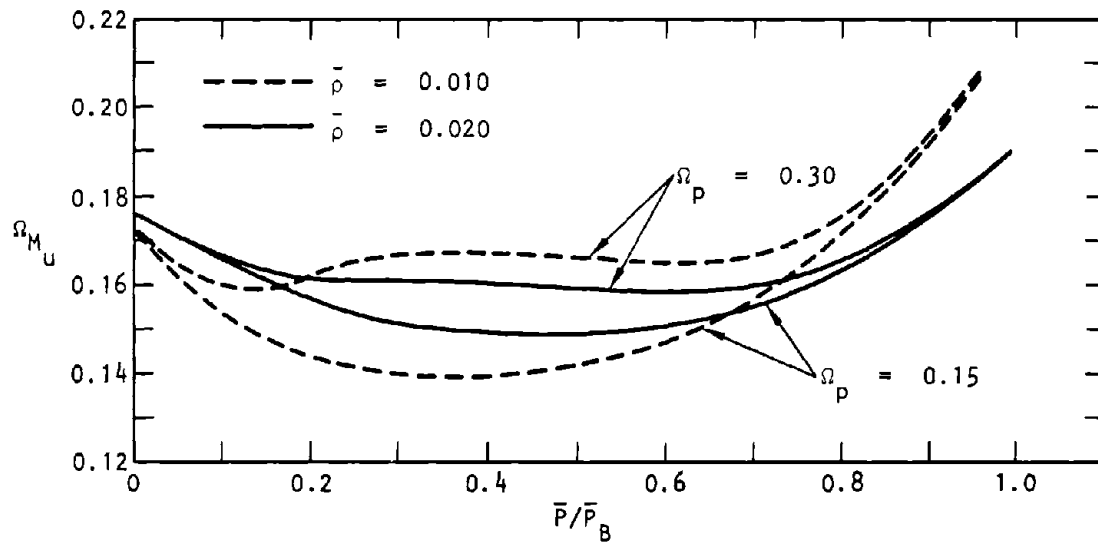
d. In selection of tolerances, a cost-effectiveness evaluation will show for each case if the use of larger uncertainties in design will be more economical than adherence to stricter tolerances in order to reduce the design uncertainties. Sensitivity studies will be required. Uncertainties in tolerances should be estimated and their effect included in the design process.



(a) Symmetrically reinforced beam

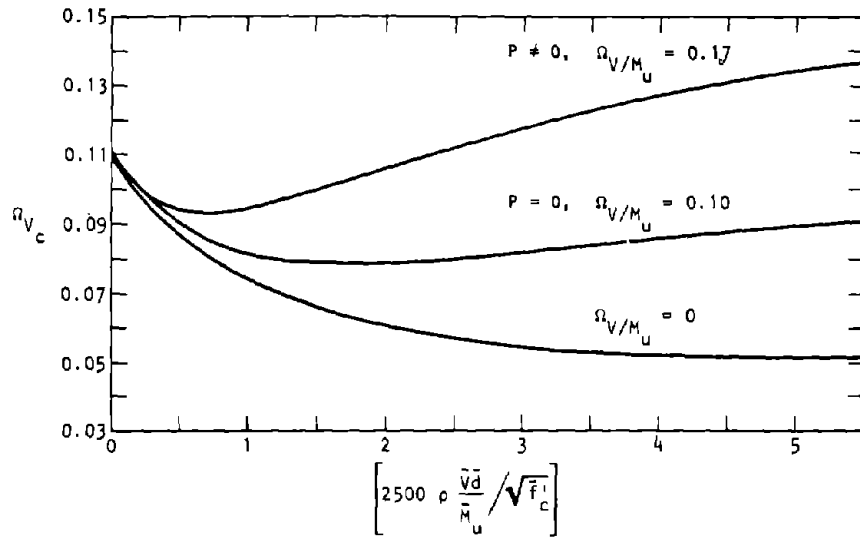


(b) Doubly reinforced beam

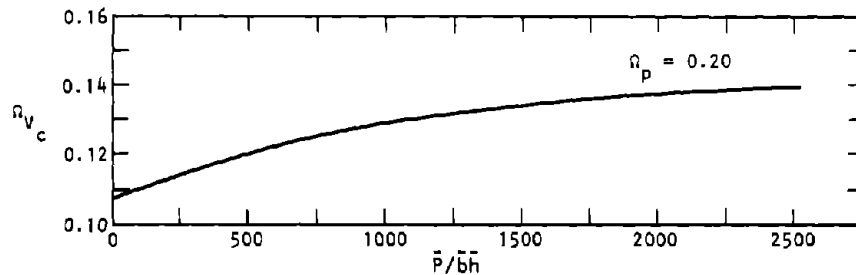


(c) Symmetrically reinforced column

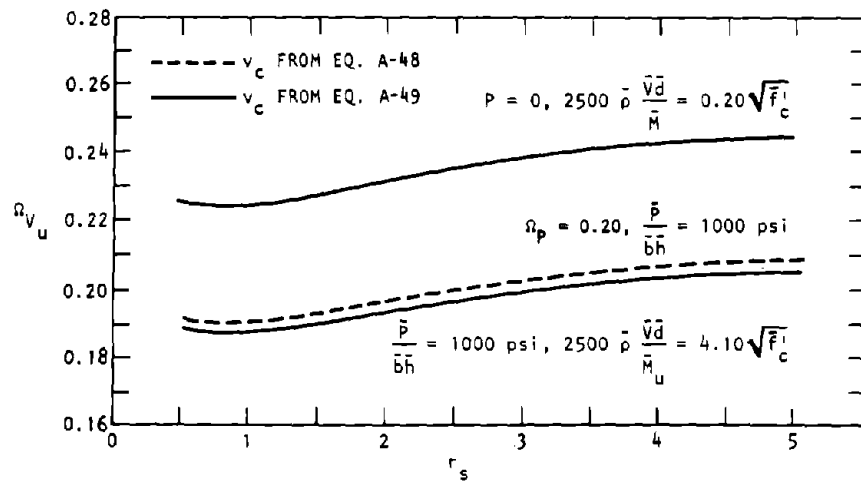
Figure A-9. Coefficients of Variation in Flexural Capacity $\bar{f}_c = 4.7$ ksi, $\bar{f}_y = 47.7$ ksi (Gallo-Ang, 1976)



(a) COV of v_c , (Eq. A-48)



(b) COV of v_c , (Eq. A-49)

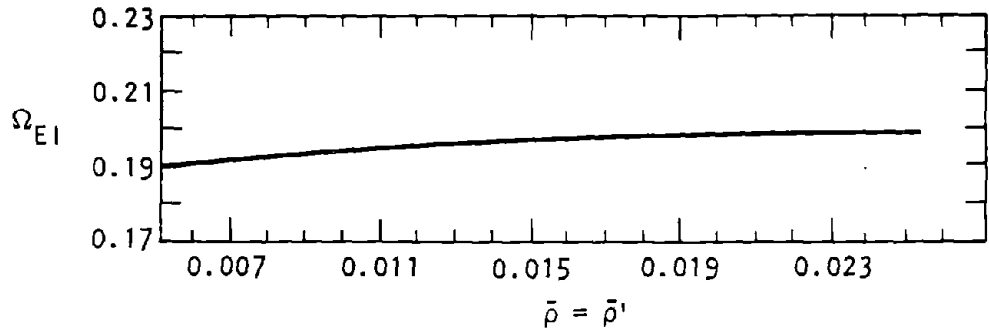


(c) COV in shear capacity

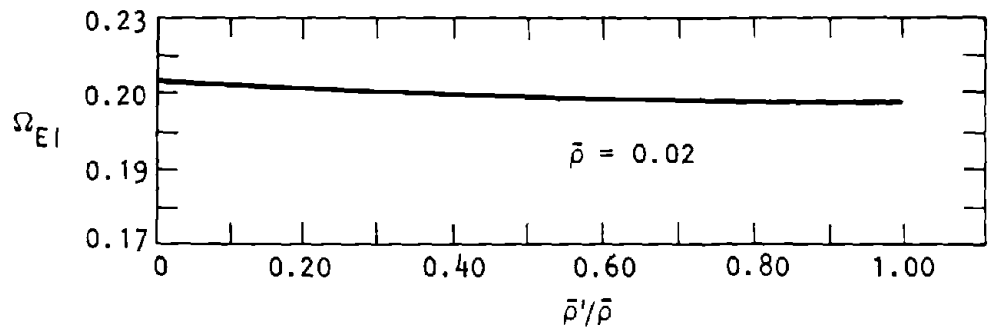
Figure A-10. Coefficients of Variations for Shear, V_c and V_u (Gallo-Ang, 1976)

Table A-3. Imperfection in the Estimation of Stiffness, EI (Gallo-Ang, 1976)

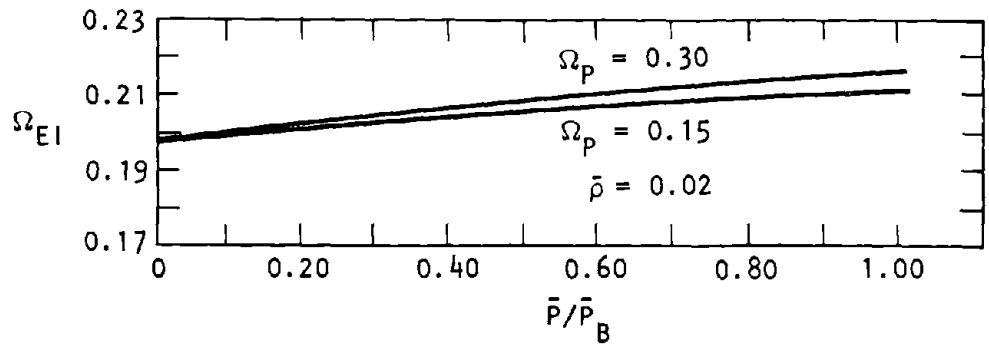
Number of Tests	Bias, \bar{N}_X	Prediction COV, Δ_X
Beams with Concentrated Loads		
31	0.79	0.20
40	0.64	0.20
19	0.79	0.15
17	0.81	0.04
12	0.93	0.14
119	0.76	0.21
Beams with Uniform Load		
30	1.08	0.11
90	1.05	0.14
107	1.02 (with top reinforcement)	0.22
	0.95 (without top reinforcement)	0.12



(a) Symmetrically reinforced beam



(b) Doubly reinforced beam



(c) Symmetrically reinforced column

Figure A-11. Coefficient of Variation of Stiffness EI; (Gallo, 1976) $f_c = 4.7$ ksi, $f_y = 47.7$ ksi

APPENDIX B FINITE ELEMENT METHOD OF STRUCTURAL ANALYSIS

B-1. Solution of simultaneous equations

Computer analysis of structures usually leads to the solution of a set of linear simultaneous equations. Numerous methods are available for the solution of these equations. One method that is used in most computer programs for structural analysis will be discussed below. This method is usually called Choleski matrix decomposition technique (Rubenstein, 1966). A system of n linear simultaneous equations may be written in the general form

$$\begin{aligned} a_{11}x_1 + a_{12}x_2 + \dots + a_{1n}x_n &= b_1 \\ a_{21}x_1 + a_{22}x_2 + \dots + a_{2n}x_n &= b_2 \\ \vdots &\vdots \\ a_{n1}x_1 + a_{n2}x_2 + \dots + a_{nn}x_n &= b_n \end{aligned} \quad (B-1)$$

The above equations can be arranged in matrix form as

$$\begin{bmatrix} a_{11} & a_{12} & \dots & a_{1n} \\ a_{21} & a_{22} & \dots & a_{2n} \\ \vdots & \vdots & \ddots & \vdots \\ a_{n1} & a_{n2} & \dots & a_{nn} \end{bmatrix} \begin{bmatrix} x_1 \\ x_2 \\ \vdots \\ x_n \end{bmatrix} = \begin{bmatrix} b_1 \\ b_2 \\ \vdots \\ b_n \end{bmatrix} \quad (B-2)$$

or simply

$$[A][X] = [B]$$

In almost all structural problems, the resulting simultaneous equations are such that the coefficient matrix [A] is symmetric and nonsingular. Thus, if [A] is symmetric and nonsingular, it can be expressed as the product of a lower triangular matrix [L], a diagonal matrix [D], and an upper triangular matrix [U], so that

$$[A] = [L][D][U] \quad (B-3)$$

In addition, the matrices [L] and [U] are such that one is the transpose of the other.

$$[L] = [U]^T \quad (B-4)$$

Therefore, [A] can be written as the product of

$$[A] = [L][D][L]^T \quad (B-5)$$

where

$$[L] = \begin{bmatrix} 1 & 0 & 0 & \dots & 0 \\ \ell_{21} & 1 & 0 & \dots & 0 \\ \ell_{31} & \ell_{32} & 1 & \dots & 0 \\ \vdots & \vdots & \vdots & \ddots & \vdots \\ \ell_{n1} & \ell_{n2} & \ell_{n3} & \dots & 1 \end{bmatrix}$$

and

$$[D] = \begin{bmatrix} d_1 & 0 & 0 & \dots & 0 \\ 0 & d_2 & 0 & \dots & 0 \\ 0 & 0 & d_3 & \dots & 0 \\ \vdots & \vdots & \vdots & \ddots & \vdots \\ 0 & 0 & 0 & \dots & d_n \end{bmatrix}$$

and therefore

$$[L]^T = \begin{bmatrix} 1 & \ell_{21} & \ell_{31} & \dots & \ell_{n1} \\ 0 & 1 & \ell_{32} & \dots & \ell_{n2} \\ 0 & 0 & 1 & \dots & \ell_{n3} \\ \vdots & \vdots & \vdots & \ddots & \vdots \\ 0 & 0 & 0 & \dots & 1 \end{bmatrix}$$

The elements of matrices [L] and [D] to satisfy equation B-5 can be obtained from the following relations

$$d_j = a_{jj} = \sum_{m=1}^{j-1} d_m \ell_{jm}^2 \quad j = 1, 2, \dots, n$$

$$\ell_{ij} = a_{ij} = \sum_{m=1}^{j-1} \ell_{im} d_m \ell_{jm} / d_j$$

$$i = j + 1, \dots, n, j = 1, 2, \dots, n \quad (B-6)$$

Using the above decomposition of [A], the simultaneous equations B-5 can be written as

$$[L][D][L]^T[X] = [B] \quad (B-7)$$

Now, defining

$$[Z] = [D][L]^T[X] \quad (B-8)$$

equation B-7 can be written as

$$[L][Z] = [B] \quad (B-9)$$

Thus, it is seen that the solution for [X] is obtained in two steps; first solving equation B-9 (forward reduction) and the equation B-8 (back substitution). The elements of [Z] and [X] are given by

$$z_i = b_i - \sum_{m=1}^{i-1} \ell_{im} z_m \quad (\text{B-10})$$

and finally

$$x_i = \frac{z_i}{d_i} - \sum_{m=i+1}^n \ell_{mi} x_m \quad (\text{B-11})$$

B-2. Force and displacement methods of structural analysis

Methods of matrix structural analysis can be divided into two categories, depending upon the nature of the unknowns used in the formulation of the problem. These methods usually are identified as force and displacement methods. In the force method, forces in the structural system are treated as unknowns, while in the displacement method, displacements are treated as unknowns. In principle, both of these methods yield the same solution, since both are based on the principle of structural mechanics. The force method is also known as the flexibility-matrix method. As mentioned before, the forces are selected as unknown in this method. A sufficient number of equations to solve for the unknowns are obtained using the equilibrium and compatibility conditions of the structural system. For statically determinate structural systems, the necessary equations are derived from the equilibrium conditions only. For the statically indeterminate systems, both the equilibrium and compatibility conditions provide sufficient number of equations for the solution. The conventional structural analysis methods for solving statically indeterminate structures such as virtual work, elastic center, and column analogy fall into this category. The displacement method is also known as the stiffness-matrix method. (Recommended textbooks are: Desai and Abel, 1972; Przemieniecki, 1968; Rubenstein, 1966; and Zienkiewicz, 1971.) In this method, the displacements of the nodes or joints are used as primary unknowns. The unknown displacements are computed by the solution of a system of linear equations obtained from the equilibrium conditions at the nodes. Since there are always as many equilibrium equations as the unknowns, no distinction is made between statically determinate and indeterminate systems by this method. The conventional structural analysis methods for solving statically indeterminate structures, such as slope-deflection or moment distribution are based on the

displacement method. Almost all of the general purpose computer programs for structural analysis that are currently being used are based on the stiffness-matrix approach. This is because for complex structures the generalization of the matrix operations becomes simpler with the stiffness method. Therefore, the force method will not be presented here and the reader is referred to available textbooks which treat matrix structural analysis. (Laurson, 1966; Martin, 1966; Przemieniecki, 1968; Rubenstein, 1966; Ural, 1971 and 1973; Wang, 1966.)

B-3. Stiffness properties of structural elements

a. Basic matrix. An important step in the stiffness-matrix method of structural analysis is the computation of the stiffness characteristics of the individual structural elements into which the structure is idealized for the purpose of the analysis. The stiffness matrix of a structural element as used in the matrix displacement method expresses a relationship between the forces and displacements in the element. Thus, the stiffness matrix is a basic and inherent property of the element and is based on the geometry and material properties of the element. In the following sections, the stiffness matrices for beam and truss elements will be derived in a form suitable for the use in the matrix stiffness method of structural analysis.

b. Stiffness matrix of a truss element. Figure B-1 shows a typical uniform truss element (or pin-jointed bar). The displacements in the bar are assumed to be completely described by the axial displacements u_1 and u_2 of its two ends, joints 1 and 2. The force distribution in the element is described by the axial forces p_1 and p_2 as shown at joints 1 and 2. The stiffness matrix [k] of the bar relates the joint displacements with the joint forces. Thus,

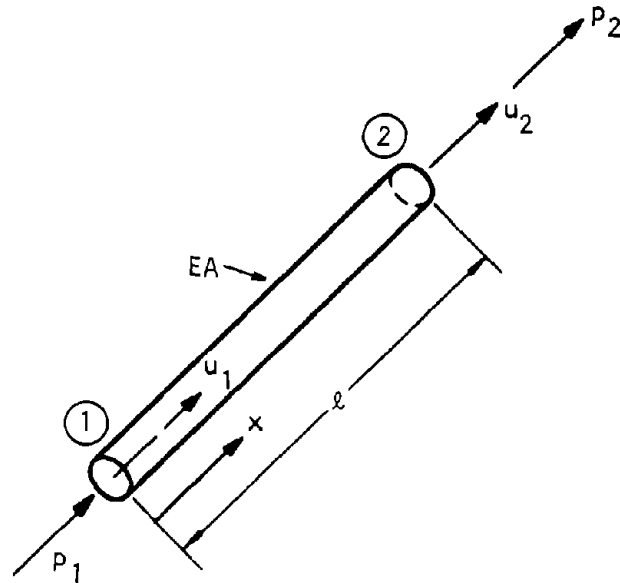
$$\begin{bmatrix} p_1 \\ p_2 \end{bmatrix} = \begin{bmatrix} k_{11} & k_{12} \\ k_{21} & k_{22} \end{bmatrix} \begin{bmatrix} u_1 \\ u_2 \end{bmatrix} \quad (\text{B-13})$$

or simply

$$[p] = [k][u]$$

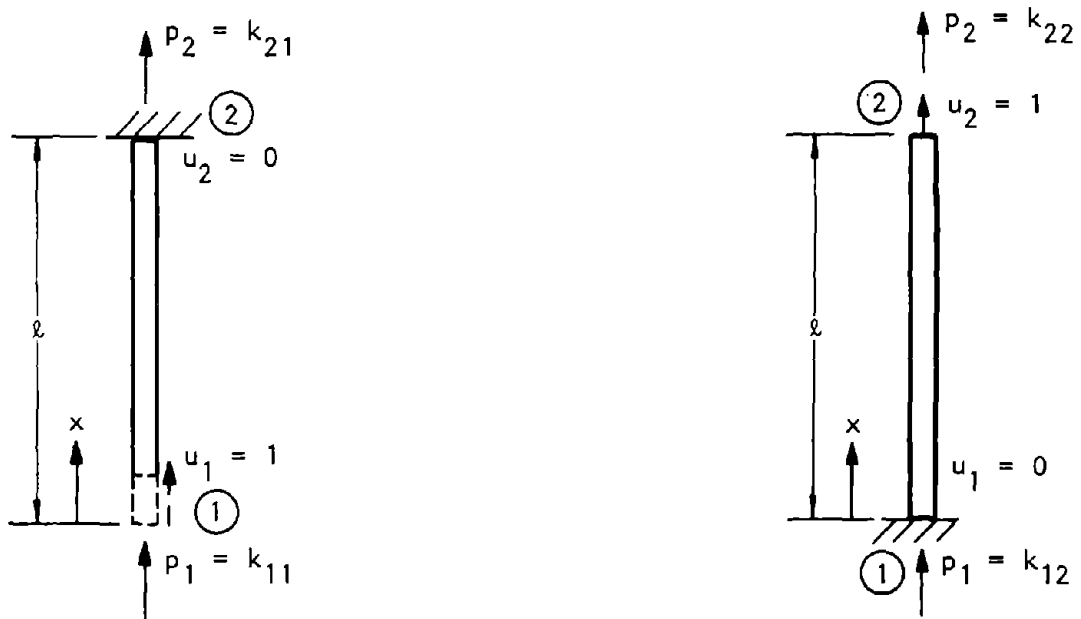
where k_{ij} , the element of the stiffness matrix [k], is defined as equal to the force p_j when $u_j = 1$ and all other u_i 's are taken as zeros. Thus, k_{11} for example can be obtained by considering the bar to be fixed at joint 2 and determining the force p_1 at joint 1 necessary to displace the joint 1 by one unit ($u_1 = 1$). If E, A and ℓ represent respectively the Young's modulus of the material, the cross-sectional area and the length of the truss member, k_{11} and k_{21} can be obtained with reference to figure B-2a as follows. The constant axial stress in the bar is given by

$$\sigma = p_1/A \quad (\text{B-14})$$



U.S. Army Corps of Engineers

Figure B-1. Uniform Truss Element



(a) Computation of k_{11} and k_{21}

(b) Computation of k_{12} and k_{22}

U.S. Army Corps of Engineers

Figure B-2. Bar Configurations for Computation of Stiffness Matrix Terms

and the constant strain is given by

$$\epsilon = \sigma/E = p_1/AE \tag{B-15}$$

Therefore, the total displacement at joint 1 is given by

$$u_1 = \epsilon \ell = \frac{P_1 \ell}{AE} \tag{B-16}$$

or

$$p_1 = u_1 AE / \ell$$

Therefore, by definition, $k_{11} = p_1$ when $u_1 = 1$

$$k_{11} = AE / \ell \tag{B-17}$$

The equilibrium of forces requires that

$$p_2 = -p_1 \text{ or } k_{12} = -AE / \ell \tag{B-18}$$

Similarly, from figure B-2b k_{12} and k_{22} can be obtained as

$$\begin{aligned} k_{12} &= -AE/\ell \\ k_{22} &= AE/\ell \end{aligned} \tag{B-19}$$

Therefore, the force displacement relationship for the element can be written as

$$\begin{bmatrix} p_1 \\ p_2 \end{bmatrix} = \frac{AE}{\ell} \begin{bmatrix} 1 & -1 \\ -1 & 1 \end{bmatrix} \begin{bmatrix} u_1 \\ u_2 \end{bmatrix} \tag{B-20}$$

and the complete stiffness matrix of the truss element is given by

$$[k] = \frac{AE}{\ell} \begin{bmatrix} 1 & -1 \\ -1 & 1 \end{bmatrix} \tag{B-21}$$

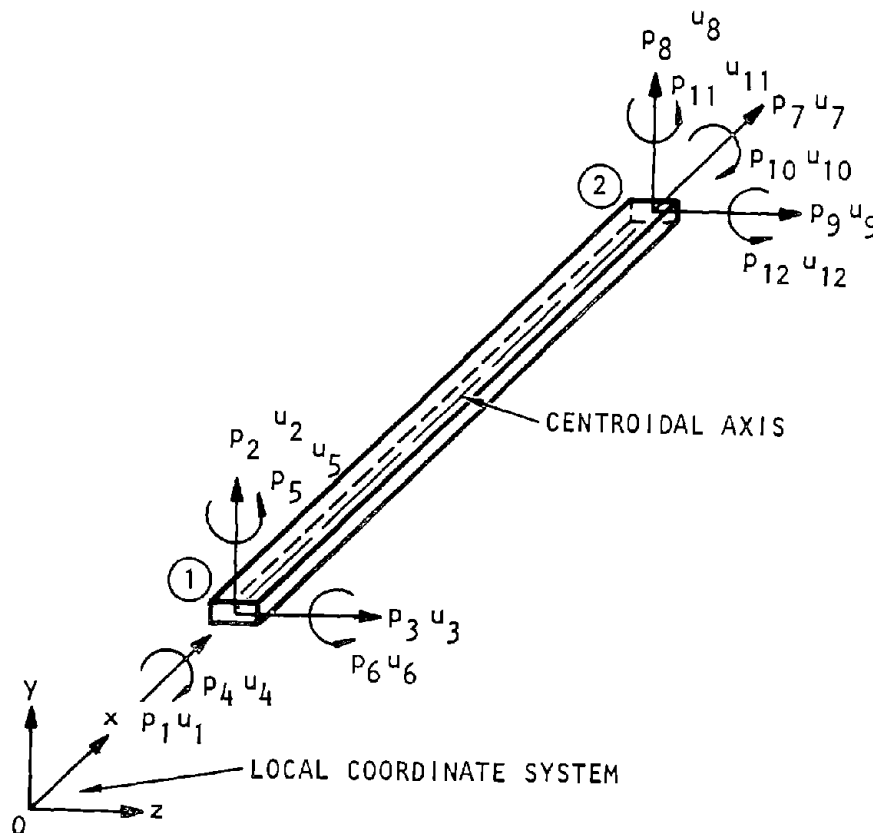
The element stiffness for the bar is derived here using only the elementary principles of strength of materials and basic definitions of the stiffness matrix. The reader is referred to textbooks (Przemieniecki, 1968; Desai-Abel, 1972; Weaver, 1967) on the finite element method or matrix structural analysis for a formal and more complete derivation of the stiffness matrix.

c. *Stiffness matrix of a beam element.* Figure B-3 shows a typical three-dimensional beam element. The beam element between the nodes is assumed to be straight and of uniform cross section. The beam is capable of resisting axial forces, bending moments about the two principal axes in the plane of its cross section, and twisting moments (torques) about its centroidal axis. The forces $p_1 \dots p_6$ act at joint 1 while the forces $p_7 \dots p_{12}$ act at joint 2. Of these forces p_1 and p_7 are axial forces; $p_2, p_3, p_8,$ and p_9 are shearing forces; $p_5, p_6, p_{11},$ and p_{12} are bending moments; and p_4 and p_{10} are twisting moments. Each of the twelve loads is associated with a corresponding displacement denoted by $u_1 \dots u_{12}$. The positive directions of the forces and displacements are shown in figure B-3. The force-displacement relation for the beam can be written as

$$\begin{bmatrix} p_1 \\ p_2 \\ p_3 \\ \vdots \\ p_{12} \end{bmatrix} = \begin{bmatrix} k_{11} & k_{12} & k_{13} & \dots & k_{1 \ 12} \\ k_{21} & k_{22} & k_{23} & \dots & k_{2 \ 12} \\ k_{31} & k_{32} & k_{33} & \dots & k_{3 \ 12} \\ \vdots & \vdots & \vdots & \ddots & \vdots \\ k_{121} & k_{122} & k_{123} & \dots & k_{1212} \end{bmatrix} \begin{bmatrix} u_1 \\ u_2 \\ u_3 \\ \vdots \\ u_{12} \end{bmatrix} \tag{B-22}$$

or

$$[p] = [k][u]$$



U.S. Army Corps of Engineers

Figure B-3. Uniform Beam Element

It is seen that the stiffness matrix for the beam is of the order 12×12 . Since k_{ij} is defined as equal to the force p_j when u_j takes a unit value and all other u_i 's are zeros, they can be computed similar to the case for a truss element. It should be noted however that by the principle of energy conservation, the stiffness matrix k must be symmetric; also, it can be seen that from the engineering theory of bending and torsion, several terms in $[k]$ become zero. As shown in the following, of the 144 terms in $[k]$, only twenty terms are nonzero and independent. The nonzero terms of the stiffness matrix are computed as follows.

d. Axial deformations. From the engineering theory of bending and torsion of a simple beam, it is seen that the axial deformations are independent of the other deformations. Therefore, the stiffness elements

$$\left. \begin{matrix} k_{11} = 0 \\ k_{77} = 0 \end{matrix} \right\} \text{except } i = 1 \text{ and } 7, j = 1 \text{ and } 7 \quad (\text{B-23})$$

The nonzero stiffness elements k_{11} and k_{77} can be evaluated from figure B-4a, similar to the computations shown in *b* above. Thus, $k_{11} = AE/\ell$ and $k_{77} = -AE/\ell$, where A , E , and ℓ represent respectively the constant cross-sectional area, Young's modulus of the material, and the length of the beam. Similarly, from figure B-4a, $k_{77} = AE/\ell$.

e. Twisting deformations. Similar to the axial deformations of beam, the twisting deformations are independent of all other deformations. Therefore, the stiffness terms associated with twisting of a beam are

$$\left. \begin{matrix} k_{i4} = 0 \\ k_{10j} = 0 \end{matrix} \right\} \text{except } i = 4 \text{ and } 10, j = 4 \text{ and } 10 \quad (\text{B-24})$$

On the basis of the engineering theory of torsion of a beam and the definitions of stiffness elements k_{44} , $k_{10\ 4}$, and $k_{10\ 10}$ are calculated as follows. From figure B-4b, the total twist of the free end of the beam is unity. Therefore, the twist per unit length is given by $1/\ell$. Therefore, the total twist at joint 1 is given by $k_{4\ 4} = p_4 = GJ/\ell$ where GJ is the torsional stiffness of the beam cross section and GJ represents the shear modulus of the material of the beam (Oden, 1967). From the equilibrium condition $k_{10\ 4} = p_{10} = -p_4 = -GJ/\ell$. Similarly, from figure B-4b, $k_{10\ 10} = p_{10} = \frac{GJ}{\ell}$.

f. Shear and bending deformations in x-y plane. Figure B-5a shows the necessary configuration for computing the terms, k_{22} , k_{62} , k_{82} and $k_{12\ 2}$. Neglecting the effect of shearing strains on deflections, it can be shown using elementary structural analysis

methods (such as Slope Deflection or Moment Distribution, AISC, 1970), that

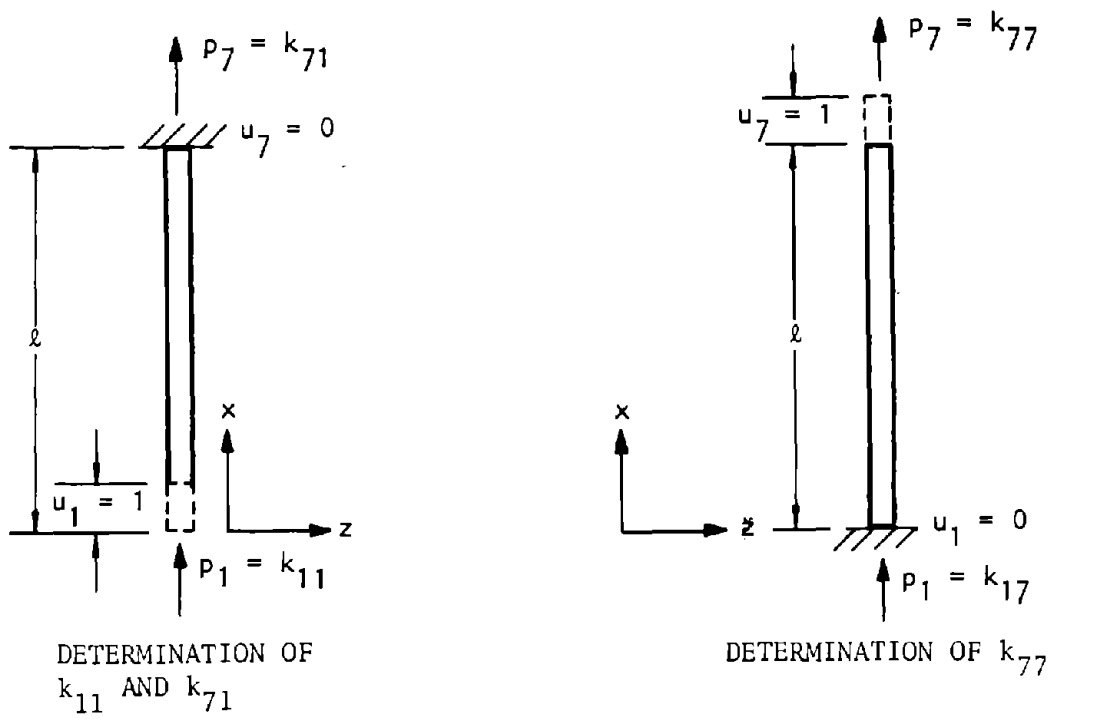
$$\begin{aligned} k_{2\ 2} &= p_2 = \frac{12\ EIz}{\ell^3} \\ k_{6\ 2} &= p_6 = \frac{6\ EIz}{\ell^2} \\ k_{8\ 2} &= p_8 = -\frac{12\ EIz}{\ell^3} \\ k_{12\ 2} &= p_{12} = \frac{6\ EIz}{\ell^2} \end{aligned} \quad (\text{B-25})$$

where I_z is the moment of inertia of the cross section of the beam associated with the bending in the xy plane (about z axis) (Oden, 1967). If the effect of shearing strains on deflection are included, the stiffness coefficients in equation B-25 modify as follows (Przenieniecki, 1968):

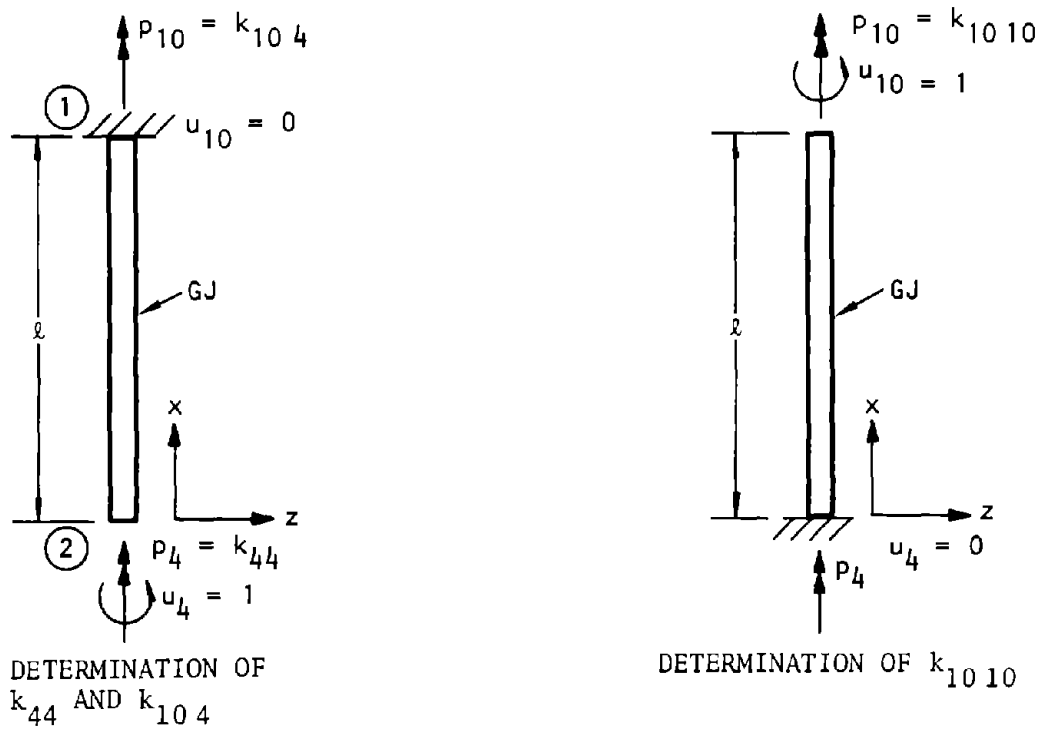
$$\begin{aligned} k_{2\ 2} &= \frac{12\ EIz}{(1 + \Phi_y)\ell^3} \\ k_{6\ 2} &= \frac{6\ EIz}{(1 + \Phi_y)\ell^2} \\ k_{8\ 2} &= \frac{12\ EIz}{(1 + \Phi_y)\ell^3} \\ k_{12\ 2} &= \frac{6\ EIz}{(1 + \Phi_y)\ell^2} \\ \text{and } \Phi_y &= \frac{12\ EIz}{G A_{sy}\ell^2} \end{aligned} \quad (\text{B-26})$$

where A_{sy} represents the effective cross-sectional area of the beam in shear. It should be noted here that if the effects of shearing strains are neglected, Φ_y is taken as zero. Shearing deformations are not significant for slender beams and hence can be neglected. However, for deep beams ($\ell/d \leq 5$) or for beams with large radius of gyration compared to length ($\ell/r \leq 20$), the effects of shear strains on the total deformations may be significant. Similarly, from figure B-5a or from the condition of symmetry

$$\begin{aligned} k_{8\ 8} &= \frac{12\ EIz}{(1 + \Phi_y)\ell^3} \\ k_{12\ 8} &= -k_{6\ 2} = -\frac{6\ EIz}{(1 + \Phi_y)\ell^2} \end{aligned} \quad (\text{B-27})$$



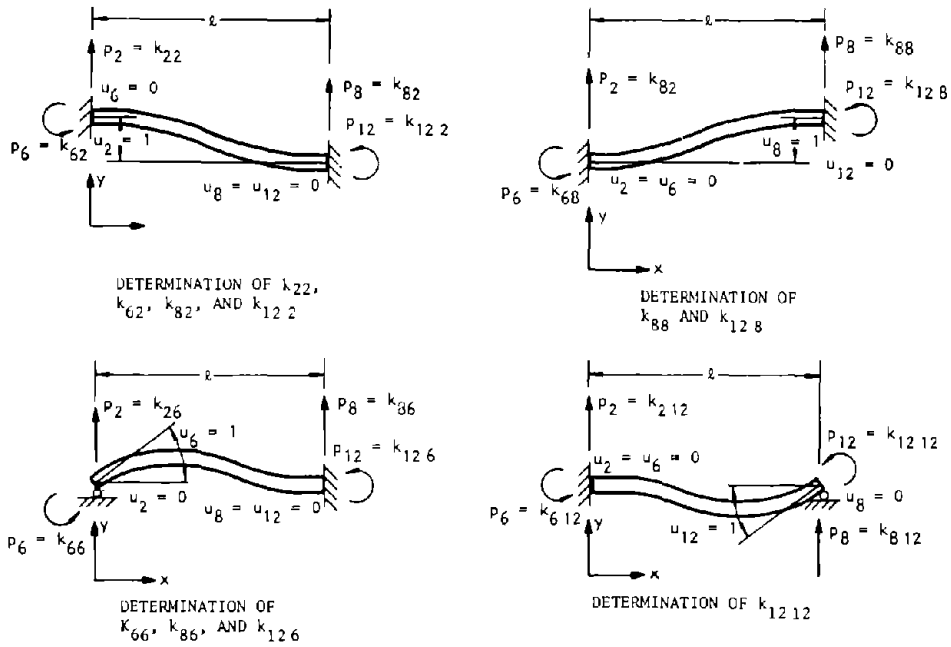
(a) AXIAL STIFFNESS TERMS



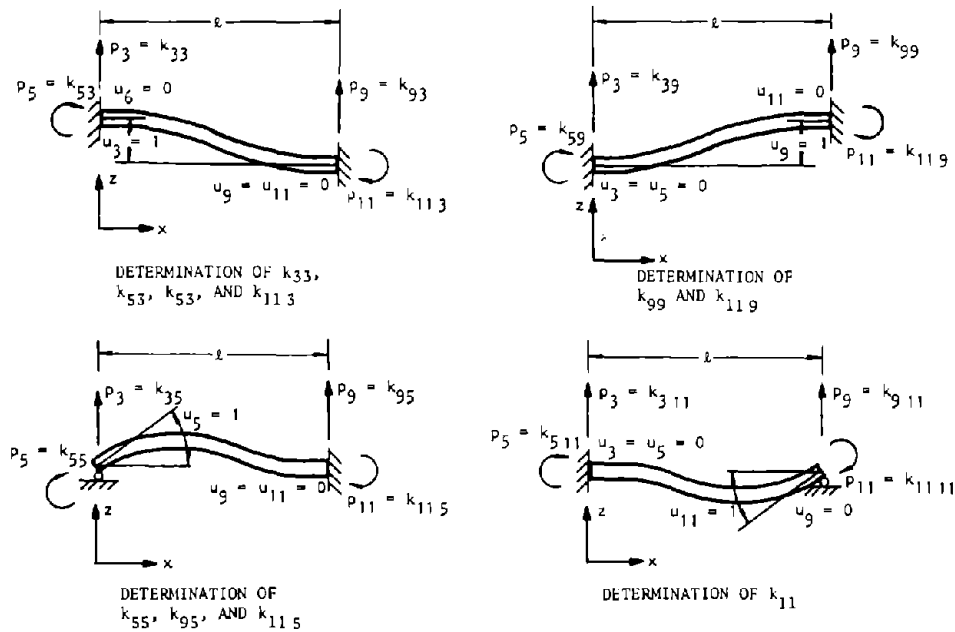
(b) Torsional stiffness terms

U.S. Army Corps of Engineers

Figure B-4. Beam Configurations for Computation of Axial and Torsional Terms in Stiffness Matrix



(a) Bending and shear terms--x-y plane



(b) Bending and shear terms--x-z plane

U.S. Army Corps of Engineers

Figure B-5. Beam Configurations for Computation of Beam Bending and Shear Terms in Stiffness Matrix

The stiffness coefficients associated with the rotations u_6 and u_{12} are computed from figure B-5a. Including the effect of shearing strains on beam deflection, the stiffness coefficients can be written as

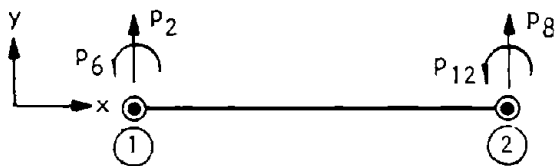
$$\begin{aligned} k_{66} &= P_6 = \frac{(4 + \Phi_y) EIz}{(1 + \Phi_y) \ell} \\ k_{86} &= P_8 = -\frac{6 EIz}{(1 + \Phi_y) \ell^2} \\ k_{126} &= P_{12} = \frac{(2 - \Phi_y) EIz}{(1 + \Phi_y) \ell} \end{aligned} \quad (B-28)$$

Similarly,

$$k_{1212} = \frac{(4 + \Phi_y) EIz}{(1 + \Phi_y) \ell} \quad (B-29)$$

g. Shear and bending deformations in x-z plane. The stiffness coefficients associated with the shear and bending deformations in the x-z plane; u_3, u_5, u_9 and u_{11} , can be derived on the basis of previous results in *f.* above. It should be noted, however, that the sign convention shown in figure B-3 assigns different positive directions for the bending moments in the yx and zx planes. These differences are illustrated in figure B-6, which shows that the positive direction of the bending moments P_5 and P_{11} is opposite to those of P_6 and P_{12} . Figure B-5b illustrates the configurations necessary for computation of the stiffness coefficients in the zx plane. From a comparison of figures B-5a and B-5b together with the sign conventions shown in figure B-6, it is seen that the stiffness coefficients including the effects of shearing strains become

$$k_{33} = \frac{12 EIy}{(1 + \Phi_z) \ell^3}$$



$$\begin{aligned} k_{53} &= -\frac{6 EIy}{(1 + \Phi_z) \ell^2} \\ k_{93} &= -\frac{12 EIy}{(1 + \Phi_z) \ell^3} \\ k_{113} &= -\frac{6 EIy}{(1 + \Phi_z) \ell^2} \\ k_{99} &= \frac{12 EIy}{(1 + \Phi_z) \ell^3} \\ k_{119} &= \frac{6 EIy}{(1 + \Phi_z) \ell^2} \\ k_{55} &= \frac{(4 + \Phi_z) EIy}{(1 + \Phi_z) \ell} \\ k_{95} &= \frac{6 EIy}{(1 + \Phi_z) \ell^2} \\ k_{115} &= \frac{(2 - \Phi_z) EIy}{(1 + \Phi_z) \ell} \\ k_{1111} &= \frac{(4 + \Phi_z) EIy}{\ell(1 + \Phi_z)} \end{aligned} \quad (B-30)$$

and

$$\Phi_z = \frac{12 EIy}{G A_{sz} \ell^2}$$

where A_{sz} represents the effective cross-sectional area of the beam in shear in the zx plane and I_y represents the moment of inertia of the cross-section of the beam associated with the bending in the zx plane (about y axis). As before, if the effects of shearing strains on the deformations are neglected, Φ_z should be taken as zero.

h. Complete element stiffness matrix. From the computations of the individual stiffness coefficients of a beam element, the complete relationship between the



U.S. Army Corps of Engineers

Figure B-6. Positive Directions of Shear Forces and Bending Moments

element forces and their corresponding displacements may be expressed as

$$\begin{bmatrix} P_1 \\ P_2 \\ P_3 \\ P_4 \\ P_5 \\ P_6 \\ P_7 \\ P_8 \\ P_9 \\ P_{10} \\ P_{11} \\ P_{12} \end{bmatrix} = \begin{bmatrix} \frac{AE}{\ell} & & & & & & & & & & & & \\ & \frac{12 \psi_z}{\ell^3} & & & & & & & & & & & \\ & & \frac{12 \phi_y}{\ell^3} & & & & & & & & & & \\ & & & \frac{GJ}{\ell} & & & & & & & & & \\ & & & & \frac{(4 + \phi_z) \psi_y}{\ell} & & & & & & & & \\ & & & & & \frac{(4 + \phi_y) \psi_z}{\ell} & & & & & & & \\ & \frac{-AE}{\ell} & & & & & & & & \frac{AE}{\ell} & & & \\ & & \frac{-12 \psi_z}{\ell^3} & & & & & & & & \frac{12 \psi_z}{\ell^3} & & \\ & & & \frac{-12 \psi_z}{\ell^3} & & \frac{6 \psi_y}{\ell^2} & & & & & & \frac{23 \psi_y}{\ell^3} & \\ & & & & \frac{GJ}{\ell} & & & & & & & & \frac{GJ}{\ell} \\ & & & & & \frac{(2 - \phi_z) \psi_y}{\ell} & & & & & \frac{G \psi_y}{\ell^2} & & \frac{(4 + \phi_z) \psi_y}{\ell} \\ & & \frac{6 \psi_z}{\ell^2} & & & & \frac{(2 - \phi_y) \psi_z}{\ell} & & & \frac{-6 \psi_z}{\ell^2} & & & \frac{(4 + \phi_y) \psi_z}{\ell} \end{bmatrix} \begin{bmatrix} u_1 \\ u_2 \\ u_3 \\ u_4 \\ u_5 \\ u_6 \\ u_7 \\ u_8 \\ u_9 \\ u_{10} \\ u_{11} \\ u_{12} \end{bmatrix}$$

SYMMETRIC

$$\psi_y = \frac{EIy}{(1 + \phi_z)} \text{ and } \psi_z = \frac{EIz}{(1 + \phi_y)} \tag{B-31}$$

B-4. Finite element method in structural mechanics

a. *Introduction.* The finite element method is essentially a generalization of matrix structural analysis methods to solve problems in continuum mechanics. The range of problems that may be solved by this method may include two-dimensional plane stress or strain distributions, plates, shells, axisymmetric solids, and three-dimensional solids. The basic concept of the finite element method is the idealization of a continuum by a structural system composed of a finite number of discrete elements. Such a structural system can then be solved using the matrix methods of structural analysis. As discussed in paragraph B-2, there are two matrix methods for

structural analysis, namely, the force method and the displacement method. These two methods along with their advantages and disadvantages are also applicable to the finite element method. However, the current usage is essentially restricted to the displacement finite element method in which the displacements of the joints are treated as unknowns of the problem. Thus, the finite element method hereafter refers to only the displacement method. The interested reader may refer to numerous textbooks and technical papers on the subject for a review of the historical development and a comprehensive background of the finite element method: Przemieniecki, 1968; Ural, 1973; Desai-Abel, 1972; Clough, 1965; Zienkiewicz, 1971; Argyris, 1968.

b. *General formulation.* To describe the general steps necessary in the mathematical formulation of the displacement finite element method, a rectangular plate under tension as shown in figure B-7 is selected as an example. The plate located in XY plane is divided into triangular (finite) elements. The state of stress in the plate is called plane stress. It is recognized that the nature of the problem requires only two degrees of freedom (DOF) per node, namely the displacements in the X and Y directions.

c. *Discretization.* The basic step in the finite element analysis is the idealization of the structure by an assembly of finite elements whose elastic properties can be obtained. In the example selected, the structure is divided into a sufficient number of triangular elements connected at the nodes only. The elements and nodes are usually numbered consecutively. Let N and M denote respectively the total number of nodes and total number of elements in the structure.

d. *Nodal displacements.* For a typical finite element, e, defined by corner nodes 1, 2, and 3, the unknown displacements of the nodes are

$$\{\delta\} = \begin{Bmatrix} \delta_1 \\ \delta_2 \\ \delta_3 \end{Bmatrix} \quad (B-32)$$

Since each node is associated with two displacement components (DOF)

$$\{\delta_m\} = \begin{Bmatrix} u_m \\ v_m \end{Bmatrix}, \quad m = 1, 2, 3 \quad (B-33)$$

where u_m and v_m are the displacements at node m in X and Y directions. When equation B-33 is substituted into equation B-45, a complete nodal displacement matrix is generated. For the example, this matrix becomes

$$\{\delta\} = \begin{Bmatrix} u_1 \\ v_1 \\ u_2 \\ v_2 \\ u_3 \\ v_3 \end{Bmatrix} \quad (B-34)$$

or

$$\{\delta\}^T = \{u_1 \ v_1 \ u_2 \ v_2 \ u_3 \ v_3\}$$

e. *Displacement functions.* To describe the internal behavior of the elements, general displacement expressions (also called shape functions) as functions of nodal displacements are assumed. This is an approximation on the actual behavior of the element. The assumptions of displacement variations should be consistent with theory. In the example, the displacement functions are written as

$$\{\Phi\} = \begin{Bmatrix} u(x,y) \\ v(x,y) \end{Bmatrix} = [A]\{\delta\} \quad (B-35)$$

where $u(x,y)$ and $v(x,y)$ describe the displacements in X and Y directions at any interior point of the element and $[A(x,y)]$ represents a matrix whose elements are the assumed shape functions of the element.

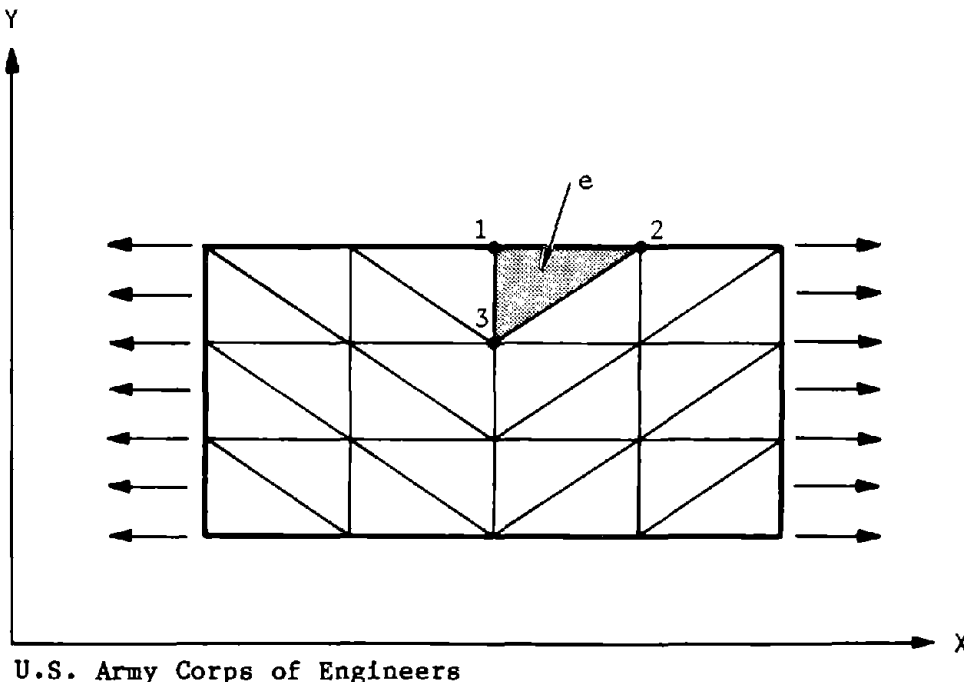


Figure B-7. Two-Dimensional Plate Under Pure Tension

f. *Strain-displacement relation.* Having computed the displacement distribution within the element, the strain components at any point can be computed in terms of the nodal displacements, $\{\delta\}$. The strain displacement relations can be written as

$$\{\epsilon\} = [B]\{\delta\} \tag{B-36}$$

in which $\{\epsilon\}$ is the strain matrix (vector) at any point within the element and $[B]$ is a matrix that is obtained from $[A]$ by appropriate differentiation. For the example problem, the strains are (Zienkiewicz, 1971)

$$\{\epsilon\} = \begin{Bmatrix} \epsilon_x \\ \epsilon_y \\ \gamma_{xy} \end{Bmatrix} = \begin{Bmatrix} \frac{\partial u}{\partial x} \\ \frac{\partial v}{\partial y} \\ \frac{\partial u}{\partial y} + \frac{\partial v}{\partial x} \end{Bmatrix} \tag{B-37}$$

g. *Stress displacement relation.* With the strains known at any point within the element, the stresses (or forces and moments for some type of elements) in the element may be calculated. Thus

$$\{\sigma\} = \begin{Bmatrix} \sigma_x \\ \sigma_y \\ \tau_{xy} \end{Bmatrix} = [D]\{\epsilon\} \tag{B-38}$$

where $\{\sigma\}$ is the stress matrix and $[D]$ is the elasticity matrix for the material. For the example problem the $[D]$ matrix from the usual isotropic stress-strain relationship is given by

$$[D] = \frac{E}{1-\nu^2} \begin{bmatrix} 1 & \nu & 0 \\ \nu & 1 & 0 \\ 0 & 0 & \frac{(1-\nu)}{2} \end{bmatrix} \tag{B-39}$$

where E is the Young's modulus and ν is the Poisson's ratio of the material of the plate.

h. *The element stiffness matrix.* With the strain-displacement and stress-displacement matrices computed, the next step is to compute the element stiffness matrix which expresses the force-displacement relationship for the element. The derivation of the element stiffness matrix $[k]$ by using the virtual work principle (Zienkiewicz, 1971) gives

$$[k]_e = \int_V [B]^T [D] [B] dv \tag{B-40}$$

where the integral is taken over the volume of the element. If the stress distribution is uniform, i.e., if the $[B]$ matrix is not dependent on the coordinates, the element stiffness matrix is given by

$$[k]_e = [B]^T [D] [B] V \tag{B-41}$$

where V is the volume of the element.

i. *Global stiffness matrix.* Having computed element stiffness matrices for all the individual elements, the global stiffness matrix $[K]$ which expresses relationship between all the nodal displacements and forces is obtained. The global stiffness matrix is assembled by summing up all the element stiffness matrices. Thus

$$[K] = \sum_{e=1}^M [k]_e \tag{B-42}$$

and the force-displacement relationship for the whole structure becomes

$$[K]\{U\} = \{F\} \tag{B-43}$$

when $\{U\}$ contains displacements of all the nodes and $\{F\}$ contains all the nodal forces. If the loads are distributed on the structure, they are appropriately lumped at the nodes.

j. *Displacements and stresses.* Since the nodal forces $\{F\}$ are given, equation B-43 forms a set of simultaneous equations in which $\{U\}$ are the unknowns. These equations are usually solved in most finite element computer programs using the Choleski decomposition method described in matrix algebra textbooks. Finally, knowing the nodal displacements, the stresses in individual elements are computed using equation B-38 for each element.

k. *Local and global coordinate systems.* The stiffness properties of trusses and beams derived in paragraphs B-3b and c above, are in terms of coordinate systems naturally associated with the members. These are referred to as the local coordinate systems. In order to sum the individual element stiffness properties as in equation B-42 to form the global stiffness matrix a common coordinate system must be established. The common coordinate system is referred to as the Global Coordinate System. Before the summation of the element stiffnesses are taken place, the element stiffness matrices expressed in terms of the local coordinate system must be expressed or transformed into the global coordinate system so that all the displacements and forces will be referred to a common system. Let $[k]$ and $\{U\}$ represent respectively the element stiffness matrix and element displacements in a local system and $[\bar{k}]$ and $\{\bar{U}\}$ represent the corresponding quantities in a global system. The relationship between $\{U\}$ and $\{\bar{U}\}$ can be expressed as

$$\{U\} = [R]\{\bar{U}\} \tag{B-44}$$

where $[R]$ is a transformation matrix whose coefficients are obtained by resolving the global displacements in the directions of local coordinates. The elements of $[R]$ are obtained from the direction cosines of angles between the local and global systems (Przemieniecki, 1968). By considering the virtual work quantity in both the local and global systems, it can be shown that (Przemieniecki, 1968)

$$[\bar{k}] = [R]^T[k][R] \tag{B-45}$$

Consider as an example, a two-dimensional truss element as shown in figure B-8 with the indicated local and global coordinate systems. The element stiffness matrix of order 2×2 in the local system can be written from equation B-21 as

$$[k] = \frac{AE}{L} \begin{bmatrix} 1 & -1 \\ -1 & 1 \end{bmatrix} \tag{B-46}$$

The global displacements $\bar{u}_1, \bar{v}_1, \bar{u}_2,$ and \bar{v}_2 can be resolved into the local components u_1 and u_2 as follows:

$$\begin{aligned} u_1 &= \bar{u}_1 \cos \theta + \bar{v}_1 \sin \theta \\ u_2 &= \bar{u}_2 \cos \theta + \bar{v}_2 \sin \theta \end{aligned}$$

or

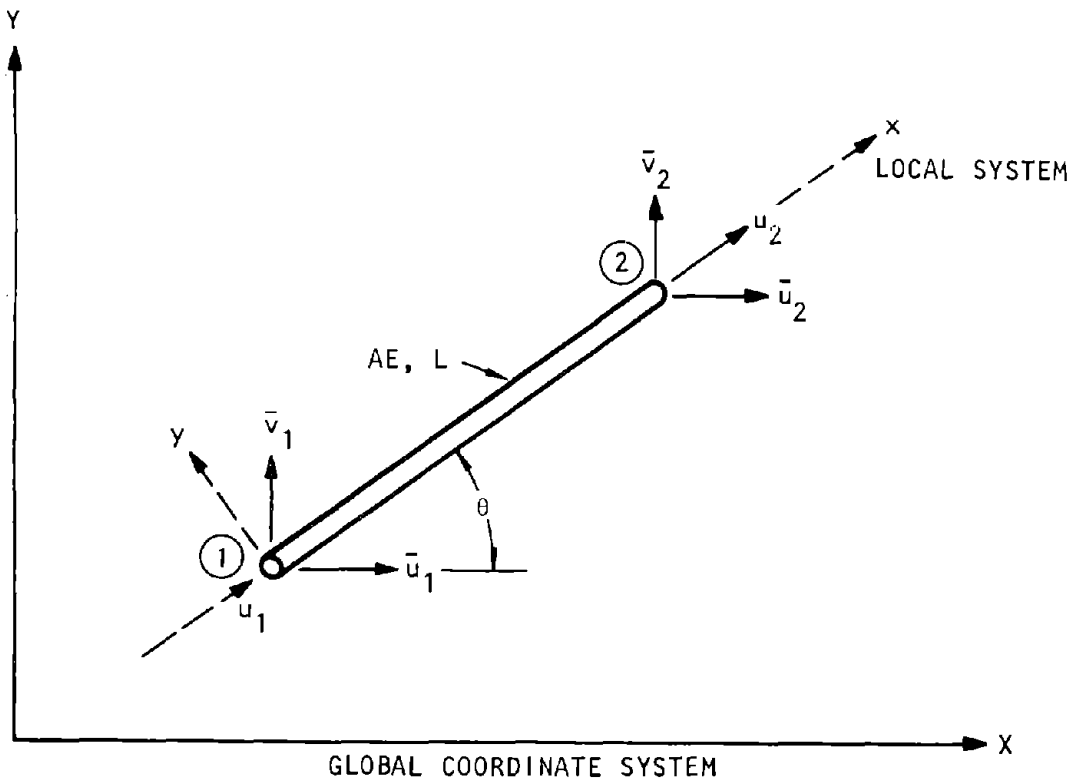
$$\begin{Bmatrix} u_1 \\ u_2 \end{Bmatrix} = \begin{bmatrix} \cos \theta & \sin \theta & 0 & 0 \\ 0 & 0 & \cos \theta & \sin \theta \end{bmatrix} \begin{Bmatrix} \bar{u}_1 \\ \bar{v}_1 \\ \bar{u}_2 \\ \bar{v}_2 \end{Bmatrix} \tag{B-47}$$

By comparing equations B-44 and B-47, the transformation matrix can be written as

$$[R] = \begin{bmatrix} \cos \theta & \sin \theta & 0 & 0 \\ 0 & 0 & \cos \theta & \sin \theta \end{bmatrix} \tag{B-48}$$

The element stiffness matrix in global system is of order 4×4 (associated with $\bar{u}_1, \bar{v}_1, \bar{u}_2,$ and \bar{v}_2) and is given from equation B-45 as

$$\begin{aligned} [\bar{k}] &= \frac{AE}{L} \begin{bmatrix} \cos \theta & 0 \\ \sin \theta & 0 \\ 0 & \cos \theta \\ 0 & \sin \theta \end{bmatrix} \begin{bmatrix} 1 & -1 \\ -1 & 1 \end{bmatrix} \begin{bmatrix} \cos \theta & \sin \theta & 0 & 0 \\ 0 & 0 & \cos \theta & \sin \theta \end{bmatrix} \\ &= \frac{AE}{L} \begin{bmatrix} \cos^2 \theta & \cos \theta \sin \theta & -\cos^2 \theta & -\cos \theta \sin \theta \\ \cos \theta \sin \theta & \sin^2 \theta & -\cos \theta \sin \theta & -\sin^2 \theta \\ -\cos^2 \theta & -\cos \theta \sin \theta & \cos^2 \theta & \cos \theta \sin \theta \\ -\cos \theta \sin \theta & -\sin^2 \theta & \cos \theta \sin \theta & \sin^2 \theta \end{bmatrix} \end{aligned} \tag{B-49}$$



U.S. Army Corps of Engineers

Figure B-8. Local and Global Coordinate Systems for a Plane Truss Element

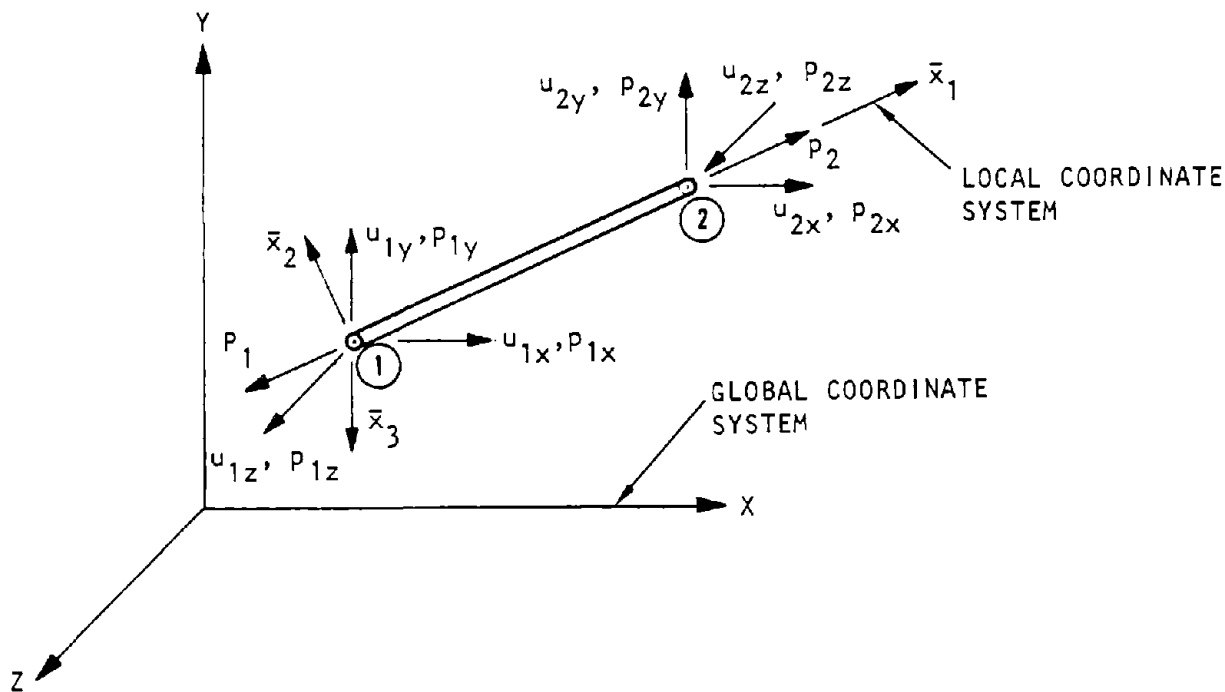
B-5. Finite elements

a. *SAP*. There are numerous types of finite elements in use for solving continuum and structural mechanics problems. The following is a brief description of the elements available in *SAP* (Wilson, 1970).

b. *Three-dimensional truss element*. The truss element is the conventional space truss member than can resist compression or tension along its axis. The truss member is subject to three translations at each end of the member as shown in figure B-9, which also shows the local and global coordinate systems. The global coordinate axes are denoted by \bar{X} , \bar{Y} , and \bar{Z} , and the local coordinates by \bar{x}_1 , \bar{x}_2 , and \bar{x}_3 . The coordinate axis \bar{x}_1 coincides with the line joining the end nodes of the element. The axes \bar{x}_2 and \bar{x}_3 are arbitrary. The member stiffness matrix is of order 6×6 . The material and geometrical properties are defined by the Young's modulus, the mass density, the cross-sectional area, the coefficient of thermal expansion, and the weight per unit length of the element. A uniform temperature change and inertia loads in three directions can be considered as the basic element loads. Axial forces and stresses may be computed. Tensile forces are considered positive.

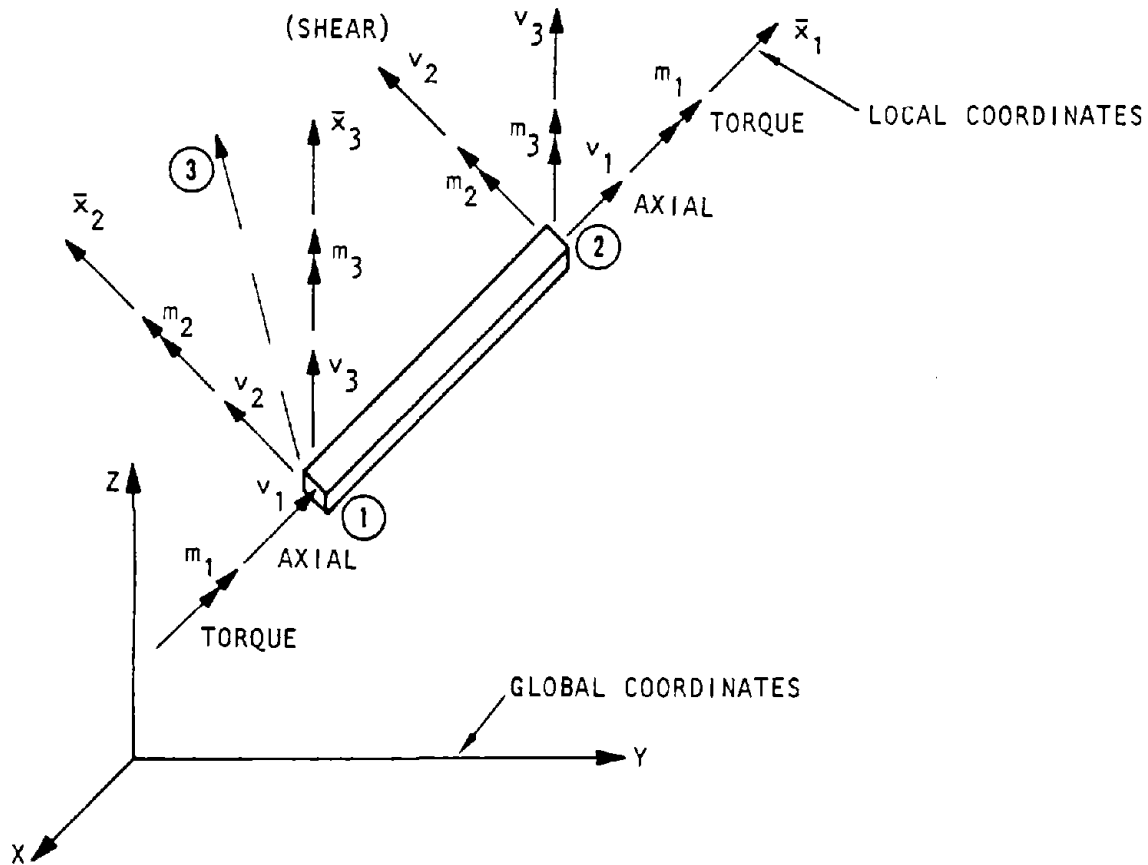
c. *Three-dimensional beam element*. The three-dimensional beam element is a straight, prismatic

member and is subject to three translations and three rotations at each end. The generalized forces and the generalized displacements associated with the six degrees of freedom (DOF) at each end are shown in in figure B-10, which also shows the local and global coordinate systems. The local coordinate axis \bar{x}_1 coincides with the line joining the end nodes of the element. The \bar{x}_2 -axis is selected so that it is normal to the \bar{x}_1 -axis. Finally, the \bar{x}_3 axis is chosen to be normal to \bar{x}_1 and \bar{x}_2 axes to form a right-handed system. The geometrical properties of the beam element are specified by an axial and two shear areas, and three principal moments of inertia, two associated with bending and one with torsion. The Young's modulus, Poisson's ratio, and mass density are required to define the material properties of the beam element. The element stiffness matrix is of the order 12×12 and is obtained from the classical beam theory including the effects of the shear deformations. A provision for the member and boundary conditions accounts for hinges and other releases. The element loads consist of inertial loading (i.e., gravity) in three directions and specified fixed end forces. Forces (one axial and two shears) and moments (one torsional and two bending) are calculated in the beam local coordinate system.



U.S. Army Corps of Engineers

Figure B-9. Three-Dimensional Truss Element

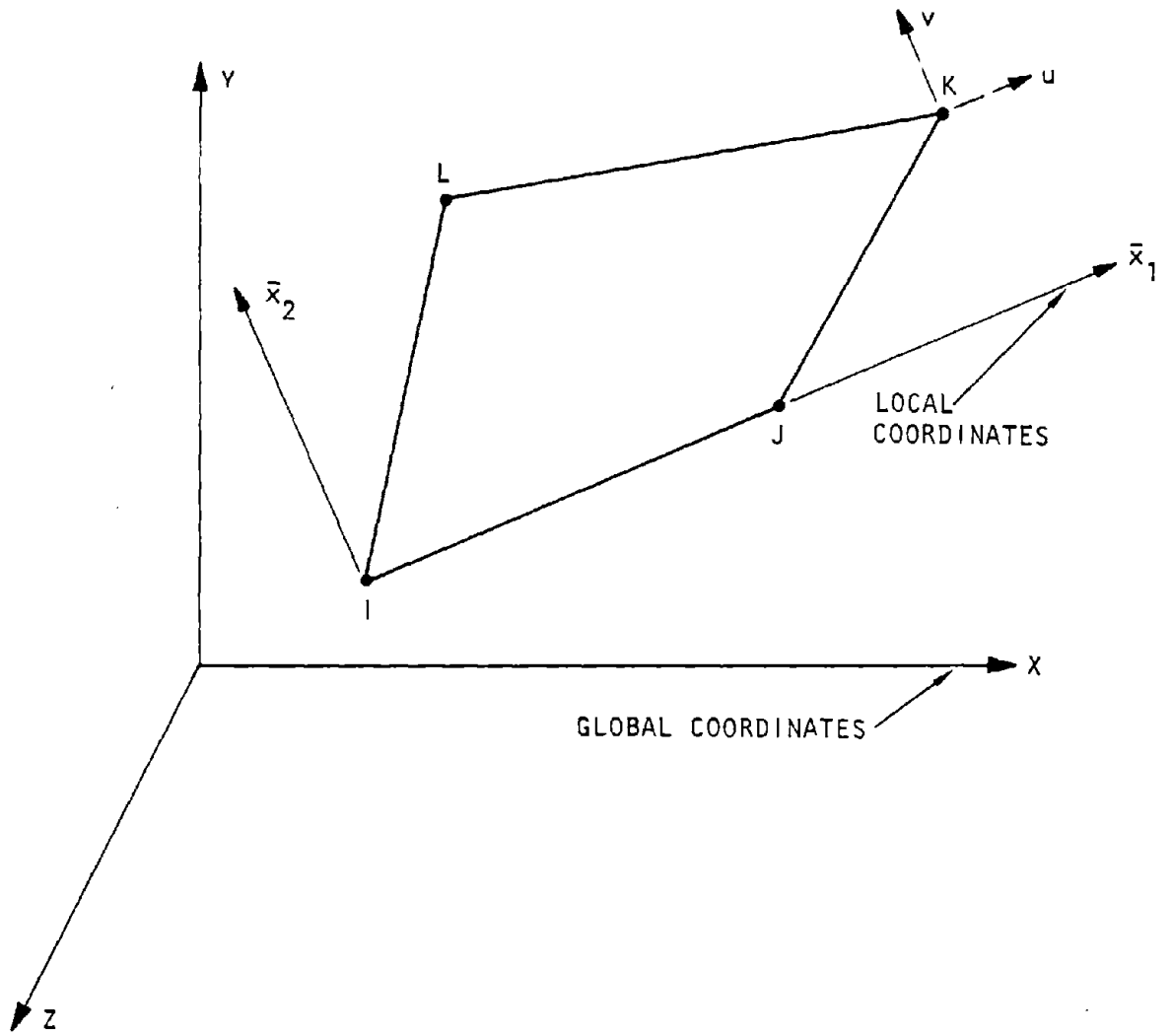


U.S. Army Corps of Engineers

Figure B-10. Three-Dimensional Beam Element

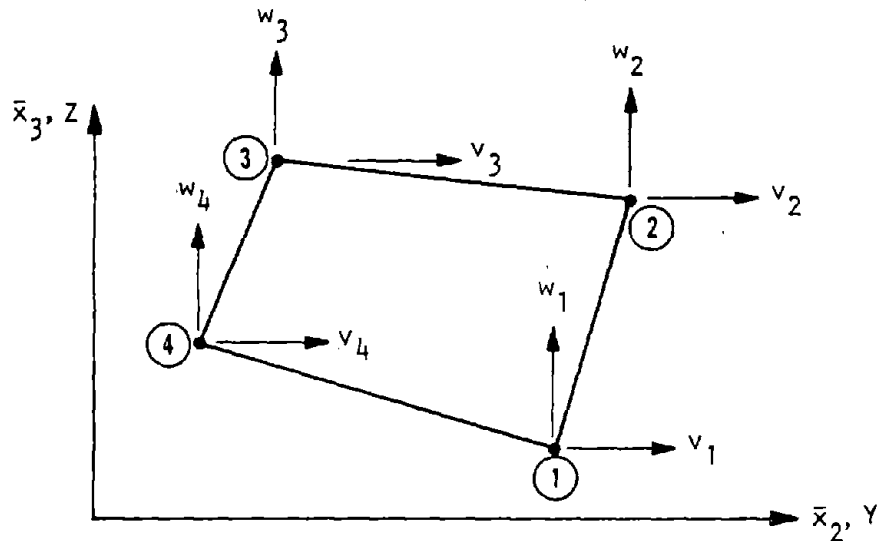
d. *Plane stress and plane strain element.* The plane stress and plane strain finite elements (membrane elements) are useful in representing an elastic continuum that is subjected to in-plane forces only. The quadrilateral is the basic membrane. While triangular elements are available, they are not recommended for general use. The general quadrilateral has twelve external DOF's (global), three per node. The displacement functions within the quadrilateral membrane may be represented by two second-degree polynomials. In addition to the twelve external DOF's three internal DOF may be chosen to define the two polynomials. The three internal DOF's are associated with the displacements at the center of the quadrilateral. The local coordinate system for a membrane element is shown in figure F-11. The local coordinate axis \bar{x}_1 coincides with the line joining the nodes I and J. The \bar{x}_2 axis is normal to the \bar{x}_1 axis and lies in the plane of the element, which may lie in any direction. If the plane of the element coincides with the global XY-plane, the element stiffness matrix is of order 8×8 ; otherwise it is of order 12×12 . The element loads may consist of gravity, inertia and temperature loadings. The stress components are computed at the center of the element and are referenced to the global coordinate system.

e. *Axisymmetric solid element.* The axisymmetric solid elements are useful in representing an elastic body symmetrical about one of the coordinate axes. The quadrilateral is the basic axisymmetric element. Triangular elements are available, but they are not recommended for general use. As shown in figure B-11, the axisymmetric element consists of two DOF per node point. Thus, the quadrilateral element has a total of eight external DOF's. The displacements within the quadrilateral axisymmetric element are assumed to vary parabolically. In addition to the eight external DOF's four internal DOF's are chosen to uniquely define the two displacement functions. Two of the four internal DOF are arbitrary and cannot be associated with the displacements of any set of interior points. The element stiffness matrix for the quadrilateral is of order 8×8 and is obtained by the "static condensation" technique applied to a 12×12 matrix. The element must be axisymmetrical about the global Z-axis and the Y direction is considered radial. Thus, the local $\bar{x}_2 \bar{x}_3$ -plane always coincides with the global YZ-plane (fig. B-12). The element loads consist of temperature, surface pressure, and inertia (in Z direction only) loadings. Stresses are computed at the center of the element and refer to the global coordinate system.



U.S. Army Corps of Engineers

Figure B-11. Plane Stress and Plane Strain Element



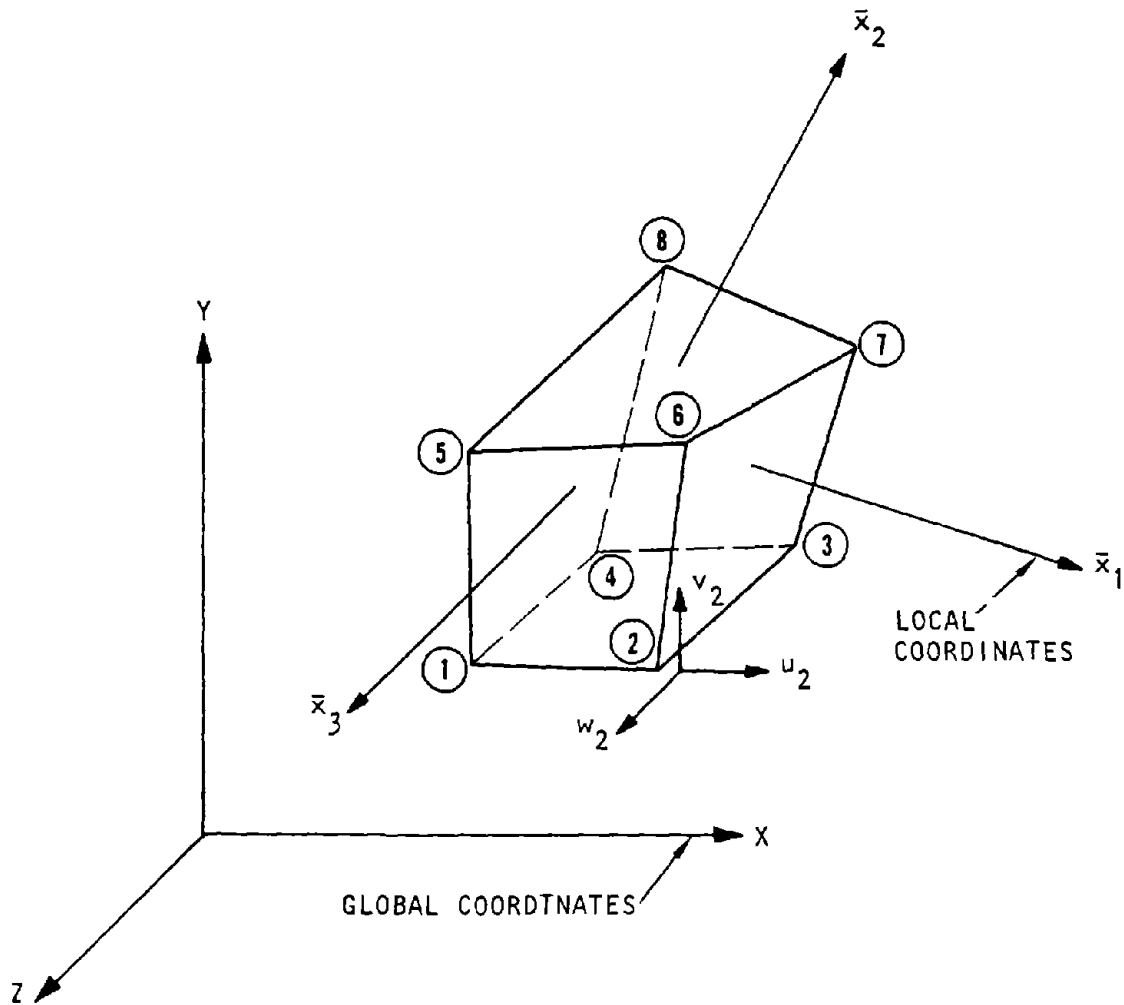
U.S. Army Corps of Engineers

Figure B-12. Axisymmetric Solid Element

f. *Three-dimensional solid element.* The three-dimensional solid element is an eight-node hexahedral element shown in figure B-13 with three translational DOF's per node point. The displacement functions within the element are represented by three complete second-order polynomials by arbitrarily choosing nine internal DOF's. As in the case of the axisymmetric element, the internal DOF's are not associated with the displacements of any set of interior points. The final 24×24 element stiffness matrix is obtained from a 33×33 stiffness matrix by eliminating the nine internal DOF's by the "static condensation" technique. In representing an elastic continuum by the solid elements, the mesh should be selected to give regular elements (cubes or rectangular prisms) as far as possible, since regular elements generally produce superior results as compared to skewed elements. The local coordinate system is a natural system for the element in which

the element maps into a unit cube. Element loading consists of temperature, surface pressure, and inertia loading in three directions. Static stresses (six components) are computed at the center of the element and at the center of each face. For the dynamic case, stresses only at the center of the element are computed. All stresses refer to the global coordinate system.

g. *Plate and shell element.* The plate and shell element is useful in modeling a thin shell or plate type of structure in which in-plane and out-of-plane forces and moments act upon the structure. A general quadrilateral element (24 DOF's) and a flat triangular element (18 DOF's) with six DOF per node are used. The triangle should be used only for refining and/or completing certain mesh layouts. Anisotropic material properties may be defined for the stiffness computation. Lateral pressure, temperature loading, and gravity loading are typical element loads. The



U.S. Army Corps of Engineers

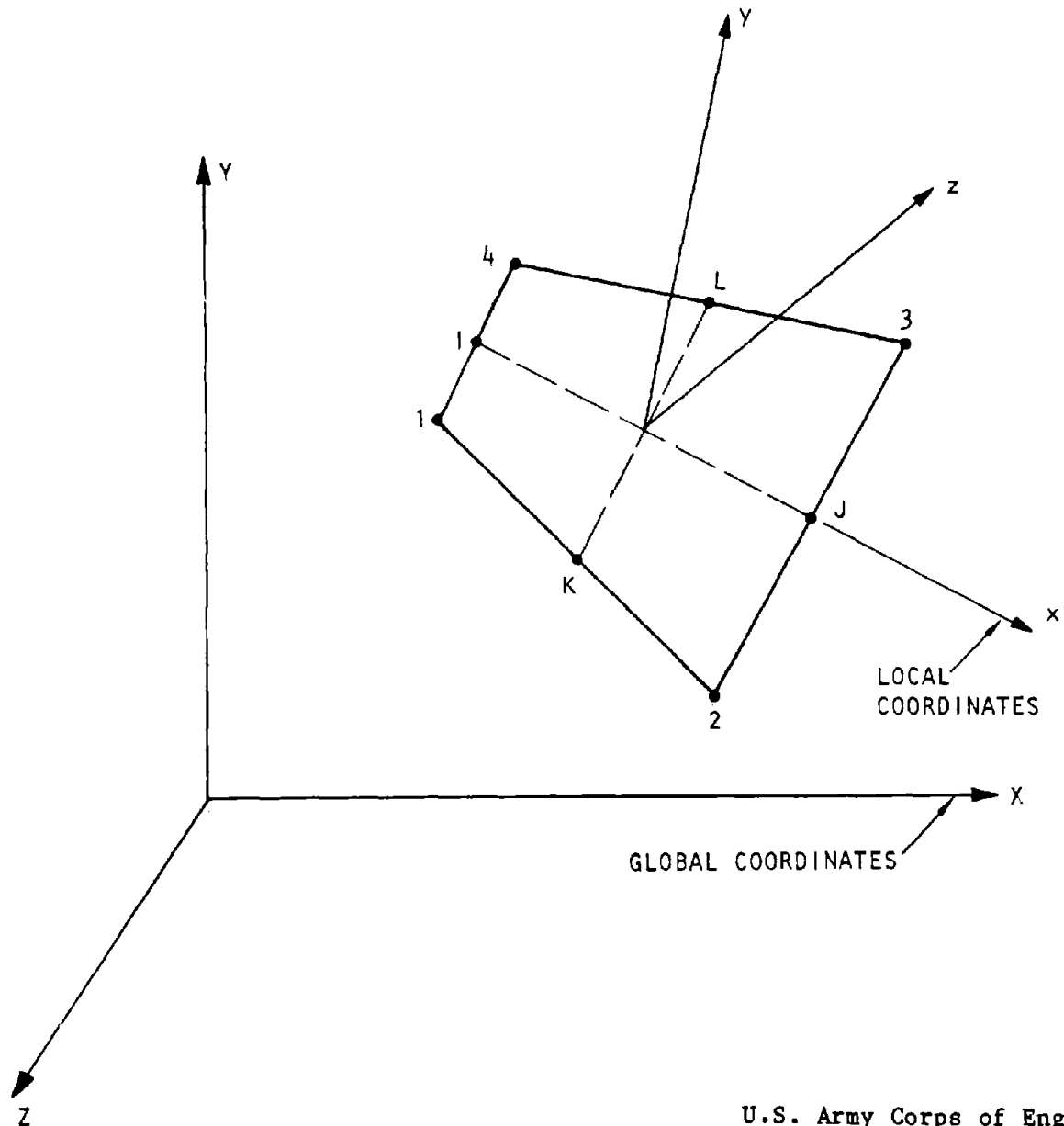
Figure B-13. Three-Dimensional Solid Element

local coordinate system for a quadrilateral shell element (1,2,3,4) is shown in figure B-14 and is defined as follows:

- x specified by I-J, where I and J are midpoints of sides 1,4 and 2,3.
- z normal to x and to the line joining midpoints K and L.
- y normal to x and z to complete the right-handed system.

This system is used to express all physical and kinematic shell properties (stresses, strains, and material law), except that the body force density (gravity, etc.) is referred to the global coordinate system (X, Y, Z). The final element stiffness matrix

for the quadrilateral is of order 24×24 and is obtained from a 42×42 matrix by eliminating the internal DOF by the "static condensation" technique. For the purpose of computing the element stiffness matrix, a quadrilateral is divided into four triangles. Each of these constituent triangles consists of a membrane element and an overlaid bending element. Each membrane triangle is the constrained linear strain triangle with a total of ten DOF's. Each bending triangle is a linear curvature compatible triangle with a total of 14 DOF's (Clough-Felippa, 1968). When the four constituent triangles are assembled together, a quadrilateral element with a total of 42 DOF's, 24 external and 18 internal. The internal DOF's are then eliminated by the "static condensation" procedure to result in the final element stiffness matrix. For static



U.S. Army Corps of Engineers

Figure B-14. Shell and Plate Element

or dynamic cases, stresses (three components) are computed at the center of the element. All stresses and moments are referred to the local coordinate system. The three stresses or moment components are expressed as force or moment values per unit length of the plate.

h. Boundary spring element. The boundary element is a one-dimensional spring element that can be used to impose displacement boundary conditions, to constrain displacements at the nodes in any arbitrary direction, and to compute support reactions. If the stiffness of this element is not provided as input, a large stiffness spring is assumed. This element is also useful in constraining the normal degrees of freedom in a plane stress or plane strain problem in which the plane region is not parallel to any of the coordinate planes. Axial force and moment about the axis of the element are computed.

i. Boundary dashpot. This is a one-dimensional damping element and is available only in conjunction with the linear or nonlinear dynamic analysis by direct integration method. The element can be used to provide structural damping and to provide a quiet boundary (i.e., a nonreflecting boundary). One end of this damping element is connected to a node; the other end is assumed to be fixed. The direction of the element must be in one of the three global coordinate axes. Thus, there can be a maximum of three damping elements connected to a joint. The damping provided by this element is linear and is proportional to the velocity in the direction of the element.

j. Nonlinear elements. Nonlinear elements may be combined with all types of linear elements to model a complex structure with the nonlinear behavior present in certain of its members. The nonlinear element connects to any two nodes. The stress in the element (spring) is a function of the relative displacement of the two nodes, whereas the damping force is a function of the relative velocity of the two nodes. For a translational spring the axis of the element is defined by a vector from the first node to the second. A rotational spring connects any two rotational components of the two joints. The material properties of the nonlinear elements are arbitrary and must be supplied by the engineer, according to the data that are appropriate for the application. The necessary input consists of the coordinates of as many points as required for defining the loading and unloading modulus. Outside the limits of the specified points, the curve is linearly extrapolated. Some examples are shown for a one-dimensional nonlinear spring element.

(1) General Nonlinear Elastic Element. Loading and unloading are on the same curve. The spring may be gapped with different compression and tension gaps as shown in figure B-15a.

(2) Nonlinear Loading-Linear Elastic Unloading Elements. Loading is on a general nonlinear curve but unloading is linear elastic with the specified unloading modulus. Permanent plastic deformations can develop and accumulate. This spring type is shown in figure B-15b.

(3) Nonlinear One-Way Spring with Linear Elastic Unloading. Loading is on a general nonlinear curve but unloading is linear elastic with the specified unloading modulus. The element is effective only in tension or compression. The spring may be gapped. Permanent plastic deformations can develop but cannot accumulate. This type of spring, as shown in figure B-16a, is useful for representing cables and other one-way members.

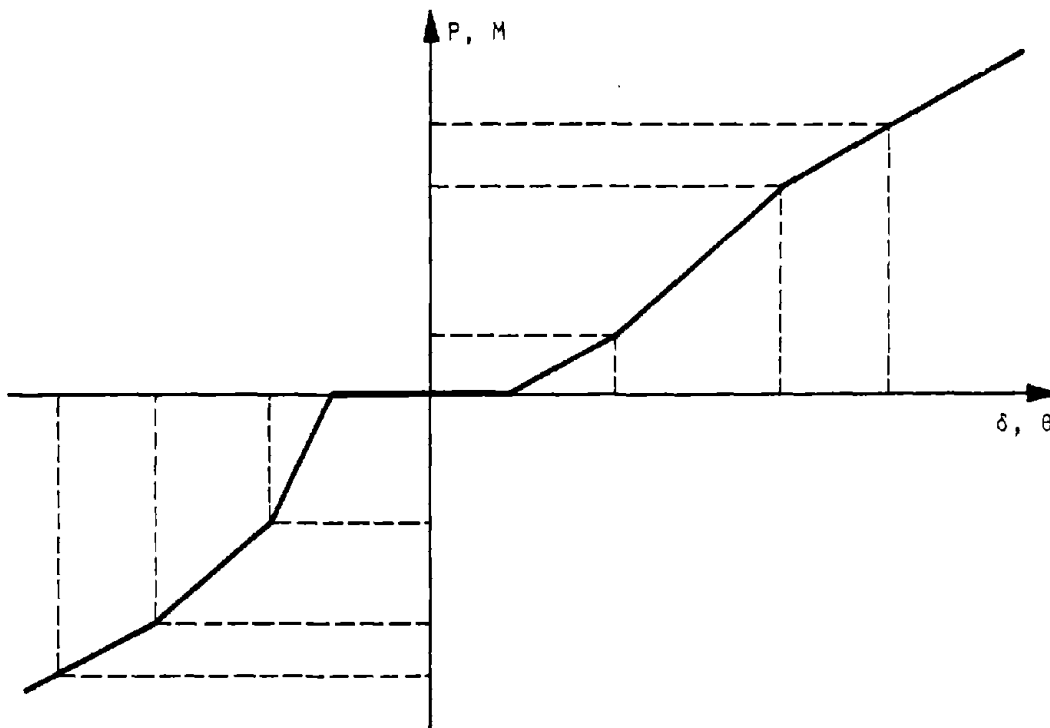
(4) Plastic-Hysteretic Element. This element, as shown in figure B-16b, can be used to model an elastic-perfectly-plastic hinge or an elastic-plastic hinge with strain hardening. The element is also useful in representing certain soil models.

B-6. Example problem solution

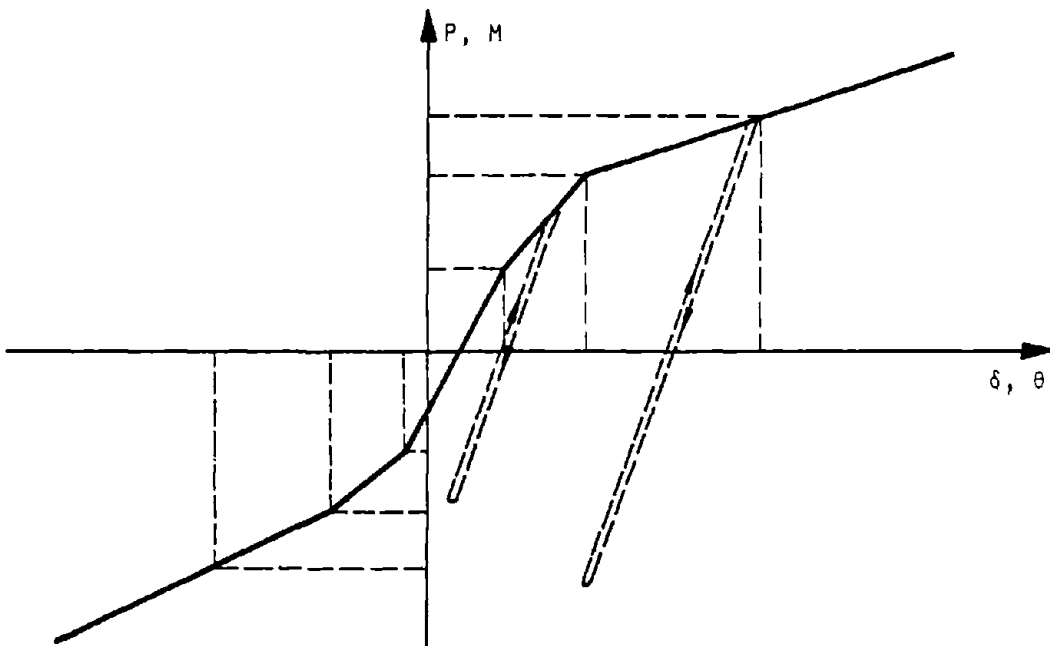
To illustrate the finite element method, the example shown in figure B-17a is selected. The cantilever beam carries a point load P at center. The beam is idealized into two beam elements as shown in figure B-17b. The global coordinate system is chosen to coincide with the beam axis so that the global and local axes coincide for each element. Therefore, the element stiffness matrices do not require any transformation. Neglecting axial deformations, we assign two DOF (rotation and transverse displacement) to each joint. The displacements (including rotations) are denoted by U_i , while the forces are denoted by P_i . Since the transverse displacements at joints 1 and 3 and the rotation at joint 3 are constrained, there are only 3 unknown displacements ($U_2, U_3,$ and U_4). The stiffness matrix for elements 1 and 2 can be obtained from the general expression given by equation B-31 after deleting the rows and columns corresponding to axial, torsional, and out-of-plane bending DOF. The element stiffness matrices for the two elements are given by Przemieniecki (1968):

$$[k]_1 = \frac{EI}{\ell^3} \begin{matrix} & \begin{matrix} 1 & 2 & 3 & 4 \end{matrix} & \leftarrow \text{DOF} \\ \begin{bmatrix} 12 & 6\ell & -12 & 6\ell \\ 6\ell & 4\ell^2 & -6\ell & 2\ell^2 \\ -12 & -6\ell & 12 & -6\ell \\ 6\ell & 2\ell^2 & -6\ell & 4\ell^2 \end{bmatrix} & \begin{matrix} 1 \\ 2 \\ 3 \\ 4 \end{matrix} & \begin{matrix} \checkmark \\ \\ \\ \end{matrix} \end{matrix} \tag{B-50}$$

$$[k]_2 = \frac{EI}{\ell^3} \begin{matrix} & \begin{matrix} 3 & 4 & 5 & 6 \end{matrix} & \leftarrow \text{DOF} \\ \begin{bmatrix} 12 & 6\ell & -12 & 6\ell \\ 6\ell & 4\ell^2 & -6\ell & 2\ell^2 \\ -12 & -6\ell & 12 & -6\ell \\ 6\ell & 2\ell^2 & -6\ell & 4\ell^2 \end{bmatrix} & \begin{matrix} 3 \\ 4 \\ 5 \\ 6 \end{matrix} & \begin{matrix} \checkmark \\ \\ \\ \end{matrix} \end{matrix}$$



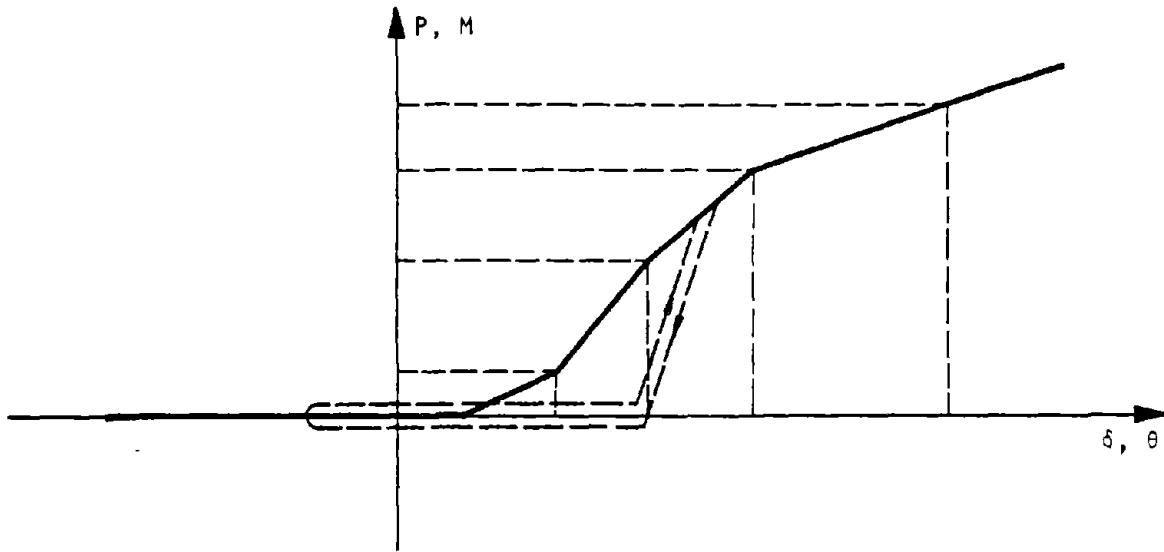
(a) General nonlinear elastic element



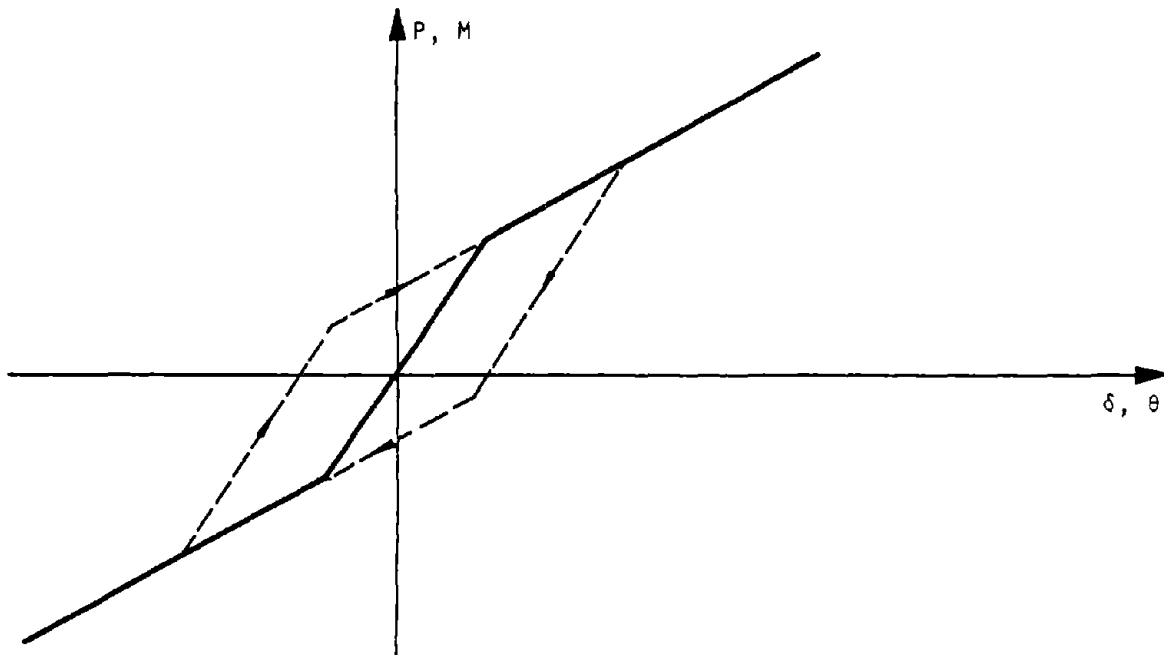
(b) Nonlinear loading--linear elastic unloading element

U.S. Army Corps of Engineers

Figure B-15. Sample Nonlinear Elements



(a) Nonlinear one-way--linear elastic unloading element



(b) Plastic--hysteretic element

U.S. Army Corps of Engineers

Figure B-16. Additional Sample Nonlinear Elements

The global stiffness matrix [K] is formed by adding the appropriate rows and columns in [k]₁ and [k]₂. It should be noted here that [K] is of order 3 × 3 corresponding to the three unknowns U₂, U₃, and U₄. Thus

$$[K] = \frac{EI}{\ell^3} \begin{matrix} & \begin{matrix} 2 & 3 & 4 \end{matrix} & \leftarrow \text{DOF} \\ \begin{bmatrix} 4\ell^2 & -6\ell & 2\ell^2 \\ -6\ell & 24 & 0 \\ 2\ell^2 & 0 & 8\ell^2 \end{bmatrix} & \begin{matrix} 2 \\ 3 \\ 4 \end{matrix} & \checkmark \end{matrix} \quad (\text{B-51})$$

The load vector consists of external loads P₂, P₃, and P₄ corresponding to U₂, U₃, and U₄. It is seen that P₂ = P₄ = 0 and P₃ = -P. Therefore, the force displacement relation for the whole structure becomes

$$\frac{EI}{\ell^3} \begin{bmatrix} 4\ell^2 & -6\ell & 2\ell^2 \\ -6\ell & 24 & 0 \\ 2\ell^2 & 0 & 8\ell^2 \end{bmatrix} \begin{bmatrix} U_2 \\ U_3 \\ U_4 \end{bmatrix} = \begin{bmatrix} 0 \\ -P \\ 0 \end{bmatrix} \quad (\text{B-52})$$

Using the Choleski matrix decomposition technique, the above equations can be written as

$$\frac{EI}{\ell^3} \begin{bmatrix} 1 & 0 & 0 \\ -3/2\ell & 1 & 0 \\ 1/2 & \ell/5 & 1 \end{bmatrix} \begin{bmatrix} 4\ell^2 & 0 & 0 \\ 0 & 15 & 0 \\ 0 & 0 & 32\ell^2/5 \end{bmatrix} \begin{bmatrix} 1 & -3/2\ell & 1 \\ 0 & 1 & \ell/5 \\ 0 & 0 & 1 \end{bmatrix} \begin{Bmatrix} U_2 \\ U_3 \\ U_4 \end{Bmatrix} = \begin{Bmatrix} 0 \\ -P \\ 0 \end{Bmatrix} \quad (\text{B-53})$$

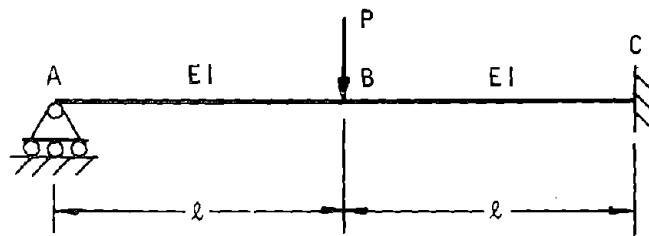
from which we can solve for U_i's as

$$\begin{Bmatrix} U_2 \\ U_3 \\ U_4 \end{Bmatrix} = \frac{\ell^2}{96 EI} \begin{Bmatrix} -12 \\ -7\ell \\ 3 \end{Bmatrix} \quad (\text{B-54})$$

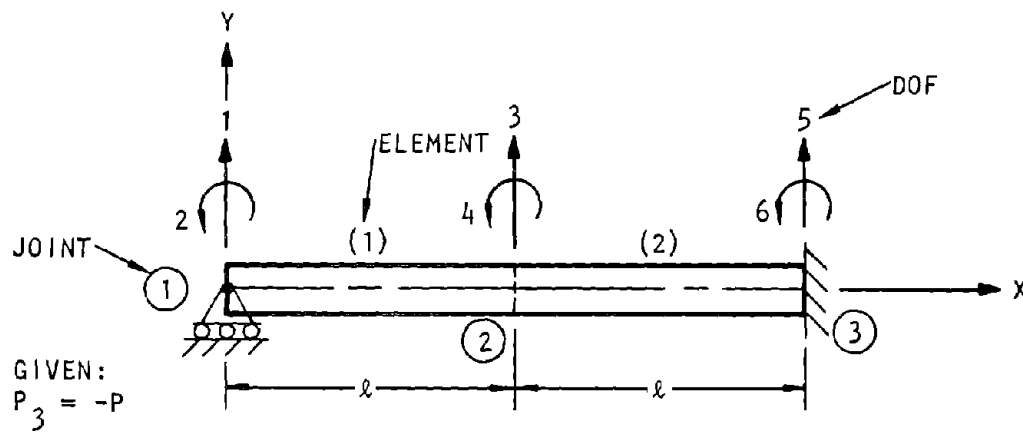
Having computed the unknown displacements U₂, U₃, and U₄, the forces P₁, P₅, and P₆ can be computed using [k]₁ and [k]₂. Thus

$$\begin{aligned} P_1 &= 5 P/16 \\ P_5 &= 11 P/16 \\ P_6 &= -3 P\ell/8 \end{aligned}$$

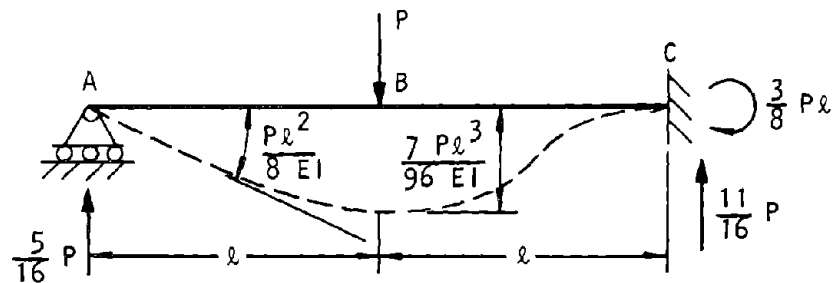
The solution for the example problem is illustrated in figure B-17c.



(a) Problem



(b) Finite element model



(c) Results

U.S. Army Corps of Engineers

Figure B-17. Cantilever Example

APPENDIX C

COMPUTER SOFTWARE FOR FINITE ELEMENT ANALYSIS

C-1. The engineer may select from many software programs available for direct application to the analysis of structure/medium interaction or structure response calculations. A compilation of most of the available software is given in this appendix (table C-1). Continuous updating of software makes such a compilation rapidly out of date. The engineer should check with the source of the software for the latest version.

C-2. Program characteristics, range of application, element library, and other features of the software are summarized. (Classification of software characteristics and data on some of the software were supplied by Information Systems Design, Inc., Santa Clara, California.) Originators of the software programs are listed in table C-2.

Table C-1. Computer Software for Finite Element Analysis

Item		Program Name												
		ADINA	ANSYS	MARC	NASTRAN	NISA	NONSAP	SAGA	SAP	SPAR	STAR DYNE	STRUDL	TRAMAL	TRI/SAC
Finite Element Program Applications	General structures	•	•	•	•	•	•	•	•	•	•	•	•	•
	Structural members	•	•	•	•	•	•	•	•	•	•	•	•	•
	Thick shells	•	•	•			•	•	•	•	•	•		•
	Thin shells	•	•	•	•	•	•	•	•	•	•	•		•
	Ship structures	•	•	•				•	•	•	•	•		•
	Building and civil engineering	•	•	•	•	•		•	•	•	•	•		•
	Piping systems	•	•	•	•	•		•	•	•	•	•		•
	Structure/medium interaction	•	•	•	•	•	•	•	•	•	•	•	•	•
Range of Application	Linear elastostatics	•	•	•	•	•	•	•	•	•	•	•	•	•
	Nonlinear statics	•	•	•	•		•	•				•		•
	Linear dynamics	•	•	•	•	•	•	•	•	•	•	•	•	•
	Nonlinear dynamics	•	•	•			•	•					•	•
	Heat transfer	•	•	•	•	•							•	•
Phenomena	Stress Analysis	Small displacement	•	•	•	•	•	•	•	•	•	•	•	•
		Large displacement	•	•	•	•		•		•		•		•
		Small strains	•	•	•	•	•	•	•	•	•	•	•	•
		Large strains	•	•	•			•						•
		Thermal Effect	•	•	•	•	•	•	•	•	•	•		•
		Plasticity	•	•	•	•		•	•				•	
		Viscoelasticity	•	•	•			•						
	Stability Analysis	Buckling			•	•		•			•			
		Instability		•	•	•		•			•			
	Vibrations and Dynamic Response	Modal vibrations		•	•	•	•	•	•	•	•	•		•
Nonlinear vibration			•	•	•	•	•	•	•	•	•		•	
Linear dynamic response		•	•	•	•	•	•	•	•	•	•	•	•	
Nonlinear dynamic response		•	•	•			•					•		
	Damping	•	•	•	•	•	•	•	•	•	•	•	•	
Optimization											•			
Material Properties	Isotropic	•	•	•	•	•	•	•	•	•	•	•	•	•
	Anisotropic	•	•	•	•	•	•	•	•	•	•	•	•	•
	Linear elastic	•	•	•	•	•	•	•	•	•	•	•	•	•
	Nonlinear elastic	•	•	•			•					•		•
	Temperature-dependent	•	•	•	•	•	•	•						•
	Elastoplastic	•	•	•	•	•	•	•				•		•
	Viscoelastic		•	•			•						•	
	Creep		•	•			•							
Material Wall Construction	Monocoque	•	•	•	•	•	•	•	•	•	•	•	•	•
	Layered	•	•	•	•	•	•	•	•	•	•	•	•	•
	Sandwich	•	•	•	•	•	•	•	•	•	•	•	•	•
	Composite Material	•	•	•	•	•	•	•	•	•	•	•	•	•

U.S. Army Corps of Engineers

Table C-1. (Continued)

Item		Program Name												
		ADINA	ANSYS	MARC	NASTRAN	NTSA	NONSAP	SAGA	SAP	SPAR	STARDYNE	STRUDL	TRAMAL	TRI/SAC
Loading	Axisymmetric variation <i>only</i>	•	•	•	•	•	•	•	•	•	•	•	•	•
	General variation	•	•	•	•	•	•	•	•	•	•	•	•	•
	Static	•	•	•	•	•	•	•	•	•	•	•	•	•
	Function of time	•	•	•	•	•	•	•	•	•	•	•	•	•
	Deformation-dependent	•	•	•	•	•	•	•	•	•	•	•	•	•
	Contact	•	•	•	•	•	•	•	•	•	•	•	•	•
Types of Loads	Point loads	•	•	•	•	•	•	•	•	•	•	•	•	•
	Line loads	•	•	•	•	•	•	•	•	•	•	•	•	•
	Surface loads	•	•	•	•	•	•	•	•	•	•	•	•	•
	Volume loads	•	•	•	•	•	•	•	•	•	•	•	•	•
	Initial stress/strain	•	•	•	•	•	•	•	•	•	•	•	•	•
	Thermal	•	•	•	•	•	•	•	•	•	•	•	•	•
	Centrifugal	•	•	•	•	•	•	•	•	•	•	•	•	•
Element Library	Rod; bar; truss	•	•	•	•	•	•	•	•	•	•	•	•	•
	Beam	•	•	•	•	•	•	•	•	•	•	•	•	•
	Plane membrane	•	•	•	•	•	•	•	•	•	•	•	•	•
	Membrane in space	•	•	•	•	•	•	•	•	•	•	•	•	•
	Plate	•	•	•	•	•	•	•	•	•	•	•	•	•
	Shell	•	•	•	•	•	•	•	•	•	•	•	•	•
	Three-dimensional continuum	•	•	•	•	•	•	•	•	•	•	•	•	•
	Axisymmetric	•	•	•	•	•	•	•	•	•	•	•	•	•
	Crack--tip	•	•	•	•	•	•	•	•	•	•	•	•	•
Isoparametric	•	•	•	•	•	•	•	•	•	•	•	•	•	
Formulation	Displacement	•	•	•	•	•	•	•	•	•	•	•	•	•
Assembled Structure	Random arrangement of nodes	•	•	•	•	•	•	•	•	•	•	•	•	•
	Automatic renumbering of nodes	•	•	•	•	•	•	•	•	•	•	•	•	•
	Substructuring possible	•	•	•	•	•	•	•	•	•	•	•	•	•
	Substructure iteration--different loads	•	•	•	•	•	•	•	•	•	•	•	•	•
	Modification w/o complete recalculation	•	•	•	•	•	•	•	•	•	•	•	•	•
	Joining of elements with different DOFs	•	•	•	•	•	•	•	•	•	•	•	•	•
	Local system of axes	•	•	•	•	•	•	•	•	•	•	•	•	•
	Prescribed displacement possible	•	•	•	•	•	•	•	•	•	•	•	•	•

U.S. Army Corps of Engineers

Table C-1. (Concluded)

Item		Program Name											
		ADINA	ANSYS	MARC	NASTRAN	NISA	NONSAP	SACA	SAP	SPAR	STARDYNE	STRUDEL	TRAVEL
Support Condition	Axisymmetric	•	•	•	•	•	•	•	•	•	•	•	•
	General	•	•	•	•	•	•	•	•	•	•	•	•
	At boundaries <i>only</i>	•	•	•	•	•	•	•	•	•	•	•	•
	At internal points	•	•	•	•	•	•	•	•	•	•	•	•
	Elastic foundation	•	•	•	•	•	•	•	•	•	•	•	•
	Contact	•	•	•	•	•	•	•	•	•	•	•	•
Friction	•	•	•	•	•	•	•	•	•	•	•	•	
General Software Information	Restart capability	•	•	•	•	•	•	•	•	•	•	•	•
	Possibility for selective output	•	•	•	•	•	•	•	•	•	•	•	•
	Free format input	•	•	•	•	•	•	•	•	•	•	•	•
Data Preparation	Automatic mesh generation	•	•	•	•	•	•	•	•	•	•	•	•
	Automatic coordinate generation	•	•	•	•	•	•	•	•	•	•	•	•
	Automatic loading generation	•	•	•	•	•	•	•	•	•	•	•	•
	Plot routines	•	•	•	•	•	•	•	•	•	•	•	•
	Interactive graphics	•	•	•	•	•	•	•	•	•	•	•	•
Output	Numeric results	•	•	•	•	•	•	•	•	•	•	•	•
	Graphical	•	•	•	•	•	•	•	•	•	•	•	•
	Interactive postprocessor	•	•	•	•	•	•	•	•	•	•	•	•
Diagnostics	Minimal	•	•	•	•	•	•	•	•	•	•	•	•
	Extensive	•	•	•	•	•	•	•	•	•	•	•	•
Documentation	Data preparation manual	•	•	•	•	•	•	•	•	•	•	•	•
	Programmer's manual	•	•	•	•	•	•	•	•	•	•	•	•
	Theory--Mathematical formula	•	•	•	•	•	•	•	•	•	•	•	•
	Comparative sample problem solution	•	•	•	•	•	•	•	•	•	•	•	•
Operational	IBM	•	•	•	•	•	•	•	•	•	•	•	•
	CDC	•	•	•	•	•	•	•	•	•	•	•	•
	Univac	•	•	•	•	•	•	•	•	•	•	•	•
	GE	•	•	•	•	•	•	•	•	•	•	•	•
Other	•	•	•	•	•	•	•	•	•	•	•	•	
Program Status	Fully operational	•	•	•	•	•	•	•	•	•	•	•	•
	Being developed	•	•	•	•	•	•	•	•	•	•	•	•

U.S. Army Corps of Engineers

Table C-2. Originators of Computer Programs

Program Name	Originator	Maintained By
ADINA	U.S. Bureau of Mines/ Massachusetts Institute of Technology (MIT)	Prof. Bathe, MIT
ANSYS*	Swanson Analysis Systems, Inc.	Swanson Analysis Systems, Inc.
MARC	Marc Analysis Research Corp.	Marc Analysis Research Corp.
NASTRAN	NASA/The MacNeal-Schwendler Corp. (updates by Universal Analytics, Inc.)	NASTRAN/MSC version is by the MacNeal-Schwendler, Corp. NASTRAN/COSMIC version is by Universal Analytics, Inc.
NISA	Engineering Mechanics Research Corp.	Engineering Mechanics Research Corp.
NONSAP	University of California, Berkeley (UCB)	None
SAGA	Agbabian Associates	Agbabian Associates
SAP*	University of California, Berkeley (UCB)	University of Southern California
SPAR	Engineering Information Systems, Inc. (EISI)	Engineering Information Systems, Inc.
STARDYNE	Mechanics Research, Inc. (MRI)	Mechanics Research, Inc.
STRUDL*	Massachusetts Institute of Technology (MIT)	STRUDL/UNIVAC by the Univac Corp. STRUDL/IBM by Multisystems, Inc. and McDonnell Douglas Automation Co. (MCAUTO)
TRANAL	Weidlinger Associates	Weidlinger Associates
TRISAC	Agbabian Associates	Agbabian Associates

*These programs are recommended for use by the Corps of Engineers as the programs are maintained and easily available to the Corps.

U.S. Army Corps of Engineers

APPENDIX D

GLOSSARY

Aboveground Facility:	Facility in which all or a portion of the structure projects above the ground surface.
Absorbent Boundary:	An artificial boundary in the continuum representing the soil or rock surrounding a structure where reflections of propagating waves are canceled by an energy absorbing device such as a dashpot.
Artificial Reflection:	The reflection of energy from a finite element model boundary acting as an artificial free surface.
Availability:	The probability of a structure being in a functional state at the start of attack at any point in time.
Backpacked Liner:	Liner separated from the rock by a layer of relatively deformable material.
Backpacking:	The placement of an energy absorbent material between a structure and surrounding medium.
Balanced Load:	Axial load capacity at simultaneous assumed ultimate strain of concrete and yielding of tension steel (balanced conditions).
Balanced Moment:	Moment capacity at simultaneous assumed ultimate strain of concrete and yielding of tension steel (balanced conditions).
Bedding Constant:	A function of the compaction of soil beneath a horizontally placed cylindrical structure, its value used in determining the flattening (horizontal deflection) of the structure under load.
Breakdown Stress:	A shear stress limit in soils above which the shearing resistance increases as a result of grain crushing.
CEP:	Circular probable error of weapon strike-distance, i.e., the radius of the circle, centered at the aim point, within which half the weapons of a statistically large number of weapons would strike.
Closed Form:	Mathematical solutions that do not need numerical approximations. Numerical methods may be used to obtain solutions from "closed form" formulations.
Coefficient of Variation (COV):	The rates of the variance to the mean value of a parameter.
Compression Mode Loading:	A loading distribution on a curved member such as an arch or a dome that causes uniform compression in the member.
Deep Beams:	Flexural members of small length-to-depth ratio where shear deformations are of the same order as bending moment deformations.
Deep-buried Facilities:	Facility buried deeply enough in the earth so that the prime-mission materiel/personnel will physically survive when weapons of the anticipated threat are delivered with great accuracy and detonated overhead.
Deflection Mode Loading:	An antisymmetrical loading of a curved member such as an arch or a dome that causes a flexural deflection, usually with a point of inflection at the crown.

Design Reliability:	The probability of a structure surviving a given level of weapon effects considering all the uncertainties in material properties, loading, analysis and construction procedures.
Deterministic Design:	A design procedure that does not consider the randomness associated with loads, material properties, structural behavior, and construction tolerances, or the probabilities that are associated with the occurrence of various loads or their possible combinations.
DIF:	Dynamic increase factors.
Discrete Interactors:	Springs and dashpots discretely placed along the structure/medium interface to represent the stiffness and energy absorbing or radiating characteristics of the medium.
Downdrag Forces:	The shear force between a structure and surrounding medium due to the greater compressibility of the medium under weapon effect loading.
Drag Coefficients:	A factor relating to shape, texture, and orientation of a surface in a dynamic air stream to the attendant air drag force on the surface.
Ductility Ratio:	The ratio of the total deflection to the maximum elastic deflection for a material.
Dynamic Design Factors:	A factor of design equivalence given as a multiplier of a static response parameter to produce the corresponding dynamic response.
Dynamic Increase Factor (DIF):	The ratio of the dynamic to the static load capacity of a structural member.
Dynamic Pressure:	The dynamic air pressure associated with the air blast from a weapon detonation.
ELF:	Extremely low frequency.
EMP:	Electromagnetic pulse, associated primarily with the high intensity radiation and conduction fields induced by nuclear explosions, can produce extremely high currents in conducting elements or disrupting or destroying electronic components.
Endurance:	Combined transattack and postattack time frames in which the facility must fulfill its functions.
Energy-Absorption Capacity:	The amount of energy that a structure can absorb during weapon-effect loading without collapse or failure of the structure.
Failure Probability:	The probability of a structure failing to survive a given level of weapon-effect loading considering all the uncertainties in material properties, loading, analysis and construction procedures.
Fiber-Reinforced Concrete:	Concrete containing high-strength fibers randomly oriented in the aggregate material.
Flush Facility:	Facility countersunk in the ground so that the structure roof is level with the ground surface.
Free-Field Overpressure:	The change in the static air pressure at a receiver location caused by the air blast from a weapon detonation.
Hardened Structures:	Structures that have been designed to survive a given level of weapon effects and remain functional.

Hardness:	The degree to which a structure survives an attack, usually expressed in terms of the level of airblast overpressure corresponding to the weapon effects that a structure can withstand and remain functional.
HRSD:	Hard Rock Silo Development
Hysteresis Loop:	The area between the loading and unloading curves on a stress/strain diagram for a material, usually signifying the occurrence of plastic deformation of the material in question.
Hysteretic Cycles:	Sequential loading and unloading cycles where each deflection causes plastic deformation of the material in question.
Integral Liner:	Liner placed directly against the rock.
Lacing:	Diagonal reinforcing steel provided to carry shear loads in reinforced concrete structures.
Mach Number:	The ratio of a shock wave velocity to the velocity of sound in the ambient air.
Material Failure (rock):	Occurs when the in situ yield strength of the intact rock with the interaction zone is exceeded and when mechanical failure is precluded.
Mechanical Failure (rock):	Characterized by relative movement along macroscopic planes of weakness lying within the interaction zone.
Partially Buried Facility:	Facility beneath a soil cover deep enough to defeat radiation and ejecta/debris impact, but shallower than one structure diameter.
Plastic Design:	A design method for continuous steel structural elements that defines the ultimate load as a function of the strength of steel in the plastic range.
Plastic Hinges:	A yielded zone in a flexural element where the moment resisting capacity is attained based on elastoplastic behavior of the material.
PMMP:	Prime-mission materiel/personnel.
Postattack:	The time frame beginning after the last burst.
Probabilistic Design:	Consideration of the uncertainties in material properties, loading, analysis and construction procedures during the design of a structure, relating safety and serviceability criteria to a rationally defined risk level.
Prolate Spheroid:	Formed by the rotation of an ellipse about its major axis.
Protective Facilities-Subsystems:	Facilities/subsystems that protect the prime mission, materiel/personnel and other facility subsystems from the weapons effects.
Rebonding:	The ability of a concrete section that has cracked under tensile forces to resist transient compressive stresses as a result of the closing of the crack under cyclic load reversals.
Rebound:	The movement or load of a structure caused by the release of strain energy during unloading.
Reflected Pressure:	The increase in the static air pressure at a structure surface caused by the interception of an air shock wave with the structure.

TM-5-858-3

Response Spectrum:	The peak response of single-degree-of-freedom systems (SDOF) to dynamic inputs, usually plotted as peak response absolute accelerations, pseudo-velocities, and relative displacements as functions of the frequency of the SDOF. Also referred to as shock spectrum.
Service Life:	The minimum period during which a structure remains functional without requiring major rehabilitation.
Shallow Buried:	A structure covered with at least one structure diameter of soil, but not deep enough to withstand a direct overhead weapon burst.
Shear Walls:	Structural walls whose load resistance is determined by deformation due to shear as well as bending moment.
SDOF:	Single-degree-of-freedom
Threshold of Collapse:	Limit of structural usefulness.
Transattack:	The time frame between the first burst (or button-up) and the last burst.
Uncertainty:	The amount (estimated) by which the predicted value for a parameter may vary from the observed or true value.
Yield Stress:	The average stress during yielding in the plastic range. For structural steel the strain corresponding to this stress usually is 0.005 in./in. and for concrete this value is usually taken as 0.002 in./in.

APPENDIX E BIBLIOGRAPHY

- Abbott, L.S.; Claiborne, H.C.; and Clifford, C.E. (editors). *Weapons Radiation Shielding Handbook*, DASA-1892. Oak Ridge, TN: Oak Ridge National Laboratory, 1971.
- Agbabian associates (AA) *Nuclear Geoplosics, A Sourcebook of Underground Phenomena and Effects of Nuclear Explosions, Part Two: Mechanical Properties of Earth Materials*, DNA-1285H1. El Segundo, CA: AA, Nov 1972.
- _____. *Reinforced Concrete Constitutive Relations*, AFWL-TR-74-72. El Segundo, CA: AA, Feb 1975 (AD A007 886).
- _____. *Equivalent Viscous Damping for Seismic Analyses of Nuclear Plants*, SAN/1011-103. El Segundo, CA: AA, Apr 1975.
- _____. *Hardness Assessment of Composite Closures*, DNA-4039F. El Segundo, CA: AA, Feb 1977.
- _____. *Low-Cycle Fatigue Tests of Hollow Concrete Spheres with Implications for the Survivability of Deep-Underground Rock Openings*, DNA 4433F, El Segundo, CA: AA, April 1978.
- Agbabian-Jacobsen Assoc. (AJA) *Protective Structure Backpacking and In-Structure Shock Isolation System Analysis and Design*, SAMSO-TR-68-355, Vol. 2. El Segundo, CA: AA, Nov 1968 (AD 843 559).
- _____. (AJA) *Hardened Facilities Design and Verification Test Studies (U)*, SAMSO-TR-70-427. Los Angeles, CA: AJA, Nov 1970 (AD 512 782L) (SECRET).
- _____. (AJA) *Dynamic Analysis of Buried MSRPP Heat Sink Tank Using DEPS Code*, M-6820-1747. El Segundo, CA: AJA, Jan 1971.
- Allgood, J.R. "The Behavior of Shallow-Buried Cylinders," *Proc. Symp. on Soil/Structure Interaction*. Univ. of Arizona, Tucson, AZ, Sep 1964.
- _____. "State-of-the-Art Report on Fiber Reinforced Concrete," *ACI Jnl*, 70:11, 1973.
- _____. *Fiber Reinforced Concrete*, ACI-SP-44. Detroit, MI: ACI, 1974.
- _____. *Building Code Requirements for Reinforced Concrete*, ACI-318-77, Detroit, MI: ACI, 1977.
- Amer. Inst. of Steel Construction (AISC) *Manual of Steel Construction*. New York: AISC, 1970.
- _____. *Specification for the Design, Fabrication and Erection of Structural Steel for Buildings* and supplements. New York: AISC, 1969.
- Amer. Machine & Foundry (AMF) *Transient Drag and Its Effect on Structures*. Santa Barbara, CA: AMF, Feb 1955.
- Amer. Soc. of Civil Eng. (ASCE) *Commentary on Plastic Design in Steel*, Manual of Eng. Practice 41. New York: ASCE, 1961.
- Amer. Soc. of Civil Eng. (ASCE) *Structural Analysis and Design of Nuclear Plant Facilities* (draft). New York: ASCE, 1976.
- Amer. Soc. for Testing & Materials (ASTM) *Notched Bar Impact Testing of Metallic Materials*, E-23-72. Philadelphia, PA: ASTM, 1972.
- Ang, H.H-S "Risk and Reliability Analysis in Engineering Design," in *Structural and Geotechnical Mechanics*. Englewood Cliffs, NJ: Prentice-Hall, 1977.
- _____. and Cornell, C.A. "Reliability Bases of Structural Safety and Design," *Proc. ASCE Struct. Div.* New York: ASCE, 100:ST9, Sep 1974.
- _____. and Tang, W.H. *Probability Concepts In Engineering Planning and Design, Vol 1-Basic Principles*. New York: Wiley, 1975.
- Archer, J.S. "Consistent Mass Matrix for Distributed Mass Systems," *Proc. ASCE Struct. Div.* New York: ASCE, 89:ST4, Aug 1963.
- Argyris, J.M. "Continua and Discontinua," *Proc. Conf. on Matrix Methods in Struct. Mech.* Wright-Patterson AFB, Oct. 26-28, 1965. (AD 646 300).
- Bagge, C.F. *Design Consideration for Deep Underground Protective Facilities*, R-7020-1760. Los Angeles: Agbabian-Jacobsen Assoc. Mar. 1972 (AD 744 790).
- Bathe, K-J. *Solution Methods for Large Generalized Eigenvalue Problems in Structural Engineering*, UC-SESM-71-20. Berkeley, CA: Univ. of Calif., Nov 1971 (PB 208 853).
- Battelle Memorial Inst. *Prevention of the Failure of Metals under Repeated Stress*. New York: Wiley, 1941.
- Benjamin, J.R. and Williams, H.A. "The Behavior of One-Story Reinforced Concrete Shear Walls," *Proc. ASCE Struct. Div.* 83:ST3, May 1957.
- Biggs, J.M. *Introduction to Structural Dynamics*. New York: McGraw-Hill, 1964.
- Birkeland, P.W., and Westhoff, L.J. "Dimensional Tolerances in a Tall Concrete Building," *ACI Jnl Proc*, 68:8, Aug 1971.
- Bresler, B.; Lin, T. Y.; and Scalzi, J.B. *Design of Steel Structures*. New York: Wiley, 1968.
- Britt, J.R. *Charts for Preliminary Design of Deep Underground Structures Subjected to Dynamic Loads*, Misc. P N-77-3. Vicksburg, MS: Army Eng. Waterways Exp. Station, Apr 1977.
- Brode, H.L. *Height of Burst Effects at High Overpressures*, DASA-2506. Santa Monica, CA: Rand Corp., Jul 1970 (AD 874 060).
- Clough, R.W. "Analysis of Astructural Vibrations and Dynamic Response, in *Recent Advances in Matrix*

- Methods of Structural Analysis and Design*, edited by R.H. Gallagher. Huntsville, AL: Univ. of Alabama Press, 1969.
- _____. "The Finite Element Method in Structural Mechanics," *Stress Analysis*, Chap. 7: O.C. Zienkiewicz and G.S. Holister (eds.). New York: Wiley, 1964.
- _____. and Felippa, C.A. "A Refined Quadrilateral Element for Analysis of Plate Bending," *Proc. 2nd Conf. on Matrix Methods in Struct. Mech.* Wright-Patterson AFB, OH, Oct 15-17, 1968 (AD 703 685). Concrete Reinforcing Steel Inst. (CRSI *CRSI Handbook, 3rd ed.* Chicago, IL: CRSI, 1978.
- Connolly, J.P. and Brown, D.M. "Construction Tolerances in Reinforced Concrete Beams/Joists," *ACI Jnl*, Nov 1976.
- Corps of Eng. Dept. of the Army (COE). *Structural Elements Subjected to Dynamic Loads*, TM 5-856-7. Washington, DC: COE, Mar 1957.
- _____. (COE). *Shear Wall Structures*, TM 5-856-7. Washington, DC: COE, Jan 1958.
- _____. (COE). *Multistorey Frame Buildings*, TM 5-856-7. Washington, DC: COE, Jan 1960.
- _____. (COE). *Arches and Domes*, TM 5-856-8. Washington, DC: COE, Jan 1960.
- _____. (COE). *Strength of Materials and Structural Elements*, TM 5-856-2. Washington, DC: COE, Mar 1965.
- _____. (COE). *Collective Protection against Chemical, Biological, and Radiological Warfare*, TM 5-855-2. Washington, DC: COE, 1977.
- Costantino, C.J.; Robinson, R.R.; and Salmon, M.A. "A Simplified Soil/Structure Interaction Model to Investigate the Response of Buried Silos and Cylinders," *Proc. Symp. on Soil/Structure Interaction*, Univ. of Arizona, Tucson, AZ, Sep 1964.
- Coulson, J.H. *The Effects of Surface Roughness on the Shear Strength of Joints in Rock*, MRD-2-70. Omaha, NE: Corps of Engineers, Missouri River Div., 1970.
- Crawford, R.E.; Higgins, C.L.; Bultman, E.H. *The Air Force Manual for Design and Analysis of Hardened Structure, Final*, AFWL-TR-74-102. Albuquerque, NM: Civil Nuc. Systems Corp., Oct 1974 (AD B004 904L)
- Crist, R.A. and Vaughan, R.G. *Dynamically Loaded Circular Composite Slabs. Phase I: Project GOLIATH*, AFWL-TR-68-9. Kirtland AFB, NM: Air Force Weapons Lab., Oct 1968 (AD 845 483).
- Deere, D.E. et al. "Design of Surface and Near-Surface Construction in Rock," in *Failure and Breakage of Rock* edited by C. Fairhurst. New York: Amer. Inst. of Mech. Eng., 1967.
- Dept. of the Army, the Navy, and the Air Force (A/N/AF). *Structures to Resist the Effects of Accidental Explosions*, TM-5-1300; NAVFAC-P-397; AFM-88-72. Washington, DC: A/N/AF, Jun 1969.
- Dept. of Defense (DOD). *Process for Welding Metal Arc and Gas, Steels, and Corrosion and Heat Resistant Alloys*, MIL-W-8611A. Washington, DC: DOD, Jul 1957.
- _____. (DOD) *Process for Welding of Aluminum Alloys*, MIL-W-8604(1). Washington, DC: DOD, Oct 1959.
- Desai, C.S. and Abel, J.F. *Introduction to the Finite Element Method*. New York: Van Nostrand Reinhold, 1972.
- Distefano, C.J. et al. *Response of Tunnel Liners, Project Officers Report—Project 3.1, Operation FLINT LOCK, Shot PILE DRIVER* (U), WT-4010. Omaha: Corps of Engineers, Omaha District, Nov 1970 (AD 512-515L) (SECRET).
- Domaschuk, L. and Wade, N.H. "A Study of Bulk and Shear Moduli of a Sand," *Proc. ASCE Soil Mech. Div.* 95:SM2, Mar 1969.
- Donath, F.A. "Some Information Squeezed Out of Rocks," *Amer. Sci.* 58:1, 1970.
- Drake, J.L. and Britt, J.R. *A Method for Designing Deep Underground Structures Subjected to Dynamic Loads*, TR-N-76-9. Vicksburg, MS: Army Eng. Waterways Exp. Station, Sep 1976.
- Drysdale, R.G. "Placement Errors for Reinforcing in Concrete Columns," *ACI Jnl*, Jan 1975.
- Ellingwood, B. "Statistical Analysis of RC Beam-Column Interaction," *Proc. ASCE Struct. Div.* 103:ST7, Jul 1977.
- Endebrook, E.G., and Traina, L.A. *Static Constitutive Relations Based on Cubical Specimens*, AFWL-TR-72-59. Kirtland AFB, NM: Air Force Weapons Lab, Dec 1972.
- Faddeeva, V.N. *Computational Methods of Linear Algebra*. New York: Dover, 1959.
- Flathau, W.J. and Meyer, G.D. *Static and Dynamic Tests of Buried Unreinforced Concrete Arches*, Misc P 1-809. Vicksburg, MS: Army Eng. Waterways Exp. Station, Apr 1966 (AD 633 339).
- _____; Sager, R.A.; and Luzi, F.R. *The Design and Analysis of Underground Reinforced Concrete Arches*, TR-2-590. Vicksburg, MS: Army Eng. Waterways Exp. Station, 1962.
- Fox, L. *An Introduction to Numerical Linear Algebra*. New York: Oxford Univ. Press, 1965.
- Franklin, J.N. *Matrix Theory*. Englewood Cliffs, N.J.: Prentice-Hall, 1968.
- Frazer, R.A.; Duncan, W.J.; and Collar, A.R. *Elementary Matrices*. Cambridge, MA: Cambridge Univ. Press, 1955.
- Fung, Y.C. *Foundations of Solid Mechanics*. Englewood Cliffs, NJ: Prentice-Hall, 1965.
- Gallo, M.P. and Ang, A.H.S. *Evaluation of Safety of Reinforced Concrete Buildings to Earthquakes*, UILU-ENG-76-2018. Urbana-Champaign, IL: Univ. of Illinois, Oct. 1976.

- Gaston, J.R.; Siess, C.P.; and Newmark, N.M. *An Investigation of the Load-Deformation Characteristics of Reinforced Concrete Beams up to the Point of Failure*, Struct. Res. Series No. 40. Urbana, IL: Univ. of Illinois, Dec 1952.
- Gaylord, E.H. and Gaylord, C.N. *Structural Engineering Handbook*. New York: McGraw-Hill, 1968.
- Gaylord, J.M.; and Weaver, W., Jr. *Matrix Algebra for Engineers*. New York: Van Nostrand Reinhold, 1965.
- Glasstone, S. *Effects of Nuclear Weapons*, DOA Pamphlet 50-3. Washington, DC: DOA, 1977.
- Glasstone, S., and Dolan, P.J. *The Effects of Nuclear Weapons*, 3rd edition. Washington, D.C.: USGPO, 1977.
- Greenspan, M. "Effect of a Small Hole on the Stresses in a Uniformly Loaded Plate," *Quarterly Appl. Math.*, Vol 2, 1944.
- Hardin, B.O. and Music, J. "Apparatus for Vibration of Soil Specimens During the Triaxial Test," *Instruments and Apparatus for Soil and Rock Mechanics*, ASTM-STP-392. New York: Amer. Soc. for Testing and Materials, 1965.
- Haynes, H.H. *Handbook for Design of Undersea, Pressure-Resistant Concrete Structures*. Port Hueneme, CA: Naval Civil Eng. Lab, Sep 1976.
- Hendron, A.J. and Aiyer, A.K. *Stresses and Strains around a Cylindrical Tunnel in an Elasto-Plastic Material with Dilatancy*, TR-10, Mahomet, IL: Alfred J. Hendron Found. Eng., Sep 1972. (AD 748-030)
- Heyman, J. "The Stone Skeleton," *Int. Jnl of Solids & Struct.* 2:2, Apr 1966.
- Hoerner, S.F. *Fluid Dynamic Drag*. Published by the author at 148 Buserd Drive, Midland Park, NJ, 1958.
- Howland, F.L. and Newmark, N.M. *Static Load Deflection Tests of Beam-Columns*, Struct. Res. Series No. 65. Urbana, IL: Univ. of Illinois, Dec 1953.
- Jaeger, J.C. and Cook, N.G.W. "Friction in Granular Materials," in *Structure, Solid Mechanics and Engineering Design*, Pt. 1, edited by M. Te'eni. New York: Wiley, 1971.
- Keenan, W.A. "Shear Stress in One-Way Slabs Subject to Blast Load," in *Proc. 17th Explosives Safety Seminar, Denver, CO*, Sep 14-16, 1976.
- _____, and Feldman, A. *The Yield Strength of Intermediate Grade Reinforcing Bars Under Solid Loading*, AFSWC-TR-59-72, Pt. 6. Port Hueneme, CA: Naval Civil Eng. Lab., Mar 1960.
- Kennedy, R.P. "A Review of Procedures for the Analysis and Design of Concrete Structures to Resist Missile Impact Effects," in *Proc. 3rd Int. Conf. on Struct. Mech. in Reactor Tech.* London, Sep 1-5, 1975, edited by T.A. Jaeger.
- Kent, D.C. and Park, R. "Flexural Members with Confined Concrete," *Proc. ASCE Struct. Div.* 97:ST7, Jul 1971.
- Ko, H.K. and Scott, R.F. "Deformation of Sand in Shear," *Proc. ASCE Soil Mech. Div.* 93:SM5, Sep 1967.
- Laursen, H.I. *Matrix Analysis of Structures*. New York: McGraw-Hill, 1966.
- Lee, L.C. and Agbabian, M.S. "Crack Pattern of an Underground Cylindrical Reinforced Concrete Structure Under an Axial Blast Loading," *Shock & Vibration Bull.* 47:Oct 1976.
- Liu, T.C.Y.; Nelson, A.H.; and Slate, F.O. "Biaxial Stress-Strain Relations for Concrete," *Proc. ASCE Struct. Div.* 98:ST5, May 1972.
- Luscher, U. *Behavior of Flexible Underground Cylinders*, AFWL-TR-65-99. Cambridge, MA: Mass. Inst. of Tech., Sep 1965 (AD 621 145).
- Lysmer, J. and Kuhlemeyer, R.L. "Finite Dynamic Model for Infinite Media," *Proc. ASCE Eng. Mech. Div.* 95:EM4, Aug 1969.
- Martin, H.C. *Introduction to Matrix Methods of Structural Analysis*. New York: McGraw-Hill, 1966.
- Mazanti, B.B. and Holland, C.N. *Study of Soil Behavior under High Pressure*, CR-4-70-2,3 Vols. Vicksburg, MS: Army Eng. Waterways Exp. Station, Feb 1970.
- McDonald, J.R. *Thickness of Reinforced Concrete Wall and Roof Panels Required to Resist Tornado-Generated Missiles*. Lubbock, TX: McDonald, Mehta and Minor Consulting Engineers, Sep 1977.
- Merritt, J.L. and Newmark, N.M. *Nuclear Geoplosics: Pt. 5: Effects on Underground Structures and Equipment*, DASA-1285(V). Washington, DC: Def. Atomic Support Agency, May 1964 (AD 443 589).
- Mogi, K. "Pressure Dependence of Rock Strength and Transition from Brittle Fracture to Ductile Flow," *Bull. Earthq. Res. Inst.* 44, 1966.
- _____. "Effect of the Intermediate Principal Stress on Rock Failure," *Jnl of Geophys. Res.* 72:20, 1967.
- Mosborg, R.J. and Talda, P.M. *An Experimental Investigation of the Arching Phenomenon Occurring over a Buried Rectangular Plate*, AFWL-TR-65-78. Urbana, IL: Univ. of Illinois, Jun 1966 (AD 484 717).
- Nat'l Tech. Information Service (NTIS). *Concrete Polymer Composites, A Bibliography*. Springfield, VA: NTIS, Jun 1978.
- Newmark, N.M. *Design of Rock Silo and Rock Cavity Linings*, TR-70-114. SAMSO, Norton AFB, CA, Aug 1970.
- _____, and Haltiwanger, J.D. *Air Force Design Manual: Principles and Practices for Design of Hardened Structures*, AFSWC-TDR-62-138. Urban, IL: Univ. of Ill., Dec 1962 (AD 295 408).
- _____, and Rosenblueth, E. *Fundamentals of Earthquake Engineering*. Englewood Cliffs, NJ: Prentice-Hall, 1971.

- Norris, C.H. et al. *Structural Design for Dynamic Loads*. New York: McGraw-Hill, 1959.
- Oden, J.T. *Mechanics of Elastic Structures*. New York: McGraw-Hill, 1967.
- Olsen, R.E. and Parola, J.F. "Dynamic Shearing Properties of Compacted Clay," *Proc. Int. Sym. on Wave Propagation and Dynamic Properties of Earth Materials*, Albuquerque, NM, Aug 1967.
- Parducci, A. and Ferreti, A.S. "Prismatic Reinforced Concrete Members Alternate Bending Beyond the Yielding of the Reinforcement under Axial Loads," *Proc. 5th World Conf. on Earthquake Eng.* Rome, Italy, June 1973.
- Park, R. and Paulay, T. (1973) "Behavior of Reinforced Concrete External Beam-Column joints under cyclic loading," *Proc. 5th World Conf. on Earthquake Eng.*, Rome, Italy, June, Paper 248.
- Paul S.L., and Sinnamon, G.K. *Concrete Tunnel Liners: Structural Testing of Segmented Liners*, UILU-ENG-75-2013. Urbana, IL: Univ. of Ill., Aug 1975 (PB 252 934).
- Paulay, T. "Some Seismic Aspects of Coupled Shear Walls," *Proc. 5th World Conf. on Earthquake Eng.* Rome, Italy, Jun 1973, Paper 88.
- Plamondon, M.A. "Appendix, Preliminary Methods for Analysis and Design of Composite Circular Slabs," in *Dynamically Loaded Circular Composite Slabs, Phase I: Project GOLIATH*, R.A. Crist and R.G. Vaughan, AFWL-TR-68-9. Kirtland AFB, NM: AFWL, Oct 1968 (AD 845 483).
- Popov, E.P.; Bertero, V.V.; and Krawinkler, H. *Cyclic Behavior of Three R.C. Flexural Members with High Shear*, EERC-72-5. Berkeley, CA: Univ. of Calif. Earthquake Eng. Res. Center, Oct 1972 (PB 214 555).
- _____, and Pinkney, R.B. *Behavior of Steel Building Connections Subjected to Inelastic Strain Reversals*, AISI Bull. 13. Berkeley, CA: Univ. of Calif., Nov 1968.
- _____, and Stephen, R.M. *Cyclic Loading of Full-Size Steel Connections* EERC-70-3. Berkeley, CA: Univ. of Calif. Earthquake Eng. Res. Center, Jul 1970 (PB 213 545).
- Portland Cement Assoc. (PCA). *Design of Deep Girders*. Skokie, IL: PCA, 1946.
- _____. *Analysis of Small Reinforced Concrete Buildings for Earthquake Forces*. Chicago, IL: PCA, 1955.
- Przemieniecki, J.S. *Theory of Matrix Structural Analysis*. New York: McGraw-Hill, 1968.
- Ralph M. Parsons Co. *A Guide for the Design of Shock Isolation Systems for Underground Protective Shelters*. AFSWC-TDR-62-64 Los Angeles, CA: Ralph M. Parsons Co., Dec 1962.
- Richart, F.E.; Brandtzoeg, A.; and Brown, R.L. *A Study of the Failure of Concrete Under Combined Compressive Stresses*, Eng. Exp. Station Bull. No. 185. Urbana, IL: Univ. of Ill, 1928.
- Richart, F.E. Jr. "Some Effects of Dynamic Soil Properties in Soil/Structure Interaction," *Proc. ASCE Geotech. Div.* 101:GT12, Dec 1975.
- _____; Hall, J.R.; and Woods, R.D. *Vibrations of Soils and Found.* Englewood Cliffs, NJ: Prentice-Hall, 1970.
- Rosen, R. "Matrix Bandwidth Minimization," *Proc. 23rd Nat'l Conf. Assoc. for Computing Machinery*. Princeton, NJ: Brandon Systems Press, 1968.
- Rubenstein, M.F. *Matrix Computer Analysis of Structures*. Englewood Cliffs, NJ: Prentice-Hall, 1966.
- Rutishauser, H. "Deflation bei Bandmatrizen," *ZAMP* 10, 1969.
- Ruzik, J.M. et al. *Welded Portal Frame Tested to Collapse*. Bethlehem, PA: Lehigh Univ., Feb 1952.
- Saucier, K.L. et al. *High Compressive Strength Concrete*, AFWL-TR-65-16. Vicksburg, MS: Army Waterways Exp. Station, 1965 (AD 622 445).
- Seed, H.B. and Idriss, I.M. *Soil Moduli and Damping Factors for Dynamic Response Analyses*, EERC-70-10, Berkeley: Univ. of Calif. Earthquake Eng. Res. Center, Dec 1970 (PB 197 869).
- Shubinski, R.P.; Wilson, E.L.; and Selna, L.G. "Dynamic Response of Deepwater Structures," *Proc. Civil Eng. in the Oceans*, San Francisco, CA, Sep 6-8 1967. New York: Amer. Soc. of Civil Eng.
- Skempton, A.W. (1961) "Effective Stress in Soils, Concrete, and Rocks," in *Pore Pressure and Suction in Soils*. London: Butterworth, 1960.
- Spangler, M.G. *Soil Engineering*, Scranton, PA: Int'l Textbook Co., 1960.
- Struct. Eng. Assoc. of Calif. (SEAOC) *Recommended Lateral Force Requirements and Commentary*. San Francisco, CA: SEAOC, 1975.
- Swanson, S.R. *Development of Constitutive Equations for Rocks*, Ph.D. Thesis, Univ. of Utah, Salt Lake City, Utah. Ann Arbor, MI: Univ. Microfilms, 1969.
- Swolfs, H.G. *Influence of Pore Fluid Chemistry and Temperature on Fracture of Sandstone Under Confining Pressure*, Ph.D. Thesis, Texas A & M University. Ann Arbor, MI: Univ. Microfilms, 1971.
- The Ralph M. Parsons Co. (RMP) *Guide for the Design of Shock Isolation Systems for Underground Protective Structures*, AFSWC-TDR-62-64. Los Angeles: RMP, Dec 1962 (AD 298 578).
- Tracy, F. *An Interactive Graphics Finite Element Methods Grid Generator for Two Dimensional Problems*, MPK-77-5. Vicksburg, MS: Army Eng. Waterways Exp. Station, 1977.
- Ural, O. *Matrix Operations and Use of Computers in Structural Engineering*. Scranton, PA: International Textbook, 1971.
- _____. *Finite Element Method: Basic Concepts and Applications*. New York: Intext Educational Pub, 1973.

- Van Horn, D.A. "A Study of Loads on Underground Structures," *Proc. Symp. on Soil/Structure Interaction, Univ. of Arizona, Tucson, AZ*, Sep 1964.
- Vesic, A.S. and Clough, W.G. "Behavior of Granular Materials Under High Stresses," *Proc. ASCE Soil Mech. Div.* 94:SM3, May 1968.
- Viest, I.M.; Siess, C.P. et al *Full-Scale Test of Channel Shear Connectors and Composite T-Beams*, Eng. Exp. Station Bull. 405. Urbana, IL: Univ. of Ill., Dec 1952.
- Wallace, G.B.; Slebir, E.J.; and Anderson, F.A. "Foundation Testing for Auburn Dam," in *Rock Mechanics—Theory and Practice* edited by W.H. Somerton. New York: Amer. Inst. of Mech. Eng., 1970.
- Wang, C.K. *Matrix Methods of Structural Analysis*. Scranton, PA: International Textbook, 1966.
- Watkins, R.K. "Structural Design Trends in Buried Flexible Conduits," *Proc. Symp. on Soil/Structure Interaction, Univ. of Arizona, Tucson, AZ*, Sep 1964.
- Weaver, W. Jr. *Computer Programs for Structural Analysis*. Princeton, NJ: Van Nostrand, 1967.
- Watestein and Borezi, *The Effect of Loading Rate on the Compressive Strength and Elastic Properties of Plain Concrete*. National Bureau of Standards Report No. 1523, Washington, D. C., March 1952.
- Wiehle, C.K. "Review of Soil/Structure Interaction," in *Proc. Symp. on Soil/Structure Interaction, Univ. of Arizona, Tucson, AZ*, Sep 1964.
- Wilson, E.L. *A Computer Program for the Dynamic Stress Analysis of Underground Structures*, UCSWSM-68-1. Berkeley: Univ. of Calif. Struct. Eng. Lab., Jan 1968 (AD 832 681).
- _____. *SAP a General Analysis Program*. Berkeley: Univ. of Calif. Struct. Eng. Lab., Report No. 70-20, Sep 1970.
- _____; Farhoomand, I.; and Bathe, K-J. "Nonlinear Dynamic Analysis of Complex Structures," *Earthq. Eng. & Struct. Dyn.* 1:3, Jan-Mar 1973.
- Winter, G. and Nilson, A.H. *Design of Concrete Structures*, 8th ed. New York: McGraw-Hill, 1973.
- Zienkiewicz, O.C. *The Finite Element Method in Engineering Science*. London: McGraw-Hill, 1971.

The proponent agency of this publication is the Office of the Chief of Engineers, United States Army. Users are invited to send comments and suggested improvements on DA Form 2028 (Recommended Changes to Publications and Blank Forms) direct to HQDA (DAEN-ECE-T), WASH DC 20314.

By Order of the Secretary of the Army:

JOHN A. WICKHAM, JR.
General, United States Army
Chief of Staff

Official:

ROBERT M. JOYCE
Major General, United States Army
The Adjutant General

Distribution:

Army: To be distributed in accordance with DA Form 12-34B, requirements for TM 5-800 Series: Engineering and Design for Real Property Facilities.

